COMBUSTION AERODYNAMICS AND POLLUTION FORMATION IN GAS-FIRED FURNACES

by

Asaad M A Kenbar

B.Sc (Basrah) & M.Sc (Glasgow)

Thesis submitted for the degree of

Doctor of Philosophy

Department of Mechanical Engineering

University of Glasgow

February 1991

Glasgow, Scotland

ACKNOWLEDGEMENTS

I would like to thank most sincerely my supervisor Dr N R L Maccallum for all his help, advice and inspiration throughout the course of this work, also with regard to the presentation of this thesis.

In particular, I am deeply indebted to Dr S A Beltagui (Glasgow University and National Engineering Laboratory) for his continuous assistance, numerous stimulating discussions and willingness to give his expertise.

I would especially like to thank Mr T Ralston (project manager) for his support, encouragement and the provision of all the facilities at NEL. Thanks are also due to other members of his team, Mr R N F Fuggle and Mr M S L McLEAN.

I am grateful to Dr C N B Martin for lending me his portable PC which I used at home.

Thanks are also due to the supporting staff at NEL, especially those in the Rankine building, purchasing section and the workshop.

Finally I would like to thank sincerely Dr H J Edrees for his inspiration during the course of my studies.

SUMMARY

This thesis presents a combined experimental and theoretical study of the combustion aerodynamics and pollutant formation in confined swirling flames. The fuel used in this study was natural gas.

In the experimental part of the work, two fuel injection modes are examined as alternatives to the conventional central axial fuel injection mode. These alternatives are (a) introducing the fuel around the periphery of the swirled air jet, and (b) injection radially outwards from the central axis, across the entering swirled air flow. The measurements were performed in a semi-industrial size furnace with a movable-block swirl generator. Four swirl settings were examined, covering swirl number range of 0 to 2.25. The flow patterns (as defined by three time-averaged velocity components and static pressure), combustion patterns (as defined by temperature and species concentrations) and pollutant formation (CO and NO_x) were investigated for these two alternative injection modes as well as for the conventional central axial mode to assess the merits of the three systems. The formation of NO_x has been studied in greater detail in these three systems. For the flow and combustion patterns, measured along the furnace, the main input variable was swirl, while for the pollutants, measured in the stack, the main input variables were fuel equivalence ratio and swirl.

The investigations showed that with the radial fuel injection system, a stable flame was achieved without swirl, while for the peripheral and central axial injection systems, a minimum swirl number of 0.8 was required to establish a stable flame. By introducing some of the combustion air radially outward through a central gun with the peripheral fuel injection system, a stable flame was achieved without swirl.

With the central radial and peripheral fuel injection modes, complete combustion can be guaranteed with 5% excess air, while for the central axial fuel injection at least 10% excess air was required to achieve complete combustion.

The results of flow and combustion patterns demonstrate that the highest rates of mixing, combustion efficiency and heat transfer from the flame were achieved with the peripheral fuel injection. Increasing the degree of swirl was found to improve these characteristics by

producing a more uniform and intense flame. The measurements of NOx at lean and rich conditions showed that this system offers wider scope for NOx reduction through lean combustion and staged combustion (ie both air and fuel staging).
The radial fuel injection has also produced much improved mixing and combustion efficiency compared with the central axial fuel injection. However, with this system and with the central axial injection, only air staging can be used to reduce NOx formation.
In all fuel injection modes, the strong dependence of NOx generation on flame temperature confirms that its principal formation is by the thermal mechanism. Locally, the effect of swirl on NOx formation was significant, however, its effect on the overall values was small.

In the theoretical part of the work, predictions of the overall NOx formation are made using a well-stirred reactor model based on the extended Zeldovich mechanism. The model takes account of the fluctuations of the concentrations of fuel and oxidant in NOx reaction zone. A stochastic analysis has been introduced by the author to calculate the effect of these fluctuations on the NOx formation rate. The results of these predictions compare satisfactorily with the experimental measurements for the three methods of fuel injection.

As part of the validation process of existing computational fluid dynamics (CFD) codes, an assessment is made of the ability of a CFD code to model swirling flames. The peripheral fuel injection mode applied to natural gas swirling flame is a novel test case (Beltagui and Maccallum (1988)). The predictions were made using the PHOENICS code, with turbulence and combustion represented by the k-ε and the 'eddy break-up' models respectively. The main changes in the combustion patterns caused by switching from central axial to peripheral fuel injection were qualitatively well predicted.
For the peripheral fuel injection system, the predicted flow patterns were in reasonable agreement with those previously measured. The quantitative agreement for combustion patterns, however, was good for the non-swirled flow only. This is attributed to the simplified turbulence and combustion models used.

CONTENTS

NOMENCLATURE

A	Eddy break-up constant, Eqn 7.5	-
A_1, A_3, A_5	Constants, Eqn 3.13	-
B_0, B_2, B_4	Constants, Eqn 3.14	-
C_k	Constant, Eqn 7.6	-
C_ε	Constant, Eqn 7.6	-
C_p	Specific heat at constant pressure	J/kg K
d	Swirler diameter	m
D	Furnace diameter, or	m
	Constant, Eqn 3.15	-
E	Efficiency factor, suction pyrometer	-
f	Mixture fraction	-
F	Shape factor, suction pyrometer	-
G	Total axial momentum flux	N
G_d	Axial momentum flux, dynamic component	N
$\bar{G}_d$	Normalised axial momentum flux	-
h	Specific sensible gas enthalpy	J/kg
H	Sensible enthalpy flux	J/s
k	Kinetic rate constant, or	cm^3/mole.s
	Kinetic energy of turbulence	m^2/s^2
K_δ	Ratio, $(\delta_{in}/\delta_{cal})$	-
K_ϕ	Flow angle coefficient (5-hole probe calibration)	-
K_p	Static Pressure coefficient (5-hole probe calibration)	-
K_U	Velocity coefficient (5-hole probe calibration)	-
l	Characteristic Dimension, Eqn 7.7	m
m	Mass fraction	kg/kg
p	Pressure	N/m^2

p_o to p_4	Pressure readings (5-hole probe)	mm H_2O
r	Radius	m
R	Rate of chemical reaction, or	kg/m^3s
	Universal gas constant	J/K mole
s	Stoichiometric air-fuel ratio	-
S	Source term, or	
	Burner Swirl Number (Based on swirler radius) $= \dfrac{\int 2\pi r^2 \rho u w \, dr}{r_b \int 2\pi r \rho u^2 \, dr}$	-
S_d	Burner Swirl Number (Based on swirler diameter) $= \dfrac{\int 2\pi r^2 \rho u w \, dr}{d \int 2\pi r \rho u^2 \, dr}$	-
S^*	Furnace swirl number (Based on furnace diameter) $= \dfrac{\int 2\pi r^2 \rho u w \, dr}{D \int 2\pi r \rho u^2 \, dr}$	-
S_o	Mixedness factor	-
t	Residence time	s
T	Temperature, or	K
	Axial flux of tangential momentum	N m
$\bar{T}$	Normalised tangential momentum flux	-
T_m	Suction pyrometer measured gas temperature	K
T_o	Suction pyrometer equilibrium gas temperature	K
T_g	True gas temperature	K
u,v,w	Time-averaged axial, radial and tangential components of velocity	m/s
V	Velocity vector	m/s
X	Axial distance along the furnace	m
x	Number of carbon atoms in hydrocarbon	-
y	Number of hydrogen atoms in hydrocarbon	-
Z	Fluctuation parameter, Eqn 6.6	-

Subscripts

b	Burner
cal	Calculated
cor	Corrected
fu	Fuel
in	Input
ox	Oxidant
pr	Product
ref	Reference
st	Static

Greek letters

α	5-hole probe yaw angle	-
β	5-hole probe pitch angle	-
Γ_{φ}	Turbulent exchange coefficient	-
δ	5-hole probe dihedral angle	-
ε	Rate of dissipation of kinetic energy of turbulence	m^2/s^3
ξ	Completeness of combustion	-
ρ	Density	kg/m^3
σ	Standard deviation	-
ϕ	Fuel/air equivalence ratio, or	-
	5-hole probe conical flow angle	-
$\overline{\phi}$	Mean value of fuel/air equivalence ratio	-
φ	Dependent variable	-

LIST OF TABLES

LIST OF PHOTOGRAPHS

LIST OF FIGURES

CHAPTER 1

INTRODUCTION

There are numerous requirements which must be considered when designing an industrial burner. These requirements include: wide stability limits, wide turn-down ratio, high combustion efficiency, high intensities of heat release, high heat transfer rates from the flame, low burner pressure drop, low noise and low emissions of pollutants. Some of these requirements are conflicting and the design has to be based on compromise. In order to achieve the best compromise, maximum use must be made of our knowledge of the key processes. One such key process is the mixing between the fuel and air. The fuel can be thoroughly mixed with the air prior to entering the combustion chamber- the "pre-mix" configuration, or the mixing can occur within the combustion chamber itself- the "non-premix" configuration. As "pre-mix" combustion systems are not generally favoured in industrial applications for reasons of safety, attention must be directed towards mixing in "non-premix" combustion systems.

In the systems which are of the "non-premix" type, there are two physical processes that can be adopted to achieve mixing within the combustion chamber. These are respectively shear layer mixing and centrifugal mixing. Shear layer mixing is effectively utilised if the fuel is injected into the regions of maximum shear in the air stream. Centrifugal mixing effects can be utilised by swirling the flow and creating favourable density gradients within flow of air, fuel and products. The employment of the full benefits of these two physical processes in a practical combustor depends significantly on the method of fuel injection. The review of the literature (Chapter 2) has shown

that the most common method of fuel injection is axially at the centre of the burner. This method of fuel injection suffers some disadvantages in terms of mixing and combustion efficiency. As an alternative to the central axial fuel injection, the fuel can be injected at the periphery of entering air jet. This system offers the possibility of employing both shear layer and centrifugal mixing, thus resulting in efficient mixing and hence high combustion intensity. Another variation from conventional central axial fuel injection is to inject the fuel radially from the centre axis across the entering air jet. This method also has some attractive features in stability and mixing. Although each of the three basic methods of fuel injection indicated above has been investigated in different combustion applications, complete and detailed information are not available to provide reliable comparisons between their performance, particularly in an industrial application. The main objectives of this work are therefore twofold:

First objective

To acquire complete and reliable data to compare the following fuel injection methods in a semi-industrial scale application:

1- Central axial fuel injection

2- Peripheral axial fuel injection

3- Central radial fuel injection

These comparisons should provide the information needed to optimise both the fuel injection mode and swirl to achieve the best characteristics of combustion and the lowest formation of pollutants. The investigations were carried out in a cylindrical upshot process fired heater (furnace hereafter) with a movable-block swirl generator. The furnace was fired by natural gas fuel. The furnace and all support equipment were located at the National Engineering Laboratory (NEL),

East Kilbride. The work was carried out as part of collaborative programme between Glasgow University and the NEL.

Flow and combustion patterns were assessed by the following measurements at different radial locations on cross-section along the furnace:

1- Three time-average velocity components and static pressure, using 5-hole pitot probe.

2- Temperatures using suction pyrometer.

3- Concentrations of carbon monoxide (CO), carbon dioxide (CO_2), oxygen (O_2), hydrocarbons (HC) and oxides of nitrogen (NO_x), using a modified sampling probe.

Measurements of main pollutant (ie CO and NO_x) were also performed in the stack under a wide range of fuel equivalence ratio.

Second objective

In addition to the knowledge acquired from the above experimental measurements, they also provide an extensive data bank which is valuable in developing and testing theoretical models of furnace flow, heat transfer and pollutant formation. Confidence in program predictions requires detailed comparison with reliable experimental measurements. Such data are vital as furnace flow and heat-transfer mathematical models are developed to handle realistic geometries. As part of the present investigations, the following theoretical modelling work has also been performed:

1- Predictions of the overall NO_x formation using a well-stirred reactor model based on the extended Zeldovich mechanism. The model takes account of the fluctuations of the concentration of fuel and oxidant in the NO_x reaction zone. A stochastic analysis has been adopted to calculate the effect of these fluctuations on the NO_x

formation rate.

2- Predictions of aerodynamic and combustion patterns using the computational fluid dynamic (CFD) code, PHOENICS. The immediate objectives of this work were to assess the ability of PHOENICS to:

   a- Model the combustion aerodynamic of swirling flames. The peripheral fuel injection mode (Beltagui and Maccallum (1988)) is a novel test case and therefore considered in this study.

   b- Predict the main changes caused by switching from the traditional central axial fuel injection to the peripheral injection considered in (a) above.

An outline of the work presented in this thesis is summarised below:

In Chapter 2, a survey of the literature is presented with special emphasis on the areas of fuel injection modes, NOx formation and CFD which are directly related to the present work.

Description of the experimental set-up, test equipment and sampling conditions are presented in Chapter 3.

Results of the experimental measurements showing the detailed picture of flow patterns, combustion patterns and pollutant formation are described in Chapter 4.

In Chapter 5, the results of the three fuel injection modes are compared and discussed to assess the merits of each system relative to the other.

The modelling work of NOx formation is presented in chapter 6. Model

results are compared with the experimental measurements performed in the stack for each of the three fuel injection modes.

In chapter 7, the predictions of flow and combustion patterns of swirling flames are presented as indicated above.

In the final Chapter, the major conclusions of the work are summarised, and suggestions are made for further work.

CHAPTER 2

LITERATURE REVIEW

2.1 INTRODUCTION

For many years, concentrated research effort has been expended on understanding and characterising the combustion aerodynamics of swirl-flow burning processes of gaseous, liquid and solid fuels. Economical design and operation of practical combustion equipment can be facilitated greatly by estimates made from complementary experimental and modelling studies. Detailed survey of the vast range of research work in this field is outside the scope of this thesis, thus, the survey of the literature presented below will only cover the areas directly related to the present work.

The survey will be started with applications where different methods of fuel injection have been studied in swirling flow. Where experimental results offering comparisons are available, they are introduced to highlight the points of weakness and strength in each method of fuel injection.

A detailed review is then given of the generation and control of NOx in swirling flames. The review will be focused on studies of the effect of burner parameters on NOx generation in furnaces and gas turbine systems, including studies covering the use of different fuel injection methods to reduce NOx formation. The different prediction models of NOx formation are also summariesed.

To complement the review of experimental work indicated above, a brief review of the theoretical predictions of flow and combustion of

swirling flows are presented.

It is important to indicate that this survey will be mainly concentrated on the 'non-premixed' combustion systems as indicated in Chapter 1.

2.2 FUEL INJECTION MODES IN SWIRLING FLAMES

Swirling flows are found in many combustion systems, notably, gas turbines, boilers, furnaces and incinerators. Experimental studies in these flows (eg, Bafuwa and Maccallum (1970), Syred and Beer (1974), Beltagui and Maccallum (1976-a), Lilley (1977), Claypole and Syred (1981), Gupta et al (1984), Gouldin et al (1985), and Beltagui and Maccallum (1988)) show that swirl has large scale effects on flow field in reacting flows. For example, it affects the flame size, shape, stability, combustion intensity and pollutant formation. The degree of swirl is usually characterised by a swirl number S, which is a non-dimensional number representing axial flux of tangential momentum divided by axial flux of axial momentum times equivalent dimension (either burner throat diameter or furnace diameter). In non-premixed combustion systems, the degree of swirl required to achieve the desired flame stability and degree of combustion depends significantly on the mode of fuel injection.

Several studies have been performed to assess the effect of fuel injection method on flame characteristics indicated above. Leuckel and Fricker (1976) and Fricker and Leuckel (1976) have studied the effect of swirl burner geometry and fuel injection method on stability and intensity of industrial-scale natural gas flames in furnaces. Four fuel injection arrangements were studied, all placed at the axis of the burner but varied in the method of fuel injection into the swirled air

flow. These are axial jet, annular axial jet, sixteen diverging jets and axial gas jet with sixteen throttle jets. Two distinct flame forms were observed in these tests with characteristics studied through the detailed measurements of velocity, gas compositions and temperature. The first flame type was observed with central axial fuel injection where the fuel jet in this case was able to penetrate completely the central reverse flow zone (CRZ) leading to a relatively small annular reverse flow zone between the gas and combustion air flows. Part of the fuel is recirculated with the CRZ together with hot combustion gases, and these mix with combustion air inside the burner quarl to give the first combustion zone, which stabilises the flame at the burner. The rest of the fuel is preheated in its passage through this zone and subsequently mixes and burns with the remaining combustion air giving a comparatively long flame tail. The fuel preheating occurs in an oxygen deficient zone, and this condition was found to lead to cracking and flame luminosity when residence times were increased by reducing the burner air and fuel flow rates proportionally. The flame has also been found to be highly asymmetric.

The second flame type was observed with the other fuel injection methods (ie, annular axial, sixteen divergent jets and axial gas with sixteen throttle jets). In these methods, the CRZ prevents the forward progress of the fuel jet, and causes it to spread away from the flame axis within the burner quarl to give an intense blue flame with rapid mixing. The flame in these injectors is highly symmetrical.

Hallet and Gunther (1978) have studied the influence of swirl and fuel injection mode on the shape and properties of the flame in free surroundings and in a furnace. The natural gas fuel was introduced at the axis of swirled air, axially in the first mode and radially outward

in the second mode. The flame properties were assessed by measurements of three velocity components and static pressure, temperature and species concentrations. Comparisons between the stability limits of the axial and radial gas injectors have shown that the radial gas injector leads to a higher stability at lower swirl, confirming a more efficient mixing of the gas and air near the burner. These characteristics have been achieved due to the coincidence of the radial gas jet with regions of high velocity gradients between the forward flow and the CRZ. This system of radial injection has therefore been recommended for use in combustion systems.

A method of fuel injection with some deviation from the conventional central axial injection has been investigated by Suzuki et al (1982) in high-temperature heating furnaces used in the steel industry. In this method, the fuel gas has been injected at an angle to the axis of the air stream instead of being injected axially at the centre. The heating efficiency of this combustion method was discussed from the standpoint of flame radiation, temperature and NO_x formation. Comparing the performance of this method with that of the central axial fuel injection, the authors reported improved heat transfer and energy consumption by increasing flame surface area and flame emissivity through slow combustion.

A multi-annular swirl burner design has been investigated by Gupta et al (1976), the fuel gas and air being injected alternately through a succession of annular openings. In this way the fuel injection was matched with regions of high shear in the flow. High efficiencies were reported, coupled with low emissions and low noise levels. The disadvantages of the system were its likely high cost and its pressure

loss. Also, the design could not take advantage of the centrifugal mixing effects.

The introduction of the fuel at locations other than the axis can also be used to reduce noise. For example, Gupta et al (1973) used a combination of radial and axial injection of natural gas fuel to obtain a significant noise reduction in a swirl-stabilised burner.

In a test of confined swirling non-premixed combustion, Tan and Maccallum (1983) have shown that much shorter flames and consequently much higher combustion efficiencies could be achieved when the fuel was introduced near the outer wall of the combustion chamber, instead of at the axis. Also the flame was much more easily stabilised than in the central injection case where air swirl vane inclination to the axis of higher than 45° was required.

The effect of centrifugal forces on the mixing and flame propagation in enclosed swirling systems, applicable to aerogas turbine has also been studied by Ahmad et al (1984). Central axial fuel injection was compared with fuel injected at the wall and with premixed combustion. When the fuel was injected at the centre of a swirling flow with CRZ, flame propagation was retarded by centrifugal forces returning the burnt gases to the fuel rich core of the flow. The fuel rich central core produced large unburnt hydrocarbon (UHC) and carbon monoxide(CO) concentrations which only burnt out well downstream of the CRZ. When fuel was injected at the wall, centrifugal forces moved burnt gases to the centre and displaced air towards the wall, prompting mixing and flame propagation. This system of injection has therefore resulted in better mixing, high combustion efficiency and lower pollutants

formation. The above authors have also compared their work with other investigators that have used central axial fuel injection systems. These comparisons have highlighted the poor characteristics of the central axial fuel injection in combustion devices and the superiority of the wall injection system.

In a similar study but in an adiabatic furnace, Beltagui and Maccallum (1988) have reported a novel burner where the fuel has been injected at the outer boundary of the swirled air flow. This system makes use of the shear layer mixing at the outer jet boundary together with mixing currents created by centrifugal forces associated with rotating flow. The utilisation of these effects results in a stable flame even without a CRZ. This system was studied through the detailed measurements of velocity components and static pressure, temperature and species concentrations. Comparison of the results of this system with those of the central axial fuel injection, taken on the same system, have revealed the potential of the peripheral fuel injection for producing high intensity flames with wide stability ranges.

The flame characteristics of another swirl-stabilised, non-premixed natural gas burner have been studied recently by Milosavljevic et al (1990) under a wide range of input conditions. Three quarl arrangements and three fuel injection modes were covered in this study. The fuel injector was placed at the axis and, the fuel was injected in three arrangements, axial, angled annular and radially outward. The objectives of this study were to study the stability, symmetry and sizes of CRZ's as a function of swirl and Reynolds numbers. This study has shown that when central axial and central annular fuel injection modes were used, a stable flame could not be achieved without some

degree of swirl. However when radial fuel injection was used, stable flame could be obtained without the need for swirl, due to the blockage created by the gas jet. By contrast to the angled annular and radial fuel injection modes, the central axial fuel injection achieved symmetric flame only under limited range of input conditions.
The creation of aerodynamic blockage, leading to a CRZ, by the use of radial fuel injection has been reported by Beltagui et al (1988-a and 1988-b) based on isothermal flow tests carried out at the NEL.

From the above review, it is seen that there is a strong evidence to support the use of fuel injection either radially outwards or at the outer periphery of the swirled air flow. These two fuel injection modes lead to enhanced mixing rates and generally shorter flames that can be stabilised at no swirl or low degree of swirl.
The present thesis represents a contribution to the further development of radial and peripheral fuel injection systems.

2.3 NOx GENERATION IN SWIRLING FLAMES

Combustion generated pollution is now recognised as a threat to the environment. The most obvious air pollutant is smoke, being visible to the naked eye. Other pollutants of importance are carbon monoxide, sulphur oxides (SO_x) and nitrogen oxides (NO_x). Recently attention has been focused on NO_x.

NO_x is a collective name for nitrogen oxides; N_2O , NO and NO_2. Combustion produces NO and to a lesser extent NO_2. At atmospheric temperature NO is converted to NO_2 and some N_2O. Locally NO_x is toxic and is known to act through photochemical reactions as a precursor to the formation of smog and other pollutants. On a wider scale it causes damage to plant life and soil through its contribution to acid rain. It

has a global effect, as N_2O is involved in depletion of the earth's ozone layer (OECD Reports (1979, 1984)).

Stationary combustion sources are responsible for about half the total man-produced NO_x. Emission standards progressively call for tighter control on emission levels. Early regulations specified percentage reductions of the then current emission levels, these reductions being achievable by the application of the most up to date technology. However, recent regulations for new sources prescribe specified levels of emissions in order to maintain a reasonable, healthy atmosphere (Anon (1988)).

2.3.1 Sources and formation mechanisms of NOx

The generation of NO_x in combustion requires the presence of nitrogen. This comes from two combustion elements, ie air and fuel. The removal of nitrogen from air before combustion is impossible and from fuel is impractical.

The nitrogen fixation is also dictated by the combustion environment, thus NO_x formation can be limited through careful combustion control.

It has been recognized that there are three important NO_x formation mechanisms- thermal, prompt and fuel. The understanding of the NO_x source and formation mechanism will determine the appropriate technique to be selected for NO_x reduction.

Various general reviews of combustion generated pollution have been published recently eg, Sawyer (1980), Levy (1982), Clarke and Williams (1985), Lawn (1987) and Williams (1989).

A brief review of NO_x formation mechanisms is presented below.

(i) Thermal NOx

The "thermal NO_x" refers to that formed from the free N_2 in the air as

it passes through the high temperature post-flame zone. The formation mechanism being that proposed by Zeldovich, (reactions 2.1 and 2.2) and further extended to include reaction 2.3 (Bowman (1975)),

$$O + N_2 \rightleftarrows NO + N \qquad (2.1)$$

$$N + O_2 \rightleftarrows NO + O \qquad (2.2)$$

$$N + OH \rightleftarrows NO + H \qquad (2.3)$$

The last reaction contribution is mainly at rich mixtures. In most cases the O atom concentration is assumed to be that in equilibrium with O_2. The main features of the above reactions are their relatively high activation energies, thus they are much slower than the main combustion reactions and can be decoupled from these (Sadakata et at (1980)).

Thermal NO_x is the main mechanism for NO_x generation when burning N-free fuels such as natural gas. However, its contribution is not significant when combustion zone temperatures are less than 1500 K.

The local rate of thermal NO_x formation depends upon the following three parameters:

a- Flame temperature- which is the main factor since NO temperature relation is exponential.

b- Oxygen concentration in the post-flame zone.

c- Residence time of gas in the high temperature region.

However it must be emphasised that the local spacial and temporal variations in these parameters are also important, eg locally fuel-rich or fuel-lean pockets have been shown to give different NO_x production rates from those derived by mean values as discussed by Appleton and Heywood (1972).

A contribution to the study of thermal NO_x formation is given in

chapter 6 of this thesis.

(ii) Prompt NOx

Early workers realised that the thermal mechanism failed to predict the high observed formation of NOx in the early part of some flames- especially hydrocarbon rich flames (Fenimore (1970) and Engleman et al (1972)). This led Fenimore (1970) to consider other reactions where the hydrocarbon fragments attack bimolecular nitrogen, producing atomic nitrogen, cyanides, and amines, which subsequently oxidize to nitric oxide.

$$CH + N_2 \rightleftarrows HCN + N \qquad (2.4)$$

$$C + N_2 \rightleftarrows CN + N \qquad (2.5)$$

The term "Prompt NO" was used to describe NO formed early in combustion, through such mechanism. It was found to be of minor importance relative to thermal NO for cases of lean mixtures and of H_2 or CO flames (Toof (1986)).

The rate of prompt NO formation is not temperature sensitive and cannot be separated from the HC kinetics. Sarofim and Pohl (1972) confirmed this and tried to relate the prompt NOx formation to a partial equilibrium mechanism with overshoot of O atoms in the flame. Takagi et al (1976) measured HC and HCN in flames and related these to prompt NOx.

Measurements of prompt NOx were also made by Semerjian and Vranos (1976) in rich flames. They found that prompt NOx formation was unaffected by the temperature fluctuations in the flame. In another study it was found that increasing the pressure increased the formation of prompt NOx (Heberling (1976)). A detailed review of prompt NOx

formation is given by Hayhurst and Vince (1980).

The contribution from prompt NOx is less than 5% of the total NOx in the case of gaseous fuels but is higher in cases of liquid and solid fuels, eg, Williams (1989).

(iii) Fuel NOx

The name "fuel NOx" refers to NOx from the nitrogen-containing compounds in the fuel. The chemical reaction mechanisms are more complex than the thermal NOx mechanisms and their temperature dependence is very weak (Gupta and Lilley (1985)).

The general hypothesis is that the fuel nitrogen molecules pyrolise or react to form an intermediate nitrogen containing species, designated I (HCN or NHi, i=0,1,2,3). This intermediate can then react with an oxygen containing molecule, R, to form NO, or with NO or possibly another I to form N_2.

$$\text{Fuel Nitrogen} \longrightarrow \text{I} \qquad (2.6)$$

$$\text{I} + \text{R} \longrightarrow \text{NO} \qquad (2.7)$$

$$\text{I} + (\text{NO or I}) \longrightarrow N_2 \qquad (2.8)$$

The rate of conversion of fuel nitrogen to NO decreases with increased fuel nitrogen content and is independent of the type of fuel, Sawyer (1980).

This rate is also dependant on the fuel equivalence ratio. Tang et al (1980) report that maximum conversion rates occur for lean mixtures, with equivalence ratios of 0.6 to 1.0. The measured conversion rates diminished for rich mixtures. Hence control of fuel NOx is sometimes based on the reduction of oxygen in the primary combustion zone- called "air staging".

Fuel NOx is the major contributor in the case of solid fuels, which

usually contain N-compounds. At the other extreme, natural gas is relatively free of nitrogen compounds, thus thermal NOx is the main mechanisms of formation. Liquid fuels usually fall between these bounds according to their nitrogen content and combustion conditions.

2.3.2 Control of NOx

In principle there are three general approaches to reduce NOx emissions:

1- Through the prevention of formation by combustion control. NOx is the most amenable of pollutants to prevention through modification of the combustion process, especially thermal and prompt NOx.

2- Through the promotion of destruction after formation by reducing reactions in a reburning zone.

3- If more reduction is needed, then treatment of the combustion products has to be implemented as a last resort. In this case chemicals are injected in the combustion gases and reactions may occur under catalytic conditions. The energy and running costs of implementing the above three techniques increase in the order they are listed above.

Some of these techniques may reduce efficiency, eg lower preheat, water injection. In power applications this is important but it could be of no effect in process applications if the process temperature is already low and thus not compromised (eg. Pfeiffer and Altmark (1987)).

The cost of the implementation of these measures is due to:

a- The reduction in efficiency or loading of the plant, (Thomson and Crow (1976)).

b- The initial cost of the extra equipment.

c- The cost of the materials, eg chemicals, and energy used in the process by fans, injectors etc. Some cost analysis is given in the

OECD Report (1983).

Other factors should be considered when selecting the technique for NOx control such as the effect upon the process and on the formation and control of other pollutants eg CO, SOx, HC etc.

The possibility of controlling both SOx and NOx simultaneously is under investigation, for example the reduction of both by use of ozone (Lozovskii et al (1988), and Anon (1989)).

(i) Control of combustion

The control of combustion to prevent the formation of NOx represents the most promising and cost effective of all methods of NOx control. The extensive worldwide research on NOx formation covering different areas of applications has resulted in many practical means for NOx control. Table 2.1 lists review of NOx control investigations. These are classified, according to the technique used and the proposed application. The principles of operation of these techniques are as follows:

1- Lowering the peak combustion temperature. Reduction of combustion peak temperature is very effective when dealing with thermal NOx, but not effective for fuel NOx. Techniques leading to this aim include:

   a- Off-stoichiometric combustion, through staged combustion,

   b- Very lean combustion, flame tube premixed burner, fibre burner, cyclone combustors,

   c- Reduced preheat,

   d- Increased heat transfer in the burner zone.

   e- Flue gas recirculation especially if the gases are cooled before recirculation.

Table 2.1

Review of NOx Emission Control Methods

Investigators	Techniques	Applications
OECD NOx Control for Stationary Sources, 1983.	Review of techniques.	Utility, Process.
Breen et al, 1970.	General Review.	Utility
Sawyer, 1980.	General Review.	Utility
Lefebvre, 1974.	General Review.	Gas Turbine
Foster, 1974.	General Review.	Furnaces.
Ahmad et al, 1984	Burner controlled mixing,	Gas Turbine
Andrews et al, 1988.	Shear layer fuel injection,	Process
Al-Shaikly et al,1989	both axial and radial.	
Markoski et al, 1976.	Premix-prevap swirl burner.	Gas Turbine
Gupta et al, 1974.	Fuel injection control, burner geometry and swirl.	Process
Suzuki et al, 1982.	Controled slow mixing, low temperature , internal FGR	Steel processing
Pfeiffer and Altmark, 1987.	Low temp. premixed radiant tube burner.	Process, Gas turbine, small boiler
Mirzaie and Syred, 1989.	Cyclone low temp. very lean combustion.	Process, low CV fuels
Schefer and Sawyer, 1976.	Lean combustion opposed jet system.	Gas Tubine
Meier and Vollerin, 1976.	High swirl with FGR.	Domestic Boilers.
Barnes et at, 1988.	Radiant Burner.	Domestic heating
Hadvig et al, 1988.	Fibre Burner.	Boiler.
Ritz et al, 1989.	Reburn with NH3 mixed with fuel	Boilers
Mulholland and Hall, 1987	Reburn with gas or oil fuel	Packaged boiler
Hunter et al,1978.	Combustion modification, Review.	Various Processes.
Siddiqui et al, 1976.	Review of techniques	Fired Heaters
Nutcher, 1984.	Review of air and fuel staging and FGR	Fired Heaters
Destefano, 1985.	NH3 injection	Glass furnace
Abassi et al, 1988.	Low excess air and slow mixing.	Glass furnace
Tsirul'nikov et al, 1986.	Low excess air, FGR and steam injection.	Utility
Meyer and Mauss, 1973	Stratified combustion, swirl and FGR.	Fundamental

Table 2.1 continued

Investigators	Techniques	Applications
Abdalla et al, 1989.	Stratified, well stirred reactor.	Fundamental
Oven et al, 1978.	Stratified swirl burner.	Fundamental
Waibel and Nickeson, 1986.	Fuel and Air staging with FGR.	Process Refinery.
Yamagushi et al, 1974	Air staging.	Boiler.
Kotler and Imankulav, 1986.	Air Staging, swirl.	Utility.
Hirai et al, 1987.	Air Staging, swirl.	Boiler, Process.
Sadakata et al, 1980.	Air Staging, preheat.	Model.
Knill, 1987.	Review of fuel staging, pf.	Utility
Smart and Weber, 1987	Internal Air staging and Precombustor.	Utility
Brown et al, 1973.	FGR	Boiler
Sigal et al;1986.	FGR.	Utility.
Godridge, 1986.	FGR.	Utility.
Lukoshyavichyvs et al, 1986.	Water spraying.	Utility.
Novoselov et al,1986, Lozovskii, 1988 and Simachev et al, 1988.	Reduction of NOx and SOx by Ozone.	Utility.
Skorik et al, 1986.	Ammonia Injection.	Utility.

f- Water injection into the primary combustion zone of a burner, as used in industrial turbines and boilers, utilizes the latent heat of evaporation of water droplets to reduce temperature. This method is most effective if water is injected exactly where needed, ie in the peak temperature zone.

2- Improved burner mixing thus eliminating temperature variations between lean and rich local mixtures. Uniform mixing is possible in premixed burner but stability and control may suffer. Injection of fuel in the shear layer of the air jet produces very low NOx with better stability and efficiency, eg Andrews et al (1988).

3- Reduction of excess oxygen. Low excess air combustion results in O_2 concentration being reduced, and efficiency is increased, as in the case of staged combustion. Both air staging and fuel staging can be

applied. Flue gas recirculation also dilutes the mixture thus reduces O_2 concentration.

4- Reduction of residence time in the flame zone and the peak temperature zone.

(ii) Destruction of NOx

By reburning in a second combustion stage, preferably using a low or N free fuel, oil or gas. Fuels such as CO, H_2 and hydrocarbons will react with O_2 rather than NO if both exist but when O_2 is completely used up they will reduce NO to N_2 (OECD Report (1983)).

(iii) Flue gas treatment

The processing of combustion products to remove NO_x is used as a final measure with or without the above described methods.

In the thermal "de-NO_x" process, reducing compounds eg ammonia, urea, ozone etc are injected into the flue gases under catalytic or non-catalytic conditions. Ammonia and other amines reduce NO in the primary combustion products in the presence of oxygen within a specified temperature range, (980 - 1370 K) and with certain NH_3/NO equivalence, eg Muzio et al (1976) claim 78% reduction at an optimum temperature of 1240 K with NH_3/NO = 1/1.

Table 2.1 gives a number of publications dealing with various control methods and their applications.

2.3.3 Effect of flow patterns and swirl

The review presented in the above sections dealt with general aspects of NO_x formation and control. This section deals with those aspects relevant to burner flow and mixing, particular emphasis being placed on swirl-stabilized gaseous flames.

(i) Effect of flow pattern

Aerodynamics plays a major role in the reactions in the flame since it dictates the role and conditions under which active species are brought together before the kinetics start to operate. The effects of flow will influence:

1- NOx concentration: This was found to depend on the local conditions early in the combustion process, in the developing jet in the near burner zone (Claypole and Syred (1980)).

2- Mixing effectiveness: This can lead to the suppression of NOx production due to the uniformity of the mixture, otherwise fuel-rich and fuel-lean pockets will exist causing higher local NOx production (Appleton and Heywood (1972) and Gouldin (1974)).

3- Length scale: NOx formation was found to have a length scale dependence (Peters and Donnerhack (1980)). Those workers, studying diffusion flames, correlated this effect with Reynolds Number and Froude Number. NOx formation has also been related to flame stretch in a flat laminar flame (Hahn and Wendt (1980)).

4- Residence time: The residence time of the combustion products in the various zones can only be controlled through the flow parameters.

5- The total NOx production: This is related to the integrated production by the flow and not by the local concentrations in the various zones. Thus in order to establish the total mass of pollutants in the combustor, it is essential to consider the pollutant mass flow profiles as illustrated by Sadakata and Beer (1976) and Claypole and Syred (1980).

(ii) Effect of swirl

The application of swirl to the combustion air can have a major influence on NOx production which is dependant upon the local temperature and mixing rates in the near burner zone. In general increased swirl will produce the following effects :

1- Increased entrainment of cooled combustion products and thereby less thermal NOx, due to lower temperature and O2 concentration.

2- Increased local oxygen availability and thereby more thermal and fuel NOx.

3- Increased combustion intensity and thus higher temperature and more thermal NOx.

These effects have been reported by various investigators. Some of these studies are briefly summarised below.

Owen et al (1976) studied the effect of swirl, fuel/air velocity ratio and pressure on the formation of pollutions from a combustor. They indicated that increasing swirl, in general, reduced NOx formation. They also illustrated how small fluctuations in the flow parameters can cause large scale fluctuations in the resulting NOx.

Oven et al (1978) discussed the influence of swirl on combustion and NOx formation in the light of flame quenching due to the rapid dilution and cooling of the reacting inner jet flow by mixing with the outer flow which thus reduce NOx.

The influence of the level of swirl on the aerodynamics and NOx emissions was also studied by Claypole and Syred (1980). Here again the effect of increased swirl was to reduce NOx emission. This reduction is a result of better mixing prior to combustion and the reduced flame peak temperature. The better mixing also tends to eliminate local imbalances of reactants. These imbalances, when present, produce local fuel-rich regions leading to more prompt NOx. The recirculation zone,

despite elevated temperature, did not appear to play a major role in the formation of NOx.

Similar effects of the flow pattern were also reported by Sadakata and Beer (1976) where NOx formation in a swirling flame was measured. They reported some NOx destruction in the central recirculating flow.

The second and third investigations above reported some NO reacting to produce NO2 in the combustor although the measured levels may have been enhanced by probe reactions.

2.3.4 Effect of fuel injection modes

The effect of the mode of fuel injection on NOx formation has been studied by Ahmad et al (1984), Andrews et al (1988), and Al-Shaikhly and Andrews (1989) in gas turbine combustor configurations. The main findings support the theory of improved mixing when fuel is injected in the shear layer of the air flow- wall injection, and radial injection being found to be superior to central injection. These systems, when used with swirl flow also utilise the centrifugal force in improving the mixing. The high mixing rates led to near premixed conditions producing minimum NOx, together with improved efficiency and turn down.

Gupta et al (1974) studied the effect of fuel injection mode and burner geometry on NOx formation from natural gas swirling flames. Their results indicate that higher recirculation of burnt gases led to less NOx due the lower temperature of the combustion zone. It was also shown that tangential fuel entry produced less NOx than axial/radial injection.

Markowski et al (1976) have reported 50% reduction of NOx by using a "premix-prevap" swirl burner in a gas turbine system. The inherent instability of swirling flows was exploited to enhance the premixing

process and to stir the reacting species thus approaching a lean premixed process.

The above investigators reduced NOx formation by using injection modes which gave more rapid mixing.

On the other hand, by effectively producing slow mixing, low NOx could also be achieved, as this acts as a staged system. This was implemented in the burner of Suzuki et al (1982) where fuel was injected at an angle to the axis of the air stream. A soft flame was formed and the temperature of the flame became more uniform with lower maximum temperature and oxygen concentration.

Abassi and Fleming (1988) used the same principle in tests in a glass furnace.

Stratified combustion produces lower NOx where two combustion regions are distinguishable, one in the primary air, the other associated with the secondary air. Meyer and Mauss (1973) illustrated this effect on a spray combustion system where the fuel was injected into a primary swirling air stream, surrounded by a non-swirling secondary stream. Low levels of NOx (50 ppm) were obtained at an optimum swirl number of 0.93 even when using a fuel with 0.01% nitrogen. It was also shown that flue gas recirculation could be used to reduce NOx even further.

2.3.5 NOx prediction

Different approaches have been adopted to model NOx formation in combustion systems. Table 2.2 give a summary review of the NOx modelling work and the different techniques used to simulate NOx formation.

Table 2.2

Review of NOx modeling work

INVESTIGATORS	NOx Mechanism	Hydrocarbon Kinetics	Flow Modelling	Remarks
Fletcher and Heywood,1971.	Thermal	Equilibrium	1.D.M	Fluctuations
Appleton and Heywood,1972.	Thermal & Fuel		1.D.M	Fluctuations
Fletcher, 1973	Thermal	Equilibrium	W.S.R	Fluctuations
Engleman et al,1972	Thermal	Semi-detailed	W.S.R	premixed
Shaw, 1973	Thermal & Prompt	Equilibrium	W.S.R	
Kretschmer and Odgers,1973	Thermal	1-step reaction	W.S.R	-
Tuttle et al,1976	Thermal	Emperical	W.S.R	-
Rubins and Marchionna,1976.	Thermal	Equilibrium	Multiple W.S.R	-
Mizutani and Katsuki,1976	Thermal	1-step reaction	2.D.M	-
Mellor and Washam, 1979, Mellor, 1980.	Thermal		W.S.R	-
Lewis ,1981	Thermal	Equilibrium	W.S.R	-
Sadakata et al, 1980	Thermal	Equilibrium	1.D.M	Air staging
Peters and Donnerhack,1980	Thermal	Equilibrium	2.D.M	Boundary layer
Touchton, 1984.	Thermal	Equilibrium	Multiple W.S.R	steam injection
Ahmed T et al, 1985	Thermal	1-step reaction	2.D.M	-
Toof, 1986	Thermal,prompt and fuel	Equilibrium		-
Sabo et al ,1986	Thermal & Fuel	Equilibrium/1-step	3.D.M	Cenral/peripheral
Pericleous et al,1988 Hand et al, 1989	Thermal Thermal & prompt	1-step + turbulence 1-step + turbulence	3.D.M 2.D.M	Central/peripheral. Dual liquid/gas burner
Kudryavtsev & Volkov, 1988	Thermal	1-step + turbulence	2.D.M	Boundary layer

1.D.M = One Dimensional Model.

2.D.M = Two = = .

3.D.M= Three = =.

W.S.R = Well stirred Reactor.

The early modellers applied simplifying assumptions for the flow, eg, well-stirred reactor. Recently however, more advanced programs for solving the flow equations have become available, such as TUFC (Sykes and Wilkes (1983)), PCOC (Stopford (1989)), PHOENICS (Ludwig et al (1989)), FLUENT (Weber and Visser (1990)) and FLOW3D (Burns et al (1988)).

Because of the high sensitivity of thermal NOx to temperature, it is essential that the model predictions of temperature are carefully validated.

On the other hand, chemical species concentration calculations can be performed at different levels of complexity, starting with very fast kinetics model "mixed-is-burned", then one-equation or two-equation models and most recently a full set of detailed kinetics, as described by Maas and Warnatz (1989).

While the closure of these two sets of equations, ie flow and chemistry, is possible, it may prove prohibitively expensive for cases of industrial interest, so some compromises may have to be made.

A two-step approach has been adopted by Pericleous et al (1988) to model the formation of NOx in a combustion system with swirling flow and fuel injected either tangentially or axially. The first step involves the main exothermal reaction of methane in air which is considered to be mixing controlled, and the second involves the solution of the Zeldovich reaction scheme for the generation of NOx. The results demonstrate the potential of these models to predict quantitatively the effects of burner geometry on the flame structure and consequently on NOx emission. The same approach has been adopted by Kudryavtsev and Volkov (1988) for jet flow in order to model the combustion of gaseous fuel in a steam boiler furnace. Recently Hand et al (1989) have formulated an NO formation model for a turbulent natural

gas flame, by adopting the two-step approach. Although the prediction of NO was limited by uncertainties in the kinetics mechanism and turbulence/chemistry interaction, good qualitative agreement was obtained from rigorous comparison with experiments. This study has shown that the effect of turbulence on the rate of NO formation cannot be ignored as fluctuations in temperature and burnt gas composition can strongly influence the mean rate of NO formation by the extended Zeldovich mechanism.

Modelling studies of the effect of peripheral fuel injection on NOx formation were also reported by Sabo et al (1988), indicating NOx levels of about 50% of those from equivalent central injection systems.

2.4 MODELLING OF SWIRLING FLOWS

Furnace system design requires careful characterisation and optimisation of complex flow phenomena. Traditionally, the designers of such systems have relied almost exclusively on empirical methods. New designs have usually been based on operating results from existing units while detailed information on the flow pattern within a furnace has been inferred from measurements on laboratory-scale models. However this approach can be expensive and in some cases is not capable of providing the large amount of design information required. Recently, numerical models capable of predicting the flow patterns and heat transfer characteristics have been developed and widely used for such furnaces. In addition to being required to handle turbulence and chemical reaction, these models must also be able to deal with complex geometries.

The research effort which has already been put into the development of these numerical models is very considerable. A significant part of this research have been devoted to the modelling of turbulence, combustion

and heat transfer. Also efforts have been made to improve the numerical techniques. A small selection of the many published detailed reviews of these research efforts is given in the references by Jones and Whitelaw (1984), Robinson (1985), Sloan et al (1986), Correa and Shyy (1987) and Leschziner (1989).

Details of all governing equations used in the prediction procedure (ie conservation of mass, momentum, energy and chemical species) and the models involved (ie turbulence, combustion and radiation heat transfer) are summarised by Gupta and Lilley (1985). Some of these equations are also given in Chapter 7 of this thesis.

Turning attention to the case of swirling flows in furnaces- a common situation in practice- the prediction procedures have been applied progressively. The simplest case- isothermal flow- has been studied for flows expanding into free space. Many investigators have combined experimental and modelling work to develop this prediction procedure. The aerodynamic characteristics of free, swirling, coaxial jets issuing from a divergent nozzle into stagnant-air surrounding have been studied by Dixon et al (1983) and Mahmud et al (1987) . These studies have combined experimental work with predictions obtained by numerical solution of governing conservation equations for mass and momentum supplemented by an eddy-viscosity (standard k-ε) turbulence model. A general agreement was obtained between measured and predicted velocity distributions at regions of low velocity gradients, although, some differences were reported, specially at regions of high velocity gradients and within the reverse-flow zone. These discrepancies have been explained by the weakness of the isotropic 2-equations turbulence model. A similar study for flows expanding into free space has also been reported by Weber et al (1986) with comparable degree of success.

For swirling flows expanding into a confinement, many investigators have also reported comparison between predictions and experiments. At the National Engineering Laboratory (NEL), Beltagui et al (1988-a and 1988-b) have reported measured and predicted isothermal flow patterns within the quarl and within the confinement of a model furnace with a variable-swirl burner. These studies were designed to validate the Heat Transfer and Fluid Flow Services (HTFS) mathematical models for furnace flow and heat transfer. The predictions have been performed by the program TUFC (Sykes and Wilkes (1983)) with turbulence closure by the standard k-ε model. Within the limitation of the k-ε turbulence model good overall agreement was demonstrated between TUFC predictions and experimental measurements, particularly the axial and tangential velocity components.

A modified turbulence model applicable to turbulent swirling flow in a straight pipe has been developed by Kobayashi and Yoda (1987). Two current models, the standard k-ε model, and the k-ε model with higher order terms in the Reynolds stress equations were first applied. The modified k-ε model with an anisotropic representation of turbulence was then proposed. Comparisons between the computed flow distributions and experimental data have shown that the modified k-ε model provides better predictions for the complex flow field. This study has shown that the isotropic assumption of the shear and normal stresses in swirling flow field is not accurate. This is also confirmed by Nagano and Hishida (1987) and an improved form of the k-ε model have also been suggested.

The limitations of the standard k-ε model to represent accurately the turbulence characteristics in swirling flows have also been reported by Nejad et al (1989). In this study, a two- component laser doppler

velocimetery (LDV) was used in a cold flow dump combustor model to obtain detailed mean and turbulence data for both swirling and non-swirling flows. The turbulence data were obtained to assess the turbulence predictions made with the standard k-ε model. The comparisons between the experimental data and predictions have shown similar conclusions to those reported by Mahmud et al (1987) and others described above. Honnery and Kent (1989) have also reached the same conclusion in a similar study.

As an alternative to the standard k-ε turbulence model, the algebraic stress model (ASM) has been recently used to model the turbulence. Armfield and Fletcher (1989) have reported comparison between the performance of the ASM and the k-ε model for swirling flow in diffusers. Their results demonstrated that the use of ASM model provides better prediction of mean flow quantities.

Improvements in computer power have assisted the implementation of the more detailed turbulence model, the Reynolds stress model (RSM), to represent accurately the turbulence characteristics of swirling flows. The use of this model for the calculation of a confined strongly swirling flow has been reported by Jones and Pascau (1989). A comparison of the results with experimental measurements showed the superiority of the RSM over the standard k-ε model. This is because the RSM represents the anisotropic nature of the swirling flows by solving differential equations for both shear and normal stress.

In a similar study, Weber and Visser (1990) have reported comparison between measurements and predictions of a number of isothermal swirling flows expanding into high confinement flow geometries representing gas turbine applications and also low confinement flow geometries encountered in industrial furnaces. In the computational procedure, three models of turbulence were tested- RSM, ASM and the standard k-ε

model. A major conclusion from this study is the success of both RSM and ASM to produce reliable predictions. As previously found by others, the use of the k-ε turbulence model resulted in a large discrepancies from measurements.

However, it should be indicated that the use of more sophisticated models (ie RSM) is generally not preferred due to the expensive computational time penalty involved.

From the above brief review of isothermal swirling flows, it appears clearly that in the isothermal flow modelling cases, the only major problem facing a modeller is the representation of turbulence. In swirling combusting flows, the modelling of exothermic chemical reaction and heat transfer add other two modelling tasks to the designer. In the last decade, few predictions has been reported for combusting swirling flows. Gosman et al (1978) have reported an extensive modelling study which involved the handling of non-premixed, partially-premixed and premixed combustion cases. These combustion cases represent different types of fuel injection modes. The combustion has been modelled by the fast chemistry model "mixed is burnt", using one-step global reaction, and the radiation heat transfer by the "flux" model. Predictions performed by the Imperial college program TEACH-T have been compared with data from a range of cylindrical furnaces. The qualitative nature of the predictions was good for all the cases considered. Similar modelling results have also been reported by Khalil et al (1980) and Abbas et al (1984) in furnaces with complex geometries found in engineering practice.

Recently Beltagui et al (1991) have reported an extension to the HTFS program PCOC (Stopford (1989)) to handle the partially premixed situation encountered when the central radial fuel injection mode is

used. Four combustion models were used in this study, namely, "mixed is burnt" and three forms of the "eddy break-up" model. Radiation heat transfer was modelled by a single gray gas and finite-ordinate discretisation. The authors reported good agreement between PCOC predictions and experimental data obtained in the NEL furnace with radial fuel injection mode.

It is seen from the above summary review that the number of modelling studies of combusting swirling flows in furnaces and gas turbine combustors is rather limited when compared with the isothermal flow situation. Confidence in the use of computer programs for handling the combustion and heat transfer characteristics of swirling flows increases only when these programs are validated against reliable experimental data obtained from different engineering applications. A contribution towards this objective is presented in chapter 7 of this thesis.

CHAPTER 3

EXPERIMENTAL FACILITY

3.1 INTRODUCTION

The work described in this thesis was carried out at the NEL. The experimental facility used in this work consists of the furnace and all the support equipment to carry out the work.

For safety aspects the furnace system and flow lines are installed in a separate room, hereafter referred to as the furnace block house. Part of this room is shown in Photograph 1. All analysers, data acquisition system, flame monitoring video equipment and the controls for operating the furnace are installed in another room, hereafter referred to as the control room Photograph 2. Details of the experimental facility and experimental techniques are described in details below.

3.2 THE FURNACE

The furnace is a model of a cylindrical upshot process fired heater. The apparatus consists of a 1 m diameter x 3 m high water-cooled chamber, which is having six separate cooling sections each 0.5 m long as shown in Figure 3.1.a. Cooling water flow through the sections is continuously monitored by an array of turbine meters and the temperature rise in each section is measured by platinum resistance thermometers. The furnace is equiped with probe access ports and LDA windows which provide for traversing at up to six longitudinal planes in each section as shown in Figure 3.1.b.

3.3 SWIRL BURNER AND FUEL INJECTION MODES

The furnace is fired by natural gas through a variable-swirl burner with a quarl, designed and supplied by the International Flame Research Foundation (IFRF) to operate at a maximum firing rate of 580 kW. The key feature of the burner design is the moving-block swirl generator illustrated in Figure 3.2.a. Air enters the distributor via four circular ports 48 mm in diameter. Two sets of prismatic blocks direct the air into the 110 mm diameter throat of the burner. A mechanism is provided which permits movement of one set of blocks, thereby varying the proportion of radial to tangential air to give a controlled swirl numbers between 0 and 4. The swirl number is determined as the ratio of tangential to axial momentum fluxes divided by the burner throat radius. The burner mouth consists of a divergent conical quarl of throat diameter 110 mm, length 100 mm and 25° half angle enlarging to exit diameter of 200 mm. The quarl is provided with a cooling water jacket as shown in Figure 3.2.a. The burner was mounted with the quarl exit section flush with the furnace base plate.

Three fuel injection modes have been utilised with this burner, these are described below.

3.3.1 Central axial fuel injection

In this case, a fuel gun of 32 mm inner diameter and 1.5 mm wall thickness is introduced through the centre of the burner as shown in Figure 3.2.a. The end of this gun is fully open to introduce the natural gas fuel axially at the throat of the quarl. The swirled air was introduced around the fuel gun to be mixed with the fuel. The position of fuel gun may be varied axially over a range of 200 mm but for the purpose of this study, the gas outlet was always located at the

end of the parallel throat section.

3.3.2 Central radial fuel injection

In this type of injection, the fuel gun described above was replaced by a gun of the same diameter but with the end closed. The fuel was injected radially outwards and normal to the axial air stream through 16 holes each of 5 mm diameter, spaced evenly on the periphery of the fuel gun as shown in Figure 3.2.b. The outlet velocity of gas from this gun was 30 m/s. The injection plane coincides with the end of the parallel throat.

3.3.3 Peripheral fuel injection

To achieve this type of fuel injection, the burner throat and quarl parts were redesigned and used with the original swirl generator as shown in Figure 3.2.c. The main dimensions of the throat and quarl were maintained as before. The gun shown at the centre of the burner is the same gun described for the radial fuel injection mode. This gun was introduced for two reasons. The first is to maintain the same geometry for the swirled air inlet as for other fuel injection modes. The second reason is to use this gun to introduce part of the combustion air in some of the schemes to be tested. Two main schemes were used with this fuel injection system as described below:

Scheme 1

Two arrangements were tested in this scheme:

A- In this arrangement , the fuel was injected through an annular slit of 2.5 mm width around the periphery of the swirled air as shown in Fig 3.2.c(A).

B- Same as A above, but instead of being introduced through the annular slit, the fuel gas was injected through 60 holes, each 4 mm diameter as shown in Figure 3.2.c(B). These were designed to maintain the same area of the continues slot.

In both arrangements no air was supplied through the central gun.

Scheme 2

The main change from scheme 1 is that part of the combustion air (10% of total) was supplied through the central gun in both arrangements, A and B. The outlet velocity of the air from this gun was 30 m/s.

3.4 FLOW SYSTEM AND REACTANTS

3.4.1 Gas flow line and flow rate metering

The gas flow lines which supply the pilot and main burner with natural gas are shown in Figure 3.3.a. Natural gas from the main site supply is fed into the system through a manual gas valve GV1. Part of the gas is diverted to the pilot via two solenoid valves, SV1 and SV2. The pilot utilises two supplies- a pre-mixed support flame and a neat-gas primary pilot flame. Before starting the pilot flame the valves SV1 and SV2 were checked for leakage by a special "provenseal" system. This system creates a vacuum in the space separating these valves and checks if the vacuum is maintained for a certain period of time to ensure the solenoids are leak free. The operation of valves SV1 and SV2 is controlled by the furnace main control panel. The pilot support flame utilises compressed air from the NEL site main air supply. The solenoid valve SV5 is provided to facilitate control of pilot ignition through the remote panel.

The flow of the gas to the main burner is controlled through the

solenoid valves SV3 and SV4. These were controlled remotely and checked for leaks as described for the pilot. The supply pressure to the main burner was boosted by a centrifugal blower to a maximum pressure of 300 mm water gauge to deliver the required mass flow rate. A bypass line is provided for control of the boost pressure via valve GV2. Once the main flame has been established, the pilot flame is switched off automatically by the solenoid valves SV1 and SV2.

The gas flow rate was metered by a 25.4 mm (1 in) bore square-edged orifice plate with flange tappings. The plate, tappings and pipe length upstream and downstream from the orifice were designed in accordance with British Standard 1042. The pressure differences across the plates and the pressure upstream of the plates were measured with pressure transducers. The temperature was measured by a thermocouple installed upstream of the orifice plate location where it did not disturb the pressure readings . The pressure and temperature readings were relayed to the control room using a special data acquisition system.

3.4.2 Air flow line and flow rate metering

The air supply to the main burner is shown in Figure 3.3.b. The compressed air is provided from a main facility serving the NEL site. Due to various demands on this compressed air by other users, the air supplied to the furnace suffers sometimes slight fluctuations in the flow rate. The air flow was controlled by a hand operated valve followed by a pneumatic operated one. The latter was adjusted from the control room to ensure a constant flow rate within ($\pm$ 1 %). The air flow rate was metered by a 44.45 mm (1.75 in) square-edged orifice plate with flange tappings in the same way as described for the fuel gas.

3.4.3 The composition of natural gas

Detailed natural gas analyses were obtained from British Gas. A sample of these analyses is shown in Table 3.1. The results of these analyses indicated that, over the period of the tests, the main fuel properties were constant to within $\pm$ 2 % for the calorific value and $\pm$ 1.2 % for the density and stoichiometric air requirements. The average values of these properties are calculated and given in Table 3.2.

Table 3.1

Natural gas composition

constituent	% by volume
Nitrogen	0.7330
Carbon dioxide	0.5420
Methane	94.298
Ethane	3.5980
Propane	0.6000
Iso-Butane	0.0570
N-Butane	0.1180
Neo-Pentane	0.0030
Iso-Pentane	0.0180
N-Pentane	0.0230
Hexane 1	0.0000
Hexane 2	0.0000
Hexane 3	0.0070
Hexane 4	0.0010
Heptane 1	0.0000
Heptane 2	0.0000

Table 3.2

Average properties of natural gas

Stoich fuel/air by vol.	0.101
Specific gravity, dry (relative to air)	0.600
Net calorific value $\frac{MJ}{Nm^3}$	35.32

3.5 FURNACE RUNNING AND SAFETY DEVICES

The furnace system was provided with advanced safety devices to avoid explosion and to protect all the parts serving the furnace. Extra care was taken during the starting procedure. The starting and running of the furnace was carried out remotely from the control room through a special control panel (see Photograph 2) following the schedule described below :

1- Ensuring the water supply for cooling the furnace walls and probes. When water flow rate or temperature as given by the turbine meters and thermometers go outside specified safety settings the flame is stopped automatically by temperature scan alarm and flow monitoring devices.

2- A gas alarm system type (GMI 1500) was installed to monitor the gas concentration in the furnace block house and stack. The output given from two detectors installed in the room and a third detector installed in the stack were analysed continuously by a combustibles analyser installed in the control room. The system would not allow flame starting or flame continuation when the concentration exceeds safety limits set at 20 % of the flammable mixture. In practice these concentrations were always observed to be zero.

3- Before the main manual gas valve was opened, the furnace chamber was purged using the full loading air flow rate.

4- Before supplying natural gas to the furnace, the gas flow lines were checked for leak by the special provenseal system as explained in section 3.3.1.

5- When all safety procedures explained above were successful, natural gas was supplied to the system to start the pilot flame. This flame was detected by an ultra violet sensor and monitored by a video equipment system.

6- When the main flame was finally established the pilot flame was switched off automatically and the pilot burner was withdrawn to avoid interference with the flow. The gas was then boosted by the centrifugal blower. The flow rates of gas and air were adjusted to achieve the required firing rate and percentage excess air.

3.6 VELOCITY AND STATIC PRESSURE MEASUREMENTS.

There are two means of measuring flow velocity, namely, non-intrusive means and intrusive means. The most common non-intrusive means are the particle track and laser-doppler anemometery (LDA) methods. The latter is the most promising tool for velocity measurements due to its accuracy and non-interference with the flow. The intrusive methods of determining velocity involve insertion of probes in the flow. The pitot tube method involves transfer of kinetic energy in to pressure energy, while the hot wire anemometer involves measuring the rate of heat transfer to a wire as it is affected by change in local gas velocity. By contrast to the pitot tube method, hot wire anemometery method has not been found suitable for flame measurements, as reported by Beer and Chigier (1972) and Chigier (1974-a).

The five-hole pitot type probe has been found to be the most effective and economic method for simultaneous measurements of the three components of velocity and static pressure and therefore was used in the present investigation. There is considerable evidence from LDA tests carried out on this system, Ralston et at (1984), that the probe readings are in agreement with LDA measurements. Similar work on other systems by Hillemens et al (1986) and Aoki et al (1986) support this conclusion.

(i) Five-hole probe

The water-cooled probe used is an 8 mm diameter hemispherical-nosed probe designed and supplied by the IFRF. The probe tip contains five radially drilled holes, one on the centre and at the pole of the hemisphere, the others are spaced equidistant from the first at an angle of 45° (Figure 3.4). The length A-B is exposed to the flame while

the rest of the probe passes through a water cooled probe carrier used for traversing the probe inside the furnace. The principle of operation of the probe (Chigier (1974-b)) is based upon the surface pressure distribution around the probe tip. If the probe is placed in a flow field such that the total mean velocity vector is at some angle to the axis of the probe, then a pressure differential will be set up across these holes, the magnitude of which will depend on the geometry of the probe tip, position of the holes and the magnitude and direction of the velocity vector.

In this study the pressure differentials for the five holes were read simultaneously using five pressure transducers averaged over a period of about 1 minute. Compared with micromanometers, these pressure transducers have the advantage of high sensitivity and rapid response which are required in the regions of low velocity and density encountered in the furnace. The principle of operation of these transducers is found in (Chigier (1974-a)). The Zero readings of these transducers were set to within 0.010 mm water. The pressure transducers were calibrated and found to be accurate to within $\pm$ 0.005 mm of water. The readings of these transducers were all driven by microcomputer which was programmed to calculate the velocity components values using the probe calibration equations. The calibration supplied with the probe was checked before starting the present measurements. The calibration procedure and the use of the probe for velocity and static pressure measurements are described in detail in the next section.

Due to the small size of the probe holes they are subjected to blockage by dust or condensation of water vapour from the furnace gases thus leading to erroneous reading. The probe holes were purged when required with nitrogen through a special arrangement of solenoid valves and gas

flow metering connected to the five probe holes. This arrangement was designed to isolate pressure transducers during the purge cycle and was driven remotely from the furnace control room.

3.6.1 Calibration and use of the five-hole probe

The probe calibration was checked for both velocity and static pressure measurements. The Leuckel calibration method recommended by Chedaille and Braud (1972), was employed. Calibration of the probe was obtained in terms of flow angle coefficient k_{ϕ}, velocity coefficient k_{v} and static pressure coefficient k_{p}. The flow direction was defined in terms of the conical flow angle ϕ and dihedral angle δ shown in Figure 3.5. These two angles are not known and therefore should be defined in term of another two angles, one is the yaw angle α and the other is the pitch angle β. These latter two angles define the probe position in the calibration rig. For convenience, the calibration procedure including the derivation of the relation between these angles is described first. The results of applying this calibration procedure then follow.

1- The probe is inserted in a free air jet of constant velocity. The velocity of this jet is measured by a standard pitot probe.

2- The probe is mounted in a special attachment that allows the probe to be rotated about its own axis to vary the yaw angle α and to be tilted to vary the pitch angle β.

Using Figure 3.5 the derivation of the angles ϕ and δ in terms of α and β is given below.

The axial, radial and tangential velocity components are related to the total velocity vector V and the angles ϕ and δ as follows:

$$u = V \cos \phi \qquad (3.1)$$

$$v = V \sin \phi \cos \delta \tag{3.2}$$

$$w = V \sin \phi \sin\delta \tag{3.3}$$

$$\alpha = \tan^{-1} \frac{w}{u} \tag{3.4}$$

$$\beta = \tan^{-1} \frac{v}{u} \tag{3.5}$$

From eqn. 3.4,

$$\tan \alpha = \frac{w}{u} = \frac{V \sin \phi \sin \delta}{V \cos \phi} = \tan \phi \sin \delta \tag{3.6}$$

From eqn. 3.5,

$$\tan \beta = \frac{v}{u} = \frac{V \sin \phi \cos \delta}{V \cos \phi} = \tan \phi \cos \delta \tag{3.7}$$

manipulating equations 3.6 and 3.7 gives:

$$\tan \phi = \pm \sqrt{\tan^2 \alpha + \tan^2 \beta} \tag{3.8}$$

substituting equation 3.8 in 3.6 give:

$$\sin \delta = \pm \frac{\tan \alpha}{\sqrt{\tan^2 \alpha + \tan^2 \beta}} \tag{3.9}$$

3- At each setting of ϕ and δ, the pressure differentials are measured and the values of the coefficients k_ϕ, k_υ and k_p are calculated from the following equations (Chedaille and Braud (1972)):

$$k_{\phi} = \sqrt{1 - \frac{(p_o - p_1) + (p_o - p_2) + (p_o - p_3) + (p_o - p_4)}{(p_o - p_1)^2 + (p_o - p_2)^2 + (p_o - p_3)^2 + (p_o - p_4)^2}} \qquad (3.10)$$

$$k_{\upsilon} = \frac{V^2 \rho}{g \sqrt{(p_o - p_1) + (p_o - p_2) + (p_o - p_3) + (p_o - p_4)}} \qquad (3.11)$$

$$k_p = \frac{2g\ (p_o - p_{st})}{\rho\ V^2} \qquad (3.12)$$

Where p_o to p_4 are the pressure readings for the five holes and ρ is the density calculated from the measured temperature. The values of these coefficients are calculated for a wide range of ϕ and δ settings. The results obtained are therefore used to correlate ϕ in term of k_{ϕ} also k_{υ} and k_p as function of ϕ as follows:

$$\phi = A_1\ k_{\phi} + A_3\ k_{\phi}^{\,3} + A_5\ k_{\phi}^{\,5} \qquad (3.13)$$

$$k_{\upsilon} = B_0 + B_2\ \phi^2 + B_4\ \phi^4 \qquad (3.14)$$

$$k_p = 1 + C\ [\ \exp\ (-D\ \phi^2\ ) - 1\ ] \qquad (3.15)$$

4- For a perfect sphere, it has been found that the angle δ is given by the relation:

$$\delta = \tan^{-1} \frac{(p_2 - p_4)}{(p_1 - p_3)} \qquad (3.16)$$

If the probe is sufficiently accurately manufactured, the error in the value of δ calculated from this equation should not be more than one degree. If this is not the case, a correction to the above equation should be implemented.

(i) Results of the calibration procedure

The calibration procedure described above was carried out on the 5-hole pitot probe inserted in a free jet of 2 m/s velocity. The probe was set at a range of pitch angle β from -40° to $+40^\circ$ at intervals of 10°. At each pitch angle, the yaw angle α was varied from -70° to $+70^\circ$ at intervals of 10°. The whole calibration was repeated for a jet velocity of 10 m/s to ensure the independence of the calibration from the Reynolds number. The results of both sets were identical. the coefficients k_ϕ, k_υ, and k_p were therefore plotted against ϕ. The results were compared with the suppliers calibration provided with the probe to check its validity. Figure 3.6.a shows the comparison for k_ϕ and k_υ and Figure 3.6.b for k_p. It is seen from the figures that all the coefficients are in close agreement with the supplier's calibration. The original constants shown in the figures were therefore used in equations 3.13 to 3.15 above.

Finally the values of the dihedral angle calculated from the pressures, Eqn. 3.16, (δ_{cal}) were compared to those from the yaw and pitch angles, Eqn. 3.9, (δ_{in}). The ratio $k_\delta = \delta_{in}/\delta_{cal}$ was plotted versus δ_{cal} for the range of yaw and pitch angles covered during the calibration, Figure 3.7. The figure shows that the ratio k_δ is not consistently equal to unity. Correction is therefore needed for the angle δ_{cal}. The correction equation takes the following form:

$$\delta_{cor} = (k_\delta)_\beta \quad \delta_{cal} \qquad (3.17)$$

The use of this relation represents an extension to the previous standard calibration.

(ii) The use of the probe

The probe was inserted in the furnace with its tip facing the main flow. The pressure values p_o to p_4 were taken by 5 pressure transducers. The coefficient k_ϕ was calculated from equation 3.10, and the angle ϕ was found from equation 3.13 (calibration curve, Figure 3.6.a). The angle δ was obtained from equation 3.16 and corrected by Equation 3.17 (Figure 3.7). K_v was calculated from equation 3.14 (calibration curve,Figure 3.6.a) at known value of ϕ. The total velocity vector was therefore found from Equation 3.11 and the three velocity components from equations 3.1 to 3.3.

For calculation of static pressure, the coefficient k_p was given by equation 3.15 (calibration curve, Figure 3.6.b) at known values of ϕ. The static pressure was therefore calculated from equation 3.12.

3.7 TEMPERATURE MEASUREMENTS

Gas temperature was measured using a water cooled suction pyrometer probe designed and manufactured by the IFRF. The probe consists of a 'Platinum- 10 % Rhodium Platinum' type thermocouple protected from the chemical action of the gas by an impermeable ceramic sheath and placed in a system of shields to isolate the thermocouple from the surrounding radiation (Figure 3.8). The figure also shows the probe cooling and gas extraction details. The suction rate corresponds to a gas velocity of 150 m/s at the thermocouple hot junction. Errors resulting from suction velocity, radiation and conduction were quantified through the test of probe efficiency. The efficiency factor E depends on the pyrometer construction, suction velocity and the gas temperature and is given below by Chedaille and Braud (1972):

$$E = \frac{T_m - T_o}{T_g - T_o}$$

where T_m is the measured gas temperature, T_o is the equilibrium gas temperature without suction and T_g is the true gas temperature. The value of the efficiency factor E is found from the curve of the response of the pyrometer (Figure. 3.9) where the shape factor F shown in the figure is defined by:

$$F = \frac{\tau_o}{\tau_m}$$

where τ_o and τ_m are the times necessary to achieve equilibrium for the thermocouple without and with suction respectively. The values of τ_o and τ_m were found from experimental test as shown in Figure 3.10. This test has shown that the efficiency of the pyrometer was 99 % . Temperature readings were therefore not corrected.

3.8 NOx MEASUREMENTS

The section which now follows describes the special procedures that were followed in sampling and measuring NOx concentrations.

3.8.1 NOx sampling conditions

In order to obtain a representative sample, the chemical constitution of the sampled mixture should be maintained. The mixture to be sampled is generally in a process of more or less rapid evolution. This evolution process must be stopped quickly by a suitable cooling process in order to freeze any further reaction in the probe or sampling line. Cooling the sample down to a temperature of 300°C is sufficient to freeze these reactions (Chedaille and Braud (1972)). Excessive, uncontrolled cooling of the gas sample could lead to water vapour condensation along the sampling system. The problem of surface absorption of NOx on the probe and sample line is aggravated by the

presence of films of moisture and hence is most serious when sampling wet gases from flames (Allen (1973) & de Soete (1989)). Furthermore, almost all gas analysers are subject to serious interference from water. This effect has been observed in the chemiluminescent analyser used in the current measurements. The use of desiccants has been found to absorb nitrogen dioxide NO_2 to varying degrees. Cold traps also remove NO_2 and water vapour simultaneously (Allen (1973)).

For the above reasons the sampling system used in the current measurements has been designed to maintain the sample temperature close to $150^{0}C$.

Choosing the probe material is also important for NOx sampling to ensure no probe reactions or surface ageing with the sampled gas. A system of a water cooled stainless steel probe and a teflon heated sample line has been found satisfactory for NOx measurements by Allen (1973) and Tuttle et al (1974). Stainless steel probes were also used satisfactorily by Oven et al (1978), Sadakata et al (1980), Ahmad et al (1984), and Mulholland et al (1987).

A water cooled stainless steel probe and a teflon sampling line were therefore used in the current measurements. The receiving part of the probe was lined with quartz to avoid the possibility of ageing, especially at the high temperature region.

In order to withdraw a local representative sample isokinetic sampling is generally recommended. However, in turbulent recirculating flows isokinetic sampling is difficult to achieve due to the large velocity fluctuations especially in the recirculating zones. It is reported by Oven et al (1978) that for such conditions it may be impossible to obtain a properly representative sample either with or without isokinetic sampling. In the present work, the suction velocity was

adjusted to be 15 m/s which is approximately the average flow velocity in the furnace.

3.8.2 NOx sampling system

The NOx sampling system consisted of three main parts, these parts being,

(i)- NOx sampling probe

(ii)- heated sample line

(iii)- Chemiluminescent analyser

Details of each part are described below.

(i) NOx sampling probe

The probe used was a modification of water-cooled stainless steel probe designed and supplied by the IFRF. Figure 3.11.a shows the probe in its initial configuration. The tip length A-C is exposed to the flame. The sample tube length D-E passes through the water cooled probe carrier to convey the sample to the heated sample line.

Before the measurements were started, the probe performance was tested in the furnace under a range of operating conditions. Two thermocouples were fitted to monitor the sample temperature at points D and E of Figure 3.11.b. Very low sample temperatures at D and E were observed and condensation of water vapour occurred inside the probe and the analyser. This problem is caused by the excessive cooling rate of the probe tip and further heat loss from the sample tube to the cooling water tubes within the probe carrier. The probe cooling system was therefore modified to control the sample gas temperature at D to 300 ^{o}C and at E to close to 150 ^{o}C. This control has been achieved as follows:

1- Controlling the cooling water temperature supplied to the probe. A bypass system was arranged to mix some of the hot water return from the probe with the fresh cold water supply. To protect the probe against overheating, the return water temperature was monitored to avoid evaporation, and possible probe damage, Figure 3.11.b.

2- Insulating the probe cooling water tubes in contact with the sample tube, length D-E, to prevent heat loss to the carrier and cooling water tubes.

3- To compensate for any further heat losses the sample tube D-E was electrically heated using a specially designed heating system with low voltage variable power supply.

The above sampling system provided complete control of the gas temperature under all the operating conditions considered.

(ii) Heated sample line

A teflon flexible heated sample line (type Signal 530) of 10 m long was employed to carry the gas sample from the probe to the NO_x analyser. The temperature of the sample was maintained in the heated line at 150°C using a temperature controller.

(iii) Chemiluminescent analyser

A chemiluminescent analyser (model AAL 443), manufactured by Analysis Automation Ltd was used for the NO/NO_x concentration measurements. The analyser detects and measures nitric oxide (NO) using its chemiluminescent reaction with ozone (O_3). The ozone is generated internally within the instrument and after the reaction any residual O_3 is catalytically destroyed. The analyser can also measure the sum of the concentration of NO and NO_2 (the sum being called NO_x) by means of

a catalytic converter in which the NO_2 is changed to NO before entering the measuring system.More details about the principle of operation are given by Allen (1973). The analyser was calibrated against a standard sample of 100 ppm nitric oxide (NO) concentration. The calibration was checked before and after each traverse. The maximum drift in the calibration was found to be within ± 2 % of full scale. The time-mean NO_x concentration values to be presented are those averaged over a period of one minute after allowing sufficient time for purging of the old sample from sample line and analyser.

3.9 MEASUREMENT OF CO, CO_2, O_2 and HC CONCENTRATIONS

For concentration analysis of CO, CO_2 and O_2 species, the sample was withdrawn through the NO_x sampling probe described in section 3.3.2 at the same time as for the NO_x measurements. Rather than going through the heated sample line, the sample was passed through a tee junction to a separate line containing a water trap, condenser and chemical dryers before being introduced to the gas analysis equipment. This drying process is needed to prevent water vapour interference with the gases analysed. Since the hydrocarbon sampling conditions are similar to NO_x conditions, the sample passing through the heated sample line was branched to the HC analyser for hydrocarbon measurements.

Infra-red analysers, manufactured by Analytical Development Co Ltd type (3M/24-4052) and (4L/24-4051) were used for CO and CO_2 analysis respectively. For O_2, a paramagnetic analyser, manufactured by Taylor Instrument Ltd (model OA. 570) was used. Details of the principle of operation of these analysers are found in (Chedaille and Braud (1972)). For HC analysis, a hydrocarbon analyser manufactured by Signal (series 3000) was used. All the analysers were calibrated against standard

gases of known concentrations, at least daily.

3.10 DATA ACQUISITION AND TRAVERSE SYSTEM

The acquisition of aerodynamic, temperature and concentration data was largely automated and carried out as shown in Figure 3.12. For each measurement, the required probe was mounted on a special traverse system driven by a stepping motor which facilitate accurate positioning of the probe. The traversing system was controlled by a microcomputer through a traverse controller which gives probe positioning within $\pm$ 1 mm. The data was scanned by a Hewlett-Packard (HP) scanner of 80 channels each controlled by the computer for a certain reading. The acquisition of aerodynamic, temperature and concentration data is summarised below:

1- Temperature measurements were carried out first using the suction pyrometer. The scanned data was processed by the computer using the thermocouple calibration.

2- The aerodynamic measurements were carried out next using the 5-hole probe . The reading of the pressure were taken by the 5 pressure transducers, which gave voltage signals scanned by the HP scanner and processed by the computer using the probe calibration described in section 3.5

3- Finally concentrations measurements were taken using the sampling probe. The readings given by the analysers were scanned continuously and processed by the computer using the calibration of each analyser.

All the data acquired were stored on disk for further analysis.

CHAPTER 4

EXPERIMENTAL RESULTS

4.1 EXPERIMENTAL PROGRAMME AND TEST CONDITIONS

This chapter reports the experimental measurements performed in the present work for the three fuel injection modes, central axial, central radial and peripheral fuel injection. Two schemes of peripheral fuel injection were tested. The main purpose was to study the flow and combustion patterns and how they change with the input parameters, particularly swirl.

This section is designed to define the range of the measurements and also give a brief description of general flame behaviour in each method of fuel injection.

The experimental measurements could be classified into two main groups:

1- In-furnace measurements:-

These correspond to the experimental measurements covering complete mapping of the aerodynamic patterns (three time-average velocity components and static pressure) and the combustion patterns (temperature and species concentrations- usually NO_x, CO, CO_2, O_2 and HC) in the furnace. These measurements were taken under fixed firing rate of 400 KW and fuel equivalence ratio (ϕ) of 0.95 (5% excess air). The range of swirl numbers studied in these tests was S=0.0, 0.45, 0.9 and 2.25. In each method of fuel injection, measurements covered the swirl settings where stable flames were possible.

2- Stack measurements:-

Concentrations of NO_x, CO, CO_2 and O_2 were measured for 400 KW firing rate under variable input fuel equivalence ratio, ϕ. since the

objective of these measurements is to study the pollutant formation, the discussion will be focused on NOx and CO measurements. These measurements were repeated for a lower firing rate of 360 KW. The tests carried out at the lower firing rate have shown no major differences from those performed at 400 KW. An example will be given in Sec 4.3.4. The conditions under which the measurements were taken for the three fuel injection systems are summarised in Table 4.1.

Table 4.1

Test conditions

Fuel injection mode	Conditions for in-furnace measurements	Conditions for stack measurements
Peripheral		
Scheme 1- A	ϕ = 0.95, 400 KW, S = 0.9, 2.25, complete mapping of flow patterns and combustion patterns	ϕ = 0.76 to 1.33, 360 and 400 KW, S =0.9, 2.25
Scheme 1- B	-	Same as above
Scheme 2- A	-	ϕ = 0.76 to 1.33, 360 and 400 KW, S =0.0, 0.45, 0.9 and 2.25
Scheme 2- B	-	Same as above
Central axial	ϕ = 0.95, 400 KW, S = 0.9, 2.25, combustion patterns (near burner zone)	ϕ = 0.83 to 1.11, 360 and 400 KW, S= 0.9, 2.25
Central radial	ϕ =0.95, 400 KW, S=0.0, 0.45, 0.9 and 2.25, complete mapping of NOX	ϕ = 0.71 to 1.33, 360 and 400 KW, S =0.0, 0.45, 0.9 and 2.25

The following sections describe the range of measurements performed for each of the three fuel injection modes. A brief description of the

flame behaviour in each case is also given.

4.1.1 Peripheral fuel injection

Two main schemes have been tested in this system as indicated in section 3.3.3:

Scheme 1

In this scheme, two arrangements were tested, as follows :

A- The fuel was injected through continuous slot, Fig 3.2.c(A).

B- The fuel injected through discrete holes instead of the continuous slot, Fig 3.2.c(B).

These two arrangements have shown virtually the same flame behaviour. In both arrangements, it was found that the flame cannot be established without a certain degree of swirl. The minimum swirl intensity required to achieve stable flame corresponded to burner swirl number, S = 0.8. Above this swirl value the flame was completely stable and blue. However it should be indicated that because one of the swirls investigated in these flames (S=0.9) was close to that minimum limit, the flame with this swirl was characterised with some non-uniformity in shape as compared with the higher swirl flame (S=2.25). Since arrangement A is regarded as the basic system, the two detailed groups of measurements, described above, were performed in this system. These measurements were taken only for S=0.9 and 2.25. The in-furnace measurements were taken for the following variables:

a- Temperature

b- Three time-average velocity components and static pressure

c- Concentrations of NOx, CO2, CO, O2 and HC.

The measurements were taken at 13 planes along the furnace, Fig 3.1.b. These planes were located at axial distance from the burner quarl exit

of 45, 80, 110, 160, 200, 300, 545, 800, 1045, 1300, 1800, 2300 and 2800 mm respectively.

Comparing the two arrangements, A and B, the flames were seen to be virtually identical in general size and appearance. The similarity in behaviour was confirmed by the stack measurements. It was considered therefore that for practical purposes the two flames were identical. Consequently full data was taken for arrangement A and only these results are presented and discussed.

Scheme 2

The main objective of testing this scheme was to investigate the possibility of achieving stable flame without the need for swirl. Part of the combustion air was introduced radially outwards from the central gun (Fig 3.2.c) with:

A- Fuel injection through continuous slot,

B- Fuel injection through discrete holes.

(these two arrangements have the same geometries as A and B of scheme 1).

Introducing part of the combustion air in these two arrangements has achieved the objective indicated above. The blockage created by this air flow allows the formation of a central recirculation zone (CRZ) which provided the required stability. In these two arrangements, only the stack measurements were taken for the four swirl numbers of S = 0.0, 0.45, 0.9 and 2.25 respectively. No significant difference was found between the results for these two arrangements, thus only the measurements for arrangement A of this scheme will be described.

4.1.2 Central Axial fuel Injection

For this type of fuel injection, it was found that the flame cannot be

established without swirl. The minimum swirl intensity required to achieve a stable flame corresponds to S = 0.8. Greater than this swirl number (S=0.9 and S=2.25) the flame was stable but virtually characterised with non-uniformity and yellow colour. Due to the observed inferior characteristics of this flame, the measurements were concentrated only on the combustion patterns (temperature and species concentrations). The in-furnace measurements were taken for temperature and NOx, CO, CO2 and O2 concentrations. These measurements were taken at two axial positions of 45 mm and 200 mm from the burner exit. Hydrocarbon measurements were not taken because the HC analyser was not available during the time of these measurements. However these results could be inferred from the CO measurements. The stack measurements of pollutant were also performed.

4.1.3 Central Radial Fuel Injection

This system had been investigated by Beltagui et al (1988-c) and (1989). It had been found that the flame was stable without and with swirl. Measurements of temperature, CO, CO2 and O2, three time-average velocity components and static pressure in this system were reported in the above references. All these measurements were carried out under the conditions described for the in-furnace measurements. The present author has contributed to some of these measurements, in particular those reported by Beltagui et al (1989) (Appendix). These results will not be described further in this chapter. However, these are used in discussions and also for the comparison with other injection modes in the next chapter. In the present work, complete mapping of NOx was carried out in this system as reported by Kenbar and Beltagui (1990). NOx measurements in the stack were also taken. Hydrocarbon measurements

were not taken for the same reason mentioned earlier.

4.2 PRELIMINARY TESTS

Before starting the detailed measurements described above and also at the conclusions of each series of measurements, tests were carried out to ensure repeatability of the measurements. These tests covered each variable measured and were carried out at the axial position of 160 mm from burner exit. Figures 4.1 - 4.3 show samples of the results taken for scheme 1-A of the peripheral fuel injection. Each figure represents measurement of one of the three probes used in this study. Figures 4.1(a,b) show the repeatability of the temperature measurements for S = 0.9 and S = 2.25 using the suction pyrometer. Figures 4.2(a,b) show the repeatability of axial velocity measurements using the five-hole probe and Figs 4.3(a,b) for the CO measurements using the sampling probe. Satisfactory repeatability was obtained for all the variables measured.

The effect of probe presence in the flame on the local value of each variable measured was also investigated by traversing the probe through two ports, radially opposite, at the 160 mm downstream position. All swirl numbers were also covered in this test. Samples of the results are shown in Figs 4.4 - 4.6 again for the three variables of temperature, axial velocity and CO concentrations. These figures also show that the probes used in the present investigation caused no noticeable disturbance to the flame.

4.3 PERIPHERAL FUEL INJECTION- SCHEME 1

The in-furnace measurements as defined in Sec 4.1 are described below in Sections 4.3.1-4.3.3 and the stack measurements in Section 4.3.4.

4.3.1 Temperature distributions

The full temperature measurements are presented as temperature contours in Figs 4.7(a,b) for S = 0.90 and S = 2.25 respectively. Samples of temperature profiles are also shown in Figs 4.8(a-c) for three axial positions along the furnace, X = 45 mm, 160 mm and 545 mm. These figures give an indication of the effect of swirl on the degree of combustion as well as the symmetry of the flame. The profiles shown in Figs 4.8(a-c) illustrate good degree of symmetry. However, it is noticed that there is slight asymmetry in the low swirl case (S = 0.9) and at planes near the burner zone. The main reason of this observation is the non-uniformity of the width of the slot used for the fuel gas injection. Similar observations were also reported by Beltagui and Maccallum (1988).

The temperature contours given in Figs 4.7(a,b) show that the maximum temperature and steepest radial temperature gradients occur nearer to the burner as swirl is increased from 0.9 to 2.25. However, further downstream, these gradients decay much more rapidly at the higher swirl. For the high swirl there is virtually no radial variations in temperature from the plane 1 m downstream of the burner, onwards. However, for the lower swirl, radial temperature gradients are evident even at furnace exit. Thus, increased swirl not only increased combustion intensity, but also enhanced the stirring of the post-flame gases.

The temperature contours also indicate that combustion starts within the quarl, a fact emphasised by the gas concentrations described in section 4.3.3.

The temperature is mostly uniform within the central recirculation zone

(CRZ). In both these cases, which are at medium to high swirl levels, the gases feeding the CRZ from downstream are products of combustion. The temperature at the centreline is always close to the maximum temperature measured at this traverse plane. Consequently the plots of centre line temperature and maximum temperature along the furnace, Figs 4.9(a,b) are virtually identical.

The temperature peak moves closer to the burner as swirl is increased from 0.9 to 2.25. Downstream from the peak it decays to the exit value at a rate which is roughly proportional to the swirl strength.

Within the peripheral recirculation zone (PRZ), Figs 4.8(a-c) show that for both swirls the gas temperature decreases from about 1000°C at 545 mm to about 600°C at 45 mm. This temperature decrease is the result of the mixing with mixtures which are still reacting and heat loss to the furnace walls.

4.3.2 Aerodynamics and static pressure distributions

Descriptions of profiles of the three time-average velocity components, flow boundaries, and static pressure distributions are given below:

(i) Axial velocity profiles

These profiles are given in Figs 4.10(a,b). The forward and reverse flow boundaries in each level are defined by these profiles. The axial velocity profiles show that for the two swirls tested, the flow patterns are essentially the same, type D, according to the classification of Beltagui and Maccallum (1976). In this pattern, near the burner, the flow consists of CRZ surrounded by an annular jet containing the main forward flow. Outside the forward flow a weak PRZ extended to the walls. The very low PRZ velocity observed here is a

result of the low confinement- manifested in a furnace to quarl diameter ratio of 5.

For the forward flow, the value of peak velocity increases with increased swirl. The high velocity gradients at the boundaries of the forward flow increase even further with increased swirl. These gradients represent enhanced shear at the jet boundaries. This explains the higher mixing and combustion rates hence the short intense flames associated with the high swirl flows.

The rate of decay of maximum velocity along the furnace is accelerated at high swirl, as shown by Fig 4.11. This indicates that the rate of jet area expansion exceeds the gas volume expansion at these points.

Figure 4.11 also demonstrates the recovery of the centreline axial velocity along the furnace. It is noted that at the higher swirl the final recovery is not quit as complete.

(ii) Flow boundaries

Figure 4.12 illustrates the boundaries of the forward flow, thus indicating the central and outer recirculation zones for the two swirls S = 0.9 and 2.25. For the first 250 mm distance from the quarl exit, the jet radial expansion is nearly the same for both swirls. Further downstream, the jet radial expansion is shown to increase with swirl, thus bringing the jet impingement point nearer to the burner- from 0.8 m at S = 0.9 to about 0.6 m for S = 2.25. A central recirculation zone (CRZ) is seen to exist in both cases. Both the length and maximum diameter of this zone are larger in the higher swirl case.

(iii) Tangential velocity profiles

These profiles are presented in Figs 4.13(a,b). The tangential velocity

values are an indication of the local swirl strength which contributes to mixing and combustion. The high swirl jet approximates to the usual Rankine-vortex flow with solid body central rotation surrounded by an outer free vortex.

At planes between the furnace inlet and about 300 mm downstream, the tangential velocity values in the high swirl case (Fig 4.13(a)) are about twice the corresponding values at the lower swirl (Fig 4.13(b)). Despite these high differences, the tangential velocities in both swirls decay to very low value by about 800 mm downstream. This indicates that when swirl increases, the rate of decay of tangential velocity along the furnace also increases.

(iv) **Radial velocity profiles**

Figures 4.14(a,b) show the profiles of the radial velocity. In these profiles, the sign convention is that in the upper half of the diagram, positive values correspond to inward radial velocity components. In the lower half of the diagram, the convention is reversed. Thus for a perfectly symmetric jet, the distributions should be diagonally symmetric.

Before describing these profiles, it should be stated that, while there is reasonable confidence in the probe measurements for the axial and tangential velocity, it is believed (Beltagui et al (1988-a) and Beltagui et al (1988-b)), that the probe measurements exaggerate the radial velocity values, particularly in the regions of peak radial velocity. Consequently, excessive reliance should not be placed on the measured radial velocity profiles.

In general the radial velocity component is an indicator of the jet spread in direction and magnitude. Both the magnitude of the radial

velocity and its rate of decay along the furnace increase with swirl. These trends are consistent with the jet expansion behaviour suggested by the axial velocity distributions.

(v) Static pressure profiles

Static pressure distributions are shown in Figs 4.15(a,b). All pressure values are below ambient pressure with minimum values near the burner. These distributions are similar to those generally observed in enclosed swirling jet flows in furnaces, with greatest depressions at and around the centre of the jet and uniform pressure distributions within the recirculation flow zones. Increased swirl increases the centreline depression resulting in a larger CRZ. In the case of the lower swirl (S = 0.9), the pressure approaches uniformity beyond 80 mm from quarl exit, while at the high swirl (S = 2.25), the pressure becomes uniform only after 300 mm downstream.

4.3.3 Species concentrations

(i) Concentrations of HC, CO, CO_2 and O_2

Complete contours of each of the above species are given in Figs 4.16 - 4.19 respectively. To study the effect of swirl on the concentration of each species, radial profiles are presented in Figs 4.20 - 4.23 for the two axial positions of 45 mm and 160 mm from quarl exit. To assist the discussion and to draw the relation between CO, CO_2 and O_2, sample profiles of these species are given in Figs 4.24 - 4.26 for axial positions of 45 mm, 110 mm and 300 mm respectively. These planes were chosen because they are close to the burner zone where it is wished to infer local combustion information. This information include how the degree of mixing, combustion intensity and flame size

are related to swirl. As shown by the contour plots (Figs 4.16 - 4.19), beyond 300 mm, concentrations of CO and HC decay to zero, and CO_2 and O_2 attain their uniform concentrations of 11.5 % and 1 % respectively. These concentrations indicate completeness of combustion at the 5 % excess air.

The concentration profiles shown in Figs 4.20 - 4.23 exhibit the same degree of symmetry as described for the temperature profiles.

On detailed analysis of the radial profiles given by Figs 4.20 - 4.23, the following comments can be drawn :

a- The flame envelope is larger in the case of S = 0.9. This is shown clearly by the contour plots of all species. From the CO contours (Figs 4.17(a,b)), it can be estimated that the flame diameter for the low swirl case (S=0.9) is about 1.3 times the flame diameter at the higher swirl.

b- The minimum value of CO_2 at the first measuring section, 45 mm from burner exit (Fig 4.22(a)), varies between 2.5% and 4.0% , indicating that combustion commences within the quarl. This is confirmed by the maximum value of O_2 concentration at this section (Fig 4.23(a)), of 14.5 percent which is significantly lower than the concentration of O_2 in air.

c- In the forward flow region, and at axial distance, X < 300 mm, the concentrations of HC and CO are higher in the case of S = 0.9. This shows that the degree of mixing and consequently completeness of combustion are lower. This is also confirmed by the lower concentrations of CO_2 and the higher concentrations of O_2 in this region as illustrated in Figs 4.24 - 4.26. As swirl is increased, high CO_2 peak concentrations are observed in the annular forward jet, and correspondingly lower O_2, CO and HC, consistent with

increased combustion intensity.

d- Within the CRZ, concentrations of HC and CO are nearly zero in the case of S = 2.25. However, for S = 0.90 small concentrations exist until the axial position of 160 mm. This is indicating that the CRZ of the lower swirl flame receives mixtures with reactions still in progress. Beyond 160 mm downstream these concentrations start to disappear.

e- In the outer recirculation region, very low concentrations of CO and HC are observed in both swirls (see Figs 4.20 and 4.24 - 4.26). This indicates that, more reactions take place at the outer boundary of the forward jet flow than at the inner boundary adjacent to the CRZ. Gases circulating in this region are therefore mainly the products of complete combustion.

(ii) NOx formation

The results of NOx measurements are presented in Figs 4.27(a,b) as contours of the NOx concentration field for the two swirl settings surveyed. Some illustrative radial NOx profiles at three planes are presented in Figs 4.28(a-c). These results are discussed in relation with the temperature and aerodynamic fields described in sections 4.3.1 and 4.3.2. For the present discussion, the flow field can be divided into four zones:

A- The main reaction zone (forward flow zone)

B- The central reverse-flow zone (CRZ).

C- The fully developed flow zone

D- The peripheral recirculation zone (PRZ).

Most of NOx formation takes place in the reaction zone (forward flow zone leading to uniform concentration distributions in the fully

developed flow zone.

The processes occurring in these zones are now discussed.

(A)- The reaction zone:

This region covers the area containing the forward flow of the fresh mixture discharged from the burner. It is regarded as extending to the point where NOx concentration becomes uniform across the whole radial profile. Figure 4.28(c) shows that with both swirls these are uniform concentrations after 500 mm downstream. The reaction zone is characterised by steep gradients of NOx concentration in both the radial and axial directions. The rate of NOx formation follows closely the rate of the main combustion reactions as indicated by the temperature and main species concentrations. Comparison of the NOx profiles at 45 mm from burner exit (Fig 4.28(a)) with those of the temperature (Fig 4.8(a)) show that NOx profiles are similar to the temperature profiles for each swirl case. On moving to the distance of 545 mm downstream from the burner exit, it seen (Fig 4.28(c)) that the NOx profiles have become much more uniform across the furnace. It is also seen that the NOx levels are significantly higher for the lower swirl case (S=0.9). The higher values with lower swirl cannot be completely explained by the temperature variation alone. The following factors must also be considered:

a- Longer residence time, due to the lower local reaction rate.

b- Higher fluctuations in the concentrations as observed generally from the shape of the flame as indicated in Sec 4.1.1.

(B)- The central reverse-flow zone (CRZ):

The flow entrained into this zone has mainly come from the forward flow

described above. Thus NOx concentrations in this zone will be the result of concentrations entrained from the forward flow and possibly due to further reactions in this zone. The profiles of NOx (Figs 4.28(a,b)) and the corresponding temperature profiles (Figs 4.8(a,b)) show that NOx concentration within this region is mainly due to the entrainment from the forward flow and not due to reactions within this zone. This is clearly shown at the 45 mm axial distance, Fig 4.28(a). It is seen from this figure that although the temperature within the CRZ is lower for S = 0.9, NOx concentrations in this region are higher. At the next axial position of 160 mm distance the temperature levels at both swirl settings are about the same, yet higher levels of NOx are observed at the lower swirl (S=0.9). These findings of higher NOx in the low swirl case are attributed to the same factors of longer residence time and greater concentration fluctuations, already described in the previous paragraph.

(C)- Fully developed flow zone:

This region covers the flow downstream from the reaction zone. In both swirl settings, constant NOx concentrations were measured throughout this region and these equal the value measured at the stack. The NOx present in this region derives primarily from the NOx formed in the reaction zone (A). Consequently one would expect from the discussion above that the lower swirl will give the higher NOx values. This is confirmed by the results where NOx concentration is 26 ppm at S=2.25 and 32 ppm when S=0.9.

(D)- The outer recirculation zone (PRZ):

The flow circulating in this region is a mixture of flows come from the

fully developed flow zone and the reaction zone. Figures 4.28(a,b) show that NOx concentrations in each swirl case changes from one plane to another until it reaches the fully developed value (Fig 4.28(c)). Since the contribution of the fully developed region to the NOx concentrations in the PRZ is higher than the reaction zone contribution, NOx values in the PRZ in the lower swirl case are higher at all planes- Figs 4.28(a-c).

From the analysis of NOx results described in paragraphs A-D above it could be summarized that:- NOx formation in these flames has been mainly affected by the flame temperature, residence time of hot gases in reaction region and the concentration fluctuations. The last two of these factors are considered to be the cause of the higher NOx values in the lower swirl case. These factors confirm that NOx has been formed mainly by the thermal mechanism in this system.

4.3.4 Stack measurements

The second group of measurements was aimed at finding the effect of fuel equivalence ratio (ϕ) upon pollutant formation (CO and NOx) as measured in the stack. The tests covered the conditions described in Section 4.1. The fuel equivalence ratio range was 0.76 (30% excess air) to 1.33 (25% deficient air). Most of the tests were carried out under the same input firing rate of 400 KW. However due to control limitations a few tests had to be performed at the lower firing rate of about 360 KW. The effect of this reduction upon the results is negligible as shown in Figs 4.29 for NOx. The results will be therefore be described for the 400 KW only.

(i) CO concentrations

The variation of CO concentrations with ϕ is given in Fig 4.30 for the two swirls tested. It is seen that the swirl change within the range tested has negligible effect on CO concentrations. For lean mixtures with excess air higher than 5 %, no CO concentration is observed, indicating completeness of combustion. At stoichiometric equivalence ratio, low concentrations of CO are observed even for the high swirl case. This is showing that, however high the swirl is, perfect mixing on the micro-scale can not be guaranteed . In this system excess air of 5% appears to be sufficient to guarantee complete combustion.

When equivalence ratio (ϕ) was increased above the stoichiometric value, CO concentrations increased proportionately. A value of 6.5% is reached at ϕ = 1.33 (25% deficient air).

(ii) NOx concentrations

The results of these measurements are shown in Fig 4.31 where concentrations of NOx are given in mg/Nm^3 (N ≡ normal) corrected to 3% O_2. At each value of ϕ, the lower swirl exhibits higher NOx concentrations which is consistent with the reasons for NOx formation within the reaction zone given in Sec 4.3.3 above. On detailed analysis of Fig 4.31, the following comments can be made:

1- In both swirls tested, maximum NOx concentrations were measured at slightly on the lean side of the near stoichiometric equivalence ratio, ie at about $\phi \approx 0.95$ (5% excess air). This is due to the condition of high temperature and availability of oxygen.

2- Increased excess air gave significant decrease in NOx formation. This trend is seen to continue to the maximum excess air tested of 30% (ϕ =0.76) in both swirls.

The formation of NOx is mainly dependant upon high temperature and to a lower extent, high O2 concentration. This condition occurs in a very localised adiabatic region where combustion products and unused oxygen coexist. Although increased excess air increases O2 concentrations, the effect of the lowering flame temperature is seen to be the controlling factor.

3- At fuel rich mixtures (ϕ > 1.0), NOx exhibits very sharp decrease as ϕ was increased, this trend being the same for both swirls.

As mentioned above, the formation of NOx is dependant upon high temperature and high O2 concentration. For rich mixtures the effects of lower temperature and lack of oxygen both work towards reducing NOx formation.

Some of the measured NOx could be formed within the flame zone by the prompt mechanism although this is unlikely within the relatively limited range of ϕ tested.

From 2 and 3 above, it is concluded that for this system, both air and fuel staging can be used to suppress NOx formation.

4.4 PERIPHERAL FUEL INJECTION- SCHEME 2

The main difference between this scheme and the one described as scheme 1 above is the introduction of part of the combustion air through the central gun, Fig 3.2.c(A). This air from the gun is introduced radially outwards across the main air stream.

Measurements were performed in the stack only. Concentrations of CO and NOx were measured for different input fuel equivalence ratio ($0.76 < \phi < 1.33$). Since the flame in this system was stable without and with swirl, four swirl values were tested, S = 0.0, 0.45, 0.90 and

2.25.

(i) CO concentrations

The results, given in figure 4.32 show that, for the range of ϕ tested, all swirls exhibit same CO concentrations variation. Complete combustion in all cases occurred at $\phi \leq 0.95$ (5% excess air and above). The discussion of CO results offered in section 4.3.4 does also apply here.

(ii) NOx concentrations

These results are given in Fig 4.33. It is seen that the maximum NOx concentrations are measured when $\phi = 0.95$ (5% excess air) in all swirls. The explanation for the peak occurring at this value is the same as that given for scheme 1 in paragraph 4.3.4(ii). It also noted that the values of NOx at this equivalence ratio are slightly higher for S = 0.0 and 0.45. The main reason for this observation is the longer residence time associated with longer flame in these swirls.

At mixtures with excess air higher than 5% ($\phi < 0.95$), all swirls except S = 0.0 show similar decrease in NOx formation. The main reason for this decrease is the lowering of flame temperature at increased excess air. However, in the case of no swirl, the effect of the decrease in mean flame temperature seems to be balanced by the greater concentration fluctuations.

At fuel rich mixtures ($\phi > 1$), a sharp decrease in NOx formation is the result of decreased O2 concentrations and reduced flame temperature simultaneously.

These results indicate that both fuel staging and air staging can reduce NOx formation in this system. However, air staging is expected

to be more effective due to the steeper decrease in NOx formation on the fuel rich side as compared with the fuel lean side. This difference between rich and lean sides had been less noticeable when using scheme 1.

4.5 CENTRAL AXIAL FUEL INJECTION

The representative samples of measuremcnts taken in this system were concentrated mainly on the pollutant formation. The aim was to quantify the poor characteristics of this flame as described in Sec 4.1.2 and to use the data for comparison with other injection modes in the next chapter. As mentioned in Sec 4.1.2 it was possible to obtain a stable flame only at medium and high swirl settings (S=0.9 and 2.25).

4.5.1 Temperature measurements

The main objective of temperature measurements in this system was to assist the analysis of NOx formation in the flame. They also indicate any departure from flame symmetry and the effect of swirl on mixing. Figures 4.34(a,b) show temperature distributions at the axial positions 45 mm and 200 mm respectively. Both figures show some asymmetry in the flame. This asymmetry indicates the poor mixing between the air and fuel in this system and explains the apparent non-uniformity of the flame. This will be illustrated further by the CO concentrations in these regions.

At 45 mm from quarl exit, Fig 4.34(a), both swirls exhibit the same steepness of temperature gradient in the forward flow region. Within both the CRZ and PRZ, the lower swirl gives lower temperature values. This indicates that the mixing in this case is slower. This slow mixing resulted in a longer flame as inferred from Fig 4.34(b) at 200 mm

downstream. In this figure the lower swirl show slightly higher temperature at the CRZ.

These two figures give a clear indication of the role of swirl in the mixing near the burner zone.

4.5.2 Species concentrations

(i) Concentrations of CO, CO_2 and O_2

Measurements of each of the above species at the axial positions, 45 mm and 200 mm are shown in Figs 4.35 - 4.37 respectively.

The combustion information obtained from these species is detailed below:

1- Concentrations of CO measured at 45 mm from quarl exit (Fig 4.35(a)) are shown to be high in both swirls with maximum values within the CRZ of 4% and 5% for S=0.9 and S=2.25 respectively. Same value is noted until 200 mm downstream for S=0.9 but reduces to only 2% for S=2.25 (Fig 4.35(b)). These high CO concentrations are a result of introducing the fuel at the centre of the air flow. At the interface between the air and fuel, the turbulence generated shear layer is small due to the small surface area of interaction. This has resulted in slow and inefficient mixing within the quarl and early sections of the furnace. As a result, the lower swirl shows a flame larger in length and diameter.

2- As expected with this method of fuel injection, maximum mixing and combustion occur at the boundary of the fuel jet as shown by the maximum concentrations of CO_2, Figs 4.36(a,b) and minimum O_2 concentrations, Fig 4.37(a,b) within the CRZ. As one moves from the centre towards the air jet boundary, concentrations of CO_2 decreases and O_2 concentrations increase, indicating the weak mixing in these

regions. The gradients of these concentrations decrease as one moves downstream along the furnace.

3- The combustion products in the outer recirculation region are those recirculated from regions downstream from the combustion zone as indicated from the maximum CO_2 and minimum O_2 in these regions. These concentration values were approximately equal to those observed in the stack.

(ii) NOx formation

Concentrations of NO_x measured at the two axial positions, 45 mm and 200 mm are given in Figs 4.38(a,b). These figures show that NO_x concentrations within the reacting forward flow are characterised by steep gradients in the radial and axial directions. These follow closely the rate of main combustion indicated by the temperature (Fig 4.34(a,b)). Within the central and outer recirculation zones, NO_x concentrations also exhibit dependence on the temperature. However, the longer residence time and higher fluctuations in the concentrations may also play an important role in the case of lower swirl. In the PRZ, NO_x concentrations are uniform with a value of nearly 18 ppm for both swirls. The NO_x concentrations recorded in the stack were also about 18 ppm for both swirl values. This indicates that the NO_x concentrations in the PRZ are the equilibrium values circulated from regions downstream from the combustion zone.

The strong dependence of NO_x on the temperature indicates that NO_x has been formed mainly by the thermal mechanism.

4.5.3 Stack measurements

Concentrations of CO and NO_x were measured for different input fuel

equivalence ratio ($0.83 < \phi < 1.11$). Outside this range it was not possible to obtain a stable flame. These measurements are presented for the 400 KW firing rate.

(i) CO concentrations

These are given in Fig 4.39. The main observation is the noticeable amount of CO measured between stoichiometry and excess air of 10 % ($\phi = 0.90$) for the lower swirl case. For high swirl, small concentrations of CO are observed even at about 5% excess air ($\phi = 0.95$). These observations indicate clearly the poor mixing characteristics of this flame and the need for more than 10% excess air to achieve complete combustion, especially for low swirl.

(ii) NOx concentrations

Figure 4.40 shows NOx variation with fuel equivalence ratio. For lean mixtures, increasing excess air up to 20% ($\phi = 0.83$) increased the stack measured NOx concentrations. This increase is seen in both swirls with small difference between them, the higher values being for the lower swirl. As indicated in Section 4.5.2, the mixing in this system is inefficient and slow. Increased excess air increases the chance of air mixing with fuel and therefore a better chance of reaction. A better reaction rate will give high peak temperature and therefore high NOx concentrations. At fuel rich mixtures ($\phi > 1$), the opposite effect occurs resulting in a lower flame temperature. The lower flame temperature together with lower O2 concentrations reduce NOx formation. This trend is more obvious at S = 2.25. The higher NOx concentrations in the case of S = 0.9 is due to the longer residence time and the greater concentration fluctuations associated with this swirl case.

4.6 CENTRAL RADIAL FUEL INJECTION

Two sets of measurements will be described for this fuel injection mode. The first set covers the in-furnace detailed measurements of NOx taken at four swirl numbers, S = 0.0, 0.45, 0.9 and 2.25. The second set covers the stack measurements of NOx. The wide range of swirl indicated above allowed the study of the effect of swirl on NOx formation in this system.

4.6.1 NOx formation and swirl

The results of the first set of measurements are presented in Figs 4.41(a-d) as contours of the NOx concentration field. Some illustrative radial NOx profiles at three planes near the burner (45 mm, 200 mm and 300 mm from quarl exit) are presented in Figs 4.42 - 4.44, together with the corresponding temperature profiles.

The above NOx contours are discussed in relation to the main data for the flow and combustion fields reported earlier by Beltagui et al (1988-c) and Beltagui et al (1989). For the present discussion, the flow field will be divided into three zones .

(A)- The reaction zone:

This region covers the area containing the forward flow of the fresh mixture discharged from the burner and extends to the point where the NOx concentration becomes uniform across the whole radial plane. The length of the reaction zone decreases from 1.15 m to 0.42 m as the swirl number increase from 0.0 to 2.25. This is in agreement with flame length values estimated from the measured CO concentration as reported by Beltagui et al (1988-c).

This region is characterised by steep gradients of NO_x concentration in both the radial and axial directions. The rate of NO_x formation follows closely the rate of the main combustion reactions as indicated by the temperature and main species concentrations.

Figures 4.42 - 4.44, show profiles of NO_x with those of temperature for three levels near the burner. The figures demonstrate the relation between NO_x concentration and temperature for the cases of swirl numbers 0.0 and 2.25. The axial distance from the burner to the position of maximum NO_x concentration decreases as swirl is increased. Figure 4.45 illustrates this further where the minimum NO_x value at any plane is plotted versus the furnace length. The increase in the minimum value of NO_x from one plane to the next indicates the newly formed NO_x. Radial profiles show higher NO_x concentrations on both sides of the minimum value due to mixing with the reverse flow on the boundaries of this region.

(B)- The central reverse-flow zone (CRZ):

As indicated earlier, the flow entrained into this zone has come from the forward flow described above. Thus reactions here depend on the length of the CRZ relative to that of the reacting zone.

Figure 4.46 shows the variation of the NO_x concentration at the centreline with axial distance along the furnace.

For low swirl the CRZ is much shorter than the reaction zone, thus the CRZ receives a mixture with reactions still in progress and with low NO_x concentration and low temperature values. In this case it is found that no more NO_x formation takes place within this zone. A decrease of NO_x concentration occurs due to dilution with fresh mixture entrained nearer the burner end, Fig 4.46.

As swirl is increased the CRZ lengthens and the reaction zone shortens but is still longer than the CRZ. Thus gases with higher NOx concentrations and at higher temperatures enter the CRZ where further NOx reactions take place producing peak concentrations near the burner, as shown in Fig 4.46, with S=2.25.

(C) Fully developed flow zone:

This region covers the fully developed forward flow downstream from the reaction zone and the reverse flow in the outer recirculating flow. At each swirl setting uniform NOx concentrations were measured throughout this region and these equaled the value measured at the stack. This value varied from about 25 ppm to 30 ppm as swirl number increased from 0.0 to 2.25.

4.6.2 NOx measurements in the stack

These tests covered the fuel equivalence ratio (ϕ) range of 0.71 (40% excess air) to 1.11 (10% deficient air) and they are presented for input firing rate of 400 KW in Fig 4.47.

(A) Lean mixtures:

Increasing the excess air up to 40% ($1.0 > \phi > 0.71$) increased the stack measured NOx concentration relative to the value at $\phi = 1$, Fig 4.47. This applies to all swirl settings tested. This suggests that for this system, the reaction zone temperature does not change significantly with excess air and the main factor contributing to the increase of NOx formation is that of increased O2 concentration.

(B) Rich mixtures:

The results, given by Fig 4.47,exhibit a very sharp decrease of NO_x as ϕ was increased, this trend being the same for all swirl settings tested.

For rich mixtures the effects of lower temperature and lack of oxygen both work together towards reducing NO_x formation. Some of the measured NO_x could be formed within the flame zone by the prompt mechanism although this is unlikely within the relatively limited range of ϕ tested in this system.

The results for lean and rich mixtures demonstrate that for this system only the air staging technique is useful for suppression of NO_x formation.

CHAPTER 5

COMPARISON OF FUEL INJECTION MODES AND DISCUSSION

5.1 INTRODUCTION

The results of the measurements presented in the previous chapter along with those reported by Beltagui et el (1988-c) and (1989) provide the data required to compare and discuss in this chapter the performance of the three fuel injection modes- central axial, central radial and peripheral. The comparison will be focused on the following points:

a- The mixing and combustion characteristics near the burner zone with swirl as the main input parameter.

b- Pollutant formation, namely CO and NOx, variation with fuel equivalence ratio as measured in the stack. Measurements of NOx taken under these conditions will be used to study the possibility of NOx reduction under fuel lean conditions or under staged combustion. The data will also be used for the validation of NOx modelling work presented in chapter 6.

Comparisons of the results will be classified into three categories according to the measurements available:

1- The flow patterns as demonstrated by in-furnace measurements of the three time-average velocity components and static pressure will be compared between the peripheral fuel injection (scheme 1) and the radial fuel injection. Momentum fluxes will be introduced and compared. Swirl number calculated from the momentum fluxes will also be discussed. These comparisons will be given in Sec 5.2.

2- The combustion patterns as demonstrated by the in-furnace measurements of temperature and species concentrations (NOx, CO, CO2

and O_2) will be compared for the three methods of fuel injection. The peripheral fuel injection method used in this case will be Scheme 1 (Sec 3.3.3). Fluxes of sensible enthalpy along the furnace will be introduced and compared between the peripheral and central radial fuel injection modes. These comparisons will be described in Sec 5.3.

3- The pollutant formation as demonstrated by stack measurements of CO and NOx concentrations will be compared over a range of equivalence ratio (ϕ). For peripheral fuel injection, this will include both Scheme 1 and Scheme 2. Section 5.4 will cover these comparisons.

5.2 FLOW PATTERNS

The profiles of the three time-average velocity components and static pressure will be compared between the peripheral fuel injection (Scheme 1) and the central radial fuel injection. Fluxes of axial and tangential momenta integrated from the experimental velocity profiles will also be introduced and compared. The swirl number calculated from these fluxes and based on the furnace diameter will also be discussed.

5.2.1 Axial velocity distributions and flow boundaries

For peripheral fuel injection (Scheme 1), the axial velocity distributions along the furnace were presented in Figs 4.10(a,b) for the swirl numbers S=0.9 and 2.25 respectively. The corresponding profiles for the radial fuel injection are shown in Figs 5.1(a,b). Generally the axial velocity distributions in both fuel injection modes exhibit some similarity. The flow in both cases consists of a CRZ surrounded by an annular jet containing the forward flow. Outside the forward flow a weak peripheral reverse flow zone extended to the walls.

The value of peak velocity in the forward flow zone increases with increased swirl. These distributions are generally observed in confined swirling flames, eg, the IFRF work (Wu and Fricker (1976), Leuckel and Fricker (1976)) and Glasgow University work (Bafuwa (1970), Beltagui and Maccallum (1976) and (1988)). Despite the general similarity in distributions, the effect of fuel injection mode in each swirl case is seen through the differences in the jet width, peak velocity values and velocity decay along the furnace. These differences are discussed below:

1- At each swirl setting, the jet in the case of the peripheral fuel injection is slightly wider. The jet width is an indication of flow expansion due to the sudden change in the area when the jet leaves the quarl and also due to the density change by combustion. The mixing in the case of peripheral fuel injection depends on the turbulence generated at the shear layer between the fuel jet and outer boundary of the swirled air jet. At these locations, combustion and maximum radial expansion occur. For the central radial fuel injection, the mixing is provided by the penetration of the high velocity fuel jets through the air stream, thus creating a status of partial mixing before combustion. Combustion in this case is expected to be relatively close to the centre. However, because combustion in both systems commences within the quarl (Sec 4.3.3(i) and Beltagui et al (1988-c)), the presence of the quarl seems to reduce these differences inside the furnace. From the boundaries of the forward flow shown in Fig 4.12 (for the peripheral injection) and Fig 5.2 (for radial injection), it is obvious that because the jet redial expansion is higher in the case of peripheral injection, the jet impingement with the walls is much earlier. For example, for

peripheral fuel injection, the jet impingement point in the case of high swirl occurs at axial distance of 0.6 m, while for the radial fuel injection, it occurs only after 1 m downstream. This earlier jet impingement explains the earlier decay of the axial velocity along the furnace observed with the peripheral injection system.

2- Radial fuel injection leads to higher peak axial forward velocities. The highest differences from those of the peripheral injection system are seen at planes near the burner zone. Figure 5.3 shows the maximum axial velocity distributions along the furnace for both fuel injection modes. At the lower swirl case (S=0.9) and X=45 mm, the peak axial velocity in the radial injection case is about twice the corresponding value of peripheral injection. Beyond 200 mm, these differences are lower and remains nearly constant to the last measuring section. At the high swirl case (S=2.25), the differences are much less. The peak velocities with the two injection modes are seen to decrease at a similar rate along the furnace. The high velocity values associated with the radial fuel injection suggest that the flow expansion in the axial direction is higher than that with peripheral injection. Figure 5.3 also shows that the differences in the peak axial velocity between the two swirls when using radial injection are much lower than their counterparts for the peripheral injection cases, especially at planes near the burner zone. This observation indicates that the contribution of swirl to the combustion in the radial fuel injection is less pronounced than its contribution with the peripheral injection system. As indicated earlier, the mixing in the radial fuel injection mode depends not only on the swirl generated shear stresses, but also on the partial mixing generated by the penetration of the small fuel jets through

the air stream. In addition to its contribution to the mixing, the latter contributes also to the provision of the aerodynamic blockage which promotes the CRZ and thus flame stability even without swirl (Beltagui et al (1989)).

3- With peripheral fuel injection, the introduction of swirl causes greater centrifugal effects than in the radial injection case (Ahmad et al (1984) and Beltagui and Maccallum (1988)). Thus for example at high swirl (S=2.25) in the present work, with peripheral fuel injection there is a pronounced CRZ (Fig 4.12) which is noticeably wider and longer than when radial fuel injection is being used (Fig 5.2). However with radial fuel injection the aerodynamic blockage described in the previous paragraph also aids the formation of the CRZ. When swirl is reduced to S=0.9, one would expect the effect in the peripheral fuel injection case to be more pronounced. This is in fact the case and the CRZ with the two injection systems now of about the same size.

4- Beyond the axial distance of about 500 mm, the lower swirl (S=0.9) coupled with radial fuel injection shows axial velocity values higher than those in all other cases. This is seen clearly in Figs 5.3 and 5.4. This case therefore represents the lowest jet expansion and lowest velocity decay along the furnace.

5.2.2 Tangential velocity distributions

The tangential velocity distributions for the peripheral fuel injection were presented in Figs 4.13(a,b) for S=0.9 and 2.25 respectively. For the radial fuel injection these are shown in Fig 5.5(a,b).

In the rotating flow field near the axis, the tangential velocity increases proportionally with the radius of the furnace, according to

the principle of solid body rotation. After having reached the maximum value, potential rotation occurs and the tangential velocity decreases as one moves towards jet boundary. The centrifugal forces caused by the rotation produces a pressure depression, which increases in the direction of the axis. Since the maximum values of the tangential velocity in the case of the peripheral fuel injection are higher than those of the radial injection especially at locations near the burner (X < 300 mm), the effect of the centrifugal forces is higher, leading to the larger CRZ at high swirl. Beyond the axial position of 300 mm, the tangential velocity at the low swirl of both injections systems decays to small values. For the high swirl, these start to decay downstream after about 550 mm from burner exit.

By contrast to the axial velocity distributions described above, the effect of introducing the fuel in the outer boundary of the air flow is seen to cause an increase in the tangential velocity. The benefit of this is to increase the centrifugal forces and thus the mixing rates. This will be confirmed by the combustion patterns in Sec 5.3.

5.2.3 Radial velocity distributions

The radial velocity distributions for the peripheral fuel injection system were presented in Figs 4.14(a,b). For radial fuel injection, these are shown in Figs 5.6(a,b). The trends of the radial velocity profile are consistent with the jet expansion behaviour suggested by the axial velocity distributions. The distributions in both injection modes show that, close to the burner, the radial components are of the same order as the axial velocity components. The effect of fuel injection mode on the radial velocities are similar to the effects on the axial velocities, previously described. Beyond 300 mm downstream,

the redial velocity values in both injection modes decay to very small values, with no noticeable differences between them.

5.2.4 Static pressure distributions

These were presented in Figs 4.15(a,b) for the peripheral fuel injection. For the radial fuel injection these are shown in Fig 5.7(a,b). All pressure values are sub-atmospheric with minimum values near the burner. These profiles also exhibit maximum depression at and around the axis of the jet. The CRZ and the PRZ are zones of uniform pressure. For the radial fuel injection, increasing the swirl from 0.9 to 2.25 resulted in a very small increase in the static pressure depression. This explains the small differences between the reverse flow velocities of the two swirls of this injection mode as described in Sec 5.2.1. For the peripheral fuel injection, increased swirl resulted in a significant increase in the static pressure depression, thus high differences in the reverse flow velocities observed between the two swirls of this injection (Fig 5.4). The high differences observed here are related to the centrifugal forces explained in Sec 5.2.1 and 5.2.2.

The static pressure distributions also show that for S=0.9, the static pressure in both injection systems start to be uniform beyond X=80 mm, while at high swirl, these are uniform only after 300 mm downstream.

5.2.5 Momentum fluxes

The experimental profiles of axial and tangential velocities compared in Sec 5.2.1 and 5.2.2 have been integrated to give the fluxes of axial and tangential momentum respectively. The main objective of these integrations was to assist the study of the effect of fuel injection on

the flow development in the furnace. These fluxes also provide a good measure for swirl which is often used as scaling parameter in swirling flames.

(i) Axial momentum flux

The total axial momentum flux across any plane is give by :

$$G = 2\pi \int_0^{D/2} [\rho u^2 + (p_{st} - p_{ref})] \, r \, dr \qquad (5.1)$$

where D, ρ, u, p_{st}, p_{ref}, and r are furnace diameter, density, axial velocity component, static pressure, reference pressure and radius respectively.

The axial momentum flux contains two terms, the dynamic term (G_d), obtained by integrating the group (ρu^2) and the static pressure term obtained by integrating the group ($p_{st} - p_{ref}$).

It is widely accepted (Beltagui and Maccallum (1976-b), Gupta and Lilley (1984), Hagiwara and Bortz (1986), Criesta (1987), and Dugue and Weber (1989)) that it is the dynamic component G_d, of the axial momentum flux which has greatest bearing on flow development in a confined furnace. Therefore, the present work has been focused on the dynamic component (G_d) of the axial momentum flux.

Figure 5.8 shows integrated flux values for the peripheral and radial fuel injection modes, normalised by the theoretical axial momentum flux at the swirler exit assuming uniform velocity. The two swirls of both injections show increase in the normalised flux at positions in the region of the flame front. In each injection method, the difference in the normalised value of the flux within these positions shows the effect of swirl on this momentum flux. This effect is more significant with the peripheral injection and is the result of the higher jet area

and the volume expansion associated with the higher swirl. It is also seen that after reaching the maximum value, all momentum fluxes decrease to a final normalised value which is much lower than unity. The main reason for this decrease is the significant loss of momentum due to the impingement of the jet on the furnace walls, the highest loss being always for the high swirl.

Since these fluxes were integrated from the axial velocity profiles, the differences between the two injection modes follow closely the differences indicated for the axial velocity (Sec 5.2.1). Some of the important comments are presented below:

1- At furnace inlet, the lower swirl case of the radial fuel injection (S=0.9) and the higher swirl of the peripheral injection (S=2.25) show similar momentum flux values. These are consistent with the axial velocity values in these regions (Fig 5.1(a) and 4.10(b)). Since the highest reverse flow velocities are associated with the high swirl of the peripheral injection, the momentum flux beyond X=160 mm is much smaller and decays quickly to a very low value at X=1 m. This is also confirmed by the high decay of maximum axial velocity shown in Fig 5.3 and the lowest recovery of the centre line velocity shown in Fig 5.4.

2- The high values of momentum flux observed with the lower swirl using radial injection at positions beyond 500 mm from quarl exit is the result of the high axial velocity observed in this region, as described in Sec 5.2.1.

3- For both injection modes it is expected that the final value of the axial momentum should be the same in both swirl cases. It was not possible to observe this due to the inability to obtain reliable velocity measurements at the low velocities which predominate at the

axial distance beyond 1 m.

(ii) Tangential momentum flux

The axial flux of tangential momentum across any plane is given by:

$$T = 2\pi \int_{0}^{D/2} \rho u w \, r^2 dr \qquad (5.2)$$

where w is the tangential velocity component. The fluxes integrated by the above equation are shown in Fig 5.9 for both fuel injection modes. These fluxes were normalised ($\overline{T}$) by the theoretical tangential momentum of the flow leaving the swirler. This theoretical flux was calculated from the input swirl number, based on the burner throat radius and assuming that the axial velocity at that plane is uniform. From Fig 5.9, it is seen that all tangential momentum fluxes emerge from the quarl to the furnace with normalised values of less than unity. This is indicating that a significant part of this momentum was lost within the quarl due to friction. At the flame front region, where maximum expansion occurs, all momentum fluxes attain maximum values depending on the fuel injection mode and on swirl. Since the differences between the axial velocities of the two injection modes were much higher than those for the tangential velocities, the differences seen in the momentum fluxes are mainly attributed to the differences in the the axial velocity values in these regions. After reaching the maximum value, all momentum fluxes decay. In each injection mode the final value in both swirls should be the same. However these final values were not found for the same reason mentioned for the axial momentum flux.

5.2.6 Swirl number

For modelling swirl flames a scaling parameter is needed as a measure of the swirl intensity given to the flow. There have been a number of definitions for this parameter. The two most commonly recognised are:-

A- Burner swirl number, defined as:

$$S = T / G_d r_b \qquad (5.3)$$

where T is the axial flux of tangential momentum at the swirler exit, G_d is the flux of axial momentum, dynamic component, at the swirler exit, and r_b is the burner throat radius.

This parameter gives a good indication of the degree of swirl imparted to the flow within the swirler. It is successful in correlating the flow close to the swirler in isothermal free flows. However, it does not account for the effects created by expansion into a furnace confinement, suddenly or via a quarl. Nor are the effects of the flow expansion caused by combustion accounted for.

The effect of area expansion, for isothermal flows, was introduced by using a swirl number based on the quarl exit diameter (Criesta et al (1987)), or the furnace diameter (Beltagui and Maccallum (1976-b), Beltagui and Ralston (1984) and Hagiwara and Bortz (1986)).

B- Furnace swirl number, defined as:

$$S^* = T / G_d D \qquad (5.4)$$

where T and G_d are the integrated fluxes of tangential and axial momenta measured at the furnace exit respectively and D is the furnace diameter.

This definition was proposed by Beltagui and Maccallum (1976-b) where

it was applied successfully to characterise the general flow patterns in two furnaces for isothermal and premixed combustion conditions.

This number proved to be a better index of the flow pattern in furnaces (eg Hagiwara (1986)). It takes account of the furnace to burner area ratio as well as the effect of combustion. However its evaluation requires more experimental measurement.

The value of the integrated S^* for the combustion flow is lower than for the isothermal flow. It is also a function of the equivalence ratio, or temperature rise due to combustion, being lower for the higher equivalence ratio. A value of $S^* = 0.1$ was found to define the onset of a CRZ in the flow, for both isothermal and premixed combusting flows, in two furnace confinements ratios (D/d) (Beltagui and Maccallum (1976-b)) and for non-premixed combusting flows (Beltagui et al (1991)).

In the present work, although the data are limited to the peripheral and radial fuel injection modes, it is found that S^* is also a function of fuel injection mode.

The values of S^* calculated from the experimental data for the present work are given in Fig 5.10 where they have been plotted against the burner swirl number (ie input swirl number). The results highlight the following points

1- Both fuel injection modes indicate a linear relationship between the furnace swirl number S^* and burner swirl number S.

2- For the peripheral fuel injection systems, the initial value of S^* for CRZ establishment is 0.1 which is in line with previous findings of Beltagui and Maccallum (1976-b) and Beltagui et al (1991)).

3- For the radial fuel injection, the results show that the onset of the CRZ starts at S^* which is much less than 0.1. This finding is

very interesting since CRZ in this fuel injection was observed even at no swirl. In this case, the CRZ is caused by the mode of fuel injection (aerodynamic blockage) rather than by swirl.

These results along with previous results therefore confirm the validity of S^* in characterising the flow patterns of swirling flows.

5.3 COMBUSTION PATTERNS

A good assessment of the relative combustion patterns is given by comparing the temperature rise profiles and the gas sampling results between the three fuel injection modes. The most important information required to assess the performance of these flames is obtained from the results of measurements near the burner zone. The information inferred from these results includes, mixing, combustion intensity, flame symmetry, heat release and pollutant formation. The comparisons are therefore presented for two planes near the burner at, X=45 mm and X=200 mm.

5.3.1 Temperature distributions

Comparison of the temperature distributions at the two planes indicated above are given in Figs 5.11(a,b) and 5.12(a,b). For each plane, temperature profiles are shown for the two swirls, S=0.9 and 2.25 respectively. These are presented to indicate the effect of swirl on mixing and combustion intensity in each of the three fuel injection modes.

From Figs 5.11 and 5.12, the following remarks are made:

1- Flame symmetry:-

In both planes and swirl intensities, the central axial fuel injection show high degree of flame asymmetry as opposed to the other fuel

injection modes. The highest degree of asymmetry is noted at the plane nearest to the burner, X=45 mm, and at the lower swirl, S=0.9, Fig 5.11(a). This asymmetry was caused by a tendency for the gas jet to be deflected to one side rather than to be spread uniformly radially outwards. These observations has also been reported in a similar work by Leuckel and Fricker (1976). The tendency towards flame deflection is seen to exist even at increased swirl. This observation is attributed to the inefficient mixing characterising this system. This inefficient mixing is the result of introducing the fuel at the centre of the flame. The mixing in this case depends mainly on the turbulence generated at the shear layer between the air and fuel jet. Since the surface area of the fuel jet is small, the area of interaction between the air and fuel is therefore small, resulting in weak and slow mixing. This slow mixing also explains why the flame is the longest compared with other fuel injection modes.

2- The main reaction zone (forward flow):-

In all fuel injection modes, the steepest temperature gradients occur at the plane nearest to the burner, X=45 mm and the temperature gradients increase as swirl is raised from 0.9 to 2.25 (Fig 5.11(a,b)). The temperature results are the time-averaged values, and they are the values measured after heat transfer has occurred. This heat transfer effect increases further if the combustion starts at locations closer to the furnace walls, as is the case with the peripheral fuel injection. The temperature also decreases due to the high rate of entrainment and subsequent rapid mixing of the relatively cool externally recirculated gases just downstream of the burner exit. Although the radial fuel injection gives reaction zone temperature

values which are higher than with the peripheral injection, these do not necessarily reflect higher combustion intensity, rather, they reflect lower heat transfer to the furnace walls. This fact will be confirmed further by the concentrations of CO, CO_2 and O_2 presented in the next section. For the axial fuel injection, the comparatively low reaction zone temperature is the result of inefficient mixing described in (1) above, and will also be confirmed by species concentrations.

3- Central recirculation zone (CRZ):-

Recirculating flow has a considerable effect on the properties of swirling flames. It transports hot gases from the downstream region back to the base of the flame. The energy which they bring into the regions of air and fuel mixing assist the ignition. This outweighs any effects of the dilution produced by these gases. In addition, recirculating flow creates a steep velocity gradient inside the jet, leading to a high turbulence and consequently good mixing in this region. The gases entrained into the CRZ are those with the maximum temperature, as shown by Figs 5.11 and 5.12. At X=45 mm all injection modes show significant increase in this temperature as swirl increased from 0.9 to 2.25. The temperature distribution within this zone becomes also more uniform with increased swirl. These observations are the result of enhanced stirring of the gases at increased swirl.

As the flow entrained into the CRZ come from the forward flow, the differences in the temperature described for the reaction zone are responsible for the differences within the CRZ.

4- The peripheral recirculation zone (PRZ):-

In all cases, the gases circulated in this zone come mainly from the

fully developed flow region further downstream. The slower the combustion, the longer is the flame, but also the less rapid is the temperature decrease by heat transfer. Consequently the higher is the gas temperature in the fully developed zone and thus the higher is the temperature in the PRZ. The longest flame was observed with the central axial fuel injection, and consequently the highest temperature in the PRZ is seen for this system. The temperature in all cases decreases during the upstream travel of the gases from the 200 mm to 45 mm planes, due to heat transfer to the furnace walls.

5.3.2 Sensible enthalpy fluxes

The sensible enthalpy flux (H) at any plane can be found from integrations of the axial velocity and temperature traverses (T) as given below:

$$H = 2\pi \int_{0}^{D/2} \rho u h \, r \, dr \qquad (5.5)$$

where h is the specific sensible gas enthalpy given by:

$$dh = C_p \, dT$$

where C_p is the specific heat of the gases at constant pressure taken to be a function of temperature.

The results of these integrated fluxes are given in Fig 5.13, for the peripheral and radial fuel injection modes. The fluxes have been normalised by the input energy. In both injection modes, the values of these fluxes are seen to progress from a minimum value at the furnace first inlet plane, to a maximum value at the end of the reaction zone. The maximum value in both injections is less than unity. The main reason for this observation is the high heat loss from the flame to the water-cooled walls of the furnace. It is also noted that the two swirls

in each injection mode exhibit almost identical values of enthalpy flux.

The figure also shows that the sensible enthalpy fluxes of the peripheral fuel injection are much lower than those observed with the radial fuel injection. This is because combustion in the peripheral fuel injection case starts at the outer boundary of the air flow and closer to the furnace wall, thus higher heat transfer to the furnace walls occurs.

Beyond the maximum enthalpy values, the sensible enthalpy fluxes in both injection modes decay to a similar normalised value of about 0.6 at 1 m downstream.

5.3.3 Concentrations of CO, CO_2 and O_2

Comparative profiles for each species are given at X=45 mm and X=200 mm respectively. For CO, these are given in Figs 5.14(a,b) and 5.15(a,b), for CO_2 in Figs 5.16(a,b) and 5.17(a,b) and for O_2 in Figs 5.18(a,b) and 5.19(a,b).

For all fuel injection modes, the effect of increased swirl is to increase mixing and combustion intensity as seen through the reduction of CO concentrations in both planes. This is also confirmed by the increase of the CO_2 concentrations and the decreased O_2 concentrations at all radial locations. It is also noted that combustion in all fuel injection modes commences within the quarl, as demonstrated by the minimum concentrations of CO_2 of 2% for S=0.9 and 4% for S=2.25 at the first plane of the furnace, X=45 mm. This is also confirmed by the maximum O_2 concentration which is significantly less than 20%. This observation has also been reported in a similar work by Leuckel and Fricker (1976).

At both planes, the lower swirl in the peripheral fuel injection exhibits a flame envelope which is wider than other fuel injection modes (Figs 5.14(a) and 5.15(a)). When swirl was increased from 0.9 to 2.25, all fuel injections exhibited nearly the same flame diameter. It is seen from all CO profiles that the lowest concentrations of CO within the flame are observed with the peripheral fuel injection mode. These are significantly lower than the CO concentrations with the radial and axial fuel injection modes. The lower CO concentrations indicate higher rates of mixing and thus the high combustion intensities characterising the peripheral fuel injection. This is confirmed further by the higher CO_2 concentrations and the lower O_2 concentration (figs 5.16-5.19). These observations are the result of the full utilisation of the benefits of centrifugal forces together with the benefits of density gradients occurring in the peripheral fuel injection system as reported by Ahmad et al (1984) and Beltagui and Maccallum (1988).

Within the forward flow region, the lowest O_2 concentrations and the highest CO_2 concentrations are observed with the peripheral injection mode. This is due to the initiation of combustion at the outer boundary of the air flow. For the same reason, the highest O_2 concentrations in the CRZ are observed with peripheral injection, Figs 5.18-5.19. This high O_2 concentrations are accompanied by the lowest values of CO, indicating the highest combustion efficiency.

In the outer recirculation zone, the low concentrations of CO and O_2 and the high concentrations of CO_2 observed with all injection modes indicate that the gases circulated in these regions are mostly the products of complete combustion. It is to be noted that the highest values of CO_2 and the minimum values of CO are observed with the

peripheral fuel injection thus, confirming the conclusion that this injection system gives the highest combustion efficiency.

5.3.4 NOx concentrations

Comparative profiles of NOx concentrations are given in Figs 5.20(a,b) and 5.21(a,b). These profiles are now discussed in relation with the temperature and species concentrations described in Sections 5.3.1 and 5.3.2.

Detailed discussion is presented below for the three main zones, the reaction zone, the CRZ and the PRZ.

(A) The reaction zone (forward flow)

All fuel injection modes show steep gradients of NOx concentrations in both radial and axial directions. The rate of NOx formation follows closely the rate of the main combustion reaction as indicated by the temperature and main species concentrations. The increase in the minimum NOx value within this zone when moving from X=45 mm to X=200 mm indicates the newly formed NOx (Figs 5.20-5.21). The maximum NOx concentrations are seen to increase towards the boundary of the CRZ as the maximum mixing and combustion intensity are increased in this region.

The effect of swirl on the concentrations of NOx depends not only on the flame temperature but also on the residence time and concentration fluctuations as described in the previous chapter. The effect of concentration fluctuations appears to depend on the type of fuel injection, as will be shown clearly in the CRZ below.

(B) The central reverse-flow zone (CRZ)

Since the flow entrained into this zone has come from the forward flow, the concentrations of NOx here depend on the length of the CRZ relative to that of the reaction zone. It depends also on whether there are further reactions within this zone or not. In both planes the low swirl with the radial fuel injection shows the minimum values of NOx compared with other injection modes. These low concentrations indicate that this zone receives mixtures which are still reacting, as confirmed by the high CO concentrations shown in Figs 5.14(a) and 5.15(a). When swirl is increased from 0.9 to 2.25, NOx concentrations for the radial fuel injection system have increases significantly. This increase indicate that gases with higher temperature and thus higher NOx concentrations enter the CRZ. It also indicates that further NOx reactions take place in the CRZ, resulting in the highest NOx concentrations compared with other fuel injections, Figs 5.20(b) and 5.21(b)).

For the peripheral fuel injection, both planes show that increased swirl has resulted in some decrease in NOx formation even though the temperature has increased. These observations were discussed in Section 4.3.3, where the high NOx concentrations observed with low swirl were related to the higher fluctuations in concentrations and to the longer residence time.

For the axial fuel injection, increased swirl shows no effect on NOx values at the first plane (X=45 mm), however, moving downstream to the axial position of 200 mm, the increased swirl resulted in a significant decrease in the NOx formation. It is suggested that this decrease follows for the same reasons as described for the peripheral fuel injection system.

It appears from this analysis that introducing the fuel jet, either at

the outer or inner boundary of the air flow (ie peripheral and central axial fuel injections) results in a significant decrease in local NOx formation when high swirl is used. It is expected that increased swirl contributes to more enhanced mixing and thus reduced local fluctuations in the concentrations, which had been observed at low swirl. The effect of concentration fluctuations on the local NOx values is discussed further in the next chapter.

(C) The peripheral recirculation zone (PRZ)

As indicated in section 5.3.1, the gases circulated in this region come mainly from the fully developed flow region. At the fully developed flow region, the minimum NOx concentrations, as indicated from stack measurements were observed with axial fuel injection. This explains the minimum values of NOx observed in the PRZ. For the peripheral fuel injection, the low swirl produced the highest NOx values in the fully developed region, while the high swirl with this injection demonstrated NOx values less than those of the radial fuel injection. NOx values in the PRZ therefore reflect those at the fully developed flow region.

All NOx values in the fully developed flow zone are the same as the values measured in the stack and these will be discussed in the next section.

5.4 POLLUTANT FORMATION

An overall measure of the total formation of CO and NOx is given by measurements in the stack at the furnace exit. Concentrations of these gases were therefore measured in the stack over a range of fuel equivalence ratio (ϕ). For CO, these measurements were performed to investigate the minimum excess air required to achieve complete

combustion for each of three fuel injection modes.

For NOx these were carried out to investigate the effect of swirl and fuel injection mode on NOx formation. The method of fuel injection will also highlight the possibility of adopting one or more of the following means of reducing NOx formation.

1- Lean combustion

2- Air staging

3- Fuel staging

As fuel rich combustion produces CO, it is not practical to use it alone to reduce NOx formation.

The data obtained from NOx measurements were also needed to validate the NOx modelling work to be presented in the next chapter.

5.4.1 CO concentrations

At the normal firing rate of 400 KW and 5% excess air, the peripheral and radial fuel injection modes gave zero CO concentrations in the stack. This was observed in all swirl cases of the two injections, including both schemes of the peripheral fuel injection. Concentrations of CO started to appear at zero excess air and, as expected when at deficient air conditions. This observation indicates that 5% excess air is sufficient to guarantee complete combustion in these two types of fuel injection.

For the central fuel injection, 5% excess air did not appear to guarantee complete combustion even for the high swirl case. The minimum excess required to guarantee complete combustion was 10%.

The above analysis confirms the comments made on the mixing efficiency in each of the three fuel injection modes in Section 5.3.

5.4.2 NOx concentrations

The results obtained for the two schemes of the peripheral fuel injection will be compared first to study the effect of introducing part of the combustion air through the central gun in the second scheme. Since the radial fuel injection and the second scheme of the peripheral fuel injection showed stable flame with and without swirl, NOx results at zero swirl and S=0.45 will be compared between these two system. For other swirls (ie S=0.9 and 2.25), the comparison is possible for all fuel injection modes.

(i) Peripheral fuel injection

Comparative NOx profiles for the two schemes of this system are shown in Fig 5.22. The two swirls in the second scheme and the high swirl in the first scheme exhibit same NOx concentrations as a function of ϕ. The lower swirl of the second scheme indicates that the introduction of part of the combustion air through the central gun contributed to a significant decrease in NOx formation as compared to the low swirl of the first scheme. This air has contributed to enhanced mixing, thus, significant decrease in the concentration fluctuations and residence time. In the first scheme this decrease could be achieved only by increasing the swirl from 0.9 to 2.25. The decrease in NOx formation at lean and rich combustion in both schemes offers all the means of NOx reduction listed in Sec 5.4. Depending on the industrial application, it is therefore possible to chose lean or staged combustion (ie both air or fuel staging) to achieve virtually equal effect of NOx reduction.

(ii) Peripheral versus radial fuel injection

Figure 5.23 show the comparison between the radial fuel injection and the second scheme of the peripheral injection at S=0.0 and 0.45. At normal firing conditions where combustion is completed at the minimum excess air of 5% (ϕ = 0.95), the two swirls with both injections show the same NOx concentrations. The high values recorded here are explained by the high flame temperature and availability of oxygen. At excess air greater than 5% (ϕ < 0.95), the differences in NOx values are very significant. The peripheral fuel injection gave significant decrease in NOx formation while the radial fuel injection gave increase in NOx formation. The differences observed here are mainly dependent on the flame temperature. For the peripheral fuel injection, increased excess air contributes to some decrease in the flame temperature and thus NOx formation . For the radial fuel injection, increased excess air does not appear to decrease the flame temperature significantly, thus the increase in O2 concentrations seems to be the controlling factor. It should be indicated that these observation are valid only to the maximum excess tested (40%).

At fuel rich conditions (ϕ >1), both fuel injection modes exhibits sharp decrease in NOx formation. This decrease is the result of both decreased temperature and O2 concentrations.

From the above argument, it can be concluded that NOx reduction in the case of redial fuel injection could be achieved only by air staging.

(iii) All fuel injections

The results are shown in Fig 5.24(a) for S=0.9 and in Fig 5.24(b) for S=2.25. The differences between the radial and peripheral injection follow those described in Section (ii) above. For the central axial

fuel injection, both swirls show lower NOx concentrations at all values of ϕ. These differences are explained mainly by the lower combustion efficiency which resulted in a lower flame temperature in the reaction zone. As observed from CO concentrations the minimum excess air required to achieve complete combustion with the central axial fuel injection was 10%. Thus increasing excess air to this limit increases the combustion intensity and therefore NOx formation. Above this limit of excess air the change in the flame temperature seems to be small, thus NOx increases due to increased O2 concentrations.

It appears from the above analysis that the peripheral fuel injection is the only method which offers both air and fuel staging scopes to suppress NOx formation. In applications when lean combustion can be used, only peripheral fuel injection offers the possibility of reducing NOx formation compared with other fuel injection modes.

CHAPTER 6

THE MODELLING OF NOx FORMATION

6.1 INTRODUCTION

The main objective of the work described in this chapter is to develop a model which can adequately predict the overall NOx formation in gas-fired furnaces to suffice practical engineering purposes. The aim is to assist the designer by reducing the amount of experimental work required to quantify the amount of NOx released into the environment. The model was developed through the identification of the main mechanism of NOx formation in the system being considered. The model formulation was based on both published research and the understanding provided by the present experimental measurements.

The main parameters, namely flame temperature, oxygen concentration, residence time and the effect of concentration fluctuation, contributing to this mechanism were therefore incorporated. The model illustrated that the consideration of the concentration fluctuations is critical to the accuracy of NOx predictions. The model was tested through the comparison of predictions with experimental measurements for the three types of fuel injection modes considered in this study.

6.2 NOx MODEL

The review of NOx formation mechanisms introduced in Sec 2.3.1 has revealed that in the application being presently considered, the NOx formation is mainly attributed to the thermal mechanism and to a much lower extent to the prompt mechanism.

The thermal NOx modelling equations, 1, 2 and 3 in Table 6.1, are well established and understood. However, their application to a particular

situation requires two sets of information. The first set includes the rate constants of the reaction equations (Table 6.1).

Table 6.1

Rate constants for extended Zeldovich mechanism

NO	Reaction	Rate constant (Forward) cm^3/mole s	Rate constant (Reverse) cm^3/mole s
1-	$O + N_2 \rightleftarrows NO + N$	$k_1 = 1.82 \times 10^{14} \exp(\frac{-38370}{T})$	$k_{-1} = 1.6 \times 10^{13}$
2-	$N + O_2 \rightleftarrows NO + O$	$k_2 = 6.4 \times 10^{9}\ T \exp(\frac{-3150}{T})$	$k_{-2} = 1.5 \times 10^{9}\ T \exp(\frac{-19500}{T})$
3-	$N + OH \rightleftarrows NO + H$	$k_3 = 1.0 \times 10^{14}$	$k_{-3} = 2.0 \times 10^{14} \exp(\frac{-23650}{T})$

Predictions are particularly sensitive to the value of rate constant (k_1). The uncertainty in determining these rate constants (Williams (1989)) is large and recent measurements have demonstrated the need for more accurate determination of these constants. The most recently accepted value for the reaction rate constant k_1, as measured by Monat et al (1978), is about 2.2 times the values for the previous decade (Bowman (1975)). The values of the reaction constants given in Table 6.1 are the most recent values used for the three NOx reaction equations.

The second set of information covers the local values of flow conditions, the most critical being the flame temperature and concentrations of oxygen and nitrogen. The determination of these values requires the solution of the momentum, heat-and mass- transfer equations together with the chemical reaction equations for the main species (Caretto (1976)). While the closure of these two sets of equations, ie flow and chemistry, is possible, it may prove

prohibitively expensive for the industrial application especially when NOx formation rate is the only variable of interest. Simplified approaches may prove cheaper and sufficient for practical engineering requirements. In the present modelling study, the well-stirred reactor concept was therefore adopted with an appropriate stochastic technique to account for the fluctuations of concentrations of fuel and oxidant.

6.2.1 Thermal NOx modelling

The formulation of the model described here was based on the following assumptions:

a- NO formation when firing lean and near-stoichiometric gaseous fuels is mainly thermal and strongly dependent on temperature.

b- NO formation rate is slower than the hydrocarbon reaction rate and that most of NO is formed after the hydrocarbon reactions reach equilibrium.

c- The calculation of NO (nitric oxide) is sufficient for determining NOx. NO_2 (nitrogen dioxide) may also form in the furnace, however the route to NO_2 is through NO.

Thermal NO was calculated via the extended Zeldovich mechanism, reactions 1 to 3, Table 6.1. Additional reactions involving NO formation from N_2O are sometimes considered but usually account for less than 1 % of the NOx formed thus they are not included here (Toof (1986)).

Assuming a steady-state concentrations of N and H atoms, and that reactions 1 and 2 are both equilibrated, the rate of NO formation becomes (Westenberg (1971)):

$$\frac{d[NO]}{dt} = 2k_1\ [O]_{eq}\ [N_2]_{eq} \left\{ \frac{1 - [NO]^2/k[O_2]_{eq}[N_2]_{eq}}{1 + k_{-1}[NO]/(k_2[O_2] + k_3[OH])} \right\} \qquad (6.1)$$

where

$$k = (k_1/k_{-1})(k_2/k_{-2})$$

The applicable rate constants are listed in table (6.1).

At this stage, for lean mixtures the contribution of reaction 3 can be neglected as mentioned in Section 2.3.1 (1). Assuming that the initial concentration of $(NO) << (NO)_{eq}$, the rate of NO formation could be approximated by:

$$\frac{d[NO]}{dt} = 2k_1\ [O]_{eq}[N_2]_{eq} \qquad (6.2)$$

Assuming O/O2 equilibrium, then (O) concentration is given by the reaction:

$$1/2\ O_2 \leftrightarrows O$$

where

$$[O]_{eq} = \frac{K_o}{(RT)^{1/2}}\ [O_2]_{eq}^{1/2} \qquad (6.3)$$

where R is universal gas constant, and

$$K_o = 3.6 \times 10^3 \exp\ (-31\ 090/T)^{1/2} \qquad (atm)^{1/2}$$

Substituting these rate constants in Eqn 6.2, the NOx production-rate equation (in ppm/s) becomes:

$$\frac{d[NO]}{dt} = 1.575 \times 10^{22}\ T^{-1/2} \exp\ (-69460/T)\ [O_2]^{1/2}\ [N_2] \qquad (6.4)$$

The application of this equation requires values of all the variables in the RHS as they exist within the NO reaction zone. Since the rate of this reaction is slower than the main combustion reactions (assumption b above), the values of temperature and concentrations of O_2 and N_2 can be taken to be the theoretical values calculated for complete combustion. Using these values, however, led to either overpredictions of NO_x rate when adiabatic flame temperature is considered or underpredictons when heat transfer is taken into account.

If, on the other hand, measured time-averaged temperatures and concentrations are used instead of the theoretical values, it is found that NO was underpredicted, sometimes by two orders of magnitude (Sadakata and Beer (1976)). In the present work the predicted NO values were one order of magnitude lower than those measured when time-averaged temperature and concentrations were used.

The explanation for this lies in the existence of fluctuations of concentrations within the NO reaction zone, leading to temperature fluctuations.

The earlier attempts to measure these fluctuations were limited by the speed of response of thermocouples. Generally this is too slow to follow the temperature fluctuations beyond 1 kHz, (Sadakata and Beer (1976)). Recent measurements using CARS technique give a much better indication of the range of the temperature fluctuations, for example LaRue et al (1984) measured a 500 K peak to peak range.

Since the NO reactions take place "immediately" after the main reactions, both temperature and concentrations fluctuations have a considerable influence on the NO formation rate.

It is suggested by many investigators that the temperature in the NO reaction zone is the stoichiometric adiabatic flame temperature (Takagi

et al (1976) and Toof (1986)). Vranos (1974) assumed that the thermal NO reactions are not faster than the mixing rates so most thermal NO is formed at or near ϕ =1.0. This assumption follows from the fact that stoichiometric mixtures have the highest probability of reaction.

When using finite difference solutions of the flow and combustion equations, eg, PHOENICS, the effect of these fluctuations is taken into consideration through the solution of an extra differential equation for the concentration fluctuations, (Elghobashi and Pun (1974)). For the present work, based on a well-stirred reactor model, a stochastic approach was adopted to estimate the fluctuating components of concentration about the mean value.

By assuming the reaction zone to be one well-stirred reactor and using Eqn 6.4, the following analysis is carried out to account for the effect of concentration fluctuations. The model calculation procedure is also illustrated by the flowchart shown in Fig 6.1.

On the microscale of mixing, it is assumed that at any location within the well-stirred reactor, the fuel/air mixture will have a random distribution of parcels with values of equivalence ratio (ϕ) which have a Gaussian distribution about the mean value $\bar{\phi}$. This assumption agrees with experimental measurements in jet flows as reviewed by Chatwin and Sullivan (1990). The spread of this distribution is dependant upon the value of the standard deviation σ. The value of σ is related to the mixedness of the mixture, S_o (where S_o = 1 corresponds to perfect mixing) by the relation (Appleton and Heywood (1972) and Fletcher (1973)):

$$\sigma = (1-S_o)\ \bar{\phi} \qquad (6.5)$$

The value of S_o for a particular system depends on the flow

configuration and mixing as dictated by the fuel injection mode (see for example Backer (1974)).

The choice of S_o for the present work was based on the experimental measurements, as will be described in Sec 6.3.

Introducing Z as a non-dimensional parameter of fluctuation :

$$Z = (\phi - \bar{\phi}\ )/\ \sigma \tag{6.6}$$

The probability density function (p.d.f) of the distribution function of ϕ is written as:

$$f(\phi)= \frac{1}{\sqrt{2\pi}} \exp(- \frac{Z^2}{2}\ ) \tag{6.7}$$

Integrating the area under the above distribution function, leads to the cumulative density function (C.D.F) of ϕ;

$$F(\phi)= \int_{-\infty}^{\phi} \frac{1}{\sqrt{2\pi}} \exp\ (- \frac{Z^2}{2}\ )\ \ dZ \qquad\qquad -\infty < \phi < \infty \tag{6.8}$$

Fig 6.2.a shows the p.d.f and C.D.F for standard Gaussian distribution. The value of $F(\phi)$ is usually between 0 and 1. A stochastic process (Kenbar (1988)) has been implemented to produce the variable Z from Eqn 6.6 using randomly generated values (between 0 and 1) of $F(\phi)$ given by an appropriate random number generator (NAG library subroutine G05CCF). From Eqn 6.8 above and at known values of $\bar{\phi}$ and σ, the stochastic value of ϕ has been predicted. This process gives the Gaussian distribution of ϕ about $\bar{\phi}$ as shown in Fig 6.2.b.

Of the different fluid parcels within the reaction zone, those with ϕ close to unity (ie stoichiometric) have the maximum probability of combustion and thus react first. The products of this reaction will be at the adiabatic stoichiometric flame temperature. The NO reaction will

take place effectively at this flame temperature. The required oxygen [O2] is assumed to come from the excess air of the unburnt lean parcels with ϕ <1. The calculation of [O2] is described in details below:

(a)- Calculate oxygen concentration ($[O_2]_R$) required for the main combustion reaction assuming a global one-step reaction given by the stoichiometric equation:

$$\bar{\phi}CxHy + (x + \frac{y}{4})(O_2 + 3.76\ N_2) \longrightarrow \xi\bar{\phi}xCO_2 + \xi\bar{\phi}\frac{y}{2}H_2O + (1-\xi)\bar{\phi}CxHy + (1-\xi\bar{\phi})(x+\frac{y}{4})O_2 + 3.76(x+\frac{y}{4})N_2 \qquad (6.9)$$

where ξ is the degree of combustion taken as 1.0,

$$[O_2]_R = \frac{2.0}{(\bar{\phi} + 2.0 + 2.0 \times 3.76)}$$

(b)- From the distribution of parcels generated above, the fraction of parcels with excess oxygen, ie ϕ < 0.99 was calculated.

(c)- calculate the average equivalence ratio of the lean fraction ($\bar{\phi}_L$).

(d)- Calculate excess oxygen ([O2]) available for NOx reaction after the lean pockets of mixture have also reacted at equivalence ratio ($\bar{\phi}_L$):

$$[O_2] = [O_2]_R\ (1- \bar{\phi}_L)$$

Given the values of [O2], [N2] (calculated from Eqn 6.9) and the adiabatic flame temperature, the rate of NO formation was calculated from Eqn 6.4 for the fraction of pockets reacting at near stoichiometric ϕ.

Finally, to calculate NO concentration, a mean value of residence time in the reaction zone was calculated from the length of the zone and the average flow velocity in this zone, both deduced from experimental measurements.

6.2.2 Prompt NOx modelling

To date, detailed models of prompt NOx are not available, because the amounts of prompt NOx are small compared to other sources of NOx, and because it seems to accrue in very rich flames as detailed in section 2.3.1(ii). A rate equation was suggested by Fenimore (1970) as given below:

$$[NO]_{prompt} = f(\phi)\ p^{1/2}\ [NO]_{eq} \qquad (6.10)$$

$f(\phi)$ is an empirical function of ϕ, given for ethylene-air combustion, as:

$$f(\phi) = 1.190 \times 10^{-6} \exp(9.287\ \phi)$$

This function was found by taking the ratio of experimental NO mole fraction which could not be accounted for by Zeldovich kinetics to equilibrium NO mole fraction for ethylene. The parameter p is the pressure in atmospheres and $[NO]_{eq}$ is the equilibrium concentration of NO corresponding to the adiabatic flame temperature.

Another equation, suggested by de Soete (1974) and used by Hand et al (1989), is given below:

$$\left(\frac{d[NO]}{dt}\right)_{prompt} = K_{pr}\ [O_2]^a\ [N_2]\ [fuel]\ \exp\left(\frac{E_a}{RT}\right) \qquad (6.11)$$

For ethane flames the values of $1.2 \times 10^7 (RT/P)^2$, 1.0 and 6000 cal/mole are recommended for (K_{pr}), (a) and (E_a) respectively. The residence time for prompt NOx formation is very small (ie<10 ms) (Bowman (1975)). In the present analysis, both equations given above were used to estimate prompt NOx. The results indicate that the contribution of this

mechanism to NOx formation is very small, less than 1.0 ppm compared to 25 to 40 ppm for the thermal NO. The prompt NOx formation has therefore been ignored.

6.3 MODEL RESULTS

The model described above requires as input the values of mixedness of fuel/air jets (S_o) and the mean residence time (t) within the reaction zone. The experimental study of NOx formation described in Chapter 4 has shown that these two parameters are affected more by fuel injection mode than by swirl. To test the present model, an estimate of the average value of standard deviation (σ) for each fuel injection mode was obtained from the experimental measurements of the temperature. The rate of collection of temperature measurements was 30 Hz. Thus, for 200 readings taken at each traverse position, the standard deviation was calculated for each fuel injection mode. The corresponding average values of S_o, calculated from Eqn 6.5, were 0.65, 0.7 and 0.8 for central axial, central radial and peripheral fuel injection modes respectively.

The model was applied to predict the effect of fuel/air ratio (equivalence ratio) on the overall NOx formation in the furnace for each type of fuel injection. The results are compared with the experimental measurements in the stack. The effect of swirl in all fuel injection modes on fluctuations was small. Thus the model predicts only small changes in stack NOx when swirl is changed. This prediction is confirmed by experiments. Comparison between the model predictions and experimental measurements, are given in Figs 6.3-6.5 for central axial, central radial and peripheral fuel injection modes respectively. For all cases, the agreement between the model results and measurements is

considered good. However, for the peripheral fuel injection mode, the predicted profile is slightly shifted to one side. This shift could be explained by two reasons. The first is that, for simplicity, the value of $\overline{\phi}$ in Eqn 6.5 was taken to be the input value rather than the actual mean value in the reaction zone. It is expected that during the air/fuel jets progress to the reaction zone, the value of the effective equivalence ratio will differ from the burner input value due to the dilution with flows circulating from the CRZ and the PRZ. This effect seems to be significant in the case of peripheral fuel injection due to the fact that the mixing in this system is higher than in the other fuel injection modes, as discussed in Chapter 5. The second reason is that the estimate of S_o was based on experimental measurements taken at at fixed equivalence ratio (ϕ = 0.95), and used for all value of equivalence ratios in the prediction. It is expected however that as ϕ decreases below the stoichiometric value, S_o should increase and when ϕ increases above the stoichiometric value, S_o should decrease. These changes in S_o will effect the value of σ (Eqn 6.5) and thus the predicted NOx profile. It might be appropriate for further work to be carried out to quantify these two factors.

Considering the simplicity of the model presented in this stage, it could be said that the present model is capable of giving a good prediction of the maximum value of NOx for different types of fuel injection modes. It also give the correct trend of NOx at the fuel lean and fuel rich conditions observed in the measurements. These results are valuable for practical engineering purposes.

This study has also highlighted the importance of accounting for the concentration fluctuation of species in the NOx predictions process.

CHAPTER 7

PREDICTIONS OF AERODYNAMIC AND COMBUSTION PATTERNS USING CFD CODES

7.1 INTRODUCTION

This chapter reports an assessment of the ability of a computational fluid dynamics (CFD) code to model the combustion aerodynamics of swirling flames. The extent to which such codes can be relied upon will depend on the extent to which they have been validated against practical combustion systems. The peripheral injection mode applied to a natural gas swirling flame, Fig 7.1, (Beltagui and Maccallum (1988)) is a novel test case and therefore is considered in this study.

The predictions were made using the PHOENICS code (Ludwig et al (1989)) with turbulence and combustion represented by the standard (k-ε) model and the 'eddy break-up' model respectively. The resulting predicted aerodynamic and combustion patterns are compared with the measured patterns.

Predictions were also made for the same system but with the fuel injected axially at the centre of the burner, Fig 7.2. The aim was to explore the ability of PHOENICS to predict the main changes caused by switching from the traditional central fuel injection to the peripheral injection considered in this study.

7.2 EQUATIONS SOLVED

The predictions have been made by solving the finite-difference formulations of the governing equations for the conservation of mass and three components of momentum. Turbulence is modelled by solving two differential equations for the turbulence kinetic energy and its dissipation rate (standard k-ε model). The simple chemically-reacting

scheme (SCRS) was used for the combustion representation. This scheme assumes that:

$$1\text{kg fu} + s\text{ kg Ox} \longrightarrow (1+s)\text{ kg Pr} + H_{fu} \tag{7.1}$$

$$m_{fu} + m_{ox} + m_{pr} = 1 \tag{7.2}$$

$$h = C_p T + H_{fu}\, m_{fu} + V^2/2 \tag{7.3}$$

where s is stoichiometric air/fuel ratio, m_{fu}, m_{ox} and m_{pr} are the mass fraction of fuel oxidant and product respectively, h is stagnation enthalpy, T is gas temperature (K), C_p is temperature dependant specific heat at constant pressure, H_{fu} is the net heat of reaction of fuel and V is the total velocity. This scheme requires the solution of differential equations for enthalpy (h), fuel mass fraction (m_{fu}) and mixture fraction (f).

All the above equations can be written in the general form for 3-D cylindrical polar coordinates (Gupta and Lilley (1985)):

$$\frac{\partial}{\partial t}(\rho\varphi) + \frac{1}{r}\left[\frac{\partial}{\partial x}(r\rho u\varphi) + \frac{\partial}{\partial r}(r\rho v\varphi) + \frac{\partial}{\partial \theta}(\rho w\varphi)\right]$$

$$= \frac{1}{r}\left[\frac{\partial}{\partial x}\left(r\Gamma_\varphi \frac{\partial \varphi}{\partial x}\right) + \frac{\partial}{\partial r}\left(r\Gamma_\varphi \frac{\partial \varphi}{\partial r}\right) + \frac{\partial}{\partial \theta}\left(\Gamma_\varphi \frac{1}{r}\frac{\partial \varphi}{\partial \theta}\right)\right] + S_\varphi \tag{7.4}$$

where φ stands for any dependent variable, and ρ, u, v, w, r are gas density, axial velocity component, radial velocity component, tangential velocity component and radius of the furnace respectively. The terms Γ_ϕ and S_ϕ are the turbulence exchange coefficient and source term respectively, their values for each variable being solved are given in Table 7.1 below.

For the axisymmetric flow considered in this study, the term $\partial/\partial\theta$ is zero.

Table 7.1

Governing equations-swirling axisymmetric form

φ	Γ_φ	S_φ
1	0	0
u	μ	$-\frac{\partial p}{\partial x}+\frac{\partial}{\partial x}\left(\mu\frac{\partial u}{\partial x}\right)+\frac{1}{r}\frac{\partial}{\partial r}\left(r\mu\frac{\partial v}{\partial x}\right)$
v	μ	$-\frac{\partial p}{\partial r}+\frac{\partial}{\partial x}\left(\mu\frac{\partial u}{\partial r}\right)+\frac{1}{r}\frac{\partial}{\partial r}\left(r\mu\frac{\partial v}{\partial r}\right)-2\mu\frac{v}{r}+\rho\frac{w^2}{r}$
w	μ	$-\frac{w}{r^2}\frac{\partial}{\partial r}(r\mu)-\rho\frac{vw}{r}$
h	μ/σ_h	0
m_{fu}	μ/σ_{fu}	R_{fu}
f	μ/σ_f	0
k	μ/σ_k	$G_k-\rho\varepsilon$
ε	μ/σ_ε	$C_1\varepsilon G_k/k-C_2\rho\varepsilon^2/k$

Where:

$\mu=\mu_{lam}+\mu_{turb}$ (Effective viscosity)

$\mu_{turb}=C_\mu\rho k^2/\varepsilon$ (Turbulent viscosity)

$$G_k=\mu\left[2\left\{\left(\frac{\partial u}{\partial x}\right)^2+\left(\frac{\partial v}{\partial r}\right)^2+\left(\frac{v}{r}\right)^2\right\}+\left(\frac{\partial u}{\partial r}+\frac{\partial v}{\partial x}\right)^2+\left(r\frac{\partial}{\partial r}\left(\frac{w}{r}\right)^2\right)+\left(\frac{\partial w}{\partial x}\right)^2\right]$$

$\sigma_h=0.7,\ \sigma_{fu}=0.7,\ \sigma_f=0.7,\ \sigma_k=1.0,\ \sigma_\varepsilon=1.3$ (Prandtle-Schmidt numbers)

$C_1=1.44,\ C_2=1.92,\ C_\mu=0.09$ (Turbulence model constants)

The representation of the reaction rate of fuel (R_{fu}) is discussed in the next section.

Given the values of the dependent variables p, u, v, w, k, ε, m_{fu}, f

and h obtained from the solution of the above equations, additional algebraic equations are solved to deduce other properties at any point in the field:

$$m_{ox} = (m_{fu} - f)\ s$$

The mass fraction m_{pr} is obtained from equation (7.2), and T from equation (7.3). Also

$$\rho = \frac{p\ M}{R\ T}$$

where R is the universal gas constant and M is the mean mixture molecular weight.

7.3 REACTION RATE REPRESENTATION

In turbulent reacting flows, the modelling of the rate of reaction, and consequently the heat release rate, is essential to the evaluation of the local gas temperature and density, the latter being a major factor in the momentum and mass conservation equations.

In the present non-premixed system, the flame is considered as diffusion controlled. Although the fast reaction, or 'mixed-is-burned', model (Kent and Bilger (1976)) is sometimes used to model such combustion systems, it tends to overpredict the combustion rate in forced draught systems. In the present work, therefore the 'eddy break-up' model of Spalding (1970) and Magnussen and Hjertager (1976) has been adopted. This model assumes that the reactants are homogeneously mixed in the finite-scale dissipative eddies of the turbulence. The chemical reaction is represented by a one-step reaction between the fuel and oxidant. The rate of the reaction is governed by the concentration of the limiting reactant:

$$R_{fu} = A\,\rho\,\frac{\varepsilon}{k}\;\text{Min}\left[\,m_{fu},\; m_{ox}/s\,\right] \qquad (7.5)$$

Where A is the 'eddy break-up' constant. The value of A used in the present work will be discussed in Section 7.7.

7.4 EXPERIMENTAL DATA

The experimental measurements had been taken by Beltagui and Maccallum (1988) in a refractory lined cylindrical furnace of 225 mm inside diameter and 0.9 m long. The air was introduced through a central concentric vane swirler of 93 mm inside diameter. The fuel- natural gas- was injected through an annular slit of 2 mm width around the periphery of the air swirler, see Fig 7.1. The experimental data were available for the following input variables;

(a) Swirler vane angle- θ- 0°, 15°, 22° and 30°, giving burner swirl number- S_d- (based on burner diameter), of 0.0, 0.089, 0.138 and 0.192.

(b) Inlet air velocities of 10.6 and 15.0 m/s, corresponding to Reynolds Number, based on swirler exit condition, of $6.3\text{x}10^4$ and $9.0\text{x}10^4$.

(c) Overall fuel equivalence ratio of 0.53 and 0.38. The data set consisted of normalised profiles of the three components of the time-mean velocity, static pressure, temperature, and concentrations of CO_2, O_2 and CO. These profiles were measured across the furnace diameter at seven planes along the furnace. Generally the profiles demonstrated good symmetry, which is vital for the meaningful comparison with axisymmetric program predictions.

7.5 BOUNDARY CONDITIONS

The inlet to the furnace is the exit plane of the burner, and at this plane the axial velocity component of the air was assumed uniform in the non-swirled case and to increase linearly with the radius in the swirl flow case. These assumptions were based on the experimental measurements by Beltagui and Maccallum (1988). The tangential component was assumed to follow the same profile and equal to the product of tan θ and the axial component. The radial velocity was taken always to be zero. The corresponding k and ε values have been calculated as follows;

$$k = C_k \left(u^2 + v^2 + w^2 \right) \tag{7.6}$$

$$\varepsilon = C_\varepsilon \, k^{3/2} / \, 0.09 \, l \tag{7.7}$$

where $C_k = 0.0323$, $C_\varepsilon = 0.1643$ and l is the characteristic dimension (width of jet at entry) for the flow stream (air or fuel). The values of the above constants have been deduced from experimental measurements in a similar flow systems (Nejad et al (1989)). Uniform inlet profiles were assumed for pressure, enthalpy and species concentration.

The flow boundary conditions at the solid walls have been described by the log-law and specified to be adiabatic.

7.6 COMPUTATIONAL DETAILS

The numerical solution of the differential equations for cylindrical polar coordinates was performed using the PHOENICS code. The furnace geometry was represented by an axisymmetric non-uniform grid of 41 axial by 45 radial nodes. Near the burner, particularly the fuel exit, the grid spacing in the radial direction was reduced to 0.5 mm.

The Upwind differencing scheme was used, with under-relaxation parameters for all the variables. About 300 to 500 sweeps were

required to obtain a satisfactorily converged solution with normalised mass residuals of less than 10^{-4}. A typical calculation of 400 sweeps required about 2.8 hours of CPU time on a VAX-785 computer.

7.7 RESULTS

A representative selection of the predictions is presented in Figs 7.3-7.9, together with the corresponding experimental measurements, covering the results for the 0° and 30° swirlers. These are presented in the form of normalised profiles of the three components of the time-mean velocity, static pressure, temperature, and concentrations of oxidant and product (predicted) or CO_2 (measured).

An exploratory trial was carried out to test the "mixed-is-burned" combustion model predictions. As expected, this model produced a combustion pattern corresponding to a reaction rate much faster than the experimentally measured pattern.

As explained in Section 7.3, the 'eddy break-up' model for the combustion reaction was next examined as an alternative. Tests were carried out to select the best value for the constant A, Eqn. (7.5). The value of A = 2.0 was found to lead to the best representation of the combustion patterns.

7.7.1 Axial velocity profiles

Predicted and measured axial velocity profiles are shown in Figs 7.3(a) and 7.3(b) for the 0° and 30° swirlers respectively. The general flow pattern is well predicted for both these cases. Detailed inspection of the profiles leads to the following comments:

1. The effect of swirl in modifying the flow pattern is predicted through the more rapid jet expansion and the faster decay of the peak velocities and the radial gradients of the axial velocity. For

example the jet wall-impingement point moved nearer to the burner as swirl is introduced. Also a uniform velocity profile was attained at a shorter axial distance. These effects had also been observed experimentally.

2. The predicted jet expansion is faster than that measured. This applies to the results both without and with swirl.
3. The predicted decay of the radial gradients of velocity is more rapid than measured, leading to the prediction that more uniform velocity profiles occur earlier than measured.
4. For the non-swirled flow case, Fig 7.3(a), better agreement between predictions and measurements is obtained nearer the burner than further downstream. By contrast, in the case using the 30° swirler the predictions are better further downstream from the burner.
5. The prediction of lower radial gradients of the axial velocity near the burner for the 30° swirler leads to a predicted centreline velocity which is higher than measured. This also leads to a failure to predict flow reversal at the centreline.

7.7.2 Tangential velocity profiles

Figure 7.4 illustrates the radial profiles of the tangential velocity component in the furnace chamber for the 30° swirler. Both the predicted and measured profiles approximate to Rankine-vortex flow with solid body rotation in the central region and peak tangential velocities in the vicinity of the axial velocity maxima.

Although the experimental profiles exhibit some asymmetry, the agreement between the predictions and the averaged experimental data is considered to be good.

7.7.3 Radial velocity profiles

Comparisons of predicted and measured radial velocity profiles are shown in Figs 7.5(a) and 7.5(b) without and with swirl respectively. In both cases, the predicted velocity profiles in the near-burner zone follow the shape of the experimentally measured profiles but the magnitudes of the predicted values are much lower than those measured. As the flow progresses downstream, it is noted that the predicted radial velocities decay much faster than the measured velocities. This is consistent with the predicted decay of the axial velocities in this region. Increasing swirl has little effect on the predicted radial velocity values as shown in Fig 7.5(b), although the measured values apparently increase.

As previously reported (Beltagui et al (1988-a) and Beltagui et al, (1988-b)), while there is reasonable confidence in the probe measurements for the axial and tangential velocity components it is believed that the probe measurements exaggerate the radial velocity values, particularly in the regions of peak radial velocities. Consequently, excessive reliance should not be placed on the measured radial velocity profiles.

7.7.4 Static pressure distribution

Comparison of the predicted and measured static pressure distributions are illustrated in Fig 7.6. In the unswirled case, Fig 7.6(a), the predicted static pressure differs only very slightly from atmospheric. The measured values however show some considerable differences below and above the atmospheric value. The fuel jet injection scheme may be partly responsible for this. Also there are indications of asymmetry of the jet. This is consistent with the noticeable asymmetry of the axial velocity profiles, Fig 7.3(a).

For the case using the 30° swirler (Fig 7.6(b)), there is generally good agreement between prediction and measurement, with sub-atmospheric pressure near the centreline, rising to near, or slightly above, atmospheric close to the walls. This pattern is typical of static pressure distributions associated with confined swirling flows.

7.7.5 Temperature distributions

Predicted and measured temperature profiles are shown in Fig 7.7. From these results the following comments are made:

1. For both unswirled and swirled flows the temperature profiles near the burner are well predicted with maximum temperatures at the outer recirculation zone and low temperatures in the unburned central flow. Combustion is initiated at the shear layer between the air and fuel jets.
2. The effect of swirl on the predicted temperature profiles is noted through reduced radial temperature gradients. However, the predicted effect of swirl on the temperature profiles is somewhat less than that observed.
3. For the non-swirled flow case, as the flow progresses downstream the agreement between the predicted and measured profiles remains good.
4. For the 30° swirler flow, as one moves downstream a discrepancy between the predicted and measured profiles becomes apparent. Whereas the measured profiles become uniform at about 3 furnace diameters downstream, the predicted profiles still show a marked non-uniformity, with a variation by a factor of about 3 in the temperature rise. Thus generally the effect of radial mixing between the flow streams is not yet adequately predicted.

7.7.6 Species concentrations:

Since the program solves the equations for a one-step global reaction, the results give concentrations of fuel, oxidant and product. The predicted oxidant profiles are compared with the measured O_2 concentrations in Fig 7.8. The predicted concentrations for the "product" can be compared with the measured CO_2 concentrations for the locations where combustion is complete. This comparison is shown in Fig 7.9. For complete combustion of the natural gas used (about 95% - by volume- methane), the CO_2 concentration in the dry product is 11.8% by volume. This comparison should give sufficient indication of the agreement, or otherwise, between the predictions and the measurements throughout most of the flow field. The comparison is not valid however in locations of partial combustion.

The predicted oxidant and product concentrations are consistent with each other, and with the predicted temperature profiles. Thus the agreement between the predicted and observed species concentration is the same as the agreement for the temperature profile. The comments made in section 7.7.5 concerning the temperature profiles therefore apply also to the concentration profiles.

7.8 COMPARISON OF PERIPHERAL FUEL-INJECTION WITH CENTRAL AXIAL FUEL-INJECTION

The prediction procedure was also set for the configuration where the fuel is injected in the centre of the air jet in order to asses the predicted degree of change in the results between the two fuel injection systems. Firstly though, these predicted results were compared with observed combustion patterns inferred from temperature measurements in the same furnace, with a central fuel injector. This test proved satisfactory. The predictions for the two fuel injection

systems were then compared.

A sample of the results for the predicted temperature is given in Fig 7.10, where a marked effect on the temperature field is clearly seen. In the peripheral fuel-injection system the high temperatures are in the outer recirculation zone and in the forward flow near the walls after the jet impingement point. On the other hand, for the central fuel-injection system, the high temperatures are near the centre of the flow. This prediction is in excellent agreement with the observed effect.

7.9. DISCUSSION OF RESULTS

The predictions presented above were all made with the program using the facilities available within the Code with no adjustments to its sub-models. The main features of the flow and combustion patterns are well predicted as demonstrated in the comparisons with the measured profiles. However, detailed comparisons indicate some less satisfactory agreement on a number of points.

Considering the flow pattern, the radial gradients of velocity components are underpredicted, particularly for the swirling flow. This feature of underpredicting the velocity gradients is a typical characteristic of the standard k-ε turbulence model and has been reported by other investigators (eg Mahmud et al (1987), Kobayashi and Yoda (1987), Negad et al (1989), Jones and Pascau (1989)). The underprediction is attributed to the body forces which arise from the effects of curvature, recirculation, swirl and buoyancy. These forces are known (Sloan et al (1986) and Leschziner (1989)) to interact selectively with different normal and shear stresses, making the use of the isotropic turbulence assumption inappropriate.

The present investigation is of a special flow configuration where the

body forces play an important role. In this furnace, using the peripheral fuel-injection scheme, combustion starts at the outer shear layer of the air jet. The centrifugal forces created in this system due to the density gradients are expected to increase further the effect of body forces on the turbulent flow (Leschziner (1989) and Beltagui and Maccallum (1988)).

Trials to overcome this deficiency through the use of a modified anisotropic form of the turbulent eddy viscosity based on the k-ε model have been presented for some simpler flow situations (eg Kobayashi (1987)). However, these models are not yet of a general form suitable for use with general codes.

Rigorous models solving the complete Reynolds stress equations should have the degree of generality required. However, these models have not been available in general CFD codes. Another reason for not using these is the expensive computational time penalty involved.

Considering the combustion patterns, as represented by the temperature and species concentration fields, the predictions are in good agreement for the non-swirled flow case, but less satisfactory agreement is obtained for the swirling flow. There are two reasons for these deficiencies:

1. The weakness in the turbulence modelling, as explained above, led to lower mixing rates in the radial direction as indicated by the lower degree of uniformity in the temperature and species concentration profiles, compared to the measured profiles. The underprediction of mixing is more apparent in the swirling flow case.
2. The simplified combustion model, which is also governed by the turbulence properties through the "eddy break-up" model, is probably too simple. The present formulation did not include the effect of the hot product concentration, which has proved

significant in another application (Beltagui et al (1991)).

CHAPTER 8

GENERAL CONCLUSIONS AND RECOMMENDATIONS

From the combined experimental and theoretical work presented in the previous chapters, the flowing general conclusions can be drawn:

(A)- Experimental measurements

1- Flame stability: With the use of central radial fuel injection, it was possible to achieve stable flame without swirl, due to the aerodynamic blockage created by the radial fuel jets.

For the central axial injection and the basic peripheral fuel injection (first scheme), a minimum swirl (S=0.8) was required to achieve a CRZ stabilised flame. In the second Scheme of the peripheral fuel injection, a CRZ was created by introducing some of the combustion air radially outward through a central gun, thus a stable flame could be established without swirl.

The longest flame was observed when central axial fuel injection was used. This flame was not uniform and has a yellow appearance. With the central radial and peripheral fuel injection modes, the flame was shortened in both cases by about the same amount and the flame became blue.

2- Flow patterns: The flow patterns presented for the central radial and peripheral fuel injection modes were represented by distributions of the three time-averaged velocity components and the static pressure. These measurements have given clear pictures of flow expansion in the radial and axial directions, also of the flow boundaries and thus the central and outer reverse flow zones (CRZ

and PRZ). The effect of swirl on the size of the CRZ was found to be more pronounced when peripheral fuel injection was used due to the increased effect of centrifugal forces in this system.

It is noted that the jet expansion in the radial and axial directions was dictated by the mode of fuel injection. The combustion with the peripheral injection system starts at the outer boundary of the swirled air flow. This has resulted in a higher radial jet expansion and thus earlier jet impingement with the furnace walls. However this has also led to a much lower jet expansion in the axial direction when compared with the central radial fuel injection mode.

3- Momentum fluxes and swirl number: The integrations of time-averaged values of velocities were performed to calculate the axial fluxes of axial and tangential momenta. The variations in the normalised fluxes along the furnace were caused by the jet area expansion, volume expansions due to combustion and jet impingement with the furnace walls. These variations were dependent on the mode of fuel injection. The effect of swirl on these fluxes was found to be more significant in the case of the peripheral fuel injection.

Swirl number calculated from these momentum fluxes and based on the furnace diameter was found to depend on the mode of fuel injection. The analysis confirms the validity of this swirl number in characterising the flow patterns of swirling flows.

4- Combustion patterns: An assessment of the relative combustion patterns has been obtained from the measurements of temperature and species concentrations for the three modes of fuel injection. The following points are made:

a- A good flame symmetry was obtained with the central radial and peripheral fuel injection modes. High degree of flame asymmetry

was observed with the central axial fuel injection.

b- The effect of swirl in all fuel injection modes is to increase the mixing and thus combustion intensity.

c- The measured temperature and the integrated fluxes of sensible enthalpy have shown that the highest heat transfer rates to the furnace walls occur with the peripheral fuel injection. This is the result of starting the combustion at the outer boundary of the swirled air flow.

d- From the measurements of temperature and CO, CO_2 and O_2 concentrations, it was found that the highest rates of mixing and thus combustion efficiency were achieved with peripheral fuel injection, due to the utilisation of the full benefits of shear layer and centrifugal mixing. The radial fuel injection also gave better mixing and combustion efficiency when compared with the central axial fuel injection.

e- Measurements of the local NO_x concentrations have shown that, in all fuel injection systems, NO_x formation has a strong dependence on the flame temperature, thus confirming the dominance of its formation by the thermal mechanism. In addition, the NO_x formation rate was dependent on the degree of mixing and the residence time within the reaction zone.The effect of swirl on the local NO_x values was significant. However, its effect on the overall NO_x concentrations is considered to be minor.

5- Pollutant formation: From the measurements of CO and NO_x in the stack it could be concluded that:

a- The CO measurements demonstrated that with the use of peripheral and central radial fuel injection modes, complete combustion could be guaranteed with 5% excess air. When central axial fuel injection is used, at least 10% excess air is required to achieve

complete combustion.

b- The lowest overall NOx concentrations were measured with the central axial fuel injection. This was the result of the lower area-averaged temperature levels caused by the slower combustion in this system. The peripheral and central radial fuel injection systems gave virtually the same NOx values at the normal firing rate (ie 5% excess air).

At fuel lean conditions, the peripheral fuel injection was the only method of fuel injection giving reduction in NOx formation. The other two systems gave some increase in NOx formation. At fuel rich conditions, all fuel injection modes gave sharp decrease in NOx formation. The peripheral fuel injection was therefore the only system to offer NOx reduction by the three methods- lean combustion, fuel staging and air staging. With the central radial and central axial injection modes, only air staging is useful in reducing NOx formation.

(B)- Modelling of NOx formation

By adopting a simplified model based on the well-stirred reactor along with accounting for the concentration fluctuations by a suitable stochastic technique, thermal NOx formation has been predicted satisfactorily. The model was able to predict with reasonable accuracy the maximum values of NOx for each type of fuel injection. The model also predicted the NOx trends at fuel lean and fuel rich conditions. This model has also demonstrated the importance of considering the fluctuations in concentrations when predicting NOx formation.

If the interest is only in obtaining NOx formation, the model presented here is sufficient for practical engineering purposes. However, when aerodynamic and combustion patterns are also required, it is

recommended that the concept provided by this model could be incorporated within a CFD code, in which the NOx equation (6.4) could be solved as a source term for a differential equation of the mass fraction of NOx. The effect of fluctuations is taken into account by the solution of another differential equation for the concentration fluctuation.

(C)- Modelling of swirling flames

The ability of a CFD code to model swirling flames has been assessed by a novel test case. The flow and combustion patterns of the peripheral fuel injection (Beltagui and Maccallum (1988)) have been predicted using PHOENICS code.

The general agreement between predicted and measured patterns is encouraging considering that the procedure used the standard k-ε turbulence model, and a simple combustion model ("eddy break-up"). The main changes in the combustion patterns caused by switching from central to peripheral fuel injection system were qualitatively well predicted.

For the peripheral fuel injection system, with a non-swirled air jet, the predictions are generally good. However the enhancement of mixing, caused by the combined effect of swirl and density gradients, was not adequately predicted. This weakness highlights the importance of modelling the contribution of the body forces to the turbulence exchange coefficients.

It is suggested that the use of anisotropic turbulence modelling is necessary for the prediction of swirling flows.

It is also suggested that including the effect of the hot combustion products concentrations in the combustion model may contribute to some improvements of the results.

(D)- **Suggestions for further work**

1- Similar investigation of a burner with combined central-radial and peripheral fuel injection modes: This burner may give more enhanced flame stability, mixing and hence combustion efficiency. The high rates of mixing should also reduce the fluctuations in the concentrations and the residence time and thus the overall NOx emission.

2- Investigation of NOx formation in an adiabatic furnace: The high temperature levels in such a furnace will make the effect of input parameters (eg swirl and fuel equivalence ratio) on NOx formation more significant than was observed with the water-cooled furnace studied in the present work.

3- LDA measurements: For the central radial and peripheral fuel injection systems presented in this study, measurements of turbulence characteristics, using LDA, may prove to be valuable in aiding the understanding of the structure of turbulence and in modifying theoretical models of turbulence. The study would also provide reliable data for the inlet boundary conditions required for CFD codes.

4- The NOx model presented in this study could be incorporated within a CFD code as described in paragraph (C) above.

5- Validating CFD codes : The experimental data provided for the NEL furnace in this study allow the assessment of present and future CFD codes for modelling the flow and combustion patterns when using different modes of fuel injection.

REFERENCES

- A -

ABASSI H A and FLEMING D K, (1988), " Combustion modifications for control of NOx Emissions from glass melting furnaces", Ceram. Eng. Sci. Proc., vol. 9, No. 3-4, pp. 168-177.

ABBAS A S, LOCKWOOD F C and SLOOJA A P, (1984), "The prediction of combustion and heat transfer performance of a refinery heater", Combustion and Flame, vol. 58, pp. 91-101.

ABDALLA A Y, BRADLEY D and CHIN S B, (1989), "Stratified lean combustion and NO formation", Joint meeting of the British and French Sections of The Combustion Institute, Rouen, pp. 29-32.

AHMAD N T, ANDREWS G E, KOWKABI M and SHARIF S F, (1984), "Centrifugal mixing forces in enclosed swirl flames", 20th Symp. (Int.) on Combustion, pp. 259-267.

AHMAD T, PLEE S L and MYERS J P, (1985), "Computation of nitric oxide and soot emissions from turbulent diffusion flames", J. Eng. Gas Turbine Power, vol. 107, No. 1, pp. 48-53.

ALLEN J D, (1973), "A review of methods of analysis for oxides Of nitrogen", J. Inst. of Fuel, vol. 46, pp. 123-133.

AL-SHAIKHLY A F A, ANDREWS G E and ANIAGOLU C O, (1989), "Jet shear layer turbulent diffusion flames for ultra-low NOx emission", Joint

meeting of the British and French Sections of The Combustion Institute, Rouen, pp. 5-8.

ANDREWS G E, ABDUL AZIZ M M, ABDUL HUSSAIN U S et al (1988), "High intensity burner with low NOx emissions", British Flame Days, Furnace combustion Research and its applications, Imperial college, London.

ANON, (1988), "On the limitation of emission of certain pollutants into the air from large combustion plants" Official Journal of European Communities, No. L 336, pp. 1-13.

ANON, (1989), "Control of NOx emission from large combustion plant", The Chem. Eng., March, pp. 33-40.

AOKI K, SHIBATA M and NAKAYAMA Y, (1986), "Study on the flow with a swirl flow in a cylindrical combustor", 2nd report, Characteristics of turbulence for the swirl number, Bulletin of JSME, vol. 29, pp. 4113-4121.

APPLETON J P and HEYWOOD J B, (1972), "The effects of imperfect fuel-air mixing in a burner on NO formation from nitrogen in the air", 14th Symp. (Int.) on Combustion, pp. 777-786.

ARMFIELD S W and FLETCHER C A J, (1989), "Comparison of the k-ε and algebraic Reynolds stress models for swirling diffuser flow", Int. J. for Numerical Methods in Fluids, vol. 9, pp. 987-1009.

- B -

BAFUWA G G, (1970), "Characteristics of swirling flames issuing from vane swirlers", PhD Thesis, Department of Mechanical Engineering, Glasgow University.

BAFUWA G G and MACCALLUM N R L, (1970), "Turbulent swirling flames issuing from vane swirler", IFRF, 18th Meeting of Aerodynamic Panel, Paris, Sept, Document No. G02/CA/3.

BARNES F H, BROMLY J H, EDWARDS J J and MANDYCZEWSKY R, (1988), "NO_x emissions for radiant gas burners",J. Inst. of Energy, vol. 61, pp. 184-188.

BECKER H A, (1974), "Effects of concentration fluctuations in turbulent diffusion flames", 15th Symp. (Int.) on Combustion, pp. 601-615.

BEER J M and CHIGIER N A, (1972), "Combustion aerodynamics", Applied Science and Publishers, London.

BELTAGUI S A and MACCALLUM N R L, (1976-a), "Aerodynamics of vane-swirled flames in furnaces", J. Inst. of Fuel, vol. 49, pp. 183-193.

BELTAGUI S A and MACCALLUM N R L, (1976-b), "The modelling of vane-swirled flames in furnaces", J. Inst. Fuel, vol. 49, pp. 194-200.

BELTAGUI S A and RALSTON T, (1985), "An isothermal model study of

aerodynamics and mixing in the flow issuing from a variable-swirl burner", HTFS Research Symp., RS 602, NEL/HTFS 63.

BELTAGUI S A, FUGGLE R N and RALSTON T, (1988-a), "Aerodynamic and mixing within the quarl of a variable swirl burner (experimental and theoretical study)", First European Conference on Industrial Furnaces and Boilers (INFUB), Lisbon, Portugal.

BELTAGUI S A, FUGGLE R N and RALSTON T, (1988-b), "An Isothermal study of the aerodynamics of the furnace flow issuing from a variable swirl burner", 1st World conference on Experimental Heat transfer, Fluid Mechanics and Thermodynamics, Dubrovnik, Yugoslavia. Elsevier Pub.

BELTAGUI S A, FUGGLE R N and RALSTON T, (1988-c), "Combustion pattern measurements for swirling flames in the NEL furnace", HTFS Research Symp., RS 756, NEL/HTFS 113.

BELTAGUI S A and MACCALLUM N R L , (1988), "Characteristics of enclosed swirl flames with peripheral fuel injection", J. Inst. of Energy, vol. 61, pp. 3-16.

BELTAGUI S A, FUGGLE R N, KENBAR A M A and RALSTON T, (1989), "Measurements of swirling flames aerodynamics in the NEL furnace", HTFS Research Symp., RS 826, NEL/HTFS 125.

BELTAGUI S A, FUGGLE R N, KENBAR A M A, RALSTON T, MARRIOTT N and STOPFORD P J, (1991), "Modelling a gas-fired furnace flow and combustion using the PCOC code", Parer accepted for presentation at the

Euroteck Direct 91, Birmingham, 2-4 July.

BELTAGUI S A, KENBAR A M A and MACCALLUM N R L, (1991), "Comparison of isothermal and combusting confined swirling flows - peripheral fuel injection", paper submitted to the 2nd World conference on Experimental Heat transfer, Fluid Mechanics and Thermodynamics, to be held in Dubrovnik, Yugoslavia.

BOWMAN C T, (1975), "Kinetics of pollutant formation and destruction in combustion", Prog. Energy and Comb. Sci., vol. 1, pp. 33-45,

BREEN B P, BELL A W, DE VOLO N B, BAGWELL F A and ROSENTHAL K, (1970), "Combustion control for elimination of nitric oxide emissions from fossil-fuel power plants", 13th Symp. (Int.) on Combustion.

BROWN T D, MITCHELL E R, and LEE G K, (1973), "Low NOx combustion: The effect of external flue gas recirculation on emissions from liquid fuel combustion", First European Symp. on Combustion, Sheffield, pp. 487-492.

BURNS A D, CIOFALO M, CLARKE D S et al, (1988), "Progress with the Harwell-Flow 3-D software for the prediction of laminar and turbulent flow, and heat transfer, 1987-1988", Harwell Report AERE-R 13148.

- C -

CARETTO L S, (1976), "Mathematical modelling of pollutant formation", Prog. Energy and Comb. Sci. vol. 1, pp. 47-75.

CHATWIN P C and SULLIVAN A N, (1990), "A simple and unifying physical interpretation of scalar fluctuation measurements from many turbulent shear flows", J. Fluid Mech., vol. 212, pp. 533-556.

CHEDAILLE J and BRAUD Y, (1972), "Measurements in flames", Edward Arnold publishers, London.

CHIGIER N A, (1974-a), "Pressure, velocity and turbulence measurement in flames", Flow, Its Measurements and Control in Science and Industry, vol. 1, R. B. Dowdell, ed., Instrument Society of America, pp. 409-418.

CHIGIER N A, (1974-b), "Velocity measurements in vortex flows", Flow, Its Measurements and Control in Science and Industry, vol. 1, R. B. Dowdell, ed., Instrument Society of America, pp. 399-408.

CLARKE A G and WILLIAMS A, (1985), "Industrial flames, Part 10: Pollutant formation in furnaces", HTFS Design Report DR32, Part 10.

CLAYPOLE T C and SYRED N, (1980), "The effect of swirl burner aerodynamics on NO_x formation", 18th Symp. (Int.) on Combustion, pp. 81-89.

CORREA S M and SHYY W, (1987), "Combustion models and methods for contentious gaseous turbulent combustion", Prog. Energy and Combust. Sci, vol. 13, pp. 249-292.

CRIESTA E D B, (1987), "Prediction of central recirculation zone size for a complete burner-quarl-furnace system", AIAA, 25(3), pp. 457-463.

- D -

DE SOETE G G, (1974), "Overall reaction rates of NO and N2 formation from fuel nitrogen", 15th Symp. (Int.) on Combustion, pp. 1093-1102.

DE SOETE G G, (1989), "N2O analysis techniques : Gas chromatography with EC detection: Sampling techniques", 1st Topic Oriented meeting TOTeM1, IFRF, Amsterdam.

DESTEFANO J T, (1985), "Post combustion NOx control technology for glass furnaces, update", Ceram. Eng. Sci. Proc., vol. 6, No. 3-4, pp. 241-248.

DIXON T F, TRUELOVE J S and WALL T F, (1983), "Aerodynamic studies on swirled coaxial jets from nozzles with divergent quarls", J. of Fluid Engineering, vol. 105, pp. 197-203.

DUGUE J AND WEBER R, (1989), "The effect of combustion on confined swirling flows", IFRF, Doc No. K 70/a/8.

- E -

ELGHOBASHI S E and PUN W M, (1974), "A theoretical and experimental study of turbulent diffusion flames in cylindrical furnaces", 15th Symp. (Int.) on Combustion, pp. 1353-1365.

ENGLEMAN V S, BARTOK W and LONGWELL P J, (1972), "Experimental and theoretical studies of NOx formation in a jet-stirred combustor", 14th Symp. (Int.) on Combustion, pp. 755-765.

- F -

FENIMORE C P (1970), "Formation of nitric oxide in premixed hydrocarbon flames", 13th Symp. (Int) on combustion, pp. 373-380.

FLETCHER R S, (1973), "The prediction of nitric oxide formation in combustion systems", 1st European Symp. on Combustion, Sheffield, pp. 445-450.

FLETCHER R S and HEYWOOD J B, (1971), "A model for nitric oxide emissions from aircraft gas turbine engines", (1971), AIAA Paper No. 71-123.

FOSTER P J, (1974), "Industrial flames, Part 5: Combustion control for minimising pollutant emissions", HTFS Design Report DR32, part 5.

FRICKER N and LEUCKEL W, (1976), "The characteristics of swirl-stabilised natural gas flames, Part 3: The effect of swirl and burner mouth geometry on flame stability", J. Inst. of Fuel, vol. 49, pp. 152-158.

- G -

GODRIDGE A M, (1986), "A study of pollutant production using a one-fifth scale model of a multi-burner furnace", IFRF, 8th Members Conference, Netherlands.

GOSMAN A D, LOCKWOOD F C and SLOOJA A P, (1978), "The prediction of cylindrical furnaces gaseous fueled with premixed and diffusion

burners", 17th Symp. (Int.) on Combustion, pp. 747-760.

GOULDIN F C, (1974), "Role of turbulent fluctuations in NO formations", Combustion Science and Technology, vol. 9, pp. 17-23.

GOULDIN F C, DEPSKY J S and LEE S-L, (1985), "Velocity field characteristics of swirling flow combustor", AIAA Journal, vol. 23, No. 1, pp. 95-102.

GUPTA A K, SYRED N and BEER J M, (1973), "A low-noise burner for swirl-stabilised natural gas flames", J. Inst. of Fuel, vol. 46, pp. 119-123.

GUPTA A K, SYRED N, and BEER J M, (1974), " Fluctuating temperature and pressure effects on the noise output of swirl burners", 15th Symp. (Int.) on Combustion, pp. 1367-1378.

GUPTA A K, BEER J M and SWITHENBANK J, (1976), "Concentric multi-annular swirl burner: Stability limits and emission characteristics", 16th Symp. (Int.) on Combustion, pp. 79-91.

GUPTA A K, LILLEY D G and Syred N, (1984), "Swirl flows", Abacus Press.

GUPTA A K and LILLEY D G, (1985), "Flowfield modeling and diagnostics" Abacus Press, Tunbridge Wells, Kent, England.

- H -

HADVIG S, MADSEN OLE H and JENSEN J, (1988), "Heat transfer and environmental conditions for fibre burner and conventional burners", British Flame Days, Imperial College, London.

HAGIWARA A and BORTZ S, (1986), "Studies on the near field aerodynamics of swirl burners, Flow visualization and hot wire measurements in isothermal swirling flows", IFRF, Doc. No. F259/a/1.

HAHN W A and WENDT J O L, (1980), "NOx formation in flat, laminar, opposed jet methane diffusion flames", 18th Symp. (Int.) on Combustion, pp. 121-131.

HALLET J and GUNTHER R, (1978), "The influence of burner-data on shape and properties of swirling flames", Ger., Chem., Eng. vol 1, pp. 340-346.

HAND G, MISSAGHI M, POURKASHANIAN M and WILLIAMS A, (1989), "Experimental studies and computer modelling of nitrogen oxides in a cylindrical natural gas fired furnace", Proc. 9th Member Conference, IFRF, May, the Netherlands.

HAYHURST A N and VINCE I M, (1980), "Nitric oxide formation from N_2 in flames: The importance of 'prompt' NO", Prog. Energy and Comb. Sci., vol. 6, pp. 35-51.

HEBERLING P V, (1976), "'Prompt NO' measurements at high pressures",

16th Symp. (Int.) on Combustion, pp. 159-168.

HILLEMANNS R, LENZE B and LEUCKEL W, (1986) "Flame stabilization and turbulent exchange in strongly swirling natural gas flames", 21st Symp. (Int.) on Combustion, pp. 1445-1453.

HIRAI T, NAGAI N and TAKADO J, (1987), "Reduction of NOx emissions by staged combustion in a high intensity spray combustor", Int. J. JSME, vol. 30, No. 260, pp. 303-309.

HONNERY D R and KENT J H, (1989), "Furnace flow modelling: Physical and computational", J. Inst. of Energy, pp. 169-177.

HUNTER S C, HALL R E and CARTER W A, (1978), "Evaluation of combustion modifications for emissions reduction on industrial processes", ASME paper No. 78-WA/APC-8.

- J -

JONES W P and PASCAU A, (1989), "Calculation of confined swirling flows with a second moment closure", ASME, J. of Fluids Eng., vol. 111, pp. 248-255.

JONES W P and WHITELAW J H, (1984), "Modelling and measurements in turbulent combustion", 20th Symp. (Int.) on Combustion, pp. 233-249.

- K -

KENBAR A M A, (1988), "Stochastic modelling as a design technique for predicting internal heat gains in buildings", M.Sc. Thesis, Dept. of

Mech. Eng., University of Glasgow.

KENBAR A M A and BELTAGUI S A , (1990), "The effect of burner parameters on NOx formation in the NEL furnace- measurements and modelling", HTFS Research Symp., RS 827, NEL/HTFS 123.

KENT J H and BILGER R W, (1976), "The predictions of turbulent diffusion flame fields and nitric oxide formation", 16th Symp. (Int.) on Combustion, pp. 1643-1656.

KHALIL E E, HUTCHINSON P and WHITELAW J H, (1980), "The calculation of the flow and heat-transfer characteristics of gas-fired furnaces", 18th Symp. (Int.) on Combustion, pp. 1927-1938.

KNILL K J, (1987), "A review of fuel staging in pulverised coal combustion systems", IFRF, Doc. No. G13/a/3.

KOBAYASHI T and YODA M, (1987), "Modified k-ε model for turbulent swirling flow in a straight pipe", JSME, Int. Journal, vol. 30, No. 259, pp. 66-71.

KOTLER V R and IMANKULOV E R, (1986), "The effect of the proportion of primary air on formation of nitrogen oxides when burning Ekibastuz coal", Thermal Eng., vol. 33, No. 1, pp. 12-14.

KRETSCHMER D and ODGERS J, (1973), "Modelling of combustors: The effects of ambient conditions upon performance", ASME Paper No. 73-WA/GT-6.

KUDRYAVTSEV N YU, and VOLKOV E P, (1988), "A mathematical model of the process of formation of nitrogen oxides and determination of their concentrations in the flue gases of steam boilers", Thermal Eng., vol. 35, No. 4, pp. 219-222.

- L -

LaRUE J C, SAMUELSEN G S and SEILER E T, (1984), "Momentum and heat flux in a swirl-stabilized combustor", 20th Symp. (Int.) on Combustion, pp. 277-285

LAWN C J, (Ed.), (1987), "Principles of Combustion Engineering for Boilers", Academic Press.

LEFEBVRE A H, (1974), "Pollution control in continuous combustion engines", 15th Symp. (Int.) on Combustion, pp. 1169-1180.

LESCHZINER M A, (1989), "Modelling turbulent recirculating flows by finite-volume methods - current status and future directions", Int. J. Heat and Fluid Flow, vol. 10, No. 3, pp. 186-202.

LEUCKEL W and FRICKER N, (1976), "The characteristics of swirl-stabilised natural gas flames, Part 1: Different flame types and their relation to flow and mixing patterns", J. Inst. of Fuel, vol. 49, pp.103-12.

LEVY A, (1982), "Unresolved problems in SOx, NOx, soot control in combustion", 19th Symp. "(Int.) on Combustion, pp. 1223-1242.

LEWIS G D, (1981), "Prediction of NOx emissions", ASME Paper No. 81-GT-119.

LILLEY D G, (1977), "Swirl flow in combustion: A review", AIAA Journal, vol. 15, pp. 1063-1078.

LOZOVSKII V A, NOVOSELOV S S, SVETLICHNYI V A et al, (1988), "The role of ozone in oxidising reactions when it interacts with the flue gases from thermal power stations", Thermal Eng., vol. 35, No. 8, pp. 442-443.

LUDWIG J C, QIN H Q and SPALDING D B, (1989), "The PHOENICS Reference Manual", CHAM TR/200, CHAM LTD.

LUKOSHYAVICHYVS V P, TSIRUL'NIKOV L M and SHVENCHYANAS P P, (1986), "The factors influencing the effectiveness of suppressing formation of nitrogen oxides by introducing moisture into the combustion zone", Thermal Eng., vol. 33, No. 7, pp. 358-361..

- M -

MAAS U and WARNATZ J, (1989), "Numerical simulation of ignition processes in two-dimensional geometries", Joint meeting of the British and French Sections of The Combustion Institute, Rouen, pp. 133-137.

MAGNUSSEN B F and HJERTAGER B H, (1976), "On mathematical modelling of turbulent combustion with special emphasis on soot formation and combustion", 16th Symp. (Int.) on Combustion, 719-730.

MAHMUD T, TRUELOVE J S, WALL T F, (1987), "Flow characteristics of swirling coaxial jets from divergent nozzles", ASME, J. of Fluids Eng., vol. 109, pp. 275-282.

MARKOWSKI S J, LOHMANN R P and REILLY R S, (1976), "The vorbix burner-a new approach to gas turbine combustors", ASME J. of Eng. Power, pp. 123-129.

MEIER J G and VOLLERIN B L, (1976), "The design of an integrated burner-boiler system using flue-gas recirculation", 16th Symp. (Int.) on Combustion, pp. 63-76.

MELLOR A M, (1980), "Semi-empirical correlations for gas turbine emissions, ignition, and flame stabilisation", Prog. Energy and Comb. Sci., vol. 6, pp. 347-358.

MELLOR A M and WASHAM R A, (1979), "Characteristic time correlations of pollutant emissions from an annular gas turbine combustor", ASME Paper No. 79-GT-194.

MEYER G and MAUSS F, (1973), "Nitrogen oxides production by a fuel oil burner operating with a small excess air", First European Symp. on Combustion, Sheffield, pp. 475-480.

MILOSAVLJEVIC V D, TAYLOR A M K P and WHITELAW J H, (1990), "The influence of burner geometry and flow rates on the stability and symmetry of swirl-stabilised non-premixed flames", Combustion and

Flame, vol. 80, pp. 196-208.

MIRZAIE H and SYRED N, (1989), "Ultra low NOx combustors using cyclone combustor technology", Joint meeting of the British and French Sections of The Combustion Institute, Rouen, pp. 61-64.

MIZUTANI Y and KATSUKI M, (1976), "Emissions from gas turbine combustors, Part 2, analytical model and numerical analysis", Bulletin of JSME, vol. 19, pp. 1360- 1366.

MONAT J P, HANSON R K and KRUGER C H, (1978), "Shock tube determination of the rate coefficient for reaction $N_2 + O \rightarrow NO + N$",17th Symp. (Int.) on Combustion, pp. 543-552.

MULHOLLAND J A and HALL R E, (1987), "Fuel oil reburning application for NOx control to fire tube package boilers" J. Eng. Gas Turbine Power, vol. 109, pp. 207-214.

MUZIO L J, ARAND J K and TEIXEIRA D P, (1976), "Gas phase decomposition of nitric oxide in combustion products", 16th Symp. (Int.) on Combustion, pp. 199-208.

- N -

NAGANO Y and HISHIDA M, (1987), "Improved form of the k-ε model for wall turbulent shear flows", Transactions of the ASME, vol. 109, pp. 156-159.

NEJAD A S, VANKA S P, FAVALORO S C, SAMIMY M and LANGENFELD C, (1989)

"Application of laser velocimetry for characterisation of confined swirling flow", ASME J. Eng. for Gas Turbines Power, vol. 111, pp. 36-45

NOVOSELOV S S, GAVRILOV A F, SVETLICHNYI V A et al, (1986), "The ozone method of removing SO_2 and NO_x from the flue gases of thermal power stations", Thermal Eng., vol. 33, No. 9, pp. 496-498.

NUTCHER P B, (1984), "Forced draft, low-NO_x burners applied to process fired heaters", Plant/Operations Progress, vol. 3, No. 3, pp. 168-173.

- O -

OECD Report, (1979), "Photochemical oxidants and their precursors in the atmosphere".

OECD Report, (1983), "Control technology for nitrogen oxide emissions from stationary sources".

OECD Report, (1984), "Emission standards for major air pollutants".

OVEN M J, GOULDIN F C and MCLEAN W J, (1978), "Temperature and species concentration measurements in a swirl-stabilized combustor", 17th Symp. (Int.) on Combustion, pp. 363-374.

OWEN F K, SPADACCINI L J and BOWMAN C T, (1976), "Pollutant formation and energy release in confined turbulent diffusion flames", 16th Symp. (Int.) on Combustion, pp. 105-118.

- P -

PERICLEOUS K A, CLARK I W and BRAIS N, (1988), "The modelling of thermal NOx emissions in combustion and its applications to burner design", British Flame Days, Imperial college, London.

PETERS N and DONNERHACK S, (1980), "Structure and similarity of nitric oxide production in turbulent diffusion flames", 18th Symp. (Int) on Combustion, pp. 33-42.

PFEIFFER R and ALTMARK D, (1987), "The sinox burner system", Research and Development Forum", Osaka, Japan.

- R -

RALSTON T, FUGGLE R N, PITCHER G F, LEE O K, OLD C F and SYKES J, (1984), "Velocity measurements of cold flows through a variable-swirl burner at NEL", HTFS, RS549.

RITZ J, KOLB T, JANSOHN P and LEUCKEL W, (1989), "Reduction of NOx emission by fuel staging, effect of ammonia addition to the reburn fuel", Joint meeting of the British and French Sections of The Combustion Institute, Rouen, pp. 37-40.

ROBINSON G F, (1985), "A three-dimensional analytical model of a large tangentially-fired furnace", J. Inst. of Energy, vol. 58, pp. 116-150

RUBINS P M and MARCHIONNA N R, (1976), "Evaluation of NOx prediction-correlation equations from small gas turbines", AIAA Paper

No. 76-612.

- S -

SABO SH, DVOINISHNIKOV V A and VILENSKII T V, (1988), "Mathematical modelling of fuel combustion in the furnaces of steam boilers", Thermal Eng., vol. 35, No. 9, pp. 534-537.

SADAKATA M and BEER J M, (1976), "Spatial distribution of nitric oxide formation rates in a swirling turbulent methane-air flame", 16th Symp. (Int.) on Combustion, pp. 93-103.

SADAKATA M, FUJIOKA Y and KUNII D, (1980), "Effects of air preheating on emissions of NO, HCN and NH3 from a tow-staged combustor", 18th Symp. (Int.) on Combustion, pp. 65-72.

SAROFIM A F and POHL J H, (1972), "Kinetics of Nitric Oxide formation in premixed laminar flames", 14th Symp. (Int.) on Combustion, pp. 739-754.

SAWYER R F, (1980), "The formation and destruction of pollutants in combustion processes: Clearing the air on the role of combustion research", 18th Symp. (Int.) on Combustion, pp. 1-22.

SCHEFER R W and SAWYER R F, (1976), "Lean premixed recirculating flow combustion for control of oxides of nitrogen", 16th Symp. (Int.) on Combustion, pp. 119-133.

SEMERJIAN H and VRANOS A, (1976), "NOx formation in premixed turbulent

flames", 16th Symp. (Int.) on combustion, pp. 169-179.

SHAW H, (1973), "The effect of water, pressure, and equivalence ratio on nitric oxide production in gas turbines", ASME Paper No. 73-WA/GT-1.

SIDDIQUI A A, TENINI J W and KILLION L D, (1976), "Control NOx emissions from fixed fireboxes", Hydrocarbon Processing, Oct., pp. 94-97.

SIGAL I YA, KOSINOV O I, DUBOSHII A N and NIZHNIK S S, (1986), "Increasing the effectiveness of methods of reducing the formation of nitrogen oxides in boiler furnaces", Thermal Eng., vol. 33, No. 7, pp. 6-9.

SIMACHEV V YU NOVOSELOV S S, SVETLICHNYI V A et al, (1988), "An investigation of the ozone-ammonia method of simultaneous desulphurisation and denitrification of flue gases when burning Donetsk coals", Thermal Eng., vol. 35, No. 3, pp. 171-175.

SKORIK L D IVANOV Yu V, ARZUMANYAN E N, and KHACHIKYAN R P, (1986), "Industrial checking of the method of removing nitrogen oxides from the flue gases of thermal power stations by adding ammonia to the boiler's high-temperature circuit", Thermal Eng., vol. 33, No. 7, pp. 389-391.

SLOAN D G, SMITH P J and SMOOT L D, (1986), "Modelling of swirl in turbulent flow systems", Prog. Energy and Combust. Sci., vol. 12, pp. 163-250.

SMART J and WEBER, (1987), "NOx reduction and burnout optimisation using aerodynamic air staging and air staged precombustors", IFRF, Doc. No. F 037/a/18.

SPALDING D B, (1970),"Mixing and chemical reaction in steady confined turbulent flames", 13th Symp. (Int.) on Combustion, pp. 649-658.

STOPFORD P J, (1989), "PCOC Users Manual", Harwell report, AERE-R12626.

SUZUKI T, MORIMOTO K, OTANI K, YAMAGATA T, ODAWARA R and FUKUDA T, (1982), "Development of high efficiency burners with low NOx emission", J. Inst. of Energy, vol. 55, Part 1; pp. 212-215. Part 2; pp. 216-220.

SYKES J and WILKES N S, (1983), "TUFC2 Program Users Manual", Harwell report AERE 11027.

SYRED N and BEER J M, (1974), "Combustion in swirling flows: A review", Combustion and Flame, vol. 23, pp. 143-201.

- T -

TAKAGI T, OGASAWARA M and DAIZO M, (1976), "Nox formation from nitrogen in fuel and air during turbulent diffusion combustion", 16th Symp. (Int.) on Combustion, pp. 181-189.

TAN H Y and MACCALLUM N R L, (1983), "Combustion in rotating flows", Report, Dept. of Mech. Eng., University of Glasgow.

TANG S, CHURCHIL S W and LIOR N, (1980), "The formation of thermal and

fuel NOx for radiantly stabilised combustion", 18th Symp. (Int.) on combustion, pp. 73-80.

THOMSON S T and CROW R H, (1976), "Energy cost of NOx control", Proc. API Refin. Dep. Midyear 41st Meeting, vol. 55, pp. 567-574.

TOOF J L, (1986), "A model for the prediction of thermal, prompt, and fuel NOx emission from combustion turbine", ASME J. Eng. gas turbine Power, vol. 108, pp. 340 347.

TOUCHTON G L, (1984), "An experimentally verified NOx prediction algorithm incorporating the effects of steam injection", ASME Paper No. 84-GT-152.

TSIRUL'NIKOV L M, NURMUKHAMEDOV M N, MINENKOV Yu E and KIRILLOV V G, (1986), "The effectiveness of some of the means of reducing emissions of nitrogen oxides when burning natural gas in the boilers of 300 MW power-generation units", Thermal Eng., vol. 33, n.9, pp. 503-506.

TUTTLE J H, SHISLER R A and MELLOR A M, (1974), "Nitrogen dioxide formation in gas turbine engine: Measurements and measurement methods", Combust. Sci. and Tech., vol. 9, pp. 261-271.

TUTTLE J H, COLKET M B, BILGER R W AND MELLOR A M, (1976), "Characteristic times for combustion and pollutant formation in spray combustion", 16th Symp. (Int.) on combustion. pp. 209-219.

- V -

VRANOS A, (1974), "Turbulent mixing and NOx formation in gas combustors", Combustion and Flame, vol. 22, pp. 253-258.

- W -

WAIBEL R and NICKESON D, (1986), "Staged fuel burners for NOx control", IFRF , 8th Members Conference, Netherlands.

WEBER R, BOYSAN F, SWITHENBANK J and ROBERTS P A, (1986), "Computation of near field aerodynamics of swirling expanding flows", 21th Symp. (Int.) on Combustion, pp. 1435-1443.

WEBER R and VISSER B M, (1990), "Assessment of turbulence modelling for engineering prediction of swirling vortices in the near burner zone", Int. J Heat and Fluid Flow, vol. 11, No. 3, pp. 225-235.

WESTENBERG A A, (1971), "Kinetics of NO and CO in lean, premixed hydrocarbon-air flames", Comb. Sci. and Technology, vol. 4, pp. 59-64.

WILLIAMS A, (1989), "Combustion-Generated NOx", Joint meeting of the British and French Sections of The Combustion Institute, Rouen, pp. A1-A11.

WU H L and FRICKER N, (1976), "The characteristics of swirl-stabilised natural gas flames, Part 2: The behaviour of swirling jet flames in a narrow cylindrical furnace", J. Inst. of Fuel, vol. 49 , pp. 144-151.

- Y -

YAMAGISHI K, NOZAWA M and YOSHIE T (1974), "A study of NOx emission characteristics in two stage combustion", 15th Symp. (Int.) on Combustion, pp. 1157-1166.

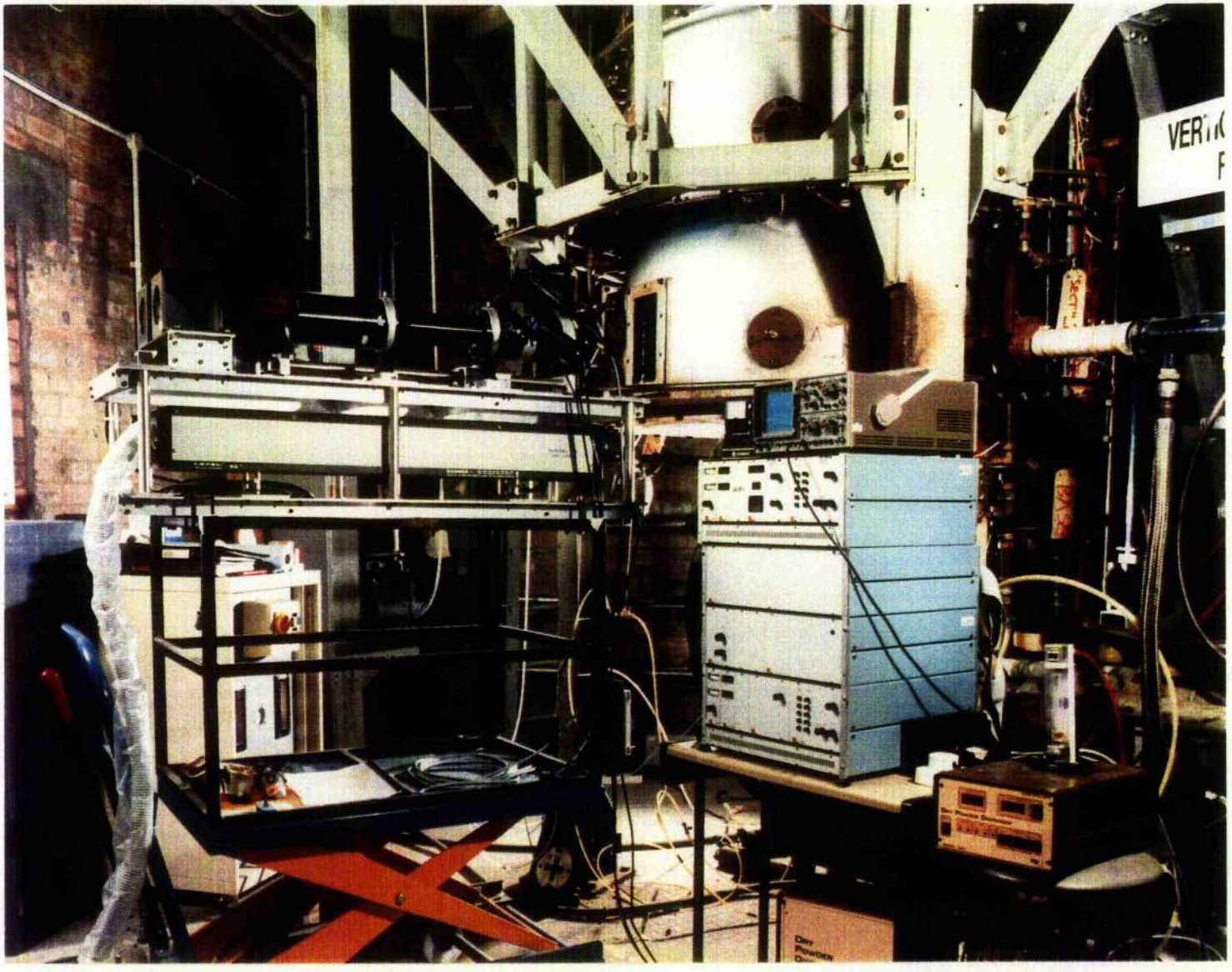

Photograph 1: Furnace block house

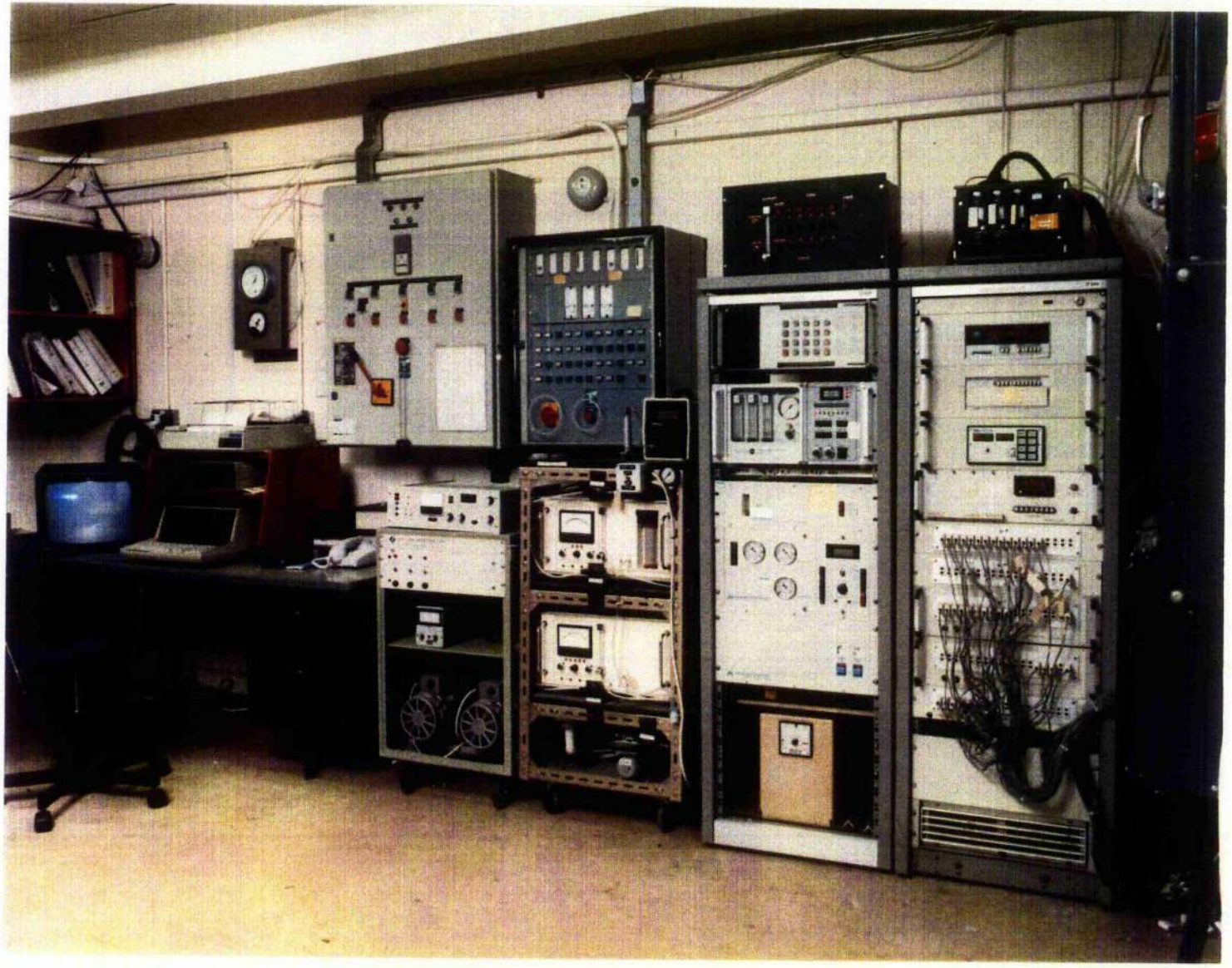

Photograph 2: Furnace control room

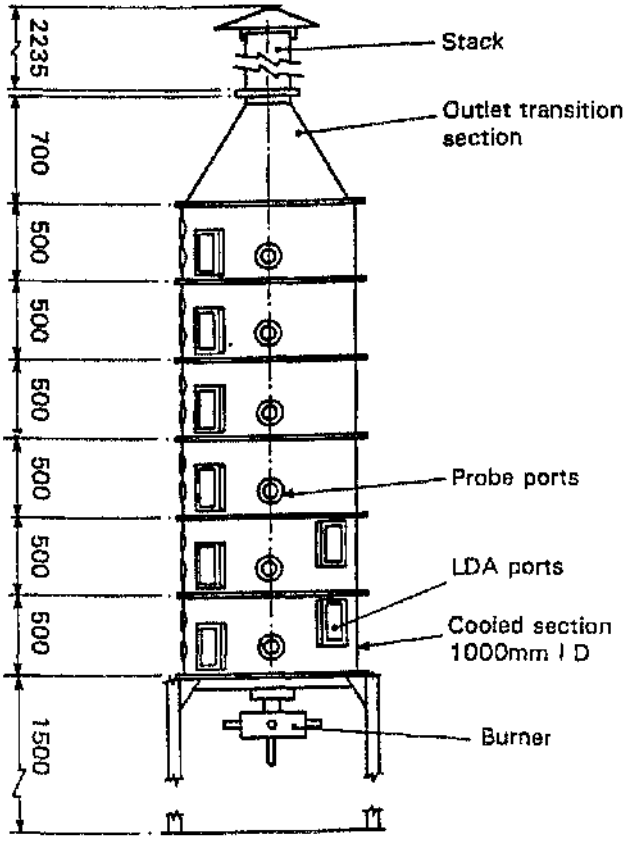

FIG 3.1.a: Schematic of the NEL furnace

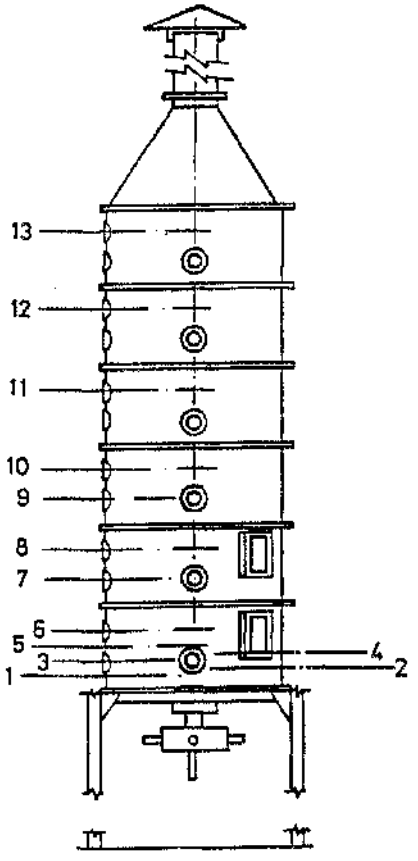

FIG 3.1.b: Furnace traversing planes

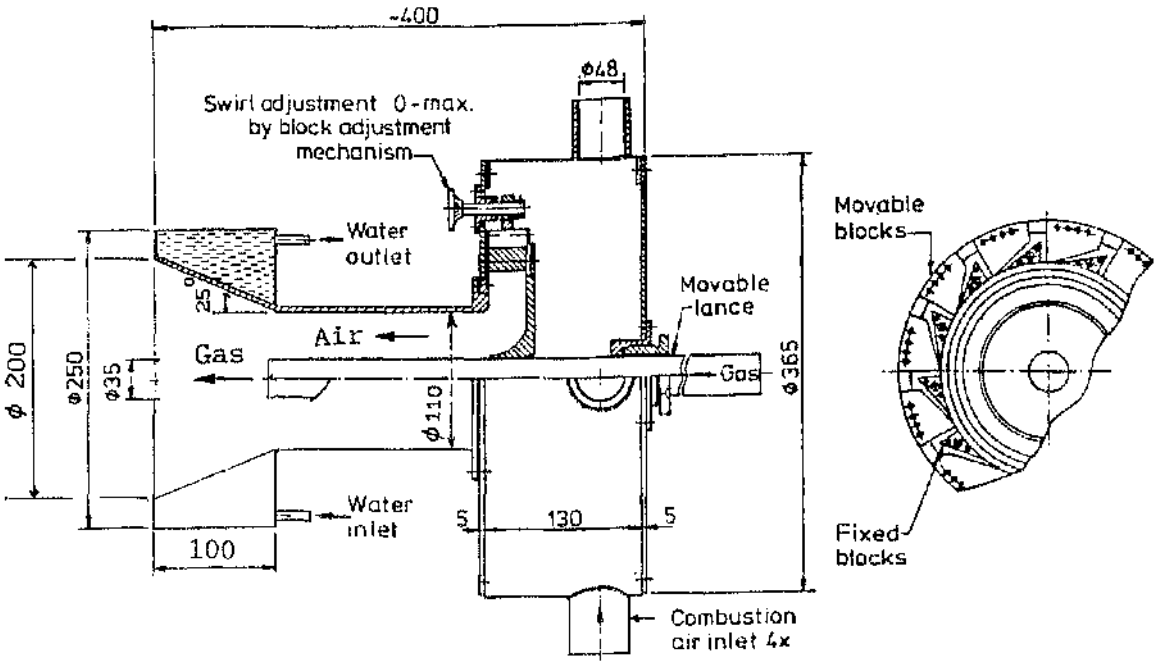

FIG 3.2.a: Central axial fuel injection

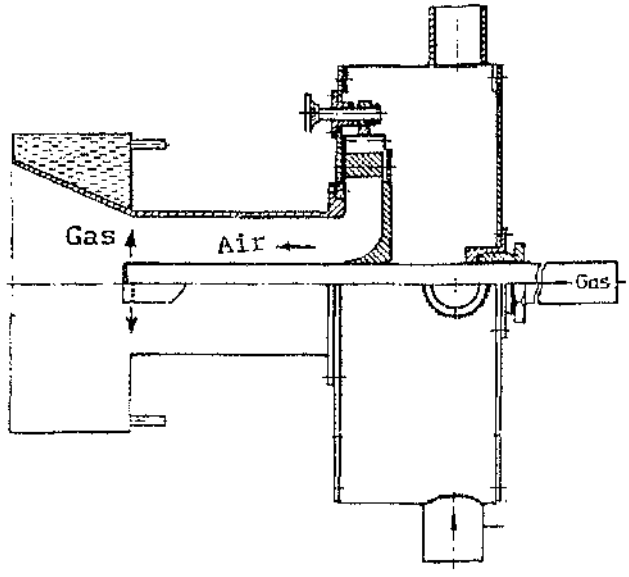

FIG 3.2.b: Central radial fuel injection

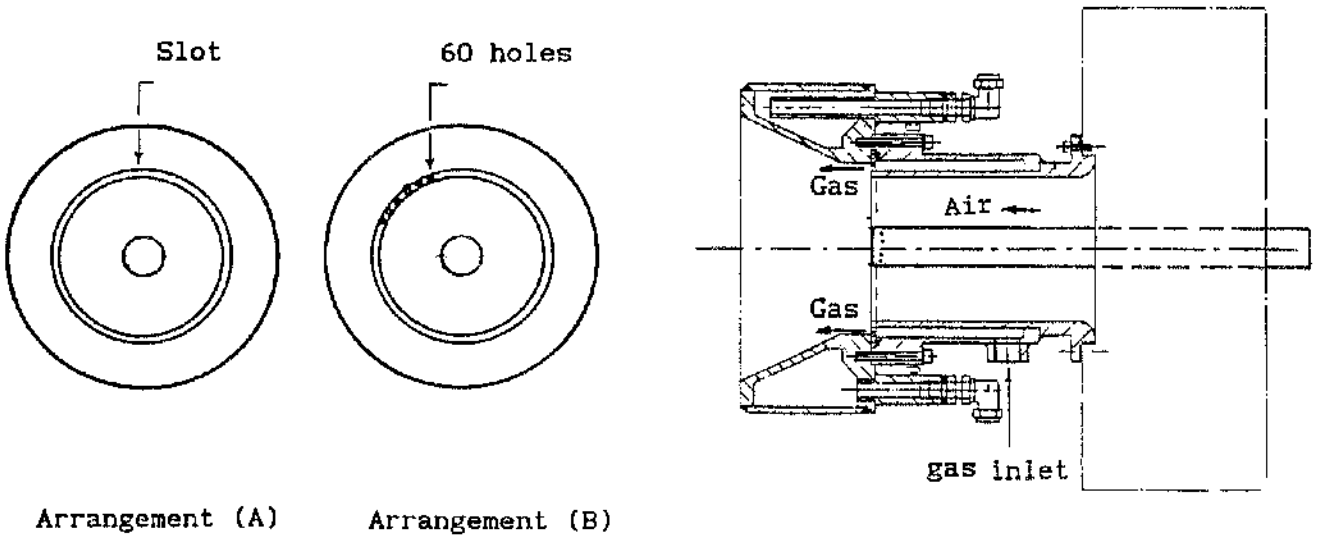

SCHEME 1

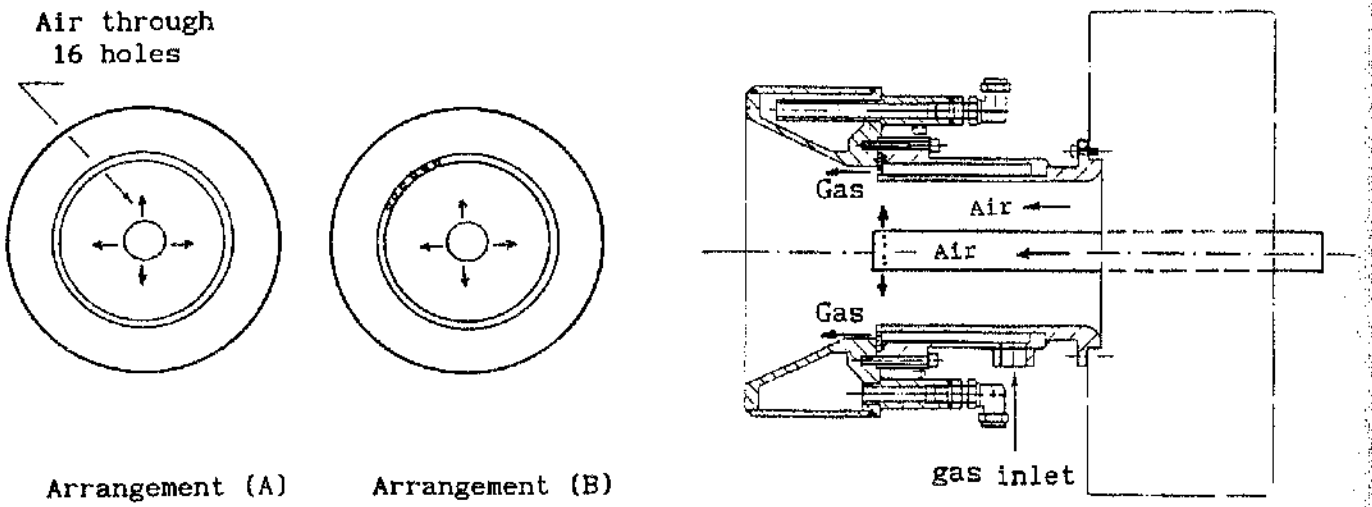

SCHEME 2

FIG 3.2.c: Peripheral fuel injection

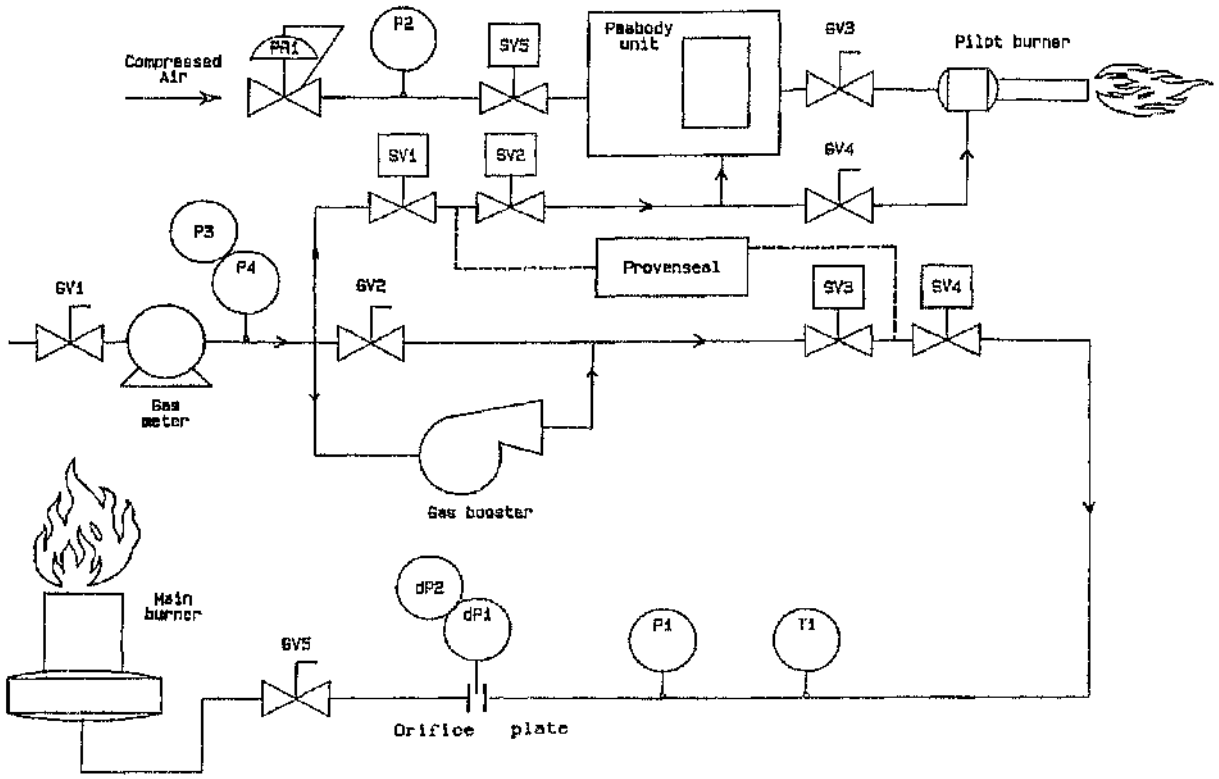

Symbol	Description
GV1	Gas supply manual shut off
GV2	Gas booster bypass control
GV3	Pilot premix manual shut off
GV4	pilot neat gas manual shut off
GV5	Main burner gas manual sut off
SV1	Pilot safety shut off
SV2	= = = =
SV3	Main burner safety shut off
SV4	= = = = =
dP1	Gas flow measurement transducer
dP2	Gas flow safety transducer
P1	Gas pressure measurement
T1	Gas temperature measurement
P2	Pilot air safety pressure switch
P3	Gas supply safety pressure switch
P4	Gas supply booster pressure switch
PR1	Pilot air pressure regulator

FIG 3.3.a: Gas flow line

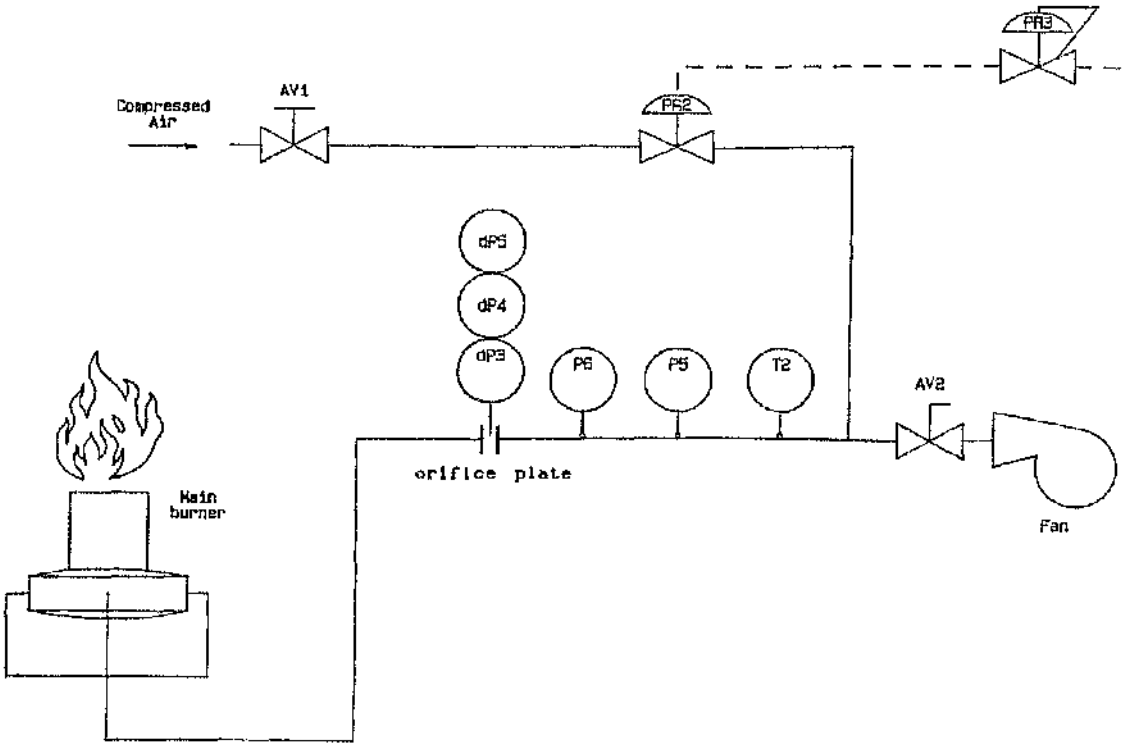

Symbol	description
AV1	Main compressed air valve
PR2	Main air pilot-operated regulator
PR3	Control regulator (control room)
AV2	Fan air control valve
T2	Air Temperature measurements
P5	Air safety pressure switch
P6	Air pressure measurements
dP3	Air flow measurement transducer
dP4	Air flow safety transducer
dp5	Air flow safety pressure switch

FIG 3.3.b: Air flow line

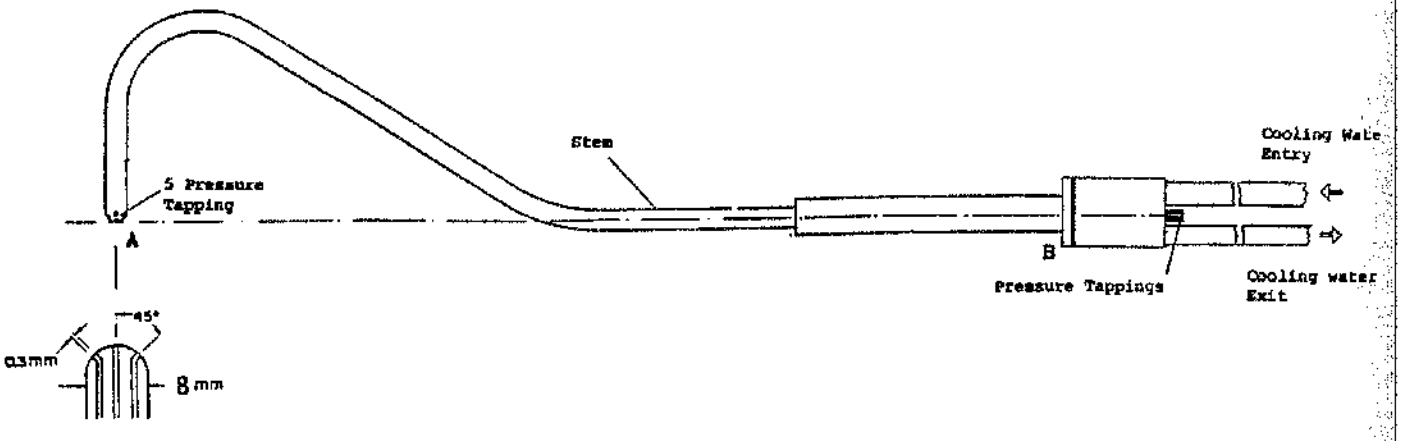

FIG 3.4: Five-hole probe

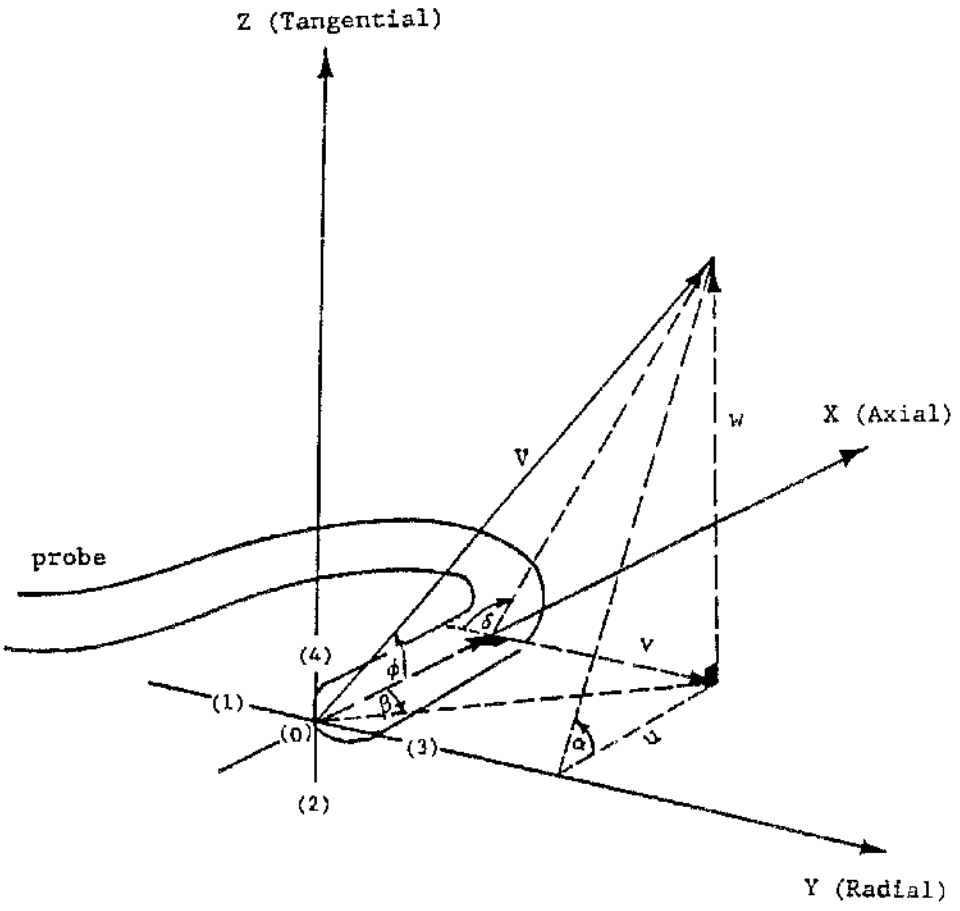

FIG 3.5: The 5-hole probe angles definition

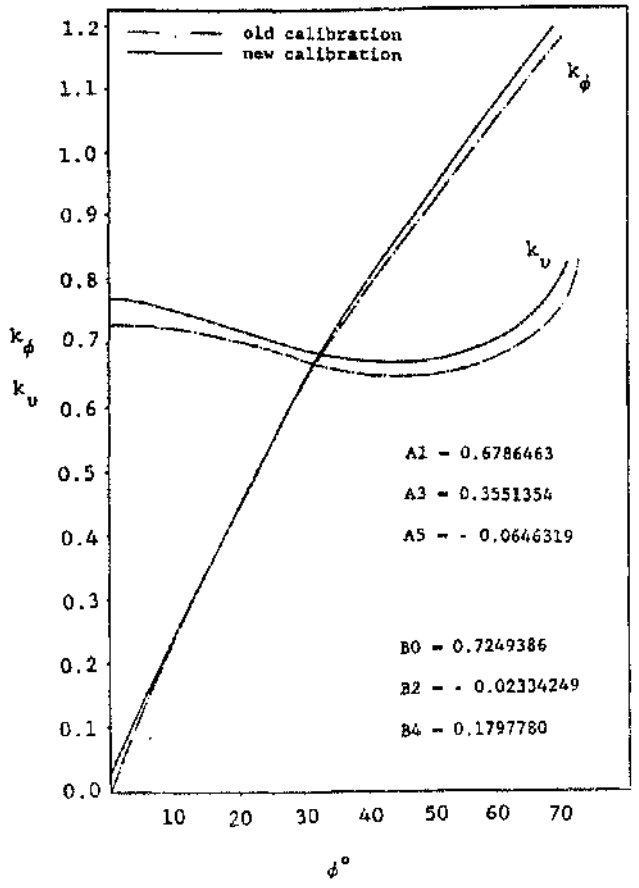

FIG 3.6.a:

Comparison of the present calibration with suppliers calibration for Kϕ and Kυ

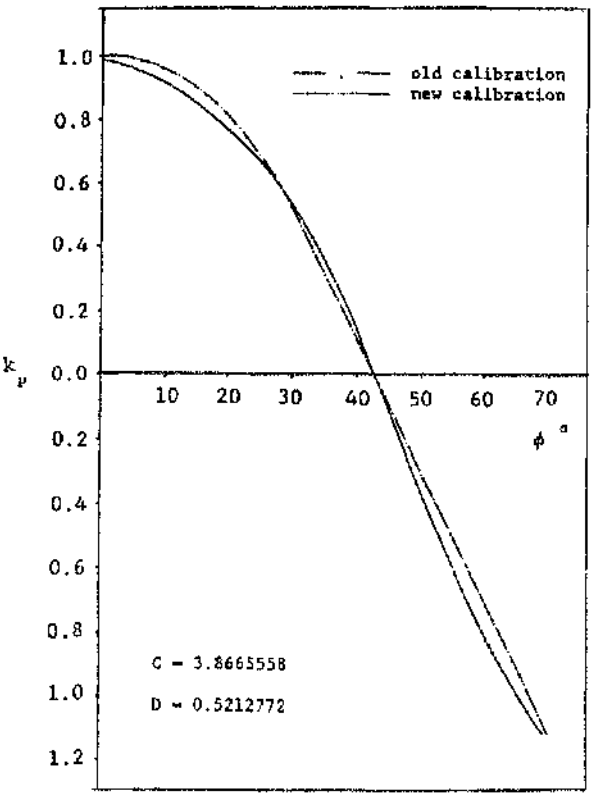

FIG 3.6.b:

Comparison of present calibration with suppliers calibration for K_p

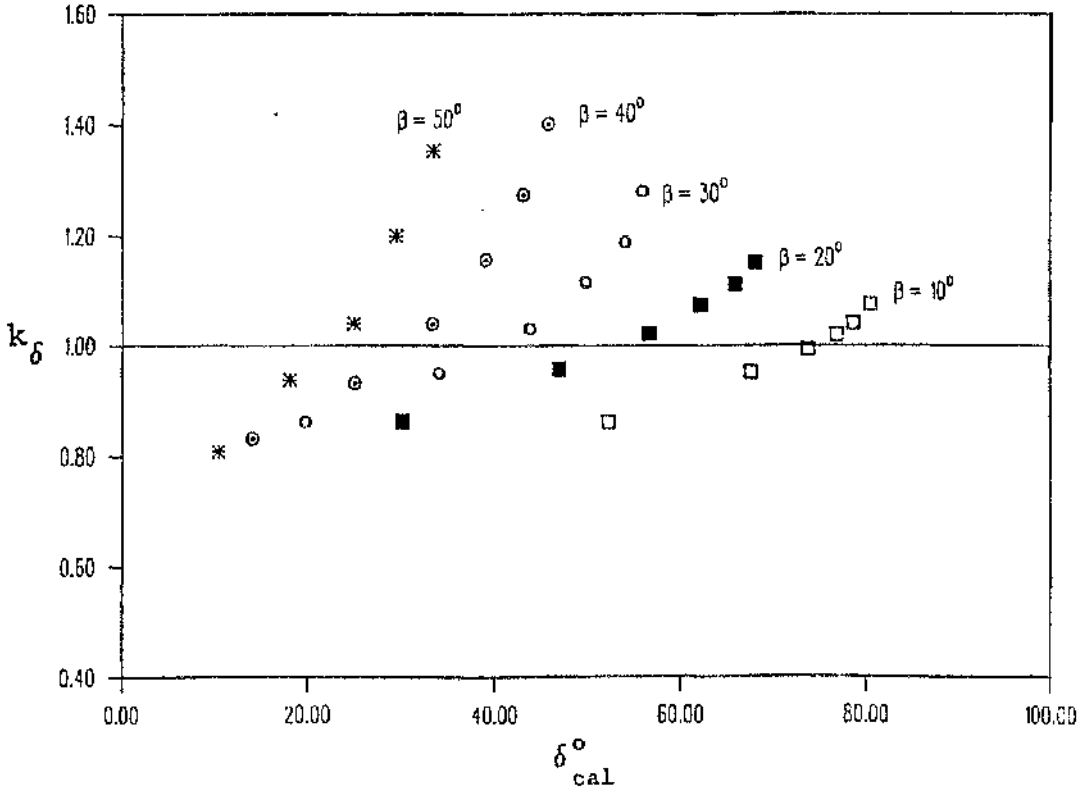

FIG 3.7: Ratio of measured to calculated δ

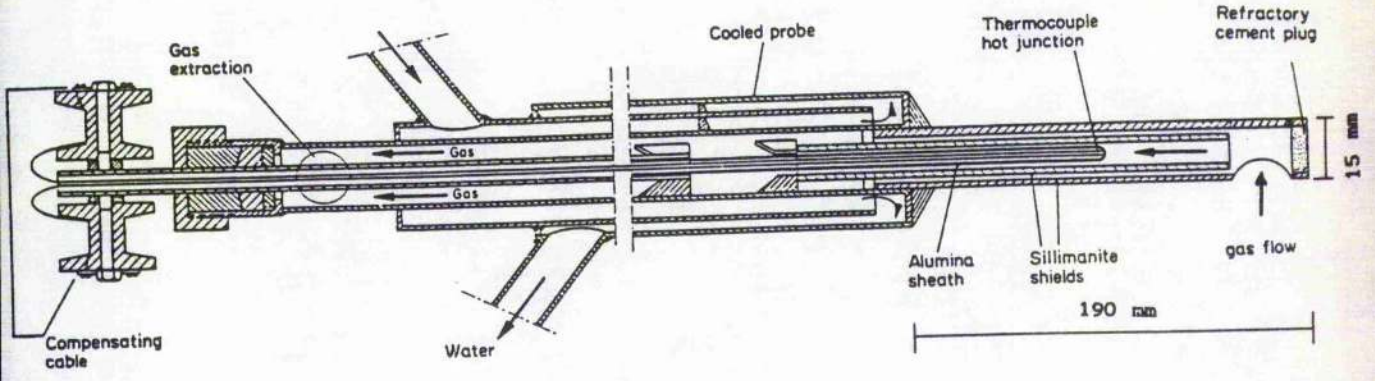

FIG 3.8: Suction pyrometer

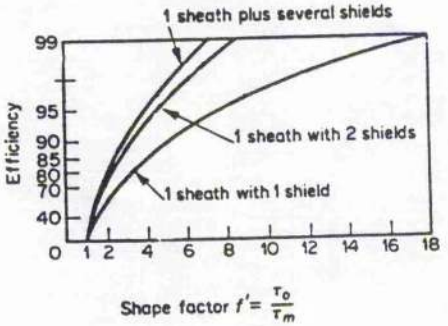

FIG 3.9: Efficiency factor for suction pyrometer (Chedaille and Braud) (1972)

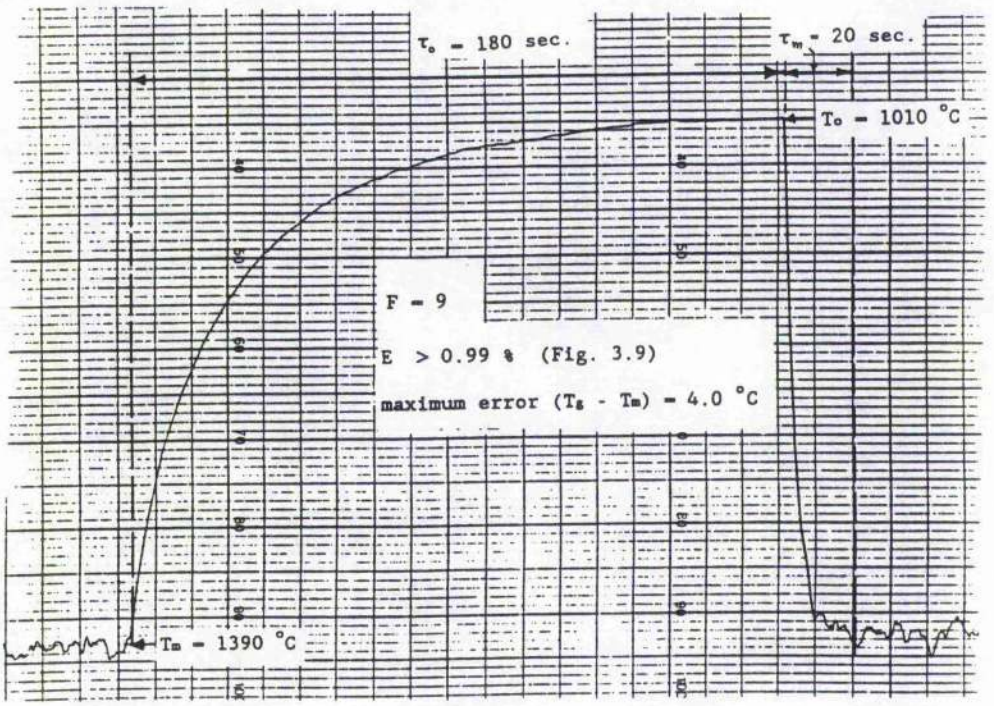

FIG 3.10: Efficiency test for suction pyrometer

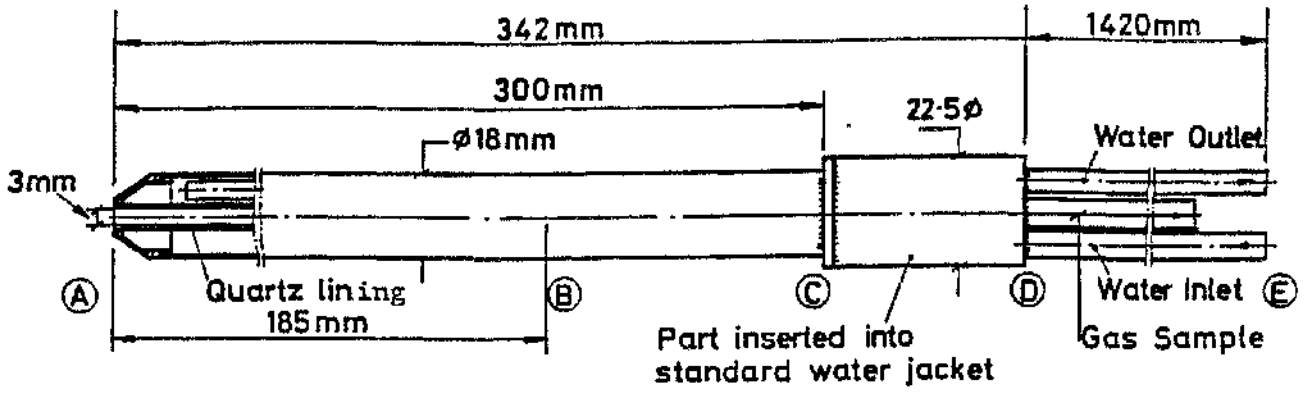

-a-

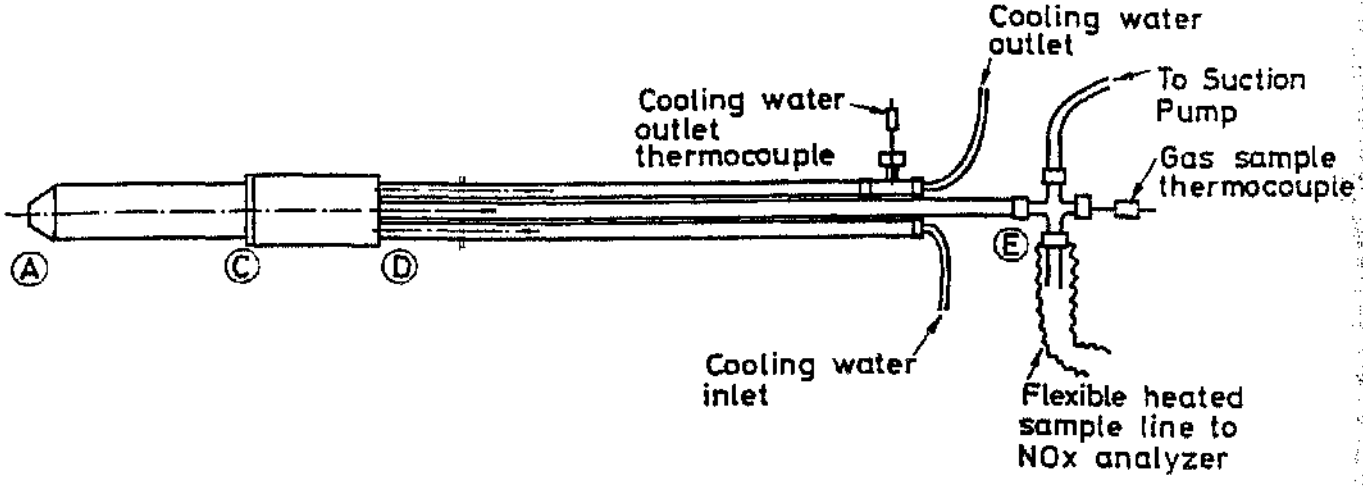

-b-

FIG 3.11: NOx sampling system

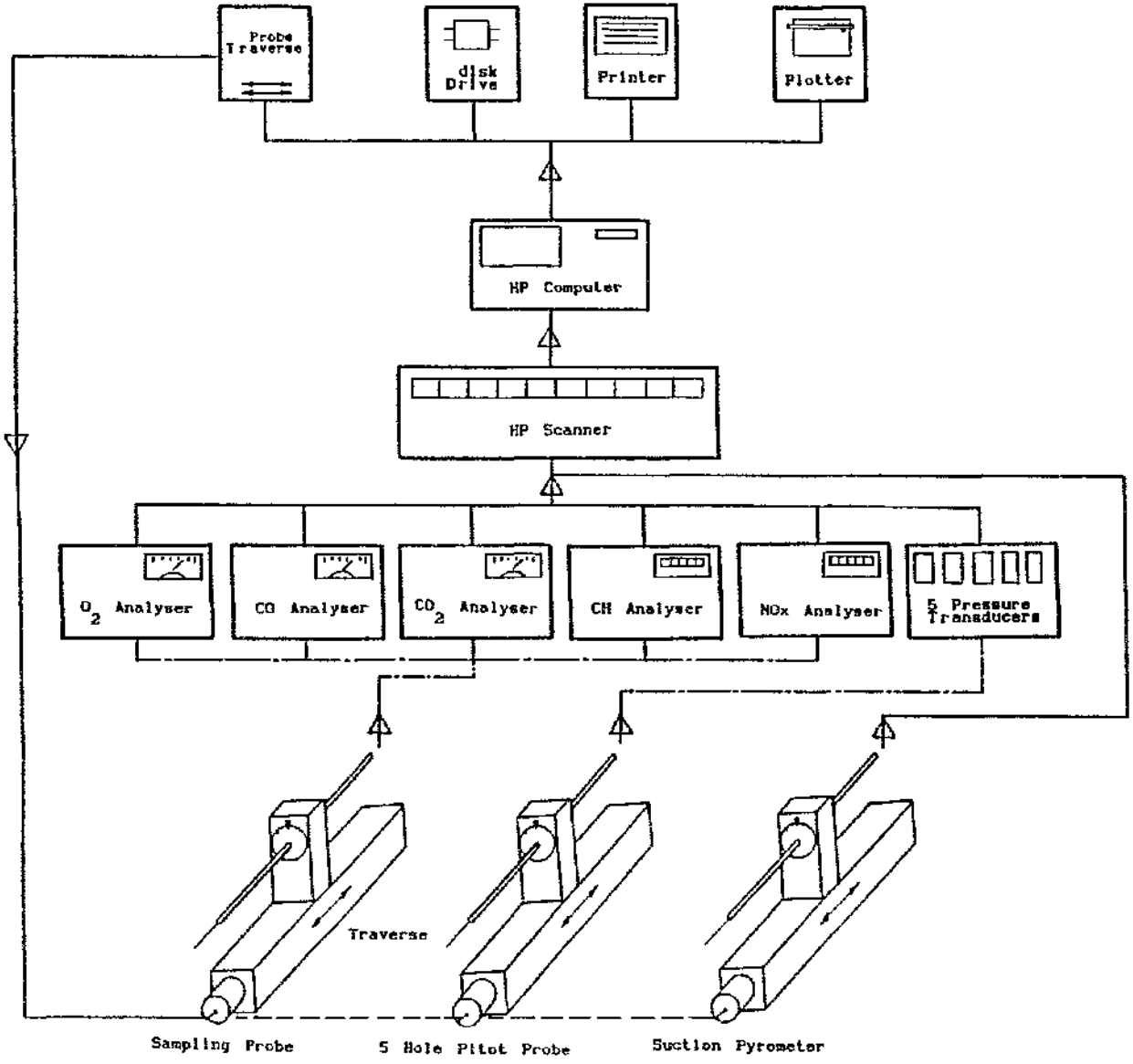

FIG 3.12: Data acquisition and traverse system

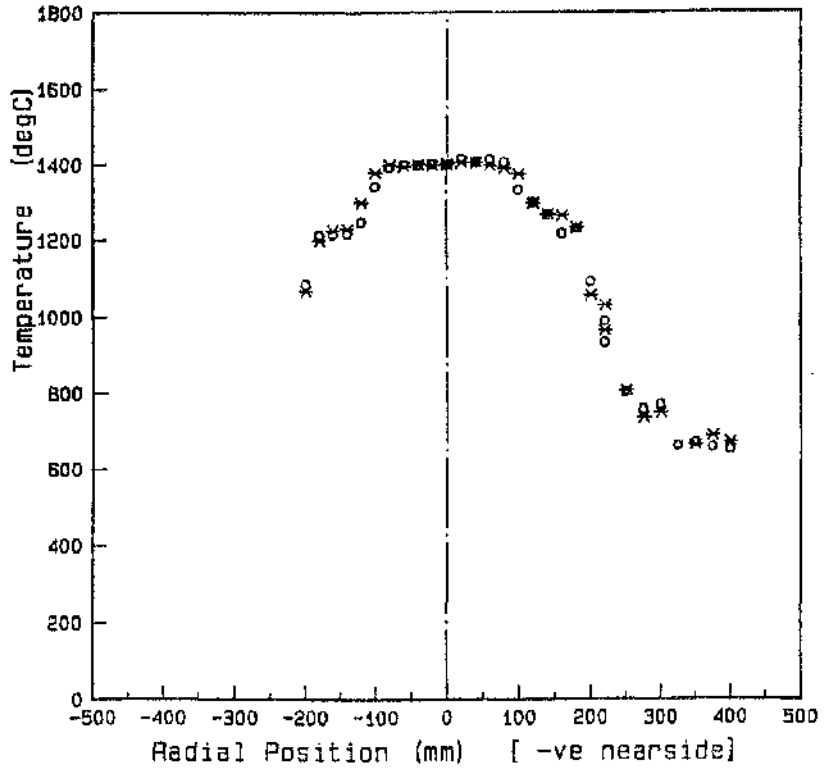

(a) S = 0.90

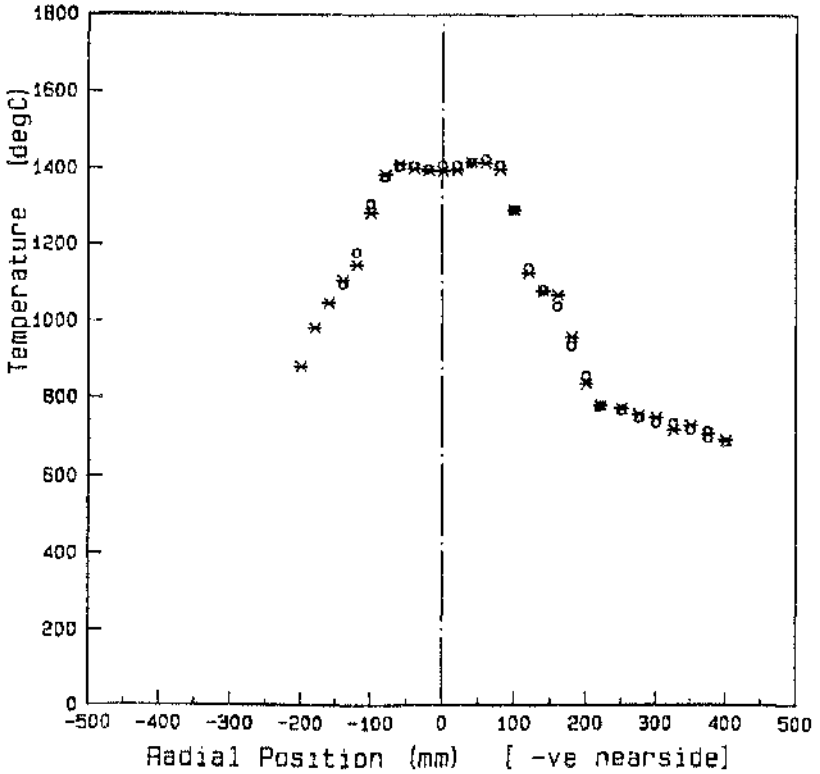

(b) S = 2.25

FIG 4.1: Repeatability test of temperature, X = 160 mm, peripheral fuel injection, Scheme 1

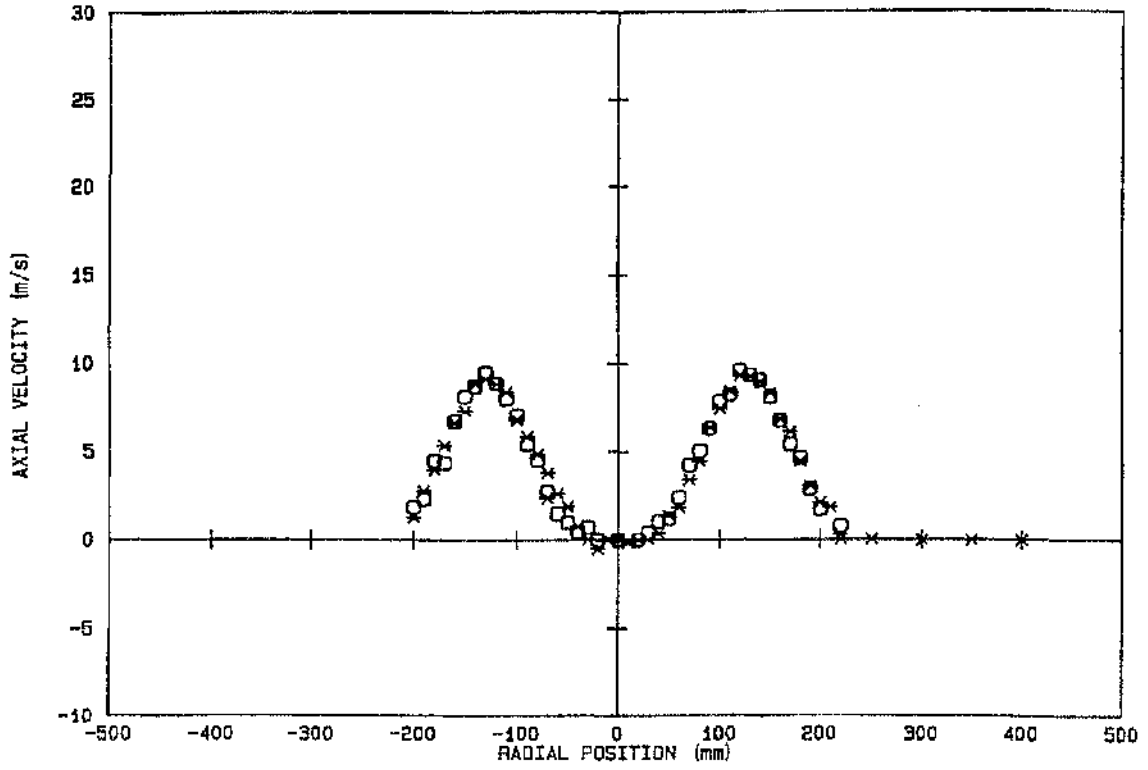

(a) S = 0.90

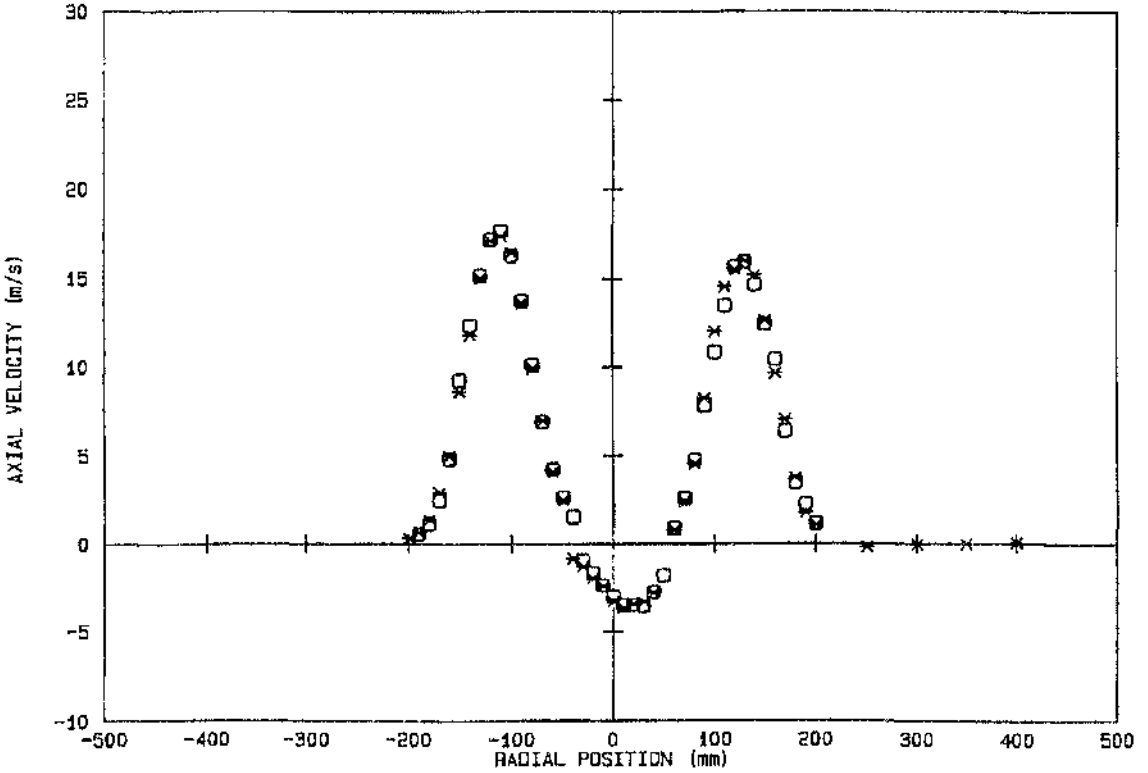

(b) S = 2.25

FIG 4.2: Repeatability test of axial velocity, X = 160 mm, peripheral fuel injection, Scheme 1

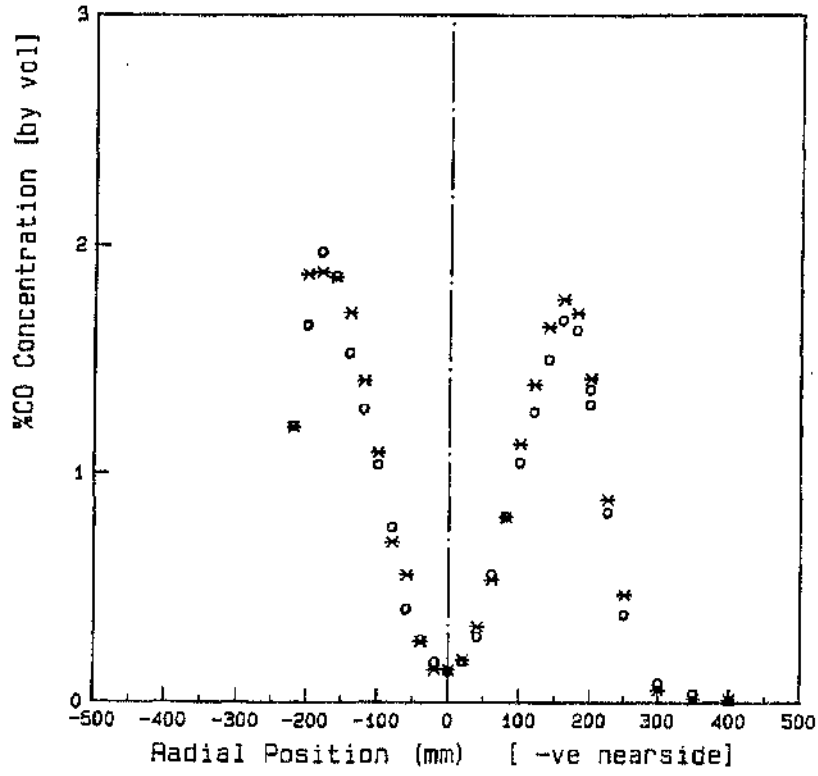

(a) S = 0.90

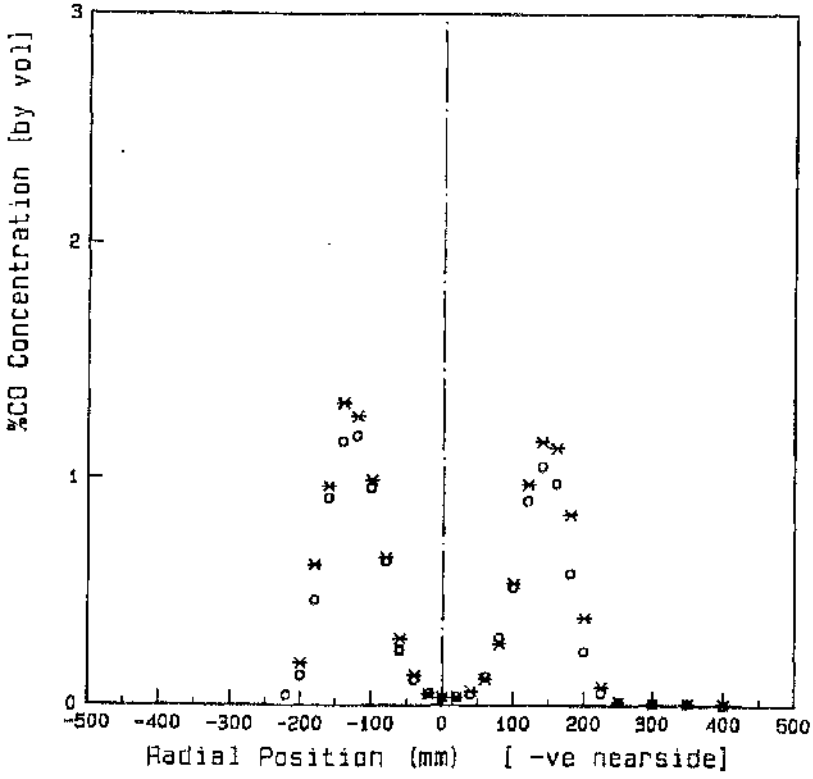

(b) S = 2.25

FIG 4.3: Repeatability test of CO, **X = 160 mm**, peripheral fuel injection, Scheme 1

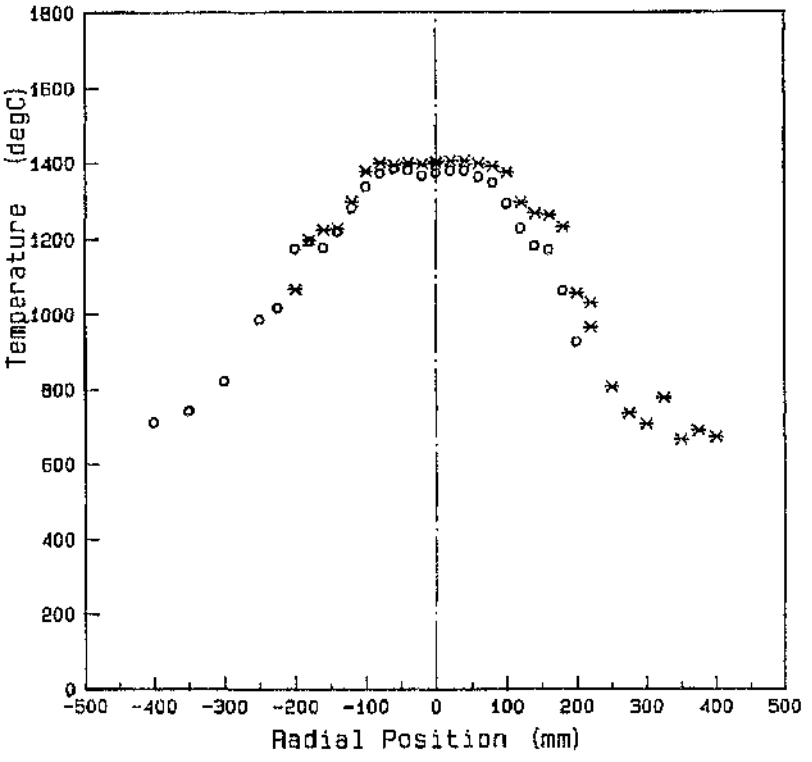

(a) S = 0.90

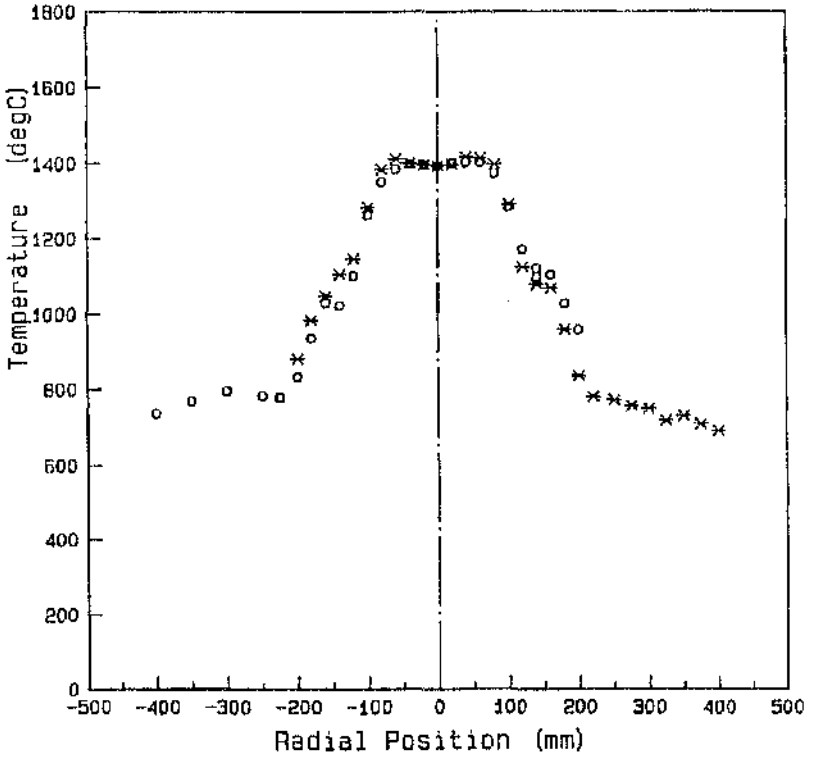

(b) S = 2.25

FIG 4.4: Test of probe effect on temperature, X = 160 mm, peripheral fuel injection, Scheme 1

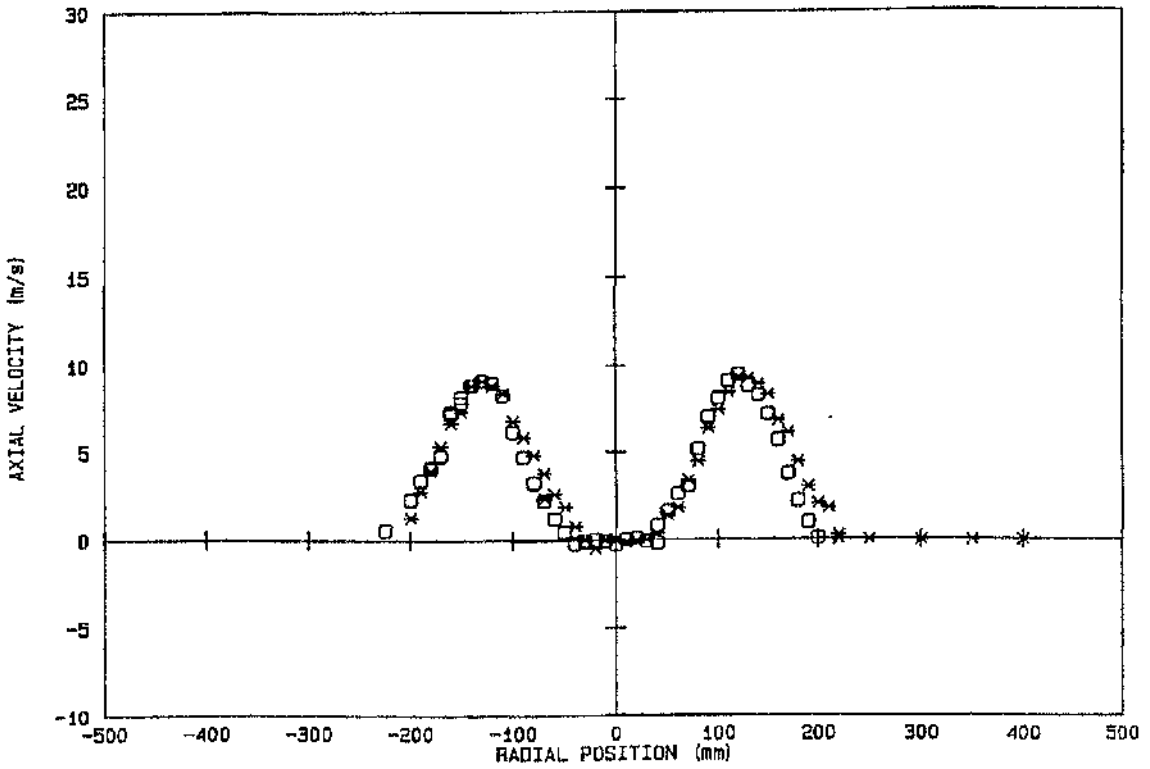

(a) S = 0.90

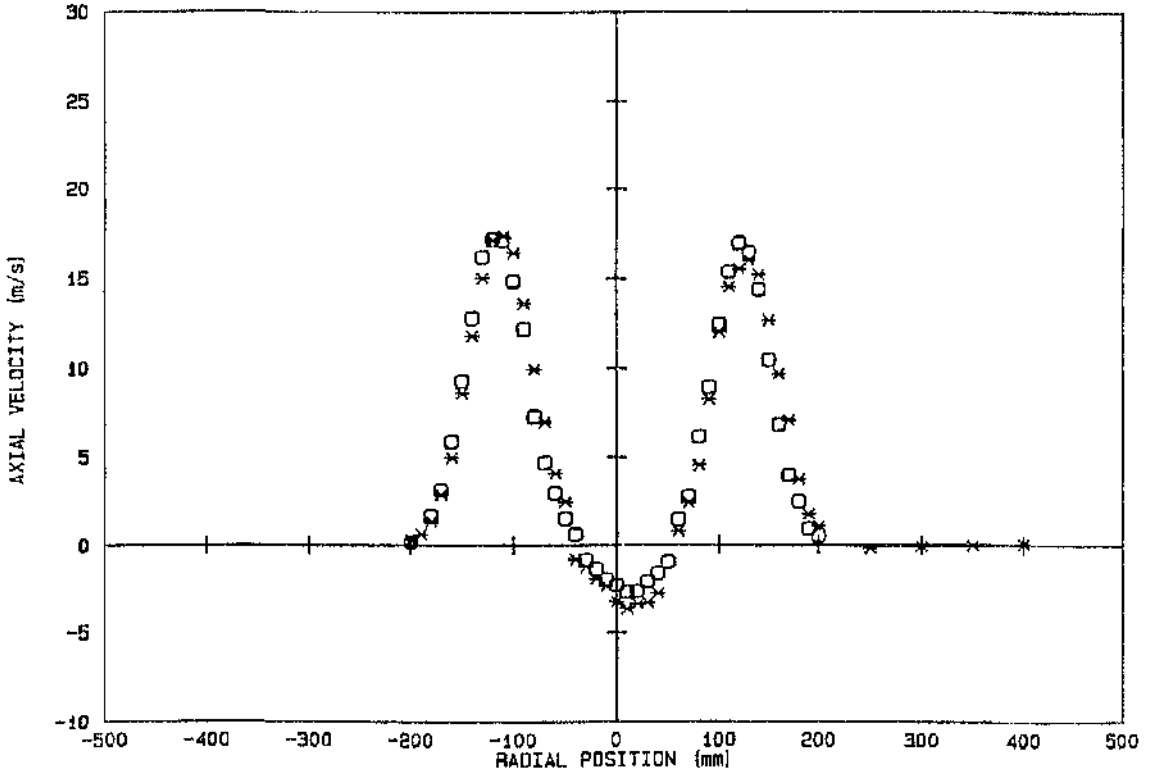

(b) S = 2.25

FIG 4.5: Test of probe effect on axial velocity, X = 160 mm, peripheral fuel injection, Scheme 1

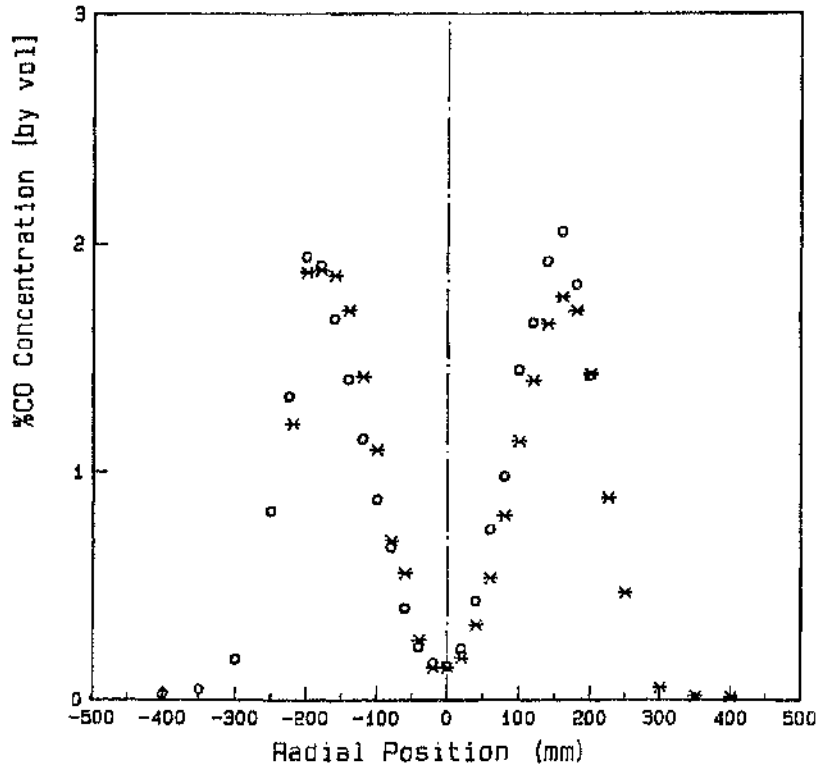

(a) S = 0.90

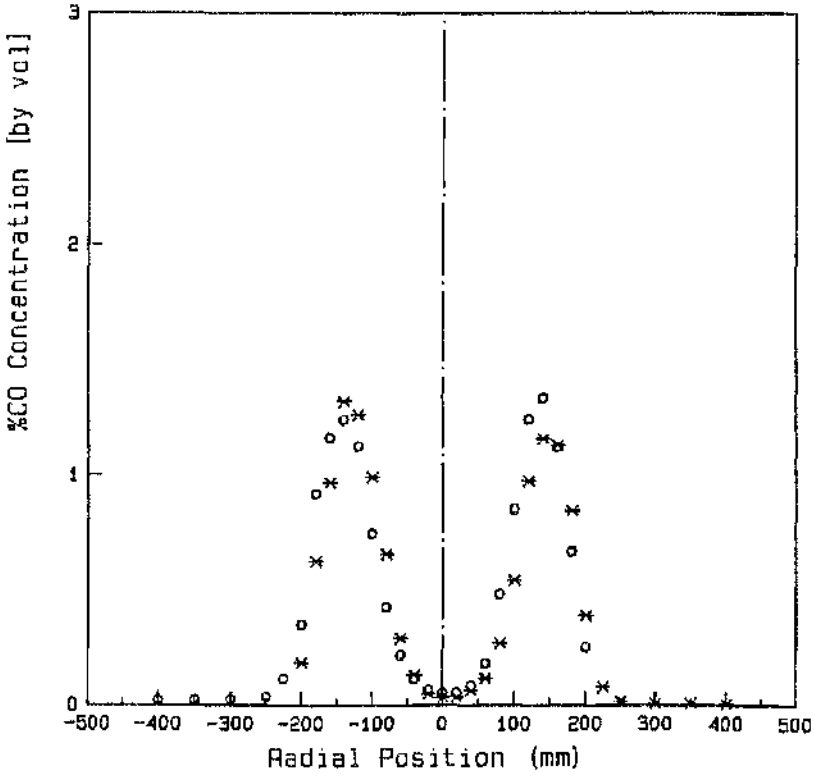

(b) S = 2.25

FIG 4.6: Test of probe effect on CO, X = 160 mm, peripheral fuel injection, Scheme 1

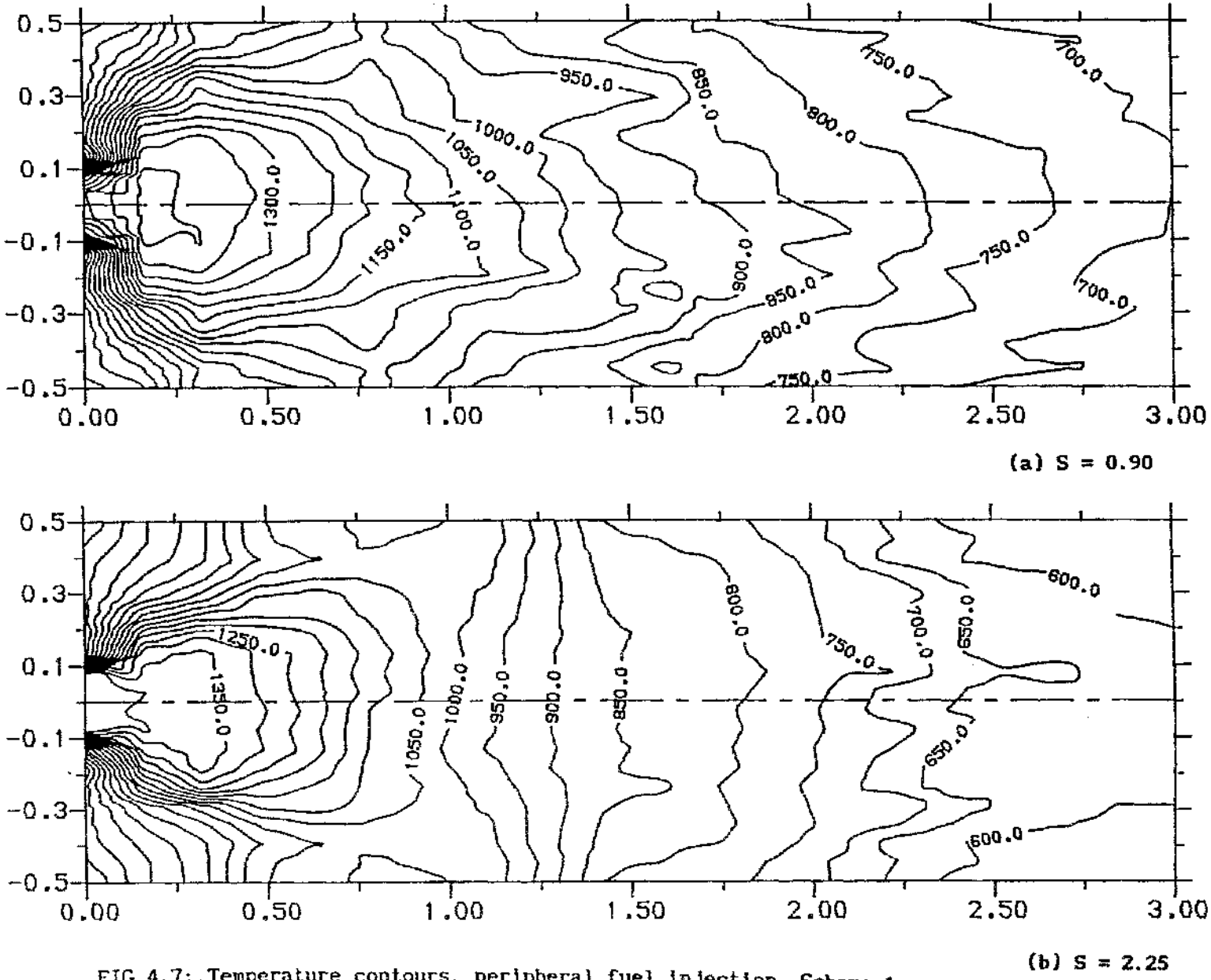

FIG 4.7: Temperature contours, peripheral fuel injection, Scheme 1

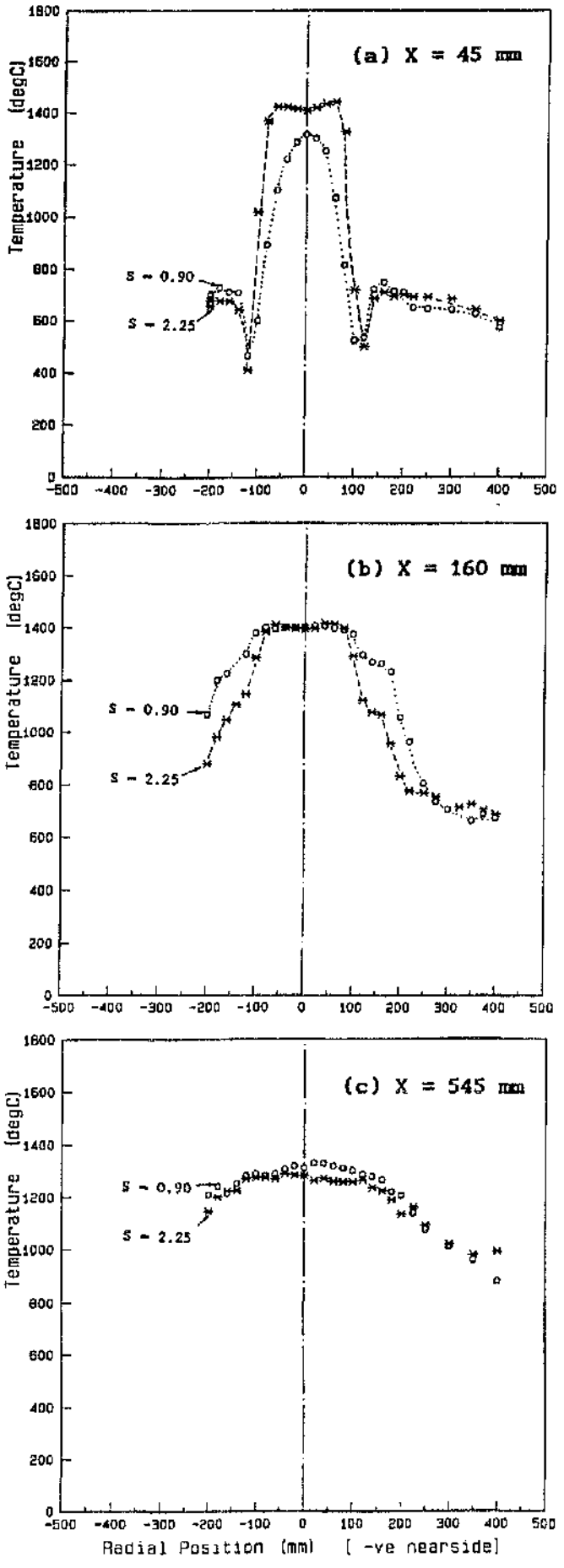

FIG 4.8: Radial temperature profiles, peripheral fuel injection, Scheme 1

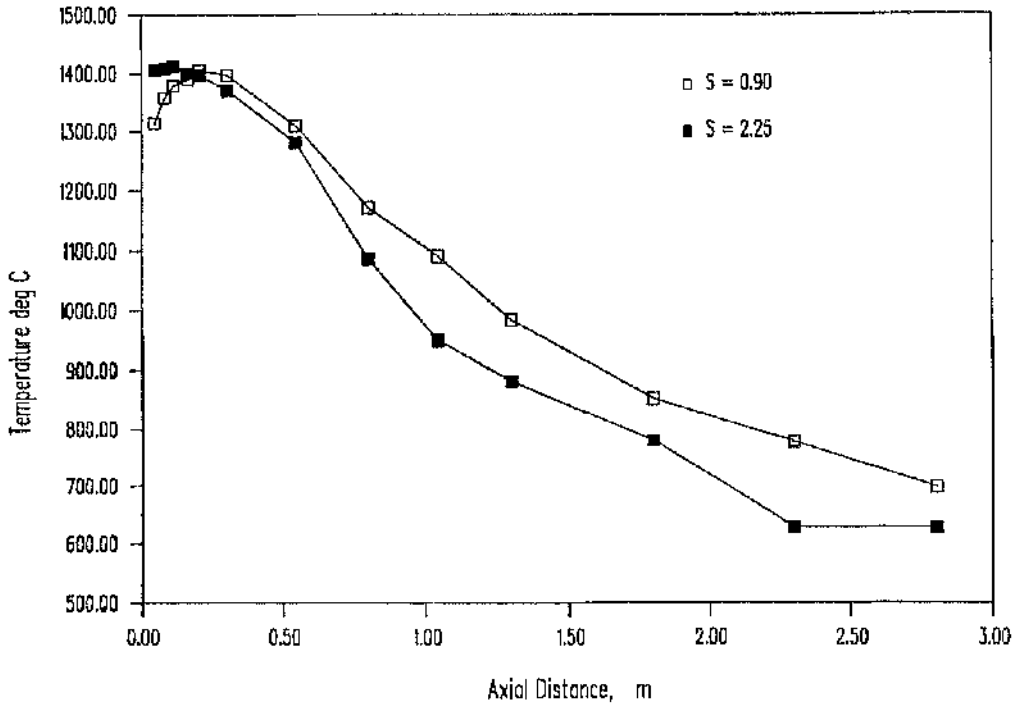

FIG 4.9.a: Variation of centre-line temperature along the furnace peripheral fuel injection, Scheme 1

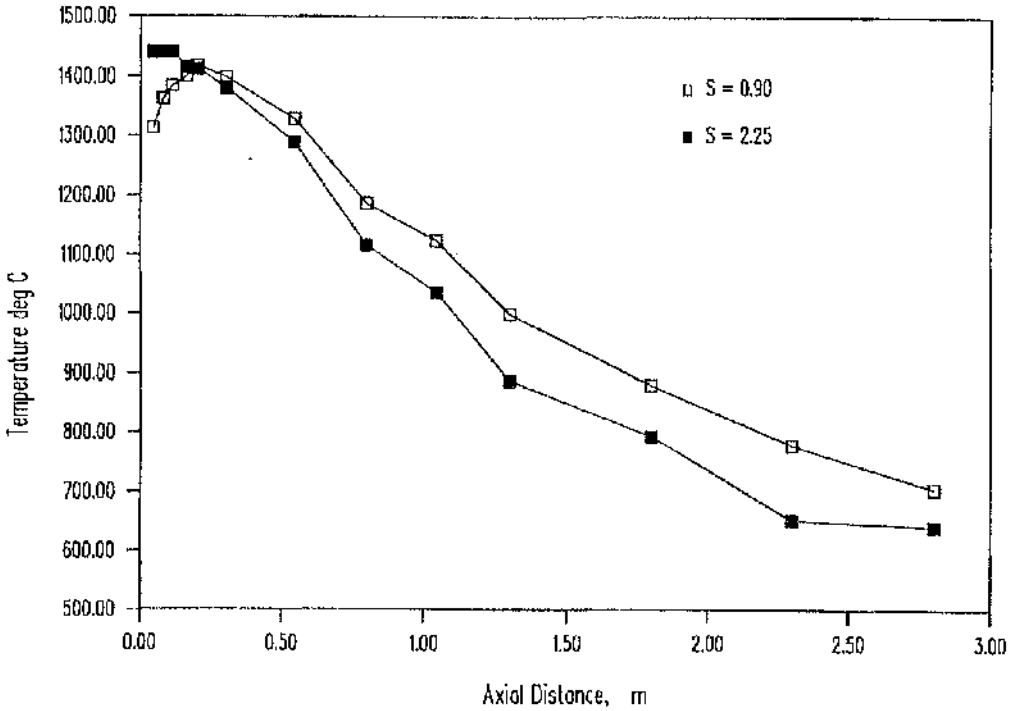

FIG 4.9.b: Variation of maximum temperature along the furnace peripheral fuel injection, Scheme 1

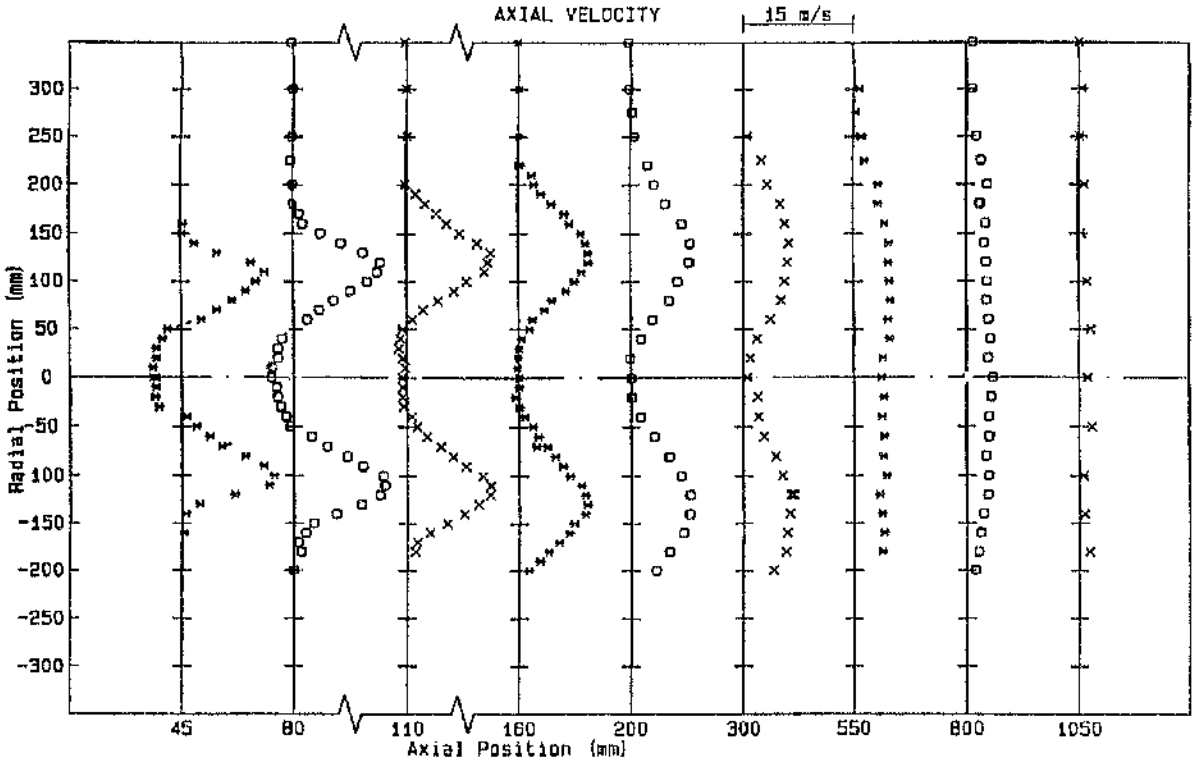

(a) S = 0.90

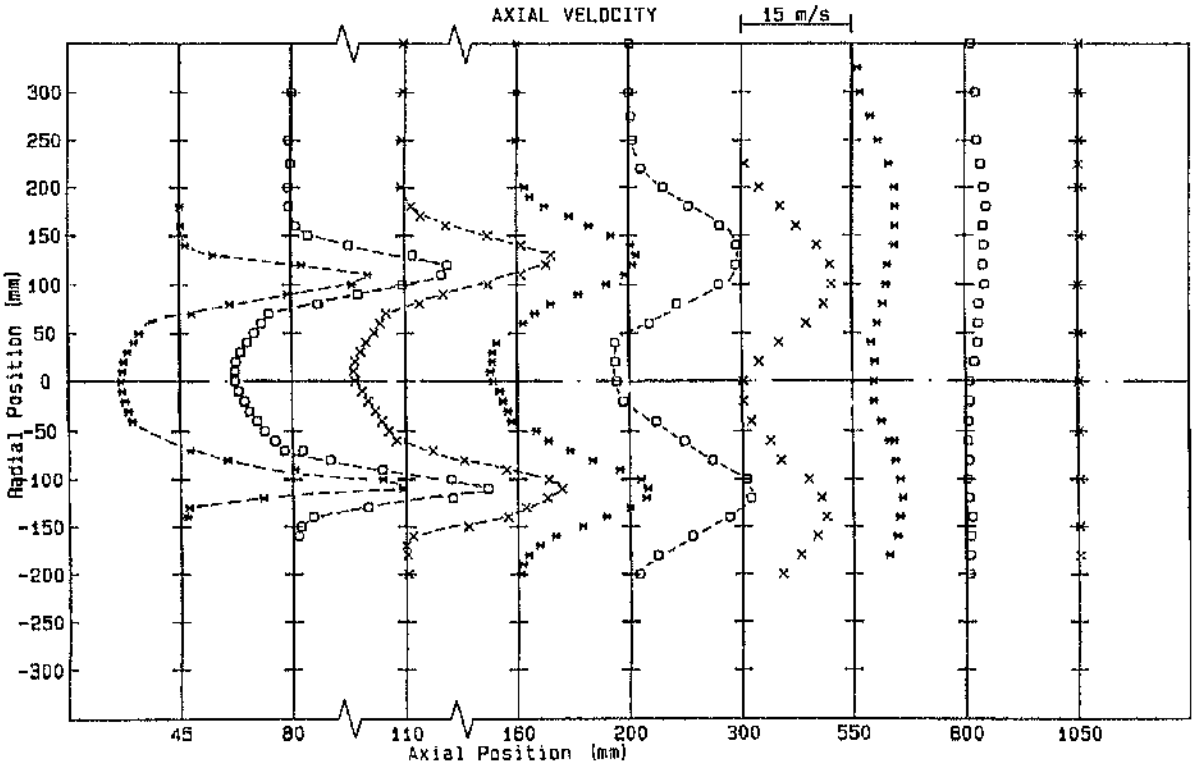

(b) S = 2.25

FIG 4.10: Axial velocity profiles, peripheral fuel injection, Scheme 1

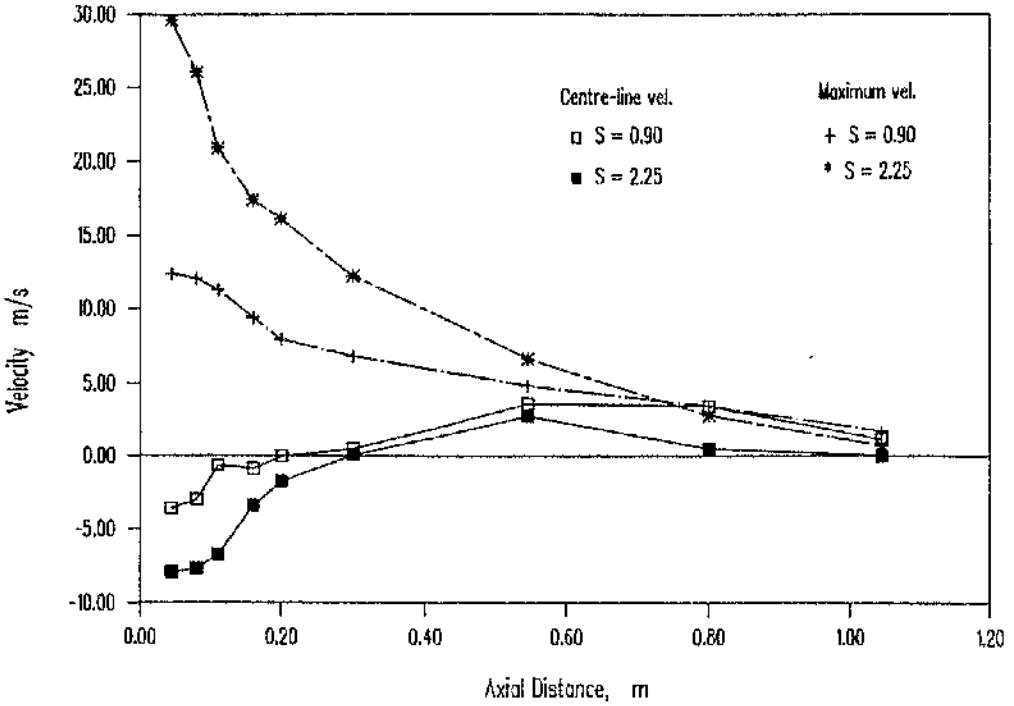

FIG 4.11: Variation of maximum and centre-line axial velocities along the furnace, peripheral fuel injection, Scheme 1

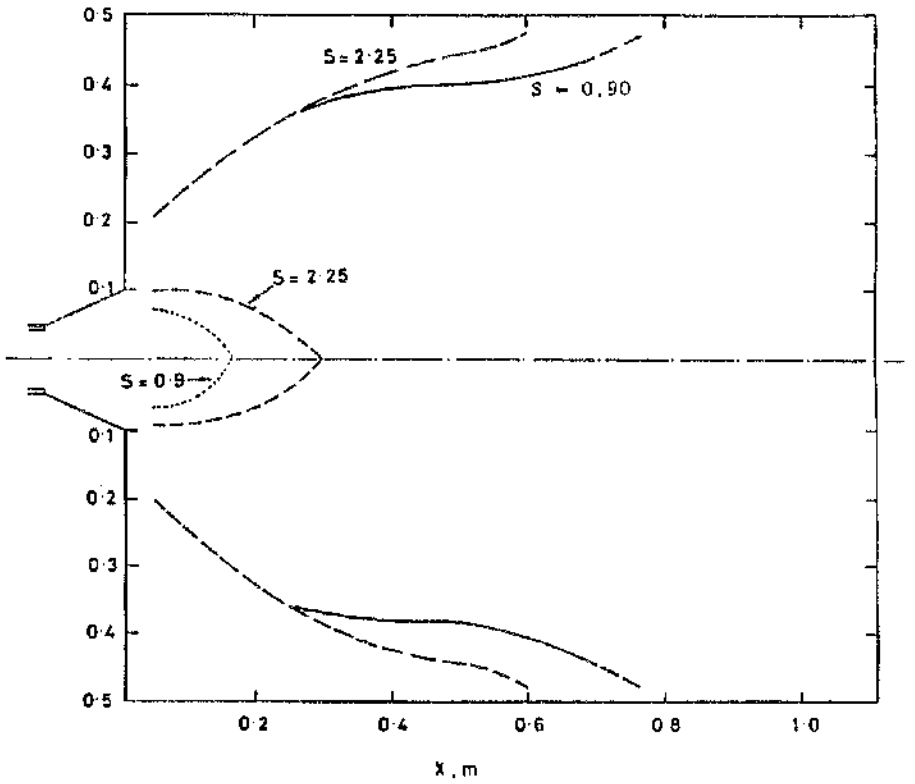

FIG 4.12: Flow boundaries, peripheral fuel injection, Scheme 1

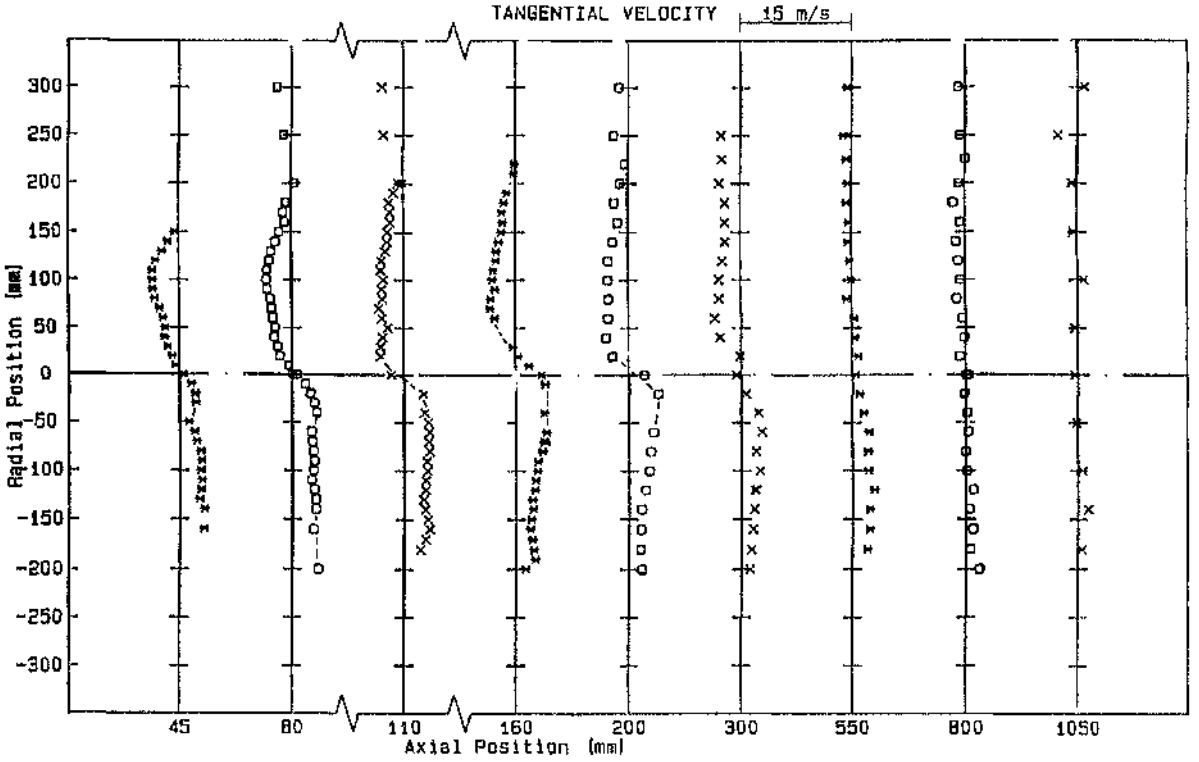

(a) S = 0.90

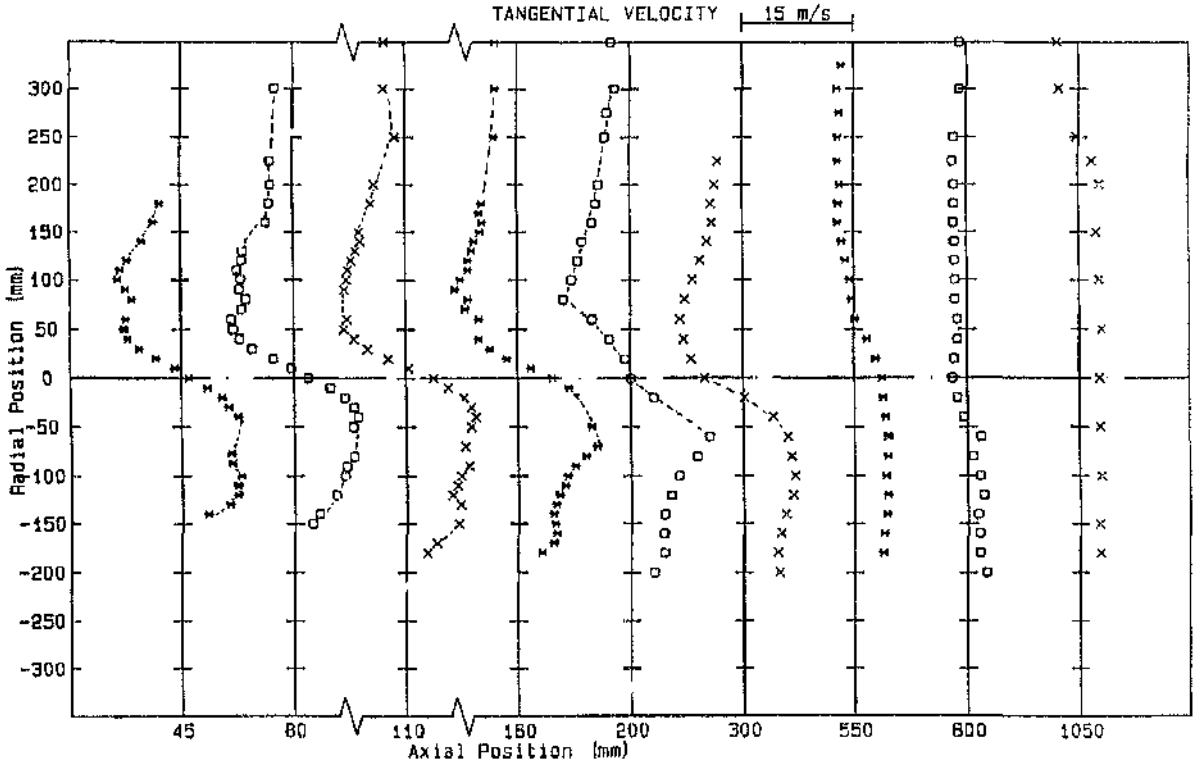

(b) S = 2.25

FIG 4.13: Tangential velocity profiles, peripheral fuel injection, Scheme 1

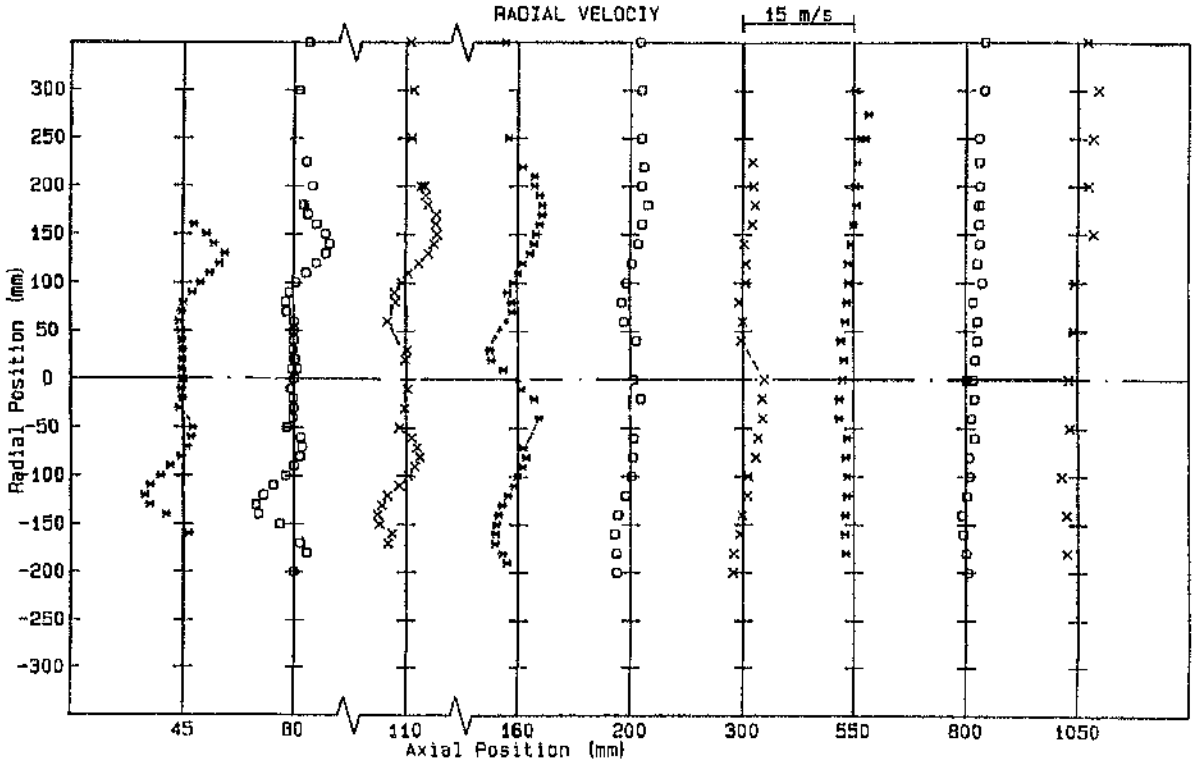

(a) S = 0.90

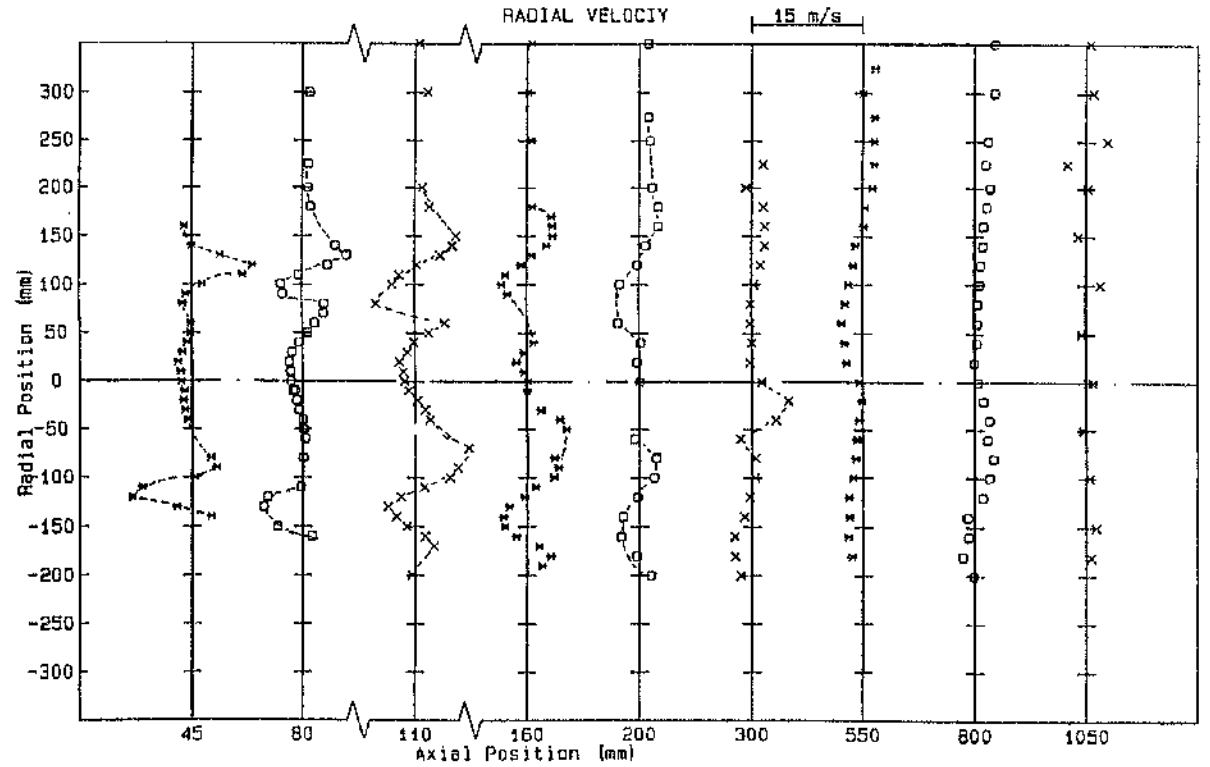

(b) S = 2.25

FIG 4.14: Radial velocity profiles, peripheral fuel injection, Scheme 1

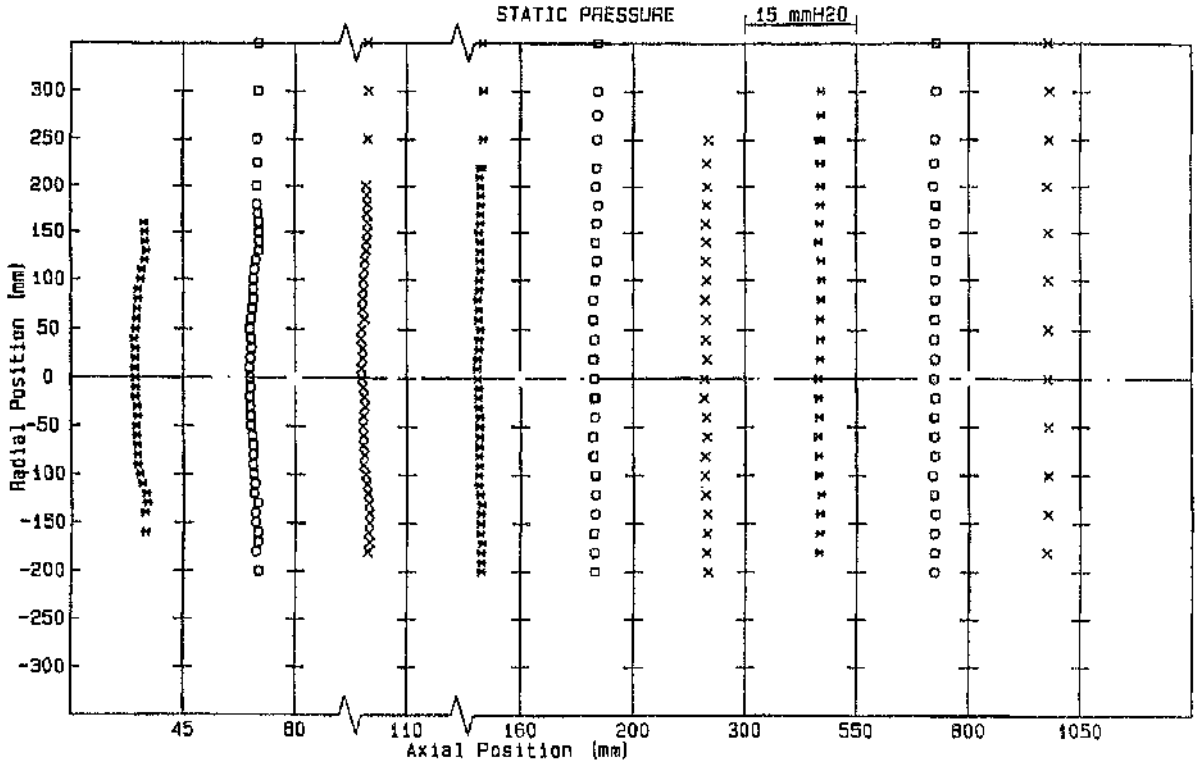

(a) S = 0.90

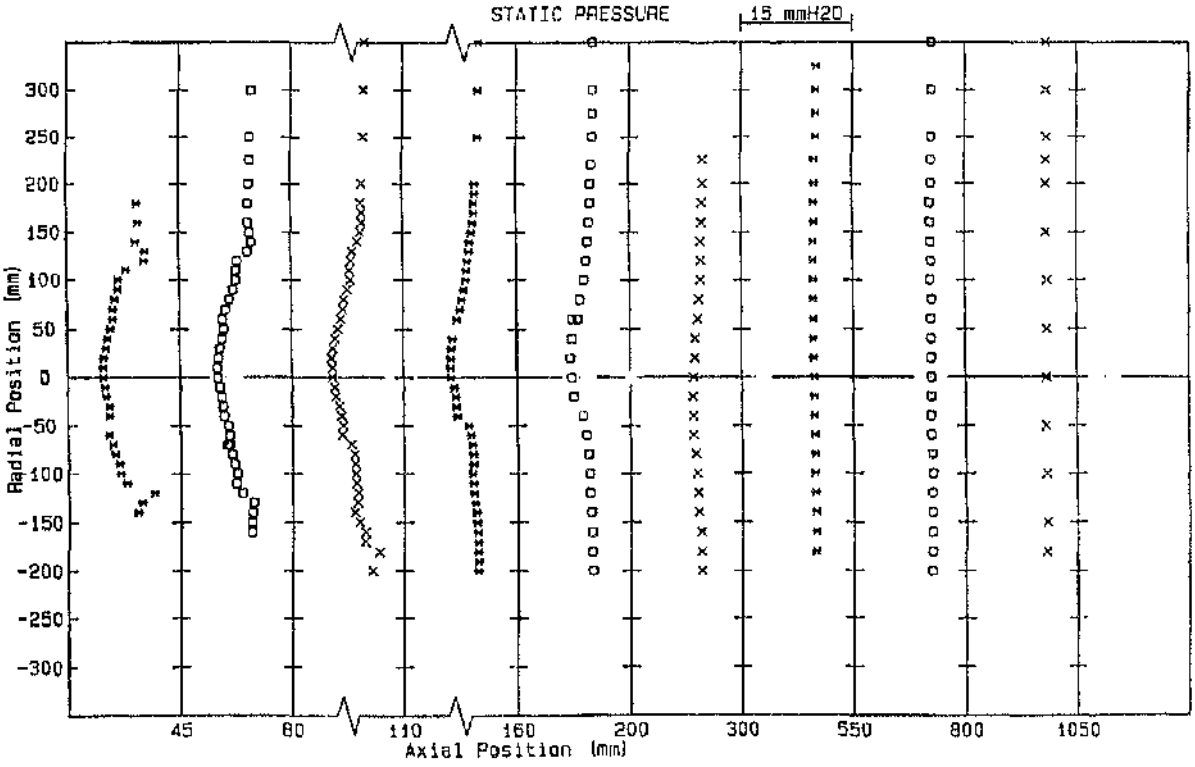

(b) S = 2.25

FIG 4.15: Static pressure profiles, peripheral fuel injection, Scheme 1

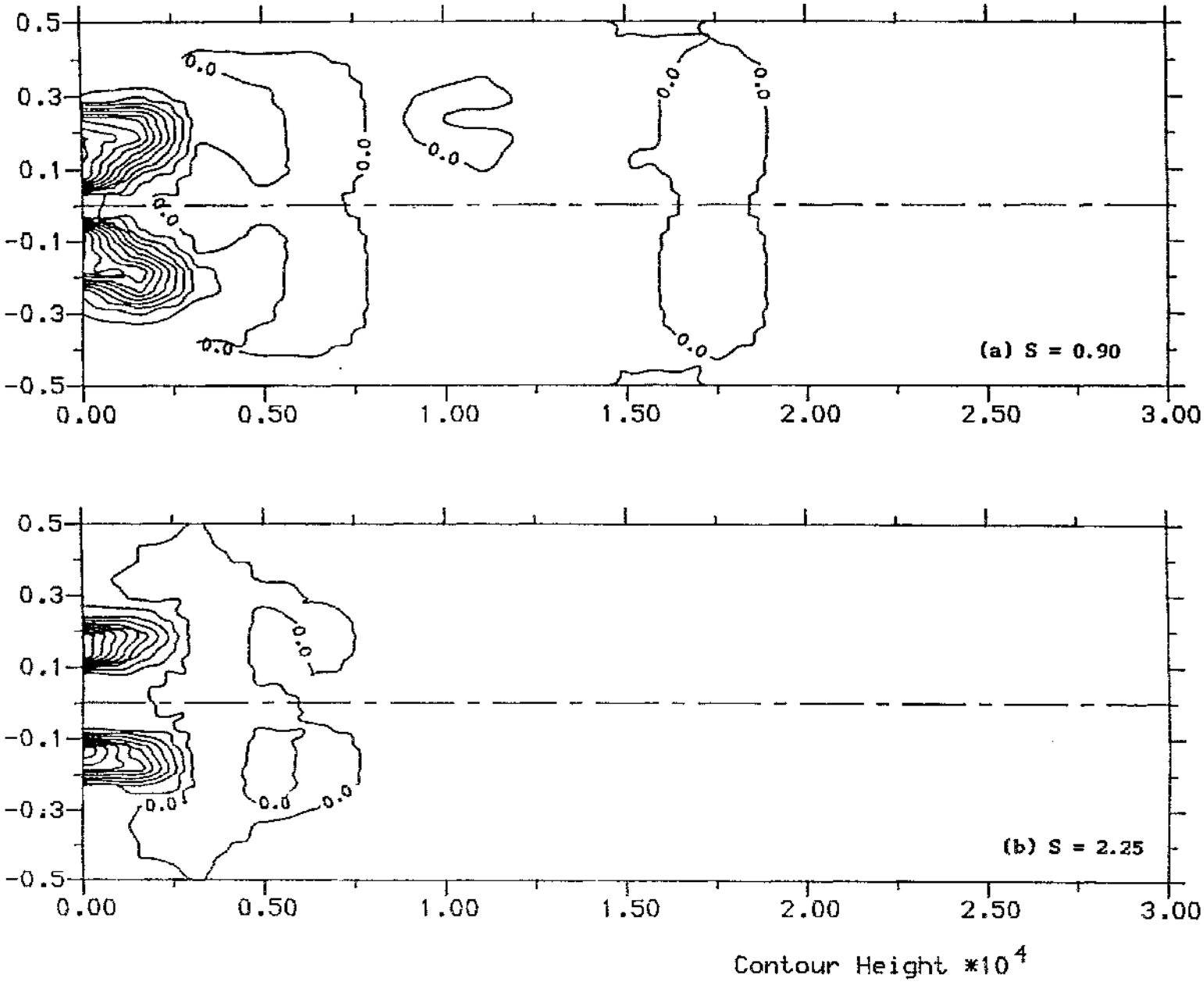

FIG 4.16: HC contours, peripheral fuel injection, Scheme 1

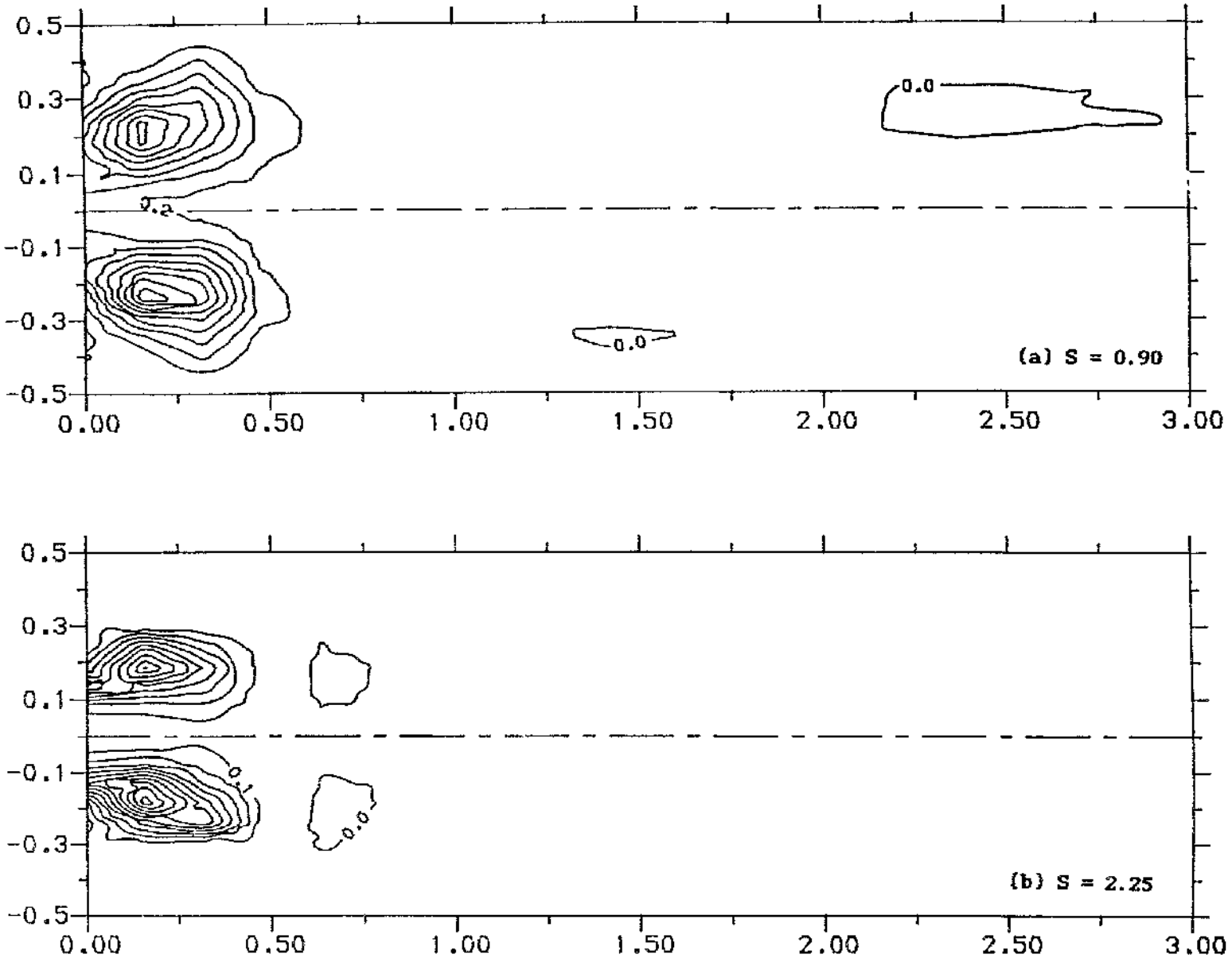

FIG 4.17: CO contours, peripheral fuel injection, Scheme 1

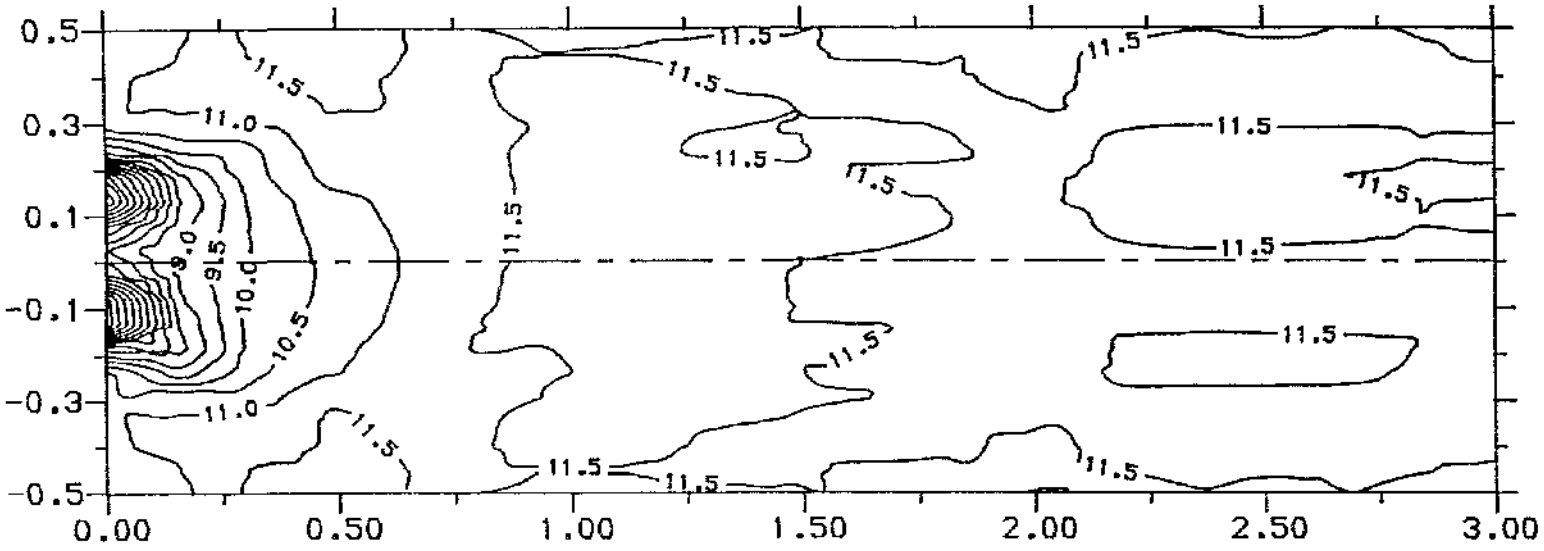

(a) S = 0.90

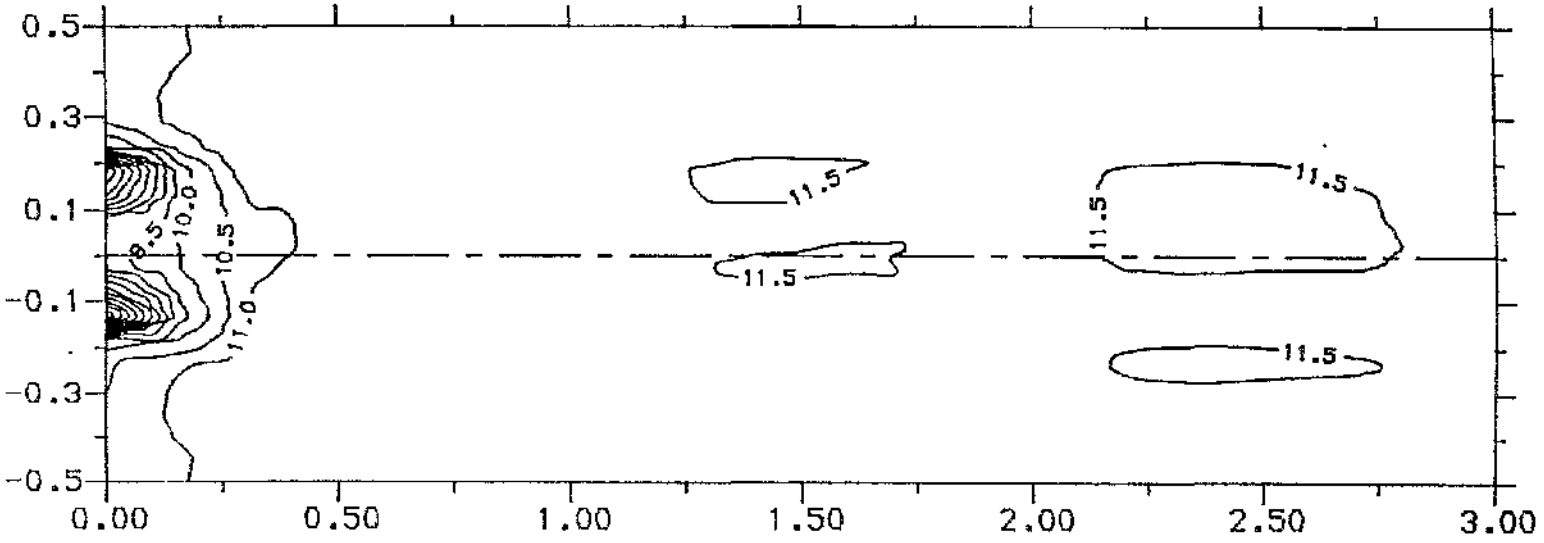

(b) S = 2.25

FIG 4.18: CO_2 contours, peripheral fuel injection, Scheme 1

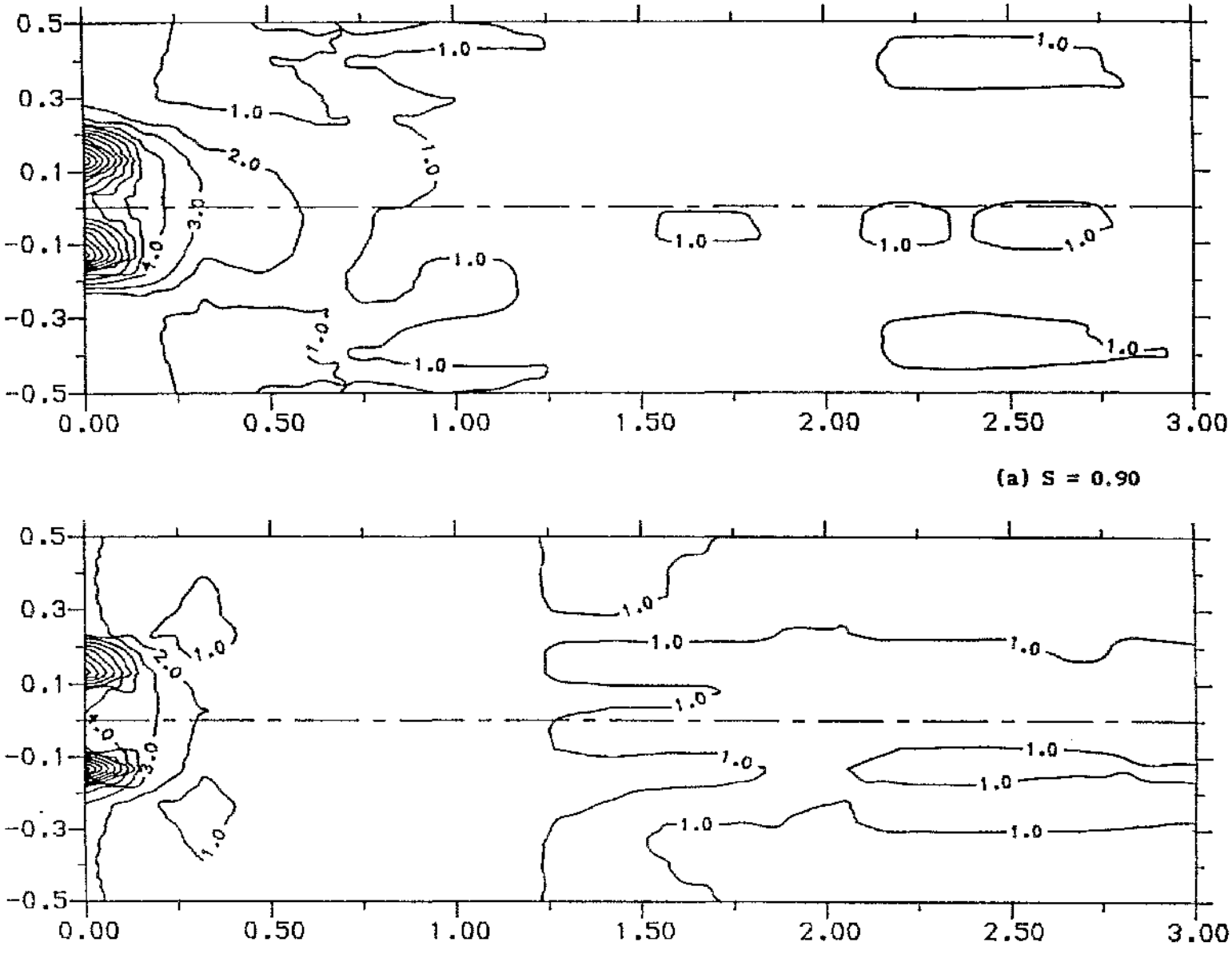

FIG 4.19: O2 contours, peripheral fuel injection, Scheme 1

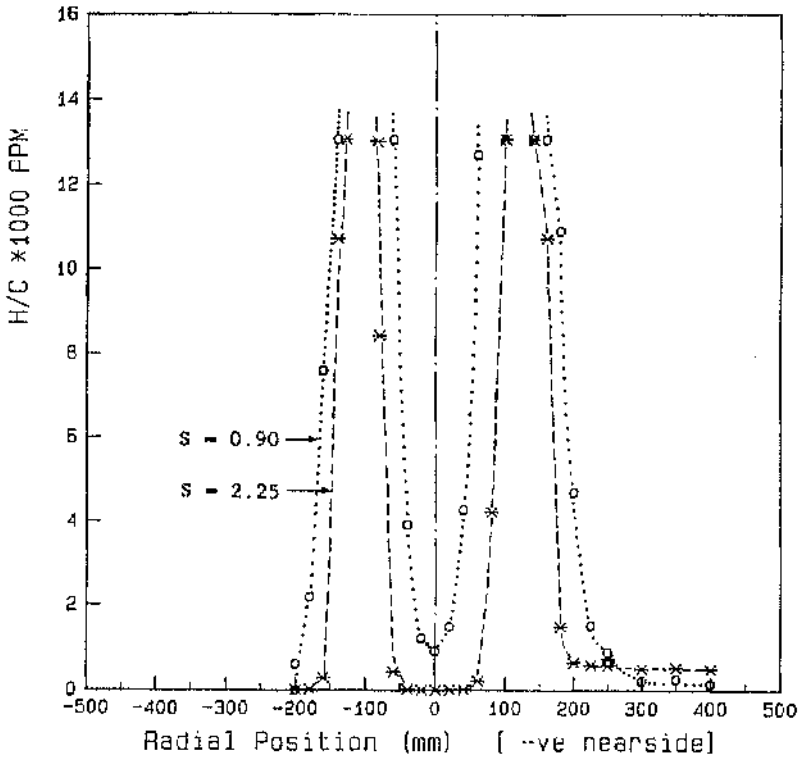

(a) X = 45 mm

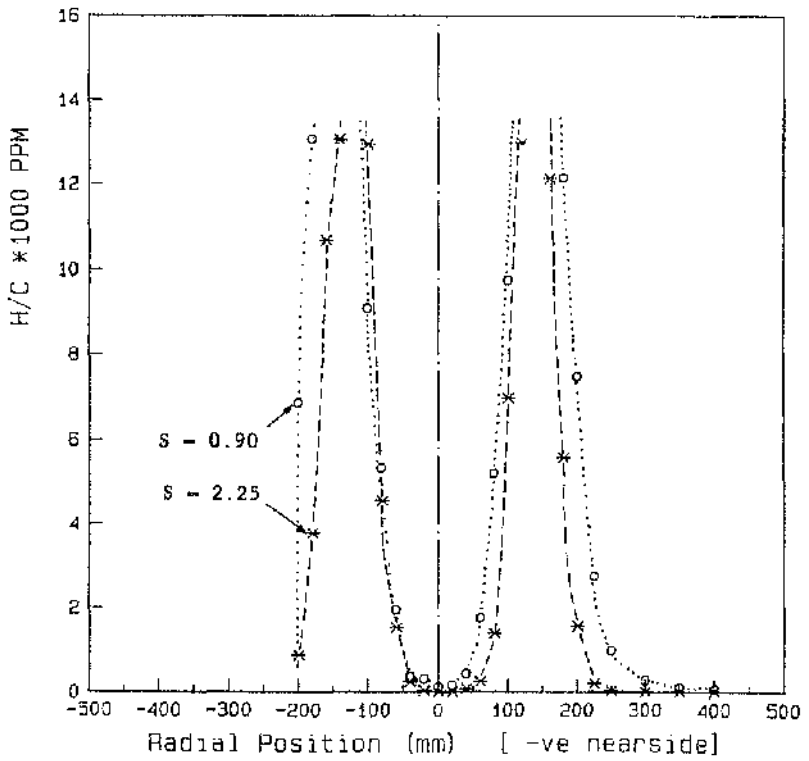

(b) X = 160 mm

FIG 4.20: Radial HC profiles, peripheral fuel injection, Scheme 1

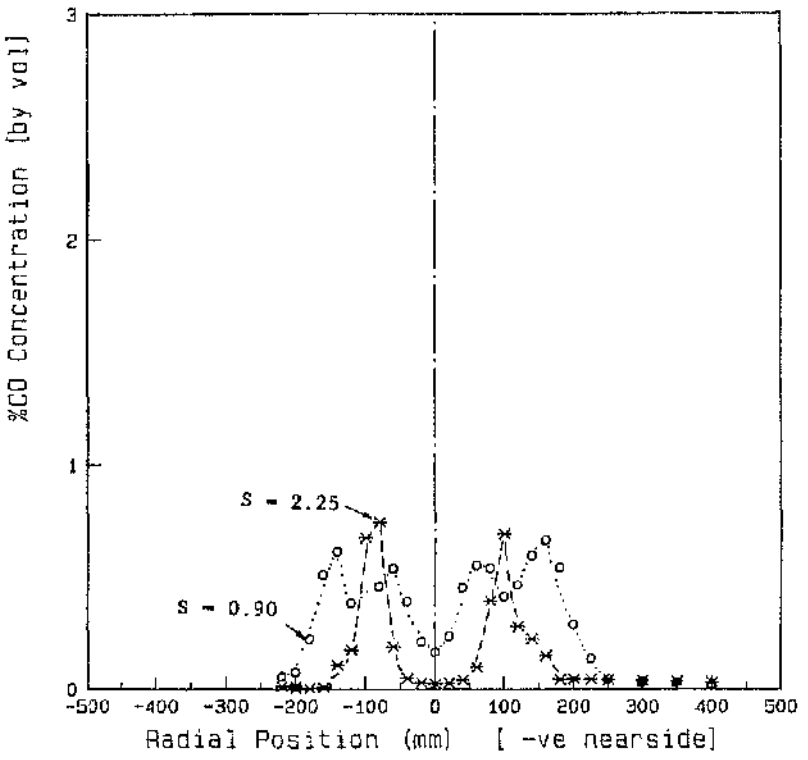

(a) X = 45 mm

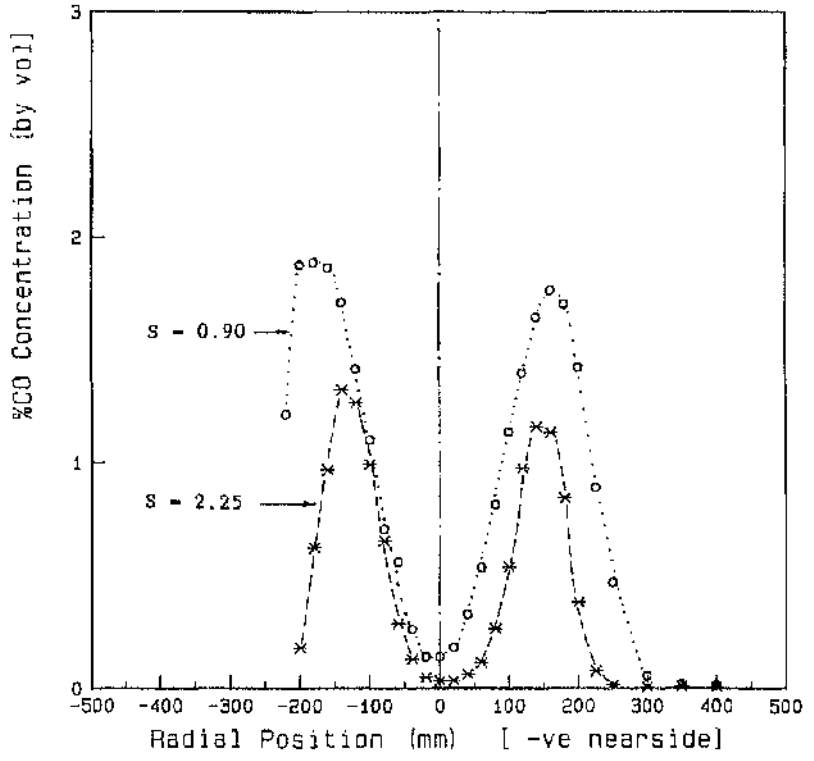

(b) X = 160 mm

FIG 4.21: Radial CO profiles, peripheral fuel injection, Scheme 1

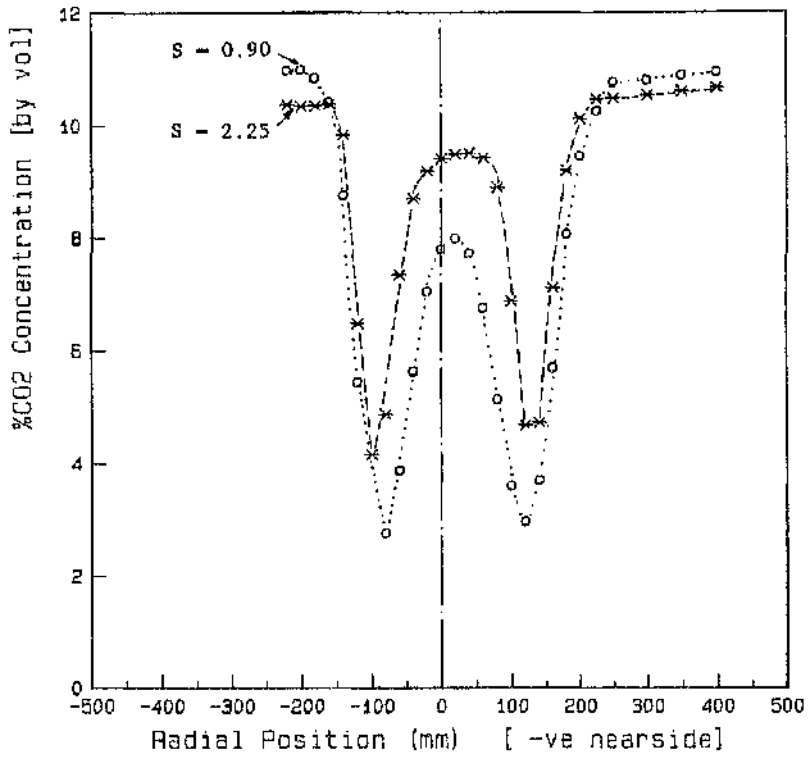

(a) X = 45 mm

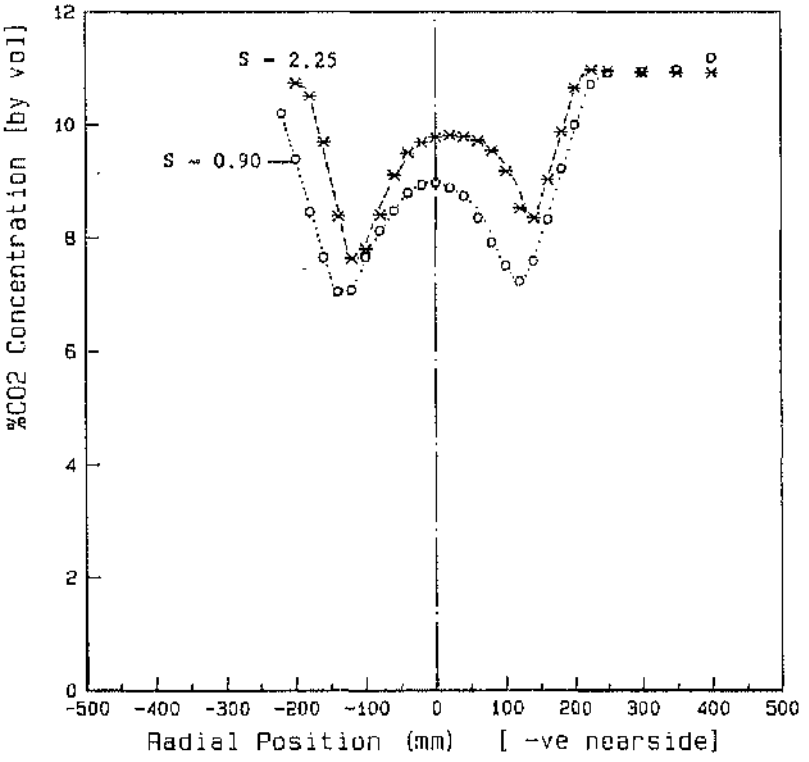

(b) X = 160 mm

FIG 4.22: Radial CO_2 profiles, peripheral fuel injection, Scheme 1

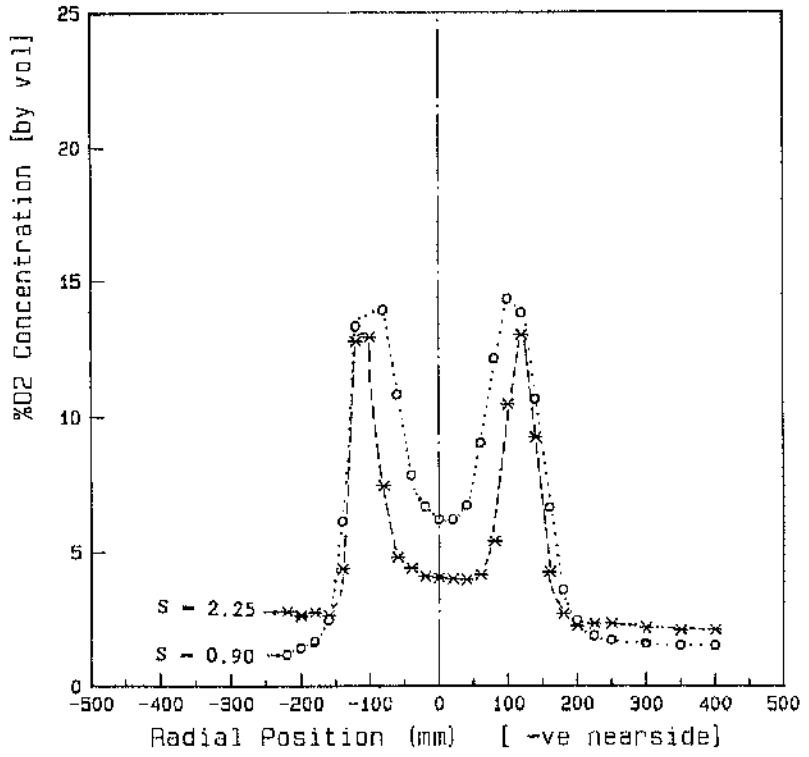

(a) X = 45 mm

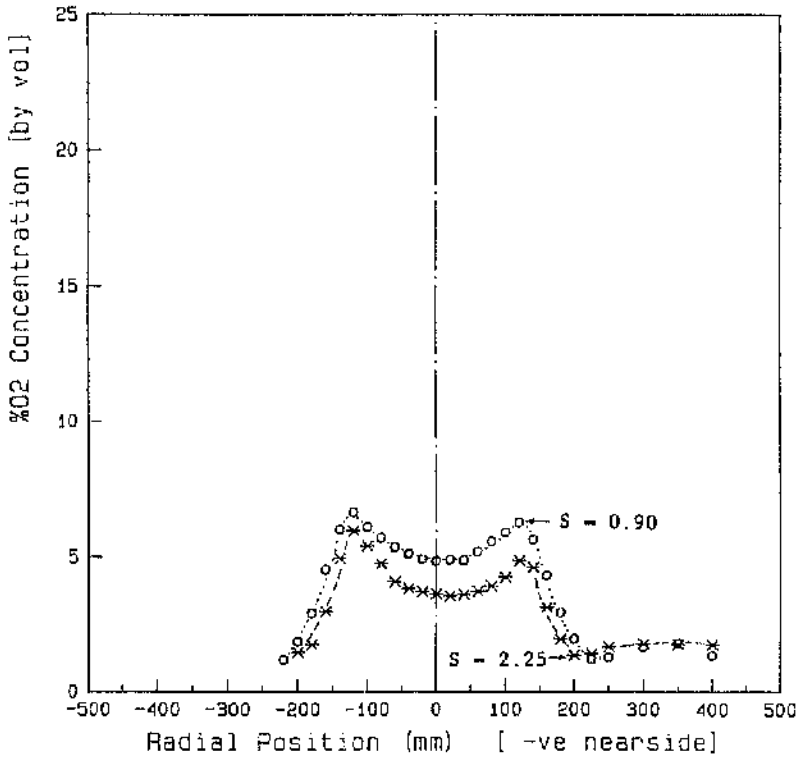

(b) X = 160 mm

FIG 4.23: Radial O_2 profiles, peripheral fuel injection, Scheme 1

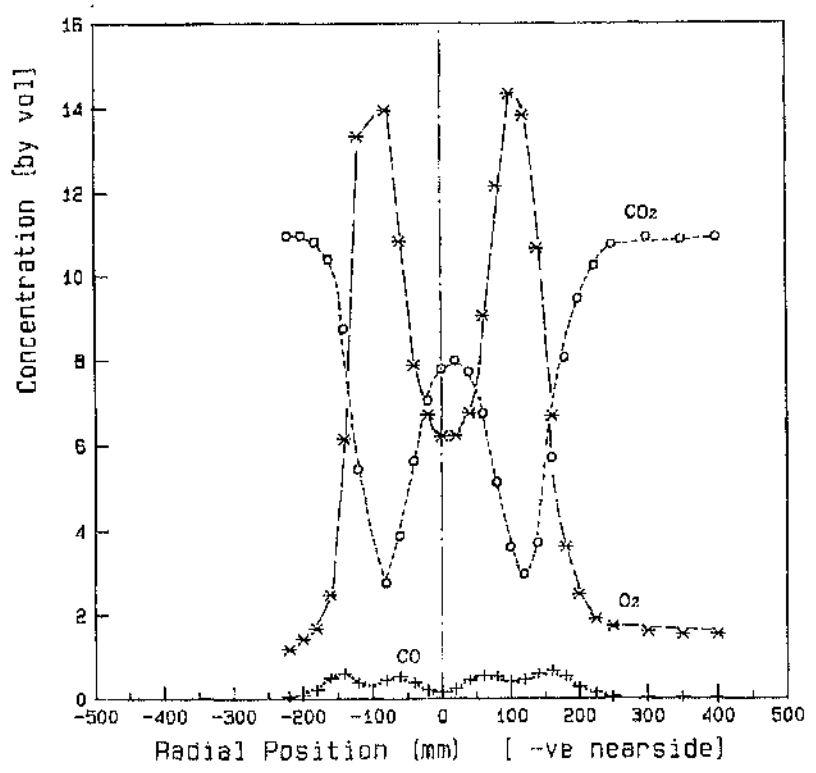

(a) S = 0.90

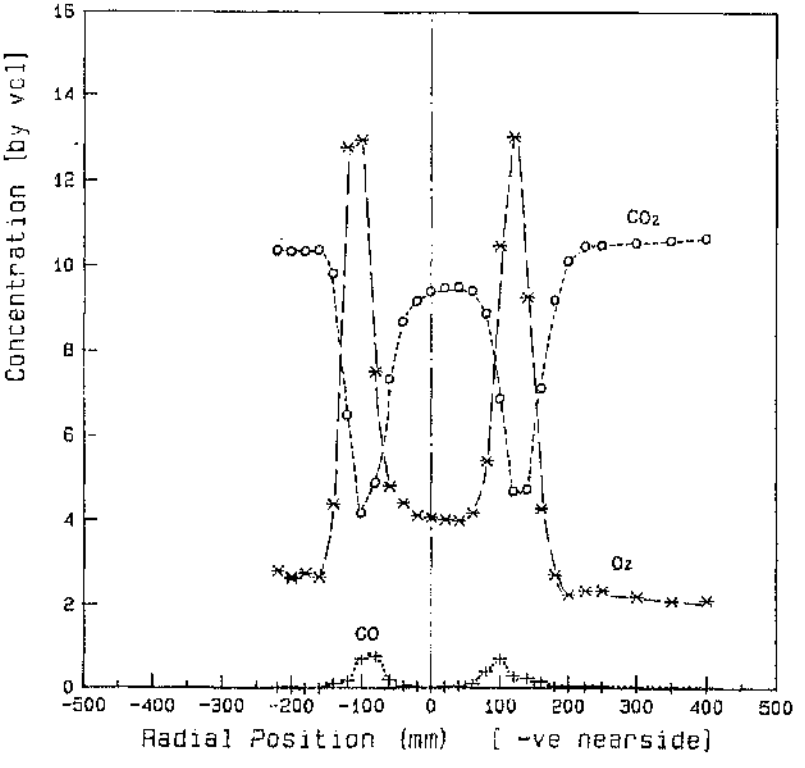

(b) S = 2.25

FIG 4.24: Sample concentration profiles, X = 45 mm, peripheral fuel injection, Scheme 1

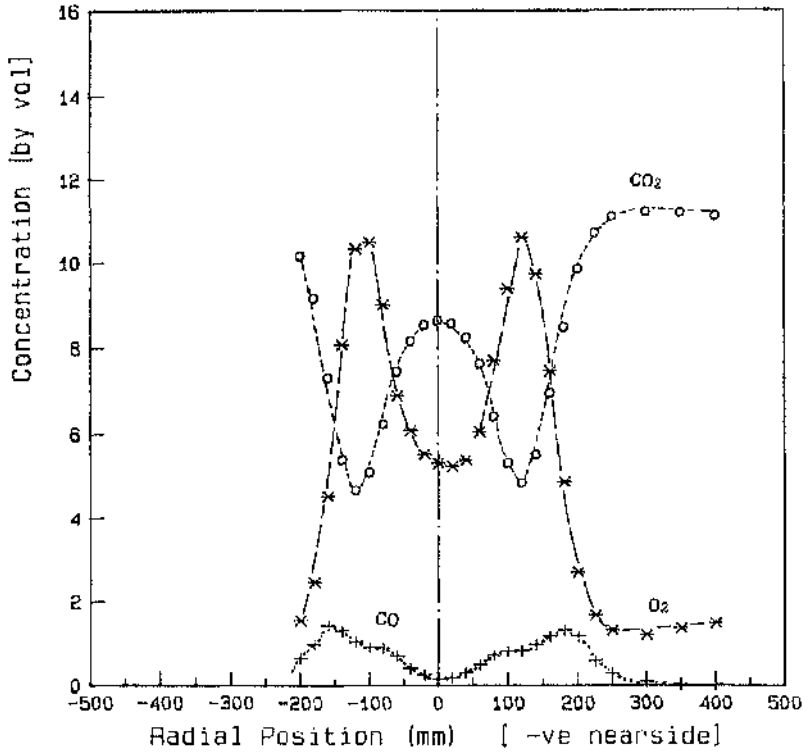

(a) S = 0.90

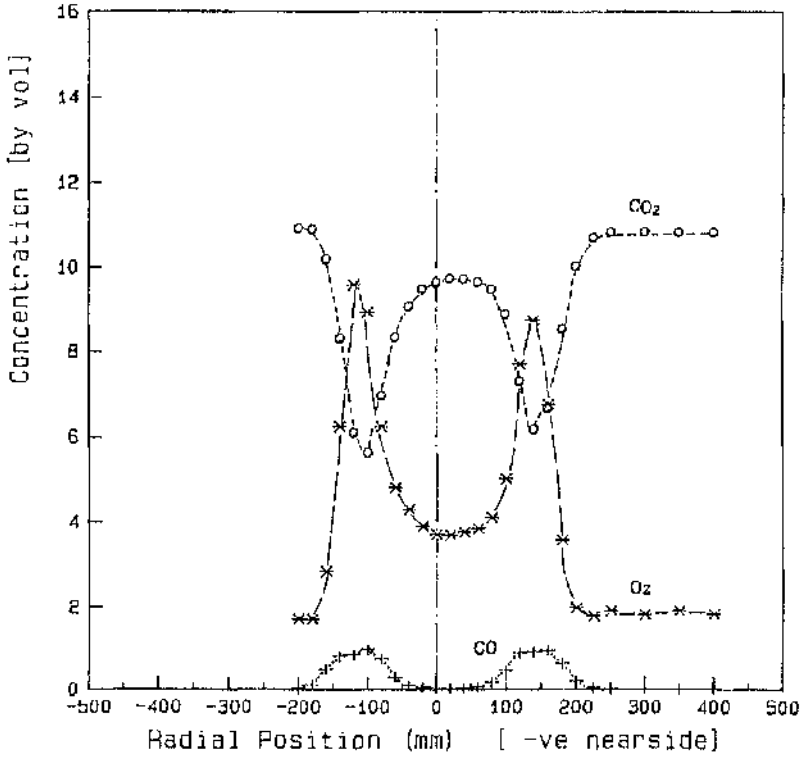

(b) S = 2.25

FIG 4.25: Sample concentration profiles, X = 110 mm, peripheral fuel injection, Scheme 1

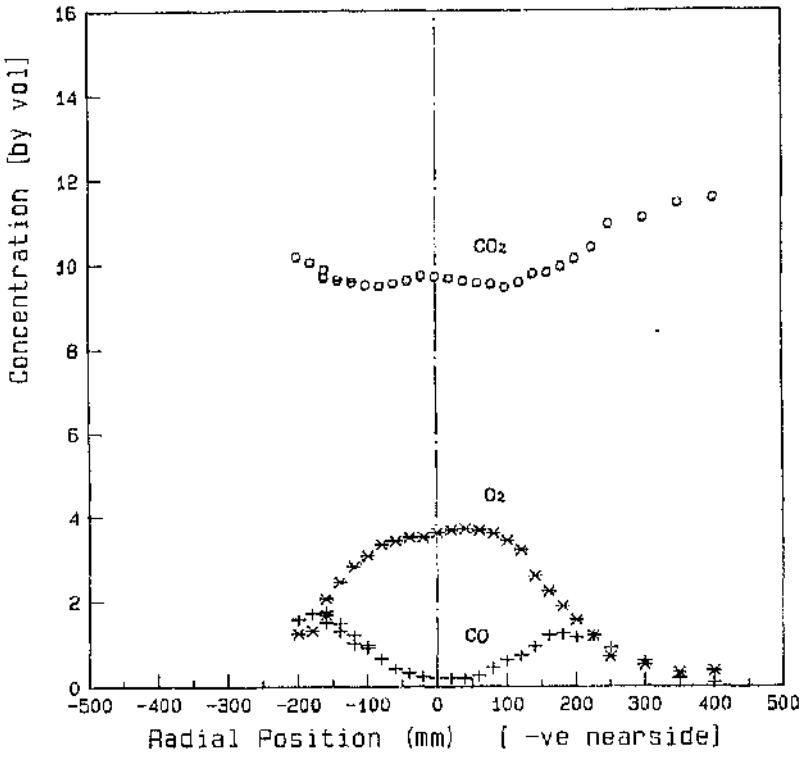

(a) S = 0.90

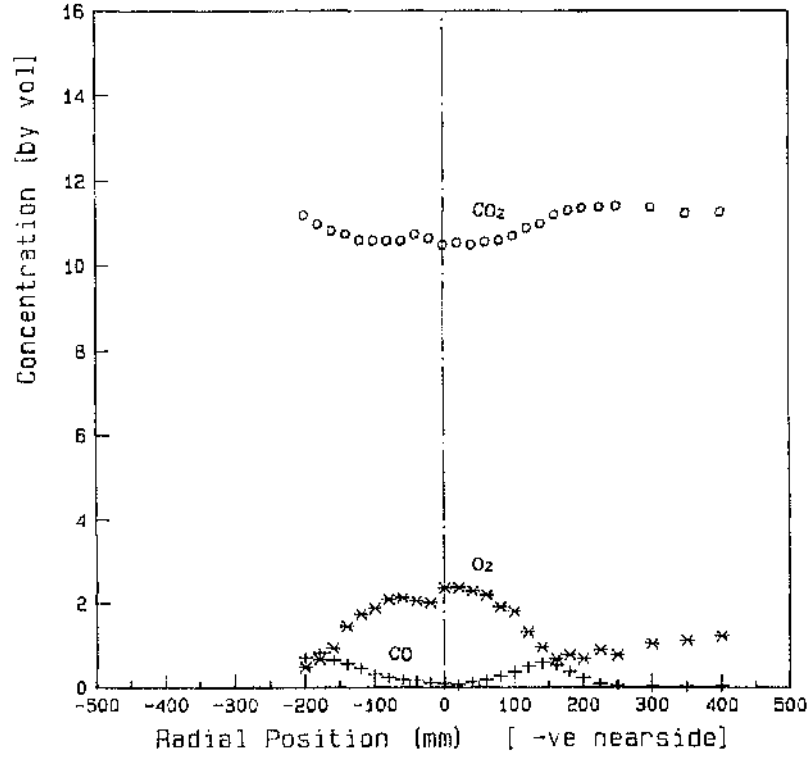

(b) S = 2.25

FIG 4.26: Sample concentration profiles, X = 300 mm, peripheral fuel injection, Scheme 1

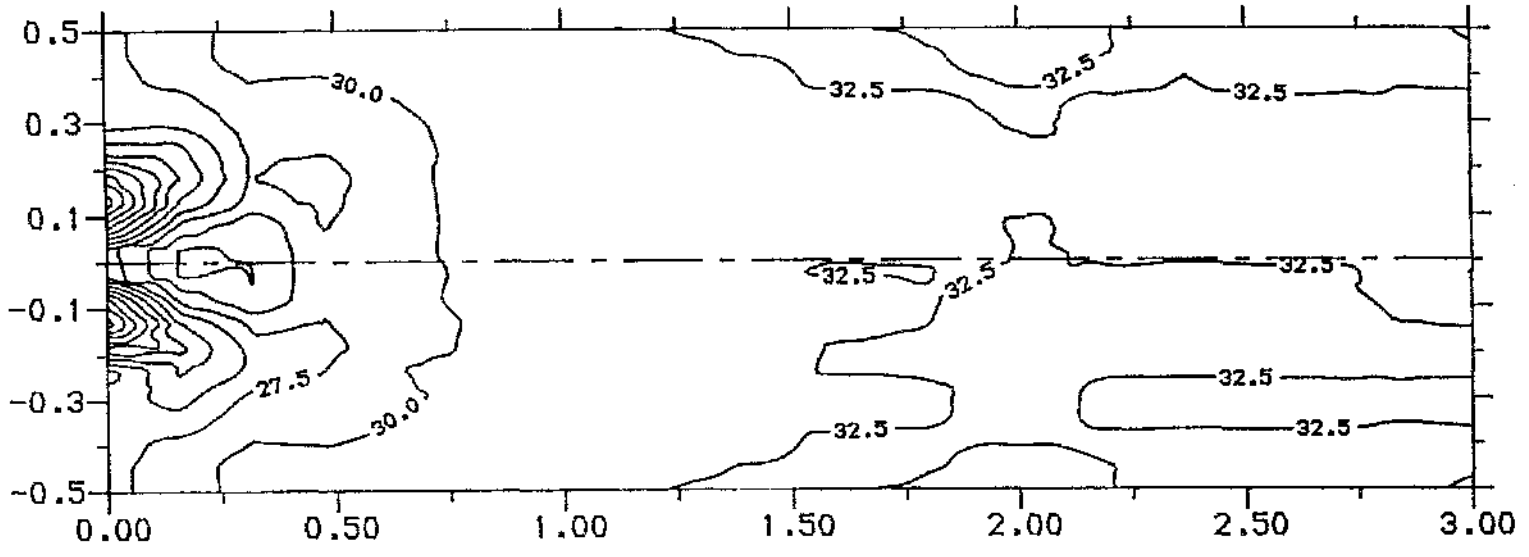

(a) S = 0.90

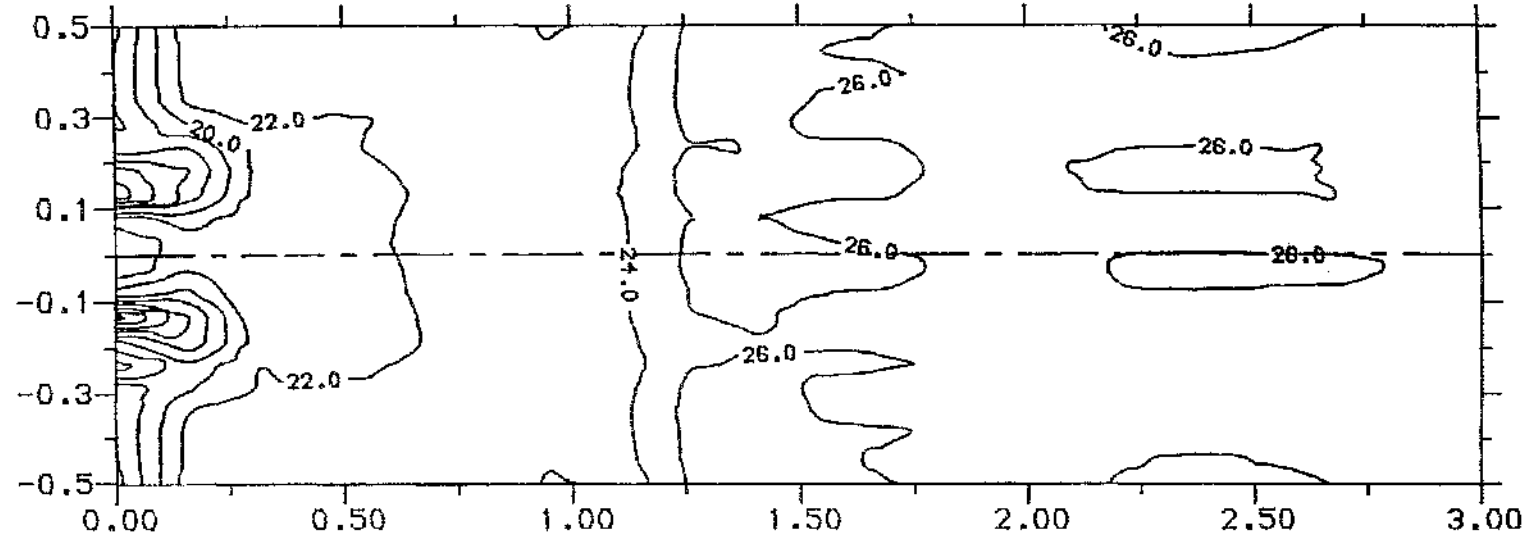

(b) S = 2.25

FIG 4.27: NOx contours, peripheral fuel injection, Scheme 1

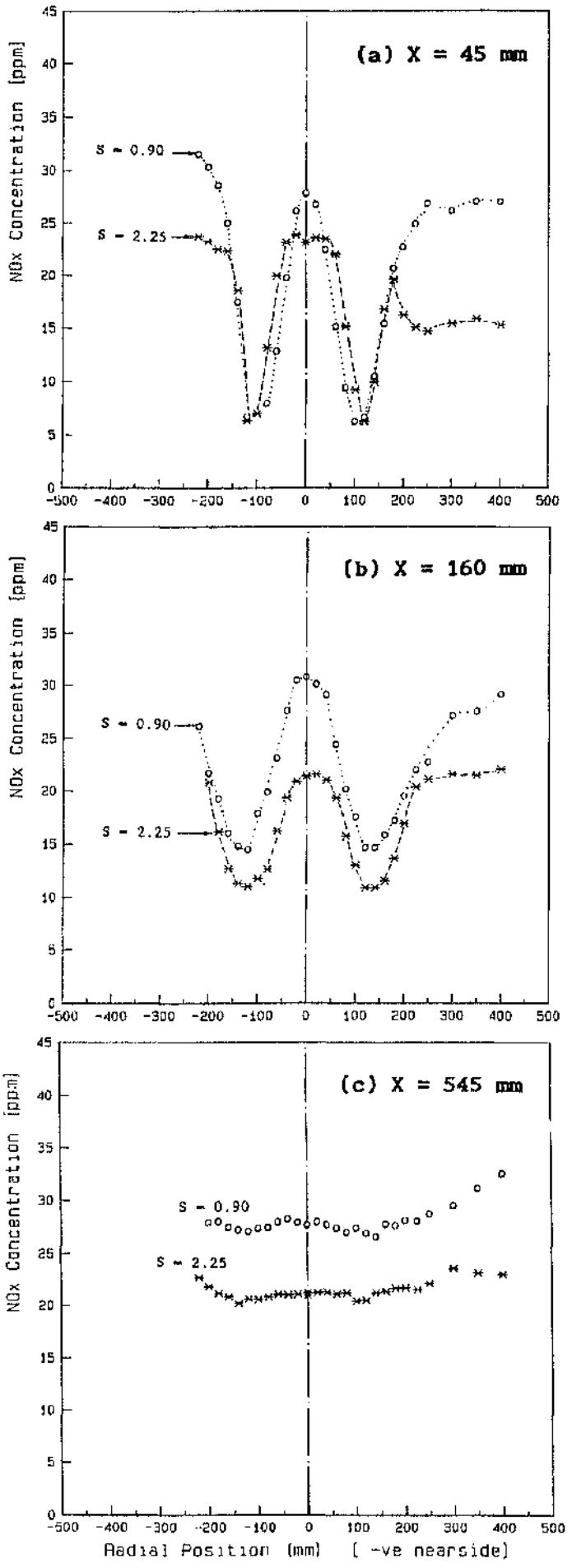

FIG 4.28: Radial NOx profiles, peripheral fuel injection, Scheme 1

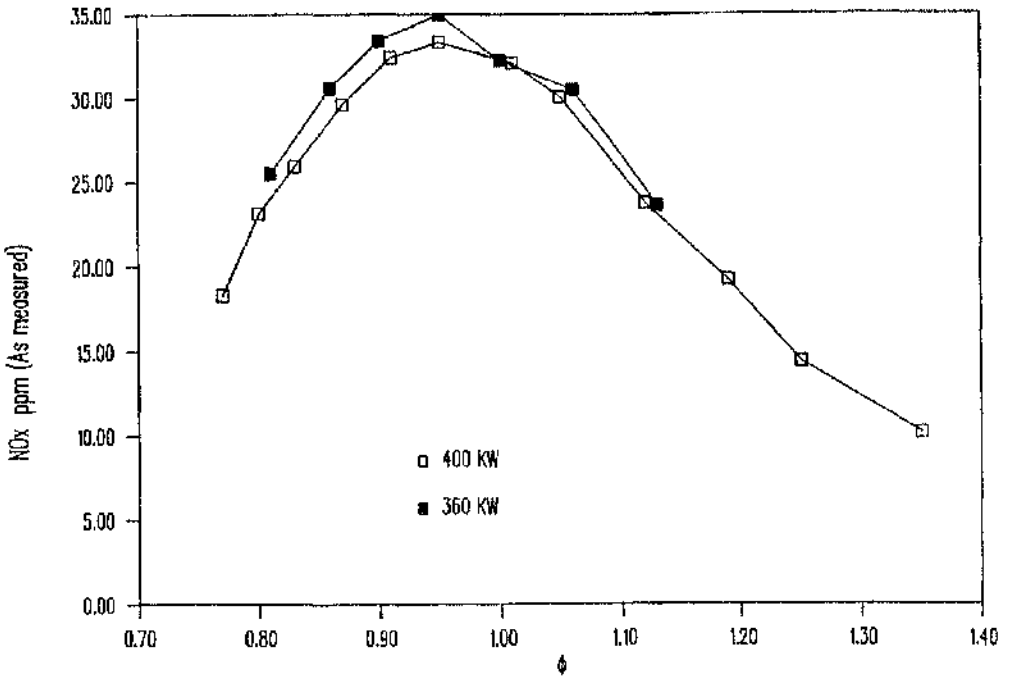

(a) S = 0.90

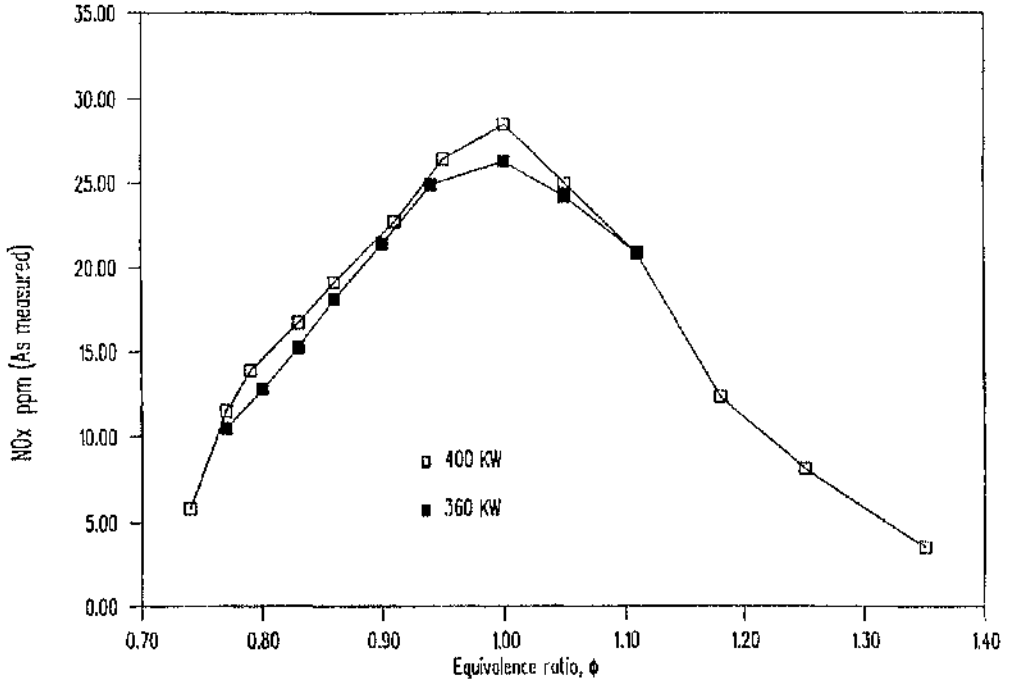

(b) S = 2.25

FIG 4.29: Effect of firing rate on overall NOx concentrations, peripheral fuel injection, Scheme 1

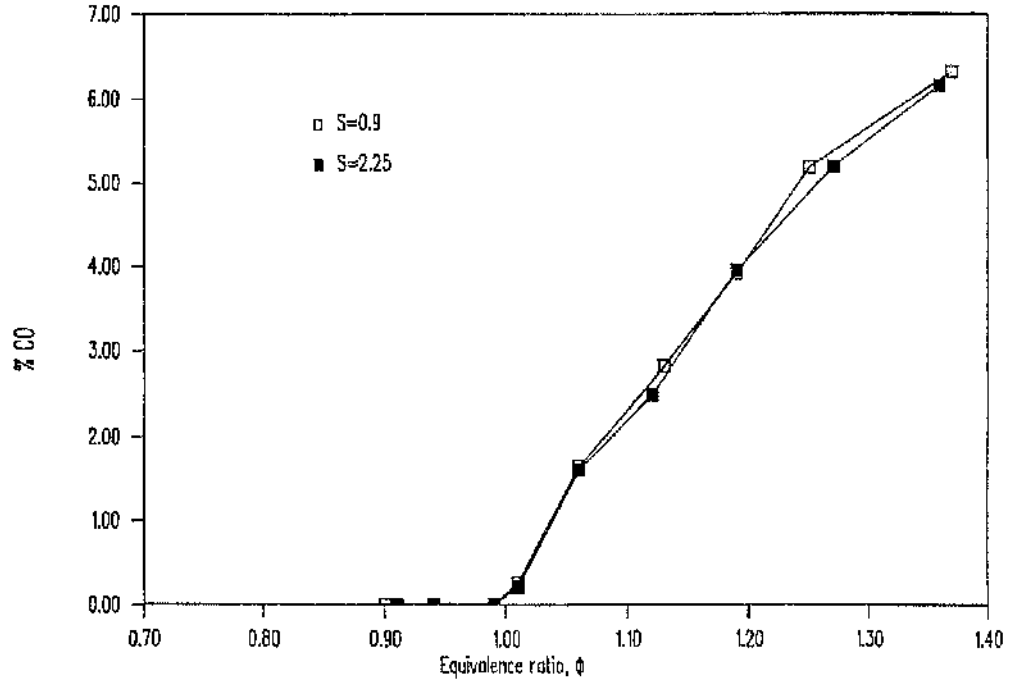

FIG 4.30: Variation of overall CO concentrations with ϕ peripheral fuel injection, Scheme 1

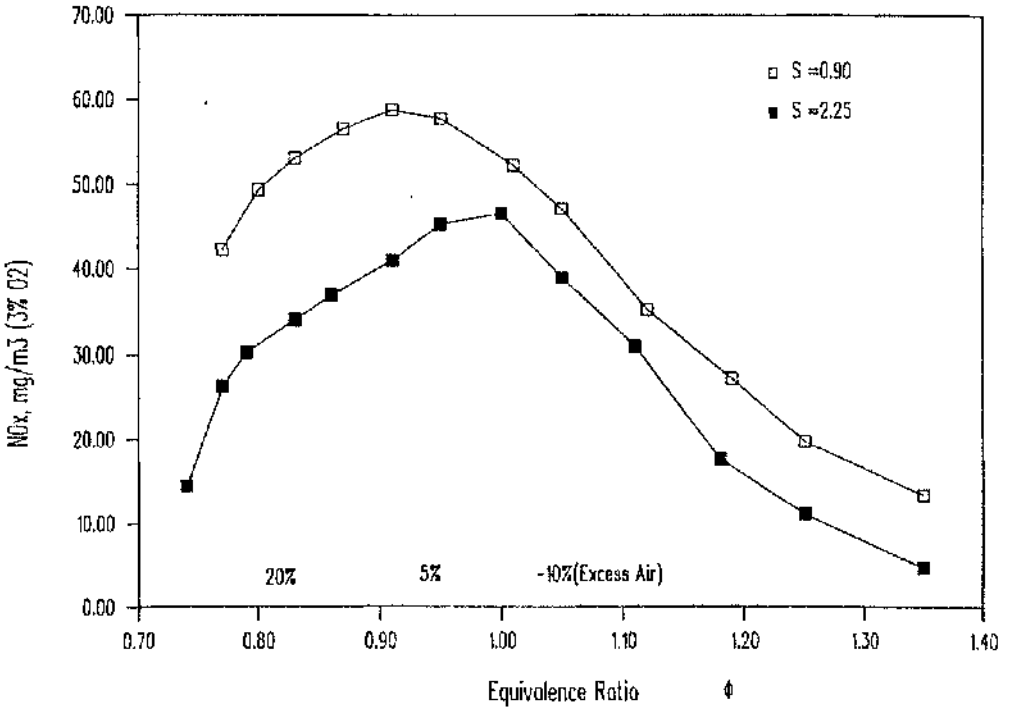

FIG 4.31: Variation of overall NOx concentrations (corrected to 3% O_2) with ϕ peripheral fuel injection, Scheme 1

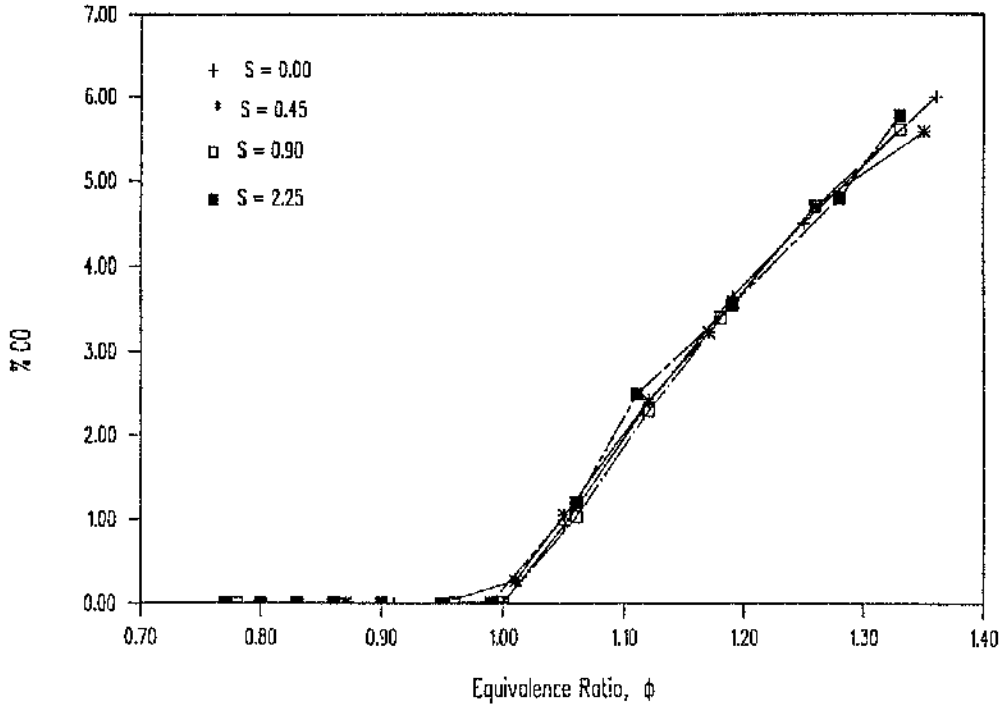

FIG 4.32: Variation of overall CO concentrations with ϕ peripheral fuel injection, Scheme 2

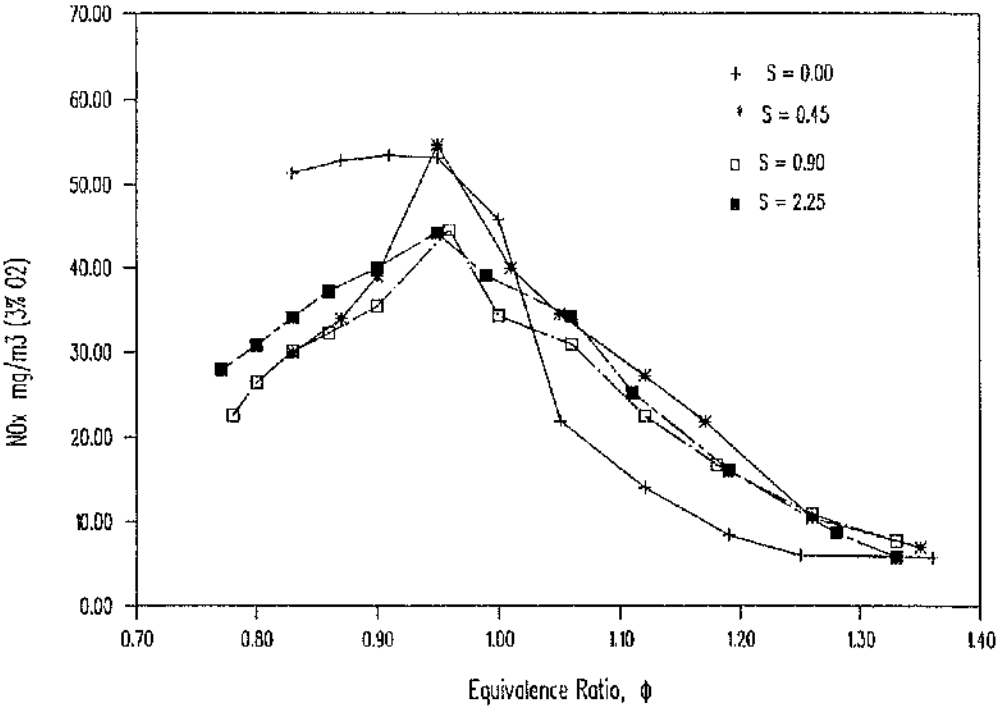

FIG 4.33: Variation of overall NOx concentrations (corrected to 3% O2) with ϕ peripheral fuel injection, Scheme 2

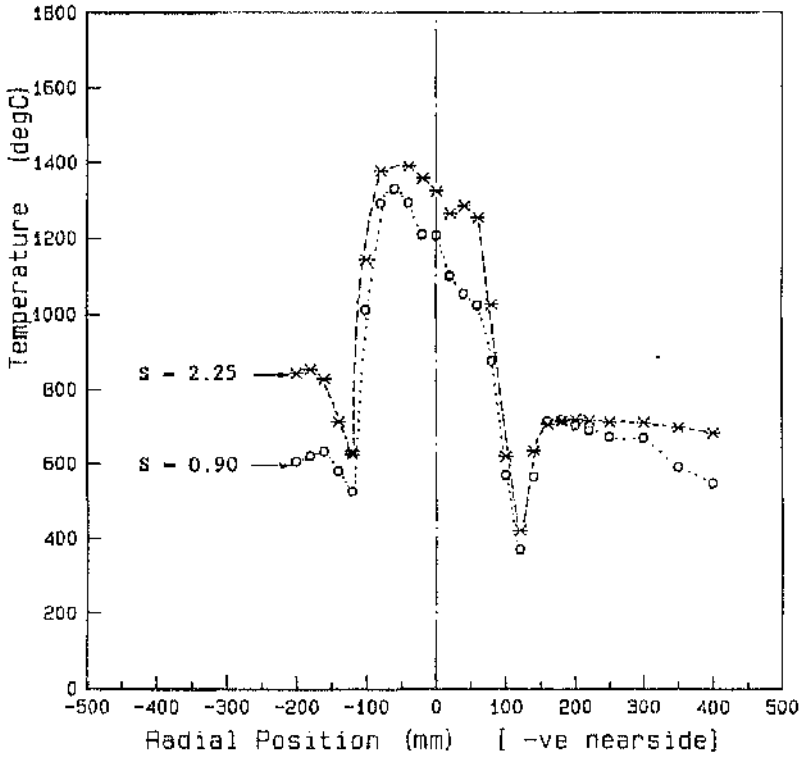

(a) X = 45 mm

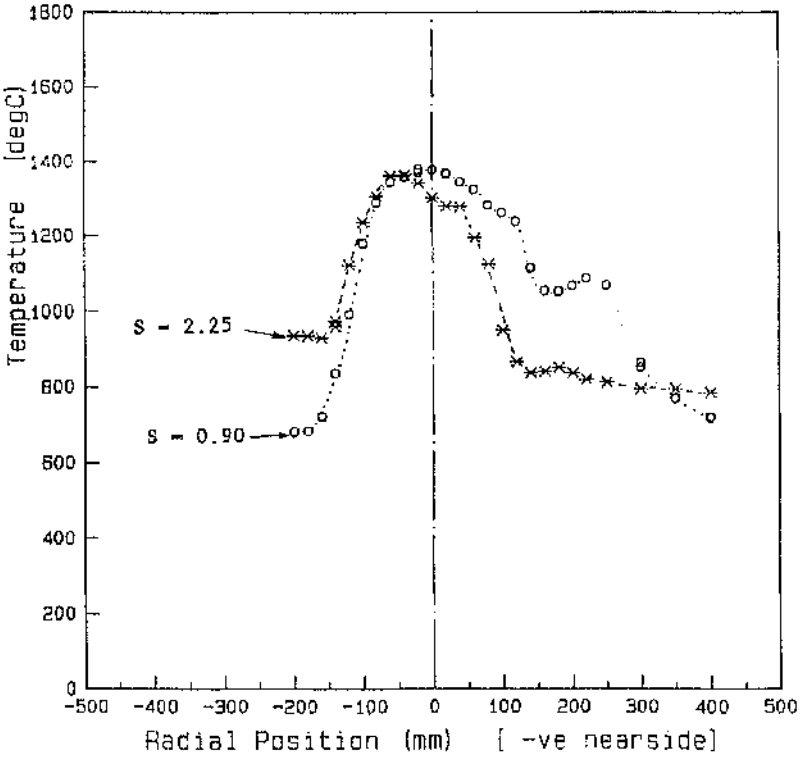

(b) X = 200 mm

FIG 4.34: Radial temperature profiles, central axial fuel injection

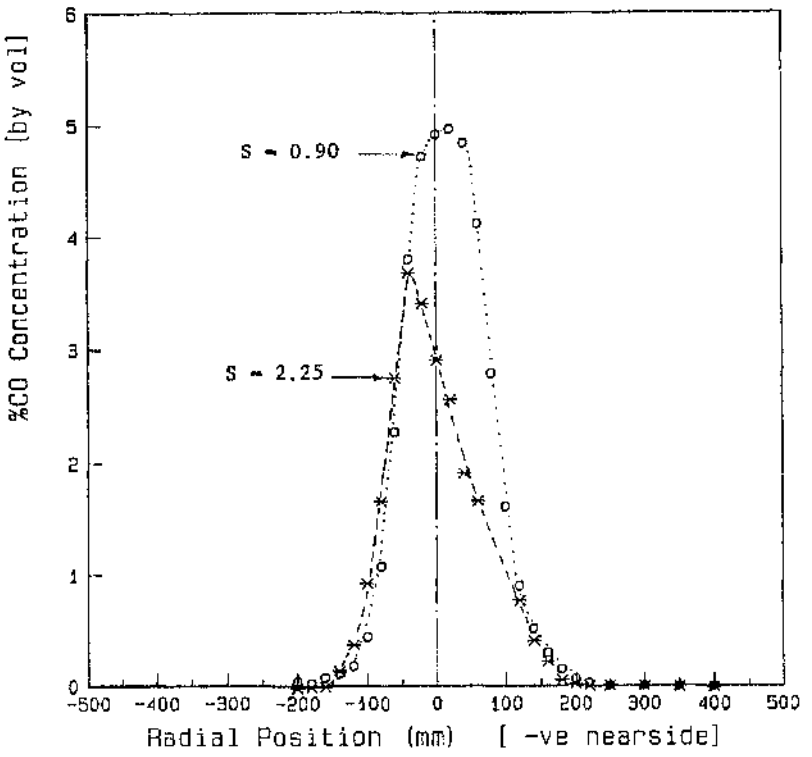

(a) X = 45 mm

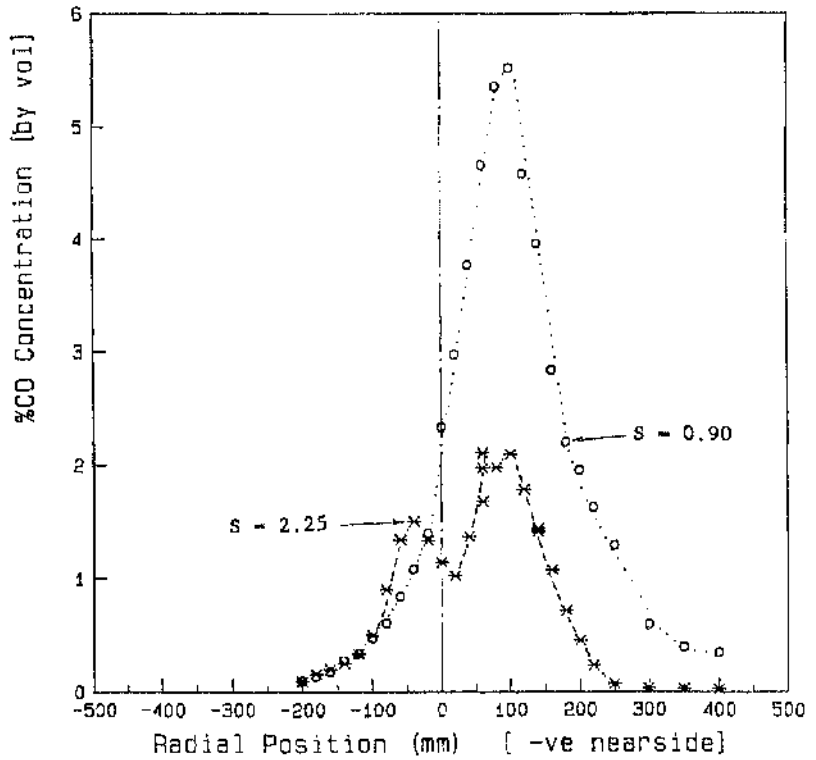

(b) X = 200 mm

FIG 4.35: Radial CO profiles, central axial fuel injection

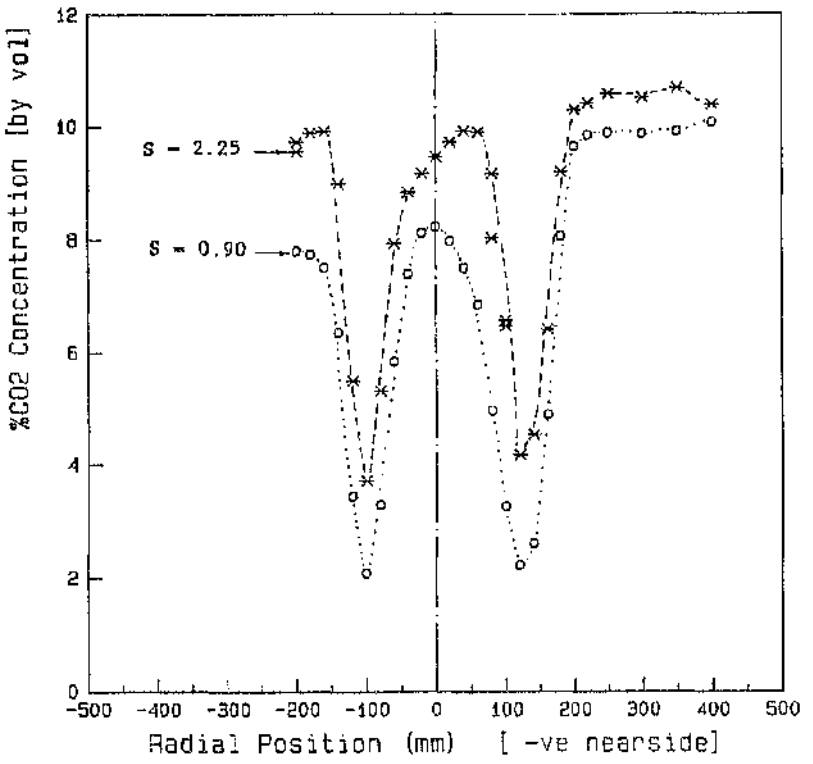

(a) X = 45 mm

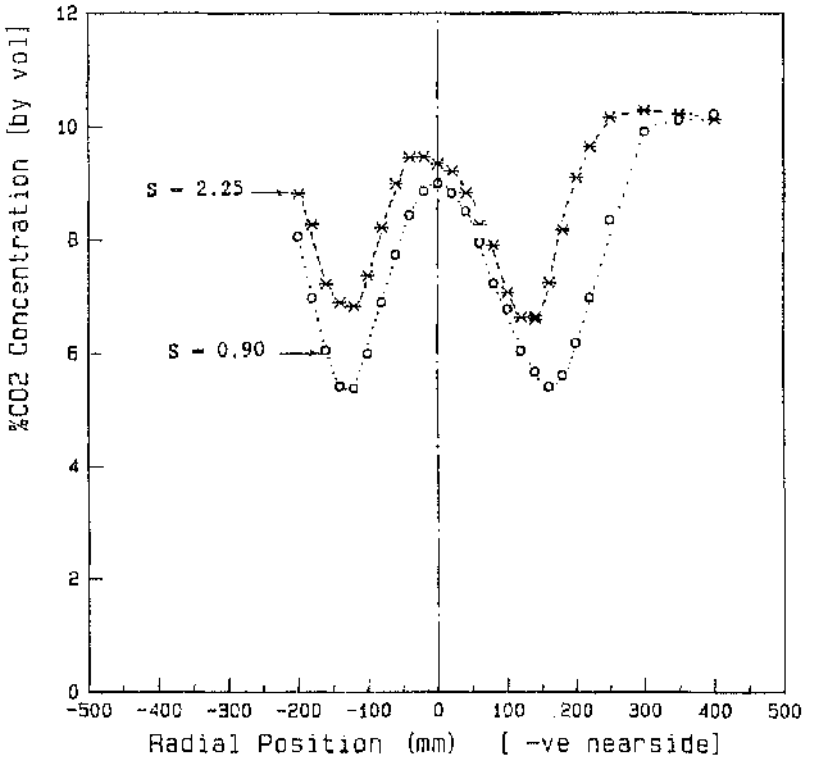

(b) X = 200 mm

FIG 4.36: Radial CO_2 profiles, central axial fuel injection

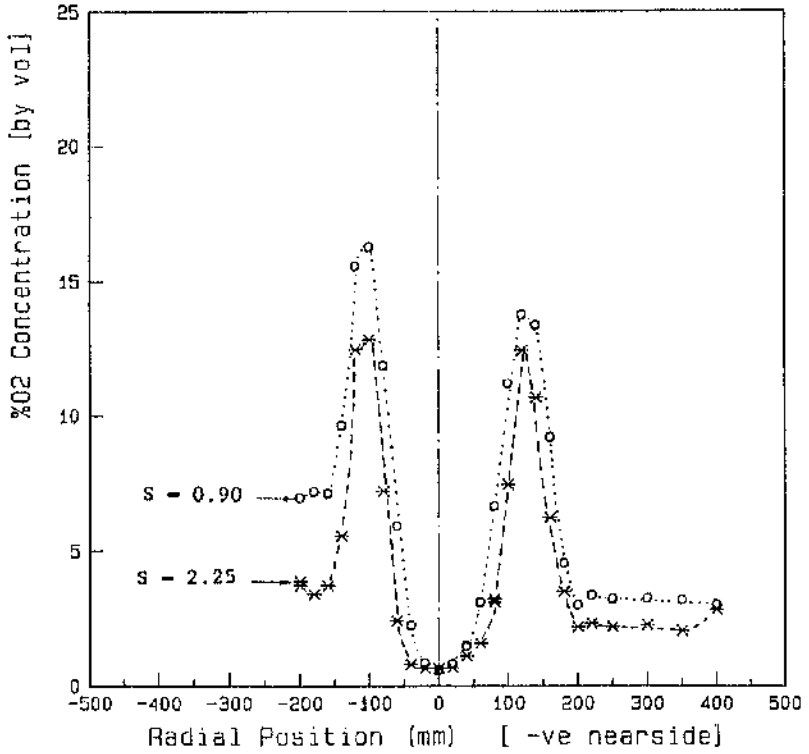

(a) X = 45 mm

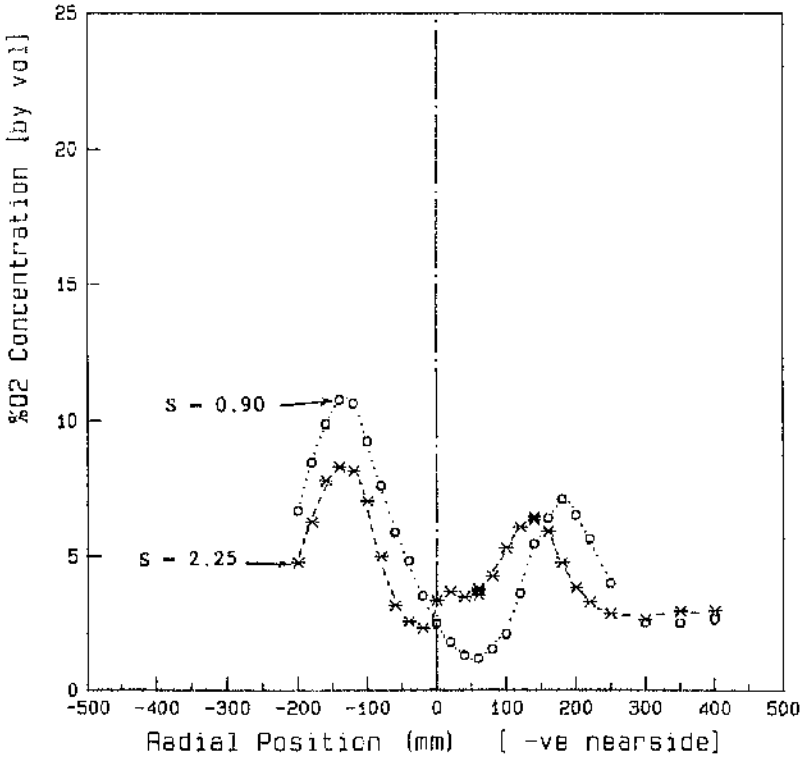

(b) X = 200 mm

FIG 4.37: Radial O2 profiles, central axial fuel injection

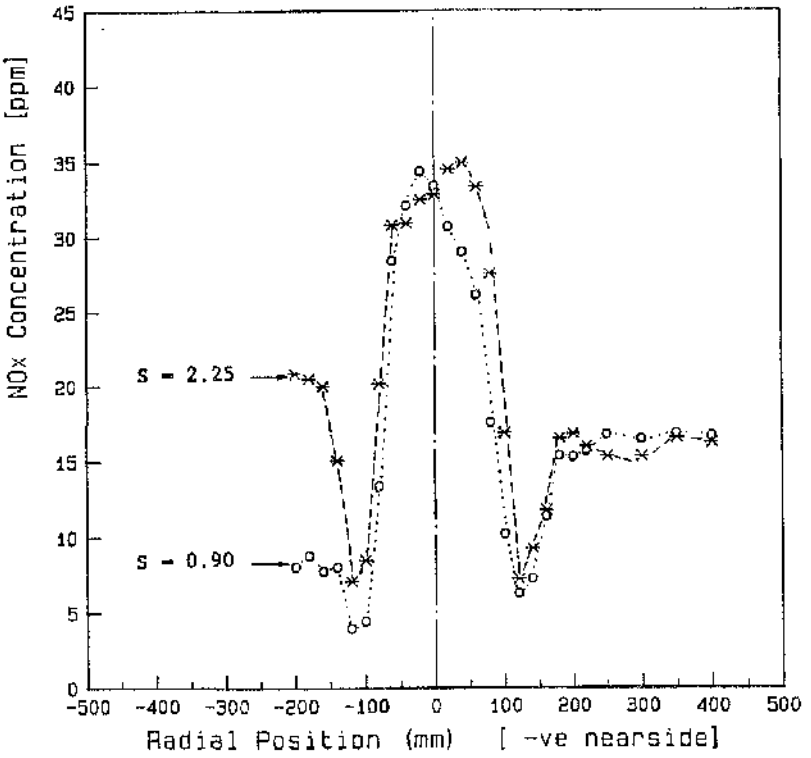

(a) X = 45 mm

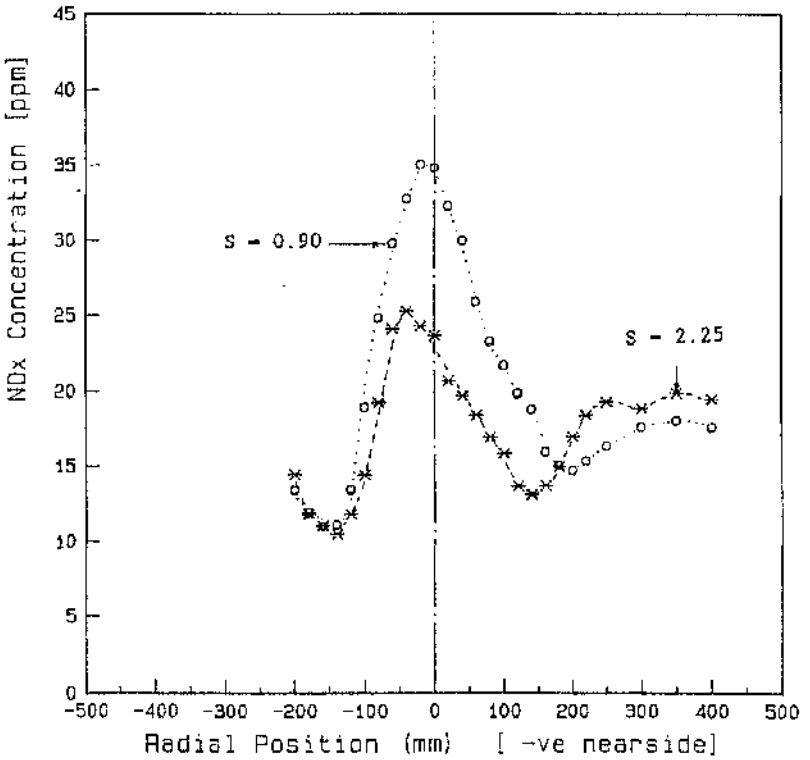

(b) X = 200 mm

FIG 4.38: Radial NOx profiles, central axial fuel injection

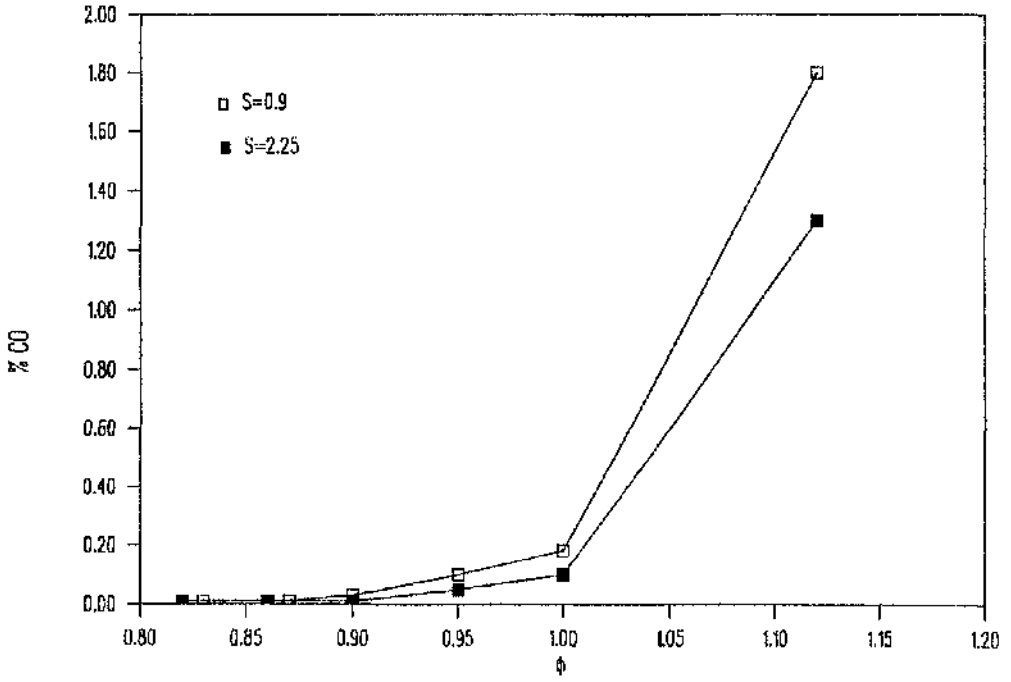

FIG 4.39: Variation of overall CO concentrations with ϕ central axial fuel injection

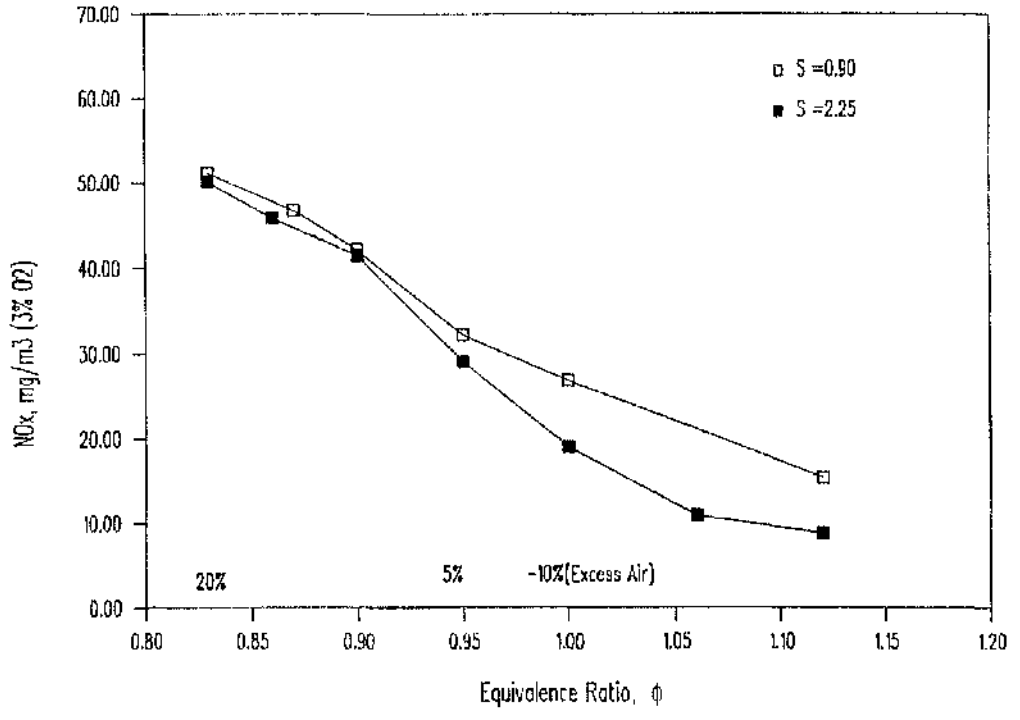

FIG 4.40: Variation of overall NOx concentrations (corrected to 3% O2) with ϕ central axial fuel injection

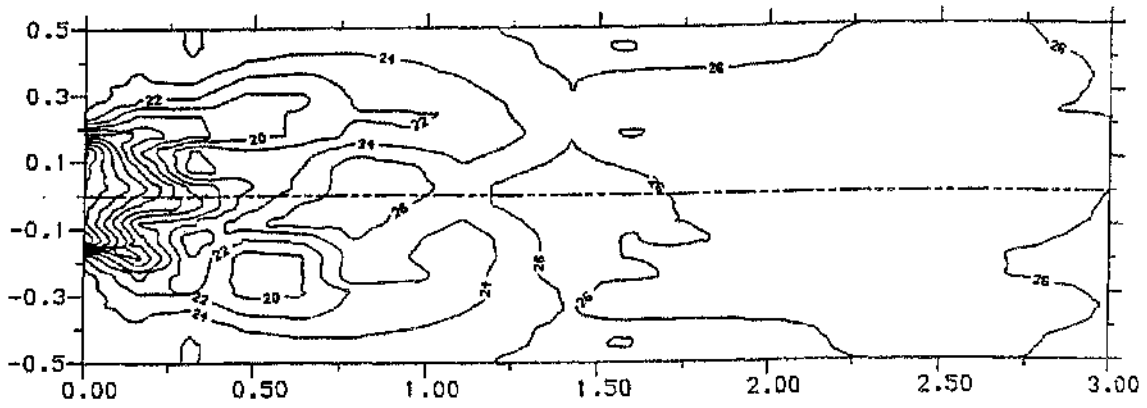

(a) S = 0.0

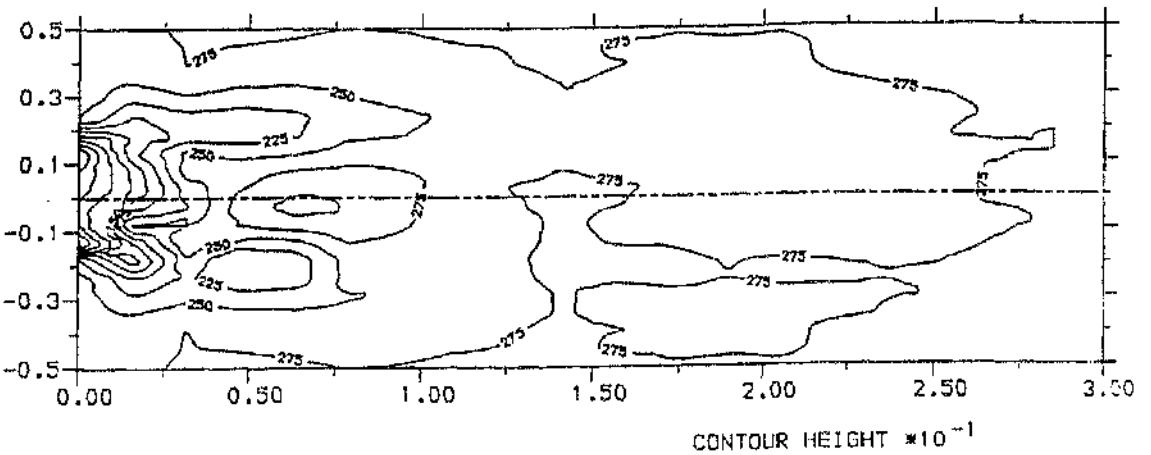

(b) S = 0.45

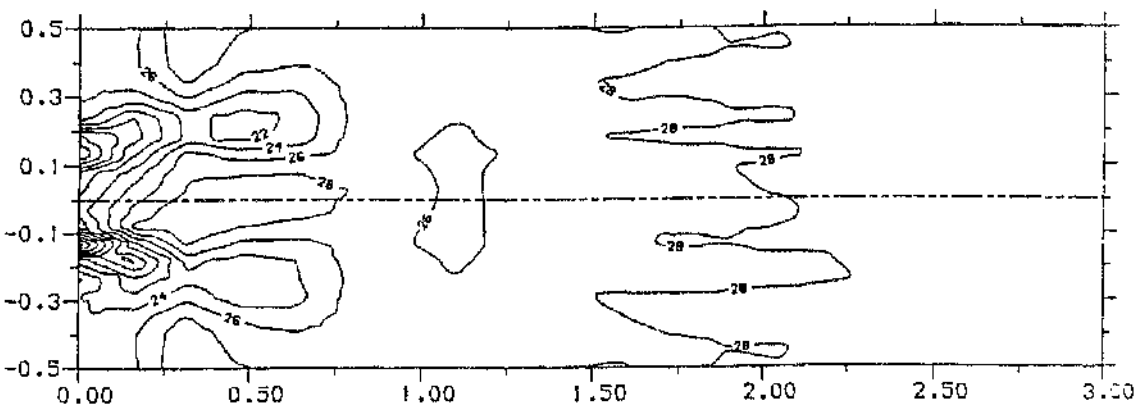

(c) S = 0.90

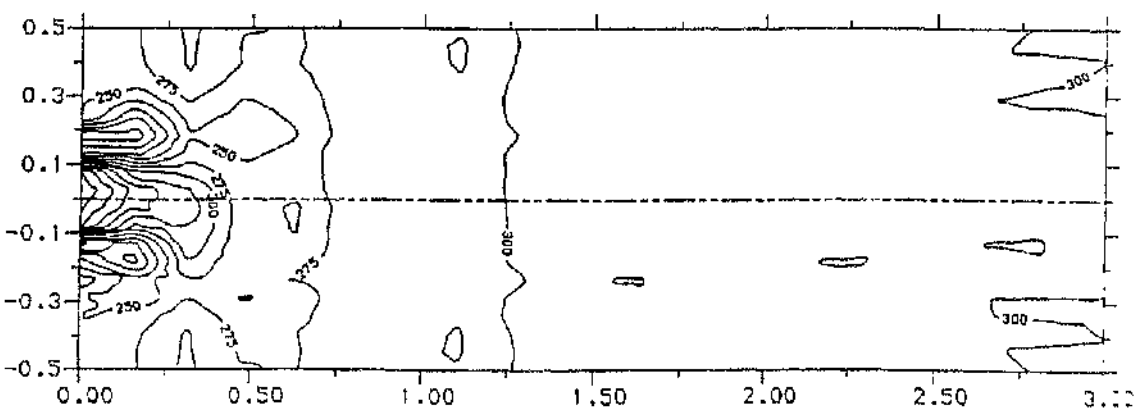

(d) S = 2.25 CONTOUR HEIGHT *10⁻¹

FIG 4.41: NOx contours, central radial fuel injection

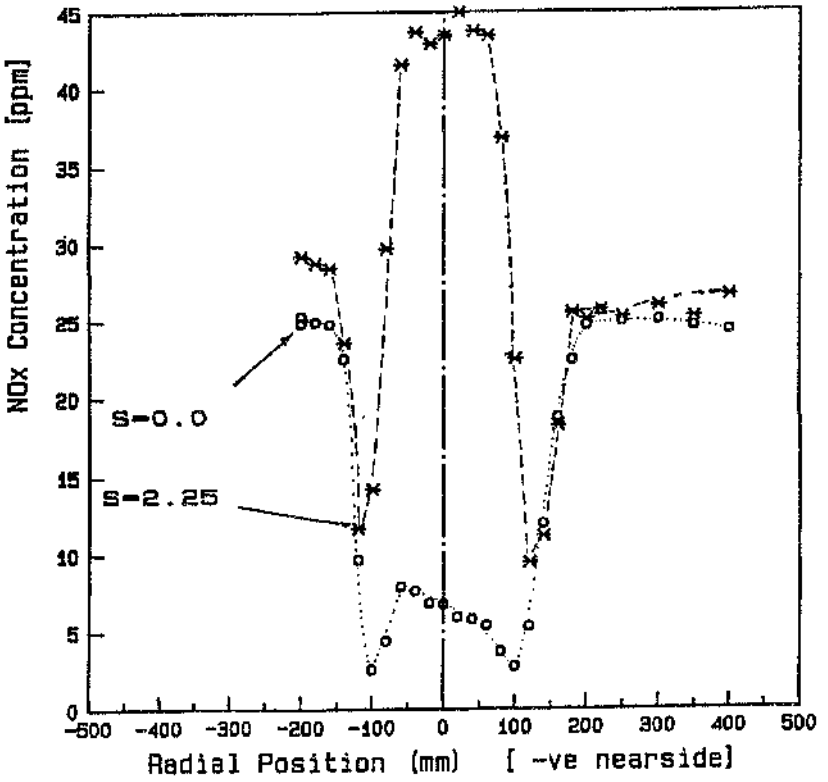

FIG 4.42.a: Radial NOx profiles, X = 45 mm, central radial fuel injection

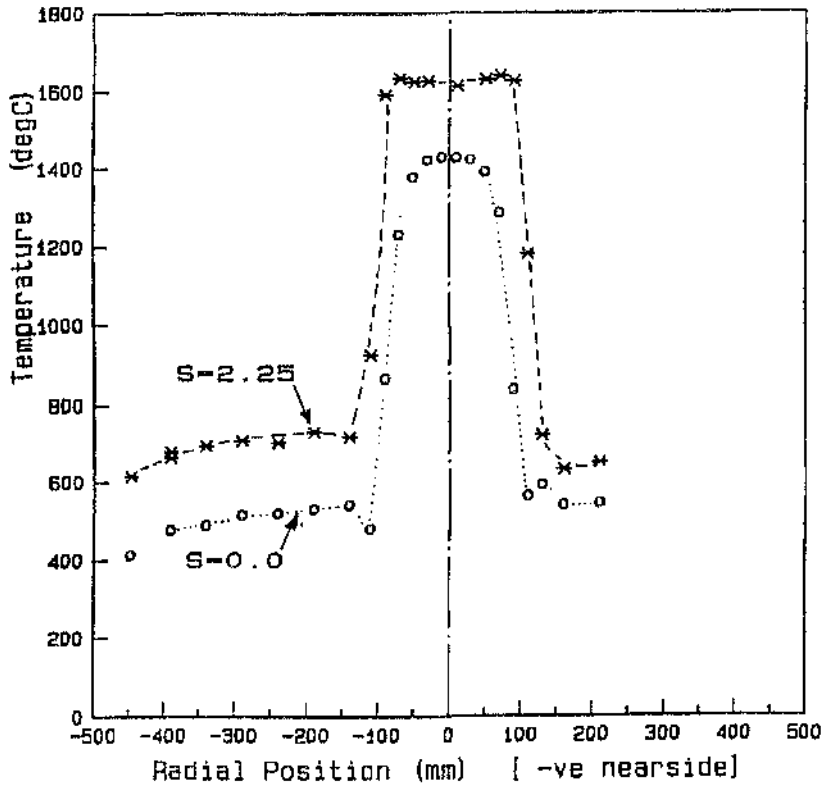

FIG 4.42.b: Radial temperature profiles, X = 45 mm, central radial fuel injection

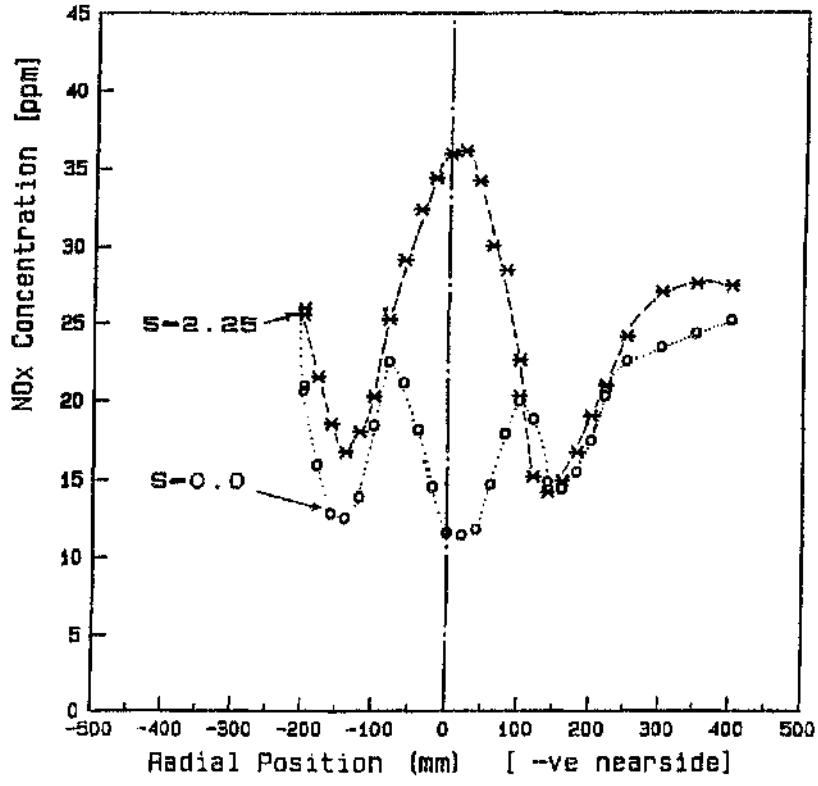

FIG 4.43.a: Radial NOx profiles, X = 200 mm, central radial fuel injection

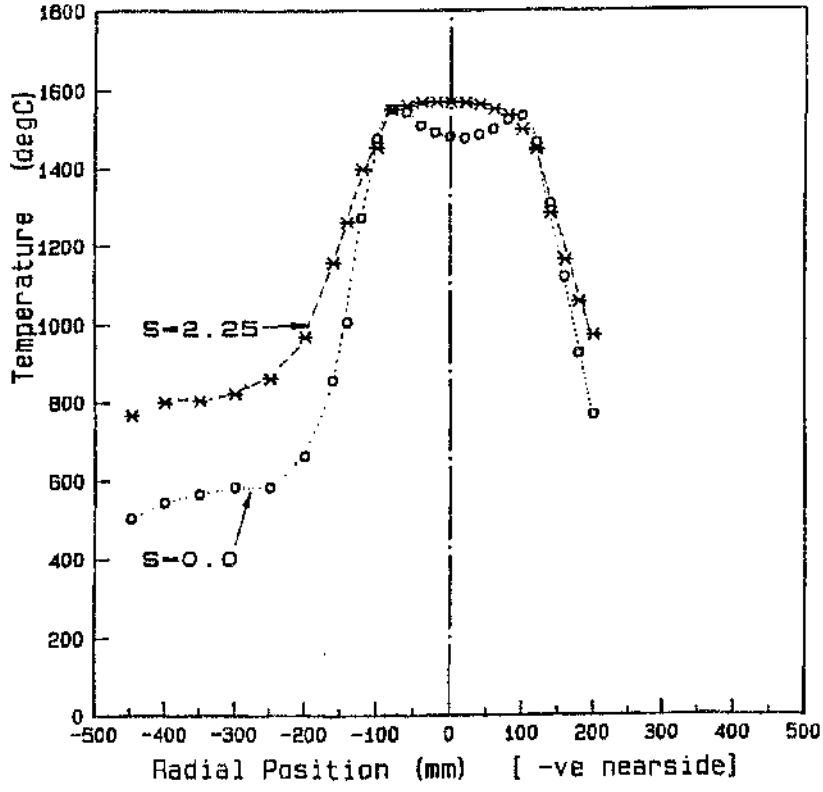

FIG 4.43.b: Radial temperature profiles, X = 200 mm, central radial fuel injection

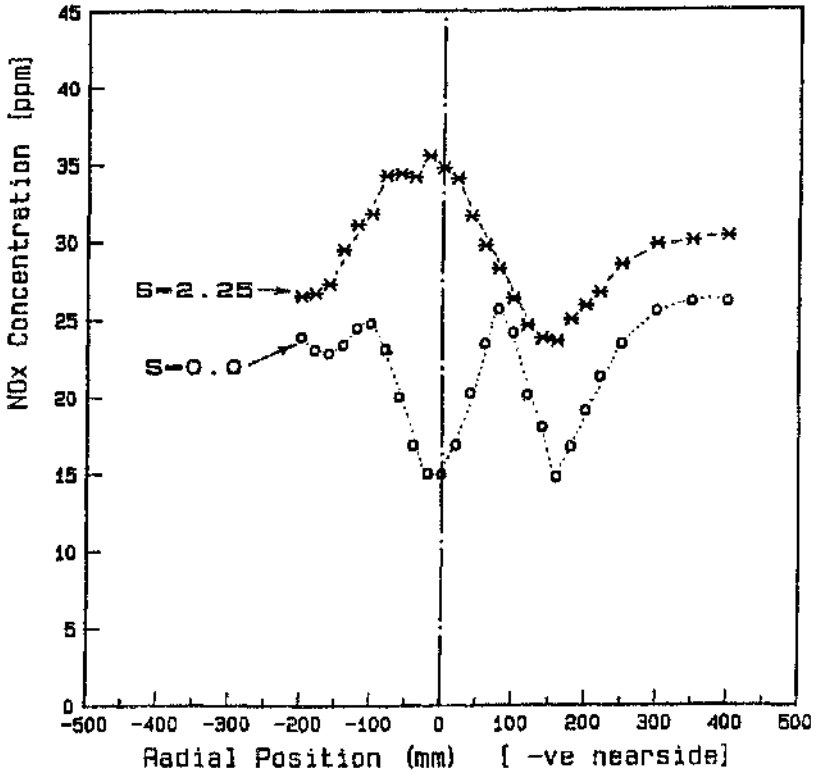

FIG 4.44.a: Radial NOx profiles, X = 300 mm, central radial fuel injection

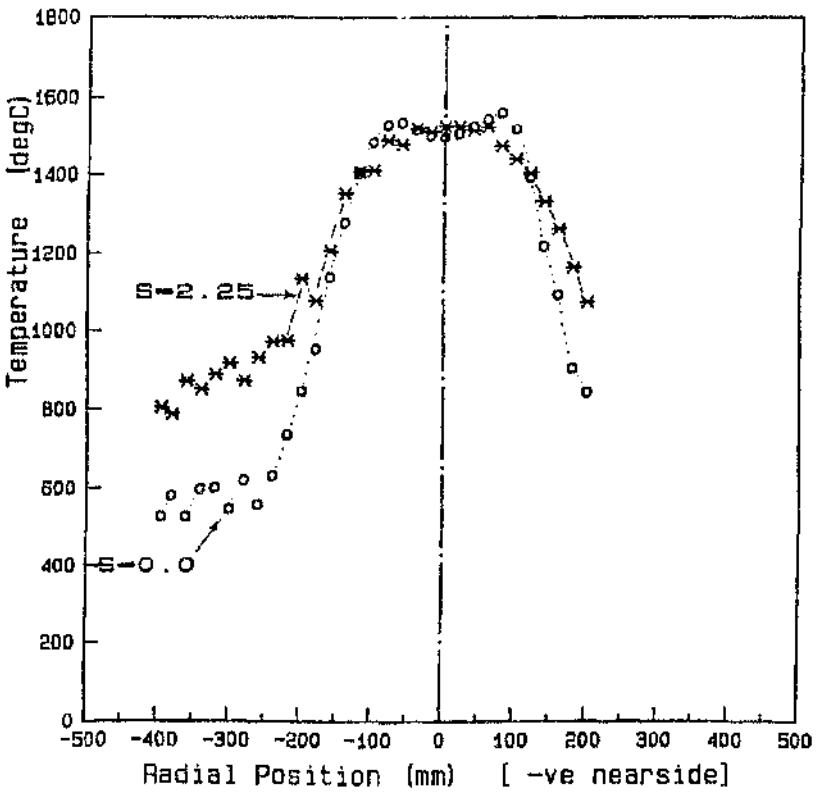

FIG 4.44.b: Radial temperature profiles, X = 300 mm, central radial fuel injection

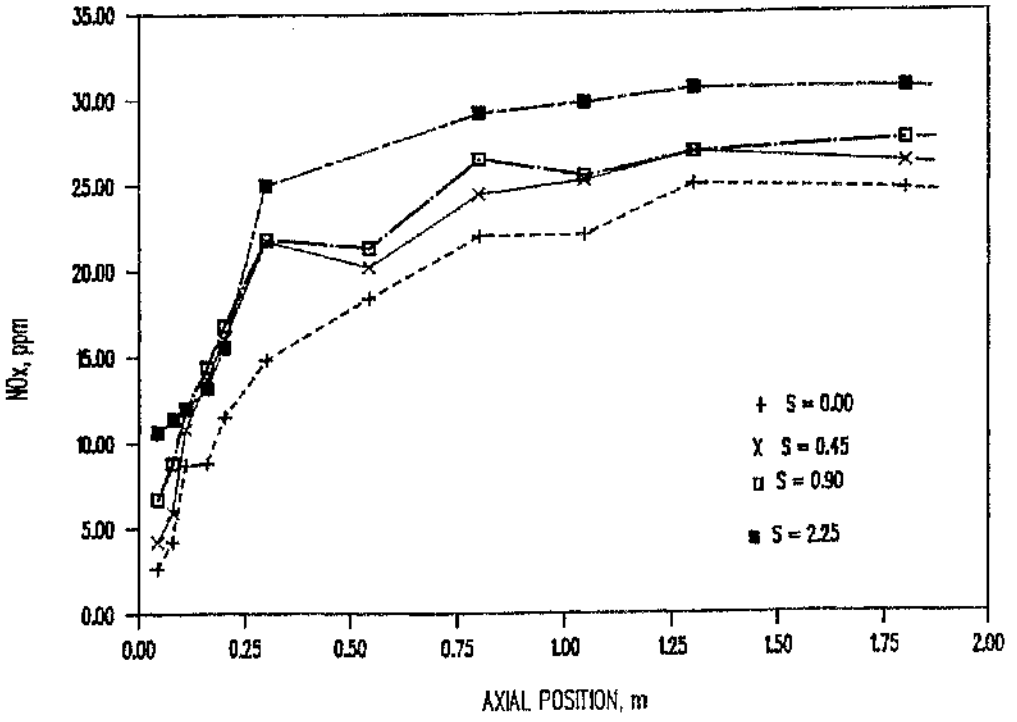

FIG 4.45: Variation of minimum NOx concentrations along the furnace central radial fuel injection

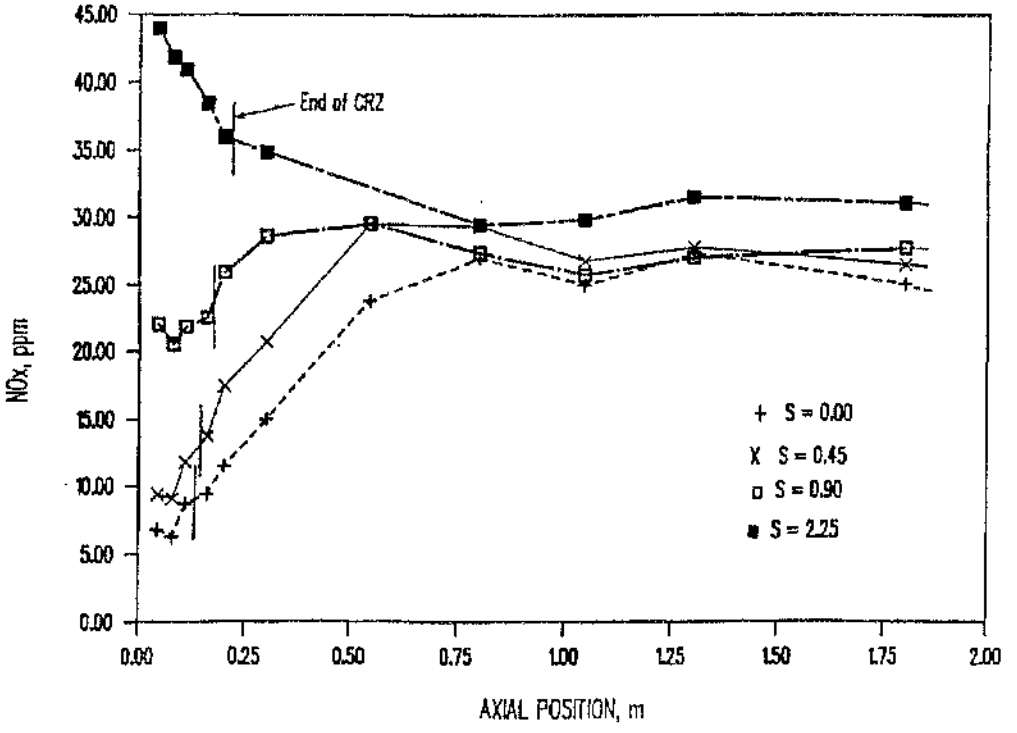

FIG 4.46: Variation of centre-line NOx concentrations along the furnace, central radial fuel injection

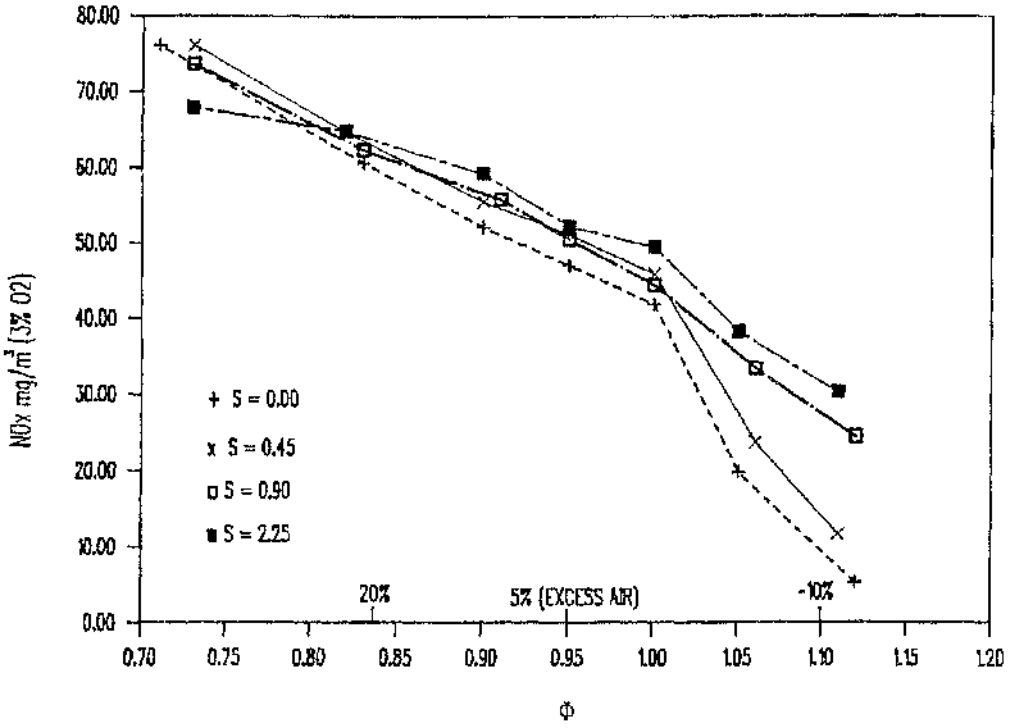

FIG 4.47: Variation of overall NOx concentrations (corrected to 3% O2) with ϕ, central radial fuel injection

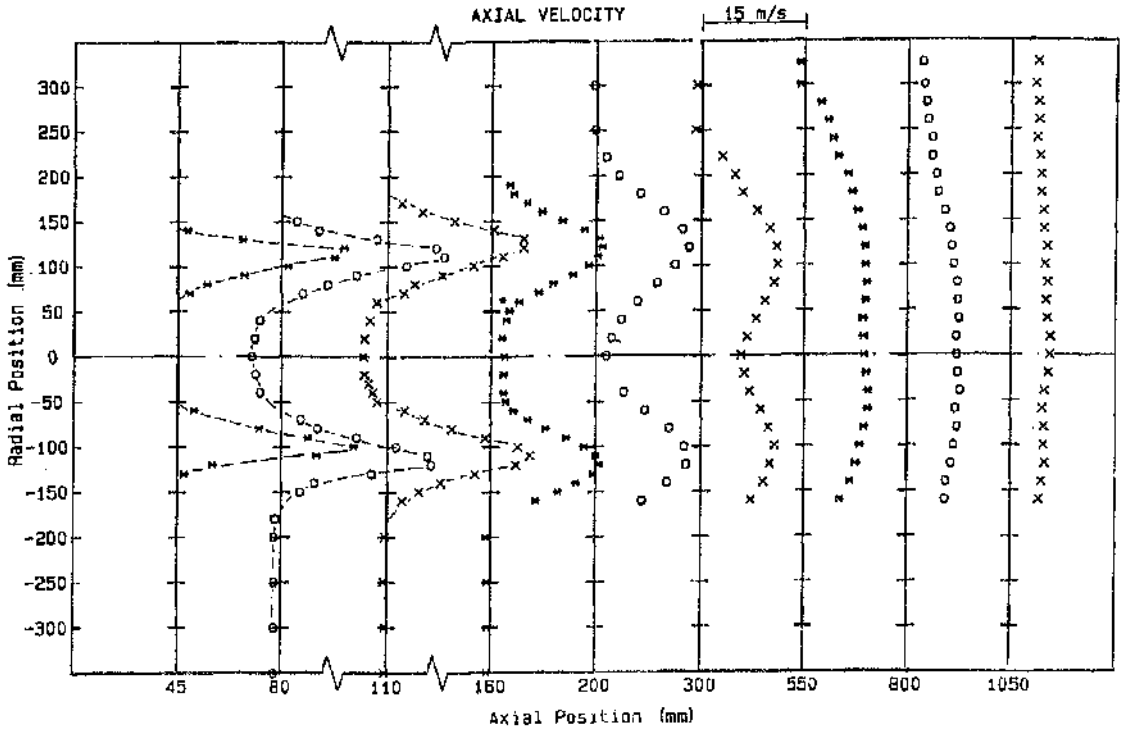

(a) S = 0.90

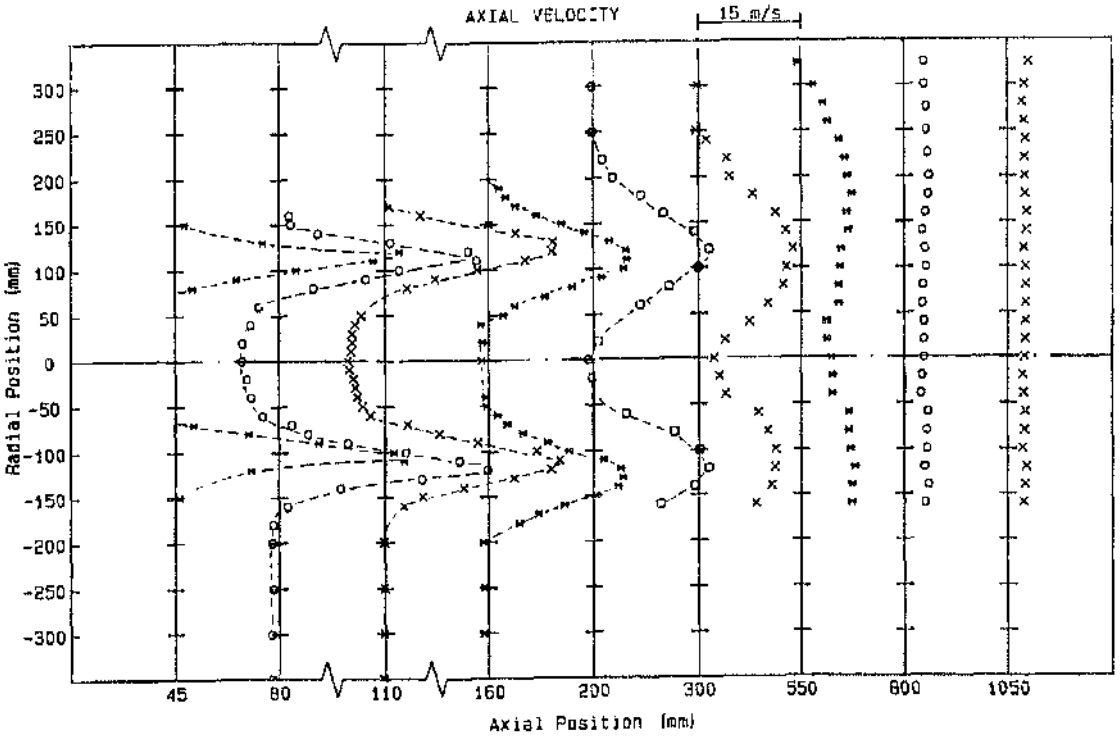

(b) S = 2.25

FIG 5.1: Axial velocity profiles, radial fuel injection

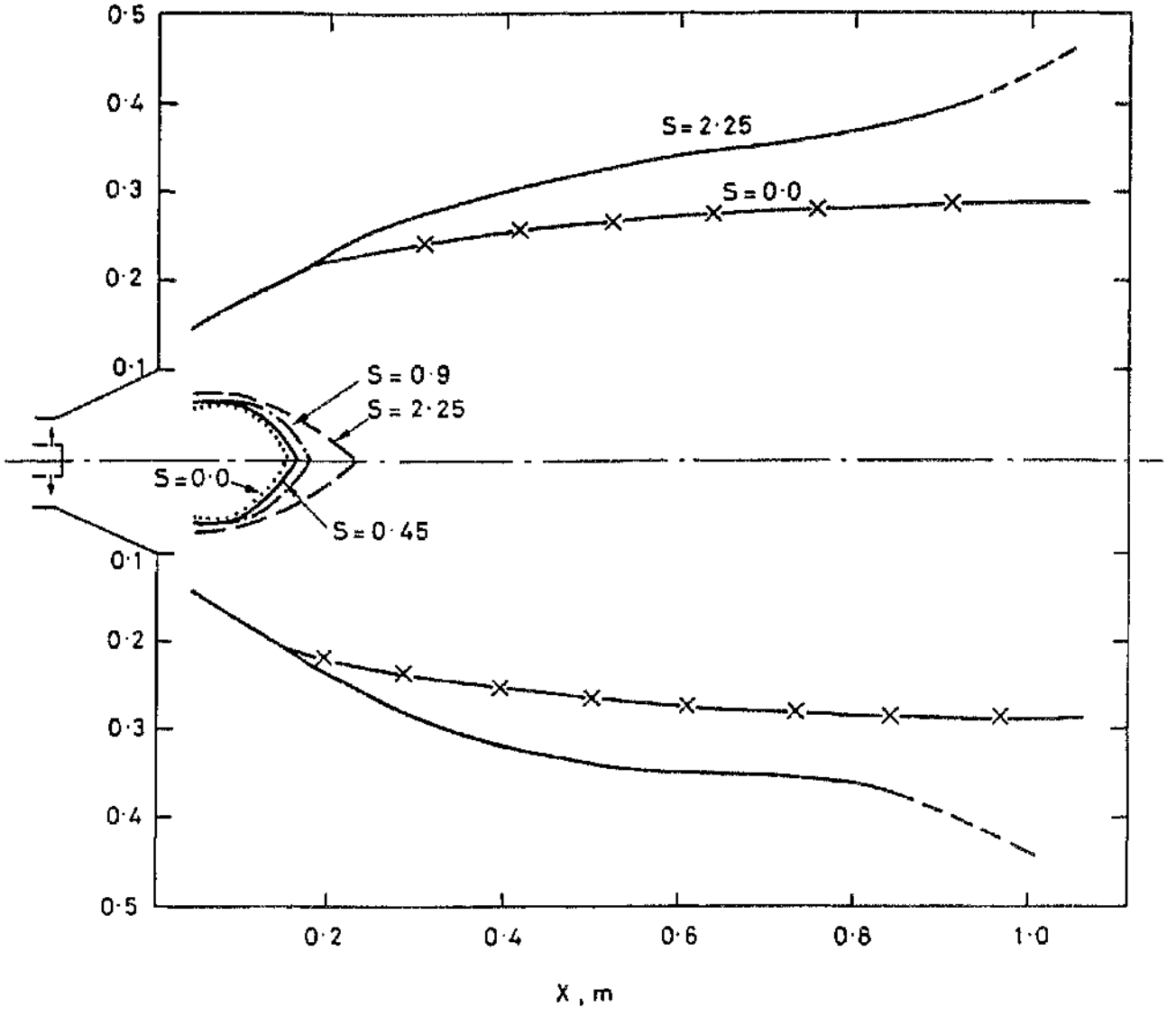

FIG 5.2: Flow boundaries, radial fuel injection

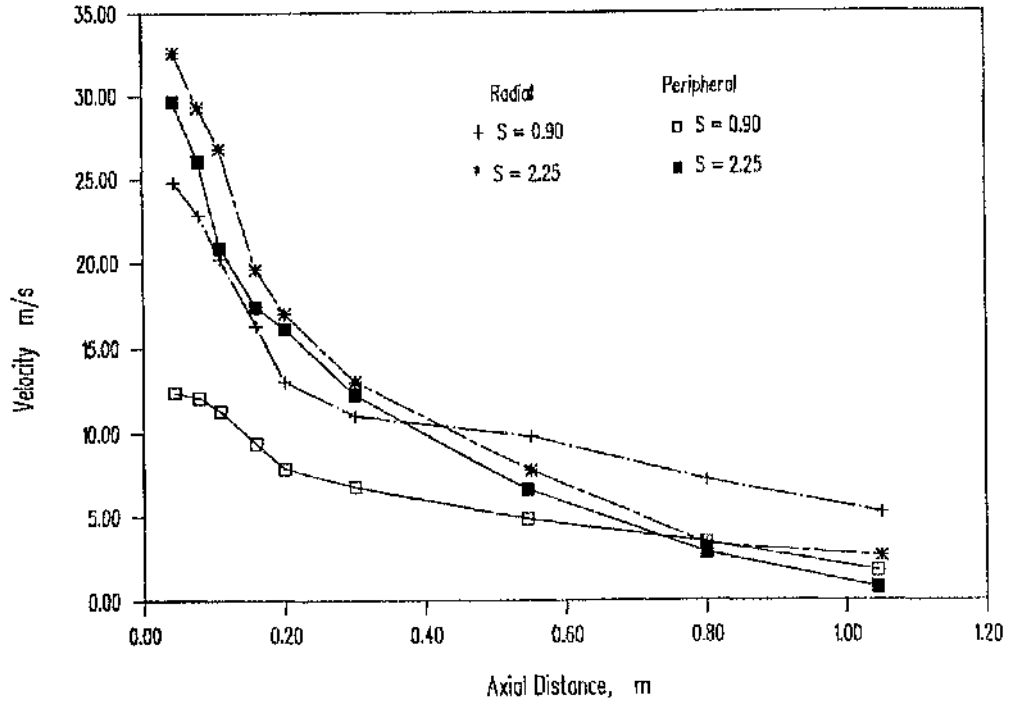

FIG 5.3: Maximum axial velocities along the furnace, peripheral versus radial fuel injection

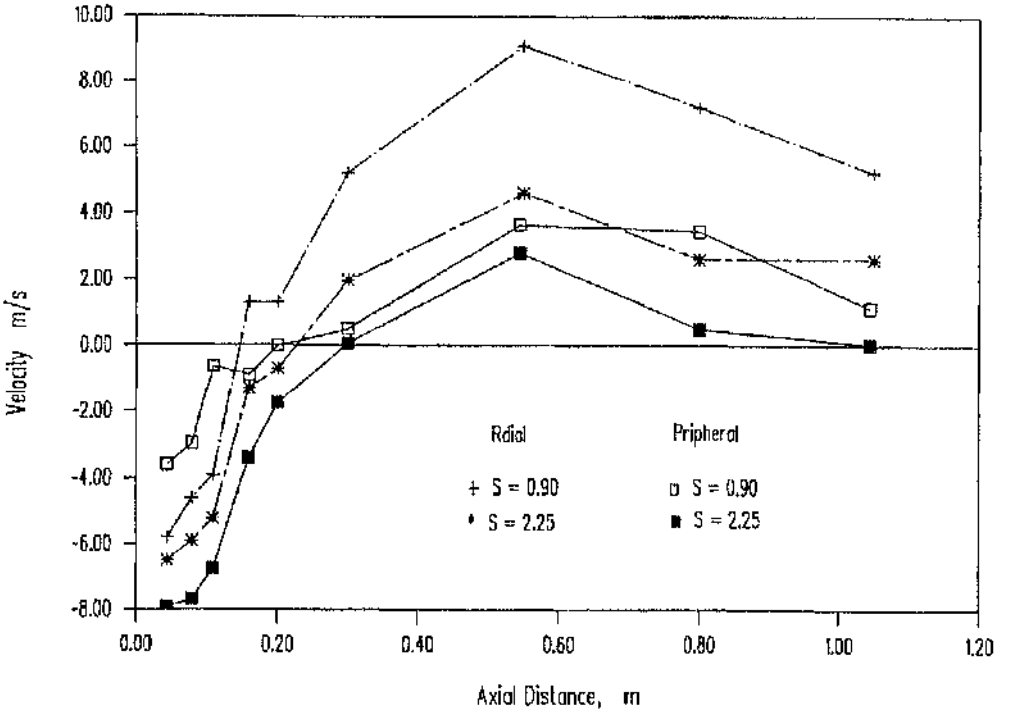

FIG 5.4 : Centre-line axial velocities along the furnace, peripheral versus radial fuel injection

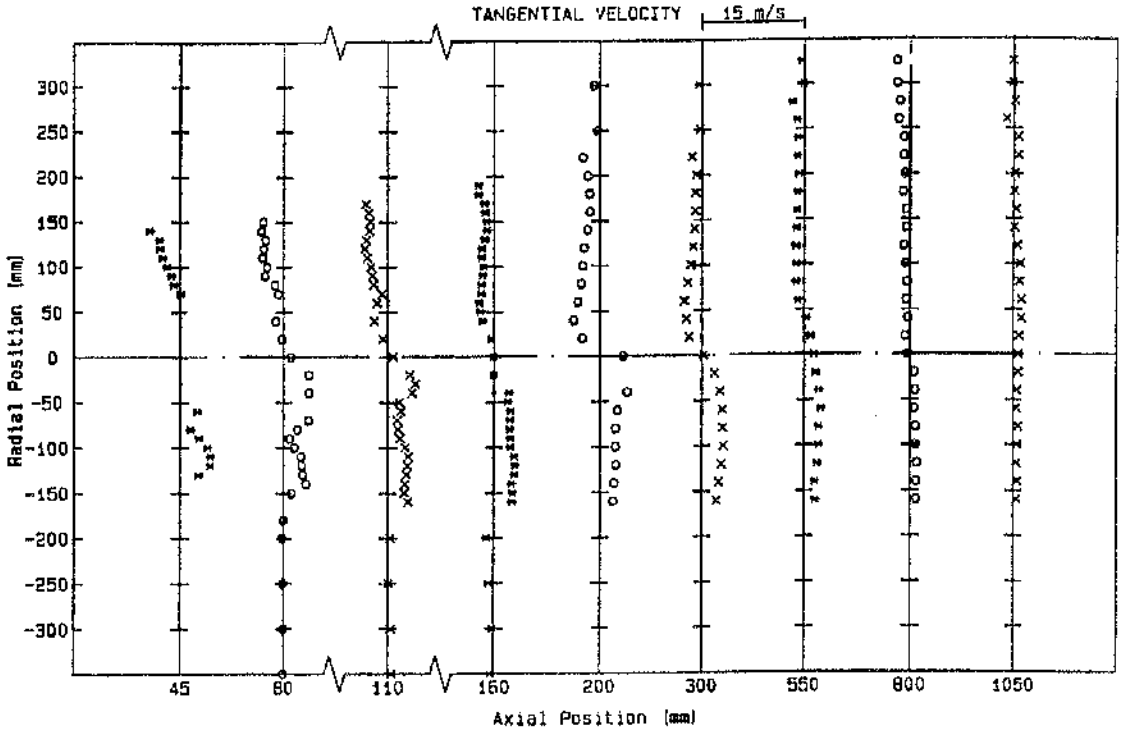

(a) S = 0.90

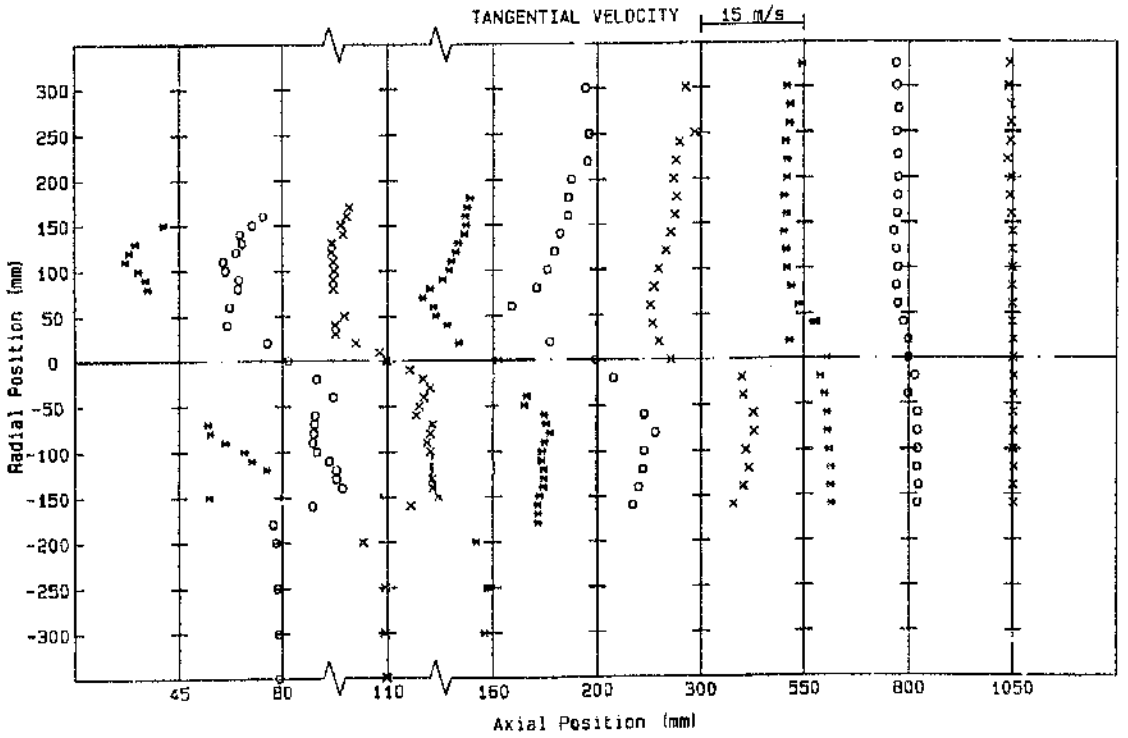

(b) S = 2.25

FIG 5.5: Tangential velocity profiles, radial fuel injection

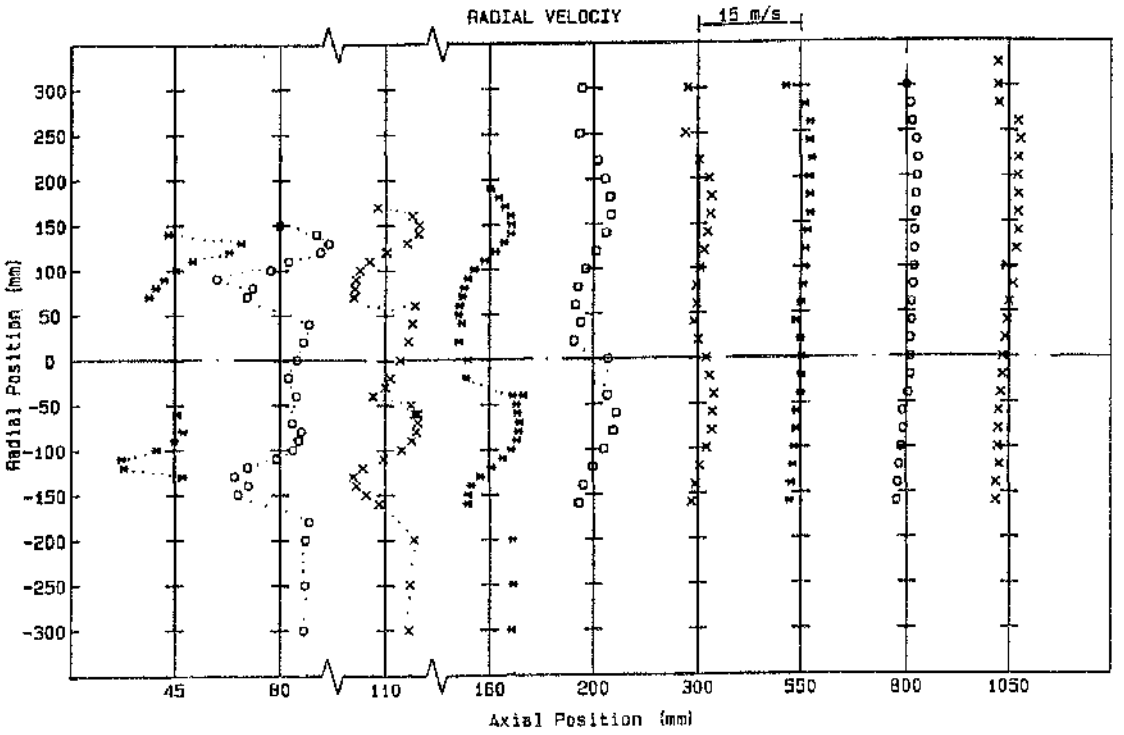

(a) S = 0.90

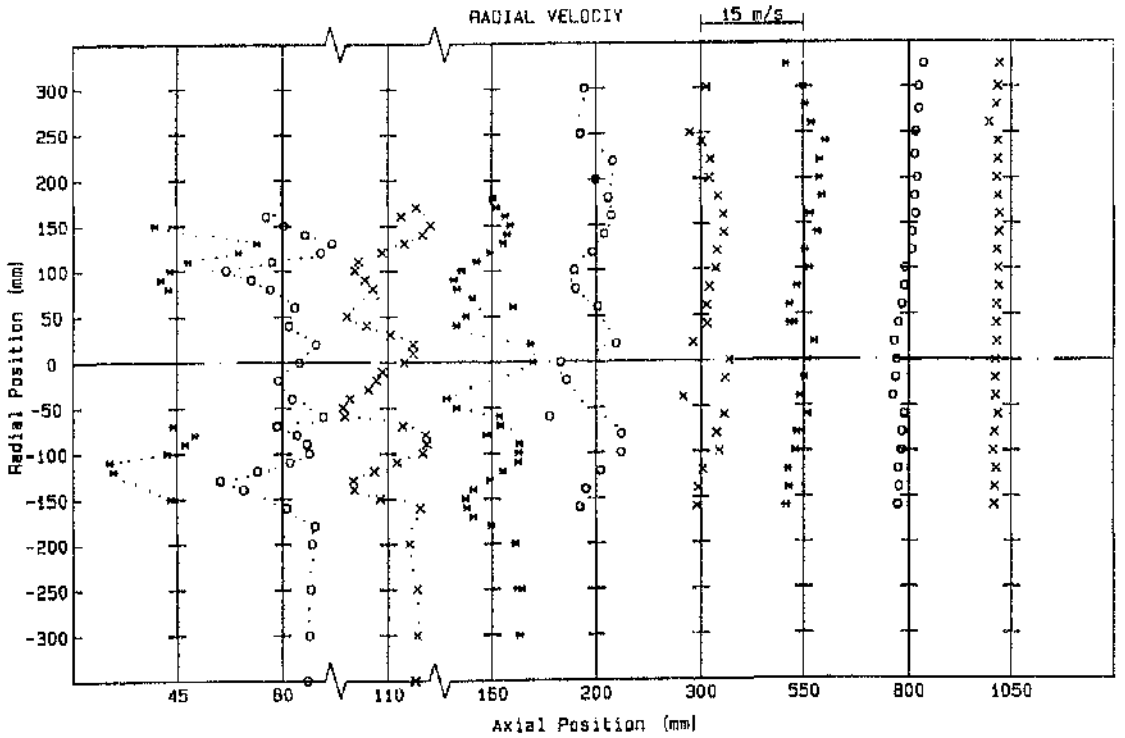

(b) S = 2.25

FIG 5.6: Radial velocity profiles, radial fuel injection

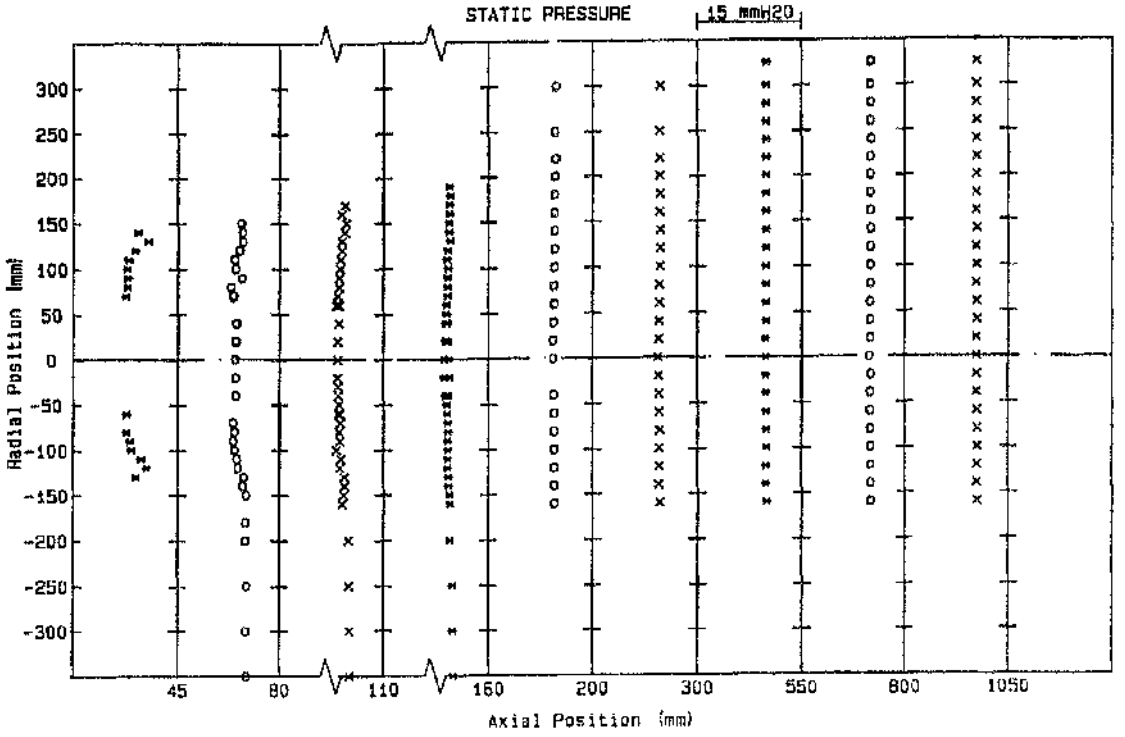

(a) S = 0.90

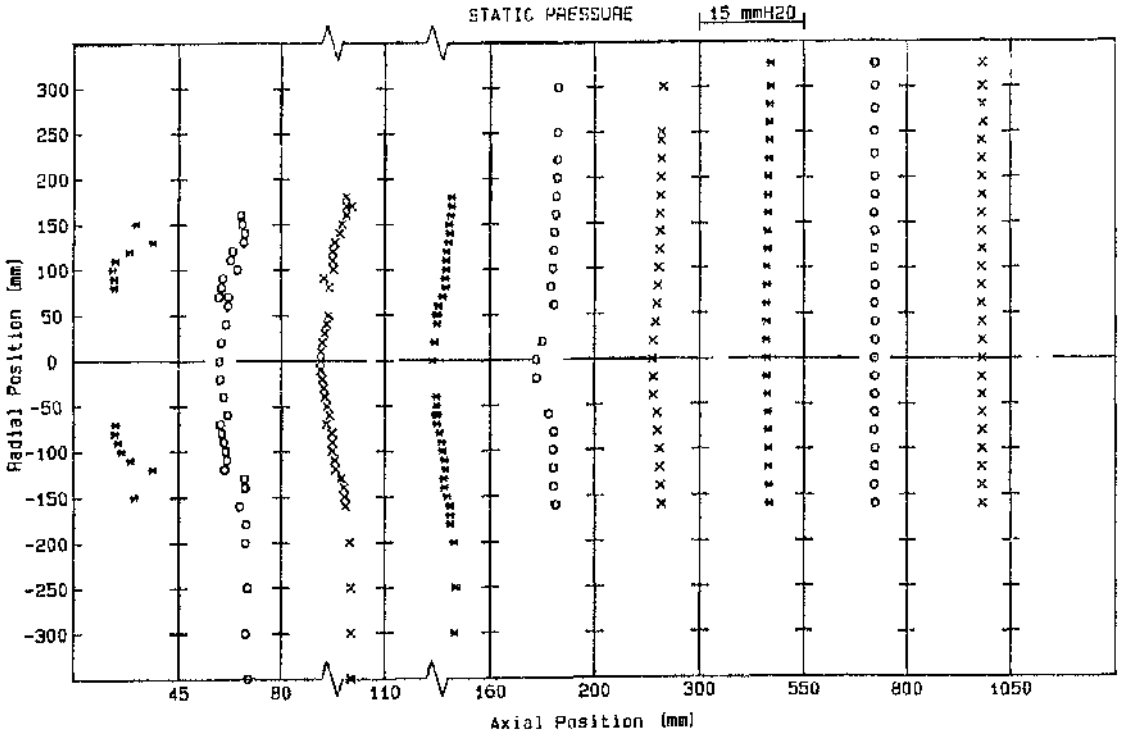

(b) S = 2.25

FIG 5.7: Static pressure profiles, radial fuel injection

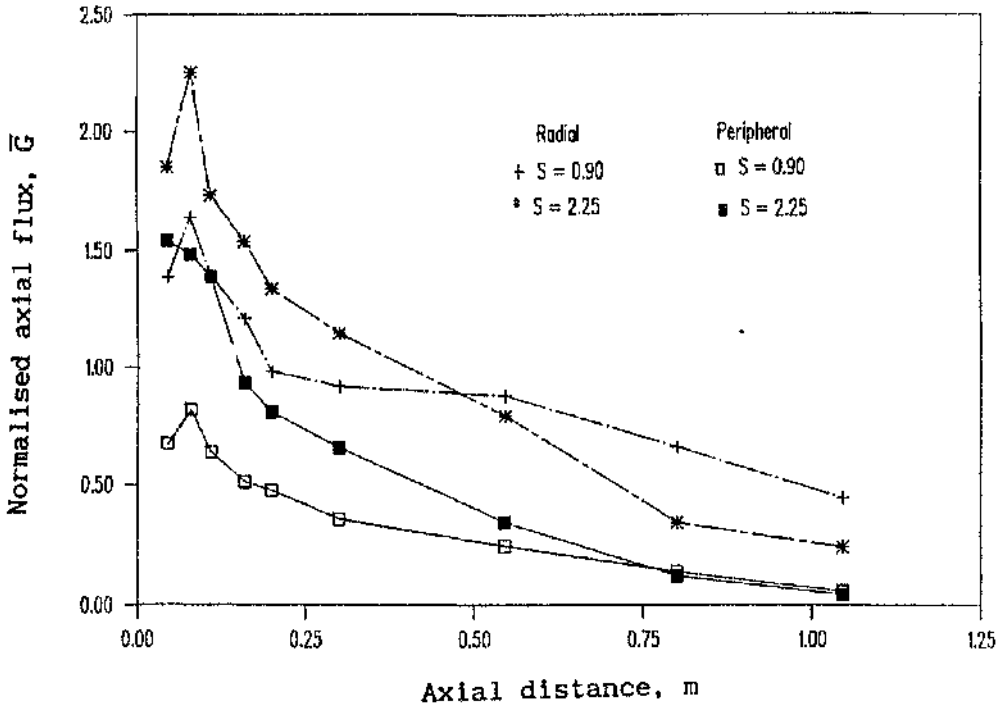

FIG 5.8: Axial momentum flux, peripheral versus radial fuel injection

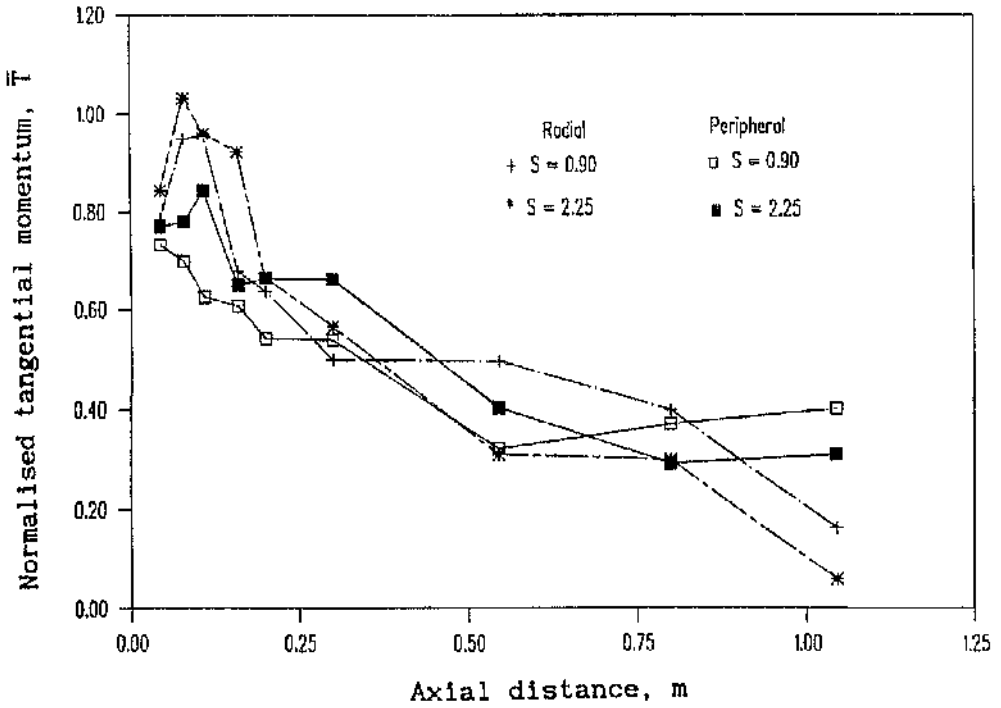

FIG 5.9: Axial flux of tangential momentum, peripheral versus radial fuel injection

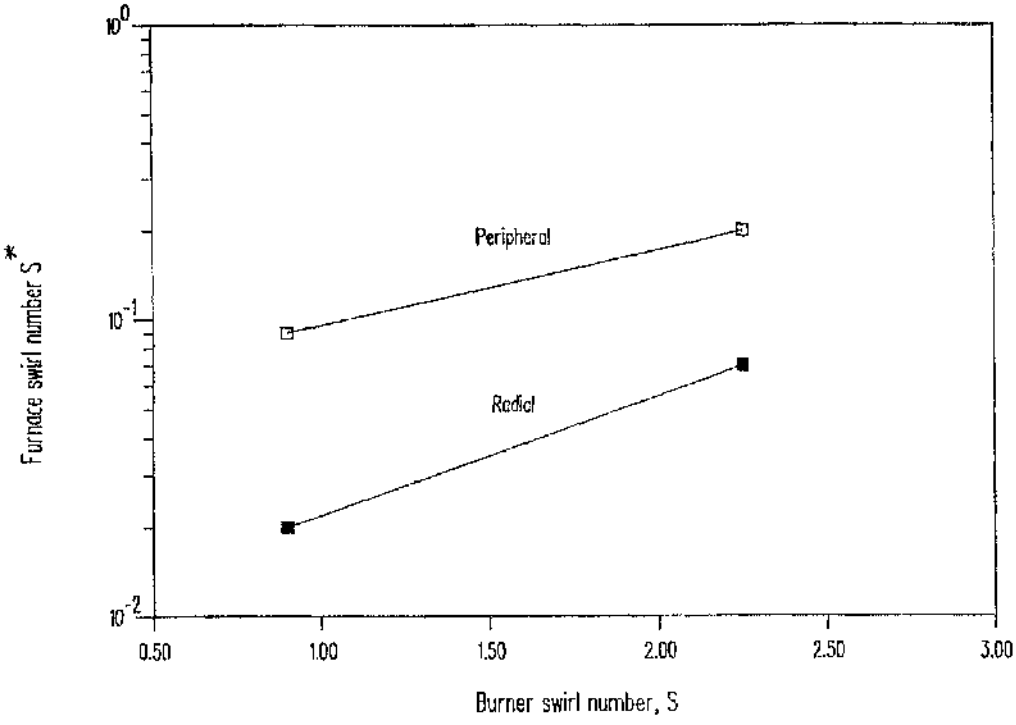

FIG 5.10: Furnace swirl number, peripheral versus radial fuel injection

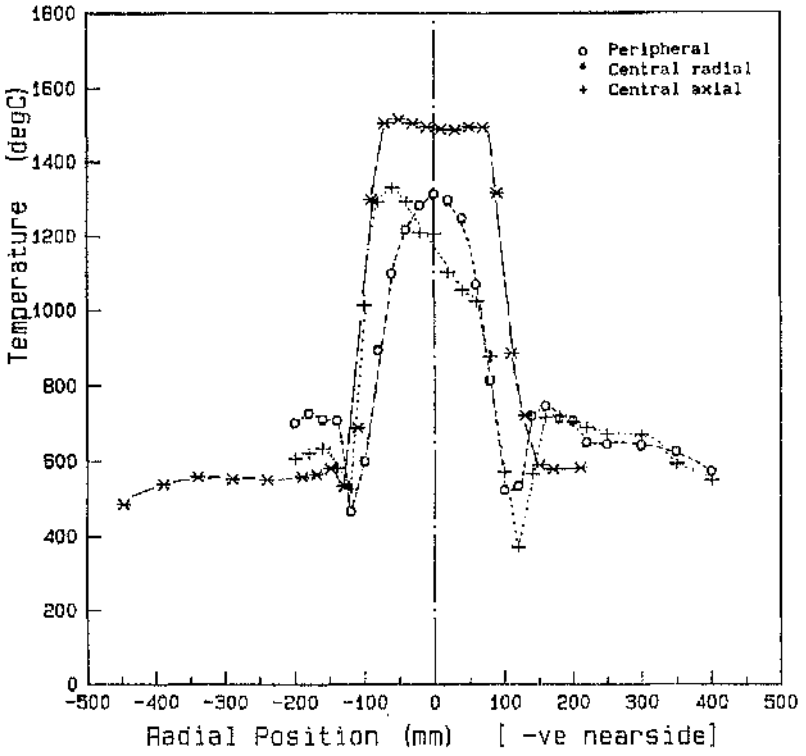

(a) S = 0.90

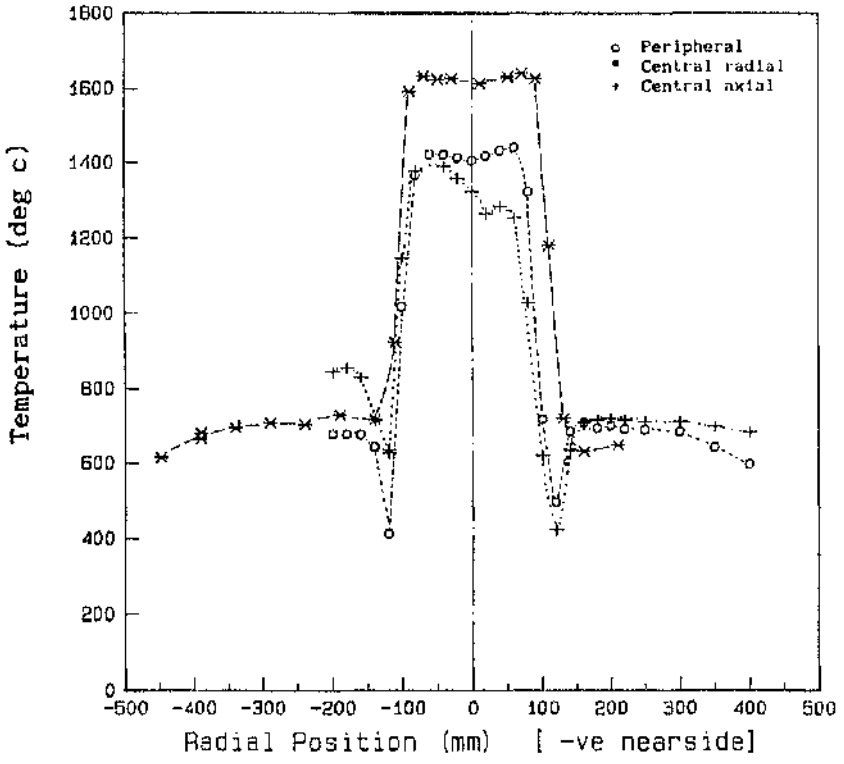

(b) S = 2.25

FIG 5.11: Radial temperature profiles, X = 45 mm, peripheral, radial and axial fuel injection modes

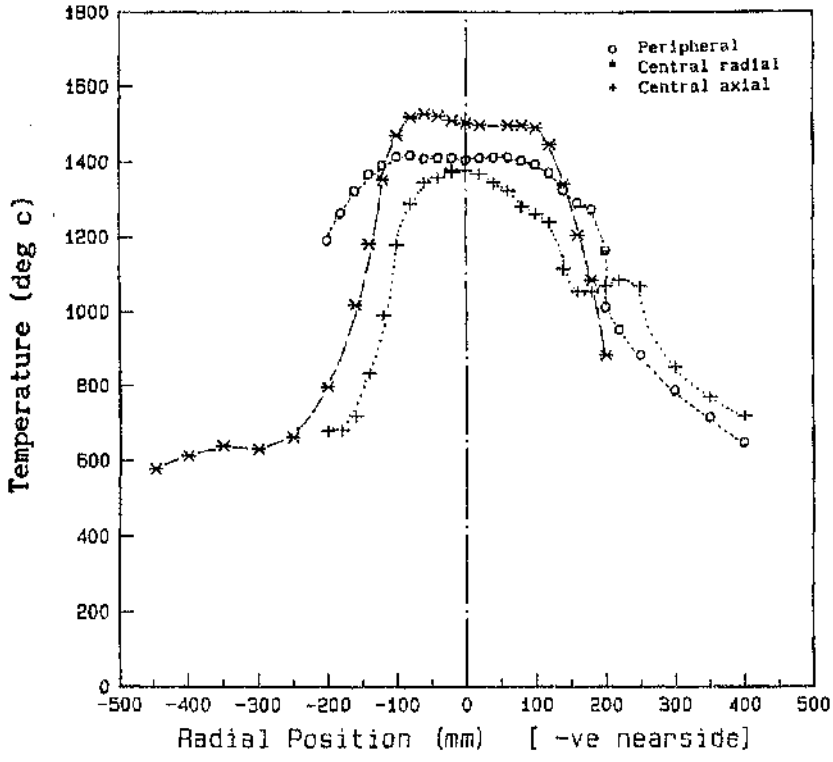

(a) S = 0.90

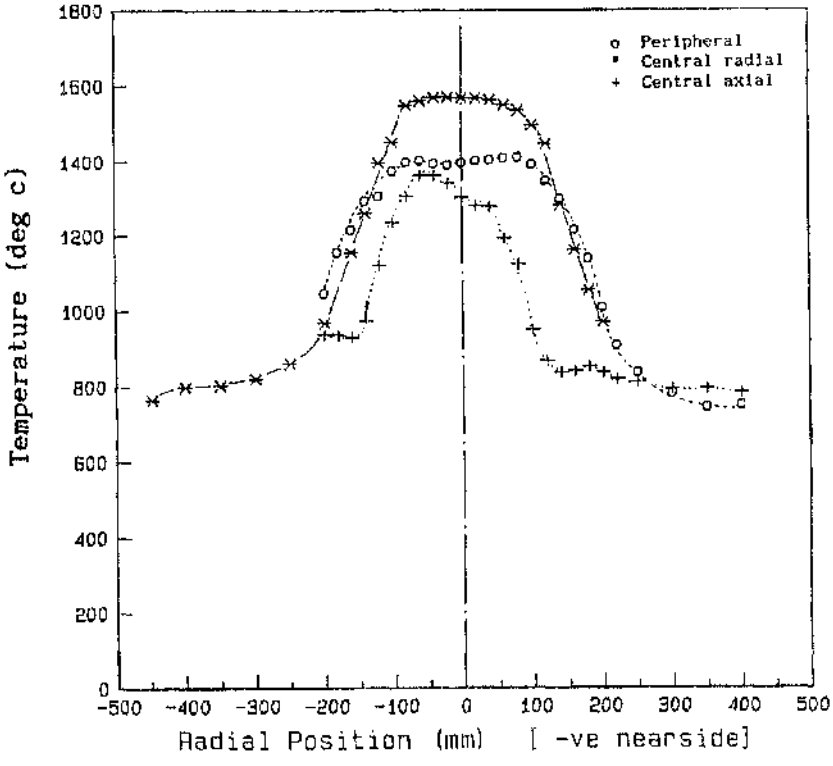

(b) S = 2.25

FIG 5.12: Radial temperature profiles, X = 200 mm, peripheral, radial and axial fuel injection modes

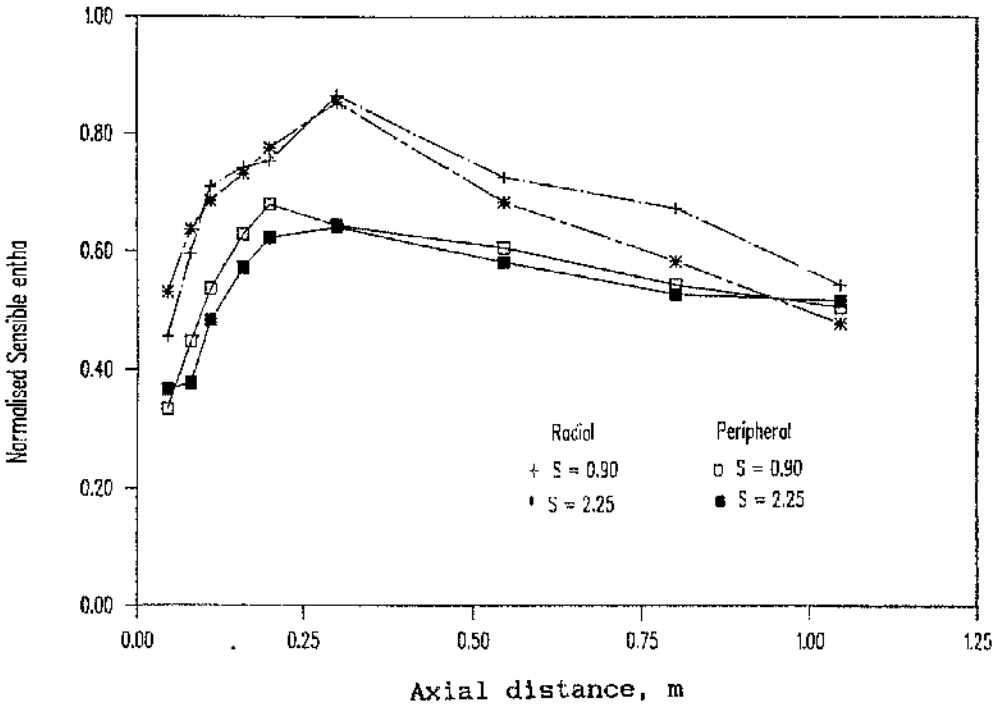

FIG 5.13: Sensible enthalpy fluxes, peripheral versus radial fuel injection

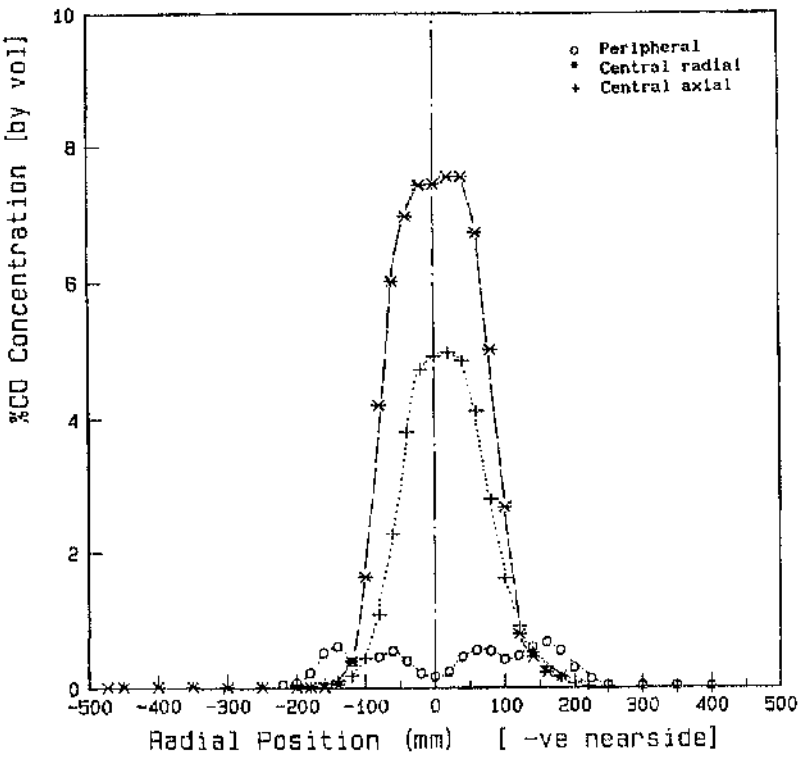

(a) S = 0.90

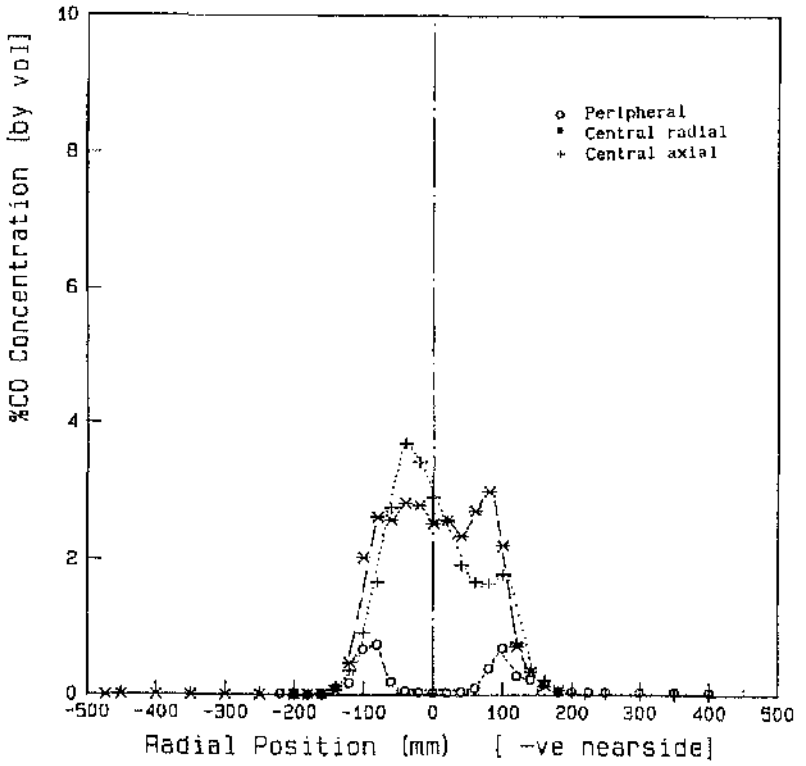

(b) S = 2.25

FIG 5.14: Radial CO profiles, **X = 45 mm**, peripheral, radial and axial fuel injection modes

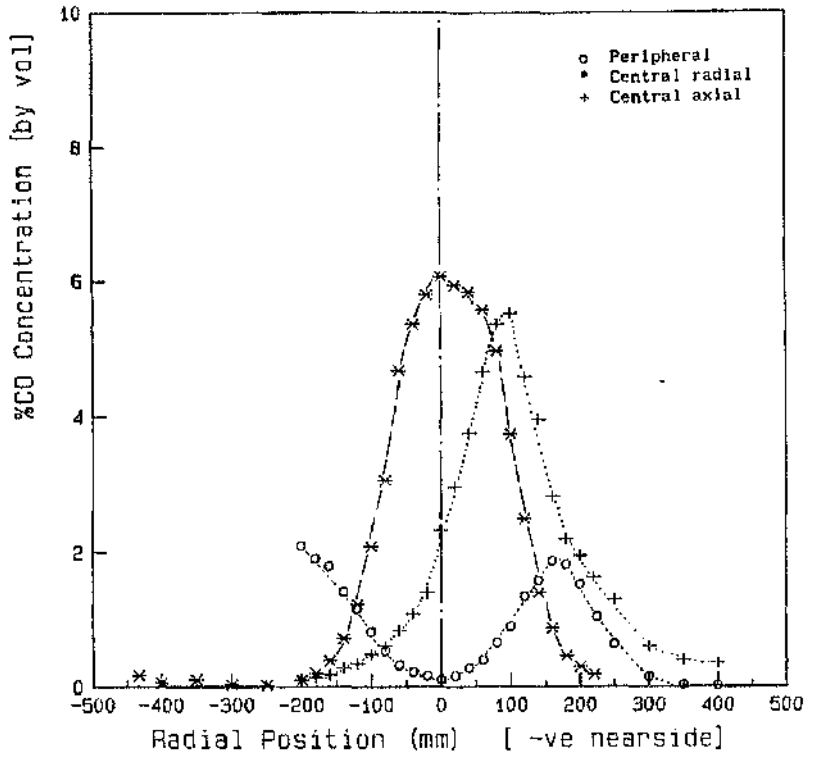

(a) S = 0.90

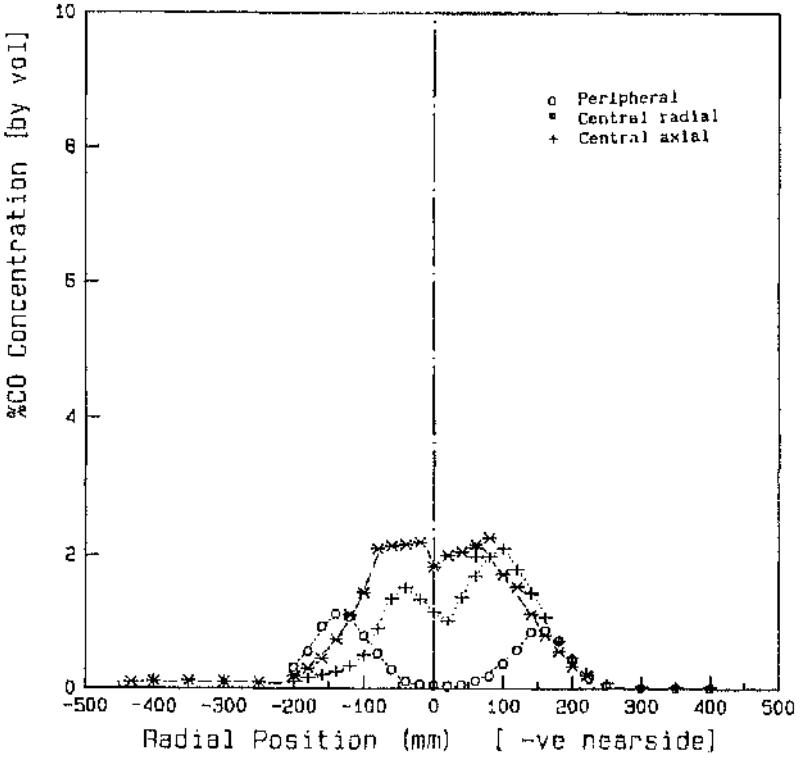

(b) S = 2.25

FIG 5.15: Radial CO profiles, X = 200 mm, peripheral, radial and axial fuel injection modes

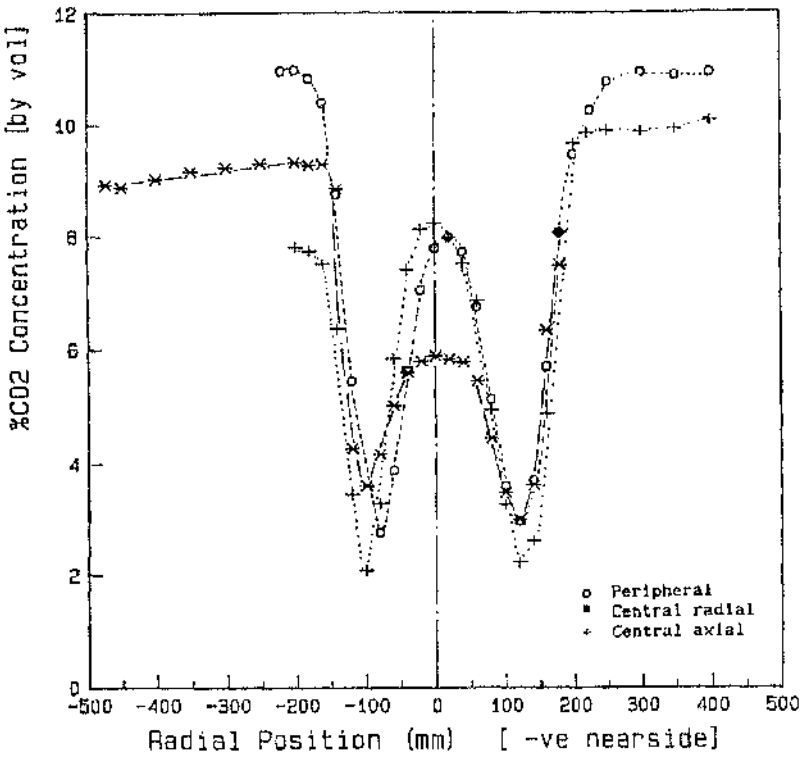

(a) S = 0.90

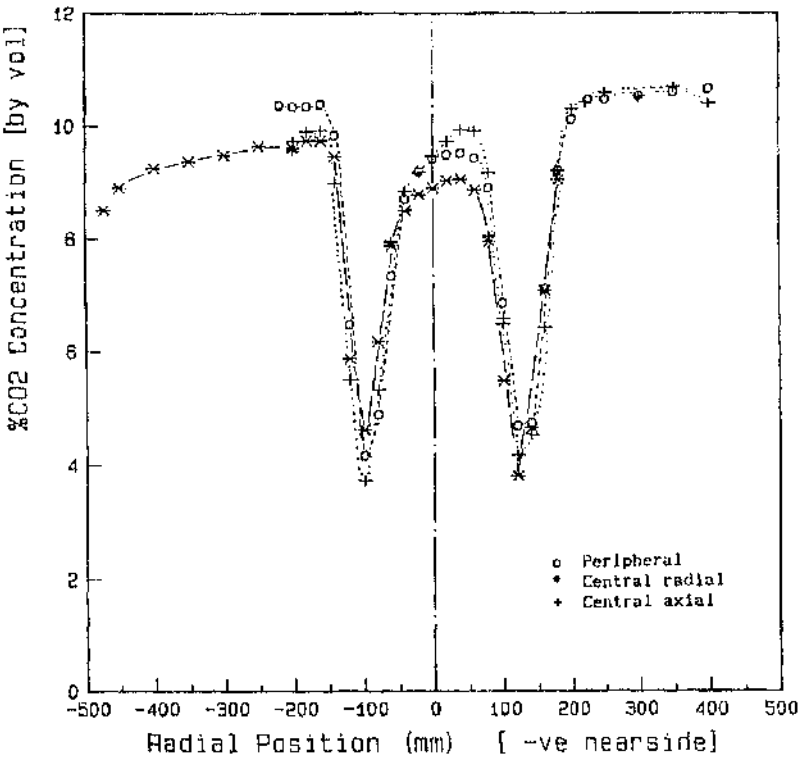

(b) S = 2.25

FIG 5.16: Radial CO_2 profiles, **X = 45 mm**, peripheral, radial and axial fuel injection modes

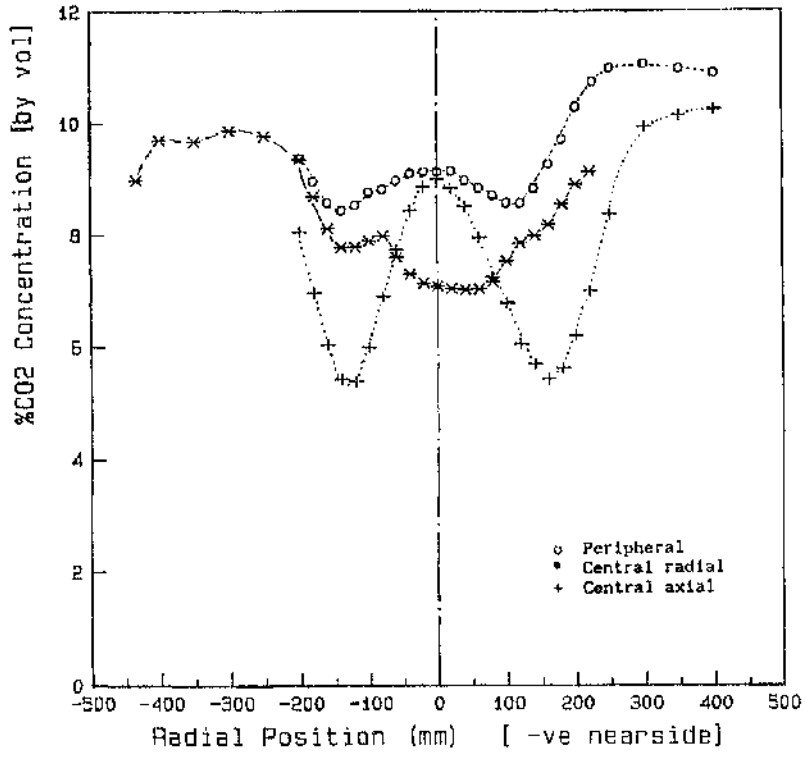

(a) S = 0.90

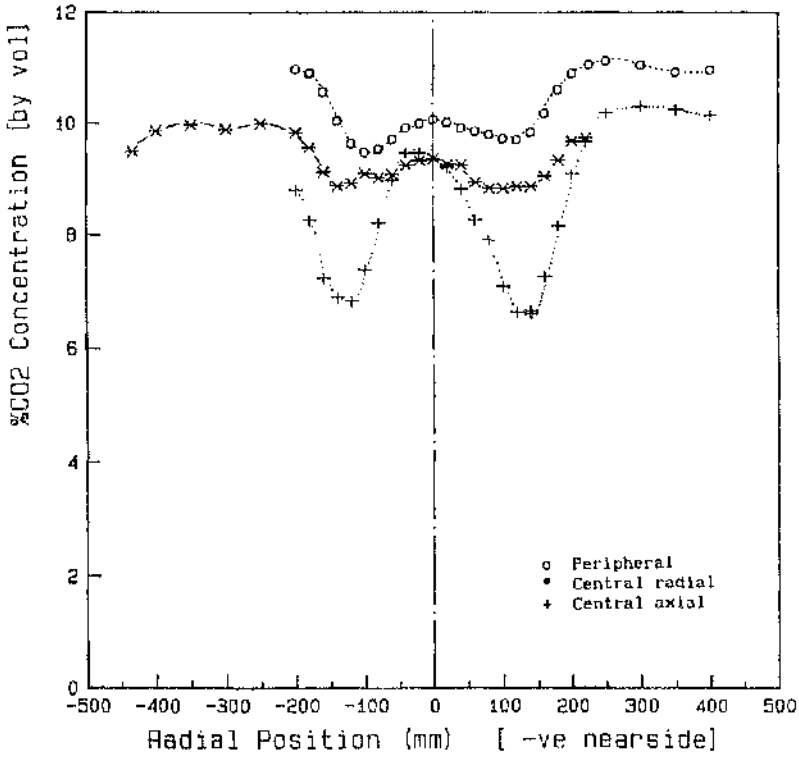

(b) S = 2.25

FIG 5.17: Radial CO_2 profiles, **X = 200 mm**, peripheral, radial and axial fuel injection modes

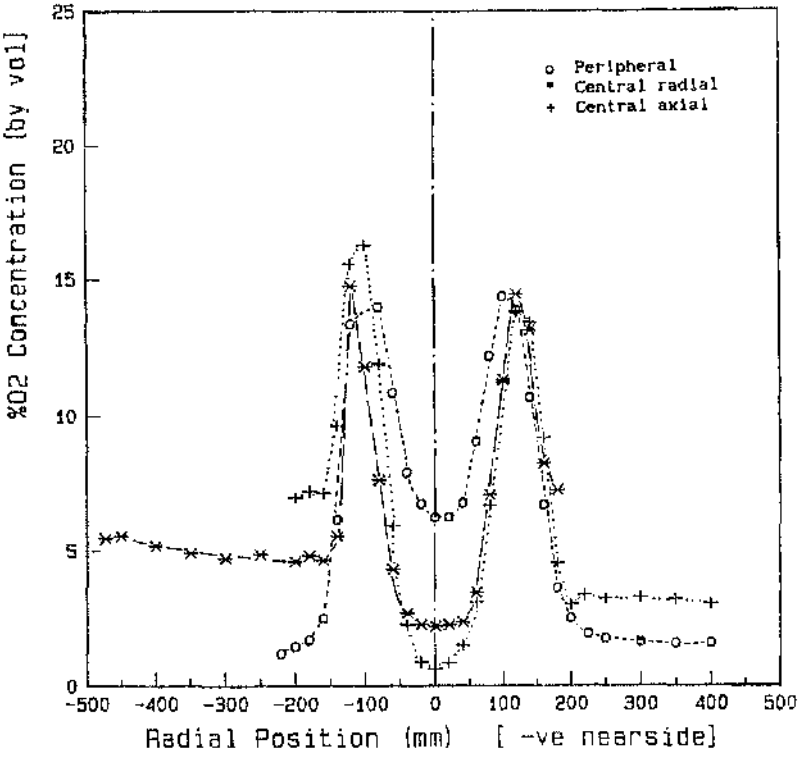

(a) S = 0.90

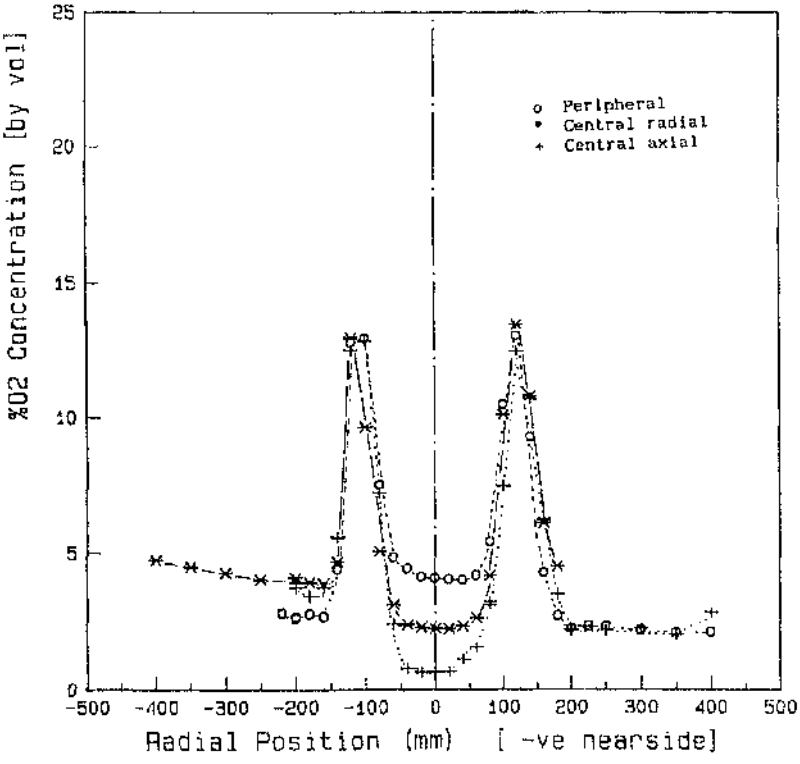

(b) S = 2.25

FIG 5.18: Radial O2 profiles, X = 45 mm, peripheral, radial and axial fuel injection modes

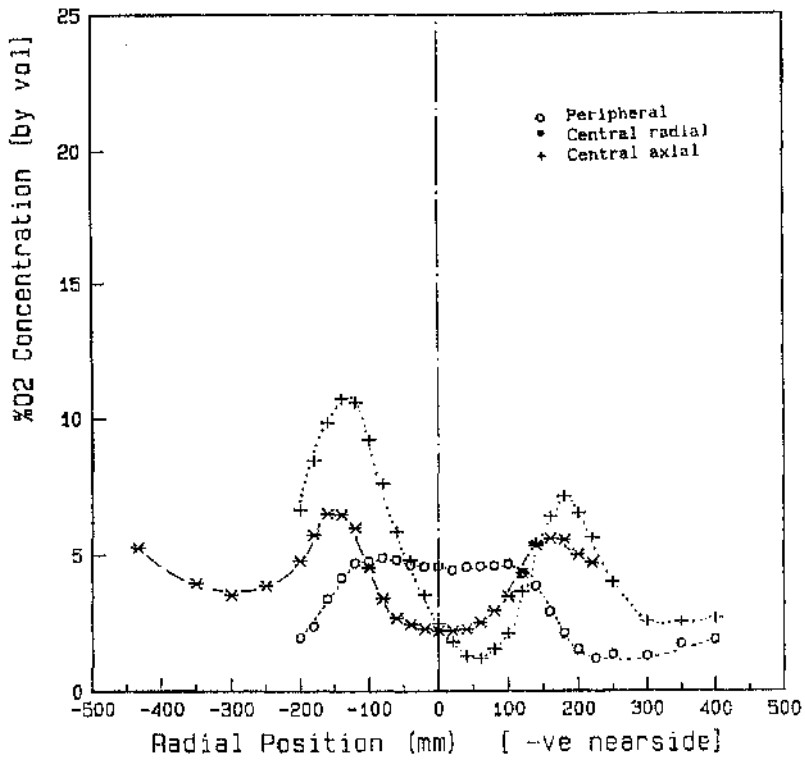

(a) S = 0.90

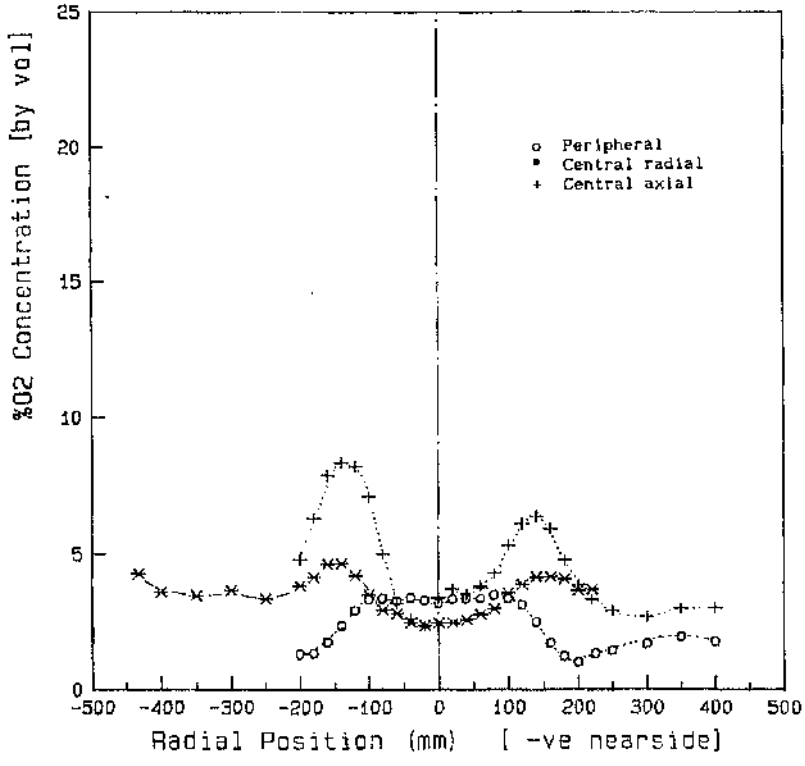

(b) S = 2.25

FIG 5.19: Radial Oz profiles, X = 200 mm, peripheral, radial and axial fuel injection modes

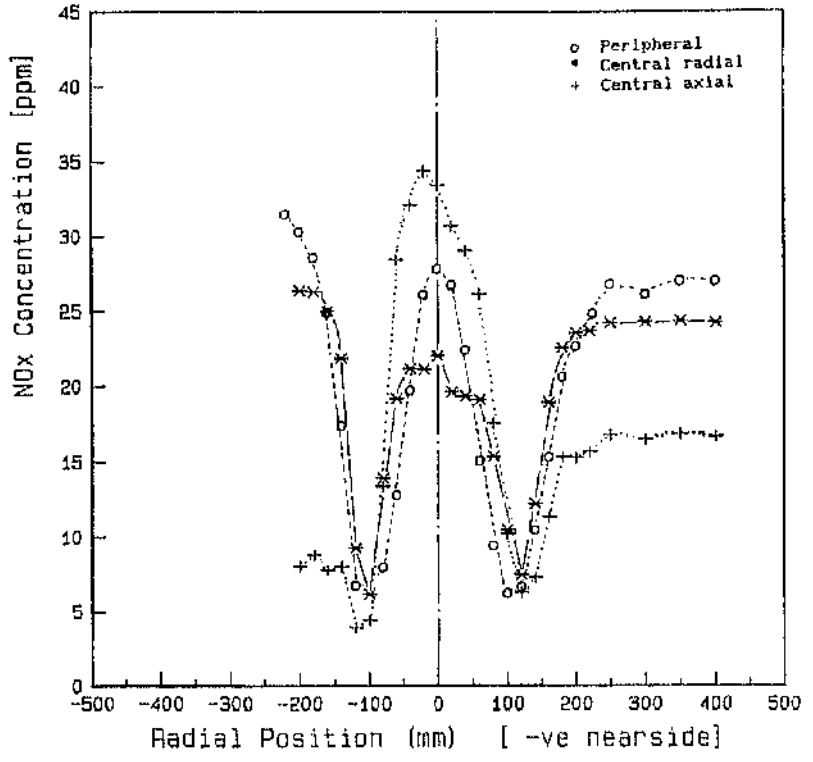

(a) S = 0.90

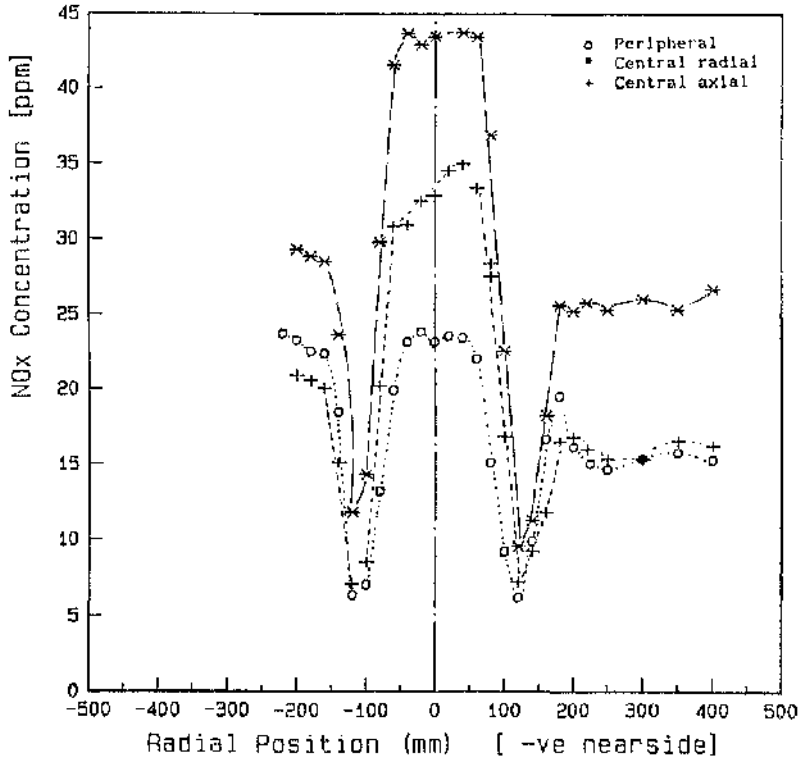

(b) S = 2.25

FIG 5.20: Radial NOx profiles, X = 45 mm, peripheral, radial and axial fuel injection modes

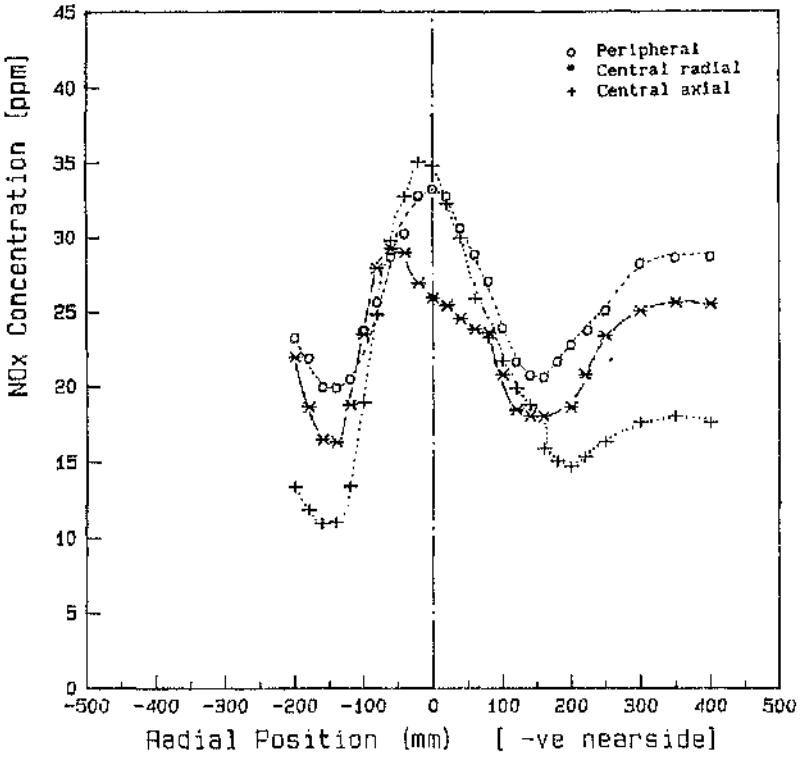

(a) S = 0.90

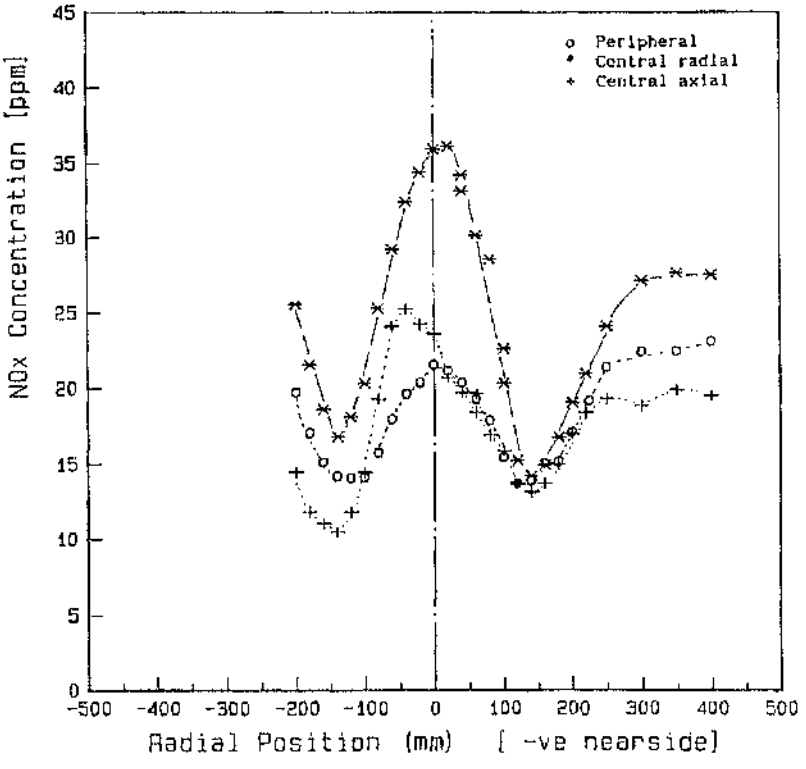

(b) S = 2.25

FIG 5.21: Radial NOx profiles, X = 200 mm, peripheral, radial and axial fuel injection modes

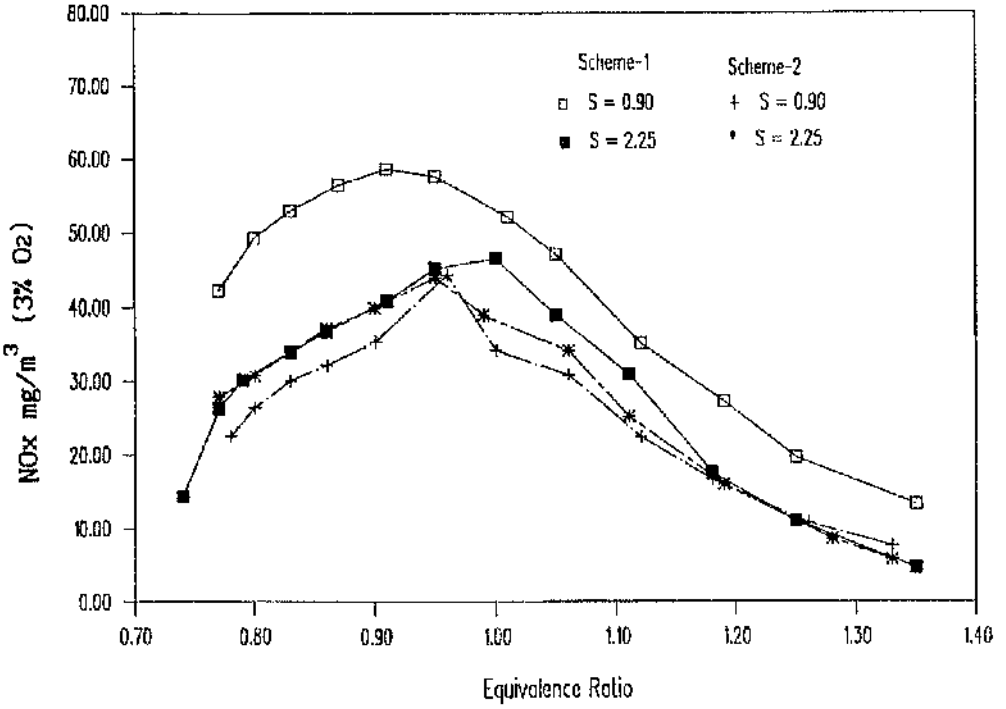

FIG 5.22: Overall NOx concentrations, peripheral fuel injection, Scheme 1 versus Scheme 2

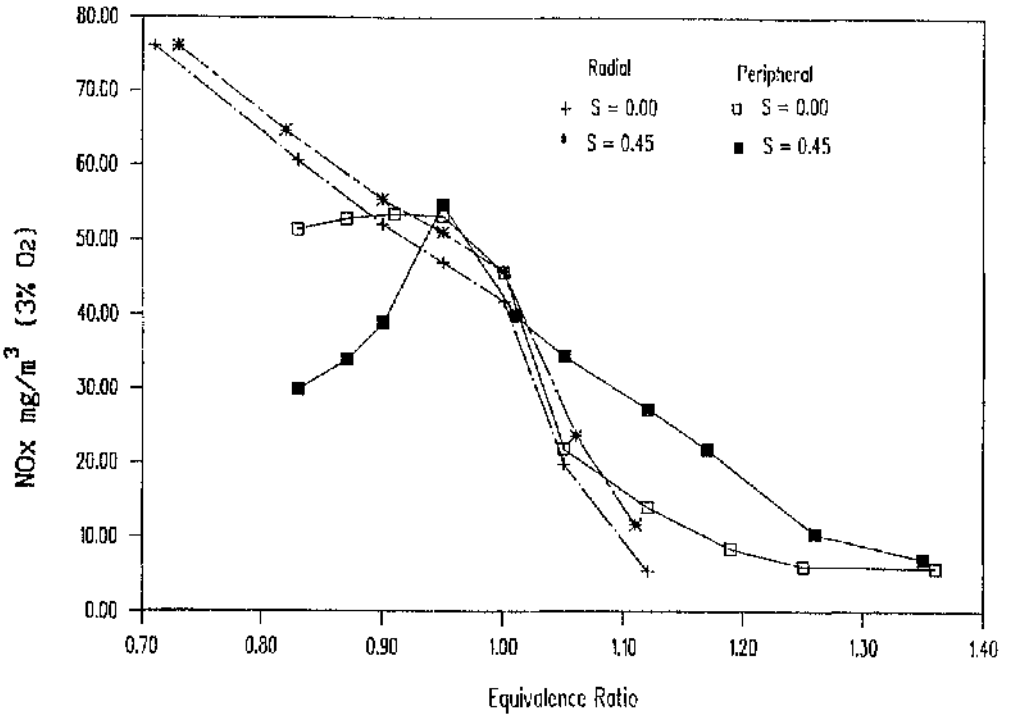

FIG 5.23: Overall NOx concentrations, peripheral (Scheme 2) versus radial fuel injection

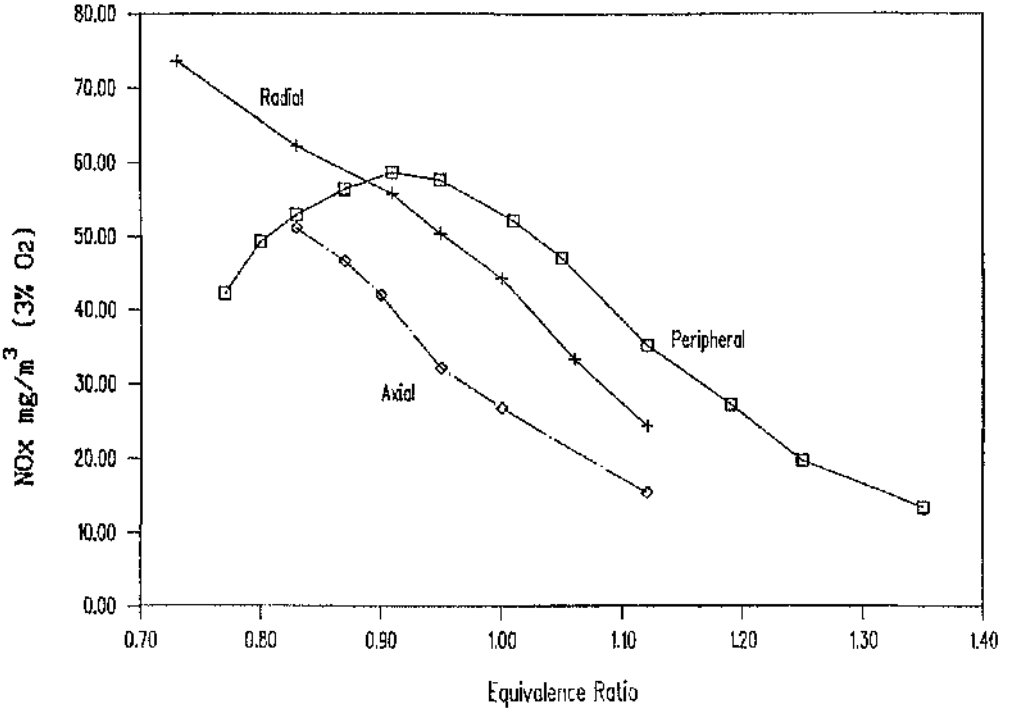

(a) S = 0.90

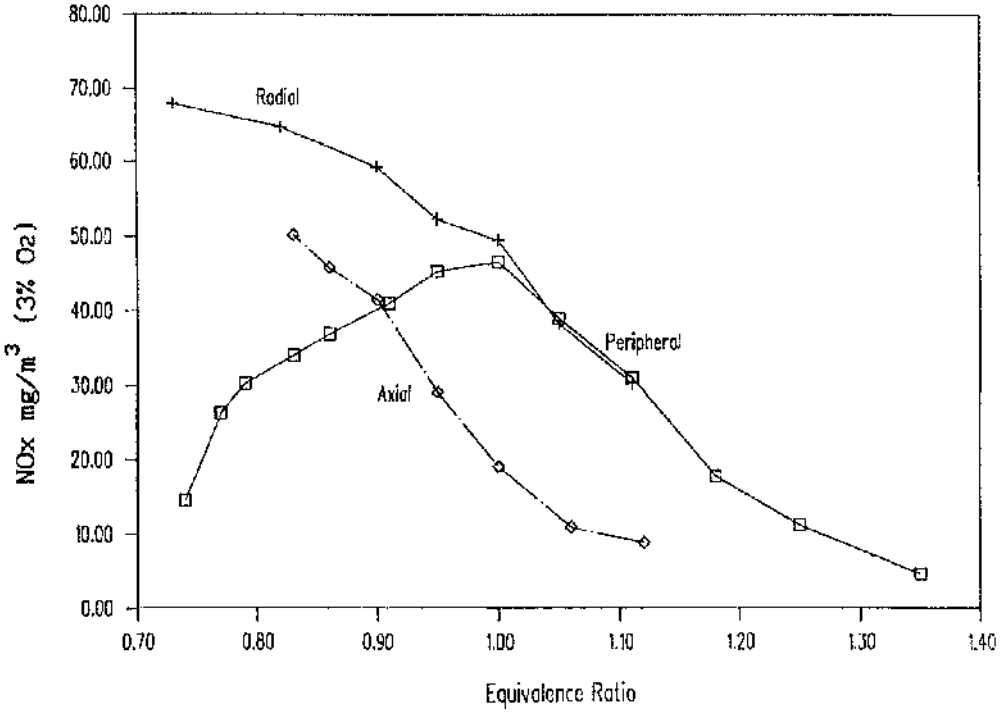

(b) S = 2.25

FIG 5.24: Overall NOx concentrations, peripheral, radial and axial fuel injection modes

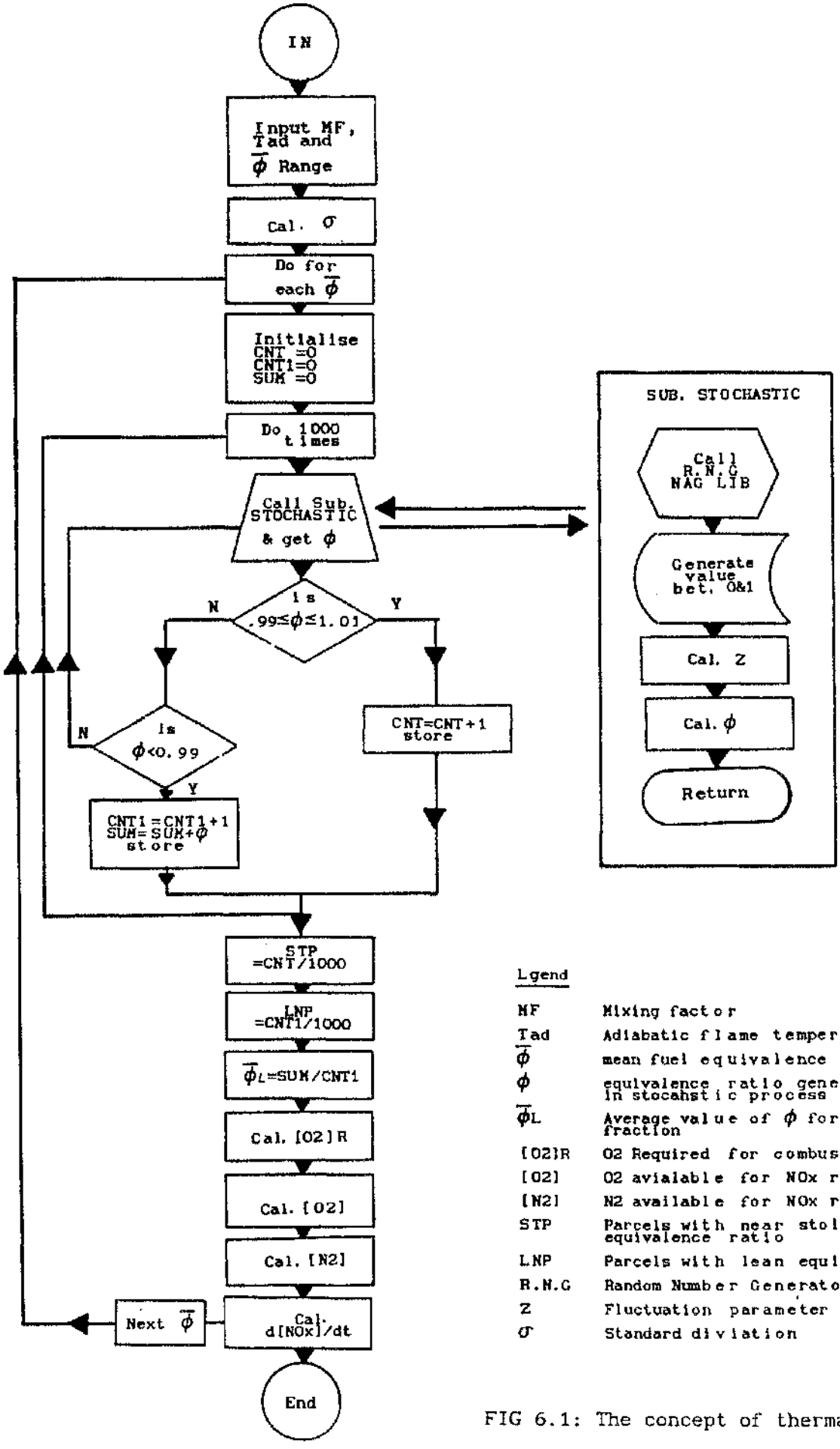

Lgend

MF	Mixing factor
Tad	Adiabatic flame temperature
$\overline{\phi}$	mean fuel equivalence retio
ϕ	equivalence ratio generated in stocahstic process
$\overline{\phi}_L$	Average value of ϕ for lean fraction
[O2]R	O2 Required for combustion
[O2]	O2 avialable for NOx reaction
[N2]	N2 available for NOx reaction
STP	Parcels with near stolchiometric equivalence ratio
LNP	Parcels with lean equivalence ratio
R.N.G	Random Number Generator
Z	Fluctuation parameter
σ	Standard diviation

FIG 6.1: The concept of thermal NOx model

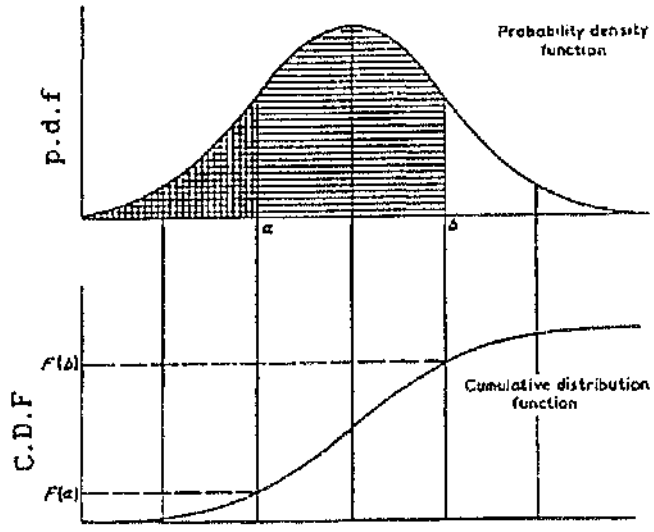

FIG 6.2.a: Probability density function (p.d.f) and cumulative density function (C.D.F) of Gaussian distribution

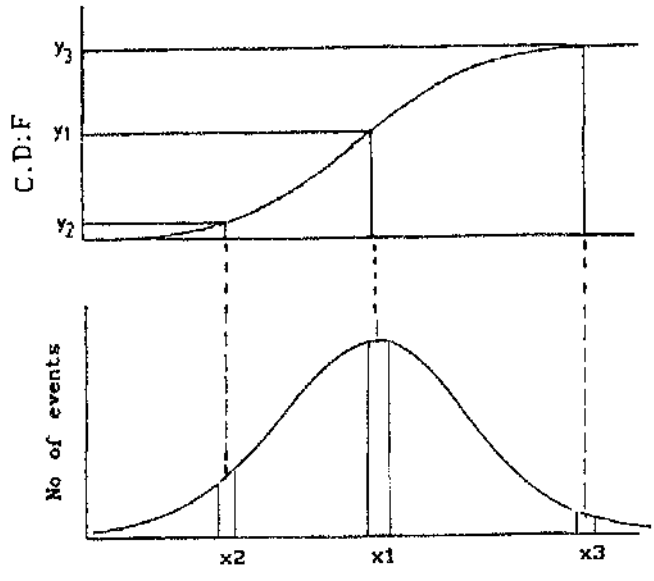

FIG 6.2.b: Graphical presentation of the method of predicting an event (equivalence ratio (ϕ) in this case)

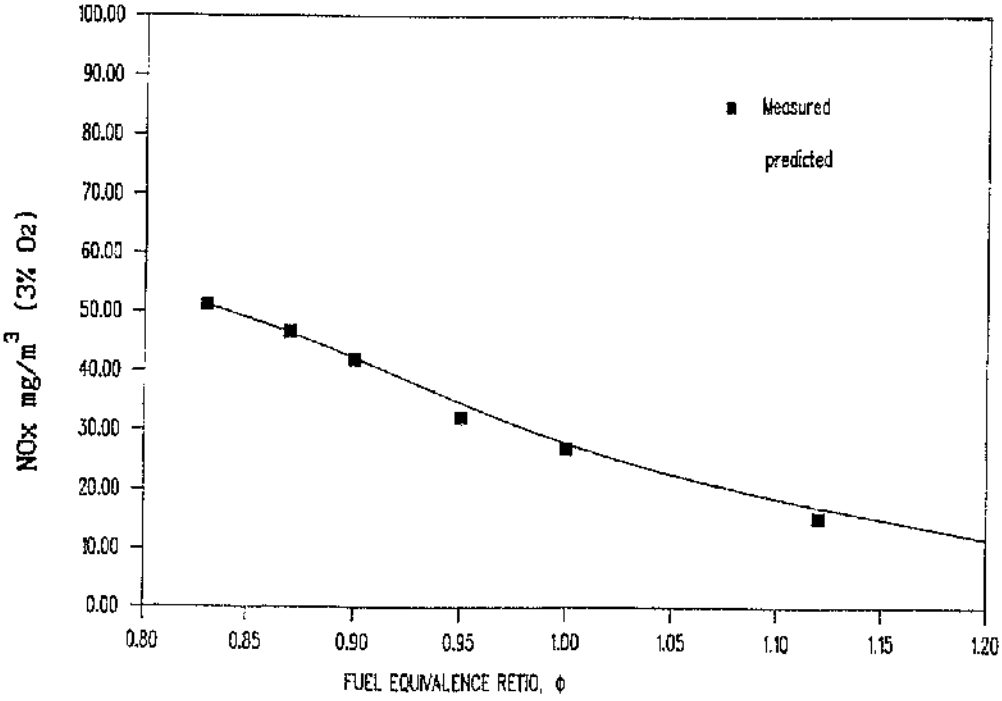

FIG 6.3: Comparison of predicted and measured NOx concentration, central axial fuel injection, S=0.90

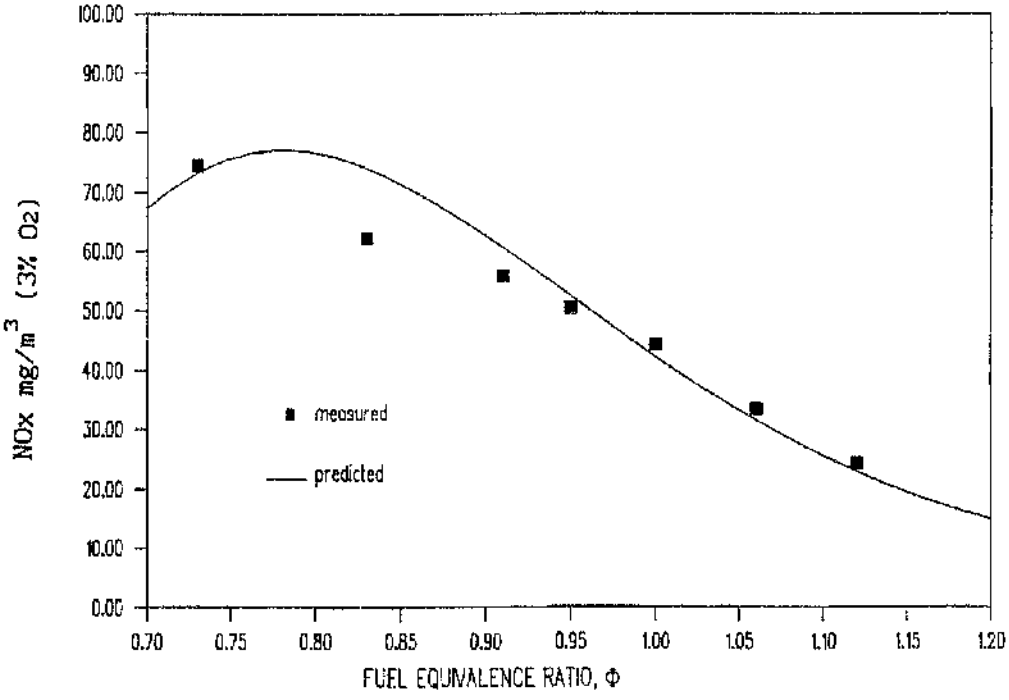

FIG 6.4: Comparison of predicted and measured NOx concentration, central radial fuel injection, S=0.90

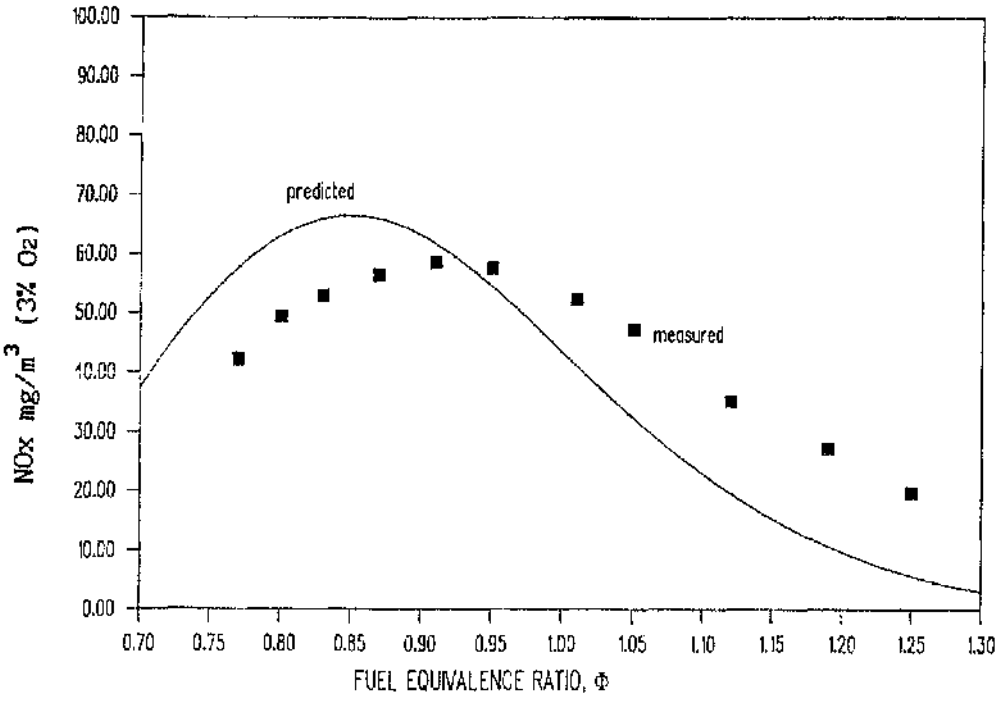

FIG 6.5: Comparison of predicted and measured NOx concentration, Peripheral fuel injection (Scheme 1), S=0.90

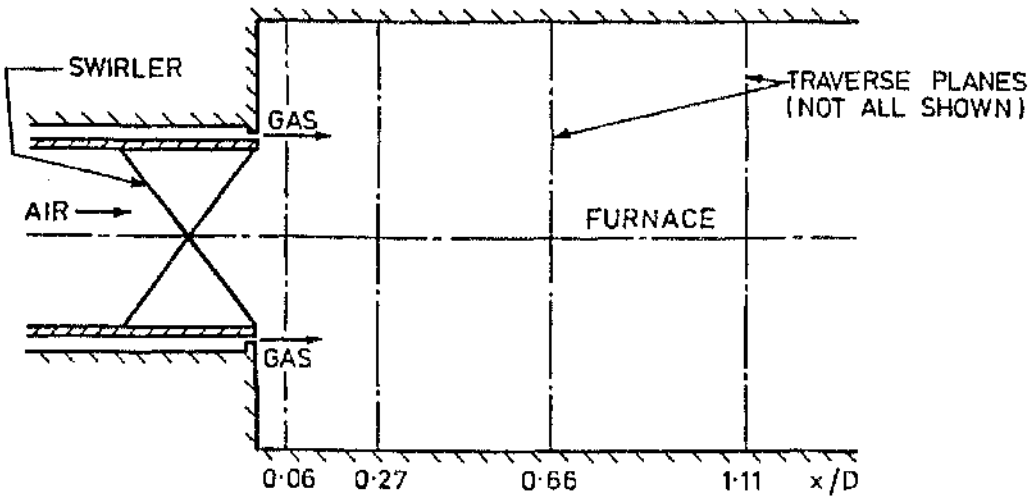

FIG 7.1: Peripheral fuel-injection burner system

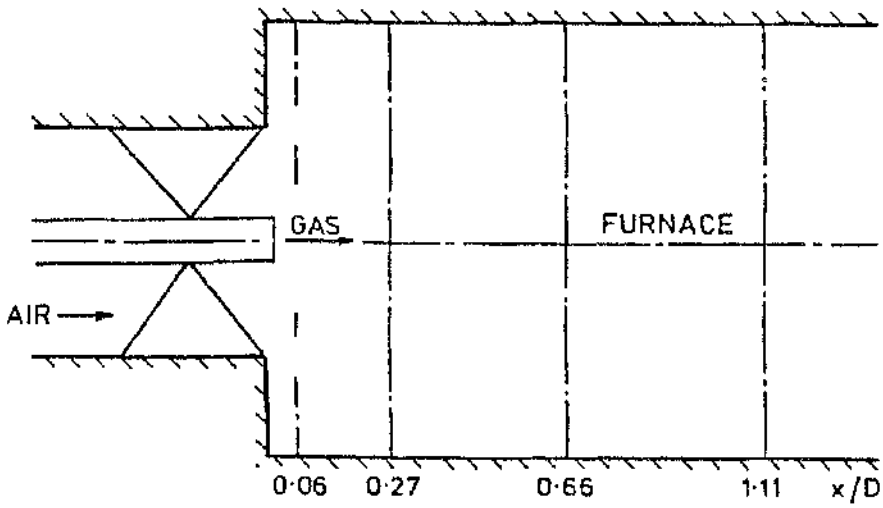

FIG 7.2: Central axial fuel-injection system

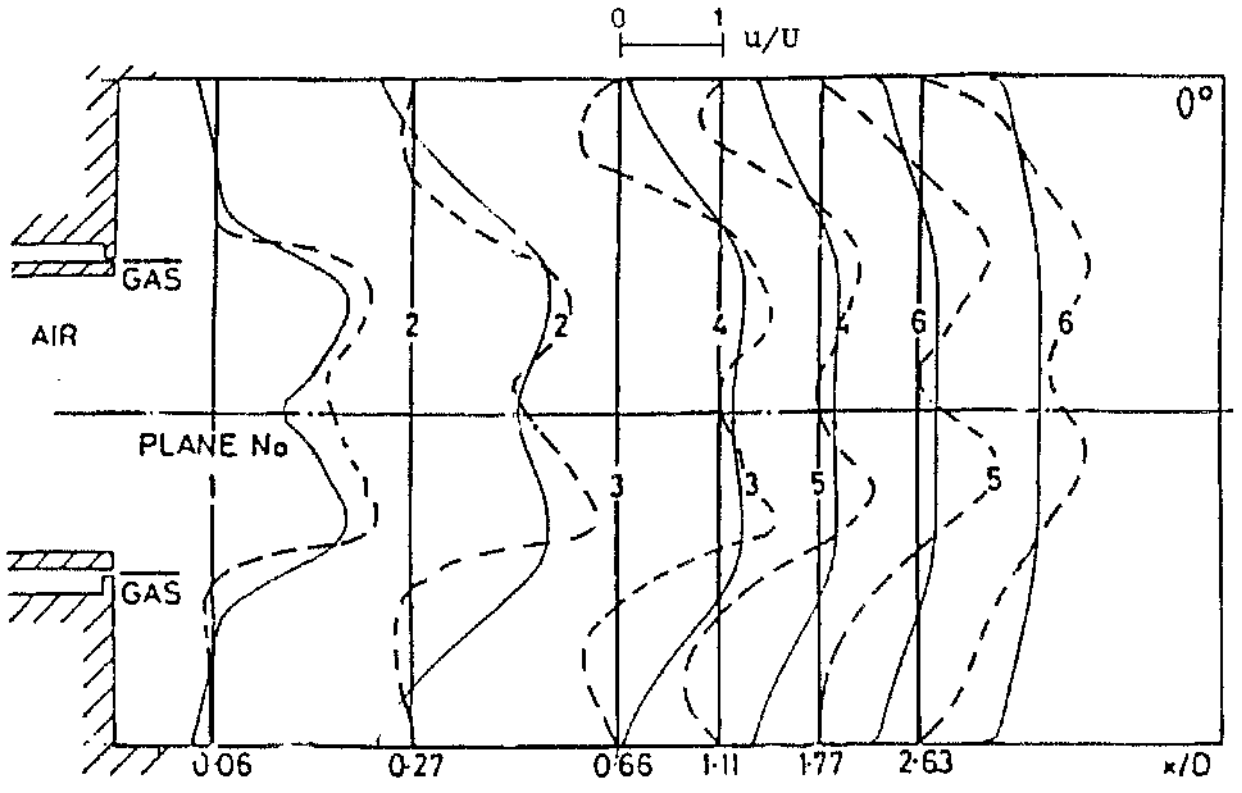

(a)

------ measurements

—— predictions

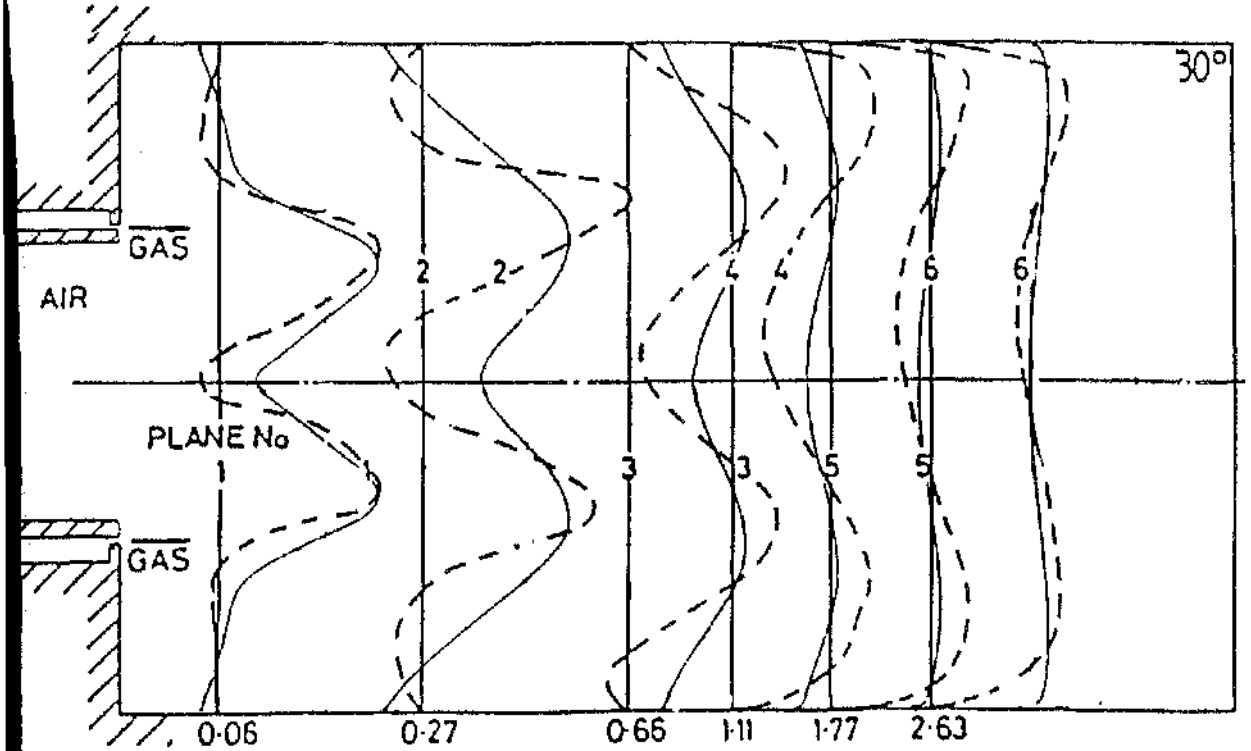

(b)

FIG 7.3: Axial velocity distributions

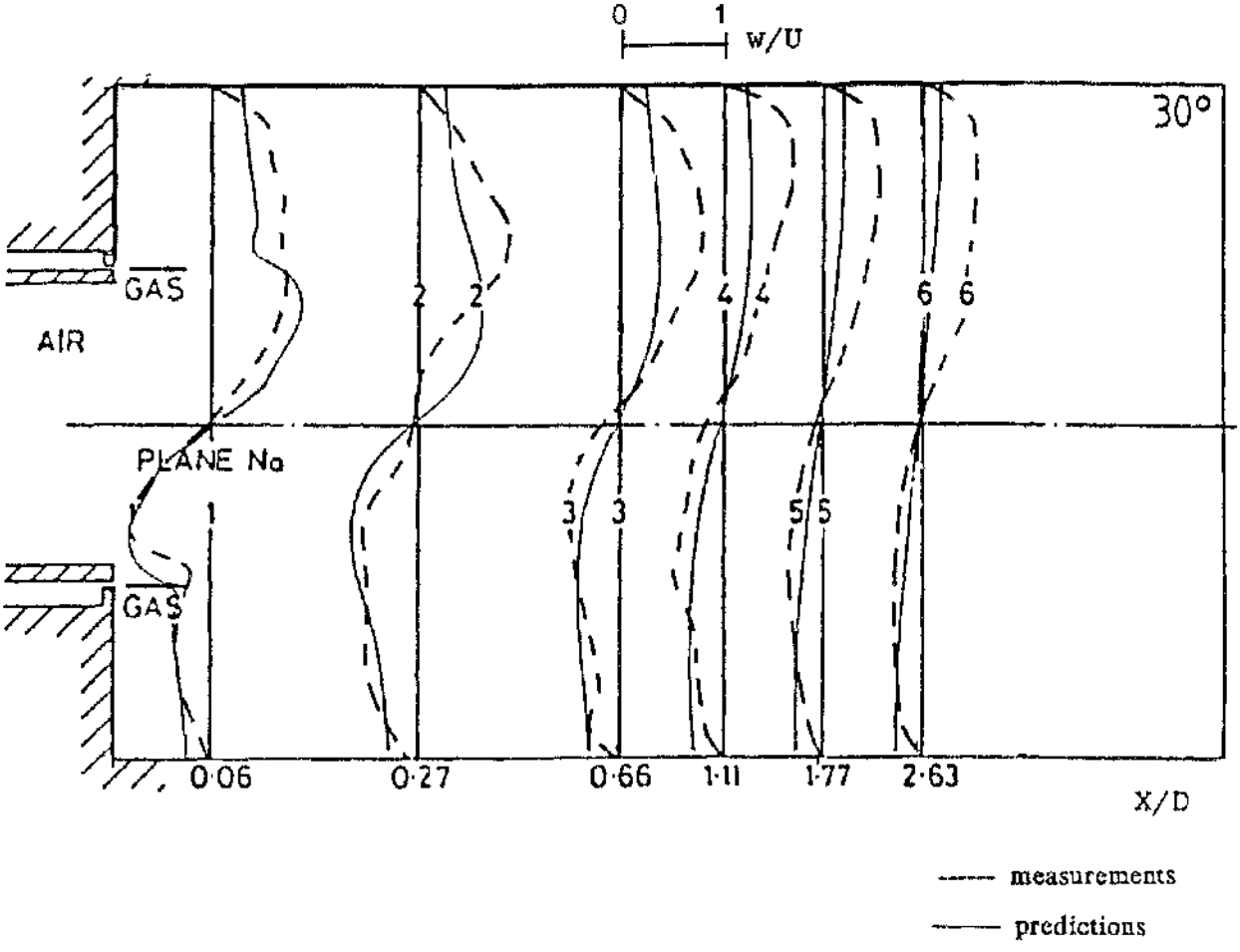

FIG 7.4: Tangential velocity distribution

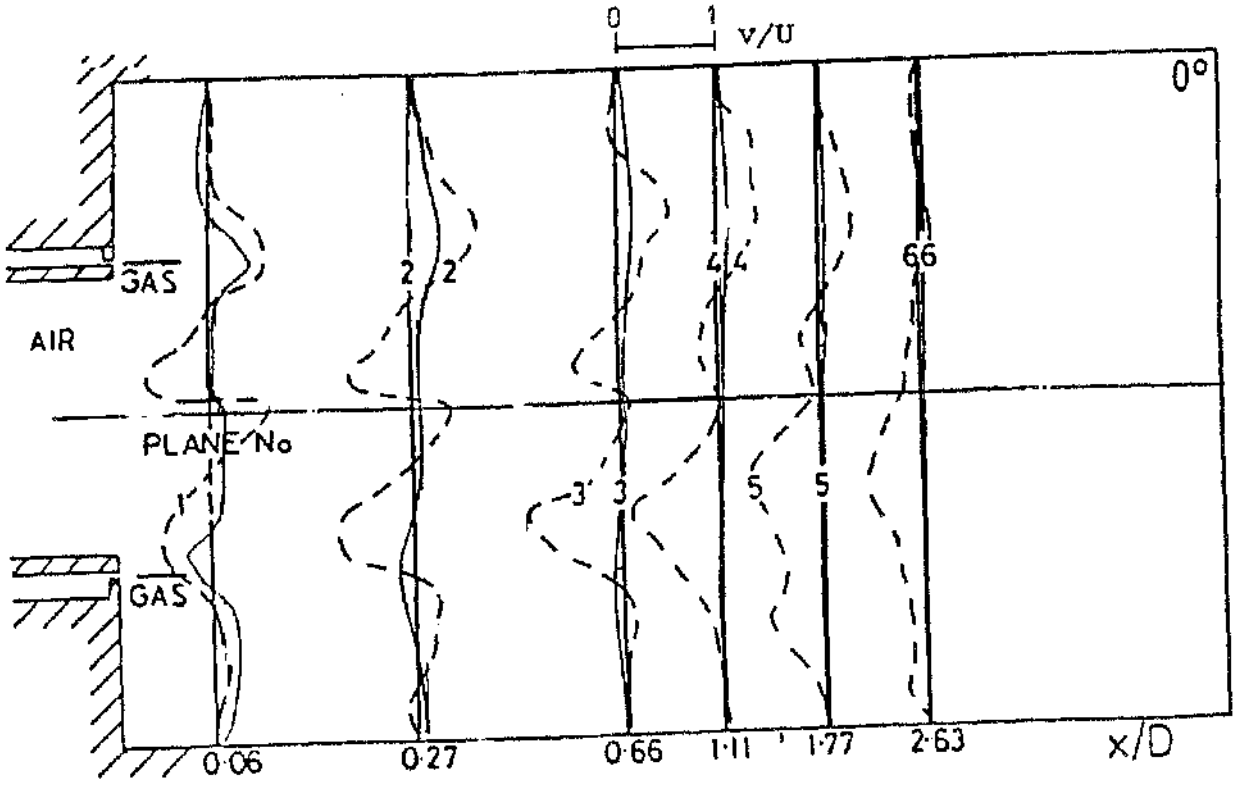

(a)

measurements

predictions

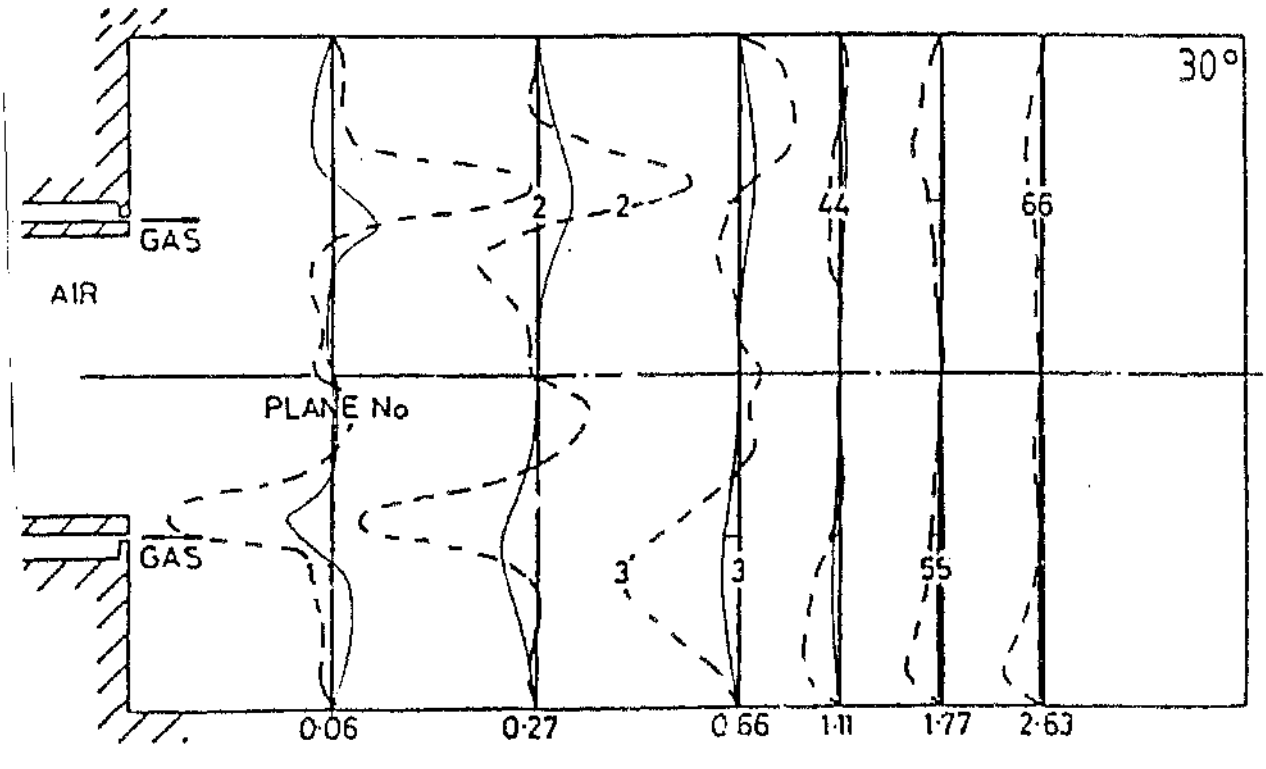

(b)

FIG 7.5: Radial velocity distributions

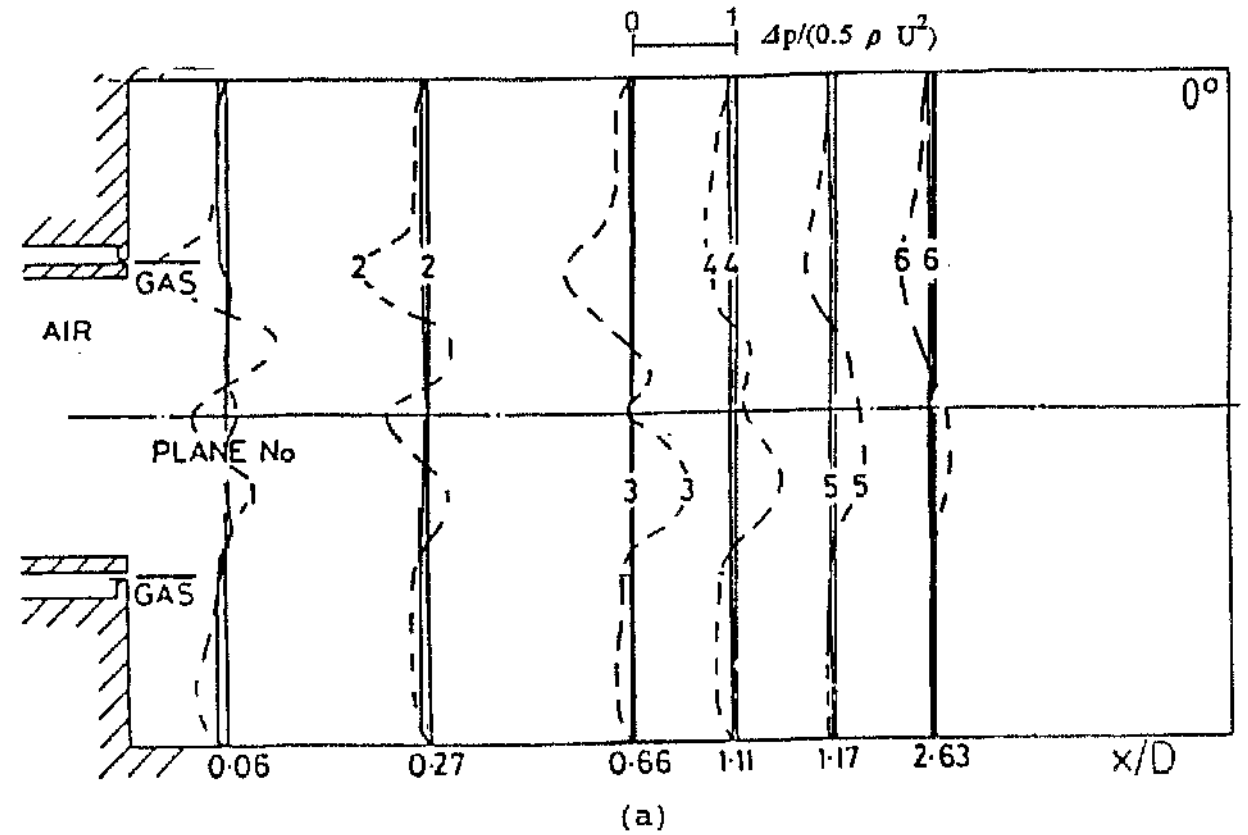

(a)

------ measurements
—— predictions

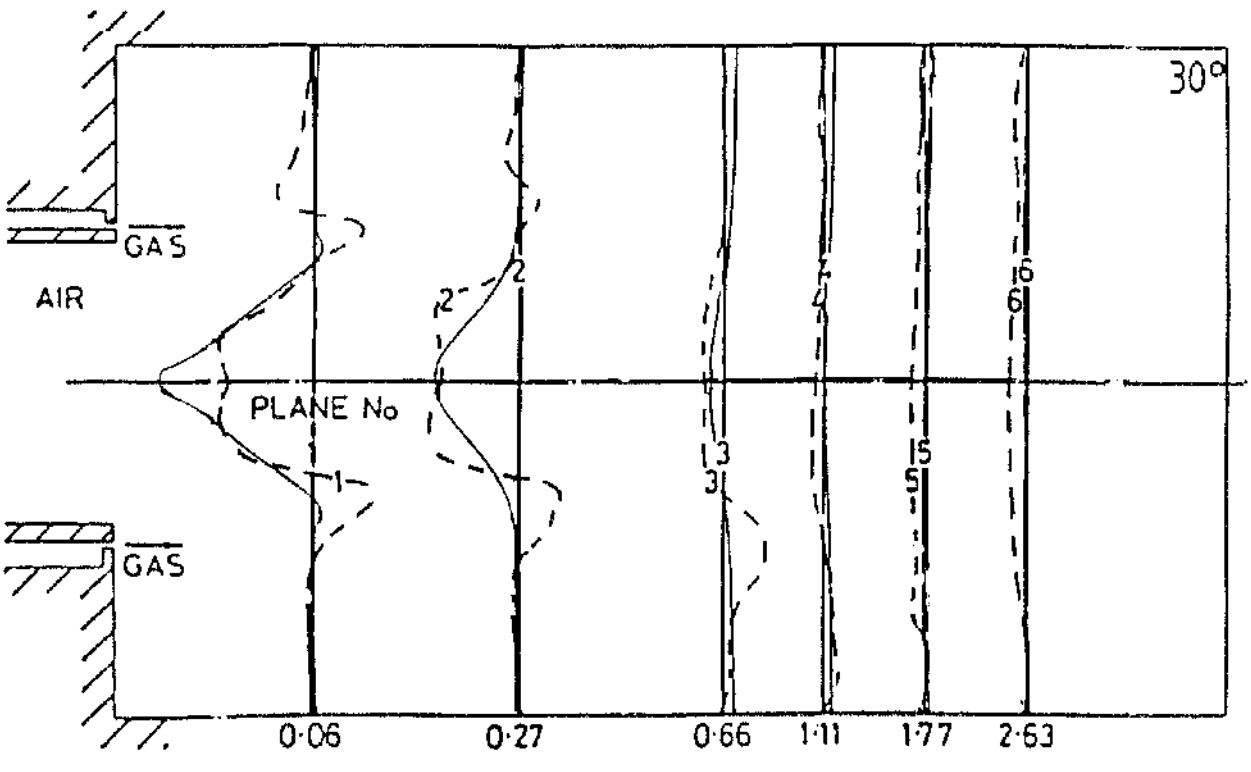

(b)

FIG 7.6: Static pressure distributions

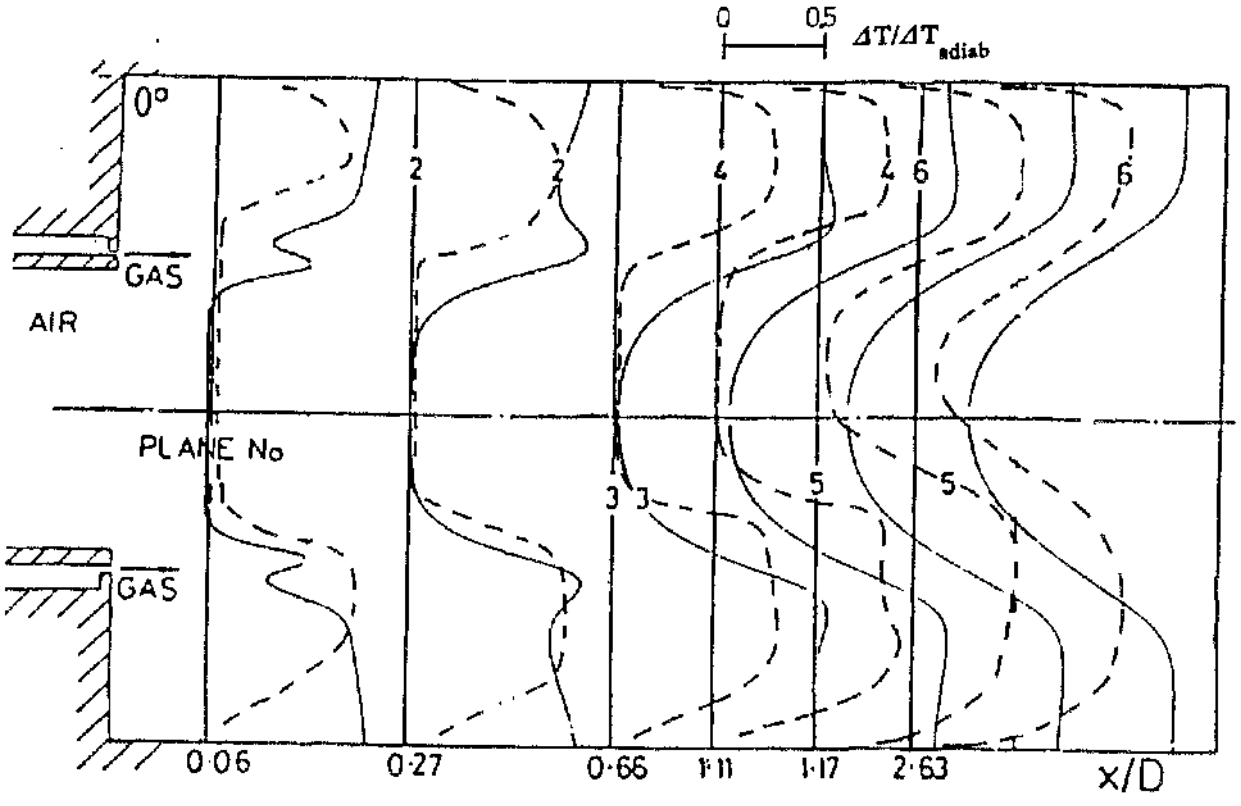

(a)

—— measurements

—— predictions

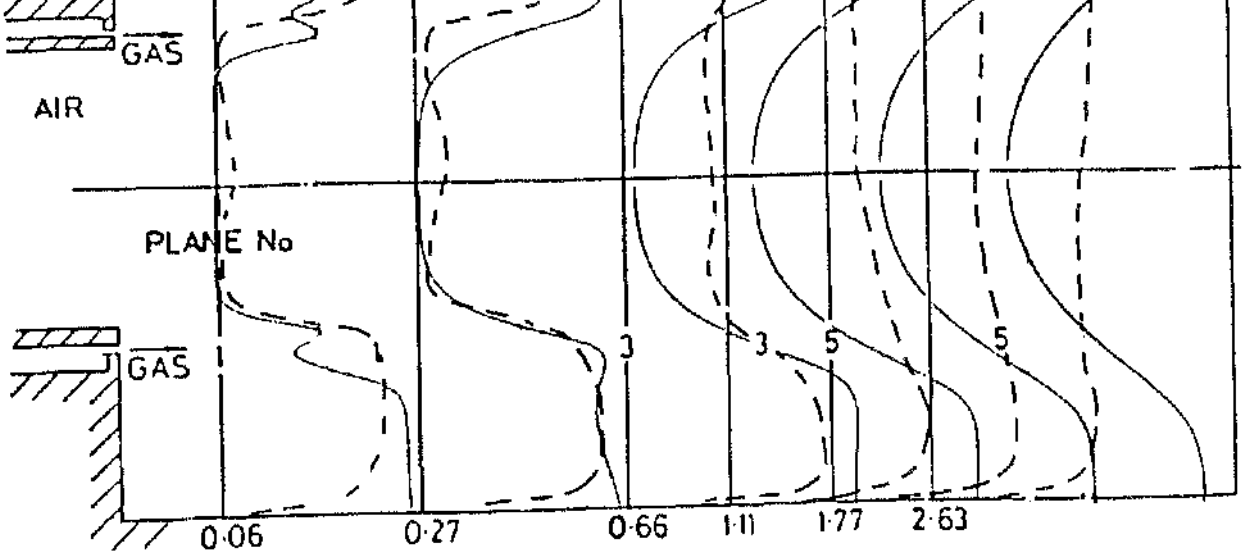

(b)

FIG 7.7: Temperature rise distributions

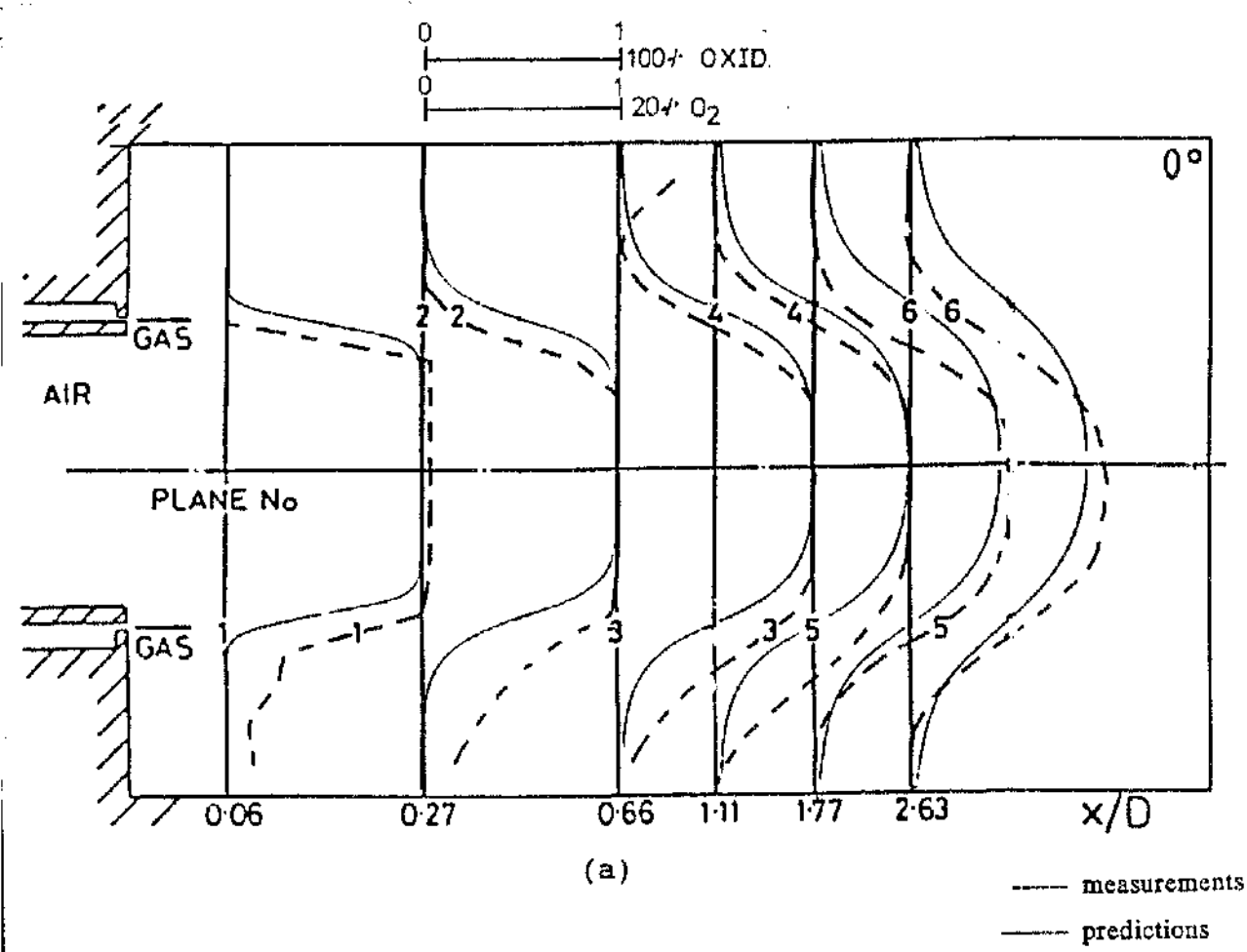

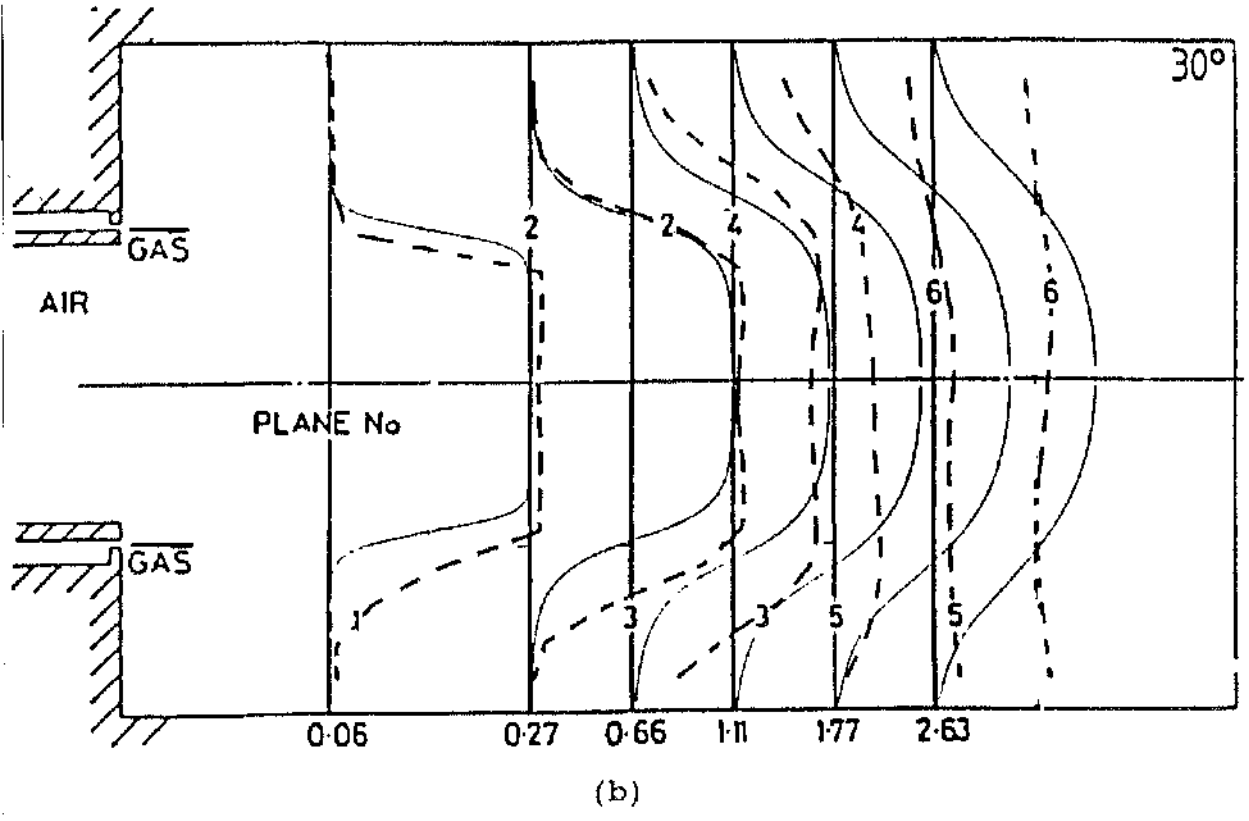

FIG 7.8: Oxidant concentration distributions

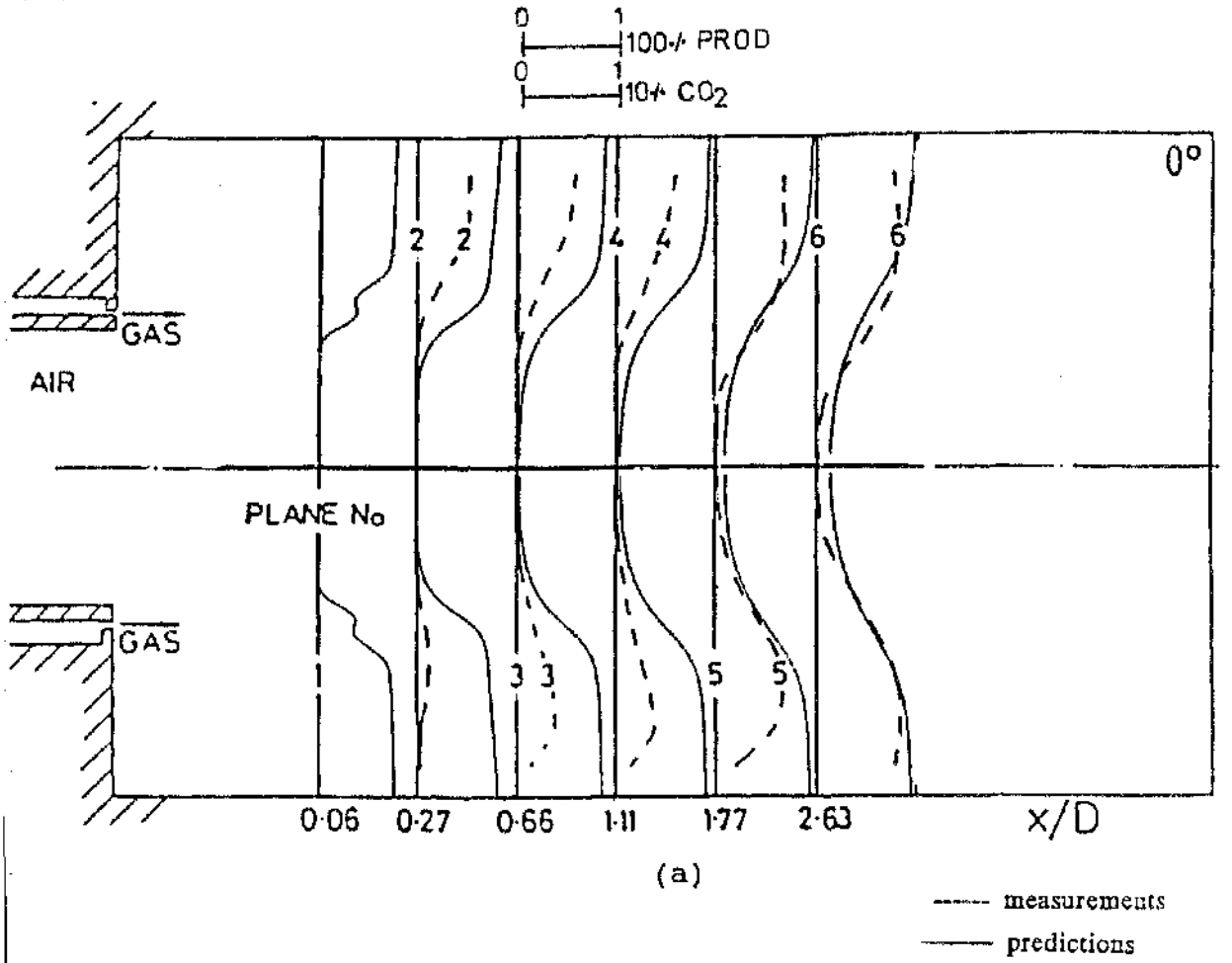

(a)

----- measurements

——— predictions

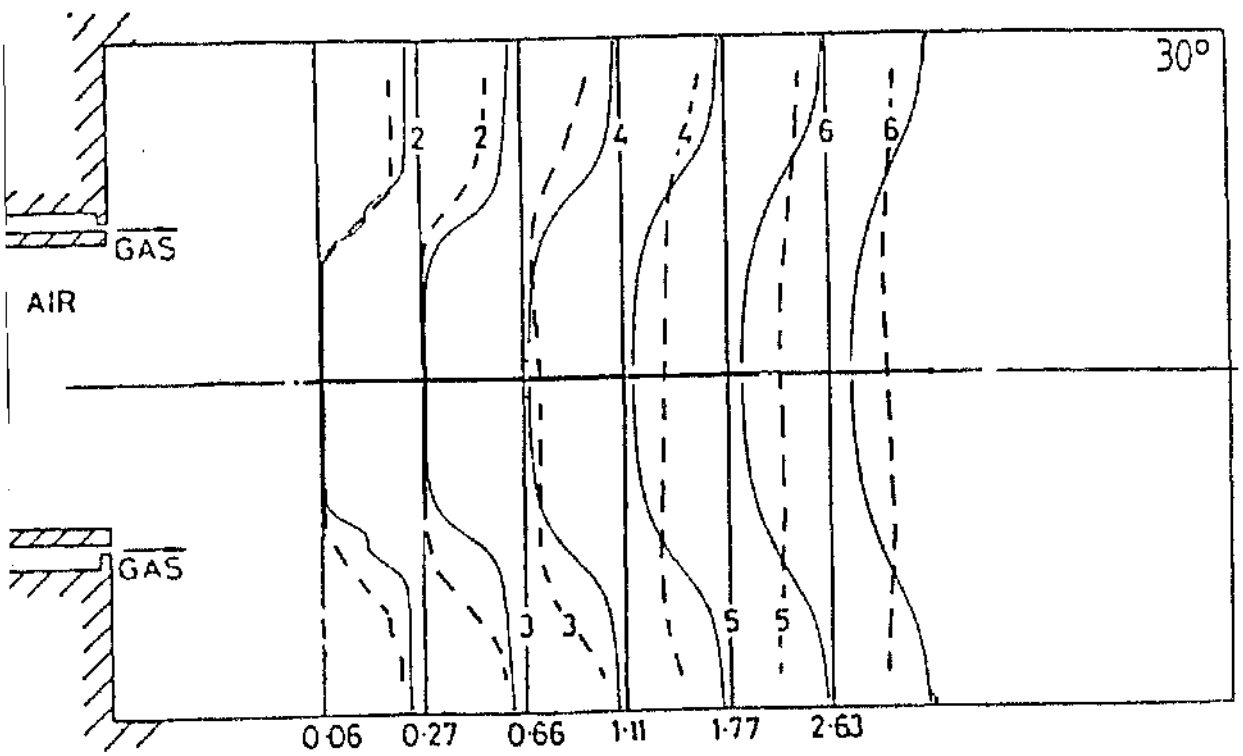

(b)

FIG 7.9: Product concentration distributions

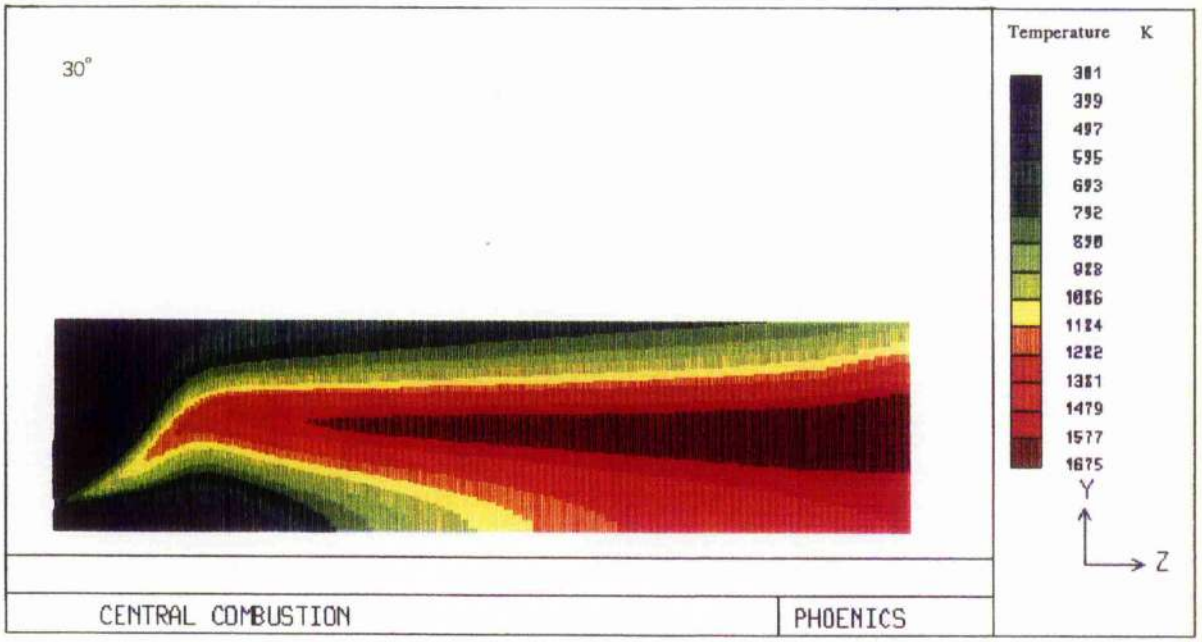

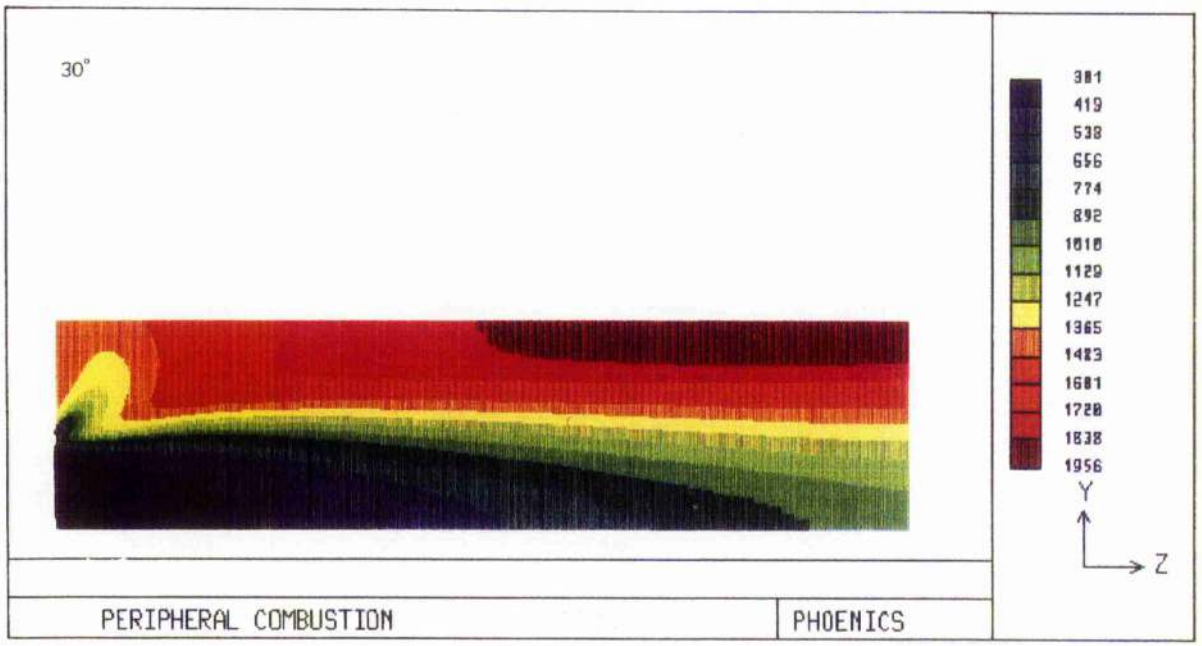

FIG 7.10: Comparison of predicted temperature rise,
Central and Peripheral fuel injection systems

APPENDIX

PUBLICATIONS

1- BELTAGUI S A, FUGGLE R N, KENBAR A M A and RALSTON T, (1989), Measurements of swirling flames aerodynamics in the NEL furnace", HTFS RS 826, NEL/HTFS 125.

2- BELTAGUI S A, KENBAR A M A and MACCALLUM N R L, (1989), "NOx generation and control in confined swirling flames-review and parametric study", HTFS RS 827, NEL/HTFS 123.

3- KENBAR A M A, BELTAGUI S A and MACCALLUM N R L, (1990), "Modelling the combustion aerodynamics for peripheral injection system", Report, Dept. Mechanical Engineering, University of Glasgow.

4- KENBAR A M A, BELTAGUI S A, RALSTON T AND MACCALLUM N R L, (1991), "The effect of burner parameters on NOx formation in a gas fired furnace- measurements and modelling", Paper submitted to the First International Conference on Combustion Technology for a Clean Environment, 3-6 Sep, Vilamoura (Algarve), Portugal.

5- BELTAGUI S A, FUGGLE R N, KENBAR A M A, RALSTON T, MARRIOTT N and STOPFORD P J, (1991), "Modelling a gas-fired furnace using the PCOC code", Parer accepted for presentation at the Euroteck Direct 91, Birmingham, 2-4 July.

6- BELTAGUI S A, KENBAR A M A and MACCALLUM N R L, (1991), "Comparison of measured isothermal and combusting confined swirling flows-Peripheral fuel injection", 2nd World conference on Experimental Heat Transfer, Fluid Mechanics and Thermodynamics, Dubrovnik, Yugoslavia.

MEASUREMENT OF SWIRLING FLAME AERODYNAMICS IN THE NEL FURNACE

S A Beltagui[1,2], R N Fuggle[1], A N A Kenbar[2] and T Ralston[1]

HTFS

1. National Engineering Laboratory, East Kilbride, Glasgow
2. University of Glasgow

ABSTRACT

This paper reports results from an extensive programme of aerodynamic and combustion measurements carried out on the NEL furnace system. The aim of these studies is to validate the HTFS mathematical models for furnace flow and heat transfer embodied in the computer programs PCDC and ZONE. Confidence in program predictions requires detailed comparison with reliable experimental measurements. Such data are vital as furnace flow and heat-transfer mathematical models are developed to handle realistic combustion system geometries. It is also necessary to provide information on the inlet profile specifications appropriate to the effective numerical modelling of such flows.

The NEL furnace is fired by natural gas through a variable-swirl burner with a quarl. Four swirl settings were considered, with burner swirl number range of 0.0-2.25.

Using a water-cooled five-hole aerodynamic probe in conjunction with a specialised data acquisition system, profiles of the three components of velocity and the local static pressure were measured at 13 planes along the chamber length.

The overall features of the swirling flow are illustrated by these profiles. The results are presented in the form of radial profiles of the three velocity components and pressure. For example, axial velocity profiles illustrate the jet boundary, degree of expansion and regions of high-velocity gradients. These also define the boundaries of the forward and reversed flow zones, the latter being fundamental to the mechanism of flame stabilization.

1. INTRODUCTION

Results reported here form part of the ongoing HTFS experimental programme of aerodynamic and combustion measurements carried out on the NEL furnace system.

These studies are aimed at the validation of the HTFS mathematical models for furnace flow and heat transfer, embodied in the

computer programs PCOC, Stopford (1989) and ZONE, Hyde et al (1984). Such validation requires comparison of computer program predictions with detailed, reliable experimental measurements. There is a continuing requirement for complete data sets which include heat transfer, combustion and aerodynamic characteristics of realistic combustion systems. These data sets will help improve the modelling capabilities of the flow and heat-transfer codes particularly when dealing with flow arrangements of significant geometric complexity, which are prevalent in industrial applications.

Measurements reported here were obtained in the NEL furnace fired by natural gas through a variable-swirl burner with a quarl. The fuel gas was radially injected through a central gun. Four swirl settings were considered, burner swirl numbers ranging from 0.0-2.25.

Earlier measurements were reported in a previous paper by Beltagui et al (1988). These described the measured boundaries of the forward and reversed flow zones which were mapped using a two-hole directional aerodynamic probe. The previous report also provided complete gas temperature contours and concentration contours for CO, CO_2 and O_2 covering the whole furnace chamber.

The present paper reports the flow patterns produced under the same firing conditions as the previous work. The results are presented in the form of profiles of the three components of velocity and the static pressure to illustrate the flow patterns associated with confined swirling flames. The data also show the effect of swirl on the flow pattern.

These flow patterns result in short intense flames with high swirl and longer flames with low or no swirl.

These measurements were made using a five-hole water-cooled probe. Radial traverses were made over 13 axial planes covering the whole furnace space.

A high degree of symmetry is evident. This is vital for the meaningful comparison with axisymmetric program predictions.

The results presented, coupled with previously reported isothermal-model data, heat transfer and combustion pattern data constitute an extremely valuable data bank for the development of the furnace modelling programs.

2. EXPERIMENTAL PROGRAMME

The NEL furnace is a model of a cylindrical upshot fired heater. The apparatus consists of a 1 m diameter x 3 m high water-cooled chamber, which is segregated into six separate cooling sections, as shown in Figure 1. The furnace is equipped with probe access ports which provide for traversing at up to six longitudinal planes in each section.

The furnace is fired by natural gas through a variable-swirl burner with a quarl. The burner used in these studies was of the moving-block swirl generator design, supplied by the International Flame Research Foundation (IFRF). This burner offers a wide, repeatable range of swirl. Figure 1 illustrates the quarl and the fuel injection geometry. The fuel is injected from 16 holes on the periphery of the fuel gun, radially outward and normal to the axial air flow. More details of the burner are given by Beltagui and Ralston (1985). Four swirl settings were considered, with

burner swirl number values of 0.0, 0.45, 0.90 and 2.25.

Air and fuel flowrates are metered at inlet by orifice plates. The furnace firing rate was set at 400 kW and an inlet air-fuel ratio corresponding to 5 per cent excess air was used. The flowrate of air and gas to the burner during each run was controlled to within ±1 per cent.

Detailed natural gas analysis was obtained from British Gas. The results indicated that, over the period of the tests, the main fuel properties were constant to within ±2 per cent for calorific value and ±1.2 per cent for density and stoichiometric air requirement.

3. MEASUREMENTS AND INSTRUMENTATION

Traverses were carried out at 13 planes along the furnace, located at axial distances from the burner quarl exit of 45, 80, 110, 160, 200, 300, 550, 800, 1050, 1300, 1800, 2300 and 2800 mm as shown by Figure 2. Additional traverses were made at some of these planes along a number of radii to check for symmetry and repeatability. Tests of the repeatability carried out at the end of the measurement campaign were satisfactory. In each plane the probe was traversed for at least 1½ radii to check the symmetry. The measurement points were spaced according to the gradients of the velocity being measured. Between 20-50 measurements were made in each plane, with increments of 10-50 mm. The absolute positioning of the probe relative to the furnace wall and baseplate was achieved to within ±2 mm. Although the probe used in this work is intrusive, there is considerable evidence from tests carried out on this system, Ralston et al (1984), that the probe readings are in agreement with laser Doppler anemometry measurements. Similar work on other combustion systems by Hillemans et al (1986) and Aoki et al (1986) also supports this conclusion.

A spherical head five-hole probe of 8 mm tip diameter, as described by Ralston et al (1984) and Chedaille and Braud (1972), was used for these measurements. The probe calibration as given by the manufacturer, IFRF (1977), was checked before the start of the measurements.

After the main part of the tests was carried out a complete calibration was undertaken. This calibration produced almost identical values for the probe calibration constants supplied by the manufacturer. However, the assumption that probe longitude angle is a simple function of the pressure differentials was rechecked. The results indicated that for non-zero pitch angles this assumption is invalid and an additional calibration factor is required, as reported by Beltagui and Kenbar (1989). The results of the measurements were reprocessed with this factor taken into consideration.

Experience with this kind of probe is that the higher are the values of yaw angle (greater than 60) and pitch angle (greater than 40) the less reliable are the probe results. This condition occurs mainly in the very low velocity zones, such as the outer recirculation zone and the jet boundary. It is also noted that for regions of low velocity associated with high pressure fluctuations the probe measurements are subject to errors. Such conditions were noted for furnace sections more than 1.0 m downstream from the burner especially at high swirl where the flow filled the whole furnace section. The expected average

axial velocity in this case is about 0.5 m/s. When the gas temperature is 900°C this velocity corresponds to total pressure of 0.004 mm water. However, at these sections the flow becomes almost uniform, thus, measurements in these sections are not reported here. Combustion pattern measurements also indicate that all the important flame developments occur before these levels.

The pressure differences were measured using pressure transducers. The zero of these transducers was set to within 0.001 mm water. The pressure transducers were calibrated and found to be accurate to within ±0.010 mm water.

The pressure differentials for the five probe readings were read simultaneously using five pressure transducers and averaged over a period of about one minute. The local gas density was calculated at each point using the temperatures measured earlier by the suction pyrometer.

The probe radial traverse and the probe pressure readings were all driven by a microcomputer which was programmed to calculate the velocity components' values using the probe calibration, Beltagui and Ralston (1985).

Due to the small size of the probe holes they are subject to blockage by dust or condensation of water vapour from the furnace gases thus leading to erroneous readings. The probe holes were regularly purged with nitrogen through a special arrangement of solenoid valves and gas flow metering connected to the five probe holes. This arrangement was designed to isolate pressure transducers during the purge cycles.

4. EXPERIMENTAL RESULTS

The results of the measurements are presented in the form of radial profiles of the three velocity components and the static pressure at the different levels surveyed. These are illustrated by Figures 3, 7, 8 and 9. In general, the profiles show a good degree of symmetry.

4.1 Axial Velocity Profiles

Figures 3a-d give the measured axial velocity profiles. The forward and reverse flow boundaries are defined by these profiles. The axial velocity profiles show that for all the four cases the flow pattern is essentially the same, Type D, according to the classification of Beltagui and Maccallum (1976). In this pattern, near the burner, the flow consists of a central reverse-flow zone (CRZ) surrounded by an annular jet containing the main forward flow. Outside the forward flow a weak peripheral reverse flow zone (PRZ) extended to the walls. The very low PRZ velocity observed here is a result of the low confinement manifest in a furnace to quarl diameter ratio of 5.

For the forward flow, both value and radial positions of peak velocity increase with increased swirl. The high velocity gradients at the boundaries of the forward flow increase even further with swirl. These gradients represent enhanced shear at the jet boundaries. This explains the higher mixing and combustion rates hence the short intense flames, associated with the high-swirl flows, as measured by Beltagui et al (1988).

The rate of decay of maximum axial velocity along the furnace is accelerated at high

swirl, as shown by Figure 4. This indicates that the rate of jet area expansion exceeds the rate of gas volume expansion at these points. Further downstream from about 0.4 m axial distance, the low swirl jets occupy the central area of the furnace whereas the high-swirl jets tend to spread over a larger area.

Figure 5 demonstrates the recovery of the centreline axial velocity along the furnace, the minimum recovery is associated with the highest swirl.

4.2 Flow Boundaries

Figure 6 illustrates the boundaries of the forward flow, thus indicating the size of the CRZ and the location of the jet outer boundary. For the first 200 mm distance from the burner, the jet radial expansion is nearly the same for all the cases measured. Further downstream the jet radial expansion is shown to increase with swirl, thus bringing the jet reattachment point nearer to the burner, from 1.5 m at zero swirl number to about 1 m when swirl number is increased to 2.25.

It was found that a central reverse-flow zone (CRZ) exists for all cases tested, even in the absence of swirl. The CRZ, in the absence of swirl and at low swirl, is promoted by the aerodynamic bluff body created by the radial fuel jets emerging from the fuel gun.

Over the range of swirl considered, both the maximum diameter and the length of the CRZ increase with swirl. These observations agree qualitatively, with the isothermal model results reported by Beltagui et al (1987, 1988). In general, the isothermal flow CRZ is wider and longer than that observed in the combusting flow results illustrated here.

4.3 Tangential Velocity Profiles

These are presented as Figures 7a-c. The tangential velocity values are an indication of the local swirl strength which contributes to mixing and combustion. The high-swirl jets produce a Rankine-type vortex. These profiles also indicate the rate of decay of swirl along the furnace. This rate of decay increases with swirl resulting in very low swirl velocities in all the cases beyond the first 1 m length of the furnace.

4.4 Radial Velocity Profiles

Figures 8a-d show the profiles of the radial velocity. The radial component is an indicator of the jet spread in direction and magnitude. Both their magnitude and rate of decay along the furnace increase with swirl.

4.5 Static Pressure Profiles

These are shown by Figures 9a-d. All pressure values are below ambient pressure with the minimum values near the burner. With high swirl some radial pressure gradients exist leading to a pressure depression at the centre of the flow. Throughout most of the CRZ and PRZ the pressure profile is almost uniform.

5. CONCLUSIONS

The overall features of the combusting swirling flow are illustrated by measured data presented here. These demonstrate a high degree of flame symmetry. They show the effect of swirl in producing flows with higher gradients of the velocity components. This produces higher shear rates,

enhanced mixing, thus more intense and shorter flames with higher heat-transfer rates in the zones nearer to the burner.

The results presented, coupled with previously reported heat-transfer and combustion data, constitute an extremely valuable data set for development of the furnace computer models. Effort is now being directed towards the comparison of these experimental data with the predictions of the PCOC program.

ACKNOWLEDGEMENTS

The work was carried out under the research programme of the Heat Transfer and Fluid Flow Service (HTFS) and was supported by the Department of Trade and Industry. A M A Kenbar wishes to acknowledge the support of the Government of Iraq. This paper is Crown copyright.

REFERENCES

ADKI, K., SHIBATA, M. and NAKAYAMA, Y., (1986), "Study of the flow with a swirl flow in a cylindrical combustor, 2nd report, Characteristics of turbulence for the swirl number", Bull. JSME, Vol. 29, pp 4113-4121.

BELTAGUI, S. A., (1986), "Prediction of heat transfer in furnaces. Part 2: Simple models and input parameters", HTFS RS657, NEL/HTFS 87.

BELTAGUI, S. A., (1987), "Prediction of heat transfer in furnaces. Part 2: ZONE 3 code predictions", HTFS RS715, NEL/HTFS 105.

BELTAGUI, S. A. and KENBAR, A. M. A., (1989), "Calibration of five-hole probe at the NEL", NEL Internal Report, to be issued.

BELTAGUI, S. A. and MACCALLUM, N. R. L., (1976), "Aerodynamics of vane-swirled flames in furnaces", J.Inst. Fuel, Vol. 49, pp 183-193.

BELTAGUI, S. A. and RALSTON, T., (1985), "An isothermal model study of aerodynamics and mixing in the flow issuing from a variable-swirl burner", HTFS RS602, NEL/HTFS 63.

BELTAGUI, S. A. and RALSTON, T., (1985), "Measurements of heat transfer from variable-swirl gas flames in the NEL furnace", HTFS RS653, NEL/HTFS 86.

BELTAGUI, S. A., FUGGLE, R. N. and RALSTON, T., (1987), "Aerodynamics and mixing within the quarl of a variable-swirl burner", HTFS RS713, NEL/HTFS 102.

BELTAGUI, S. A., FUGGLE, R. N. and RALSTON, T., (1988), "Combustion pattern measurements for swirling flames in the NEL furnace", HTFS RS756, NEL/HTFS 113.

CHEDAILLE, J. and BRAUD, Y., (1972), "Industrial flames", Vol. 1, "Measurements in flames", Edward Arnold Publishers, London.

FABER, A., (1980), "Manual and calibration sheets of the five-hole velocity tube", International Flame Research Foundation, Ijmuden, The Netherlands.

HILLEMANNS, R., LENZE, B. and LEUCKEL, W., (1986), "Flame stabilisation and turbulent exchange in strongly swirling natural gas flames", 21st International Symposium on Combustion, The Combustion Institute.

HYDE, D., TRUELOVE, J. S. and SYKES, J., (1984), "ZONE3 - Program users' manual", AERE-R 11652.

RALSTON, T., FUGGLE, R. N., PITCHER, G. F., LEE, O. K., OLD, C. F. and SYKES, J., (1984), "Velocity measurements of cold flows through a variable-swirl burner at NEL", HTFS RS549.

STOPFORD, P. J., (1989), "PCOC users' manual", AERE-R12626.

LIST OF FIGURES

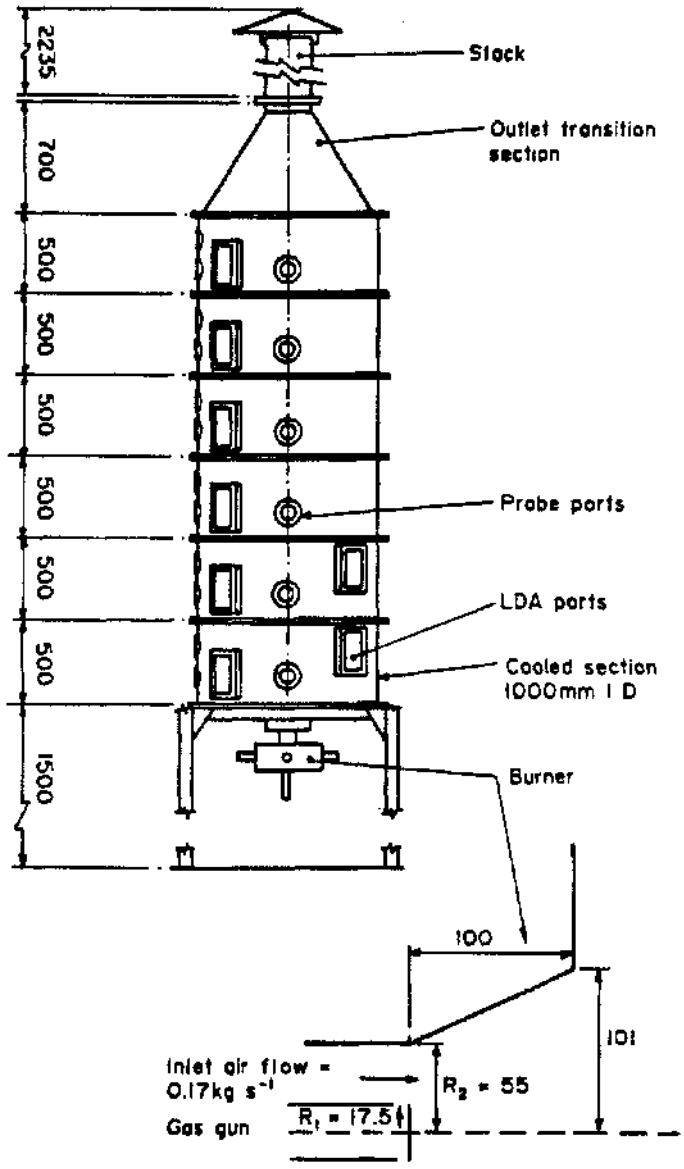

FIG 1 SCHEMATIC OF FURNACE AND BURNER

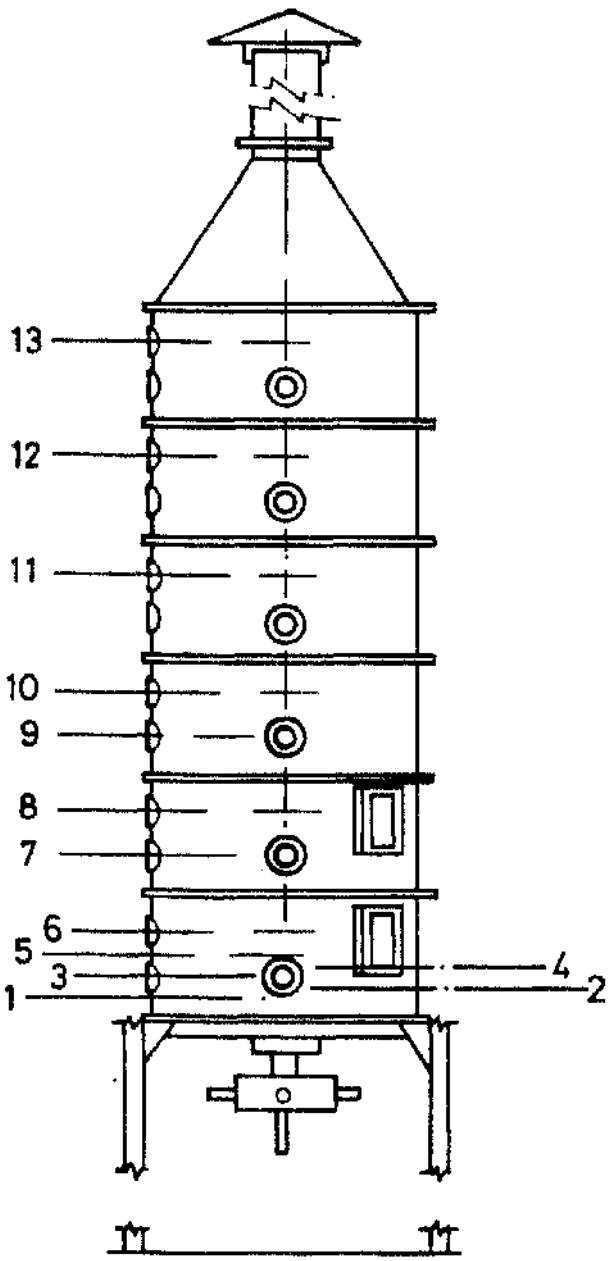

Fig 2 Furnace Traversing Planes

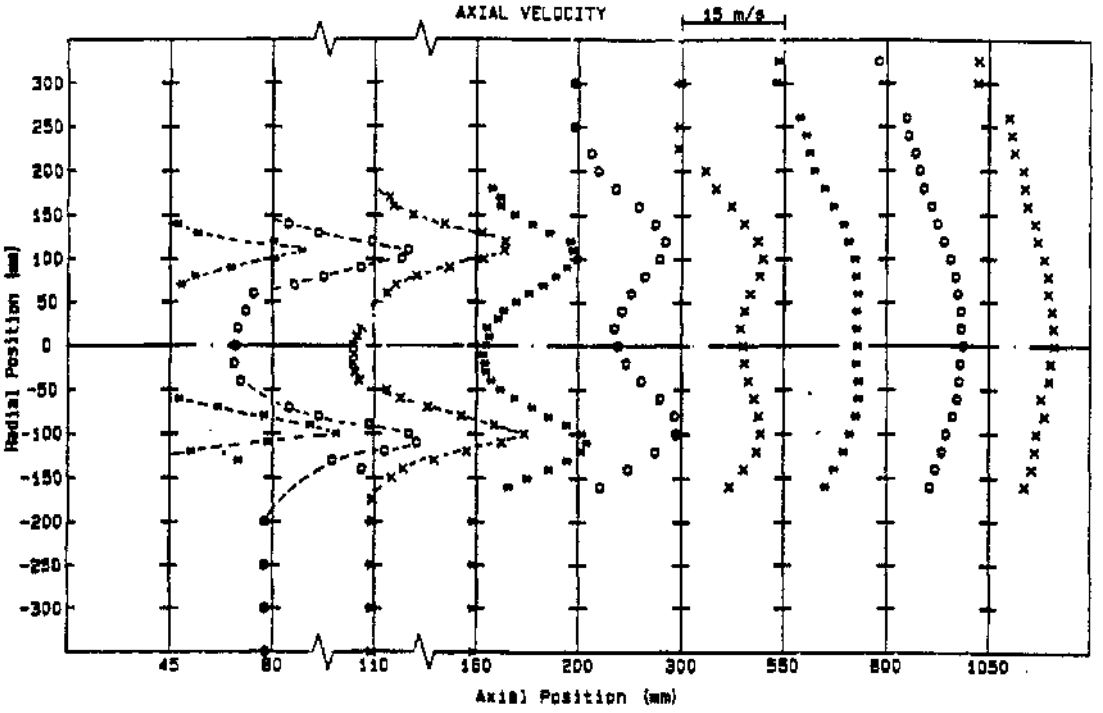

FIGURE 3-a: AXIAL VELOCITY PROFILES - S = 0.00

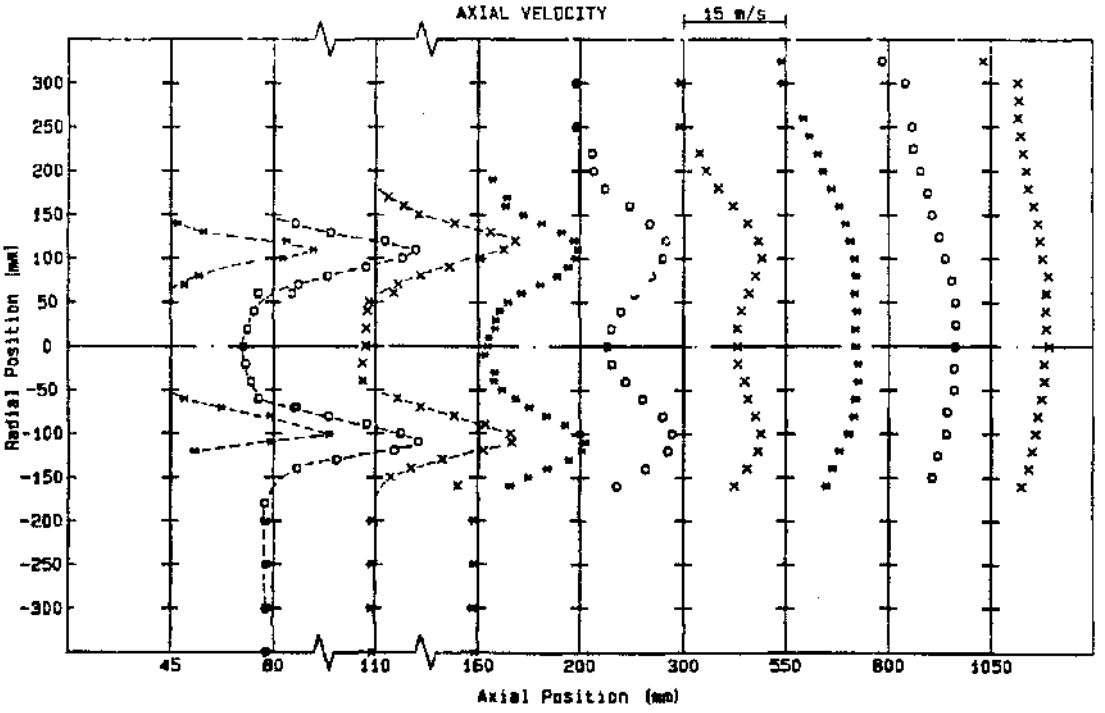

FIGURE 3-b: AXIAL VELOCITY PROFILES - S = 0.45

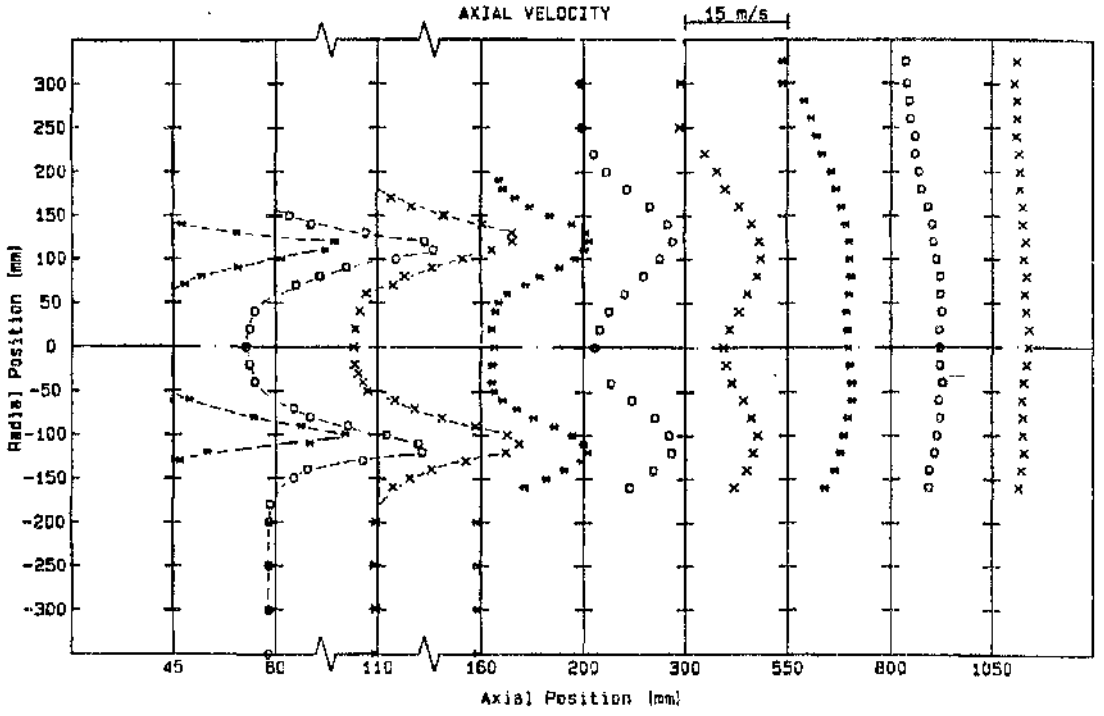

FIGURE 3-c: AXIAL VELOCITY PROFILES - S = 0.90

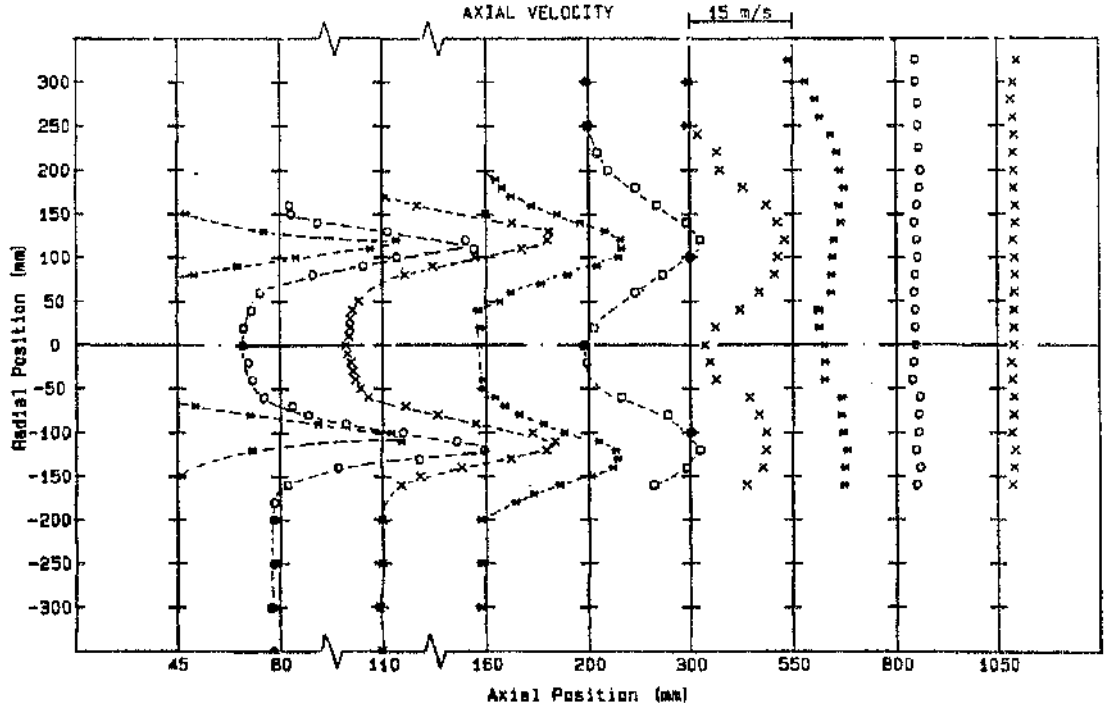

FIGURE 3-d: AXIAL VELOCITY PROFILES - S = 2.25

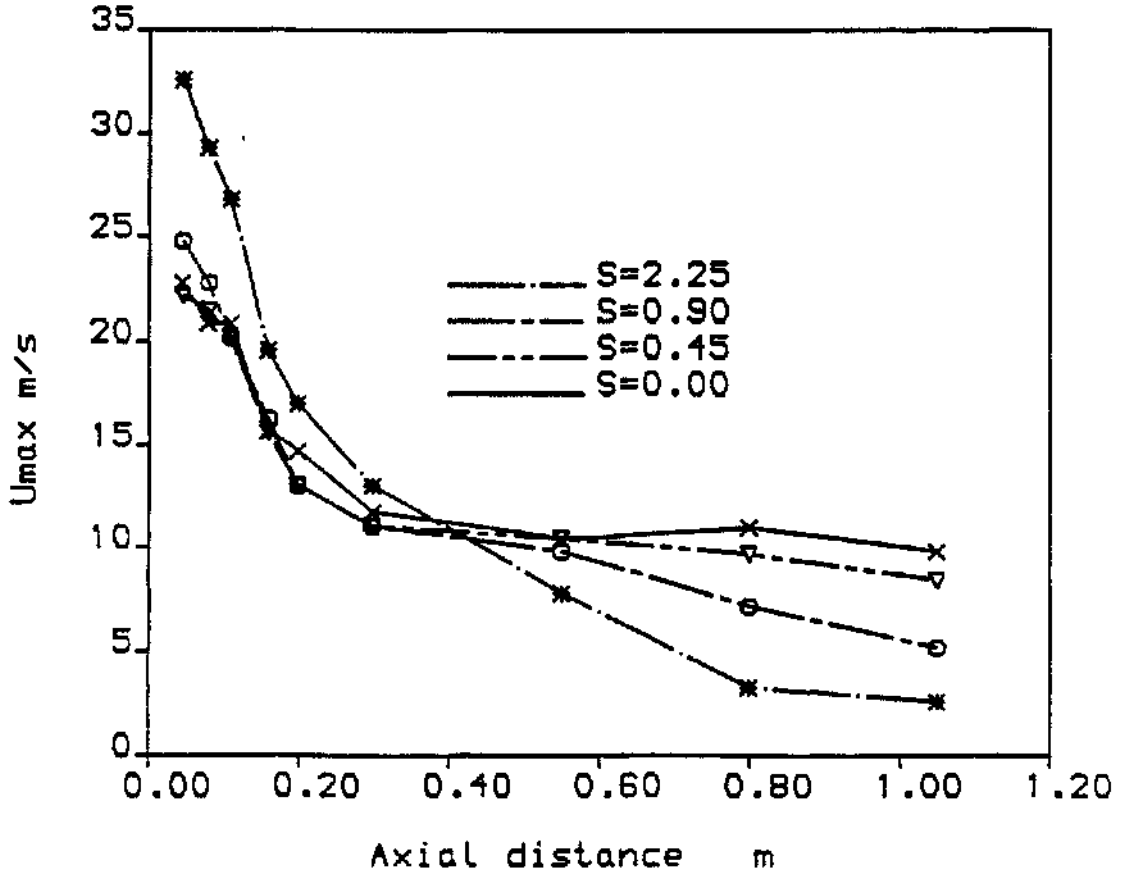

FIG.4:VARIATION OF THE MAXIMUM AXIAL VELOCITY ALONG THE FURNACE

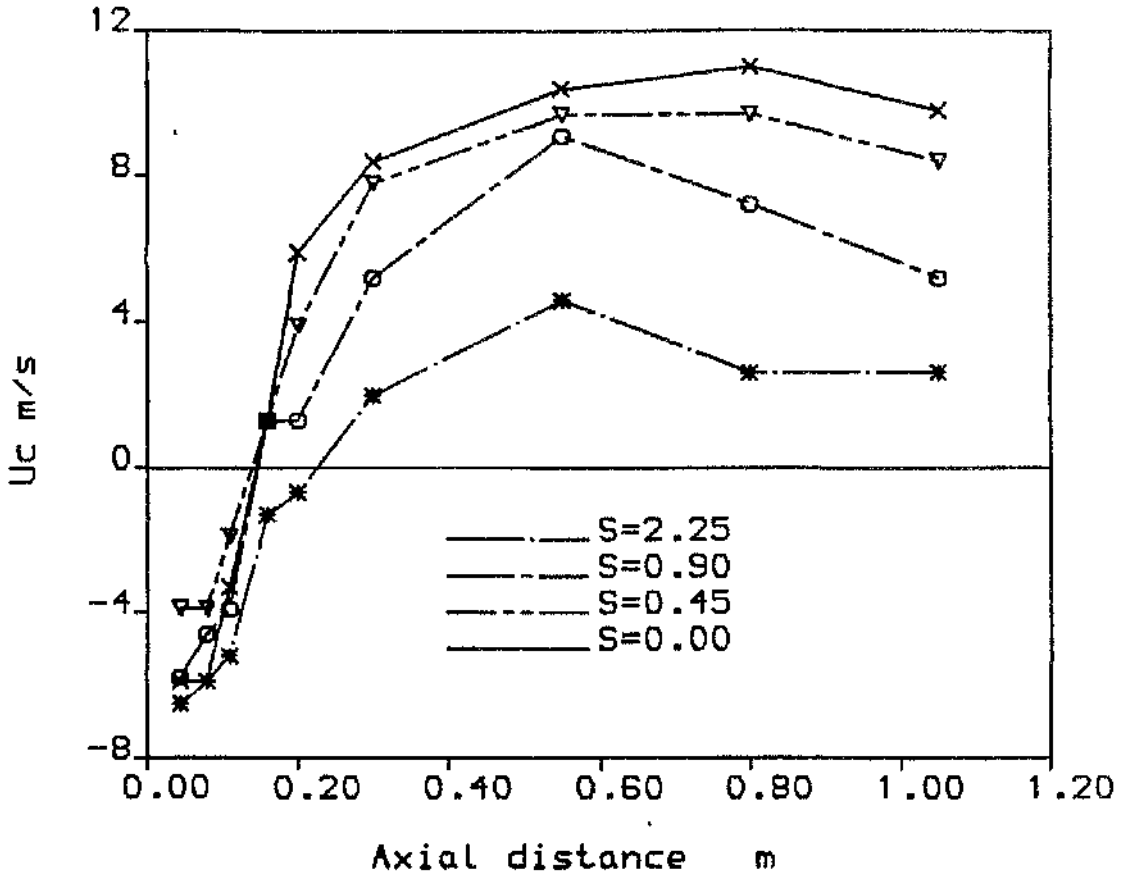

FIG.5:VARIATION OF THE CENTERLINE AXIAL VELOCITY ALONG THE FURNACE

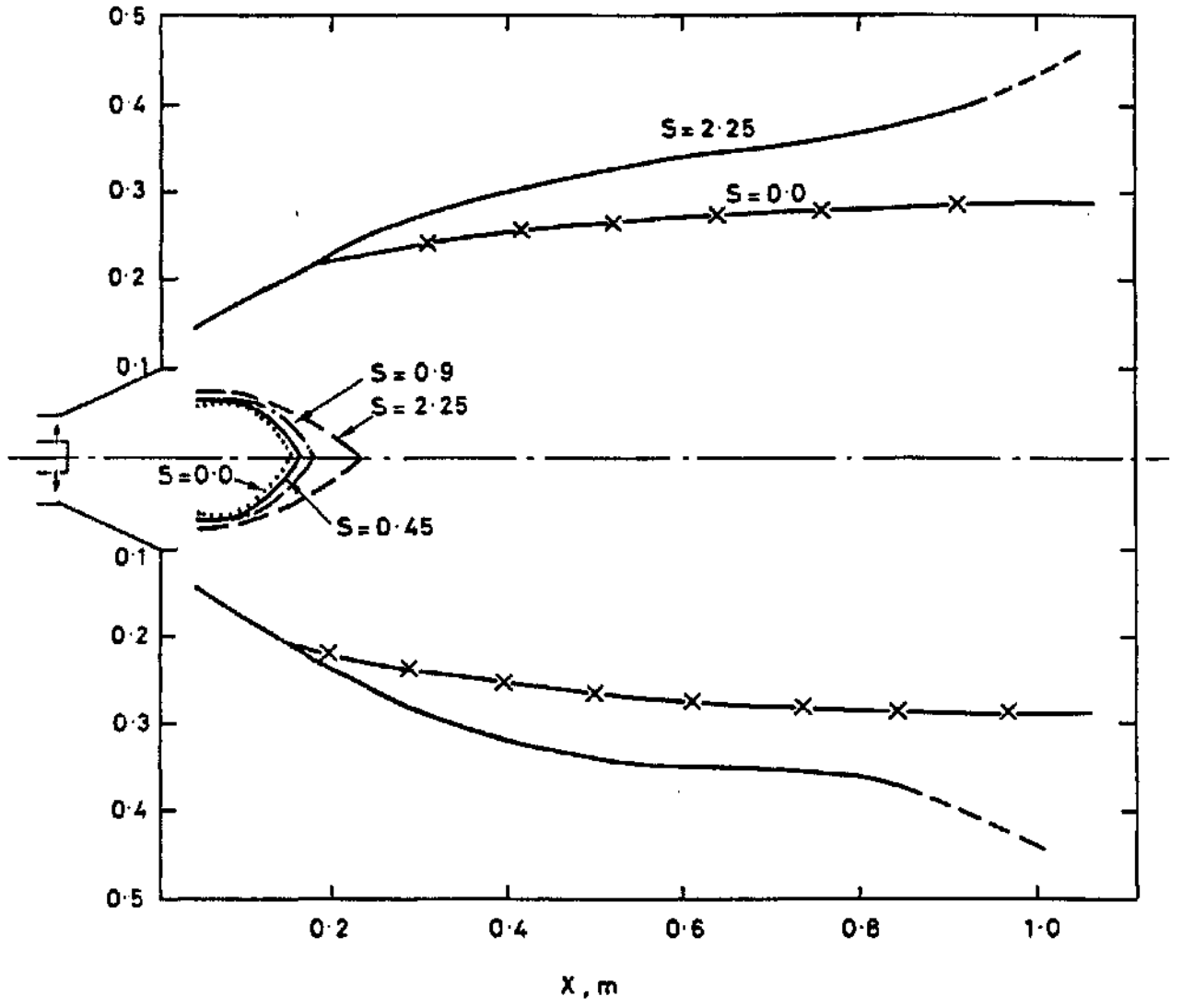

Fig. 6 FLOW BOUNDARIES

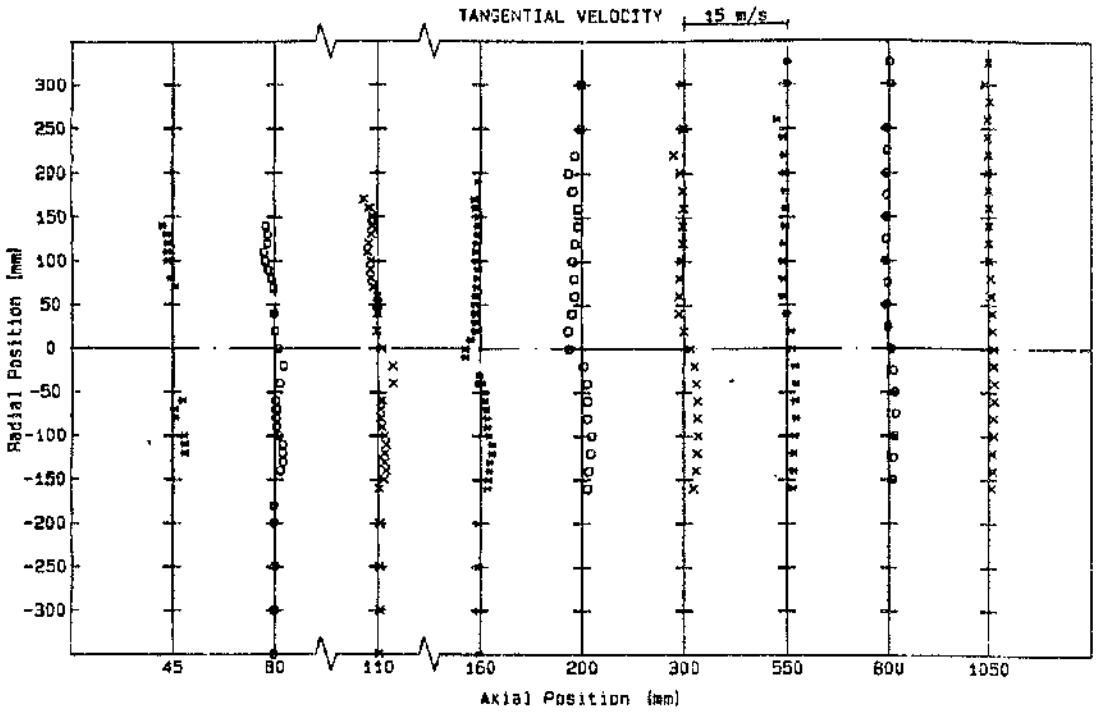

FIGURE 7-a: TANGENTIAL VELOCITY PROFILES - S = 0.45

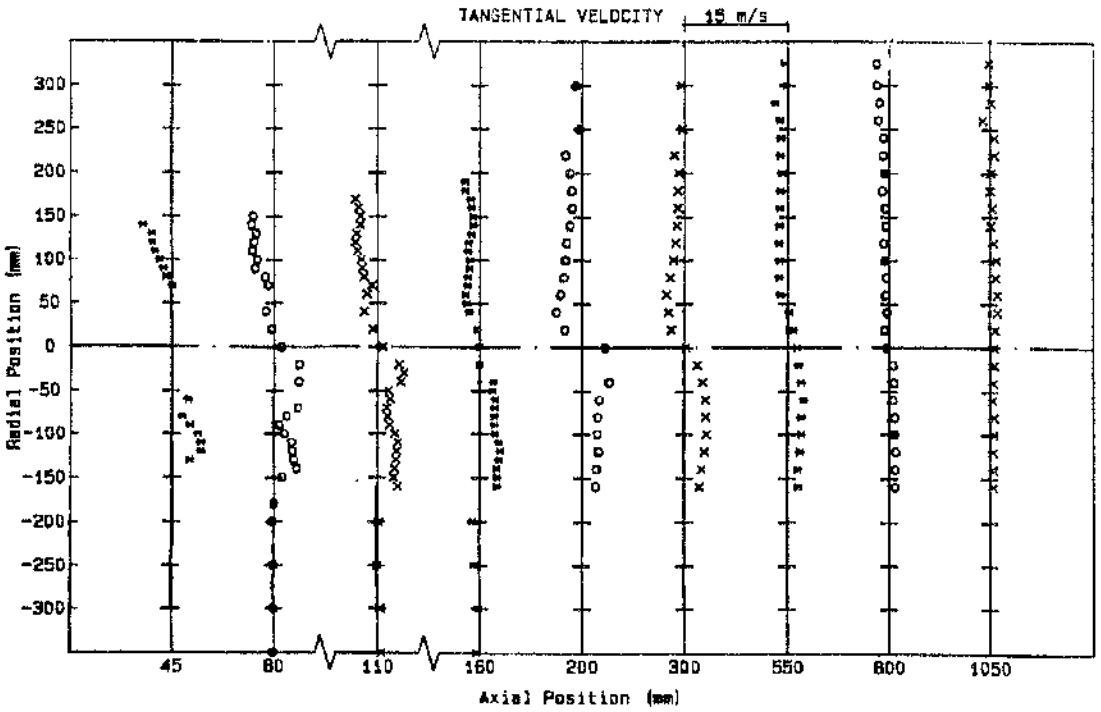

FIGURE 7-b: TANGENTIAL VELOCITY PROFILES - S = 0.90

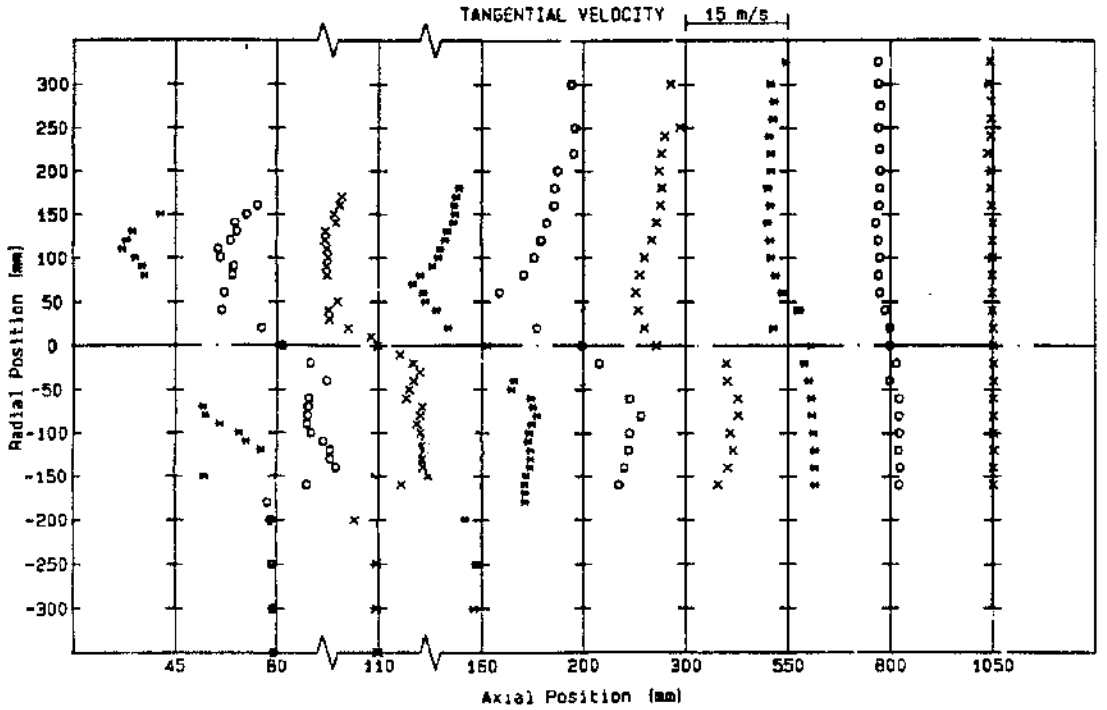

FIGURE 7-c: TANGENTIAL VELOCITY PROFILES - S = 2.25

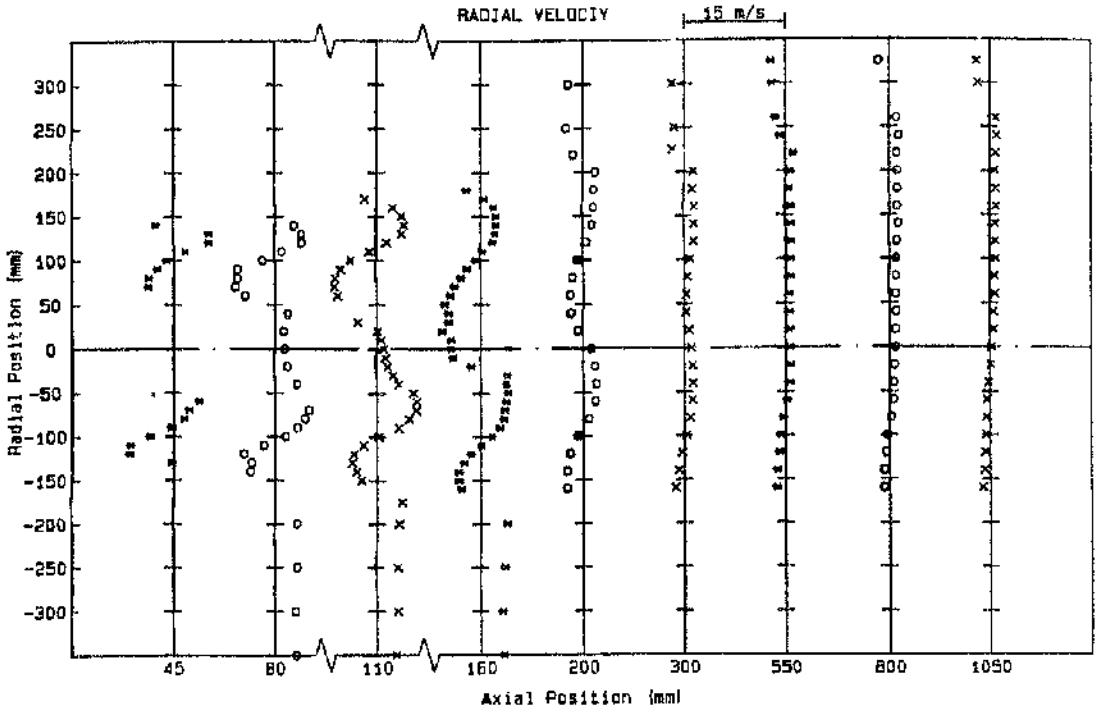

FIGURE 8-a: RADIAL VELOCITY PROFILES - S = 0.00

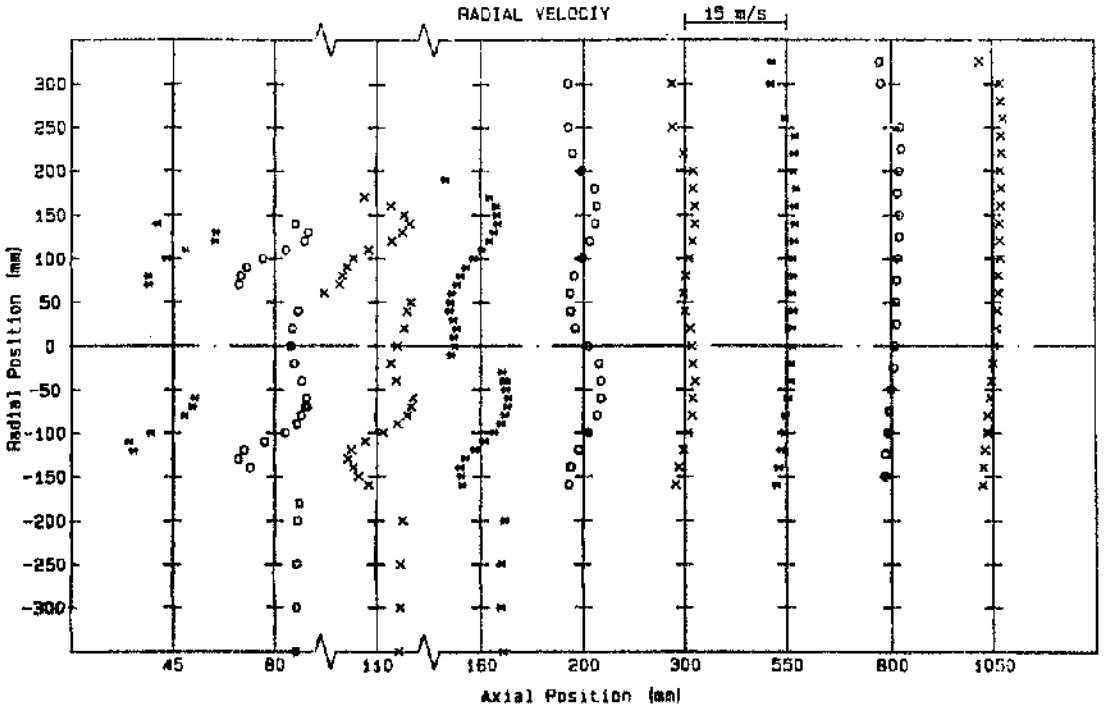

FIGURE 8-b: RADIAL VELOCITY PROFILES - S = 0.45

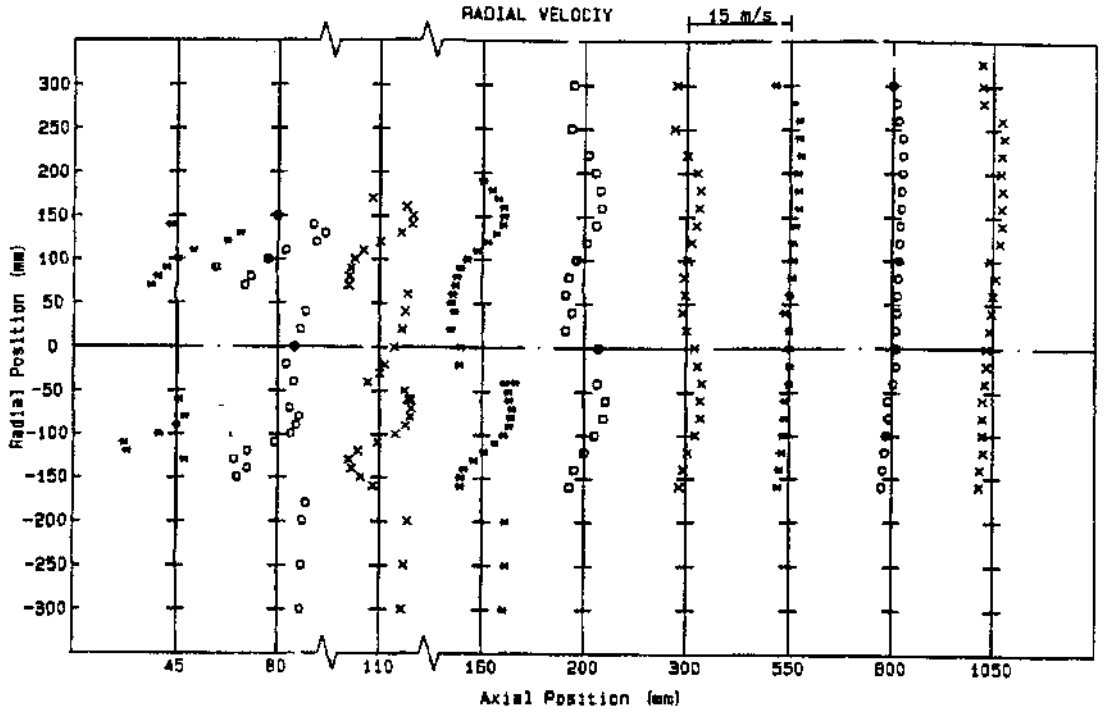

FIGURE 8-c: RADIAL VELOCITY PROFILES - S = 0.90

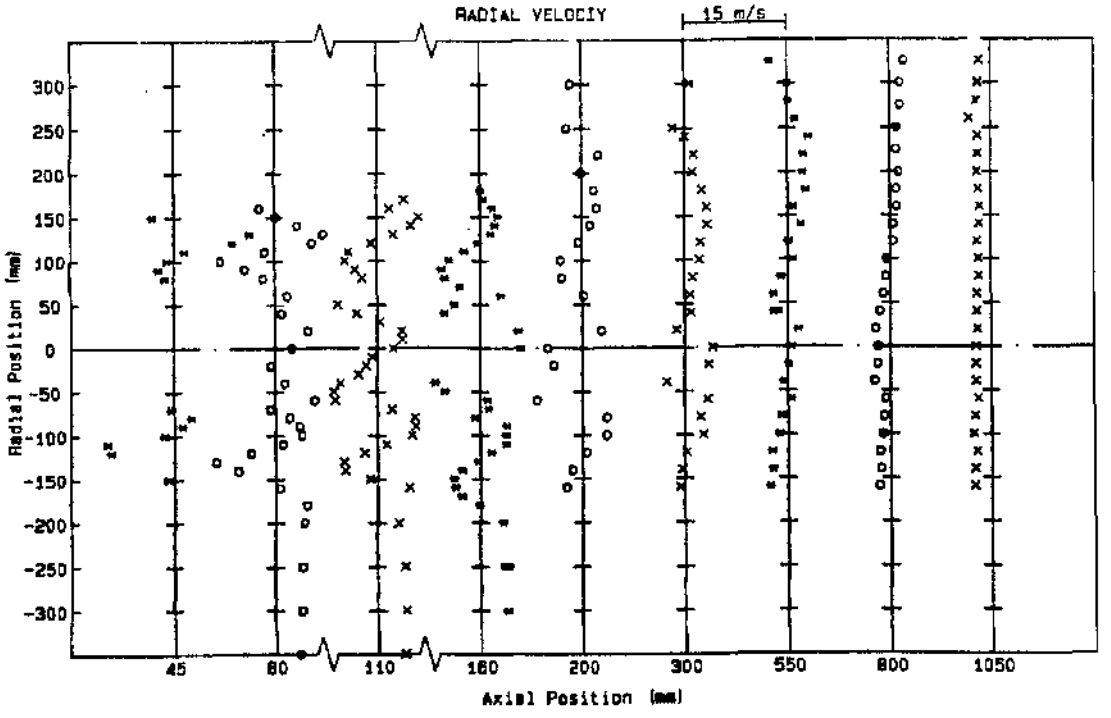

FIGURE 8-d: RADIAL VELOCITY PROFILES - S = 2.25

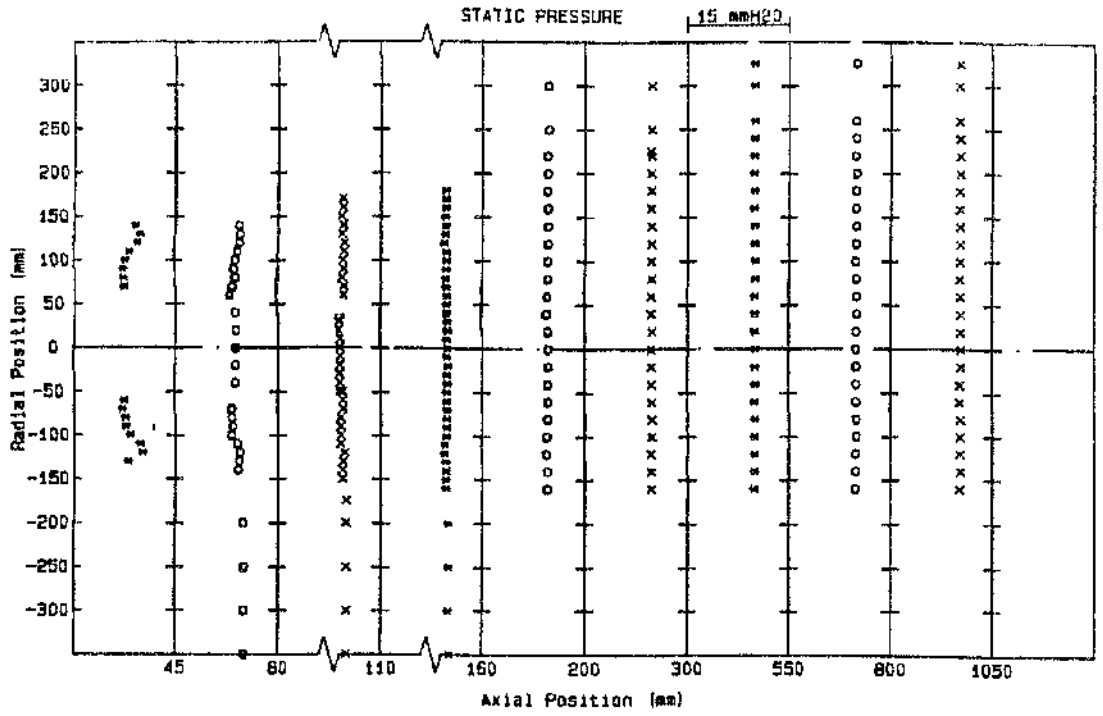

FIGURE 9-a: STATIC PRESSURE PROFILES - S = 0.00

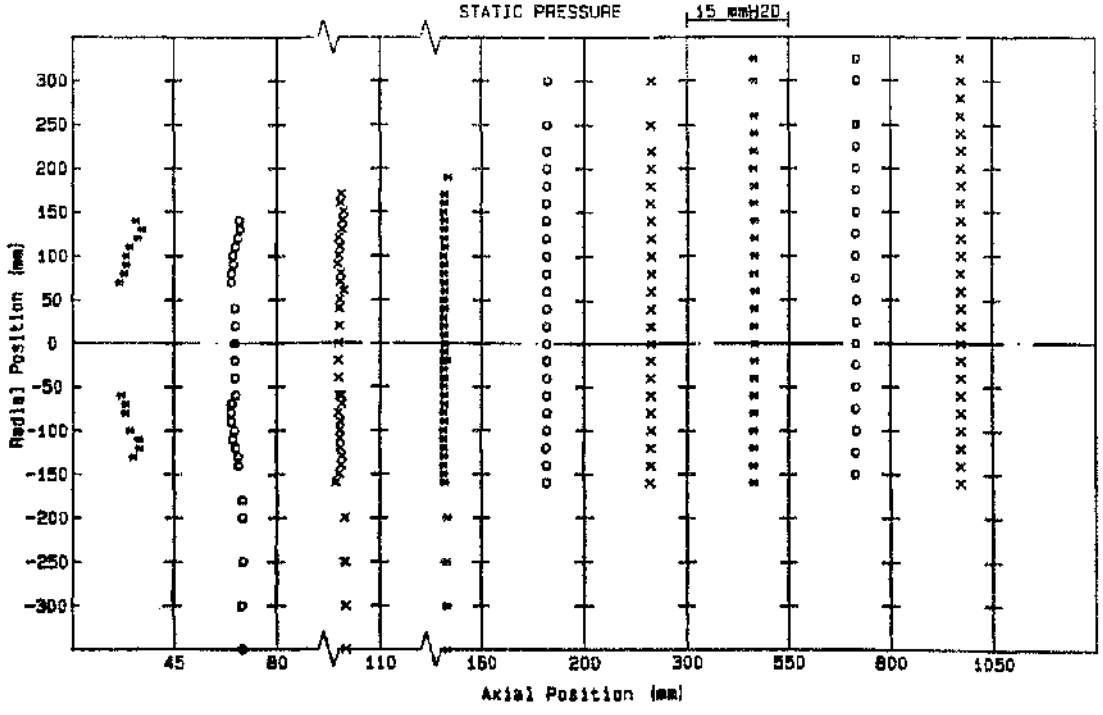

FIGURE 9-b: STATIC PRESSURE PROFILES - S = 0.45

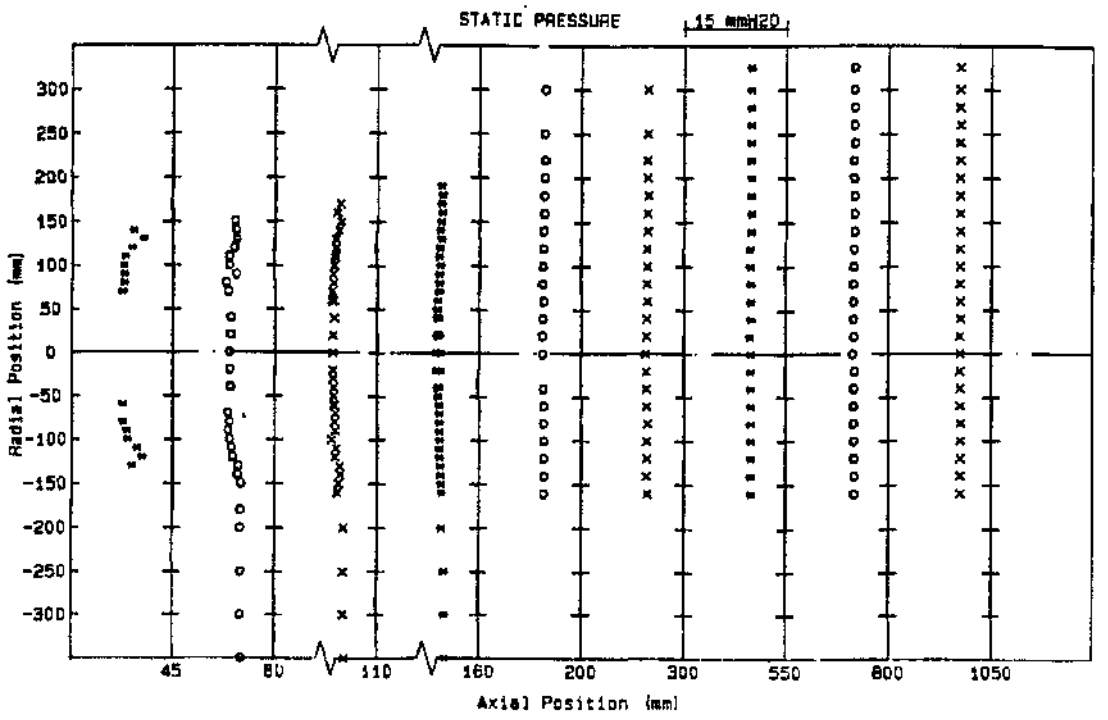

FIGURE 9-c: STATIC PRESSURE PROFILES - S = 0.90

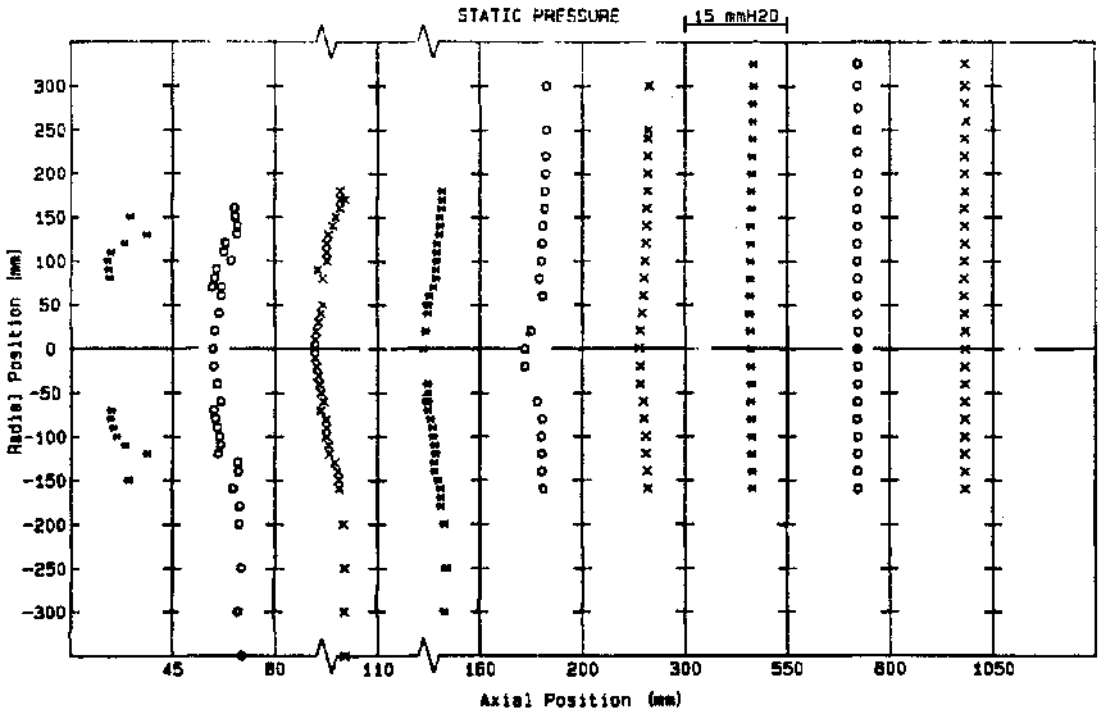

FIGURE 9-d: STATIC PRESSURE PROFILES - S = 2.25

NOx GENERATION AND CONTROL IN CONFINED SWIRLING FLAMES - REVIEW AND PARAMETRIC STUDY

S A Beltagui[1,2], A M A Kenbar[1] and N R L Maccallum[1]

1. University of Glasgow
2. National Engineering Laboratory, East Kilbride, Glasgow

ABSTRACT

A programme of work on the control of combustion-generated NOx has started at the National Engineering Laboratory (NEL) in collaboration with Glasgow University. The main emphasis is to control the NOx generation through the aerodynamic design of the burner and its fuel injection mode. The work will involve both experimental measurements in the NEL furnace and theoretical modelling, in conjunction with the HTFS flow and combustion programs.

This paper reports on the literature survey, on NOx generation and control, carried out at the start of the work. The survey focuses on studies of the effect of burner parameters on the NOx generation in furnaces and gas turbine systems. Alternative prediction models are reviewed and the recommended model is presented.

The proposed model is applied to a well-stirred reactor to illustrate the relative importance of the main contributors to the NOx generation, namely, flame temperature, oxygen concentration and residence time.

NOTATION

k	Kinetic rate constant	cm^3/mole s
t	Residence time	s
T	Flame temperature	K
x	Number of carbon atoms in hydrocarbon	-
y	Number of hydrogen atoms in hydrocarbon	-
[ ]	Concentration	mole/cm^3 s
ϕ	Fuel/air equivalence ratio, dimensionless	-
ζ	Completeness of combustion, dimensionless	-

1. INTRODUCTION

1.1 NOx and the Environment

Combustion generated pollution is now

recognised as a threat to the environment. The most obvious air pollutant is smoke, being visible to the naked eye. Other pollutants of importance are carbon monoxide, sulphur oxides (SOx) and nitrogen oxides (NOx). Recently, attention has been focused on NOx.

NOx is a collective name for nitrogen oxides; N_2O, NO and NO_2.

Combustion produces NO and to a lesser extent NO_2. At atmospheric temperature NO is converted to NO_2 and some N_2O. Stationary sources are responsible for about half the total man-produced NOx.

Locally, NOx is toxic and is known to act through photochemical reactions as a precursor to the formation of smog and other pollutants. On a wider scale it causes damage to plant life and soil through its contribution to acid rain. It has a global effect, as N_2O is involved in depletion of the earth's ozone layer (OECD Reports (1979, 1984)).

Emission standards progressively call for tighter control on emission levels. Early regulations specify percentage reductions of the current emission levels, these reductions being achievable by the application of the most up-to-date technology. However, recent regulations for new sources prescribe specified levels of emissions in order to maintain a reasonable, healthy atmosphere (OECD Reports (1979, 1983)).

1.2 Sources and Control of Combustion Generated NOx

The main origin of combustion-generated NOx is nitrogen contained in the two combustion elements, ie air and fuel. The removal of nitrogen from air before combustion is impossible and from fuel is impractical. The nitrogen fixation is a result of the combustion environment, thus, NOx formation can be limited through careful combustion control.

It has been recognized that there are three important formation mechanisms - thermal, prompt and fuel NOx - and each has its own characteristics. The understanding of the NOx source and formation mechanism will determine the appropriate technique to be selected for NOx reduction.

Various general reviews of combustion-generated pollution have been published recently eg Sawyer (1981), Levy (1982), Clarke and Williams (1985), Lawn (1987) and Williams (1989).

The present paper begins with a very brief review of NOx formation mechanisms. Methods of reduction are described, followed by a more detailed review of those methods which relate to the present work, where control is examined in the context of gaseous combustion systems.

The last part of the paper presents a parametric study of the thermal NO formation through the application of the kinetic model to a well-stirred reactor system.

2. FORMATION OF NOx

The fundamental understanding of the chemical and physical processes leading to the formation of NOx is critical to the techniques for the minimisation of its emissions.

Three categories of NOx formed in the

combustion process have been identified according to the source of the nitrogen and the chemical kinetics of the NOx formation, as shown in Figure 1.

2.1 Thermal NOx

The 'thermal NOx' refers to that formed from the free N_2 in the air as it passes through the high temperature post-flame zone. The formation mechanism being that proposed by Zeldovich, (reactions 1,2) and further extended to include reaction 3 (Bowman (1975)).

$$O + N_2 \rightleftarrows NO + N \qquad (1)$$

$$N + O_2 \rightleftarrows NO + O \qquad (2)$$

$$N + OH \rightleftarrows NO + H. \qquad (3)$$

The last reaction contribution is mainly at rich and near stoichiometric mixtures. In most cases the O atom concentration is assumed to be that in equilibrium with O_2. The main feature of the above reactions is their relatively high activation energy, thus, they are much slower than the main combustion reactions and can be decoupled from these, as will be detailed in Section 6.

An approximate formula for the overall prediction of thermal NO takes the form

$$\frac{d[NO]}{dt} = k_1(T)_{eq}^{-1/2} \exp(-E/RT) [O_2]_{eq}^{1/2} [N_2]_{eq} \text{ mole/cm}^3 \text{ s.} \quad (4)$$

Measurements by Newhall and Shahed (1971) on H_2 flames and by Engleman et al (1973) on H_2, CO and propane flames have shown that the rates of formation in the post-flame high temperature zone follow this reaction rate law. Later measurements as reviewed by Sawyer (1981) and shown in Figure 2 confirm these results.

Thermal NOx is the main mechanism for NOx generation when burning N-free fuels such as natural gas. However, its contribution is not significant when combustion zone temperatures are less than 1500 K.

The rate of thermal NOx formation depends upon the following three parameters:

a Flame temperature - which is the main factor since NO temperature relation is exponential,

b Oxygen concentration in the post-flame zone, and

c Residence time of gas in high temperature region.

The relative importance of these parameters in contributing to thermal NOx formation is illustrated in Section 6.

The control of these three parameters is the basis of the techniques for thermal NOx reduction.

However, it must be emphasised that the local spacial and temporal variations in these parameters are as important as the mean values, eg locally fuel-rich or fuel-lean pockets could lead to different NOx production rates from those derived by mean values as discussed by Appleton and Heywood (1973).

2.2 Prompt NOx

Early workers realised that the thermal mechanism failed to predict the observed

high formation rate of NOx in the early part of some flames especially hydrocarbon rich flames (Fenimore (1971), Engleman et al (1973)). This led Fenimore (1971) to consider other reactions where the hydrocarbon fragments attack bimolecular nitrogen, producing atomic nitrogen, cyanides and amines, which subsequently oxidize to nitric oxide.

$$CH + N_2 \rightleftharpoons HCN + N \qquad (5)$$

$$C + N_2 \rightleftharpoons CN + N. \qquad (6)$$

The term 'Prompt NO" was used to describe NO formed early in combustion, through such mechanism. It was found to be of minor importance relative to thermal NO for cases of lean mixtures and of H_2 or CO flames.

The rate of prompt NO formation is not temperature sensitive and cannot be separated from the HC kinetics. Sarofim and Pohl (1973) confirmed this and tried to relate the prompt NOx formation to a partial equilibrium mechanism with overshoot of O atoms in the flame. Takagi et al (1976) measured HC and HCN in flames and related these to prompt NOx.

Measurements of prompt NOx were also made by Semerjian and Vranos (1976) in rich flames. They found that prompt NOx formation was unaffected by the temperature fluctuations in the flame. In another study it was found that increasing the pressure increased the formation of prompt NOx (Heberling (1976)). A detailed review of prompt NOx formation is given by Hayhurst and Vince (1980).

The contribution from prompt NOx is about 5 per cent of the total NOx in the case of gaseous fuels but is higher in cases of liquid and solid fuels, eg Williams (1989).

Reduction of prompt NOx formation could be achieved through the reduction of residence time in the flame reaction zone and by use of lean mixtures.

2.3 Fuel NOx

The name 'fuel NOx' refers to NOx from the nitrogen-containing compounds in the fuel. The chemical reaction mechanisms are more complex than thermal NOx and their temperature dependence is very weak.

Several prediction mechanisms for fuel NOx are proposed, eg Fenimore (1972), De Soete (1975), Takagi (1976), Roslyakov (1986) and Eberius et al (1989).

The general hypothesis is that the fuel nitrogen molecules pyrolise or react to form an intermediate nitrogen containing species, designated I (HCN or NH_i i = 0, 1, 2, 3). This intermediate can then react with an oxygen containing molecule, R, to form NO, or with NO or possibly another I to form N_2.

$$\text{Fuel nitrogen} \rightarrow I \qquad (7)$$

$$I + R \rightarrow NO \qquad (8)$$

$$I + (NO \text{ or } I) \rightarrow N_2 \qquad (9)$$

The rate of conversion of fuel nitrogen to NO decreases with increased fuel nitrogen content and is independent of the type of fuel, Sawyer (1981).

This rate is also dependent on the fuel equivalence ratio. Tang et al (1981) report that maximum conversion rates occur for lean mixtures, with equivalence ratios

0.6 to 1.0. The measured conversion rates diminished for rich mixtures. Hence, control of fuel NOx is sometimes based on the reduction of oxygen in the primary combustion zone - called 'air staging'.

Fuel NOx is the major contributor in the case of solid fuels, which usually contain N-compounds. At the other extreme, natural gas is relatively free of nitrogen compounds thus thermal and prompt NOx are the main mechanisms of formation. Liquid fuels usually fall between these bounds according to their nitrogen content and combustion conditions.

3. ABATEMENT

In principle, there are three general approaches to reducing NOx emissions:

a Through the prevention of formation by combustion control. NOx is the most amenable of pollutants to prevention through modification of the combustion process, especially thermal and prompt NOx.

b Through the promotion of destruction after formation by reducing reactions in a reburning zone.

c If more reduction is needed, then treatment of the combustion products has to be implemented as a last resort. In this case, chemicals are injected in the combustion gases and reactions may occur under catalytic conditions.

The first two methods have proved sufficient in most applications.

The energy and running costs of implementing the above three techniques increase in the order they are listed above.

Some of these techniques may reduce efficiency, eg lower preheat, water injection. In power applications this is important but it could be of no effect in process applications if the process temperature is already low and thus not compromised (Pfeiffer and Altmark (1987)).

The cost of the implementation of these measures is due to

a The reduction in efficiency or loading of the plant, (Thomson and Crow (1976)),

b The initial cost of the extra equipment, and

c The cost of the materials, eg chemicals and energy used in the process by fans, injectors etc.

Some cost analysis is given in the Proceedings of the EPRI Joint Symposium on Stationary Combustion NOx Control (1982), and in OECD Report (1983).

Other factors should be considered when selecting the technique for NOx control such as the effect upon the process and on the formation and control of other pollutants, eg CO, SOx, HC etc.

The possibility of controlling both SOx and NOx simultaneously is under investigation, for example, the reduction of both by use of ozone (Lozovskii et al (1988) and Anon (1989)).

3.1 Control of Combustion

The control of combustion to prevent the formation of NOx represents the most promising and cost effective of all methods of NOx control. The extensive world-wide research on NOx formation covering different areas of applications has resulted in many practical means for NOx control. Table 1 lists the NOx control investigations reviewed. These are classified, according to the technique used and the proposed application. The principles of operation of these techniques are as follows.

a Lowering the peak combustion temperature:

A reduction of combustion peak temperature is very effective when dealing with thermal NOx but not effective for fuel NOx. Techniques leading to this aim include

i Off-stoichiometric combustion, through staged combustion,

ii Very lean combustion, flame tube premixed burner, fibre burner, cyclone combustors,

iii Reduced preheat,

iv Increased heat transfer in the burner zone,

v Flue gas recirculation, especially if the gases are cooled before recirculation, and

vi Water injection into the primary combustion zone of a burner, as used in industrial turbines and boilers, utilizes the latent heat of evaporation of water droplets to reduce temperature. This method is most effective if water is injected exactly where needed, ie in the peak temperature zone.

b Improved burner mixing thus eliminating temperature variations between lean and rich local mixtures. Uniform mixing is possible in premixed burners but stability and control may suffer. Injection of fuel in the shear layer of the air jet produces very low NOx with better stability and efficiency, eg Andrews et al (1988).

c Reduction of excess oxygen: Low excess air combustion since O_2 concentration is reduced and efficiency is increased, as in the case of staged combustion, both air staging and fuel staging are applied. Flue gas recirculation also dilutes the mixture and thus reduces O_2 concentration.

d Reduction of residence time in the flame zone and the peak temperature zone.

3.2 Destruction of NOx

By reburning in a second combustion stage, preferably using a low or N-free fuel, oil or gas. Fuels such as CO, H_2 and hydrocarbons will react with O_2 rather than NO if both exist but when O_2 is completely used up they will reduce NO to N_2.

3.3 Flue Gas Treatment

The processing of combustion products to remove NOx is used as a final measure with or without the above described methods.

In the thermal 'de-NOx' process reducing compounds, eg ammonia, urea, ozone etc are injected into the flue gases under

catalytic or noncatalytic conditions. Ammonia and other amines reduce NO in the primary combustion products in the presence of oxygen within a specified temperature range, (980-1370 K) and with certain NH3/NO equivalence, eg Muzio et al (1976) claim 78 per cent reduction at an optimum temperature of 1240 K with NH3/NO = 1/1.

Table 1 summarises a number of publications dealing with various control methods and their applications.

4. NOx IN CONFINED SWIRLING FLAMES

The review presented in the above sections dealt with general aspects of NOx formation and control. This section deals with those aspects relevant to burner flow and mixing, particular emphasis being placed on swirl stabilized gaseous flames.

4.1 Effect of Flow Pattern

Aerodynamics plays a major role in the reactions in the flame since it dictates the role and conditions under which active species are brought together before the kinetics starts to operate. The effects of flow will influence

a NOx concentration. This was found to depend on the local conditions early in the combustion process, in the developing jet in the near burner zone.

b Mixing effectiveness. This can lead to the suppression of NOx production due to the uniformity of the mixture, otherwise fuel-rich and fuel-lean pockets will exist causing higher local NOx production.

c Length scale. NOx formation was found to have a length scale dependence (Peters and Donnerhack (1981)). Those workers, studying diffusion flames, correlated this effect with Reynolds number and Froude number. NOx formation has also been related to flame stretch in a flat laminar flame (Hahn and Wendt (1981)).

d Residence time. The residence time of the combustion products in the various zones can only bé controlled through the flow parameters.

e The total NOx production. This is related to the integrated producton by the flow and not by the local concentrations in the various zones. Thus, in order to establish the total mass of pollutants in the combustor, it is essential to consider the pollutant mass flow profiles as illustrated by Sadakata and Beer (1976) and Claypole and Syred (1981)).

4.2 Effect of Swirl

The application of swirl to the combustion air can have a major influence on NOx production which is dependent upon the local temperature and mixing rates in the near burner zone. In general, increased swirl will produce the following effects.

a Increased entrainment of cooled combustion products and thereby less thermal NOx, due to lower temperature and O_2 concentration.

b Increased local oxygen availability and thereby more thermal and fuel NOx.

c Increased combustion intensity and thus higher temperature and more thermal NOx.

These effects have been reported by various

investigators. Some of these studies are briefly summarised below.

i Owen et al (1976) studied the effect of swirl, fuel/air velocity ratio and pressure on the formation of pollutions from a combustor. They indicated the effect of these parameters on NOx formation and they also illustrated how small fluctuations in these flow parameters can cause large-scale fluctuations in the resulting NOx.

ii Oven et al (1978) discussed the influence of swirl on combustion and NOx formation in the light of flame quenching due to the rapid dilution and cooling of the reacting inner jet flow by mixing with the outer flow.

iii The influence of the level of swirl on the aerodynamics and NOx emissions was also studied by Claypole and Syred (1981). The effect of higher central flow recirculation is to reduce NOx emission. This reduction is a result of better mixing prior to combustion and the reduced flame peak temperature. The better mixing also tends to eliminate local imbalances of reactants. These imbalances produce local fuel-rich regions leading to more prompt NOx. The recirculation zone, despite elevated temperature did not appear to play a major role in the formation of NOx.

The last two investigations reported some NO reacting to produce NO_2 in the combustor although the measured levels may have been enhanced by probe reactions.

iv Similar effects of the flow pattern were also reported by Sadakata and Beer (1976) where NOx formation in a swirling flame was measured. They reported some NOx destruction in the central recirculating flow.

4.3 Effects of Fuel Injection Modes

a The effect of the mode of fuel injection on NOx formation has been studied by Ahmad N T et al (1985), Andrews et al (1988) and Al-Shaikhly and Andrews (1989) in gas turbine combustor configurations. The main findings support the theory of improved mixing when fuel is injected in the shear layer of the air flow - wall injection and radial injection being superior to central injection. These systems, when used with swirl flow, also utilise the centrifugal force in improving the mixing. The high mixing rates led to near premixed conditions producing minimum NOx, together with improved efficiency and turn down.

b Gupta et al (1975) studied the effect of fuel injection mode and burner geometry on NOx formation from natural gas swirling flames. Their results indicate that higher recirculation of burnt gases led to less NOx due to the lower temperature of the combustion zone. It was also shown that tangential fuel entry produced less NOx than axial/radial injection.

c Markowski et al (1976) have reported 50 per cent reduction of NOx by using a 'premix-prevap' swirl burner in a gas turbine system. The inherent instability of swirling flows was exploited to enhance the premixing process and to stir the reacting species thus approaching a lean premixed process.

d On the other hand, by effectively producing slow mixing low NOx could be

achieved, as this acts as a system staged. This was implemented in the burner of Suzuki et al (1982) where fuel was injected at an angle to the axis of the air stream. A soft flame was formed and the temperature of the flame became more uniform with lower maximum temperature and oxygen concentration.

Abassi and Fleming (1988) used the same principle in tests in a glass furnace.

e Stratified combustion produces lower NOx where two combustion regions are distinguishable, one in the primary air, the other associated with the secondary air. Meyer and Mauss (1973) illustrated this effect on a spray combustion system where the fuel was injected into a primary swirling air stream, surrounded by a non-swirling secondary stream. Low levels of NOx (50 p.p.m.) were obtained at an optimum swirl number of 0.93 even when using a fuel with 0.01 per cent nitrogen. It was also shown that flue gas recirculation could be used to reduce NOx even further.

5. THE PROPOSED PROGRAMME

The literature reviewed above reveals that use of a system employing both centrifugal and shear-layer mixing significantly inhibits NOx formation. Earlier work at Glasgow University by Beltagui and Maccallum (1988) has shown that such an aerodynamic configuration can be achieved through the peripheral injection of fuel in a swirl burner. Radial fuel injection, as currently employed in the NEL furnace programme of aerodynamic and heat-transfer measurements, can also produce good shear-layer mixing. This latter method has the merit of stabilising the flame through promotion of a central recirculation zone even without swirl (Beltagui et al (1988)).

It is thus proposed to carry out a series of measurements of the local NOx formation in flames of the above types. The programme will cover three different modes of natural gas injection:

a Central/axial fuel injection,

b Central/radial fuel injection, and

c Peripheral/axial fuel injection.

For each mode, the effect of the swirl-burner aerodynamics on NOx formation will be studied. Comparisons should provide the information needed to optimise both the fuel injection mode and swirl to achieve the best suppression of NOx formation.

HTFS also requires data from the proposed measurements to develop and validate computer models for prediction of NOx formation. This will be carried out by incorporating the thermal NOx model in a tested flow and combustion program.

6. THERMAL NOx MODELLING

In the application being presently considered, the NOx formation is mainly attributed to the thermal mechanism. Therefore, in this section the appropriate reaction rate equations are presented. Calculations are made for NOx production for a well-stirred reactor system. The results illustrate the relative effects of the main parameters, namely, flame temperature, oxygen concentration and residence time.

6.1 Model Inputs

The thermal NOx modelling equations (1), (2), and (3), as mentioned in Section 2, are well established and understood. However, their application even using a simplified overall equation (4), requires two sets of information.

The first set includes the rate constants of the reaction equations. Predictions are particularly sensitive to the value of the rate constant for the reaction (1). The uncertainty in determining these rate constants is large and recent measurements have demonstrated the need for more accurate determination of these constants. The most recently accepted value for k1 as measured by Monat et al (1978) is about 2.2 times the values used for the previous decade (Bowman (1975)).

The second set covers the local values of the flow conditions, the most critical being temperature and concentration of the main species. The determination of these values requires the solution of the momentum, heat- and mass-transfer equations, together with the chemical reaction equations for the main species (Caretto (1976)).

The flow pattern also has to be determined. The early modellers, see Table 2, applied simplifying assumptions for the flow, eg well-stirred reactor. Recently, however, more advanced programs for solving the flow equations have become available, such as TUFC (Sykes and Wilkes (1983)), PCOC (Stopford (1989)), PHOENICS (Rosten and Spalding (1987)), FLUENT (Visser et al (1987)) and FLOW3D (Burns et al (1988)).

Because of the high sensitivity of thermal NOx to temperature, it is essential that the predictions of temperature from the flow model are carefully validated.

On the other hand, chemical species concentration calculations can be performed at different levels of complexity, starting with a very fast kinetics model (mixed-is-burned) then one or two equation models and, most recently, a full set of detailed kinetics, as described by Maas and Warnatz (1989).

While the closure of these two sets of equations, ie flow and chemistry, is possible, it may prove prohibitively expensive for cases of industrial interest, so some compromises may have to be made.

A two-step approach has been adopted by Pericleous et al (1988) to model the formation of NOx in a combustion system with swirling flow and fuel injected either tangentially or axially. The first step involves the main exothermal reaction of methane in air which is considered to be mixing controlled and the second involves the solution of the Zeldovich reaction scheme for the generation of NOx. The results demonstrate the potential of these models to predict quantitatively the effects of burner geometry on the flame structure and, consequently, on NOx emission. The same approach has been adopted by Kudryavtsev (1988) for jet flow in order to model the combustion of gaseous fuel in a steam boiler furnace. Modelling studies of the effect of peripheral fuel injection on NOx formation were also reported by Sabo et al (1988), indicating NOx levels of about 50 per cent of those from equivalent central injection systems.

6.2 The Proposed Model

6.2.1 Combustion calculations

As indicated above, gas conditions required for the calculation of thermal NOx include temperature and species concentrations. The values of these quantities were calculated for methane combustion in a well-stirred reactor assuming a global one-step reaction given by the stoichiometry equation

$$\phi C_x H_y + \left(x + \frac{y}{4}\right)(O_2 + 3.76N_2) \rightarrow$$

$$\zeta\phi x CO_2 + \zeta\phi \frac{y}{2} H_2O + (1 - \zeta)\phi C_x H_y +$$

$$+ (1 - \zeta\phi)\left(x + \frac{y}{4}\right)O_2 + 3.76\left(x + \frac{y}{4}\right)N_2 \quad (10)$$

where ϕ is the equivalence ratio and ζ is the degree of combustion.

Equilibrium conditions were assumed using a dissociation factor as given by Fairweather (1985) to calculate the adiabatic flame temperature.

The actual flame temperature was then calculated after making allowance for radiative heat transfer, with radiation parameters approximating to the NEL furnace conditions. Results are compared with adiabatic temperatures in Figure 3a. This was carried out to compare NOx formation under adiabatic and heat-transfer conditions.

6.2.2 NOx model

The formulation of the model described here was based on the following assumptions:

a NO formation when firing lean and near-stoichiometric gaseous fuels is mainly thermal and strongly dependent on temperature.

b NO formation rate is much slower than the hydrocarbon reaction rate and that most of NO is formed after the hydrocarbon reactions reach equilibrium.

c The calculation of NO (nitric oxide) is sufficient for determining NOx. NO_2 (nitrogen dioxide) may also form in the furnace. However, the total NOx (NO + NO_2) is not affected by the amount of NO_2 formed (Toof (1986)).

Thermal NO was calculated via the extended Zeldovich mechanism reactions 1, 2 and 3. Additional reactions involving NO formation from N_2O are sometimes considered but usually account for less than 1 per cent of the NOx formed thus they are not included here.

The general NO formation production equation will have the form

$$\frac{d[NO]}{dt} = 2k_1[O][N_2]\left\{\frac{1 - [NO]^2/K[O_2][N_2]}{1 + k_{-1}[NO]/(k_2[O_2] + k_3[OH])}\right\} \quad (11)$$

where $K = (k_1/k_{-1})(k_2/k_{-2})$.

At this stage for lean mixtures the contribution of reaction 3 can be neglected. Assuming steady-state concentrations of N and H atoms, the rate of NO formation could be approximated by

$$\frac{d[NO]}{dt} = 2k_1[O]_{eq}[N_2]_{eq} \quad (12)$$

where

$$k_1 = 1.82 \times 10^{14}$$

$$\exp [-38\ 370/T] \text{ cm}^3/\text{mole.s}$$

(Monat et al (1978).

Assuming O/O2 equilibrium, then (O) concentration is given by

$$[O]_{eq} = \{K_o/(RT)^{1/2}\}[O_2]_{eq}^{1/2} \qquad (13)$$

where

$$K_o = 3.6 \times 10^3 \exp(-31\ 090/T)\ (\text{atm})^{1/2}.$$

Substituting these rate constants in equation (12), the final NO production-rate equation becomes

$$\frac{d[NO]}{dt} = 1.44 \times 10^{17} T^{-1/2} \exp(-69\ 460/T)$$

$$[O_2]^{1/2}[N_2] \text{ (mole/cm}^3\text{s)}. \qquad (14)$$

6.2.3 Model results

Using the above simplified analysis, values of NO formed under various input conditions of equivalence ratio and degree of combustion are calculated. These simple model predictions are used to illustrate the relative contribution of input conditions to thermal NO production. In all cases the fuel is methane and the inlet air and fuel temperatures are 300 K.

Figure 3b shows the effect of heat transfer on NO formation at constant degree of combustion ζ of 0.95. Flame temperature values in all the subsequent figures are sensitive to O_2 concentration as it is to flame temperature. Despite the decay of O_2 concentration with the increase of equiv- those in which heat transfer is considered.

Both Figures 3b and 4 illustrate the strong dependence of thermal NO on flame temperature.

To examine the effect of the degree of combustion on NO formation, the results are shown in Figure 5 for ζ values of 0.80, 0.85 and 0.95. It is obvious that at a given value of the equivalence ratio, the increase in the degree of combustion results in a higher flame temperature and hence higher NO formation.

Figure 6 shows that NO formation is not as sensitive to O_2 concentration as it is to flame temperature. Despite the decay of O_2 concentration with the increase of equivalence ratio, NO continues to increase exponentially with the flame temperature.

Finally, the effect of residence time on NO formation is illustrated in Figure 7. It is clear that reduction in residence time of gas in the high temperature region reduces NO formation.

7. SUMMARY AND CONCLUSIONS

Nitrogen oxides are generated in combustion systems either by fixation of atmospheric nitrogen, through thermal and prompt mechanisms or by conversion from N-containing compounds in fuel. Nitrogen oxides are products of the combustion environment and their control should start with the modification of the combustion to prevent their formation. The next level of control involves the destruction of formed NOx in a reburning or second stage zone. If neither method achieves adequate reduction, treatment of combustion products through catalytic reduction or other methods has to be undertaken. Alternative techniques based on the above principles are reviewed with

particular emphasis on those based on combustion control for prevention of NOx formation.

In most gaseous combustion systems the major contributor to the overall NOx emission is thermal NOx. Methods of thermal NOx control are principally based on the reduction of one or more of the following flame parameters; temperature, excess oxygen concentration and residence time in the post-flame zone. The present review illustrates that the aim of NOx reduction can be achieved through the careful control of the aerodynamics and mixing in the near-burner zone.

An experimental program has been proposed which will focus on the effects of swirl and fuel injection modes on NOx formation in natural gas flames in a cylindrical furnace.

The mathematical modelling of NOx formation in this case is also under investigation. A first step is presented here offering a simple parametric study of the relative importance of the combustion parameters on the NOx formation. The calculations are based on the thermal NO mechanism applied to a well-stirred reactor.

ACKNOWLEDGEMENTS

The authors wish to thank colleagues at the National Engineering Laboratory and the University of Glasgow for their advice and encouragement. This work was supported in part by the Management Board of the National Engineering Laboratory.
A M A Kenbar wishes to acknowledge the support of the Government of Iraq.

REFERENCES

ABASSI, H. A. and FLEMING, D. K., (1988), Ceram. Eng. Sci. Proc., Vol. 9, No 3-4, pp 168-177.

ABDALLA, A. Y., BRADLEY, D. and CHIN, S. B., (1989), Joint Meeting of the British and French Sections of the Combustion Institute, Rouen, pp 29-32.

AHMAD, N. T., ANDREWS, G. E., KOWKABI, M. and SHARIF, S. F., (1985), 20th Internat. Symp. on Combustion, pp 259-267.

AHMAD, T., PLEE, S. L. and MYERS, J. P., (1985), J. Eng. Gas Turbine Power, Vol. 107, No 1, pp 48-53.

AL-SHAIKHLY, A. F. A., ANDREWS, G. . and ANIAGOLU, C. O., (1989), Joint Meeting of the British and French Sections of the Combustion Institute, Rouen, pp 5-8.

ANDREWS, G. E. et al, (1988), British flame days, Imperial College, London.

ANON, (1989), "Control of NOx emission from large combustion plant", The Chem. Eng., March, pp 33-40.

APPLETON, J. P. and HEYWOOD, J. B., (1973), 14th Internat. Symp. on Combustion, pp 777-786.

BARNES, F. H., BROMLY, J. H., EDWARDS, J. J. and MANDYCZEWSKY, R., (1988), J. Inst. Energy, Vol. 61, pp 184-188.

BELTAGUI, S. A., FUGGLE, R. N. and RALSTON, T., (1988), HTFS RS 756, NEL/HTFS 113.

BELTAGUI, S. A. and MACCALLUM, N. R. L., (1988), J. Inst. of Energy, pp 3-16.

BOWMAN, C. T., (1975), Prog. Energy Comb. Sci., Vol. 1, pp 33-45.

BREEN, B. P., BELL, A. W., De VOLO, N. B., BAGWEKK, F. A. and ROSENTHAL, K., (1971), 13th Internat. Symp. on Combustion, pp 391-401.

BROWN, T. D., MITCHELL, E. R. and LEE, G. K., (1973), First European Symp. on Combustion, Sheffield, pp 487-492.

BURNS, A. D. et al, (1988), Harwell Report AERE-R 13148.

CARETTO, L. S., (1976), Prog. Energy and Comb. Sci., Vol. 1, pp 47-75.

CLARKE, A. G. and WILLIAMS, A., (1985), HTFS Design Report DR32, Part 10.

CLAYPOLE, T. C. and SYRED, N., (1981), 18th Internat. Symp. on Combustion, pp 81-89.

DE SOETE, G. G., (1975), 15th Internat. Symp. on Combustion, pp 1093-1099.

DESTEFANO, J. T., (1985), Ceram. Eng. Sci. Proc., Vol. 6, No 3-4, pp 241-248.

EBERIUS, H., JUST, Th., KELM, S. and WARNATZ, J., (1989), Joint Meeting of the British and French Sections of the Combustion Institute, Rouen, pp 17-20.

ENGLEMAN, V. S. et al, (1973), 14th Internat. Symp. on Combustion, pp 755-765.

EPRI, (1982), Proc. of the Joint Symp. on Stationary Combustion NOx Control, Vols 1 and 2. Elect. Power Research Institute, Palo Alto, California.

FAIRWEATHER, M., (1985), HTFS Design Report DR32, Part 2.

FENIMORE, C. P., (1971), 13th Internat. Symp. on Combustion, pp 373-380.

FENIMORE, C. P., (1972), Combustion and Flame, Vol. 19, pp 289-296.

FLAMENT, P. and BURY, F., (1989), Joint Meeting of the British and French Sections of the Combustion Institute, Rouen, pp 239-242.

FLETCHER, R. S., (1973), 1st European Symp. on Combustion, Sheffield, pp 445-450.

FLETCHER, R. S. and HEYWOOD, J. B., (1971), AIAA Paper No 71-123, New York, N. Y.: American Institute of Aeronautics and Astronautics.

FOSTER, P. J., (1974), HTFS Design Report DR32, Part 5.

GODRIDGE, A. M., (1986), Int. Flame Research Foundation, 8th Members Conference, Netherlands.

GUPTA, A. K., SYRED, N. and BEER, J. M., (1975), 15th Internat. Symp. on Combustion, pp 1367-1378.

HADVIG, S., HADSEN O, H. and JENSEN, J., (1988), British Flame Days, Imperial College, London.

HAHN, W. A. and WENDT, J. D. L., (1981), 18th Internat. Symp. on Combustion, pp. 121-131.

HAYHURST, A. N. and VINCE, I. M., (1980), Prog. Energy Comb. Sci., Vol. 6, pp 35-51.

HEBERLING, P. V., (1976), 16th Internat. Symp. on Combustion, pp 159-168.

HIRAI, T., NAGAI, N. and TAKADO, J., (1987), Int. J. JSME, Vol. 30, No 260, pp 303-309.

HUNTER, S. C., HALL, R. E. and CARTER, W. A., (1978), ASME Paper No 78-WA/APC-8.

KNILL, K. J., (1987), Int. Flame Research Foundation Doc. No G13/a/3.

KOTLER, V. R. and IMANKULOV, E. R., (1986), Thermal Eng., Vol. 33, No 1, pp 12-14.

KRETSCHMER, D. and ODGERS, J., (1973), ASME Paper No 73-WA/GT-6.

KUDRYAVTSEV, N. Yu. and VOLKOV, E. P., (1988), Thermal Eng., Vol. 35, No 4, pp 219-222.

LAWN, C. J., (Ed.), (1987), "Principles of combustion engineering for boilers", Academic Press.

LEFEBVRE, A. H., (1975), 15th Internat. Symp. on Combustion, pp 1169-1180.

LEVY, A., (1982), 19th Internat. Symp. on Combustion, pp 1223-1242.

LEWIS, G. D., (1981), ASME Paper No 81-GT-119.

LOZOVSKII, V. A. et al, (1988), Thermal Eng., Vol. 35, No 8, pp 20-22.

LUKOSHYAVICHYVS, V. P., TSIRUL'NIKOV, L. M. and SHVENCHYANAS, P. P., (1986), Thermal Eng., Vol. 33, No 7, pp 9-12.

NAAS, V. and WARNATZ, J., (1989), Joint Meeting of the British and French Sections of the Combustion Institute, Rouen, pp 133-137.

MARKOWSKI, S. J., LOHMANN, R. P. and REILLY, R. S., (1976), ASME J. of Eng. Power, pp 123-129.

MEIER, J. G. and VOLLERIN, B. L., (1976), 16th Internat. Symp. on Combustion, pp 63-76.

MELLOR, A. M., (1980), Prog. in Energy and Comb. Sci., Vol. 6, pp 347-358.

MELLOR, A. M. and WASHAM, R. A., (1979), ASME Paper No 79-GT-194.

MEYER, G., and NAUSS, F., (1973), First European Symp. on Combustion, Sheffield, pp 475-480.

MIRZAIE, H. and SYRED, N., (1989), Joint Meeting of the British and French Sections of the Combustion Institute, Rouen, pp 61-64.

MIZUTANI, Y. and KATSUKI, M., (1976), Bulletin of JSME, Vol. 19, pp 1360-1366.

MONAT, J. P., HANSON, R. K. and KRUGER, C. H., (1978), 17th Symp. (Int.) on Combustion, pp 543-552.

MONAT, J. P., HANSON, R. K. and KRUGER, C. H., (1978), 17th Internat. Symp. on Combustion, pp 543-552.

MULHOLLAND, J. A. and HALL, R. E., (1987), J. Eng. Gas Turbine Power, Vol. 109, pp 207-214.

MUZIO, L. J. ANAND, J. K. and TEIXEIRA, D. P., (1976), 16th Internat. Symp. on Combustion, pp 199-208.

NEWHALL, H. K. and SHAHED, S. M., (1971), 13th Internat. Symp. on Combustion, pp 381-389.

NOVOSELOV, S. S. et al, (1986), Thermal Eng., Vol. 33, No 9, pp 30-33.

NUTCHER, P. B., (1984), Plant/Operations Progress, Vol. 3, No 3, pp 168-173.

OECD, (1979), "Photochemical oxidants and their precursors in the atmosphere", OECD Report

OECD, (1983), "Control technology for nitrogen oxide emissions from stationary sources", OECD Report.

OECD, (1984), "Emission standards for major air pollutants", OECD Report.

OVEN, M. J., GOULDIN, F. C. and McLEAN, W. J., (1978), 17th Internat. Symp. on Combustion, pp 363-374.

OWEN, F. K., SPADACCINI, L. J. and BOWMAN, C. T., (1976), 16th Internat. Symp. on Combustion, pp 105-118.

PERICLEOUS, K. A., CLARK, I. W. and BRAIS, N., (1988), British Flame Days, Imperial College, London

PETERS, N. and DONNERHACK, S., (1981), 18th Internat. Symp. on Combustion, pp 33-42.

PFEIFFER, R. and ALTHARK, D., (1987), Research and Development Forum, June, Osaka, Japan.

RITZ, J., KOLB, T., JANSOHN, P. and LEUCKEL, W., (1989), Joint Meeting of the British and French Sections of the Combustion Institute, Rouen, pp 37-40.

ROSLYAKOV, P. V., (1986), Thermal Eng., Vol. 33, No 1, pp 23-26 and Vol. 33, No 9, pp 499-502.

ROSTEN, H. I. and SPALDING, D. B., (1987), Phoenics Reference Manual, Cham.

RUBINS, P. M. and MARCHIONNA, N. R., (1976), AIAA Paper No 76-612, New York, N.Y.: American Institute of Aeronautics and Astronautics.

SABO, Sh., DVOINISHNIKOV, V. A. and VILENSKII, T. V., (1988), Thermal Eng., Vol 35, No 9, pp 534-537.

SADAKATA, M. and BEER, J. M., (1976), 16th Internat. Symp. on Combustion, pp 93-103.

SADAKATA, M., FUJIOKA, Y. and KUNII, D., (1981), 18th Internat. Symp. on Combustion, pp 65-72.

SAROFIM, A. F. and POHL, J. H., (1973), 14th Internat. Symp. on Combustion, pp 739-754.

SAWYER, R. F., (1981), 18th Internat. Symp. on Combustion, pp 1-22.

SCHEFER, R. W. and SAWYER, R. F., (1976), 16th Internat. Symp. on Combustion, pp 119-133.

SEMERJIAN, H. and VRANOS, A., (1976), 16th Internat. Symp. on Combustion, pp 169-179.

SHAW, H., (1973), ASME Paper No 73-WA/GT-1.

SIDDIQUI, A. A., TENINI, J. W. and KILLION, L. D., (1976), Hydrocarbon Processing, Oct., pp 94-97.

SIGAL, I. Ya., KOSINOV, O. I., DUBOSHII, A. N. and NIZHNIK, S. S., (1986), Thermal Eng., Vol. 33, No 7, pp 6-9.

SIMACHEV, V. Y. et al, (1988), Thermal Eng., Vol. 35, No 3, pp 171-175.

SKORIK, L. D. et al, (1986), Thermal Eng., Vol. 33, No 7, pp 58-59.

SMART, J. and WEBER, R., (1987), Int. Flame Research Foundation, Doc. No F 037/a/18.

STOPFORD, P. J., (1989), PCOC Users Manual, AERE-R12626.

SUZUKI, T. et al, (1982), J. Inst. Energy, Vol. 55, Part 1, pp 212-215, Part 2, pp 216-220.

SYKES, J. and WILKES, N. S., (1983), TUFC2 Program Users Manual, Harwell Report AERE-R11027.

TAKAGI, T. OGASAWARA, M., DIAZO, M. and TATSUMI, T., (1976), 16th Internat. Symp. on Combustion, pp 181-189.

TANG, S., CHURCHIL, S. W. and LIOR, N., (1981), 18th Internat. Symp. on Combustion, pp 73-80.

THOMSON, S. T. and CROW, R. H., (1976), Proc. API Refin. Dep. Midyear 41st Meeting, Vol. 55, pp 567-574.

TOOF, J. L., (1986), ASME J. Eng. Gas Turbine Power, Vol. 108, pp 340-347.

TOUCHTON, G. L., (1984), ASME Paper No 84-GT-152.

TSIRUL'NIKOV, L. M. et al, (1986), Thermal Eng., Vol. 33, No 9, pp 503-506.

TUTTLE, J. H., COLKET, M. B., BILGER, R. W. and MELLOR, A. M., (1976), 16th Internat. Symp. on Combustion, pp 209-219.

VISSER, M., BOYSAN, F. and WEBER, R., (1987), Int. Flame Research Foundation, Doc. No F 336/a/9.

WAIBEL, R. and NICKESON, D., (1986), Int. Flame Research Foundation, 8th Members Conference, The Netherlands.

WILLIAMS, A., (1989), Joint Meeting of the British and French Sections of the Combustion Institute, Rouen, pp A1-A11.

YAMAGISHI, K. et al, (1975), 15th Internat. Symp. on Combustion, pp 1157-1166.

LIST OF TABLES

LIST OF FIGURES

4	Variation of NO formation with flame temperature	6	Variation of flame temperature, O_2 and NO with equivalence ratio
5	Effect of degree of combustion on NO formation	7	Variation of NO formation with residence time.

TABLE 1

REVIEW OF NOx EMISSION CONTROL METHODS

Investigators	Techniques	Applications
EPRI 1982 NOx Symp.	Review of all techniques and applications	Utility, process.
OECD NOx Control for Stationary Sources, 1983	Review of techniques	Utility, process.
Breen et al, 1971	General review	Utility
Sawyer, 1981	General review	Utility
Lefebvre, 1975	General review	Gas turbine
Foster, 1974	General review	Furnaces
Ahmad, N. T. et al, 1985	Burner controlled mixing,	Gas turbine
Andrews et al, 1988	shear layer fuel injection,	Process
Al-Shaikly et al, 1989	both axial and radial	
Markoski et al, 1976	Premix-prevap swirl burner	Gas turbine
Gupta et al, 1975	Fuel injection control burner geometry and swirl	Process
Suzuki et al, 1982	Controlled slow mixing, low temperature, internal FGR	Steel processing
Pfeiffer and Altmark, 1987	Low temperature premixed radiant tube burner	Process, gas turbine, small boiler
Mirzaie and Syred, 1989	Cyclone low temp. very lean combustion	Process, low CV fuels
Schefer and Sawyer, 1976	Lean combustion opposed jet system	Gas turbine
Meier and Volleron, 1976	High swirl with FGR	Domestic boilers
Barnes et al, 1988	Radiant burner	Domestic heating
Hadvig et al, 1988	Fibre burner	Boiler
Ritz et al, 1989	Reburn with NH_3 mixed with fuel	Boilers
Hulholland and Hall, 1987	Reburn with gas or oil fuel	Packaged boiler
Hunter et al, 1978	Combustion modification, review	Various processes

TABLE 1 (contd)

Investigators	Techniques	Applications
Siddiqui et al, 1976	Review of techniques	Fired heaters
Nutcher, 1984	Review of air and fuel staging and FGR	Fired heaters
Destefano, 1985	NH_3 injection	Glass furnace
Abassi et al, 1988	Low excess air and slow mixing	Glass furnace
Tsirul'nikov et al, 1986	Low excess air, FGR and steam injection	Utility
Meyer and Mauss, 1973	Stratified combustion, swirl and FGR	Fundamental
Abdalla et al, 1989	Stratified, well-stirred reactor	Fundamental
Oven et al, 1979	Stratified swirl burner	Fundamental
Waibel and Nickeson, 1986	Fuel and air staging with FGR	Process refinery
Yamagushi et al, 1975	Air staging	Boiler
Kotler and Imankulav, 1986	Air staging, swirl	Utility
Hirai et al, 1987	Air staging, swirl	Boiler, process
Sadakata et al, 1981	Air staging, preheat	Model
Knill, 1987	Review of fuel staging, pf.	Utility
Smart and Weber, 1988	Internal air staging and precombustor	Utility
Flament and Bury, 1989	Fuel staging, central and peripheral injection	Boilers
Brown et al, 1973	FGR	Boiler
Sigal et al, 1986	FGR	Utility
Godridge, 1986	FGR	Utility
Lukoshyavichyvs et al 1986	Water spraying	Utility
Novoselov et al, 1986, Lozovskii, 1988 and Simachev et al, 1988	Reduction of NOx and SOx by ozone	Utility
Skorik et al, 1986	Ammonia injection	Utility

TABLE 2

REVIEW OF NOx MODELLING WORK

INVESTIGATORS	NOx Mechanism	Hydrocarbon Kinetics	Flow Modeling	Remarks
a)Fletcher and Heywood,1971. b)Fletcher,1973	a) Thermal b) Thermal	a) Equilibrium b) 2-step reaction	a) 1.D.M b) 2.D.M	a) Fluctuations b) Premixed
Appleton and Heywood,1973.	Thermal & Fuel		1.D.M	Fluctuations
Fletcher, 1973	Thermal	Equilibrium	W.S.R	Fluctuations
Engleman et al,1973	Thermal	Semi-detailed	W.S.R	premixed
Shaw, 1973	Thermal & Prompt	Equilibrium	W.S.R	
Kretschmer and Odgers,1973	Thermal	1-step reaction	W.S.R	
Tuttle et al,1976	Thermal	Emperical	W.S.R	
Rubins and Marchionna,1976.	Thermal	Equilibrium	Multiple W.S.R	
Mizutani and Katsuki,1976	Thermal	1-step reaction	2.D.M	
Mellor and Washam, 1979, Mellor, 1980.	Thermal		W.S.R	
Lewis ,1981	Thermal	Equilibrium	W.S.R	
Sadakata et al, 1981	Thermal	Equilibrium	1.D.M	Air staging
Peters and Donnerhack,1981	Thermal	Equilibrium	2.D.M	Boundary layer
Touchton, 1984.	Thermal	Equilibrium	Multiple W.S.R	steam injection
Ahmed T et al, 1985	Thermal	1-step reaction	2.D.M	
Toof, 1986	Thermal,prompt and fuel	Equilibrium		
Sabo et al ,1988	Thermal & Fuel	Equilibrium/1-step	3.D.M	Cenral/peripheral injection
Pericleous et al,1988	Thermal	1-step + turbulence	3.D.M	Central/peripheral injection
Kudryavtsev & Volkov, 1988	Thermal	1-step + turbulence	2.D.M	Boundary layer

1.D.M = One Dimensional Model.
2.D.M = Two = = .
3.D.M= Three = =.
W.S.R = Well stirred Reactor.

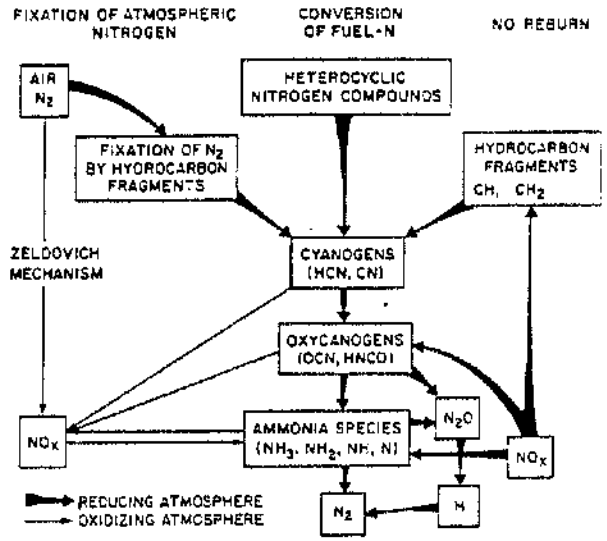

FIG.1: POTENTIAL NOx FORMATION ROUTES

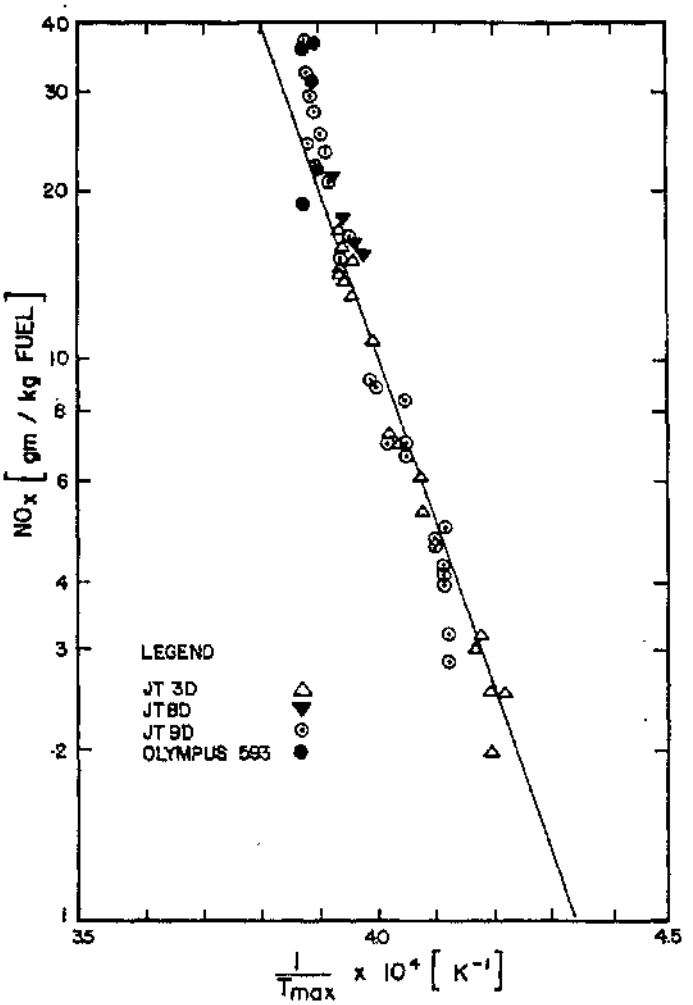

FIG.2: THERMAL NO-EXPERIMENTAL VS PREDICTIONS

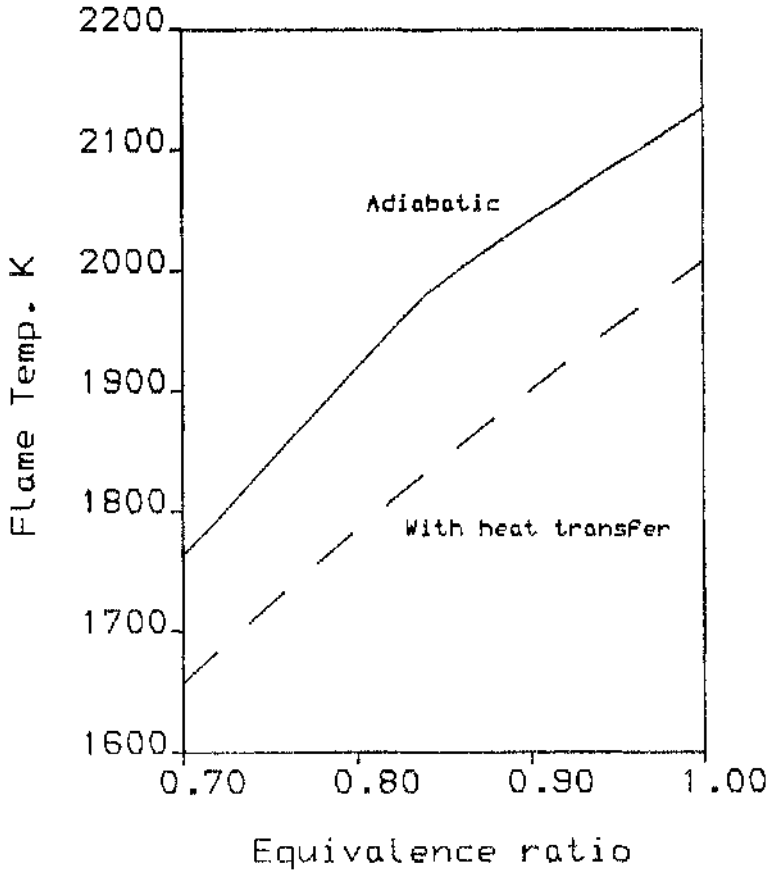

FIG.3a:EFFECT OF HEAT TRANSFER ON FLAME TEMPERATURE

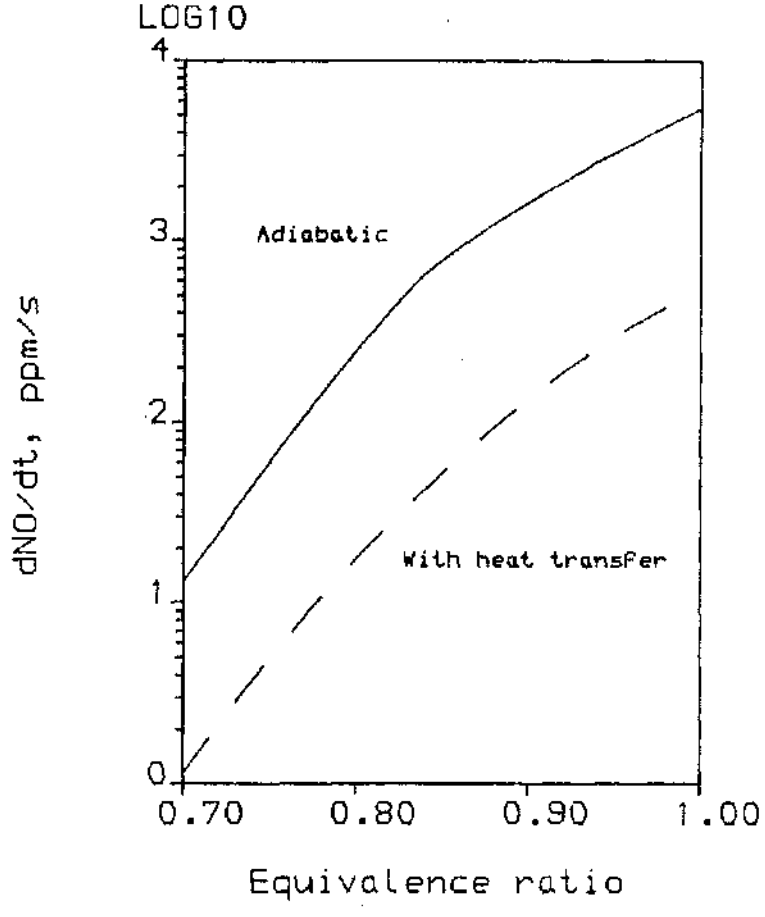

FIG.3b: EFFECT OF HEAT TRANSFER ON NO FORMATION

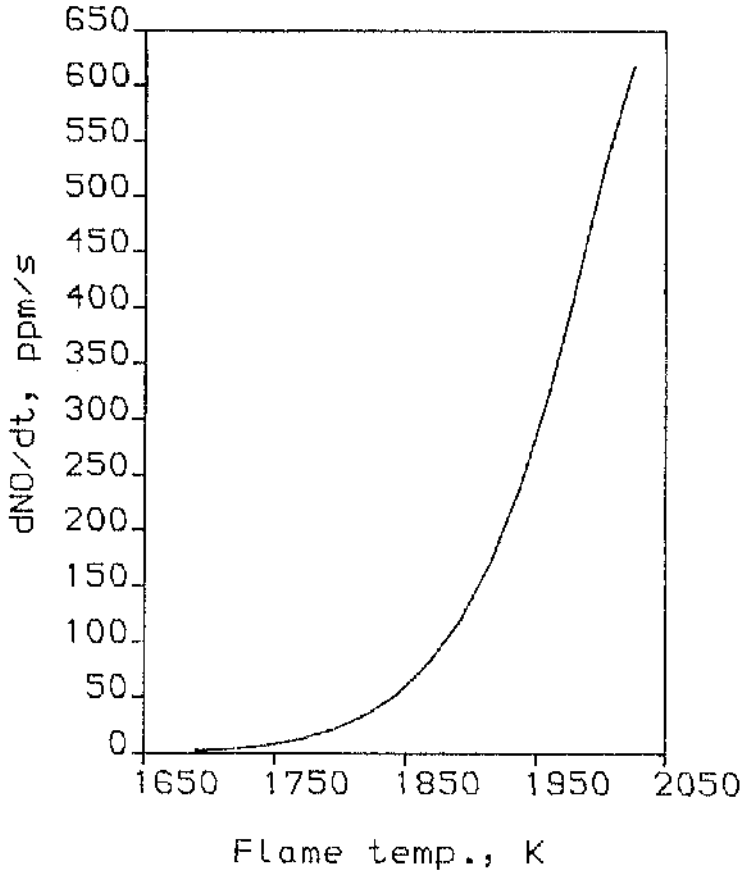

FIG.4:VARIATION OF NO FORMATION WITH FLAME TEMPERATURE

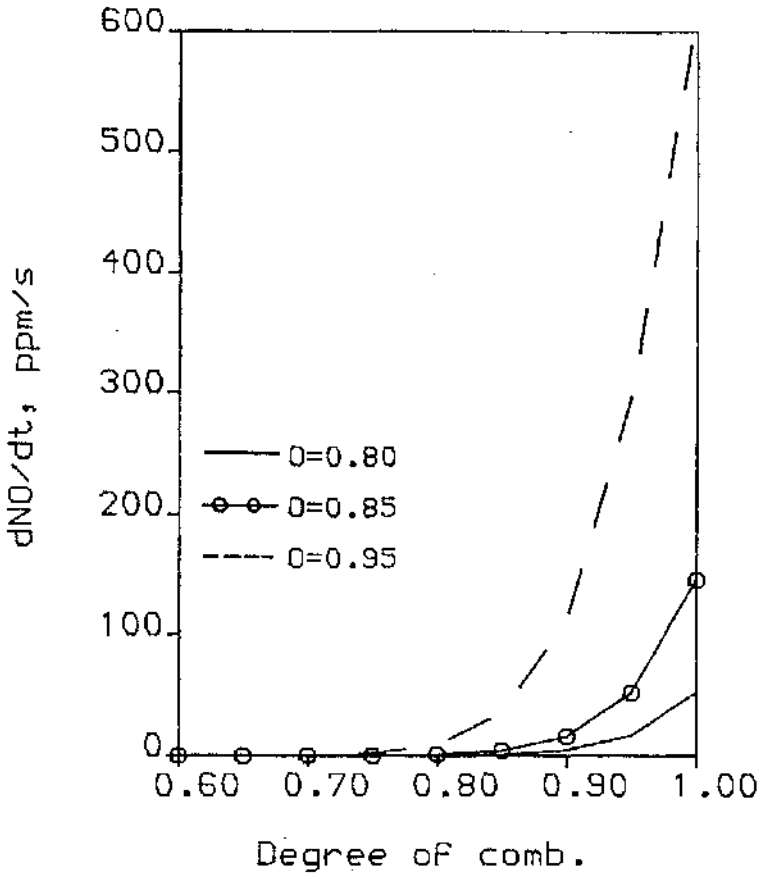

FIG.5: EFFECT OF DEGREE OF COMBUSTION ON NO FORMATION.

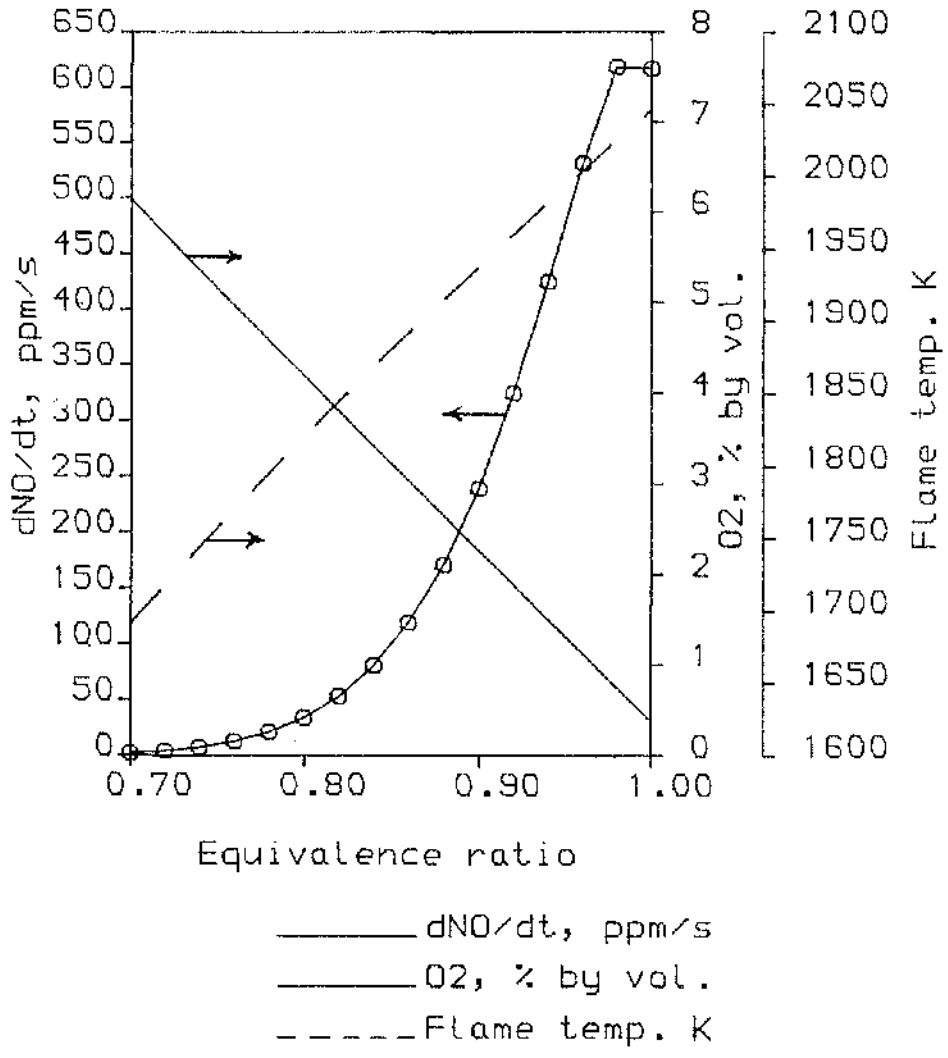

FIG.6: VARIATION OF FLAME TEMPERATURE, O2 AND NO WITH EQUIVALENCE RATIO.

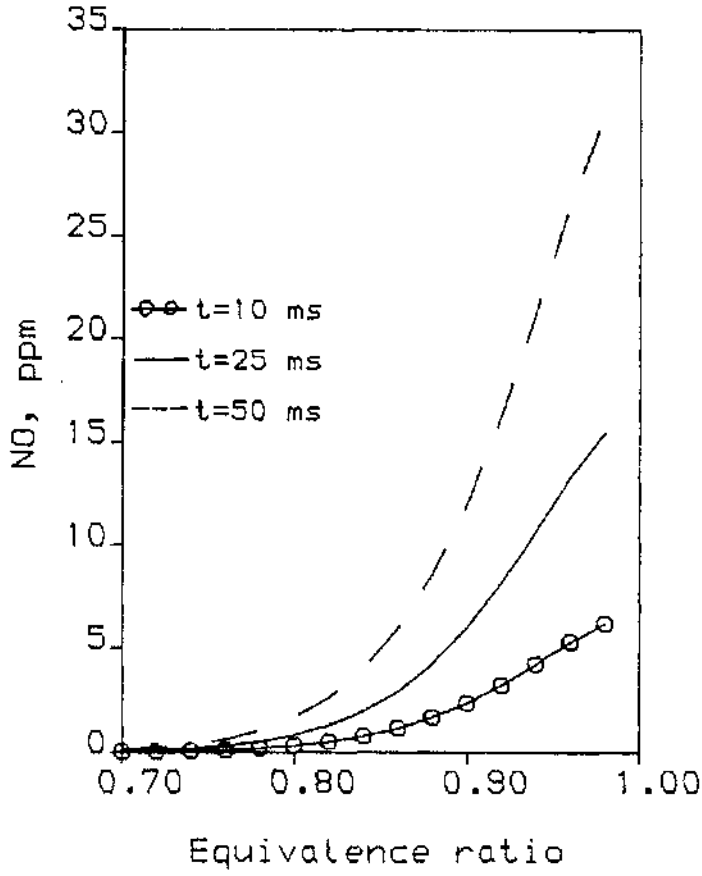

FIG.7:VARIATION OF NO FORMATION WITH RESIDENCE TIME

MODELLING THE COMBUSTION AERODYNAMICS FOR A PERIPHERAL INJECTION SYSTEM

Kenbar[1] A M A, Beltagui[1,2] S A and Maccallum[1] N R L

1- Glasgow University

2- National Engineering Laboratory

SYNOPSIS

An assessment is made of the ability of a CFD code to model swirling flames. The peripheral fuel injection mode applied to natural gas swirling flame is a novel test case. The predictions were made using the PHOENICS code, with turbulence and combustion represented by the k-ε and the 'eddy break-up' models respectively. The predicted flow patterns were in reasonable agreement with those previously measured. The agreement for combustion patterns, however, was good for the non-swirled flow only. This is attributed to the simplified turbulence and combustion models used.

NOTATION

A	Eddy break-up constant	Dimensionless
C_1	Constant, Eqn. 3	Dimensionless
C_2	Constant, Eqn. 4	Dimensionless
C_3	Constant, Eqn. 4	Dimensionless
d	Swirler diameter	m
D	Furnace diameter	m
k	Kinetic energy of turbulence	m^2/s^2
l	Characteristic Dimension	m
M	Mass fraction	kg/kg
r	Radius	m
R	Rate of chemical reaction	kg/m^3s
s	stoichiometric air-fuel ratio	Dimensionless
S	Burner Swirl Number $= \dfrac{\int 2\pi\, r^2 \rho\, U\, W\, dr}{d \int 2\pi\, r\, \rho\, U^2\, dr}$	
S_φ	Source term of variable φ, Eqn. 1	
t	time	s
U	Time-mean axial velocity	m/s
$\vec{V}$	Velocity vector, Eqn. 1.	
V	Time-mean radial velocity	m/s
W	Time-mean swirl velocity	m/s

X	Axial distance along the furnace	m
ε	Rate of dissipation of kinetic energy	m^2/s^3
ρ	Density	kg/m^3
φ	dependent variable, Eqn. 1.	
Γ_φ	Turbulent exchange coefficient	
θ	Swirler vane angle	

Subscrips

f	Fuel
o	Oxidant
φ	Dependant variable

1 INTRODUCTION.

Furnace system design requires careful characterisation and optimisation of complex flow phenomena. Traditionally, the designers of such systems have relied almost exclusively on empirical methods. New designs have usually been based on operating results from existing units while detailed information on the flow pattern within a furnace has been inferred from measurements on laboratory-scale models. However this approach can be expensive and in some cases is not capable of providing the large amount of design information required. Recently, analytical models capable of predicting the flow patterns and heat transfer characteristics have been developed and widely used for such furnaces. In addition to being required to handle turbulence and chemical reaction, these models must also be able to deal with complex geometries.

The research effort which has already been put into the development of these analytical models is very considerable. A significant part of this research have been devoted to the modelling of turbulence, combustion and radiative heat transfer. Also efforts have been made to improve the numerical techniques. A small selection of the many published detailed reviews of these research efforts is given in references (1-5)

Turning attention to the case of swirling flows in furnaces- a common situation in practice- the prediction procedures have been applied progressively. The simplest case- isothermal flow- has been studied for flows expanding into free space (eg. 6,7) and into confinement (eg. 8-11). Combusting flows have also been predicted satisfactorily (eg. 12-16). However, these combusting cases dealt with geometries where the fuel was injected in the centre of the swirled air jet.

Recent advances in burner design to meet operational and environmental requirements have resulted in burners with other modes of fuel injection. An example is a burner with fuel injected at the periphery of the swirled air flow, studied in an experimental furnace system by Beltagui and Maccallum (17). In that burner the mixing and combustion patterns are significantly different from those of the central fuel injection case due to the utilisation of the combined effects of shear-layer and centrifugal mixing. Therefore predicting the aerodynamic and combustion patterns of such a combustion system represents a new test for the generality of the modelling procedures.

The purpose of the present study is therefore to investigate the ability of a CFD procedure to deal with this peripheral fuel injection configuration (17). The system examined uses natural gas in an adiabatic furnace. The governing equations are solved by the finite difference procedure embodied in the PHOENICS Code (18). Turbulence is modeled by the standard k-ε model (19,20) and combustion by the 'eddy break-up' model

(21,22). The predictions of aerodynamic and combustion patterns are compared with the measured patterns.

2 EXPERIMENTAL DATA

The experimental measurements had been taken by Beltagui and Maccallum (17) in a refractory lined cylindrical furnace of 225 mm inside diameter and 0.9 m long. The air was introduced through a central concentric vane swirler of 93 mm inside diameter. The fuel- natural gas- was injected through an annular slit of 2 mm width around the periphery of the air swirler, see Fig 1. The experimental data were available for the following input variables;

(a) Swirler vane angle- θ- 0^0, 15°, 22° and 30°, giving burner swirl Number- S - (based on diameter), of 0.0, 0.089, 0.138 and 0.192.
(b) Inlet air velocity of 10.6 and 15.0 m/s, corresponding to Reynolds Number, based on swirler exit condition, of 6.3×10^4 and 9.0×10^4.
(c) Overall fuel equivalence ratio of 0.53 and 0.38.

The data set consisted of normalised profiles of the three components of the time-mean velocity, static pressure, temperature, and concentrations of CO_2, O_2 and CO.

In addition, a set of measurements had been taken for the isothermal flow covering all the swirl cases in (a) and the two air velocity levels (b), as reported by Beltagui et al (23).

These profiles were measured across the furnace diameter at seven planes along the furnace. Generally the profiles demonstrated good symmetry, which is vital for the meaningful comparison with axisymmetric program predictions.

3 PREDICTION PROCEDURE

The predictions have been made by solving the finite-difference formulations of the governing equations for the conservation of mass and three components of momentum. Turbulence is modelled by solving two differential equations for the turbulence kinetic energy and its dissipation rate (standard k-ε model). The combustion modelling was performed by solving differential equations for the enthalpy, fuel mass fraction and mixture fraction.

All the above equations can be written in a generalised form :

$$\frac{\partial}{\partial t} (\rho \varphi) + \text{div} (\rho \vec{v} \varphi - \Gamma_\varphi \text{ grad } \varphi) = S_\varphi \qquad (1)$$

where φ stands for any of the dependent variables, and ρ, $\vec{v}$, Γ_φ and S_φ are density, velocity vector, turbulent exchange coefficient and source term respectively. The source terms and exchange coefficients for the momentum and turbulence equations are discussed in detail in references (3,19,20) and others.

3.1 Isothermal flow simulation

The problem of devising a predictive method for turbulent reacting swirling flows can be approached by considering first the isothermal case so that attention can be focussed on the modelling of turbulent transport.

In the present work the isothermal flow simulation was performed first and then used as a basis for the reacting flow application which requires a combustion model.

3.2 Combustion model

In turbulent reacting flows, the modelling of the rate of reaction, and consequently the heat release rate, is essential to the evaluation of the local gas temperature and density, the latter being a major factor in the momentum and mass conservation equations.

In the present non-premixed system, the flame is considered as diffusion controlled. Although the fast reaction, or 'mixed-is-burned', model (13) is sometimes used to model such combustion systems, it tends to overpredict the combustion rate in forced draught systems.

In the present work, therefore the 'eddy break-up' model of Spalding (21) and Magnussen and Hjertager (22) has been adopted. This model assumes that the reactants are homogeneously mixed in the finite-scale dissipative eddies of the turbulence. The chemical reaction is represented by a one-step reaction between the fuel and oxidant. The rate of the reaction is governed by the concentration of the limiting reactant:

$$R_f = A \rho \frac{\varepsilon}{k} \text{ Min } [M_f , M_o/s] \qquad (2)$$

where M_f and M_o are the mean mass fractions of fuel and oxidant respectively, s is the stoichiometric ratio and A is the 'eddy break-up' constant. The value of A used in the present work will be discussed in Section 4.2.

The local gas temperature was calculated from the enthalpy using temperature dependant specific heat values for each of the three species, oxidant, product and fuel. The perfect gas law was used for the density calculation.

3.3 Boundary conditions

The inlet to the furnace is the exit plane of the burner, and at this plane the axial velocity component of the air was assumed uniform in the non-swirled case and to increase linearly with the radius in the swirl flow case. The tangential component was assumed to follow the same profile and equal to the product of tan θ and the axial component, where θ is the swirler vane angle. The radial velocity was taken always to be zero. The corresponding k and ε values have been calculated as follows;

$$k = C_1 (U^2 + V^2 + W^2) \qquad (3)$$

$$\varepsilon = C_2 k^{3/2} / C_3 l \qquad (4)$$

where $C_1 = 0.0323$, $C_2 = 0.1643$, $C_3 = 0.09$ and l is the characteristic dimension for the flow stream (air or fuel). The values of the above constants have been deduced from experimental measurements in similar flow systems (10). Uniform profiles were assumed for inlet pressure, enthalpy and species concentration.

The flow boundary conditions at the solid walls have been described by the log-law and specified to be adiabatic.

3.4 Computational details

The numerical solution of the differential equations for cylindrical polar coordinates was performed using the PHOENICS code (18). The furnace geometry was represented by an axisymmetric non-uniform grid of 41 axial by 45 radial nodes. Near the burner, particularly the fuel exit, the grid spacing in the radial direction was reduced to 0.5 mm.

The Upwind differencing scheme was used, with under-relaxation parameters for all the variables. About 300 to 500 sweeps were required to obtain a satisfactorily converged solution with normalised mass residuals of less than 10^{-4}. A typical calculation of 400 sweeps required about 2.8 hours of CPU time on a VAX-785 computer.

4 RESULTS

4.1 Isothermal flow simulation- peripheral fuel injection

For the isothermal flow simulation, both experimental and predicted, the fuel jet was represented by an air jet of equal velocity.
The predicted and measured flow pattern results were then compared . The comparisons, not presented here for brevity, showed that under low swirl conditions the flow boundaries and velocity profiles were well predicted. At high swirl, however, the central recirculation was underpredicted. In general, the agreement was good and this encouraged application of the prediction procedure to the combustion case.

4.2 Combusting flow simulation- peripheral fuel injection

A representative selection of the predictions is presented in Figs 2-8, together with the corresponding experimental measurements, covering the results for the 0° and 30° swirlers. They are presented in the form of normalised profiles of the three components of the time-mean velocity, static pressure, temperature, and concentrations of oxidant and product (predicted) or CO_2 (measured).

An exploratory trial was carried out to test the "mixed-is-burned" combustion model predictions. As expected, this model produced a combustion pattern corresponding to a reaction rate much faster than the experimentally measured.

As explained in Section 3.2, the 'eddy break-up' model was next examined and tests were carried out to select the best value for the constant A, Eqn. (2). The value of A = 2.0 was found to lead to the best representation of the combustion patterns.

4.2.1 Axial velocity profiles

Predicted and measured axial velocity profiles are shown in Figs 2(a) and 2(b) for the 0° and 30° swirlers respectively. The general flow pattern is well predicted for both these cases. However on detailed inspection of the profiles the following comments are made;

1. The effect of swirl in modifying the flow pattern is predicted through the more rapid jet expansion and the faster decay of the peak velocities and the radial gradients of the axial velocity. For example the jet wall-impingement point moved nearer to the burner as swirl is introduced. Also a uniform velocity profile was attained at a shorter axial distance.
2. The predicted jet expansion is faster than that measured. This applies to the results both without and with swirl.
3. The predicted decay of the radial gradients of velocity is more rapid than measured, leading to the prediction that more uniform velocity profiles occur earlier than measured.
4. For the non-swirled flow case, Fig 2(a), better agreement between predictions and measurements is obtained nearer the burner than further downstream. By contrast, in the case using the 30° swirler the predictions are better further downstream from the burner.
5. The prediction of lower radial gradients of the axial velocity near the burner for the 30° swirler leads to a predicted centreline velocity

which is higher than measured. This also leads to a failure to predict flow reversal at the centreline.

4.2.2 Tangential velocity profiles

Figure 3 illustrates the radial profiles of the tangential velocity component in the furnace chamber for the 30° swirler. Both the predicted and measured profiles approximate to Rankine-vortex flow with solid body rotation in the central region and peak tangential velocities in the vicinity of the axial velocity maxima.
Although the experimental profiles exhibit some asymmetry, the agreement between the predictions and the averaged experimental data is considered to be good.

4.2.3 Radial velocity profiles

Comparisons of predicted and measured radial velocity profiles are shown in Figs 4(a) and 4(b) without and with swirl respectively. In both cases, the predicted velocity profiles in the near-burner zone follow the shape of the experimentally measured profiles but the magnitudes of the predicted values are much lower than those measured. As the flow progresses downstream, it is noted that the predicted radial velocities decay much faster than the measured velocities. This is consistent with the predicted decay of the axial velocities in this region. Increasing swirl has little effect on the predicted radial velocity values as shown in Fig 4(b), although the measured values apparently increase.

As previously reported (8,9), while there is reasonable confidence in the probe measurements for the axial and tangential velocity components it is believed that the probe measurements exaggerate the radial velocity values, particularly in the regions of peak radial velocities. Consequently, excessive reliance should not be placed on the measured radial velocity profiles.

4.2.4 Static pressure distribution

Comparison of the predicted and measured static pressure distributions are illustrated in Fig 5. In the unswirled case, Fig 5(a), the predicted static pressure differs only very slightly from atmospheric. The measured values show some considerable differences below and above the atmospheric value. The fuel jet injection scheme may be partly responsible for this. Also there are indications of asymmetry of the jet. This is consistent with the noticeable asymmetry of the axial velocity profiles, Fig 2(a).

For the case using the 30° swirler (Fig 5(b)), there is generally good agreement between prediction and measurement, with sub-atmospheric pressure near the centreline, rising to near, or slightly above, atmospheric close to the walls. This pattern is typical of static pressure distributions associated with confined swirling flows.

4.2.5 Temperature distributions

Predicted and measured temperature profiles are shown in Fig 6. From these results the following comments are made:
1. For both unswirled and swirled flows the temperature profiles near the burner are well predicted with maximum temperatures at the outer recirculation zone and low temperatures in the unburned central flow. Combustion is initiated at the shear layer between the air and fuel jets.
2. The effect of swirl on the predicted temperature profiles is noted through reduced radial temperature gradients. However, the predicted effect of swirl on the temperature profiles is somewhat less than that

observed.
3. For the non-swirled flow case, as the flow progresses downstream the agreement between the predicted and measured profiles remains good.
4. For the 30° swirler flow, as one moves downstream a discrepancy between the predicted and measured profiles becomes apparent. Whereas the measured profiles become uniform at about 3 furnace diameters downstream, the predicted profiles still show a marked non-uniformity, with a variation by a factor of about 3 in the temperature rise. Thus generally the effect of radial mixing between the flow streams is not yet adequately predicted.

4.2.6 Species concentrations:

Since the program solves the equations for a one-step global reaction, the results give concentrations of fuel, oxidant and product. The predicted oxidant profiles are compared with the measured O2 concentrations in Fig 7. The predicted concentrations for the "product" can be compared with the measured CO2 concentrations for the locations where combustion is complete. This comparison is shown in Fig 8. For complete combustion of the natural gas used (about 95% - by volume-methane), the CO2 concentration in the dry product is 11.8% by volume. This comparison should give sufficient indication of the agreement, or otherwise, between the predictions and the measurements throughout most of the flow field. The comparison is not valid however in locations of partial combustion.

The predicted oxidant and product concentrations are consistent with each other, and with the predicted temperature profiles. Thus the agreement between the predicted and observed species concentration is the same as the agreement for the temperature profile. The comments made in section 4.2.5 about the temperature profiles therefore apply also to the concentration profiles.

4.3. Comparison of peripheral fuel-injection with central fuel-injection:

The prediction procedure was also set for the configuration where the fuel is injected in the centre of the air jet in order to asses the predicted degree of change in the results between the two fuel injection systems. Firstly though, these predicted results were compared with observed combustion patterns inferred from temperature measurements in the same furnace, with a central fuel injector. This test proved satisfactory. The predictions for the two fuel injection systems were then compared.

A sample of the results for the predicted temperature is given in Fig 9, where a marked effect on the temperature field is clearly seen. In the peripheral fuel-injection system the high temperatures are in the outer recirculation zone and in the forward flow near the walls after the jet impingement point. On the other hand, for the central fuel-injection system, the high temperatures are near the centre of the flow. This prediction is in excellent agreement with the observed effect.

5. DISCUSSION OF RESULTS

The predictions presented above were all made with the program using the facilities available within the Code with no adjustments to its sub-models.The main features of the flow and combustion patterns are well predicted as demonstrated in the comparisons with the measured profiles. However, detailed comparisons indicate some less satisfactory agreement on a number of points.

Considering the flow pattern, the radial gradients of velocity

components are underpredicted, particularly for the swirling flow. This feature of underpredicting the velocity gradients is a typical characteristic of the standard k-ε turbulence model and has been reported by other investigators (eg 7,10,11,24). The underprediction is attributed to the body forces which arise from the effects of curvature, recirculation, swirl and buoyancy. These forces are known (3,5) to interact selectively with different normal and shear stresses making the use of the isotropic turbulence assumption inappropriate.

The present investigation is of a special flow configuration where the body forces play an important role. In this furnace, using the peripheral fuel-injection scheme, combustion starts at the outer shear layer of the air jet. The centrifugal forces created in this system due to the density gradients are expected to increase further the effect of body forces on the turbulent flow (5,17).

Trials to overcome this deficiency through the use of a modified anisotropic form of the turbulent eddy viscosity based on the k-ε model have been presented for some simpler flow situations (eg 24). However, these models are not yet of a general form suitable for use with general codes.

Rigorous models solving the complete Reynolds stress equations should have the degree of generality required. However, these models have not been available in general CFD codes. Another reason for not using these is the expensive computational time penalty involved.

Considering the combustion patterns, as represented by the temperature and species concentration fields, the predictions are in good agreement for the non-swirled flow case, but less satisfactory agreement is obtained for the swirling flow. There are two reasons for these deficiencies;

Firstly, the weakness in the turbulence modelling, as explained above, led to lower mixing rates in the radial direction as indicated by the lower degree of uniformity in the temperature and species concentration profiles, compared to the measured profiles. The underprediction of mixing is more apparent in the swirling flow case.

Secondly, the simplified combustion model, which is also governed by the turbulence properties through the "eddy break-up" model, is probably too simple.The present formulation did not include the effect of the hot product concentration, which has proved significant in another application (12).

6. CONCLUSIONS

The general agreement between predicted and measured flow and combustion patterns is encouraging considering that the procedure used the standard k-ε turbulence model, and a simple combustion model.

The main changes in the combustion pattern caused by switching from central to peripheral fuel injection were well predicted.

For the peripheral fuel injection system, with a non-swirled air jet the predictions are generally good. However, the enhancement of mixing caused by the combined effect of swirl and density gradients, was not adequately predicted. This weakness highlights the importance of modelling the contribution of the body forces to the turbulence exchange coefficients.

It is suggested that the use of anisotropic turbulent modelling is necessary for the prediction of swirling reacting flows.

REFERENCES

1. JONES, W. P. and WHITELAW, J. H., "Modelling and measurements in turbulent combustion", 20th Symp. (int.) on Combustion, 1984, 233-249. The Combustion Institute, Pittsburgh, PA.

2. ROBINSON, G. F., "A three-dimensional analytical model of a large tangentially-fired furnace", J. Inst. of Energy, Sept. 1985, 116-150

3. SLOAN, D. G., SMITH, P. J. and SMOOT, L. D., "Modelling of swirl in turbulent flow systems", Prog. Energy Combust. Sci., 1986, Vol. 12, 163-250.

4. CORREA, S. M. and SHYY, W., "Combustion models and methods for contentious gaseous turbulent combustion", Prog. Energy Combust. Sci, 1987, vol. 13, 249-292.

5. LESCHZINER, M. A., "Modelling turbulent recirculating flows by finite-volume methods - current status and future directions", Int. J. Heat and Fluid Flow, 1989, Vol. 10, No. 3, 186-202.

6. WEBER, R., BOYSAN, F.,SWITHENBANK, J. and ROBERTS, P. A.,"Computation of near field aerodynamics of swirling expanding flows", 21th Symp. (Int.) on Combustion, 1986,1435-1443. The Combustion Institute, Pittsburgh, PA.

7. MAHMUD, T., TRUELOVE, J. S., WALL, T. F., "Flow characteristics of swirling coaxial jets from divergent nozzles", ASME, J. of Fluids Eng., 1987, vol. 109, 275-282.

8. BELTAGUI, S. A., FUGGLE R. N. and RALSTON, T., "Aerodynamic and mixing within the quarl of a variable swirl burner (experimental and theoretical study)", First European Conference on Industrial Furnaces and Boilers (INFUB), Lisbon, Portugal, 1988.

9. BELTAGUI, S. A., FUGGLE R. N. and RALSTON, T., "An Isothermal study of the aerodynamics of the furnace flow issuing from a variable swirl burner", 1st World conference on Experimental Heat transfer, Fluid Mechanics and Thermodynamics, 1988, Dubrovnik, Yugoslavia. Elsevier Pub.

10. NEJAD, A. S., VANKA, S. P., FAVALORO, S. C., SAMIMY, M. and LANGENFELD, C., "Application of laser velocimetry for characterization of confined swirling flow", ASME J. Eng. for Gas Turbines and Power, 1989, vol. 111, 36-45

11. JONES, W. P. and PASCAU, A., "Calculation of confined swirling flows with a second moment closure", ASME, J. of Fluids Eng., 1989, Vol. 111, 248,255.

12. BELTAGUI, S. A., FUGGLE R. N., KENBAR, A. M. A., RALSTON, T., MARRIOTT, N. and STOPFORD P. J., "Modelling a gas-fired furnace flow and combustion using the PCOC code", paper submitted to Eurotech Direct, 1991.

13. KENT, J. H. and BILGER. R. W., "The predictions of turbulent diffusion flame fields and nitric oxide formation", 16th Symp. (Int.) on Combustion, 1976, 1643-1656. The Combustion Institute, Pittsburgh, PA.

14. ABBAS, A. S., LOCKWOOD, F.C. and SLOOJA, A. P., "The prediction of combustion and heat transfer performance of a refinery heater", Combustion and Flame, 58, 91-101, 1984.

15. GOSMAN, A. D., LOCKWOOD, F.C. and SLOOJA, A. P., "The prediction of cylindrical furnaces gaseous fueled with premixed and diffusion burners", 17th Symp. (Int.) on Combustion, 1978, 747-760. The Combustion Institute, Pittsburgh, PA.

16. KHALIL, E. E., HUTCHINSON, P. and WHITELAW, J. H., "The calculation of the flow and heat-transfer characteristics of gas-fired furnaces", 18th Symp. (Int.) on Combustion, 1981, 1927-1938. The Combustion Institute, Pittsburgh, PA.

17. BELTAGUI, S. A. and MACCALLUM, N. R. .L, "Characteristics of enclosed swirl flames with peripheral fuel injection ", J. Inst. of Energy, March, 1988, 3-16.

18. LUDWIG, J. C., QIN, H. Q. and SPALDING, D. B., "The PHOENICS Reference Manual", CHAM TR/200, 1989, CHAM LTD.

19. BRADSHAW, P., CEBECI, T. and WHITELAW, J. H., "Engineering calculation methods for turbulent flow", Academic Press, 1981, London.

20. GUPTA, A. K. and LILLEY, D. G., "Flowfield modeling and dignostics" ABACUS Press, 1985, Tunbridge Wells, Kent, England.

21. SPALDING, D. B., "Mixing and chemical reaction in steady confined turbulent flames", 13th Symp. (Int.) on Combustion, 1970, 649-658.The Combustion Institute, Pittsburgh, PA.

22. MAGNUSSEN, B. F. and HJERTAGER, B. H., "On mathematical modelling of turbulent combustion with special emphasis on soot formation and combustion", 16th Symp. (Int). on Combustion, 1976, 719-730.The Combustion Institute, Pittsburgh, PA.

23. BELTAGUI, S. A., KENBAR A. M. A. and MACCALLUM N. R. L, "Comparison of isothermal and combusting confined swirling flows - peripheral fuel injection", paper submitted to the 2nd World conference on Experimental Heat transfer, Fluid Mechanics and Thermodynamics, to be held in Dubrovnik, Yugoslavia, 1991.

24. KOBAYASHI, T. and YODA, M., "Modified k-ε model for turbulent swirling flow in a straight pipe", JSME, Internat. Journal, 1987, Vol. 30, No. 259, 66-71.

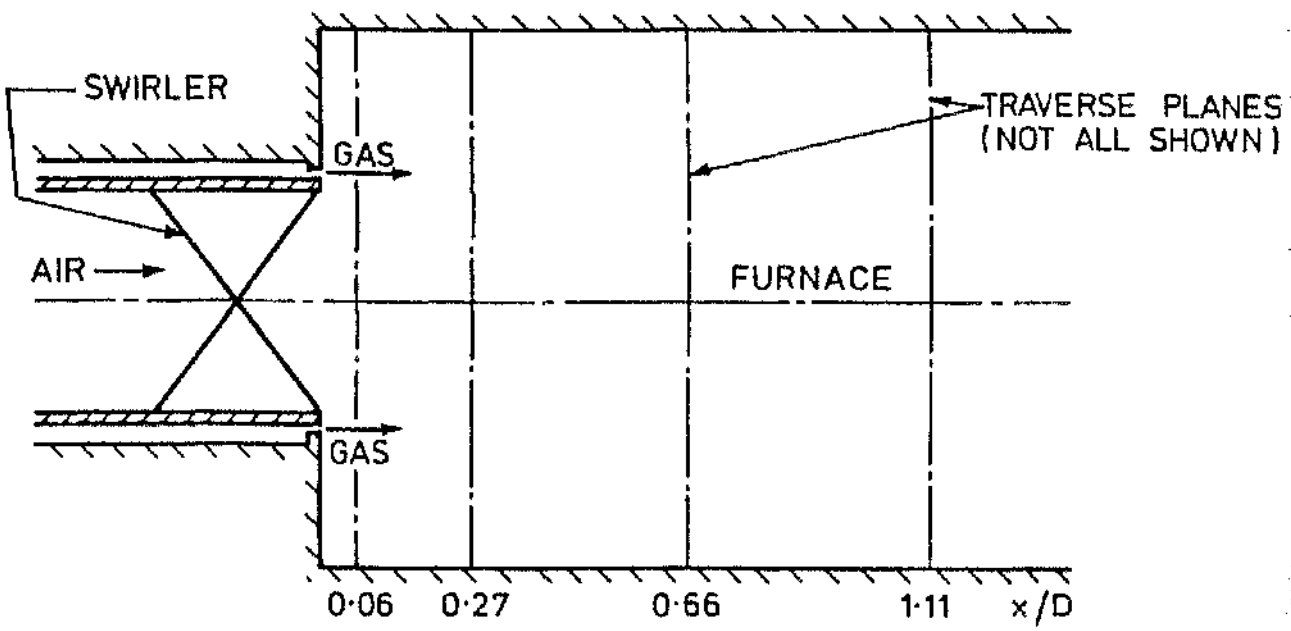

Fig. 1 : Peripheral fuel-injection burner system

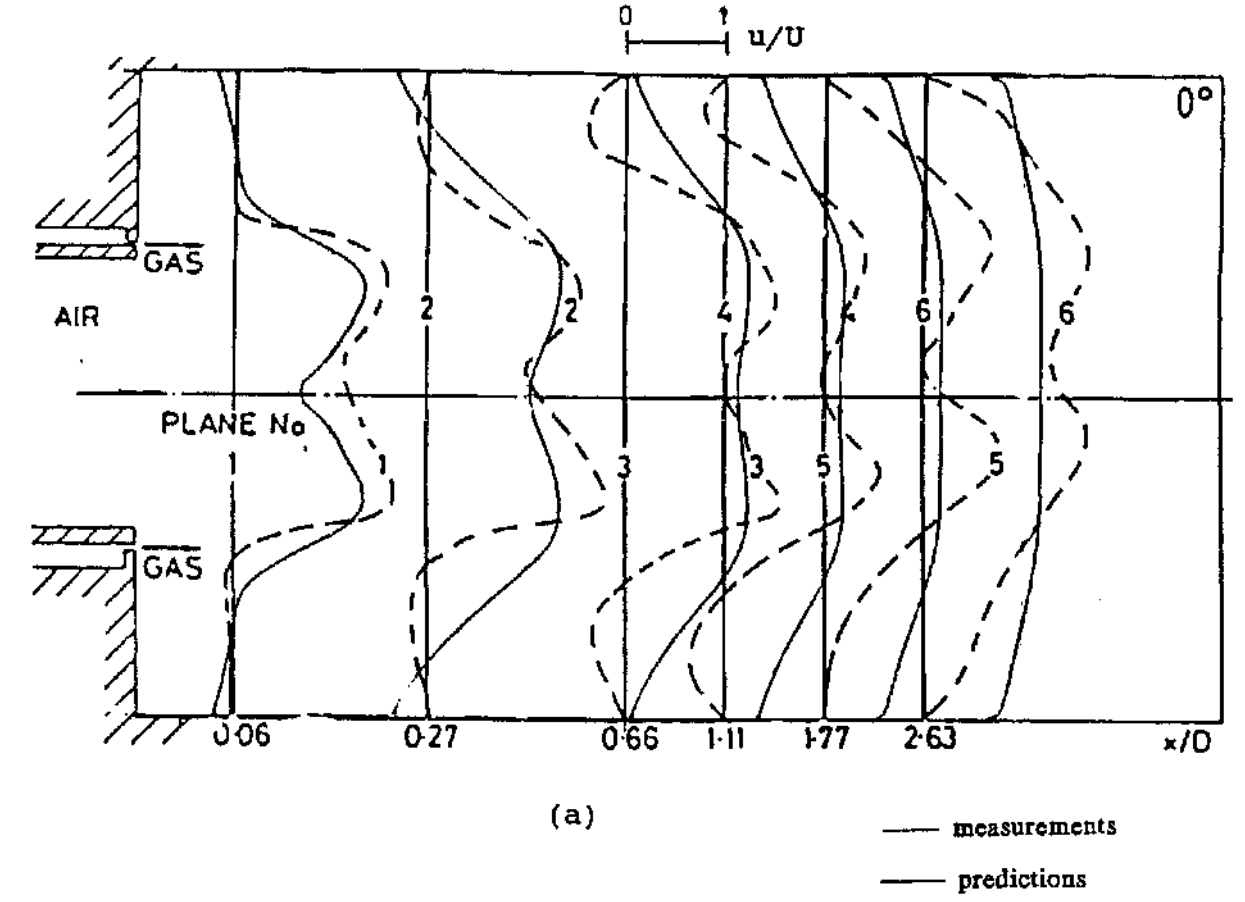

(a)

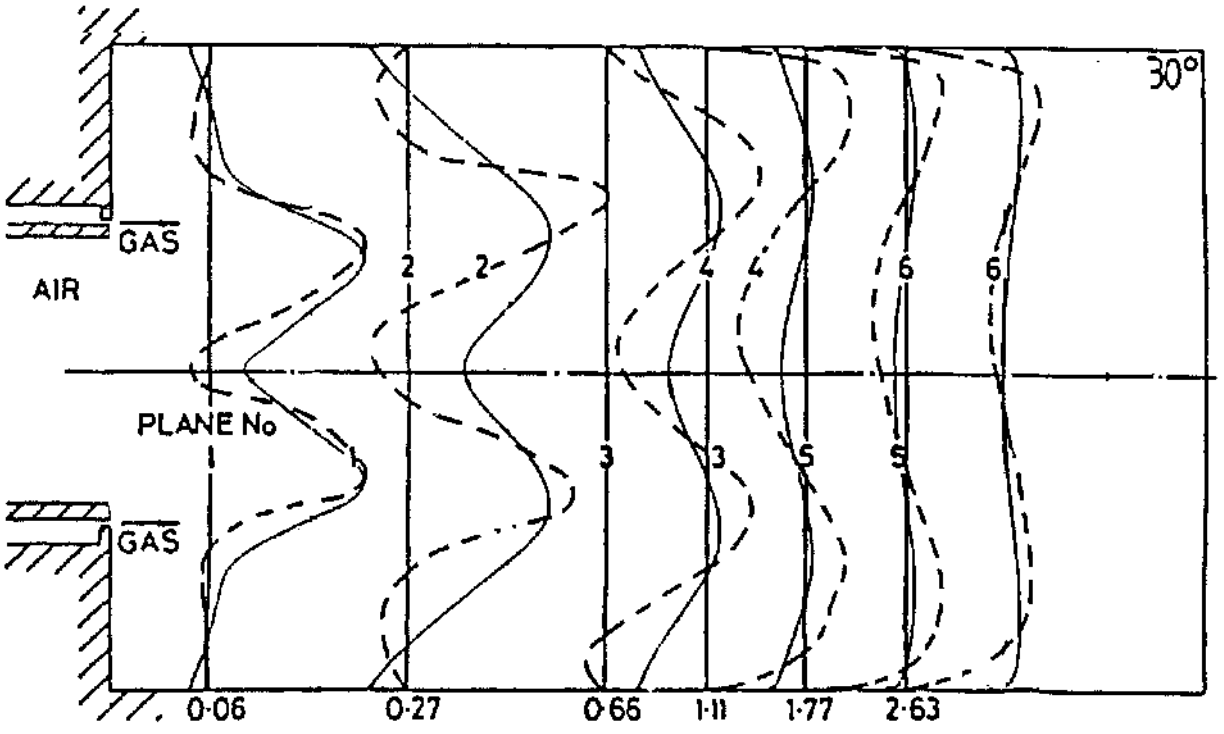

(b)

Fig. 2 : Axial velocity distributions

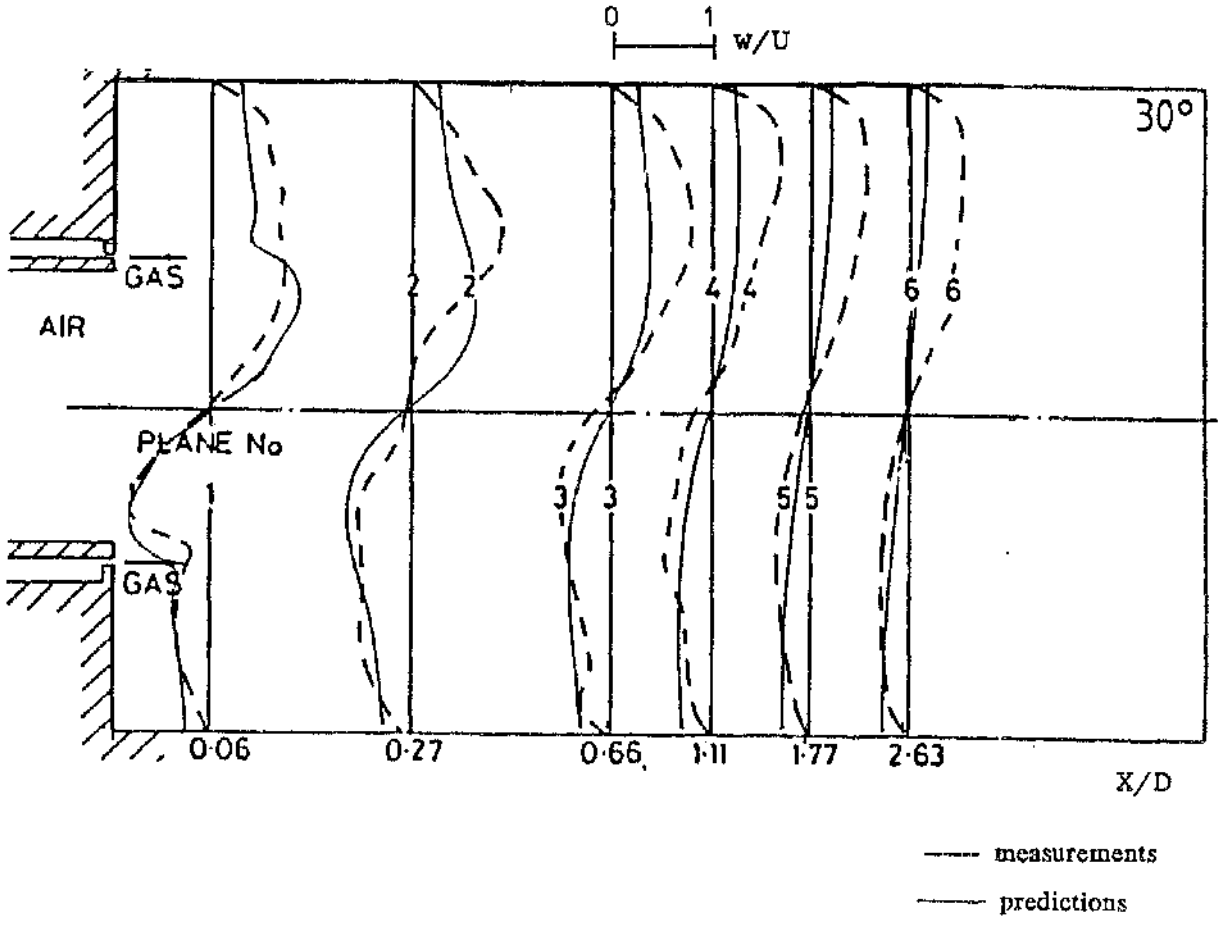

Fig. 3 : Tangential velocity distribution

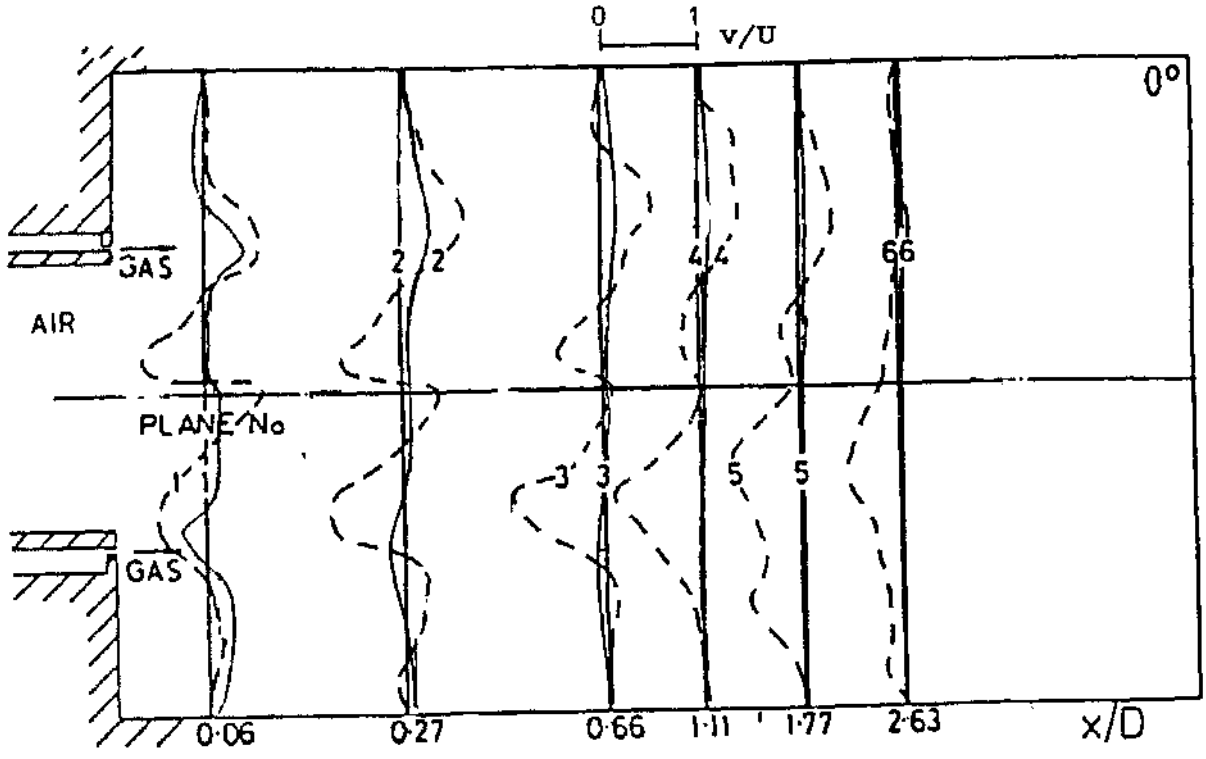

(a)

------ measurements

—— predictions

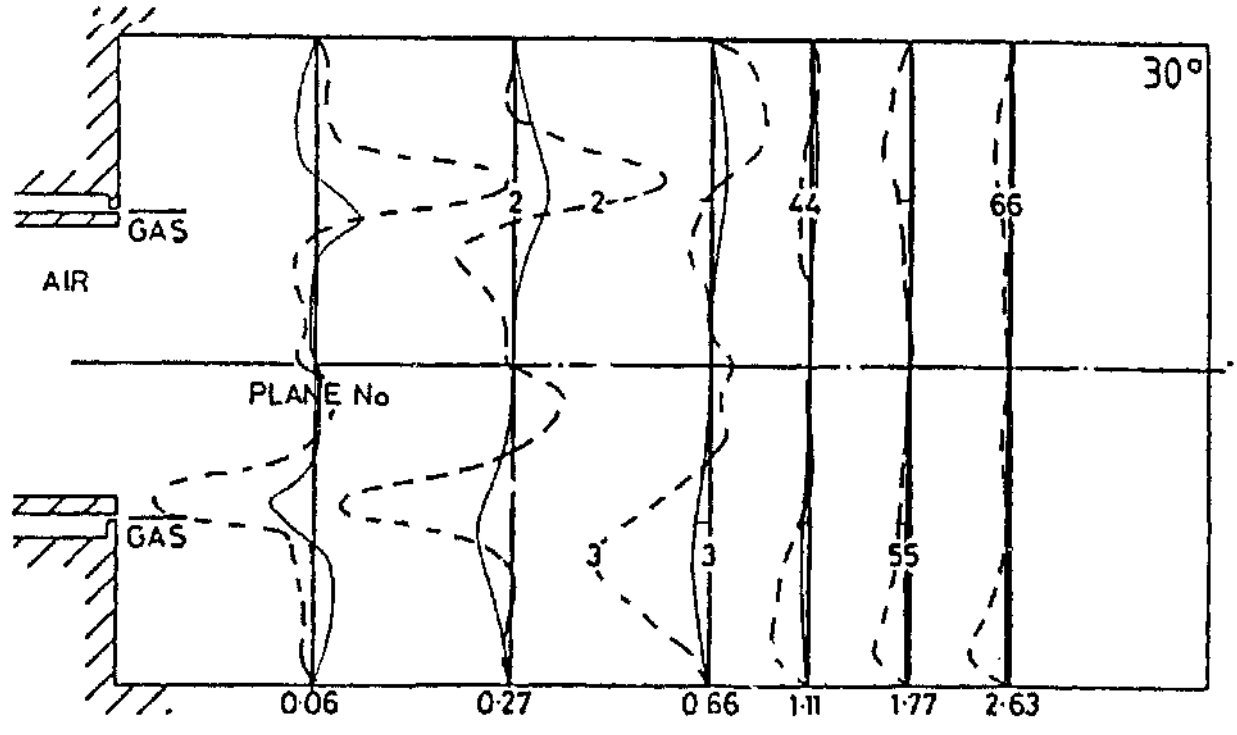

(b)

Fig. 4 : Radial velocity distributions

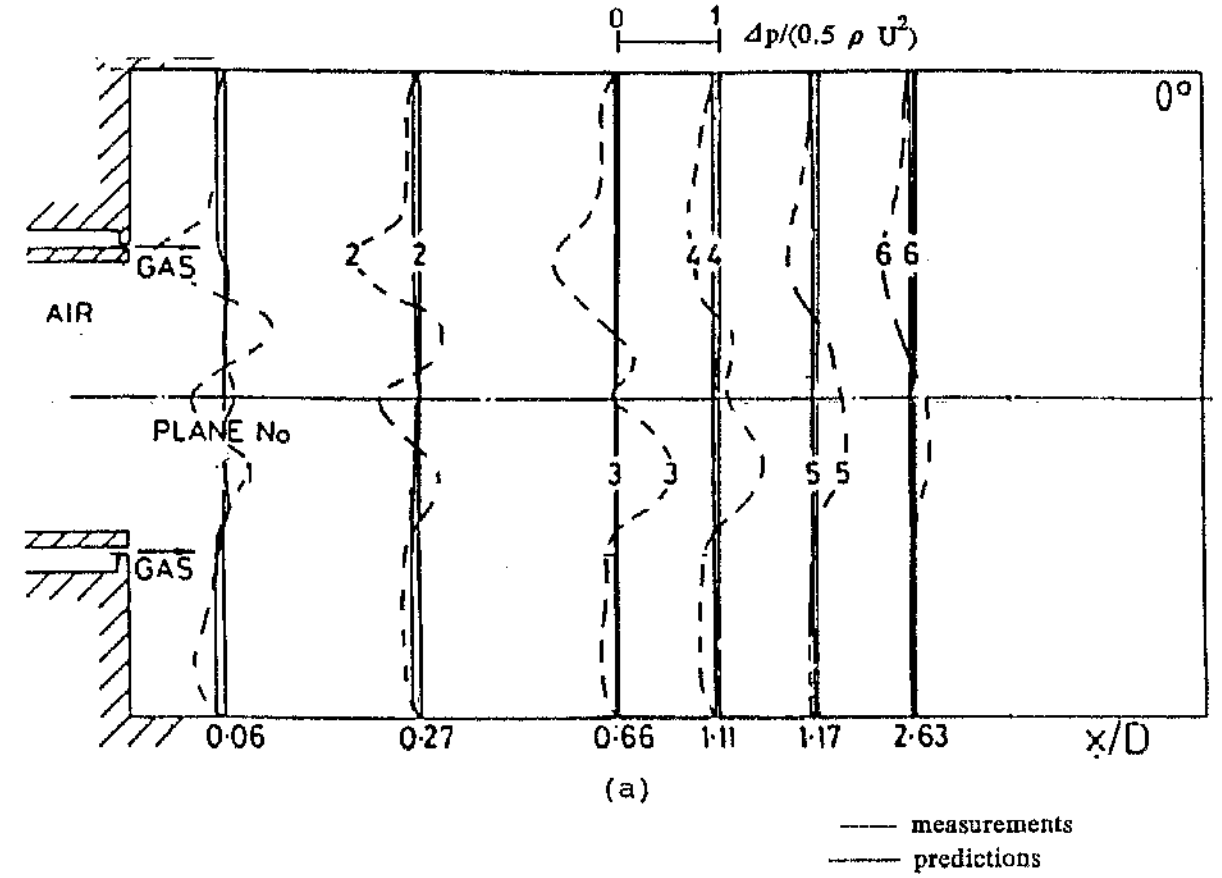

(a)

—— measurements
——— predictions

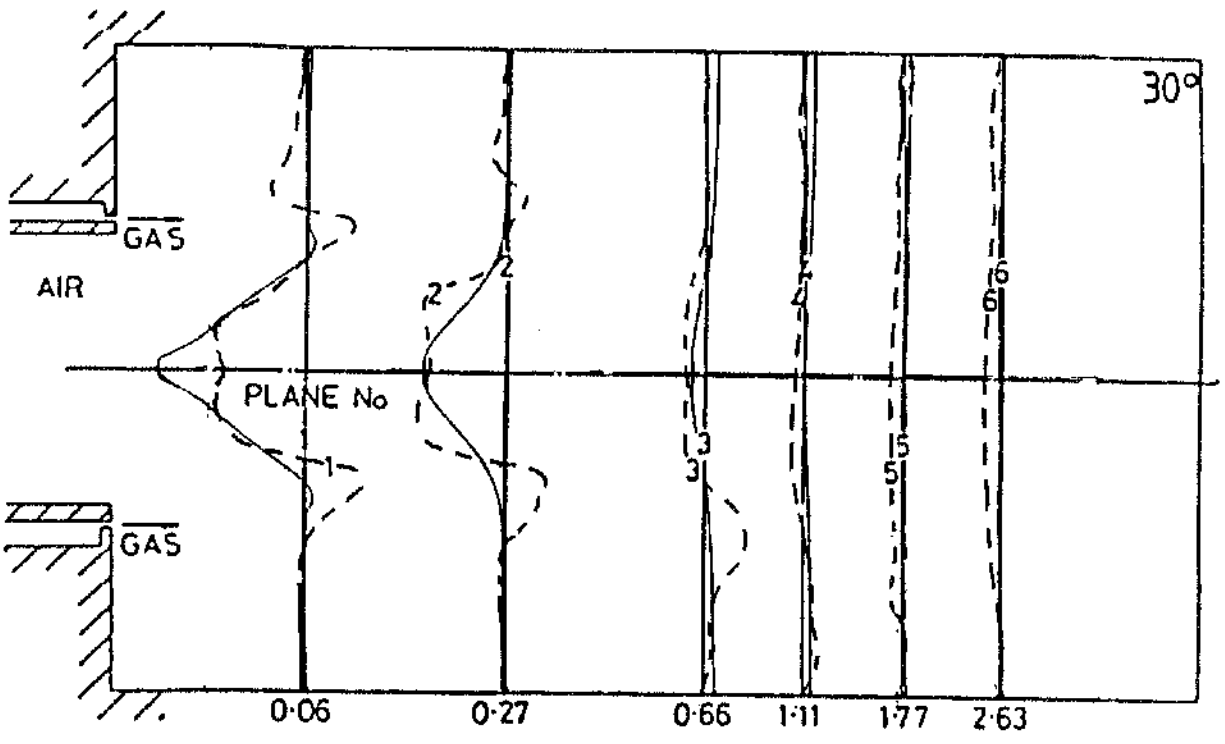

(b)

Fig. 5 : Static pressure distributions

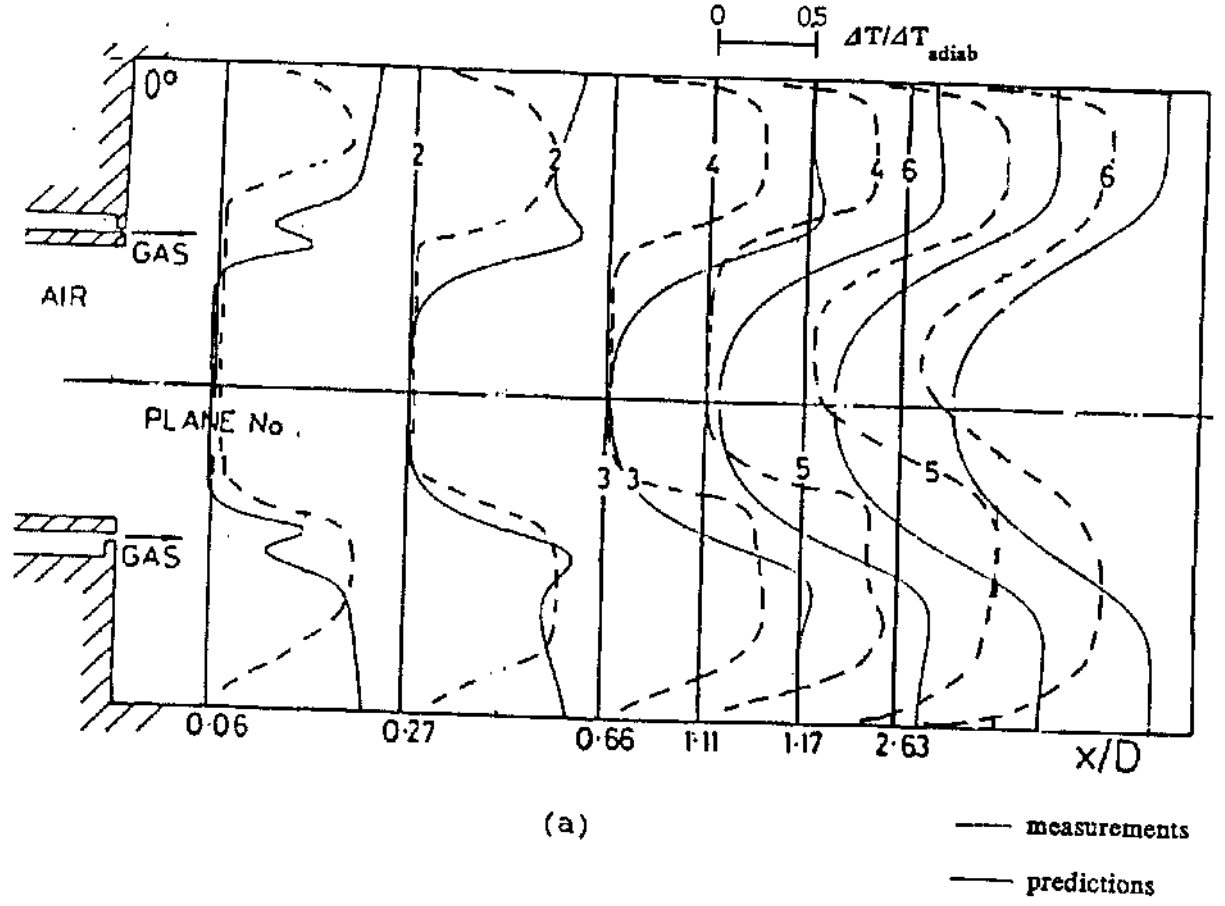

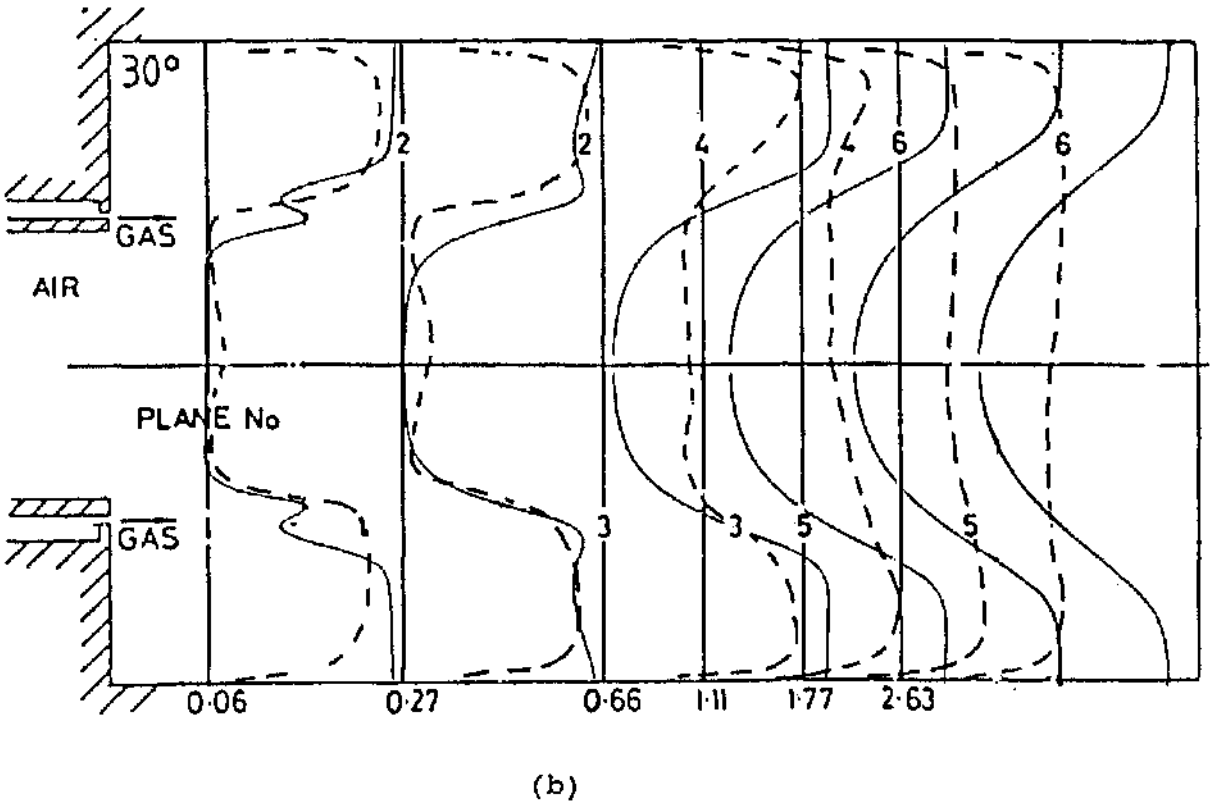

Fig. 6 : Temperature rise distributions

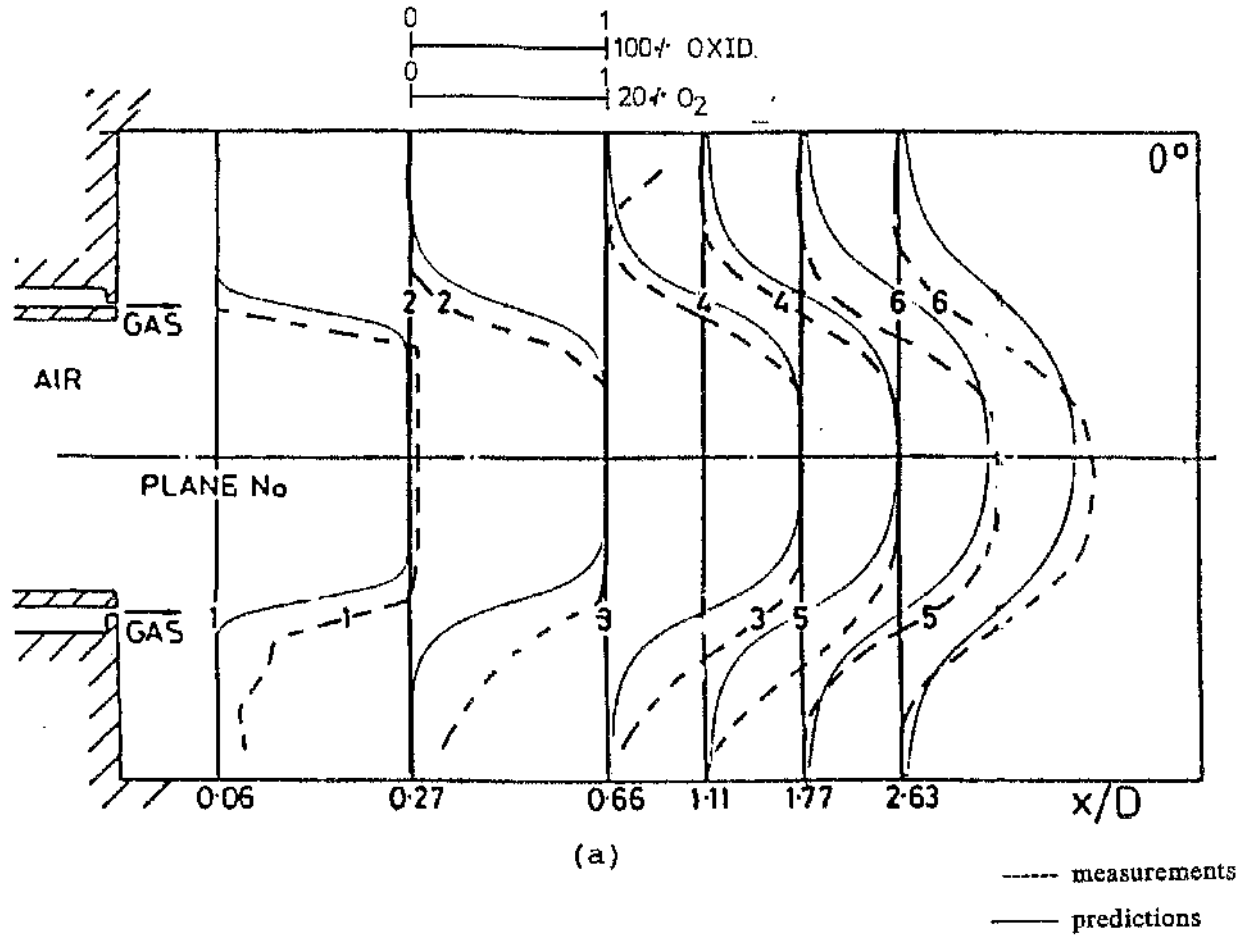

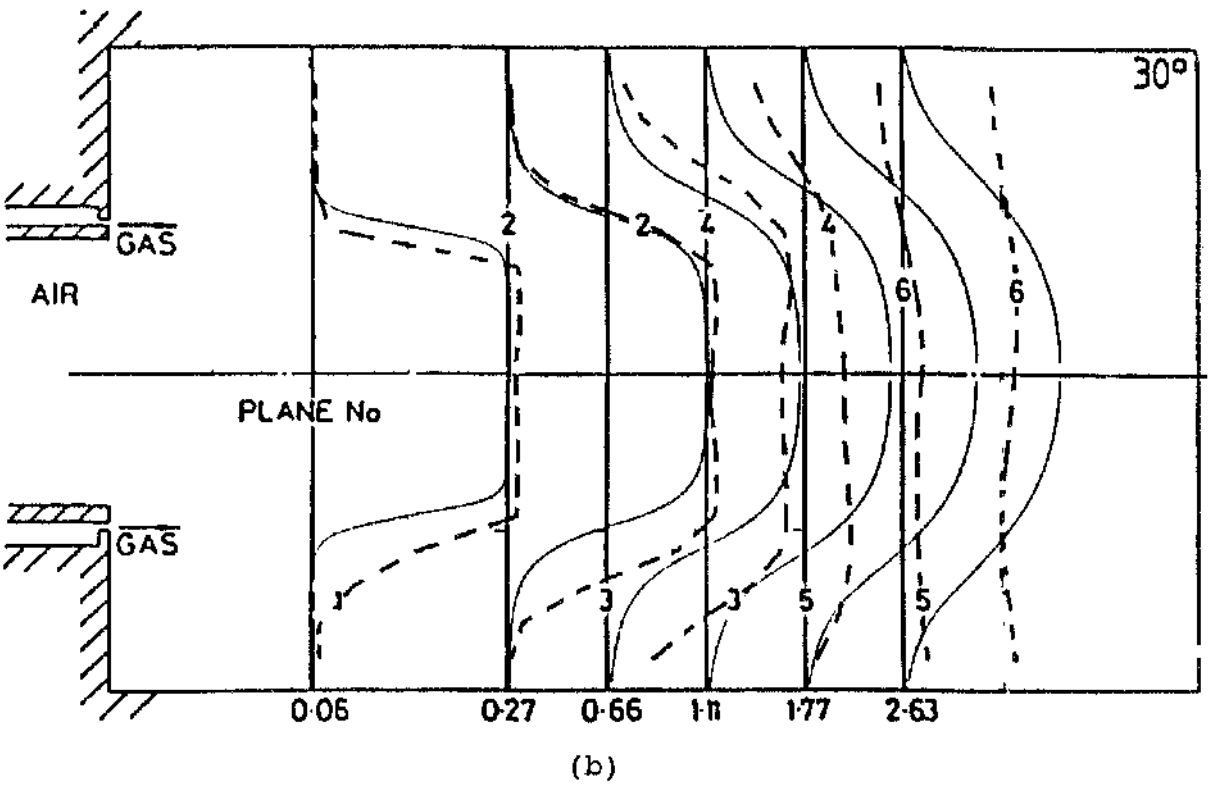

Fig. 7 : Oxidant concentration distributions

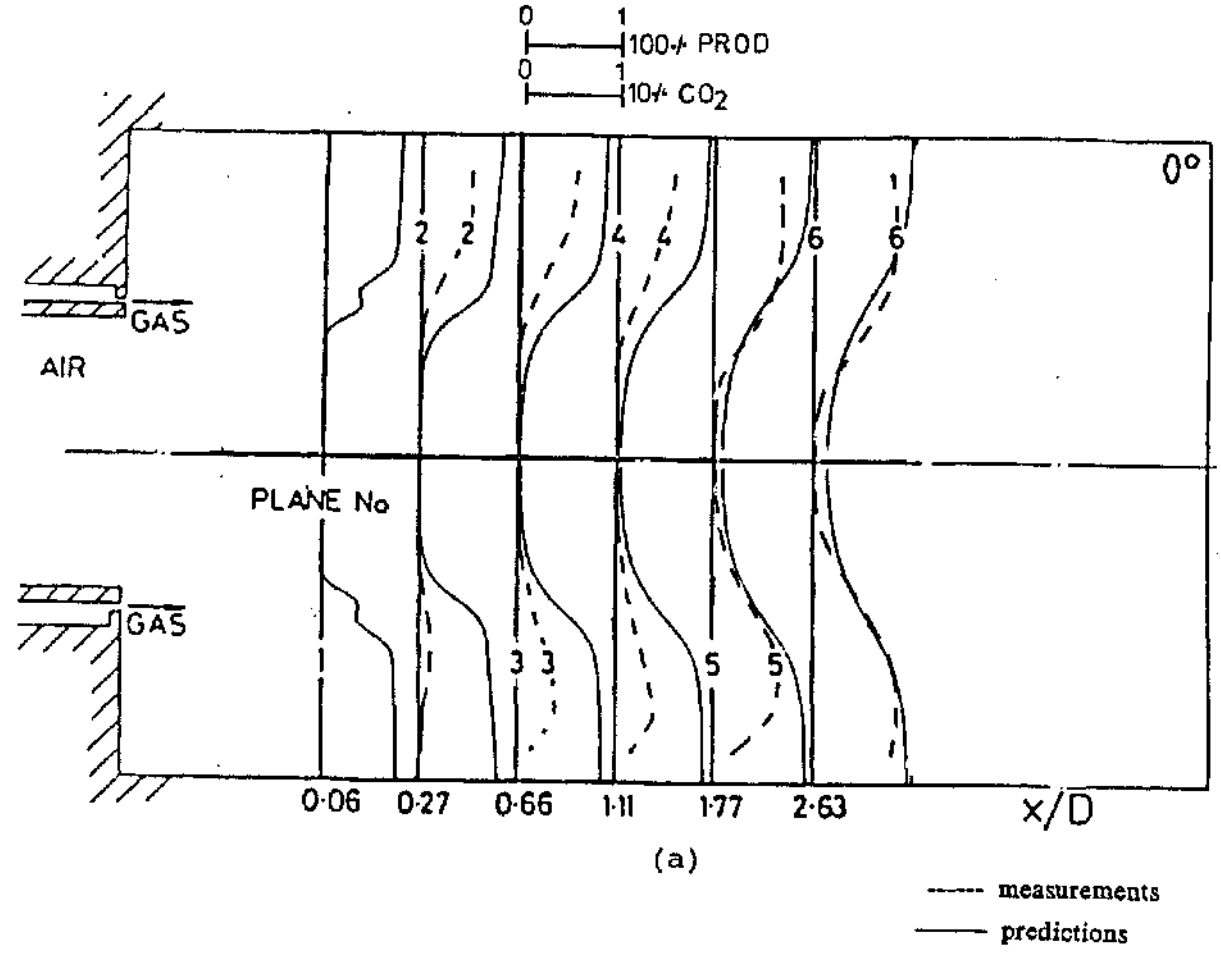

(a)

----- measurements

——— predictions

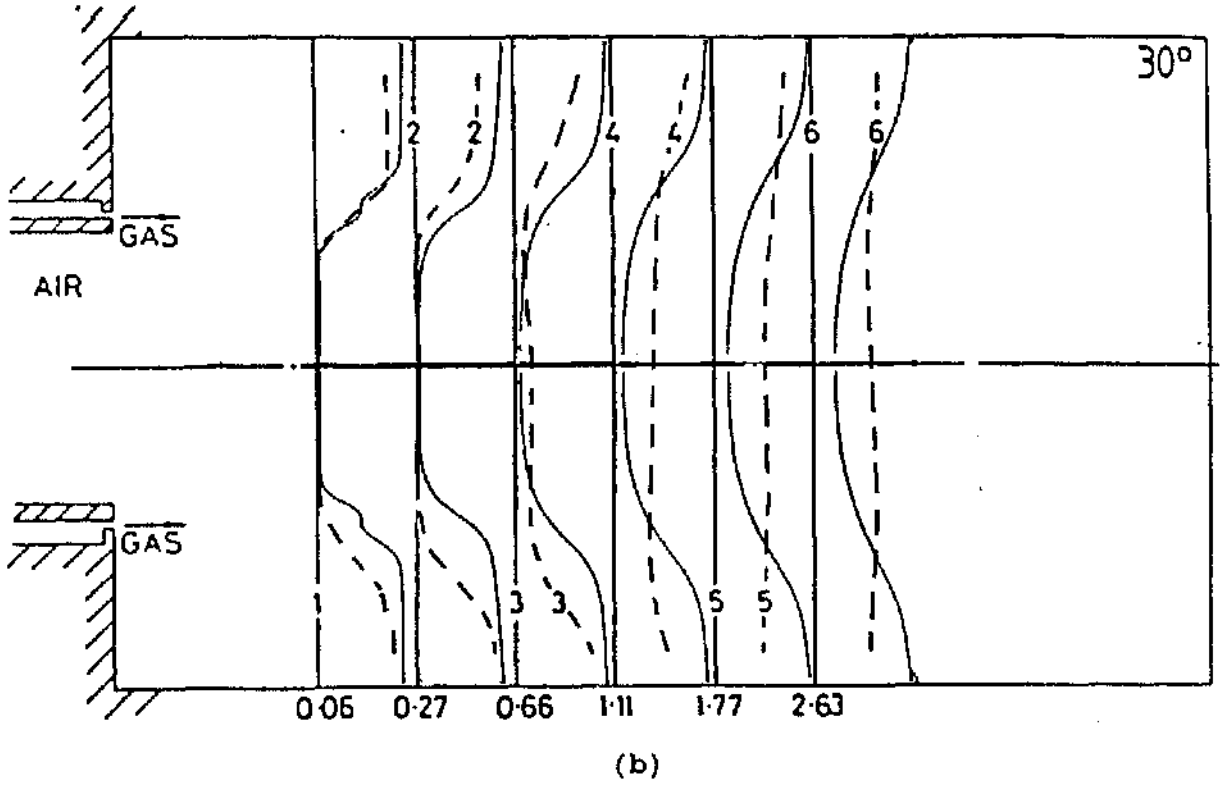

(b)

Fig. 8 : Product concentration distributions

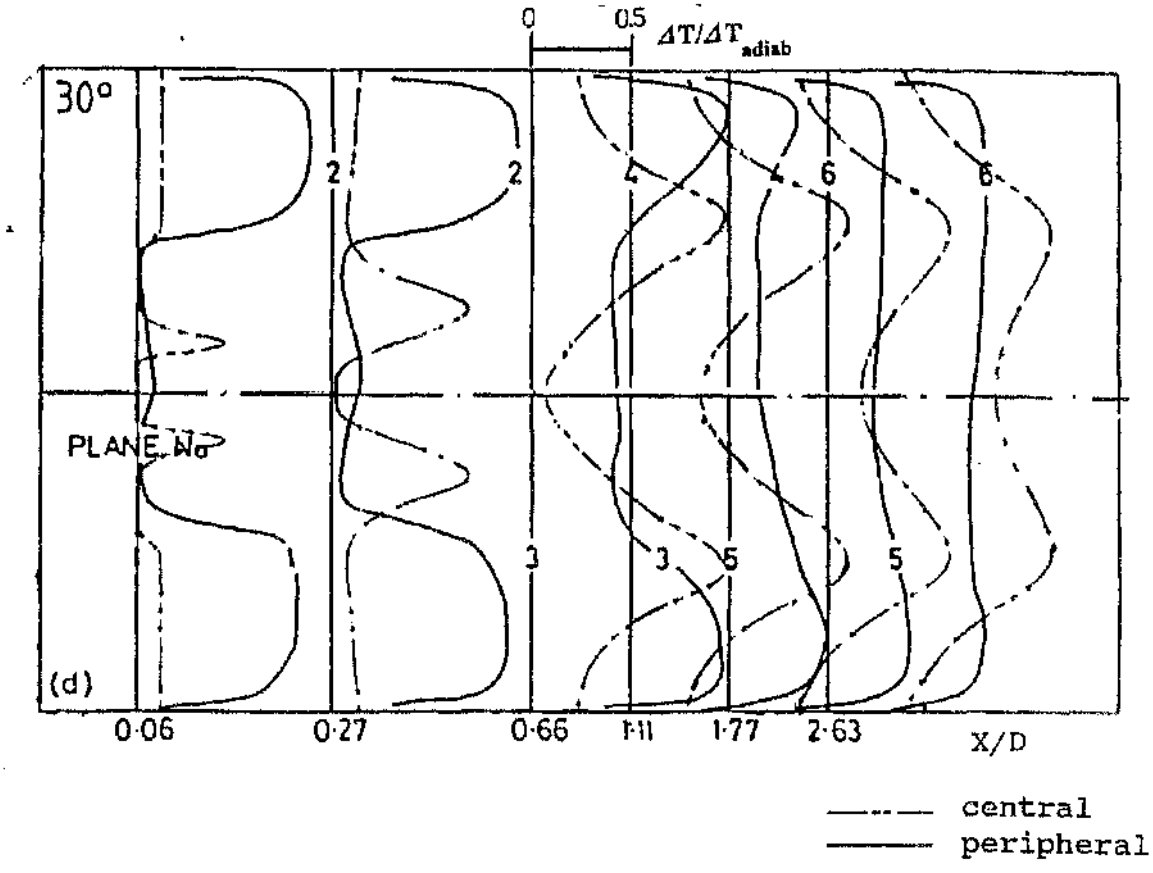

Fig. 9 : Comparison of predicted temperature rise, Central and Peripheral fuel injection systems

International Conference on Combustion Technology for a Clean Environment, 3-6 Sep, Vilamoura (Algarve), Portugal.

THE EFFECT OF BURNER PARAMETERS ON NOx FORMATION IN A GAS FIRED FURNACE- MEASUREMENT AND MODELLING

KENBAR A M A[1], BELTAGUI S A [1,2], RALSTON T[2] AND MACCALLUM N R L[1]

1-University of Glasgow
2-Heat Transfer and Fluid Flow Service (HTFS), National Engineering Laboratory, East Kilbride, Glasgow

ABSTRACT

This paper reports results of NOx measurements carried out on a gas fired furnace. The data consists of a complete mapping of NOx concentration in the furnace under variable swirl conditions. Swirl produced locally higher NOx concentrations but little overall increase. The data is needed for testing and developing theoretical models. Measured stack NOx variations with burner input conditions indicate that operating with a fuel rich mixture is more effective in suppressing NOx formation than with excess air operation.
Theoretical predictions of the overall NOx formation are made using a well-stirred reactor model based on the Zeldovich mechanism with account for the species concentration fluctuations. The model predictions compare satisfactorily with the measurements.

NOTATION

$[N_2]$	Nitrogen concentration,	mol/cm^3 s
$[O_2]$	Oxygen concentration,	mol/cm^3 s
S_o	Mixedness factor, dimensionless	-
t	Residence time ,	s
T	Flame temperature,	K
Z	Fluctuation parameter, dimensionless	-
ϕ	Fuel/air equivalence ratio, dimensionless	-
$\overline{\phi}$	Mean value of ϕ	
σ	Standard deviation, dimensionless	-

1 INTRODUCTION

The need to protect the environment from combustion generated NOx has led to considerable demand to improve burner design. Swirl is one of the important features of burner design since it provides satisfactory flame stability by creating a central reverse flow zone.
The mixture fuel/air ratio and firing rate are other parameters of importance in burner operation. These three parameters are interrelated and vary from one combustion system to another. Thus it is important to investigate their effects on the level of NOx emissions. This study makes a significant contribution to the understanding of the main

factors involved in the formation of NOx in these flames. The work also provides a valuable data-base for the assessment and validation of the theoretical models for NOx prediction.
In a previous paper (1) a review was made of the NOx formation mechanisms and methods of abatement. Previous workers have realised that the effect of swirl is linked to other parameters, such as fuel injection mode and fuel/air ratio.
The aerodynamics and combustion patterns of the swirling flames in the National Engineering Laboratory (NEL) furnace have already been extensively studied through detailed measurements of the velocity components, gas temperature and species concentrations of CO_2, CO and O_2. It is thus possible to study the NOx formation in relation to the local flow and thermal parameters, eg temperature. The availability of this complete set of data is useful in testing and developing the furnace flow and heat transfer codes.
The previous measurements mentioned above and those reported here were all obtained in the NEL furnace fired by natural gas through a variable-swirl burner with a quarl. The fuel gas was injected from a central gun radially outward. Four swirl settings were considered, burner swirl numbers ranging from 0.0 to 2.25.
The present paper presents two data sets:
1- The first illustrates complete mapping of NOx concentrations produced under different swirl levels, but with the same firing conditions, in order to study the effect of swirl on NOx formation.
2- The second illustrates the effects of the mixture fuel/air ratio and firing rate on the overall NOx emissions as measured in the stack.
Theoretical predictions of the overall NOx formation under the above test conditions have been made using a well-stirred reactor model based on the extended Zeldovich mechanism. The model takes account of the fluctuations of the concentrations of fuel and oxidant in the NOx reaction zone. A stochastic analysis has been adopted to calculate the effect of these fluctuations on the NOx formation rate. The results of these predictions are compared with the measurements.

2 EXPERIMENTAL PROGRAMME

The aims of the experimental programme were:
1- To produce complete mapping of the local NOx concentrations within the furnace under a range of swirl intensities. This set of data is required for the understanding of the NOx formation mechanism. It is also required for the assessment and development of the modelling procedures.
2- To investigate the effect of the burner parameters, namely, swirl, fuel/air ratio and firing rate on overall NOx formation as measured in the stack.
Both sets of results have been analysed and discussed in the light of the temperature, concentrations and velocity measurements carried out under the same operating conditions.
The NEL furnace is a model of a cylindrical upshot fired heater fired by natural gas through a variable swirl burner with a quarl. The burner used in this study has a moving-block swirl generator supplied by the International Flame Research Foundation (IFRF). The fuel is injected radially outward in the centre of the air jet through 16 holes on the periphery of the fuel gun. Figure 1 illustrates the quarl and the fuel injection geometry.Four swirl settings were considered, with burner swirl number values of 0.0, 0.45, 0.9 and 2.25. Air and fuel flow rates were metered at inlet by orifice plates. The flow rates of air and gas during each run were controlled to within $\pm$ 1%. Detailed natural gas analysis, obtained from British Gas, indicated that, over the period of the tests

the main fuel properties were constant to within ±2 % for the calorific value and ±1.2 %for density and stoichiometric ratio.

In the first set of measurements the furnace firing rate was constant at 400 KW and an inlet air/fuel ratio corresponding to 5 % excess air was used. In the second set, firing rates of 400 KW and 360 KW were used with a wide range of fuel air ratios, corresponding to equivalence ratio range of 0.71 to 1.1, (excess air 40 % to -10 %).

3 MEASUREMENTS AND INSTRUMENTATION.

Radial traverses were carried out at 13 planes along the furnace, located at axial distances from the quarl exit as shown in Fig 2. Additional traverses were made at some of these planes along other radii to check the flow symmetry and probe intrusive effect. Repeatability tests were also performed.
In each level the NOx sampling probe was traversed for at least 1.5 radii to confirm the flow symmetry. The measurement points were spaced 20 to 50 mm according to the gradients of the NOx concentration being measured. Between 13 - 26 measurement points were made in each plane. The absolute positioning of the probe relative to the furnace wall and base plate was achieved to within ± 2 mm.

The probe used in the measurements is a water cooled stainless steel probe. The design of the probe and sampling system is described in Sec. 3.2. After leaving the probe, the gas sample passes through a heated sample line to the NOx chemiluminescent analyser. The analyser was calibrated against a standard sample of 100 ppm nitric oxide (NO) concentration. The calibration was checked before and after each traverse. The maximum drift in the calibration was found to be within ± 2 % of the full scale.
The time-mean NOx concentration values reported are those averaged over a period of 1 minute after allowing sufficient time for purging of the old sample from the heated sample line and analyser. The probe radial traverse and the data collection rate were all controlled by a microcomputer in conjunction with a specialised data acquisition system.
Although all the results are presented in terms of NOx concentration, it should be appreciated that NO is the main constituent of the measured NOx value.

3.1 Sampling conditions

In order to obtain a representative sample, the chemical constitution of the sampled mixture should be maintained. The mixture to be sampled is generally in a process of more or less rapid evolution. This evolution process must be stopped quickly by a suitable cooling process in order to freeze any further reaction in the probe or sampling line. Cooling the sample down to a temperature of 300°C is sufficient to freeze these reactions (2). Excessive, uncontrolled cooling of the gas sample could lead to water vapour condensation along the sampling system. The problem of surface absorption of NOx on the probe and sample line is aggravated by the presence of absorbed films of moisture and hence is most serious when sampling wet gases from flames (3,4). Furthermore, almost all gas analysers are subject to serious interference from water. This effect has been noticed in the chemiluminescent analyser used in the current measurements. The use of desiccants have been found to absorb nitrogen dioxide NO_2 to varying degrees. Cold traps also remove NO_2 and water vapour simultaneously (3).
For the above reasons the sampling system used in the current measurements has been designed to maintain the sample temperature close to

150°C.
Choosing the probe material is also important for NOx sampling to insure no probe reactions or surface ageing with the sampled gas. A system of water cooled stainless steel probe and a teflon heated sample line was found satisfactory for NOx measurements by Allen (3) and Tuttle (5). Stainless steel probes were also used satisfactorily by other investigators (6,7,8,9).
A water cooled stainless steel probe and a teflon sampling line were therefore used in the current measurements. The receiving part of the probe was lined with quartz to avoid the possibility of ageing especially at the high temperature region.
In order to withdraw a local representative sample isokinetic sampling is generally recommended. However, in turbulent recirculating flows isokinetic sampling is difficult to achieve due to the large velocity fluctuations especially in the recirculating zones. It is reported by Oven et al(6) that for such conditions it may be impossible to obtain a properly representative sample either with or without isokinetic sampling. None the less in the present work, the suction velocity was adjusted to be of similar magnitude to the average flow velocity in the furnace.

3.2 Sampling probe

Figure 3(a) shows the NOx sampling probe as supplied by the IFRF. The tip length A-C is exposed to the flame. The sample tube length D-E passes through the water cooled probe carrier to convey the sample to the heated sample line.
Before the measurements were started, the probe performance was tested in the furnace under a range of operating conditions. Two thermocouples were fitted to monitor the sample temperature at points D and E of Fig (3-b). Very low sample temperatures at D and E were observed and condensation of water vapour occurred inside the probe and the analyser. This problem is caused by the excessive cooling rate of the probe tip and further heat loss from the sample tube to the cooling water tubes within the probe carrier. The probe cooling system was therefore modified to control the sample gas temperature at D to 300 °C and at E to close to 150 °C. This control has been achieved as follows;

(a)- Controlling the cooling water temperature supplied to the probe. A bypass system was arranged to mix some of the hot water return from the probe with the fresh cold water supply. To protect the probe against overheating, the return water temperature was monitored to avoid evaporation, and possible probe damage, Fig.(3-b).

(b)-Insulating the probe cooling water tubes in contact with the sample tube, length D-E, to prevent heat loss to the carrier and cooling water tubes.

(c)-To compensate for any further heat losses the sample tube D-E was electrically heated using a specially designed heating system with low voltage variable power supply.
The above sampling system provided complete control on the gas temperature under all the operating conditions considered.

3.3 Preliminary tests:

Before starting the detailed NOx measurements and also at the conclusion of the series of measurements, tests were carried out to ensure repeatability. of the measurements. These tests were carried out at axial positions of 200 and 300 mm for all swirl settings. Figure 4(a,b)

shows samples of the results. Satisfactory repeatability of the measurements was obtained at all swirl settings. The small differences in the peaks of the two profiles (about ± 2 ppm) can be attributed to slight changes in the firing conditions and/or analyser calibration drift. All the differences are within the practical limitations of the experimental measurements.
The effect of probe presence in the flame on the local NOx concentration was also investigated by traversing the probe through two ports, radially opposite, at the 200 mm downstream position. All swirl numbers mentioned earlier (0.0-2.25) were covered. The results are shown for the zero and maximum swirl cases in Figs 5(a,b). These show no noticeable probe disturbance to the flame. However an apparent shift of the profiles in the radial direction is noticed. This shift may be caused by inconsistency in the probe positioning relative to the flow centreline, due to the fact that the burner centreline is about 5mm offset from the chamber centreline.
The observation of no major flame disturbance by the probe is also reported by Oven et al (6) and Ahmad et al (8).

4 EXPERIMENTAL RESULTS AND DISCUSSION:

4.1 NOx formation and swirl:

The results of the first set of measurements are presented in Figs 6(a-d) as contours of the NOx concentration field for the four swirl settings surveyed. Some illustrative radial NOx profiles at three planes near the burner are presented in Figs (7-9), together with the corresponding temperature profiles.
The above NOx contours are discussed in relation with the temperature measurements.For the present discussion, the flow field can be divided into three zones;

1. The main reaction zone (forward flow zone)
2. The central reverse-flow zone (CRZ).
3. The fully developed flow zone

Most of NOx formation takes place in the first zone. Some further reactions occur in the second, leading to uniform concentration distributions in the third zone. The processes occurring in these zones are now discussed.

4.1.1 The reaction zone:

This region covers the area containing the forward flow of the fresh mixture discharged from the burner. It is regarded as extending to the point where NOx concentration becomes uniform across the whole radial profile. The length of the reaction zone decreases from 1.15 m to 0.42 m over the swirl range 0.0 to 2.25. This region is characterised by steep gradients of NOx concentration in both the radial and axial directions. The rate of NOx formation follows closely the rate of the main combustion reactions as indicated by the temperature and main species concentrations.
Figures (7-9), show profiles of NOx with those of temperature for three levels near the burner. The figures demonstrate the relation between NOx concentration and temperature for the cases of swirl numbers 0.0 and 2.25. The axial distance from the burner to the position of maximum NOx concentration decreases as swirl is increased. Figure (10) illustrates this further where the minimum NOx value at any plane is plotted versus the furnace length. The increase in the minimum value of NOx from one plane to the next indicates the newly formed NOx. Radial

profiles show higher NOx concentrations on both sides of the minimum value due to mixing with the reverse flow on the boundaries of this region.

4.1.2 The central reverse-flow zone:

The flow entrained into this zone has come from the forward flow described above. Thus reactions here depend on the length of the CRZ relative to that of the reacting zone.
Figure (11) shows the variation of the NOx concentration at the centreline with axial distance along the furnace.
For low swirl the CRZ is much shorter than the reaction zone, thus the CRZ receives a mixture with reactions still in progress and with low NOx concentration and low temperature values. In this case it was found that no more NOx formation takes place within this zone. A decrease of NOx concentration occurs due to dilution with fresh mixture entrained nearer the burner end, Fig 11.
As swirl is increased the CRZ lengthens and the reaction zone shortens but is still longer than the CRZ. Thus gases with higher NOx concentrations and at higher temperatures enter the CRZ where further NOx reactions take place producing peak concentrations near the burner, as shown in Fig 11, with S=2.25.

4.1.3 Fully developed flow zone:

This region covers the fully developed forward flow downstream from the reaction zone and the reverse flow in the outer recirculating flow. At each swirl setting constant NOx concentrations were measured throughout this region and these equal the value measured at the stack. This value varied from about 25 ppm to 30 ppm over the range of swirl studied.

4.1.4 Discussion of the results:

In the present system burning natural gas, free from nitrogen compounds, NOx is formed by fixation of atmospheric nitrogen . The main mechanism for this process is known to be the thermal one. This reaction mechanism, assumes post flame NOx formation and is usually modelled by the Zeldovich equations. Some additional NOx may be formed within the flame, known as prompt NOx. Previous investigators (10,11,12) suggest that prompt NOx is only significant at rich flames. The present data was obtained in a lean flame with 5 % excess air, thus little or no prompt NOx is expected. The rate of thermal NOx reaction is dependant on three parameters, namely temperature, O_2 concentration and residence time.
It is widely acknowledged that the fluctuations in temperature and oxygen concentration have to be taken into account when calculating thermal NOx, especially in continuous combustion systems such as gas turbines and furnaces. The influence of the fluctuations will be discussed in detail in Section 5.
Turning now to the experimental results, these indicate that the overall effect of swirl on the final NOx emission from the furnace is small. Over the range of swirl studied, swirl numbers 0 to 2.25, the stack NOx concentration varied from 25 to 30 ppm.
The NOx formation in the forward flow reaction zone, as shown by Fig 10, is nearly the same for all swirls, as measured by the increase of NOx over the length x = 0 to x = 1.15 m. The value of NOx at x = 0 is the result of flow from the CRZ mixing with the fresh flow. Thus it can be assumed that all the increase in NOx due to swirl is caused by the reactions taking place within the CRZ. These reactions seem to be most effective in the highest swirl case (2.25) as illustrated by Fig 11.

Thus although swirl increases the rate of the main combustion reaction resulting in a shorter flame, it does not contribute to high NOx generation within the forward flow. This is due to the reduced residence time in the shorter high temperature forward flow zone.
It is also realised that the mixing is affected more by the fuel injection system, than by swirl. The mixing pattern in the present system is governed by the radial fuel injection mode. This can be confirmed by the general similarity of the flow patterns obtained for all swirl cases tested, eg even for zero swirl a CRZ is created (13). The use of different fuel injection mode produces different stability ranges and flow patterns (13). For example using central axial fuel injection in this same burner system produced significantly lower NOx emissions for the same swirl although the stability range was seriously reduced (14). Work by Andrews et al and co-workers (15,16) also demonstrate the significant effect of fuel injection mode on NOx formation.

4.2 NOx variation with mixture fuel/air ratio:

The second set of measurements was aimed at finding the effect of fuel/air ratio upon NOx formation as measured in the stack . The tests covered the same swirl range as for the first set. The fuel equivalence ratio (ϕ) range was 0.71 (40% excess air) to 1.1 (10% deficient air). Most of the tests were carried out under the same input firing rate of 400 KW. However due to control limitations a few tests had to be performed at the lower rate of about 360 KW. The effect of this reduction upon NOx formation is negligible .

4.2.1 The effect of equivalence ratio

(a) Lean mixtures:

Mixtures with excess air up to 40% (ϕ = 1.0 - 0.71), gave only slight changes of the stack measured NOx concentration, Fig12-a. This applies to all swirl settings tested. NOx concentrations are also given in mg/Nm^3 corrected to 3% O_2 in Fig 12-b.
The formation of NOx is dependant upon high temperature and high O_2 concentration. This condition occurs in a very localised adiabatic region where combustion products and unused oxygen coexist. As the excess air is increased the opposing effects of the lower temperature and the increased O_2 concentration seem to balance each other.

(b) Rich mixtures:

Measurements were made of the NOx formed when burning fuel-rich mixtures with ϕ up to 1.11. The results, given by Fig.(12), exhibit a very sharp decrease of NOx as ϕ was increased, this trend being the same for all swirl settings tested.
As mentioned above, the formation of NOx is dependant upon high temperature and high O_2 concentration. For rich mixtures the effects of lower temperature and lack of oxygen both work together towards reducing NOx formation. Some of the measured NOx could be formed within the flame zone by the prompt mechanism although this is unlikely within the relatively limited range of ϕ tested.
This result demonstrates the effectiveness of the air staging technique in reducing NOx formation.

5 MODELLING OF NOx FORMATION:
The aim of this modelling work is to produce a simple engineering model which can be used to predict the overall NOx formation for furnaces.The

model should be able to predict the variation of NOx formation with input conditions, mainly fuel injection mode and equivalence ratio. The model is based on the well-stirred reactor concept with account being taken for local concentration fluctuations. The inputs to the model are limited to the residence time in the reaction zone and the fuel-air mixing parameter.

5.1 Thermal no:

The thermal NO formation rate, based on the extended Zeldovich mechanism, is well established. The rate equation was reduced (1) to the form:

$$\frac{dNO}{dt} = 1.44 \times 10^{17} [N_2] [O_2]^{1/2} (T)^{-1/2} \exp(-69\,460/T) \quad \text{mole/cm}^3\text{s} \quad (1)$$

The application of this equation requires values of all the variables in the RHS as they exist within the NO reaction zone. Since the rate of this reaction is slower than the main combustion reactions, it is possible to assume that reactions of the main species progress to completion before NO reactions start. Thus the values of temperature and concentrations of O_2 and N_2 can be calculated.
However when using measured time-averaged temperatures it was found that NO was underpredicted, sometimes by two orders of magnitude (17). In the present work the predicted NO values were one order of magnitude lower than those measured. The explanation for this lies in the existence of concentrations and temperature fluctuations within the NO reaction zone.
The earlier attempts to measure these fluctuations were limited by the the speed of response of thermocouples. Generally this is too slow to follow the temperature fluctuations beyond 1 kHz,(17) .Recent measurements using CARS technique give a much better indication of the range of the temperature fluctuations, for example LaRue et al (18) measured a 500 K peak to peak range.
These temperature fluctuations are caused by concentration fluctuations. Since the NO reactions take place "immediately" after the main reactions, both temperature and concentrations fluctuations have a considerable influence on the NO formation rate.
It is suggested by many investigators (19,20) that the temperature in the NO reaction zone is the stoichiometric adiabatic flame temperature.Vranos (21) assumed that the thermal NO reactions are not faster than the mixing rates so most thermal NO is formed at or near $\phi = 1.0$. This assumption follows from the fact that stoichiometric mixtures have the highest probability of reaction.
When using finite difference solutions of the flow and combustion equations,the effect of these fluctuations is taken in consideration through the solution of an extra differential equation for the concentration fluctuations, eg., (22). For the present work considering a well-stirred reactor model, a stochastic approach was adopted to estimate the fluctuating components of concentration about the mean value.

5.2 Model assumptions:

Assuming the reaction zone to be one well-stirred reactor and using Eqn. 1, the following analysis is carried out to account for the effect of concentration fluctuations.
On the microscale of mixing, it is assumed that at any location within the well-stirred reactor, the fuel air mixture will have a random distribution of parcels with values of ϕ which have a Gaussian distribution about the mean value $\overline{\phi}$ (23). This assumption agrees with experimental measurements in jet flows as reviewed by Chatwin and Sullivan

(24). The spread of this distribution is dependant upon the value of the standard deviation σ. The value of σ is related to the mixedness (S_o) of the mixture by the relation;

$$\sigma = (1-S_o) * \bar{\phi} \qquad (2)$$

Introducing Z as a non dimensional parameter of fluctuation ;

$$Z = (\phi - \bar{\phi}) / \sigma \qquad (3)$$

The probability density function (p.d.f) of the distribution function of ϕ is written as;

$$f(\phi) = \frac{1}{\sqrt{2\pi}} \exp\left(-\frac{1}{2} Z^2\right) \qquad (4)$$

Integrating the area under the above distribution function, leads to the cumulative density function (c.d.f) of ϕ;

$$F(\phi) = \int_{-\infty}^{\phi} \frac{1}{\sqrt{2\pi}} \exp\left(-\frac{Z^2}{2}\right) dZ \qquad -\infty < \phi < \infty \qquad (5)$$

For standard Gaussian distribution , the value of $F(\phi)$ is usually between 0 and 1. A stochastic process (25) has been implemented to produce the variable Z from Eqn.5 using randomly generated values of $F(\phi)$. From eqn. 3 above and at known values of $\bar{\phi}$ and σ, the stochastic value of ϕ has been predicted. This process gives the Gaussian distribution of ϕ about $\bar{\phi}$.
Of the different parcels, those with ϕ close to unity (ie stoichiometric) have the maximum probability of combustion and thus react first. The products of this reaction will be at the adiabatic stoichiometric flame temperature. The NO reaction will take place effectively at this flame temperature. The required oxygen is assumed to come from the excess air of the unburnt lean parcels with $\phi < 1$. These values are substituted in Eqn. 1.
A mean value of residence time in the reaction zone was calculated from the length of the zone and the average flow velocity in this zone.

5.3 Prompt NOx

Although prompt NOx was initially defined as NOx formed in the flame front, it sometimes refers to NOx resulting from N_2 via reactions other than the Zeldovich mechanism. Detailed models of prompt NOx are not available yet, because the amounts of prompt NOx are small compared to other sources of NOx, and because it seems to occur mainly in very rich flames. It can be important in fuel-rich pockets of diffusion flames. Rate equations were suggested by Fenimore (26) and de Soete (27).
In the present analysis both equations were used to estimate prompt NOx. The results indicate the contribution by this mechanism to be very small , less than 1 ppm.

5.4 Model results:

The above model was tested by application to the conditions of the second set of experimental measurements to predict the effect of fuel/air ratio (equivalence ratio) on the overall NOx emission from the furnace. The value for the standard deviation σ can be estimated from the measurements of the fluctuations of concentrations and temperatures in jet flows, as reported by Becker (28). His results give an estimated value of 0.7 for the parameter So in Eqn 2.
The results for the case of S=0.90 are presented in Fig. 13. The

agreement between the model predictions and measurements is considered satisfactory and very encouraging considering the simplicity of treating the reaction zone as one well-stirred reactor. Unfortunately, the effect of swirl in this system is small and could not be used as a reliable test of this model. However this model can be used for other geometries and conditions. The input data required is restricted to the knowledge of the mixedness of the fuel/air jets and the mean residence time within the reaction zone.

6 CONCLUSIONS

Two sets of experimental measurements have been carried out in the NEL furnace. The first set covers a complete mapping of NOx concentrations carried out at different swirl settings. The effect of swirl on the local NOx concentration has been presented and discussed in the light of the measured flow and combustion patterns.
In the second set, the effect of fuel/air ratio and firing rate on NOx emissions in the stack has been measured.
The reliability of these measurements has been checked by carrying out tests of repeatability and of the probe intrusion effect. Nox concentration profiles have shown reasonable degree of symmetry. This is important for the meaningful comparison with the axisymmetric program predictions.
From the experimental measurements the following conclusions can be drawn;

1 - NOx formation occurred mainly at the high temperature regions downstream of the combustion zone (flame front), hence confirming that NOx has been formed by thermal mechanism which is slower than combustion.

2 - Increased swirl did not contribute significantly to increased NOx emissions. At zero swirl, NOx concentration measured at the stack was about 25 ppm while at the high swirl (S=2.25), NOx concentration was about 30 ppm.

3 - Increased swirl has contributed only to increased local NOx concentrations in the central recirculation zone.

4 - Increased excess air, up to 40%, did not produce a significant alteration in the NOx emissions.

5 - At rich flame conditions, increased fuel equivalence ratio resulted in marked reduction of NOx emission. This finding supports the use of air-staged combustion for NOx reduction.
Theoretical predictions of the overall NOx formation under the above test conditions have been made using a well-stirred reactor model based on the extended Zeldovich mechanism. The model takes account of the fluctuations of the concentrations of fuel and oxidant in the NOx reaction zone. A stochastic analysis has been adopted to calculate the effect of these fluctuations on the NOx formation rate. The results of these predictions compare satisfactorily with the measurements.

ACKNOWLEDGEMENTS
The authors wish to thank colleagues at the National Engineering Laboratory (NEL) and the University of Glasgow for their advice and encouragement. This work was supported in part by the Management Board of the NEL .
A M A Kenbar wishes to acknowledge the support of the government of Iraq.

REFERENCES

(1) BELTAGUI, S. A., KENBAR, A. M. A. and MACCALLUM, N. R. L. NOx generation and control in confined swirling flames - review and parametric study. HTFS Research Symp., 1989, RS 827,NEL/HTFS 123.

(2) CHEADAILLE, J. and BRAUD, Y. Industrial flames. 1972, vol. 1, Measurements in flames, Edward Arnold publishers, London.

(3) ALLEN, J. D. A. review of methods of analysis for Oxides Of Nitrogen. J. Inst. of Fuel, 1973, vol.46, pp. 123-133.

(4) DE SOETE, G. G. N_2O analysis techniques : Gas chromatography with EC detection; sampling techniques. 1st topic Oriental meeting TOTeM1, 1989, IFRF, Amsterdam.

(5) TUTTLE, J. H. SHISLER, R. A. and MELLOR, A. M. Nitrogen Dioxide formation in gas turbine engine: Measurements and measurement methods. Combust. Sci. and Tech., 1974, Vol. 9, pp. 261-271.

(6) OVEN, M. J. GOULDIN, F. C. and MCLEAN, W. J. Temperature and species concentration measurements in a swirl-stabilized combustor. 17th Int. Symp. on Combustion, 1978, pp. 363-374.

(7) SADAKATA, M. FUJIOKA, Y. and KUNII, D. Effects of air preheating on emissions of NO, HCN and NH_3 from a tow-staged combustor. 18th Int. Symp. on Combustion, 1980, pp. 65-72.

(8) AHMAD, N. T. ANDREWS, G. E. KOWKABI, M. and SHARIF, S. F. Centrifugal mixing forces in enclosed swirl flames. 20th Int.Symp. on Combustion, 1984, pp 259-267.

(9) MULHOLLAND, J. A. and HALL, R. E. Fuel oil reburning application for NOx control to fire tube package boilers. J. Eng. Gas Turbine Power, 1987, v. 109, pp. 207-214.

(10) SAROFIM, A. F. and POHL, J. H. Kinetics of Nitric Oxide formation in premixed laminar flames. 14th Int. Symp. on Combustion, 1972, pp. 739-754.

(11) SEMERJIAN, H. and VRANOS, A. NOx formation in premixed turbulent flames. 16th Int. Symp. on combustion, 1976, pp. 169-179.

(12) WILLIAMS, A. Combustion-Generated NOx. Joint meeting of the British and French Sections of The Combustion Institute, Rouen, 1989, pp.A1-A11.

(13) BELTAGUI, S. A. MACCALLUM, N. R. L. and RALSTON, T. The effect of fuel injection modes on combustion. British Flame Days,1988, Imperial college, London.

(14) KENBAR, A. M. A. BELTAGUI, S. A. B. and MACCALLUM, N. R. L. The effect of fuel injection modes on NOx emissions from swirling flames. 1990, To be published.

(15) ANDREWS, G. E. ABDUL AZIZ, M. M. ABDUL HUSSAIN, U. S. et al, High intensity burner with low NOx emissions. British Flame Days, 1989, Furnace combustion Research and its applications, The Institute of Energy, London.

(16) AL-SHAIKHLY, A. F. A. ANDREWS, G. E. and ANIAGOLU, C. O. Jet shear layer turbulent diffusion flames for ultra-low NOx emission. Joint meeting of the British and French Sections of The Combustion Institute, Rouen, 1989, pp. 5-8.

(17) SADAKATA, M. and BEER, J. M. Spatial distribution of Nitric Oxide formation rates in a swirling turbulent methane-air flame. 16th Int. Symp. on Combustion, 1976, pp. 93-103.

(18) LaRue, J. C. SAMUELSEN, G. S. and SEILER, E. T. Momentum and heat flux in a swirl-stabilized combustor. 20th Int. Symp. on Combustion, 1984, pp.277-285

(19) TOOF, J. L. A model for the prediction of thermal, prompt, and fuel NOx emission from combustion turbine. ASME J. Eng. gas turbine Power, 1986, v.108, pp. 340 347.

(20) TAKAGI, T. OGASAWARA, M. and DAIZO, M. Nox formation from nitrogen in fuel and air during turbulent diffusion combustion. 16th Int. Symp. on Combustion, 1976, pp 181-189.

(21) VRANOS, A. Turbulent mixing and NOx formation in gas combustors. Combustion and Flame, 1974, Vol. 22, pp. 253-258.

(22) ELGHOBASHI, S. E. and PUN, W. M. A theoretical and experimental study of turbulent diffusion flames in cylindrical furnaces. 15th Int. Symp. on Combustion, 1974, pp. 1353-1365.

(23) FIAGAN, R. c. and APPLETON, J. P. A stochastic model of turbulent mixing with chemical reaction : nitric oxide formation in a plug-flow burner. combustion and flame, 1974, 23, 249-267.

(24) CHATWIN, P. C. and SULLIVAN, A. N. A simple and unifying physical interpretation of scalar fluctuation measurements from many turbulent shear flows. J. fluid mech., 1990, vol 212, pp. 533-556.

(25) KENBAR, A. M. A. Stochastic modelling as a design technique for predicting internal heat gains in buildings. MSc thesis, 1988, Dept. of Mech. Eng., University of Glasgow.

(26) FENIMORE, C. P. Formation of nitric oxide in premixed hydrocarbon flames. 13th Int. Symp. on combustion, 1970, pp. 373-380.

(27) DE SOETE, G. G. Overall reaction rates of NO and N2 formation from fuel nitrogen. 15th Int. Symp. on Combustion, 1974, pp 1093-1102.

(28) BECKER, H. A. Effects of concentration fluctuations in turbulent diffusion flames. 15th Int. Symp. on Combustion, 1974, pp 601-615.

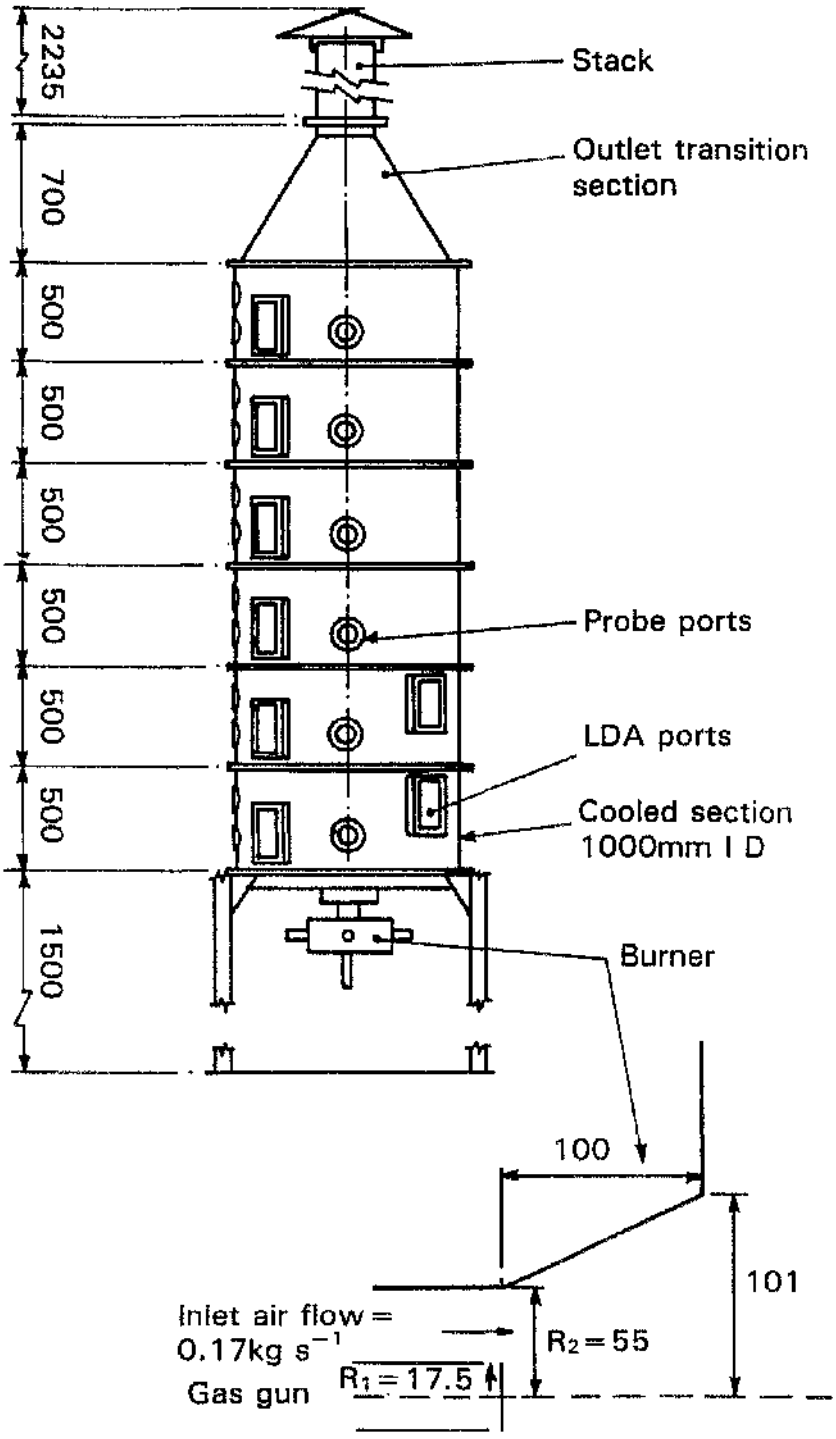

Fig.1: Schematic of furnace and burner

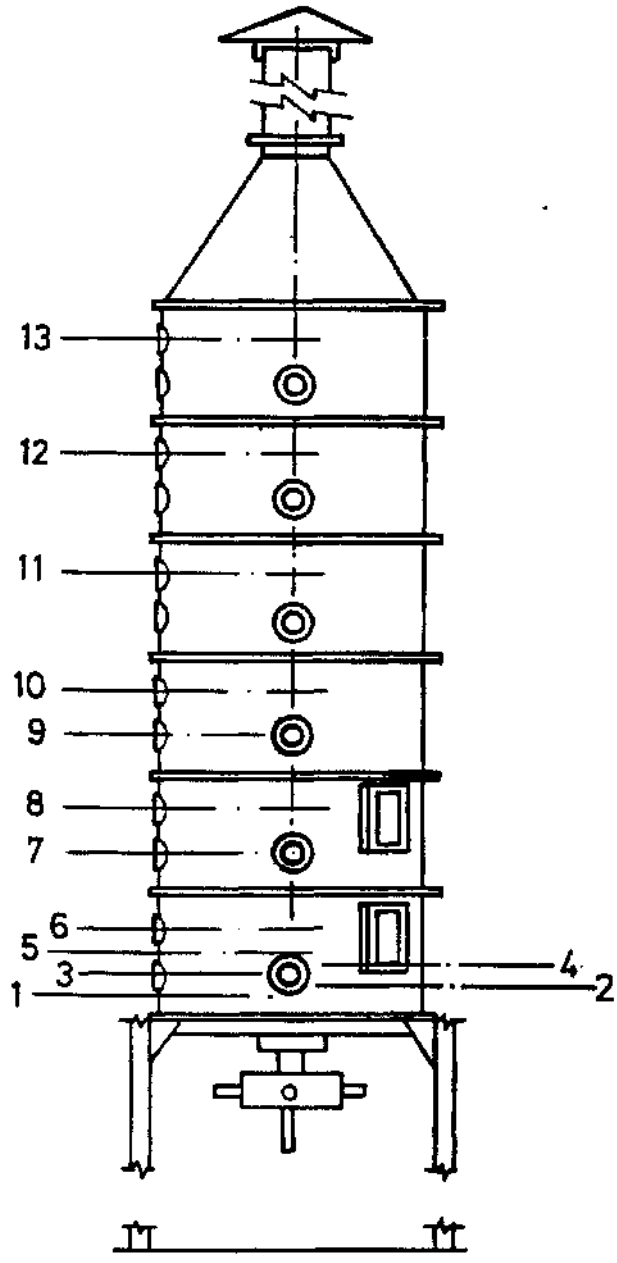

Fig.2: Furnace traversing planes

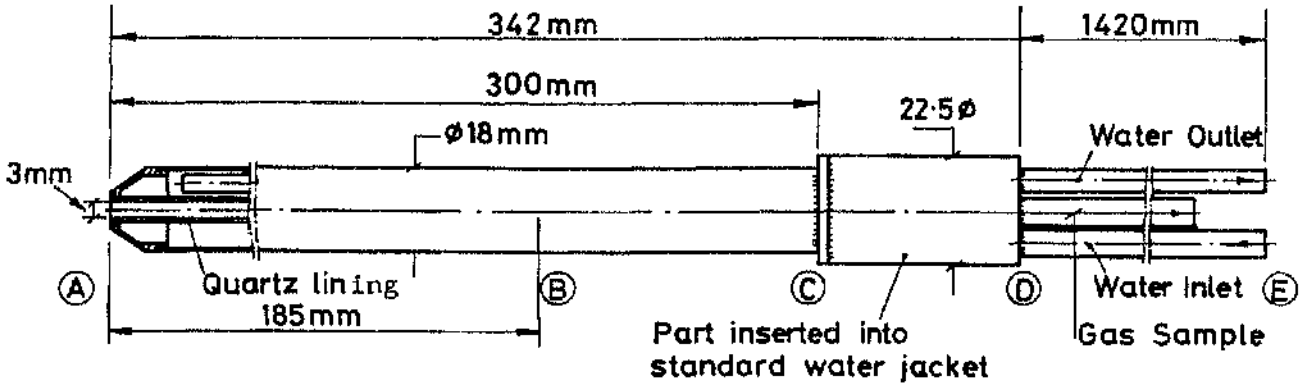

-a-

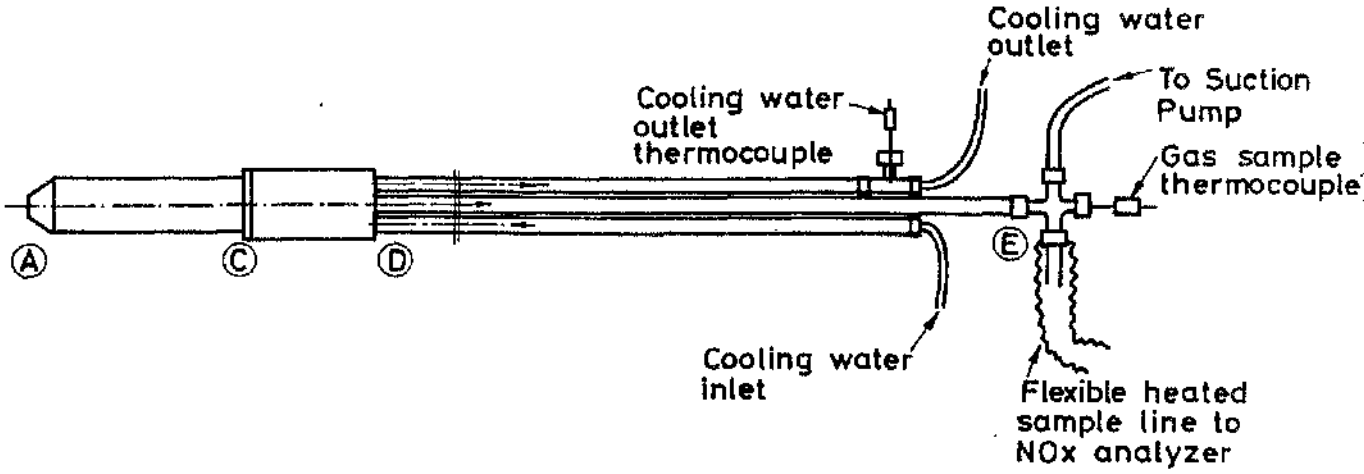

-b-

Fig.3: NOx sampling system

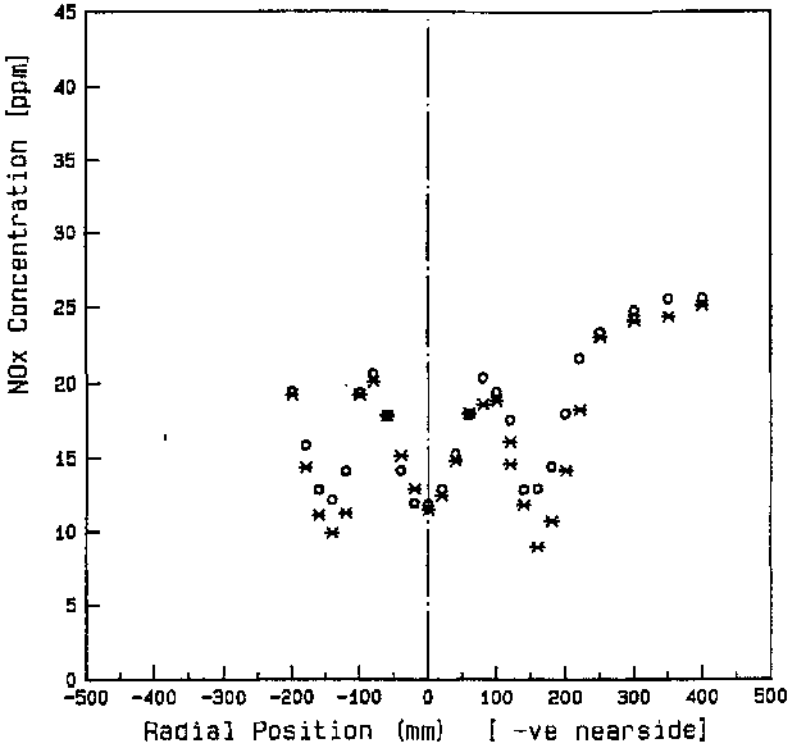

Fig.4-a: Repeatability test, axial position 200 mm, S = 0.0

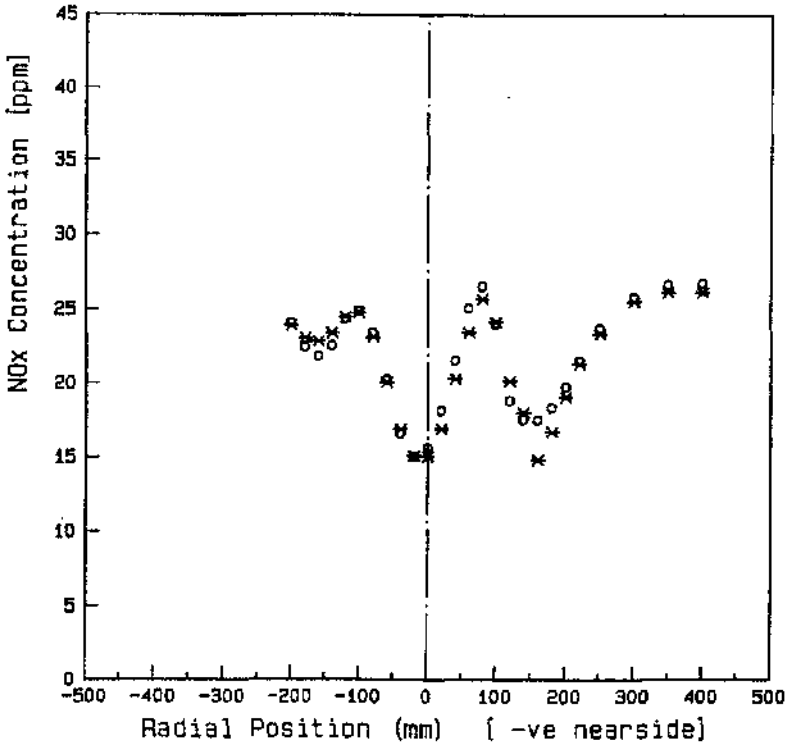

Fig.4-b: Repeatability test, axial position 300 mm, S =0.0

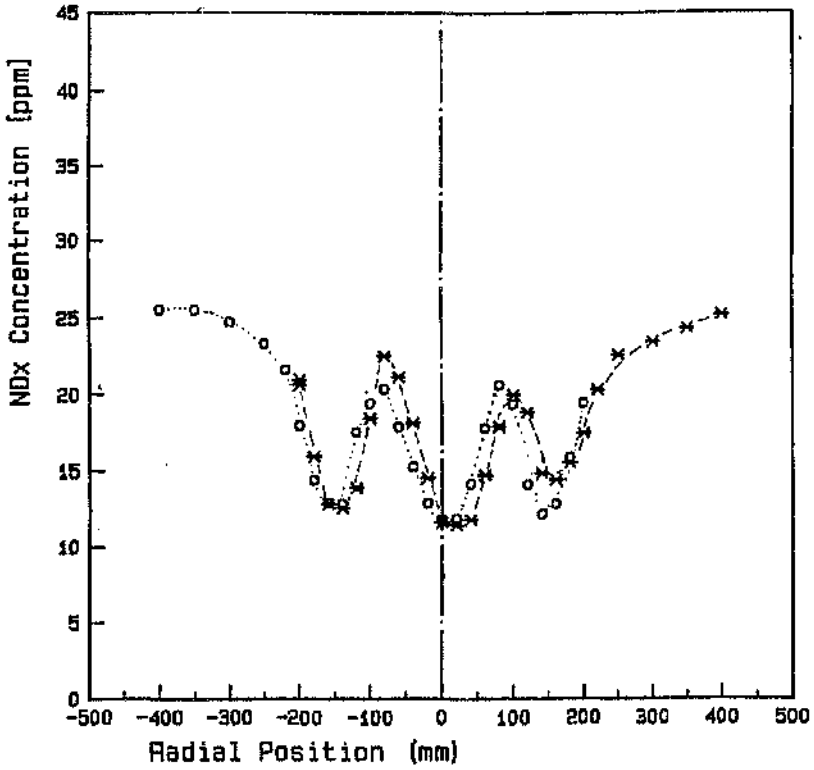

Fig.5-a: Test of probe effect on NOx measurements, axial position 200 mm, S=0.0

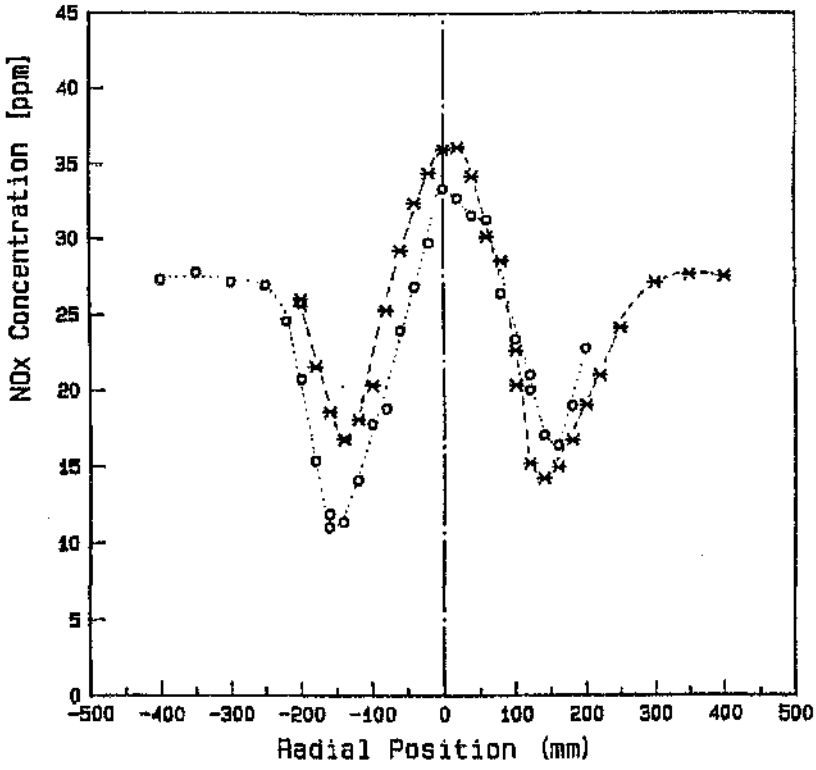

Fig.5-b: Test of probe effect on NOx measurements, axial position 200 mm, S = 2.25

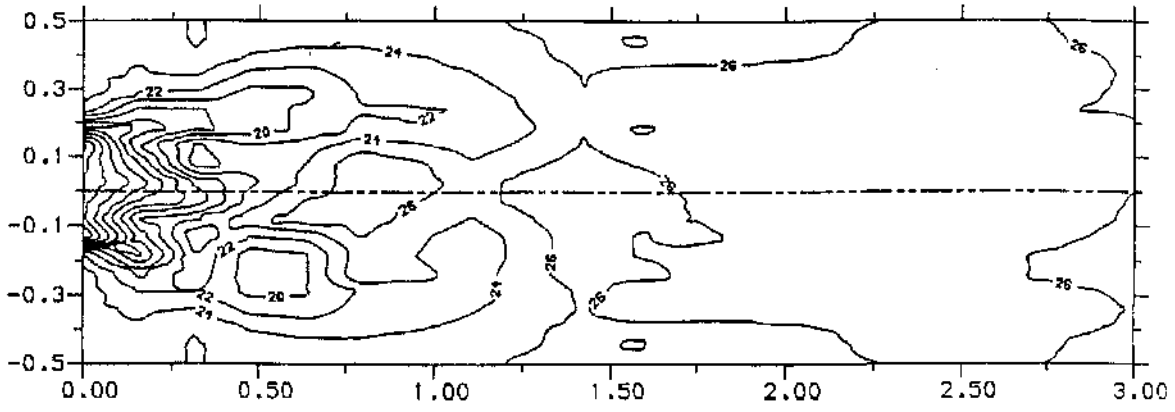

Fig.6-a: NOx contours, S = 0.0

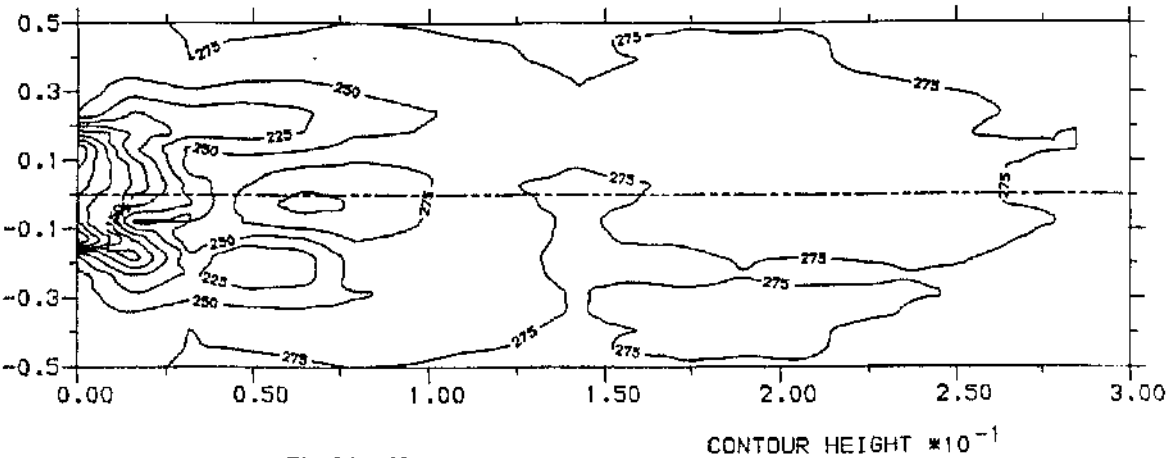

Fig.6-b: NOx contours, S = 0.45

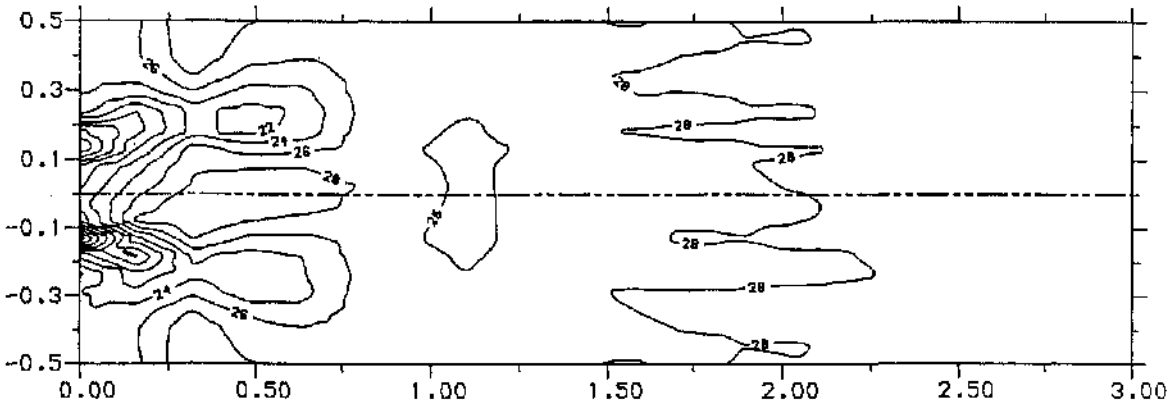

Fig.6-c: NOx contours, S = 0.90

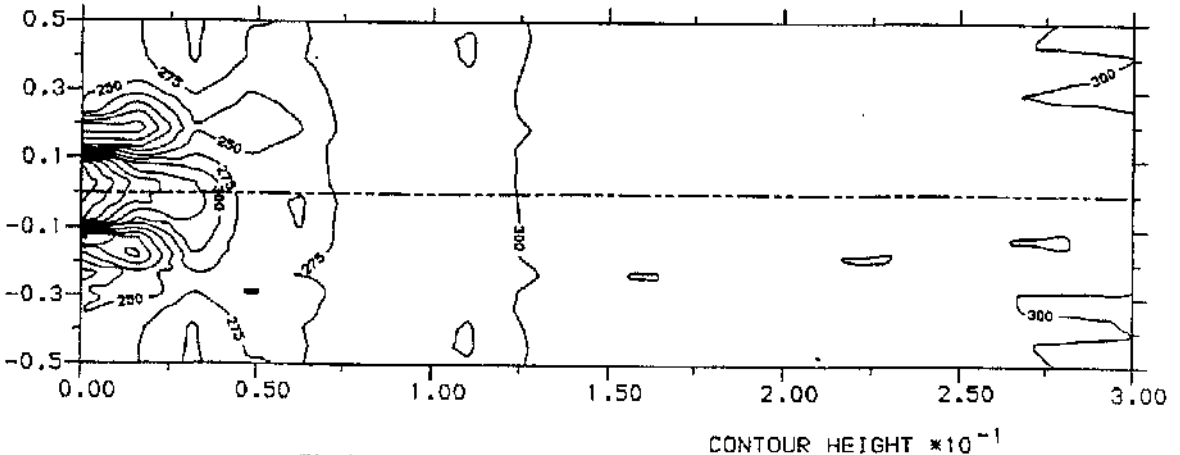

Fig.6-d: NOx contours, S = 2.25

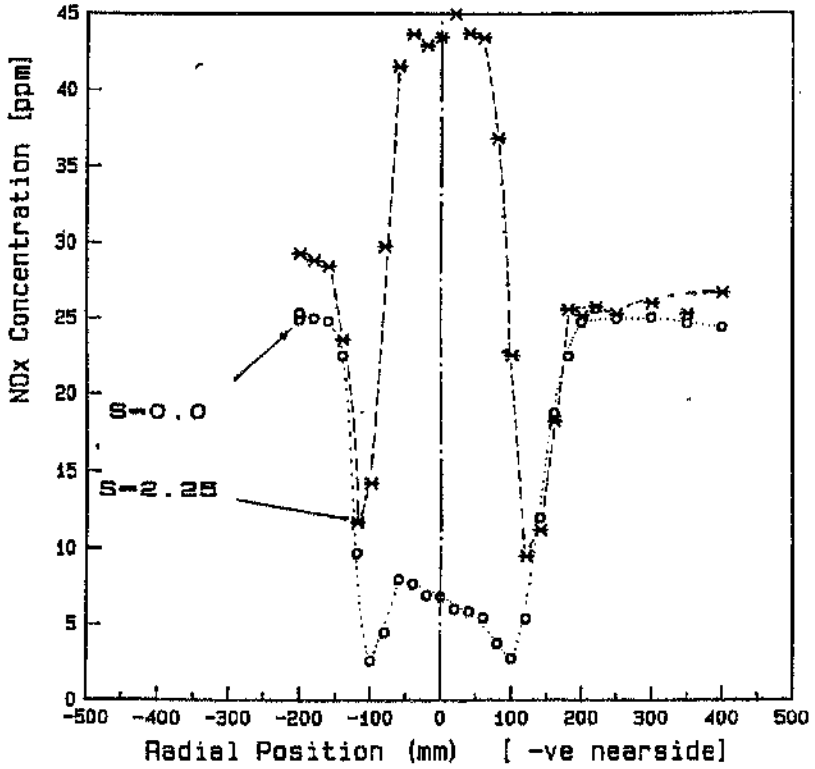

Fig.7-a: Radial NOx profile, axial position 45 mm

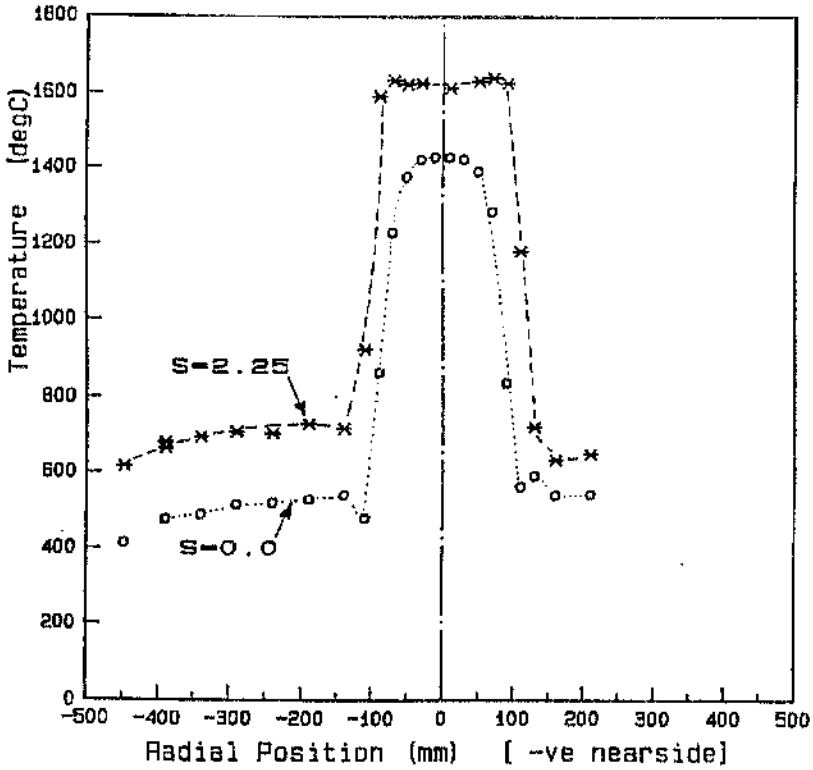

Fig.7-b: Radial temperature profile, axial position 45 mm

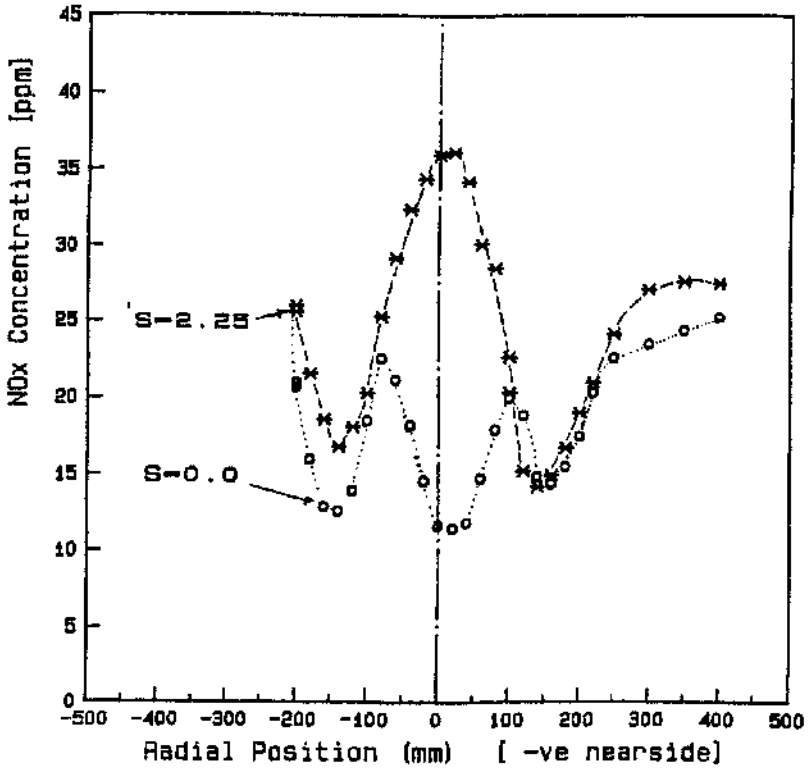

Fig.8-a: Radial NOx profile, axial position 200 mm

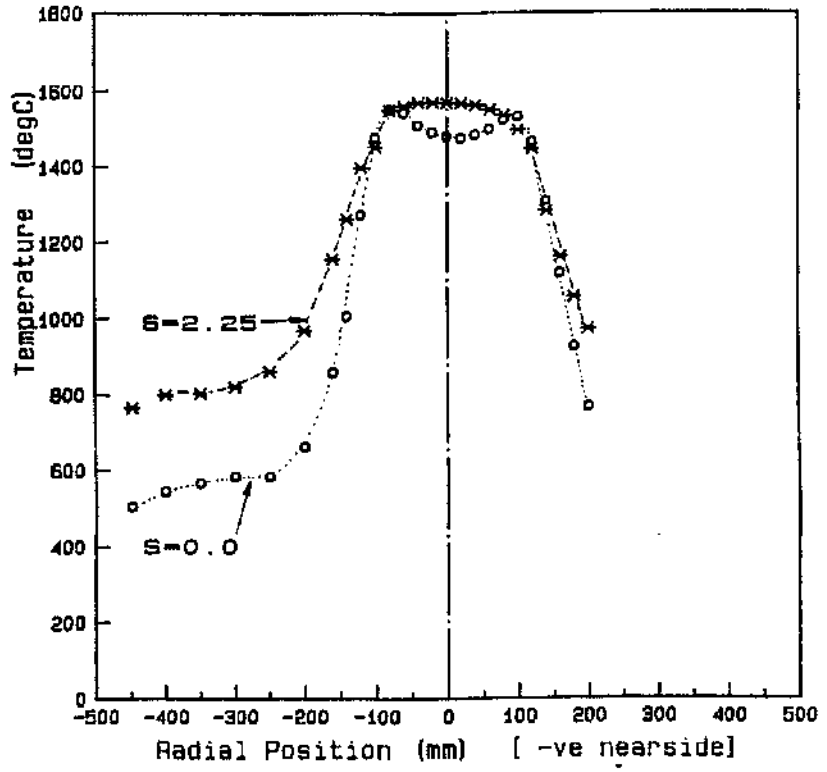

Fig.8-b: Radial temperature profile, axial position 200 mm

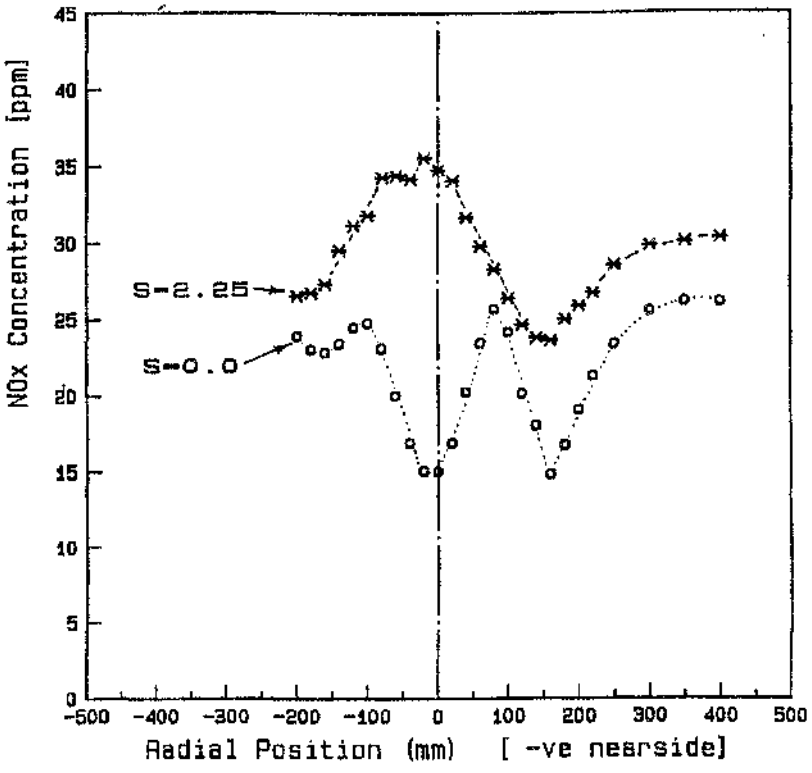

Fig.9-a: Radial NOx profile, axial position 300 mm

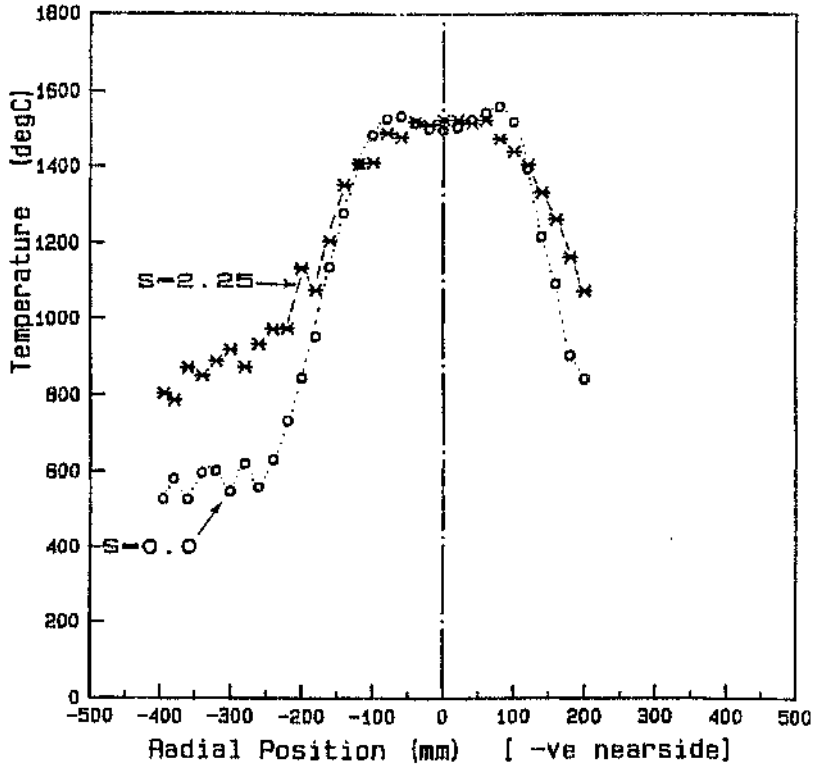

Fig.9-b: Radial temperature profile, axial position 300 mm

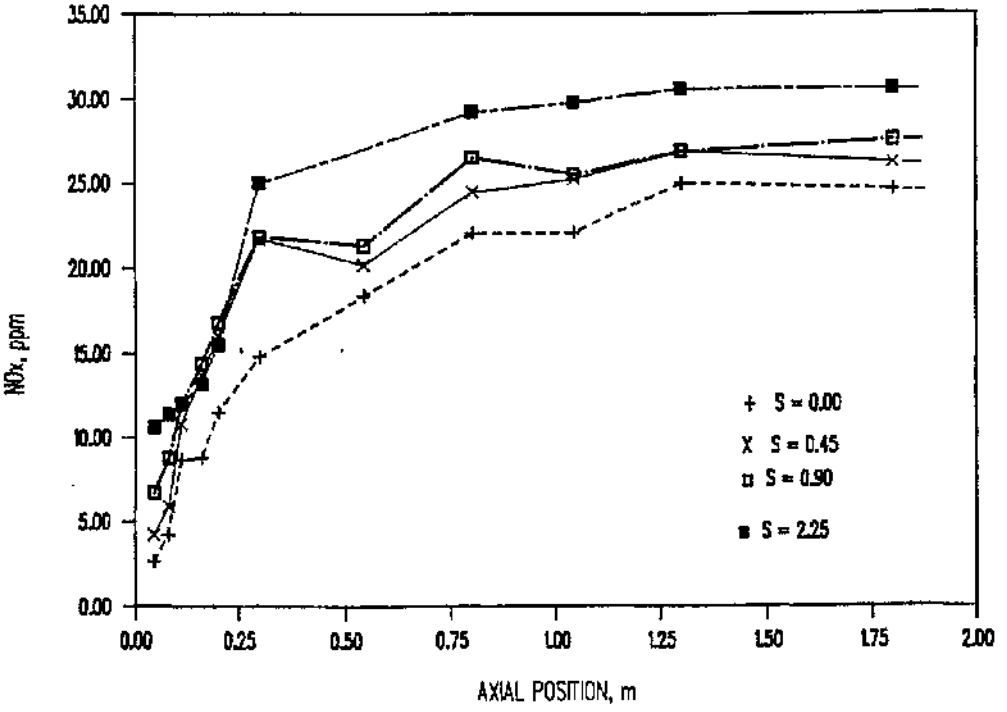

Fig.10: Variation of minimum NOx concentrations along the furnace

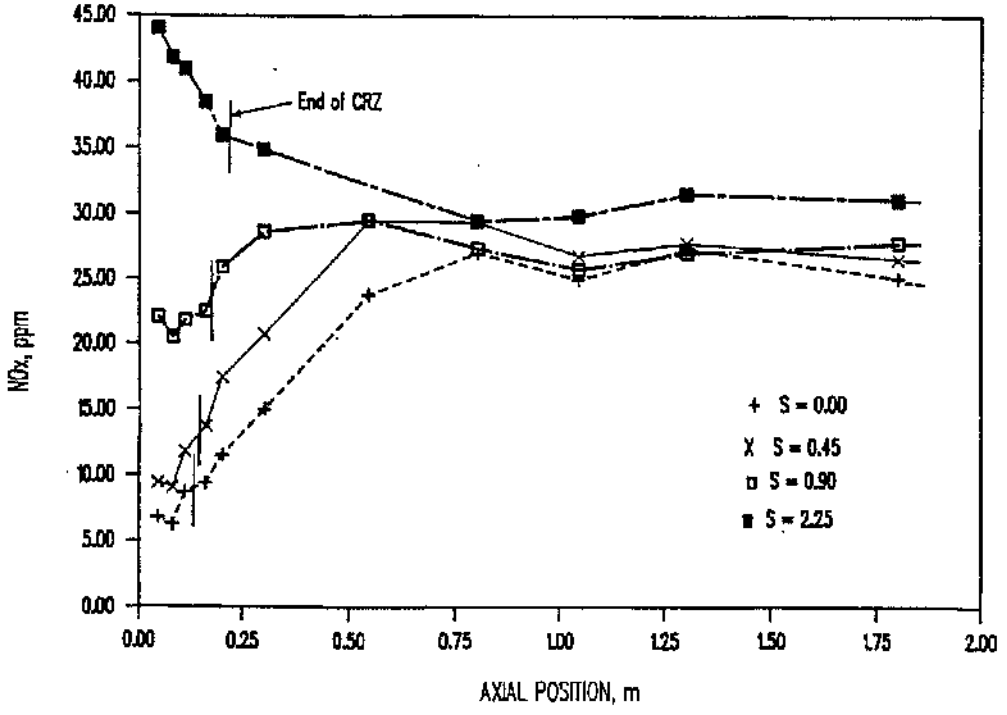

Fig.11: Variation of centerline NOx concentration along the furnace

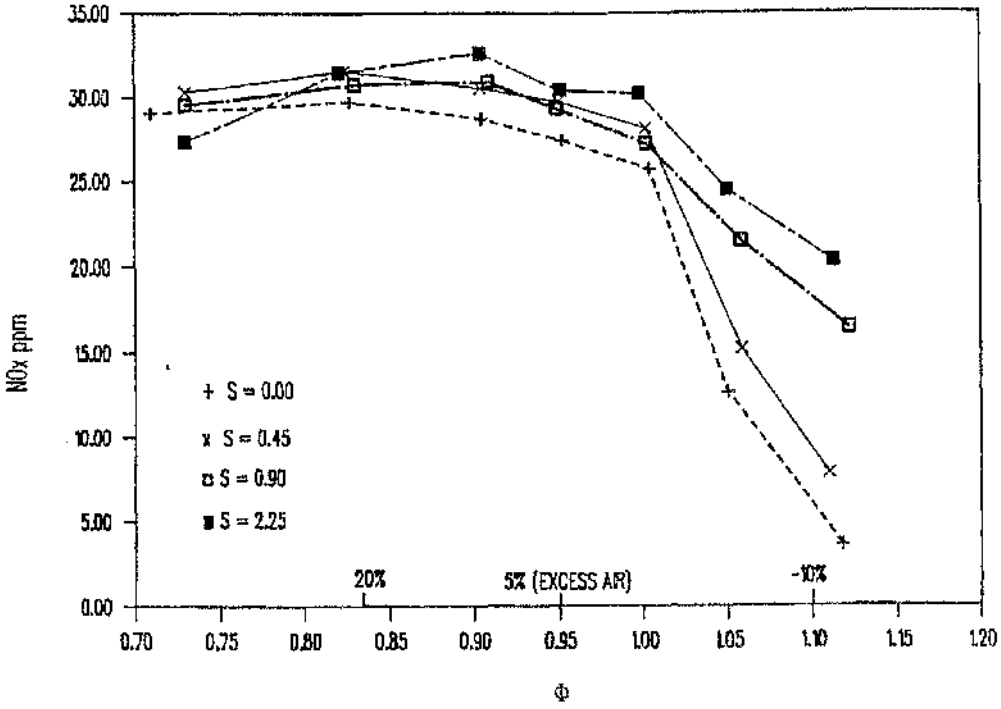

Fig.12-a: Variation of overall NOx concentration (ppm as measured) with fuel equivalence ratio.

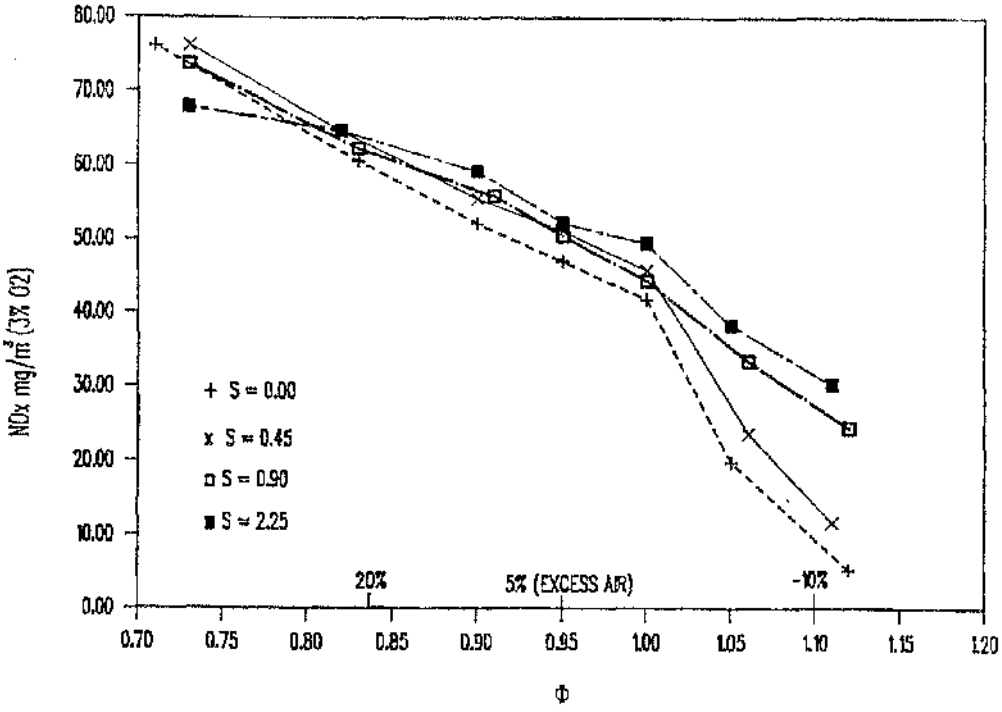

Fig.12-b: Variation of overall NOx concentration (corrected to 3 % O2) with fuel equivalence ratio.

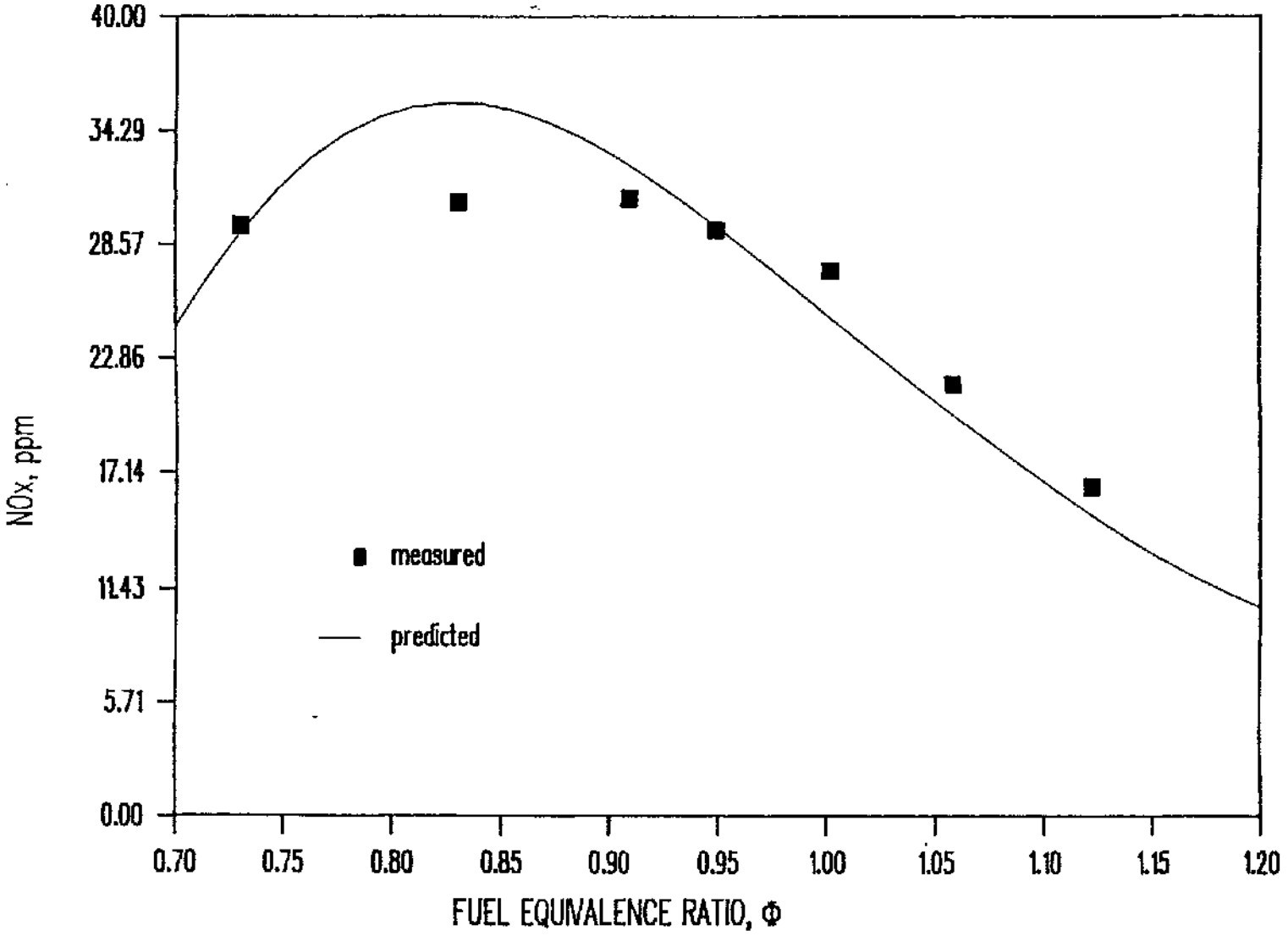

Fig.13: Comparison of predicted and measured NOx concentration, S = 0.90

Euroteck Direct 91, Birmingham, 2-4 July.

MODELLING A GAS-FIRED FURNACE FLOW AND COMBUSTION USING THE PCOC CODE

S A Beltagui[1,2], R N Fuggle[1], A M A Kenbar[2], T Ralston[1],
N Marriott[3] and P J Stopford[3]

1. Heat Transfer and Fluid Flow Service (HTFS),
   National Engineering Laboratory (NEL)
2. University of Glasgow
3. HTFS, AEA Technology, Harwell Laboratory.

ABSTRACT

This paper reports on comparisons between the predictions of the HTFS combustion modelling program, PCOC, and some of the measurements on the NEL furnace emphasising the modelling of the flow and combustion patterns.

The present burner has high-speed radial fuel-jets producing rapid turbulent pre-mixing of the reactants. Such flames have often proved difficult to predict due to limitations in the modelling of turbulence and chemical kinetics.

This paper describes calculations using the 'Eddy Break-up' combustion model. Supplementary information on inlet conditions were deduced from isothermal experiments. The predictions are compared with in-flame velocities and temperatures recently measured in the NEL furnace, with four burner swirl settings.

NOTATION

A	Eddy break-up constant (Model 1)	Dimensionless
B	Eddy break-up constant (Model 2)	Dimensionless
D	Damköhler number	Dimensionless
k	Kinetic energy of turbulence	m^2/s^2
M	Species mass fraction	kg/kg
R	Rate of chemical reaction	kg/m^3s
r	Inlet radius	m
s	Stoichiometric air-fuel ratio	Dimensionless
ε	Rate of dissipation of turbulent kinetic energy	m^2/s^3
ρ	Density	kg/m^3
τ	Time	s

Subscripts

c	Critical
ch	Chemical
f	Fuel
o	Oxidant
p	Product
t	Turbulent

1. INTRODUCTION

The successful prediction of swirling gaseous diffusion flames has been demonstrated by earlier HTFS work and others, eg (1). These works covered burner geometries consisting of two concentric pipes so that the model boundary conditions were simple and no pre-mixing was possible. In industrial applications, however, burners often consist of a central gun which introduces several high-speed jets of fuel gas radially into the swirling air flow within a surrounding pipe. This report describes an extension of the PCOC program to allow the modelling of such burners.

The immediate objective is to model a large and comprehensive set of data which has been measured on the furnace at the National Engineering Laboratory (NEL). The data comprise isothermal (2, 3) and combusting velocities, major species concentrations and temperatures as a function of the air swirl velocity.

The NEL furnace consists of a 1 m internal diameter vertical cylinder, 3 m high. The rig is watercooled in separate sections to facilitate measurement of heat-transfer distribution and is provided with ports for access by a range of probes. The facility is more fully described elsewhere (2-4).

The burner has a fuel injector which consists of sixteen radial gas jets which create intense turbulence leading to rapid mixing within the burner quarl. The resulting pre-mixing of fuel and oxidant means that the combustion rate will depend on the pre-heating and chemical kinetics of the reactants and not just their rate of mixing. Any model of this type of burner must successfully account for both the pre-mixing and combustion phases in order to obtain accurate predictions.

This report uses isothermal mixing data, (2, 3) to avoid the necessity for 3-D turbulence modelling of the radial-jet flow. The partially pre-mixed nature of the combustion is then taken into account by incorporating an 'eddy break-up' model into PCOC.

Before the calculations are described, the PCOC furnace code and the 'eddy break-up' model are briefly reviewed.

2. THE PCOC CODE

PCOC is an extension of the earlier HTFS furnace codes, TUFC and NERO, to include pulverised coal combustion. For gaseous flames, PCOC is essentially equivalent to TUFC except that the burner quarl can now be represented as a series of steps in the finite difference grid. The code solves the steady-state conservation equations for mass, momentum, energy and mixture fractions in an axisymmetric furnace. The solution is found iteratively using line relaxation and the SIMPLEC velocity-pressure coupling method of Reference (5). Turbulence is modelled by the standard k-ε model and radiative heat transfer by a single grey gas approximation and finite-ordinate discretisation. The 'mixed-is-burnt' model, used by TUFC and PCOC for gaseous diffusion flame calculations, is described briefly in the next section.

3. REVIEW OF TURBULENT DIFFUSION FLAME MODELS

Early studies of turbulent jet flames lead to the development of two different classes of model, both of which were based on the assumption that the rate of combustion was controlled by the mixing of fuel and oxidant rather than by the chemical kinetics. The 'mixed-is-burnt' model of Kent and Bilger (6) assumes that the chemical processes are so fast that fuel and oxidant do not co-exist at the same time and place. As a result, concentration fields can be described by a single conserved scalar, the 'mixture fraction'.

Turbulent fluctuations are included by assuming a shape for the pdf describing the fluctuations in mixture fraction. The model has been validated for a wide range of furnace sizes by various workers in HTFS and others eg (1).

The alternative approach is the 'eddy break-up' or 'eddy dissipation' model of Spalding (7) and Magnussen and Hjertager (8) which assumes that the reactants are homogeneously mixed in the fine-scale dissipative eddies of the turbulence. In the limit of fast chemistry, the reaction rate of the fuel is given by the concentration of the limiting reactant:

$$R_f = A\rho \frac{\varepsilon}{k} \text{Min}\left[M_f, \frac{M_o}{s}\right] \qquad \text{Model 1}$$

where M_f and M_o are the mean mass fractions of fuel and oxidant respectively, s is the stoichiometric ratio and A is a dimensionless constant which is usually obtained by fitting the predictions to the data. The choice of A is discussed below. Comparisons between the 'mixed-is-burnt' and 'eddy break-up' model, for example (9), generally indicate close agreement between the two models for near-stoichiometric conditions.

4. PARTIALLY-PREMIXED COMBUSTION MODELLING

When the fuel and oxidant co-exist in the same turbulent eddies, the reaction rate is controlled by chemical kinetics rather than by turbulent mixing. The 'mixed-is-burnt' assumed pdf shape approach depends crucially on the impossibility of the co-existence of reactants in order to uniquely define a mixture fraction. Consequently, an extension to partially-premixed conditions is difficult if not impossible. On the other hand, the 'eddy break-up' model is easily extended.

The approach adopted by Bakke and Hjertager (10) is to quench the reaction at a cut-off point determined by the value of the Damköhler number (D), defined as the ratio of the turbulent and chemical timescales (τ_t/τ_{ch}), ie

$$R_f = \frac{A\rho}{\tau_t} \text{Min}\left[M_f, \frac{M_o}{s}\right] \quad D \geq D_c \qquad \text{Model 2}$$

$$= 0 \qquad D < D_c$$

where $\tau_t = k/\varepsilon$ and $D_c = 10^{-3}$. For natural gas combustion in air, a modified Arrhenius expression for τ_{ch} is given by Beltagui and Maccallum (11). This model has the advantage that τ_{ch} and D_c have direct physical relevance so they can be easily adjusted to apply to different reactants. Ideally, τ_{ch} should be measured in a turbulent flame as the temperature in eddies containing reacting gas may be significantly higher than the bulk temperature.

One way of avoiding explicit chemical modelling is to postulate that the reaction rate in eddies containing a cold unburnt mixture of reactants is proportional to the mixing rate with the surrounding hot combustion products. This phenomenological approach lead Magnussen and Hjertager (8) to a simple extension of the 'eddy break-up' model:

$$R_f = \frac{\rho}{\tau_t} \text{Min} \left[AM_f, \frac{AM_o}{s}, \frac{B M_p}{1+s} \right] \quad \text{Model 3}$$

where M_p is the mass fraction of products and B is another constant. This model has been widely used for partially-premixed gaseous combustion, eg (12), with the constants A = 4 and B = 2 chosen empirically.

In Section 6 all three models are compared with the data from the NEL furnace.

5. COMPUTATIONAL DETAILS

The NEL furnace geometry was discretised by an axisymmetric grid of 54 axial and 42 radial intervals with 588 nodes in the quarl region. The QUICK higher-order differencing scheme was used to avoid the possibility of smearing the near-burner flow details by numerical diffusion.

The measured profiles of axial and swirl velocity at the inlet plane were used as input to the program boundary conditions. Constant profiles were assumed for the other inlet variables. The radial velocity was fixed by the requirement that the radial momentum of the fuel jet is conserved. The effect of varying the initial values of k and ε will be discussed in the next section. The mixture fraction at the inlet was measured by helium tracer experiments performed earlier (2).

The radiation model assumes an emissivity of 0.2 over the quarl and 0.85 on the furnace wall. The absorption coefficient was taken to be 0.355 m^{-1}.

The calculations were performed with under-relaxation fractions of 0.05 for density and reaction rate and 0.3-0.5 for the other variables.

About 2000-3000 iterations were required to reduce the dimensionless mass and enthalpy residuals to 3×10^{-4} and 10^{-3} respectively, at which point the calculations had effectively converged. Each calculation took about 8 minutes of CPU time on the Harwell CRAY-2 supercomputer.

6. RESULTS

The first calculations using the diffusion flame models, 'mixed-is-burnt' and the 'eddy break-up' (EBU) Model 1, greatly over-predicted the reaction rate as expected. As a result, the central recirculation zone (CRZ) was predicted to be over 1 m long compared with the measured 0.25-0.3 m.

The agreement with the data was considerably improved by switching to EBU Model 3.

Figure 1 shows the comparison of the predicted and measured flow reversal boundaries for three different swirl numbers. Examples of the detailed comparisons of temperatures and velocities can be seen in Figures 2-5.

The results obtained with the explicit chemical kinetic model (EBU Model 2) were almost identical with temperatures, for example, agreeing to within 20°C with those of Model 3.

6.1 Flow Pattern

The length of the CRZ was found to be dependent on the assumed inlet values of k and ε. The calculations shown in Figures 2-5 were based on an estimated 15 per cent turbulent velocity giving

k = 10, 13 and 24 m^2/s^2 for swirl numbers 0, 0.45 and 0.9 respectively. The energy dissipation, ε, was taken to be 3000 m^2/s^3 independent of swirl. The effect of varying k and ε on the flow boundaries predicted by Model 3 for S = 0.45 is shown in Figure 6. In general, the length of the CRZ varies approximately as $\varepsilon r^2/k^{3/2}$ where r is the inlet radius.

It is particularly encouraging that the code successfully predicts a CRZ even in the absence of swirl, a feature associated with the radial fuel injection of this burner geometry.

6.2 Temperature Distribution

Temperature distributions are illustrated in Figure 2, where 2a, 2b and 2c show results for S = 0, 0.45 and 0.9 respectively. The upper half of each figure presents the predictions of Model 3. In all three cases the predictions yield higher temperatures in restricted areas than are evident in experimental measurements. Figure 2b is typical with a predicted torroidal region, close to the burner exit, where temperatures exceed those measured by 200°C. It is also notable that the predictions suggest lower exit temperatures than recorded in the measurements. Contour shapes in predictions and measurements are very similar with large zones of the flow being reasonably predicted.

Clearly, the local gas temperatures are highly dependent on the precision of the combustion model and, to a lesser extent, on the transport of mass and radiative heat transfer in the near burner region. Future comparisons will address the heat-transfer behaviour of the predicted system.

6.3 Axial Velocity Profiles

Radial profiles of axial velocity are presented in Figures 3a and 3b. Since the region of most interest is that closest to the burner, results are confined to the first 1050 mm of the chamber. Although 3 components of velocity were measured at 4 swirl intensities, results are presented for only 2 swirl levels in this paper. For all axial locations, measurements from nearside and farside of the furnace centre line are discriminated by the use of cross and box symbols. Whilst not always coincident, a high degree of symmetry is evident in the measured data.

In general, axial velocity profiles are well predicted. In a partially-premixed flame, such as that examined here, the gas expansion associated with combustion has a major influence on the near-flame aerodynamics.

Figure 3a is typical of the set. Close to the quarl exit, very reasonable quantitative agreement in local velocity predictions is evident. PCOC predictions agreeing very closely with the experimental CRZ boundary and the boundary of the outer recirculation zone. Both forward and reversed peak velocities are well predicted up to 110 mm downstream of quarl exit. However, as the flow progresses, the predictions are seen to exaggerate peak velocity values and the associated gradients. PCOC predicts a velocity turning value on the centre line in all of the profiles illustrated, whereas, the measurements indicate that this feature disappears between 300 and 545 mm.

6.4 Radial Velocities

Figure 4 is one example to illustrate the comparison of measured and predicted radial profiles of radial velocity for S = 0.9.

As previously reported, (2, 3) the least confidence in aerodynamic measurements is ascribed to the radial components of

velocity. As with isothermal comparisons, the shape of radial profiles is well represented. It is worth noting that the position of turning points in the experimental profiles are closely represented by the predictions. In general, however, local measured radial velocity values exceed those predicted. Results at higher swirl exhibit marginally better agreement than those at low swirl.

6.5 Swirl Velocity

Figures 5 illustrates the radial profiles of swirl velocity for S = 0.9.

It is clear that, close to the quarl exit, predictions exceed measurements by as much as a factor of two for those areas of the flow where the experimental swirl velocity is well defined. As the flow progresses downstream, the predictions and measurements do exhibit improved agreement.

7. DISCUSSION

Given the complexity of the inlet conditions, the agreement between PCOC, with combustion Models 2 and 3, and data is most encouraging. In particular, the agreement between the chemical kinetic and product eddy mixing models indicate that either can be used depending on the type of reaction rate information available.

The length of the CRZ is found to be much smaller than it is in the corresponding isothermal flow. This is due to the volume expansion associated with combustion at about 0.25 m from the burner. The calculations suggest, however, that there is still some dependence on the burner aerodynamics through the inlet turbulence level.

8. CONCLUSIONS

The 'eddy break-up' model is capable of simulating the combustion of natural gas using a central-gun-type burner. The present theoretical approach should be applicable in many industrial applications which use this type of burner. The success of a combustion model based on chemical kinetics suggests that the model can also be applied in the case of other reactants for which basic kinetic data are available.

The objective of HTFS work on the NEL furnace system has been to provide detailed validation of furnace modelling on a semi-industrial scale facility. Future comparisons with PCOC will allow refinement of the predictions with access to some turbulence information from LDA measurements within the chamber. LDA work will also afford the opportunity of exploring further time-averaged velocities in the near-burner field. In addition, the heat-transfer predictions of the PCOC code will be compared with the detailed heat-flux data previously published, (13).

The local measurements of NO_x, (4), also offer scope for validation of the thermal NO_x model in the PCOC program.

ACKNOWLEDGEMENTS

This work was carried out under the research programme of the Heat Transfer and Fluid Flow Service (HTFS) and was supported by the Department of Trade and Industry. This paper is Crown copyright.

A M A Kenbar wishes to acknowledge the support of the Government of Iraq.

REFERENCES

(1) KHALIL, E. E., HUTCHISON, P. and WHITELAW, J. H., "The calculation of the flow and heat-transfer characteristics of gas-fired furnaces", Proc. 17th Symp. (Int.) on Comb., 1981, p 747, The Combustion Institute, and Harwell report AERE-R 9591.

(2) BELTAGUI, S. A., FUGGLE, R. N. and RALSTON, T., "Aerodynamics and mixing within the quarl of a variable-swirl burner", 1st European Conference on Industrial Furnaces and Boilers, Lisbon, Portugal, March 1988.

(3) BELTAGUI, S. A., FUGGLE, R. N. and RALSTON, T., "An isothermal study of the aerodynamics of the flow issuing from a variable-swirl burner", 1st World Conference on Experimental Heat Transfer, Fluid Mechanics and Thermodynamics, Dubrovnik, Yugoslavia, Sept 1988, pp 1548-1555. Edited by R. K. Shah et al. Elsevier Applied Science Publishers, London, ISBN 0444-013377.

(4) KENBAR, A. M. A, BELTAGUI, S. A., RALSTON, T. and MACCALLUM, N. R. L., "The effect of burner parameters on NO_x formation in a gas-fired furnace - measurement and modelling", paper submitted to Eurotech 91.

(5) VAN DOORMAAL, J. P. and RAITHBY, G. D., "Enhancements of the SIMPLE method for predicting incompressible fluid flows", Numer. Heat Transfer, 1984, 7, 147-163.

(6) KENT, J. H. and BILGER, R. W., "The prediction of turbulent diffusion flame fields and nitric oxide formation", Proc. 16th Symp. (Int.) on Comb., 1976, pp 1643-1656, The Combustion Institute.

(7) SPALDING, D. B., "Mixing and chemical reaction in steady confined turbulent flames". Proc. 13th Symp. (Int.) on Comb., 1970, pp 649-658, The Combustion Institute.

(8) MAGNUSSEN, B. F. and HJERTAGER, B. H., "On mathematical modelling of turbulent combustion with special emphasis on soot formation and combustion", Proc. 16th Symp. (Int.) on Comb., 1976, p 719, The Combustion Institute.

(9) WILKES, N. S., GUILBERT, P. W., SHEPHERD, C. M. and SIMCOX, S., "The application of Harwell-FLOW3D to combustion problems", Harwell report AERE-R 13508, 1989.

(10) BAKKE, J. R. and HJERTAGER, B. H., "The effect of explosion venting in empty vessel", Int. J. Num. Methods Engng., 1987, 24, 129-140.

(11) BELTAGUI, S. A. and MACCALLUM, N. R. L., "Stability limits of free swirling premixed flames. Part II. Theoretical prediction", J. Inst. Energy, 1986, 59, 165-167.

(12) LOCKWOOD, F. C., SALOOJA, A. P. and SYED, S. A., "A prediction method for coal-fired furnaces", Comb. Flame, 1980, 38, 1-15.

(13) BELTAGUI, S. A., FUGGLE, R. N. and RALSTON, T., "Measurement and prediction of heat transfer in the NEL furnace", I.Mech.E./I.Chem.E./Heat Transfer Society, 2nd UK National Heat Transfer Conference, Glasgow, 14-16 Sept, 1988, 2, Paper C163/88, pp 1219-1232, Mechanical Engineering Publications. ISBN 0-85298-667-X.

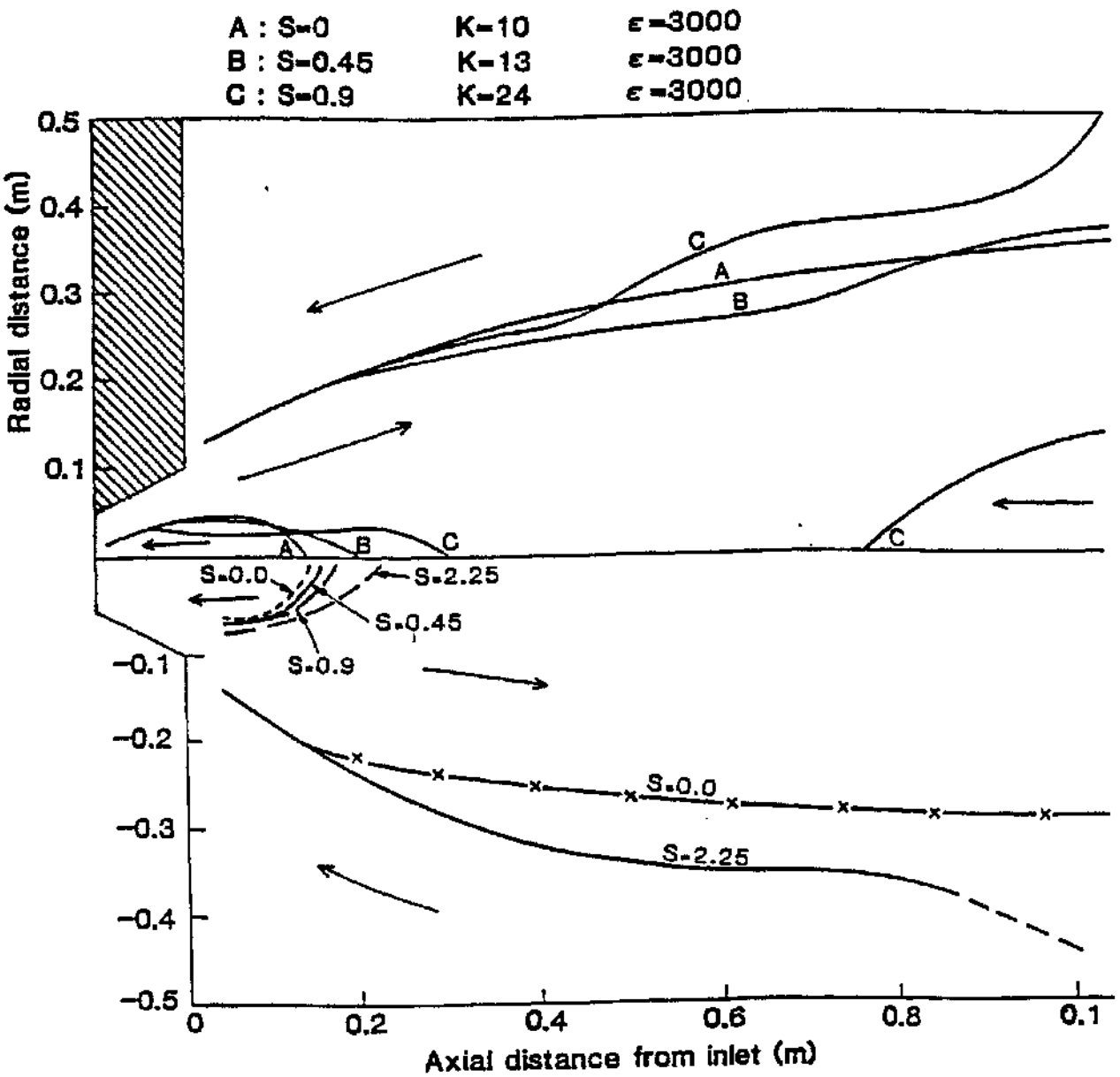

FIG.1: Comparison of predicted (EBU model 3) and flow reversal boundaries

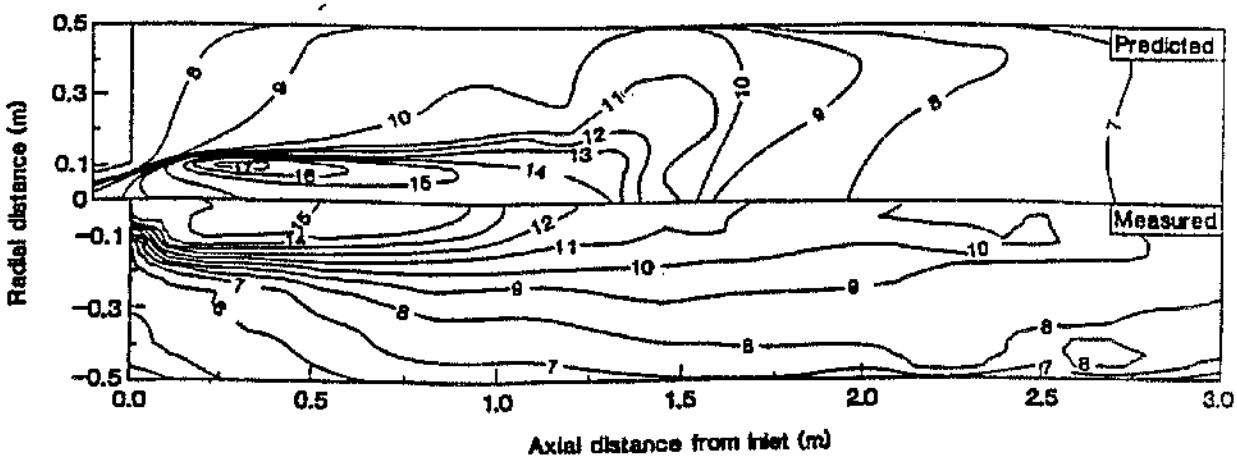

(a)

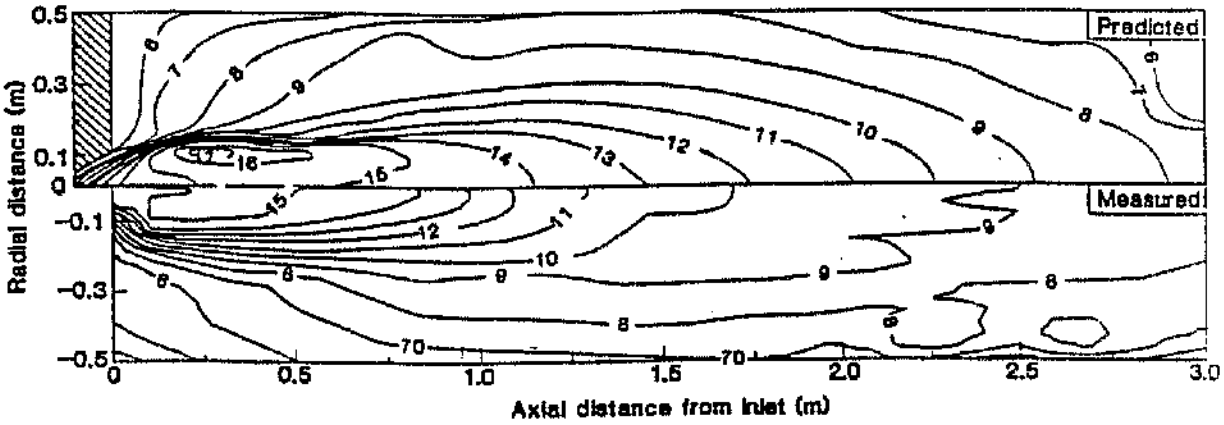

(b)

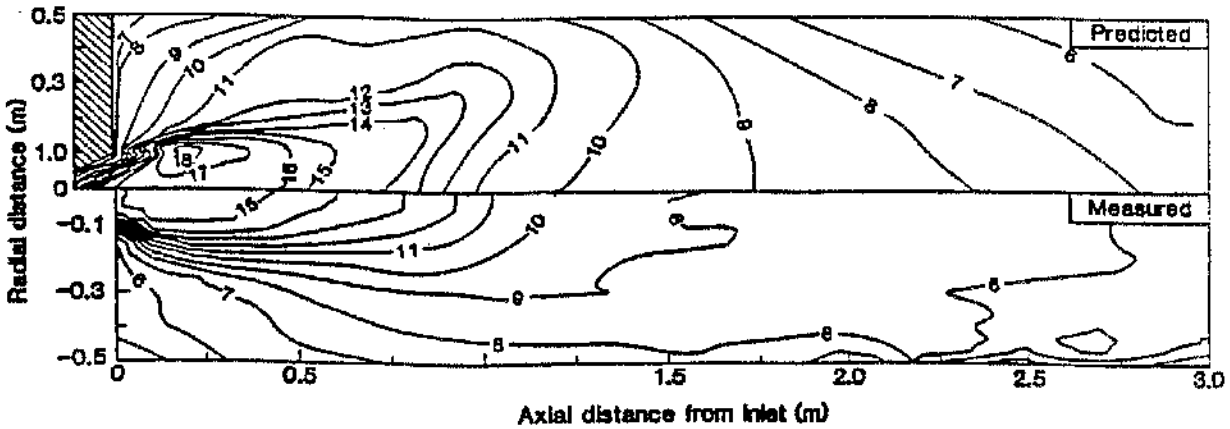

(c)

FIG.2: Temperature contours (arbitrary scale)

(a) S = 0, (b) S = 0.45, (c) S = 0.9

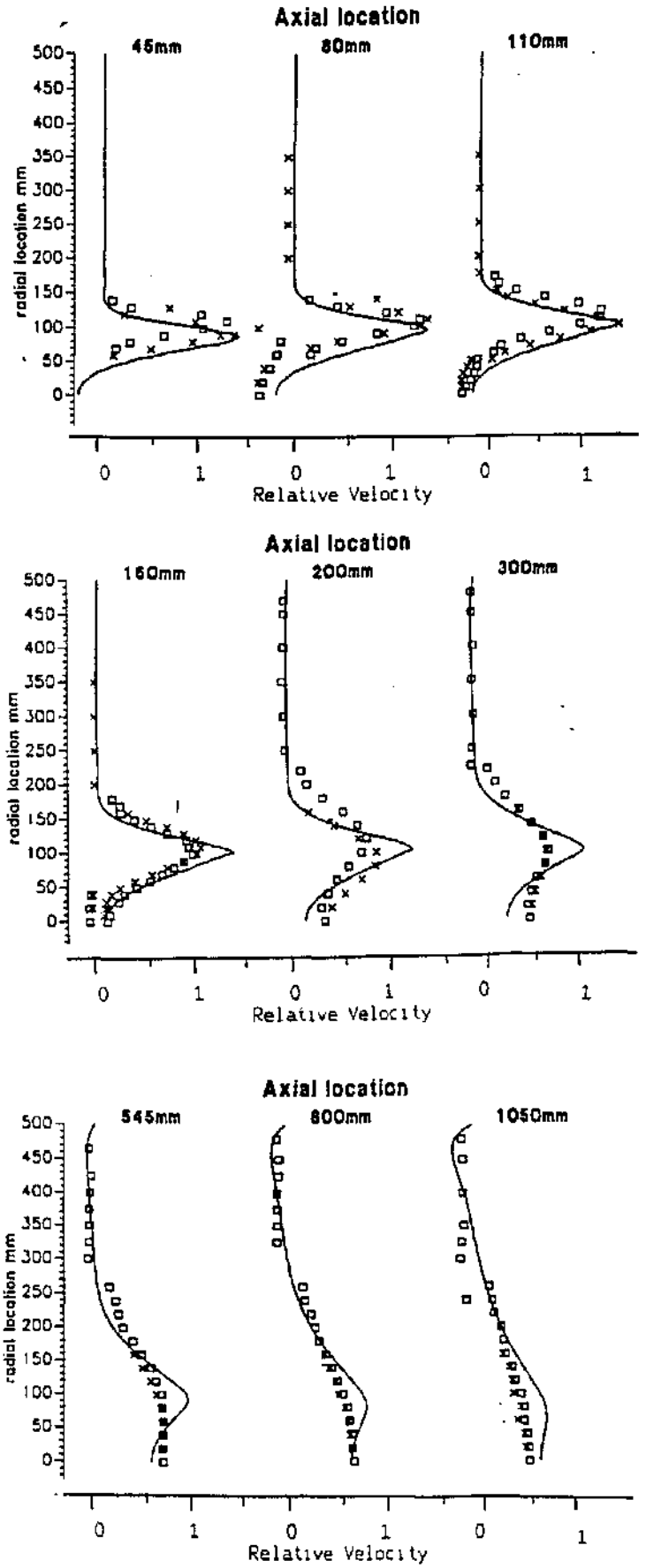

FIG.3: Radial profiles of axial velocity :

(a) S=0

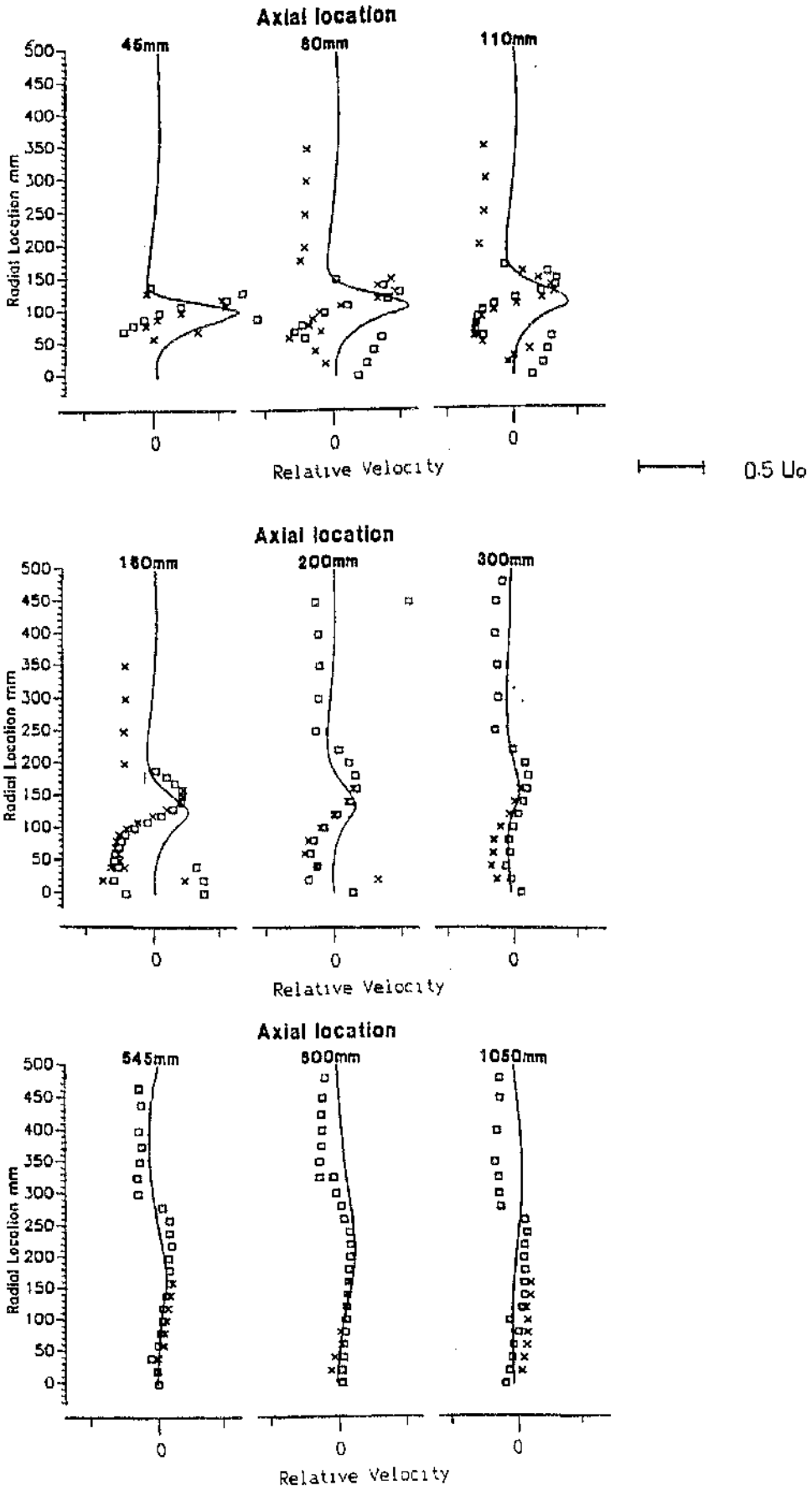

FIG.4: Radial profiles of radial velocity :

S = 0.9

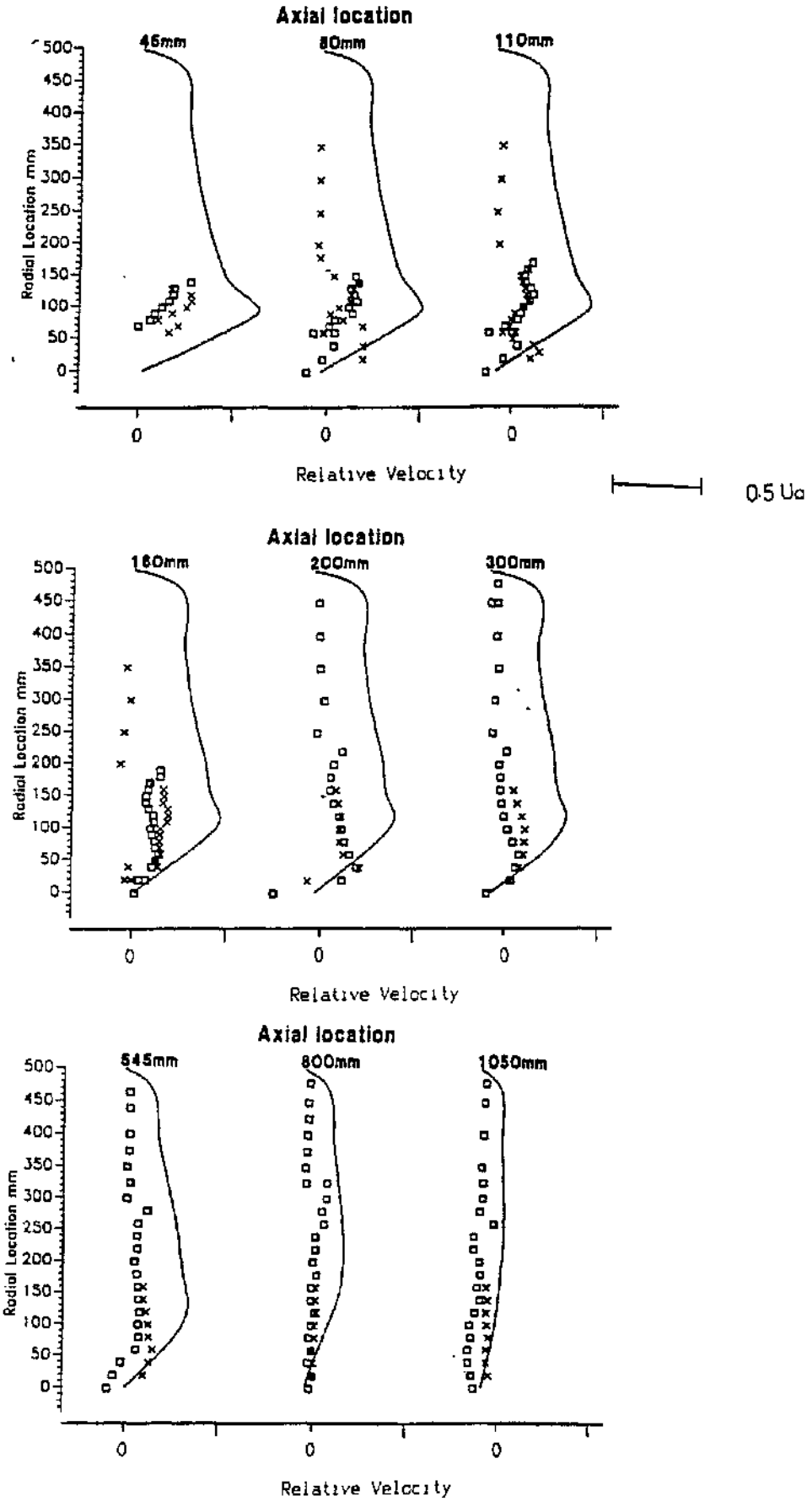

FIG.5: Radial profiles of swirl velocity :

S = 0.9

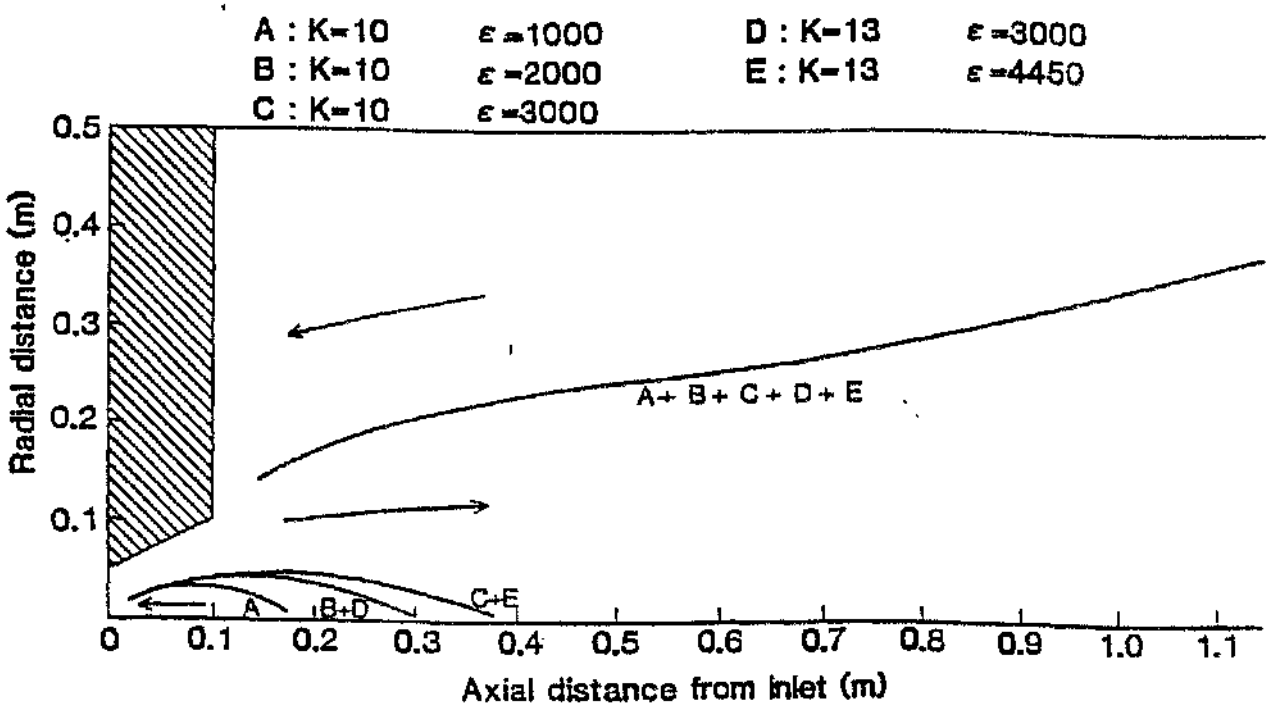

FIG.6: Flow boundaries predicted by model 3 for various choices of k and ϵ at the inlet (S = 0.45)